frontiers | Research Topics

Vaccines and breakthrough infections

Edited by
Sonia Jangra, Donald James Alcendor and Fabio Fiorino

Published in
Frontiers in Immunology

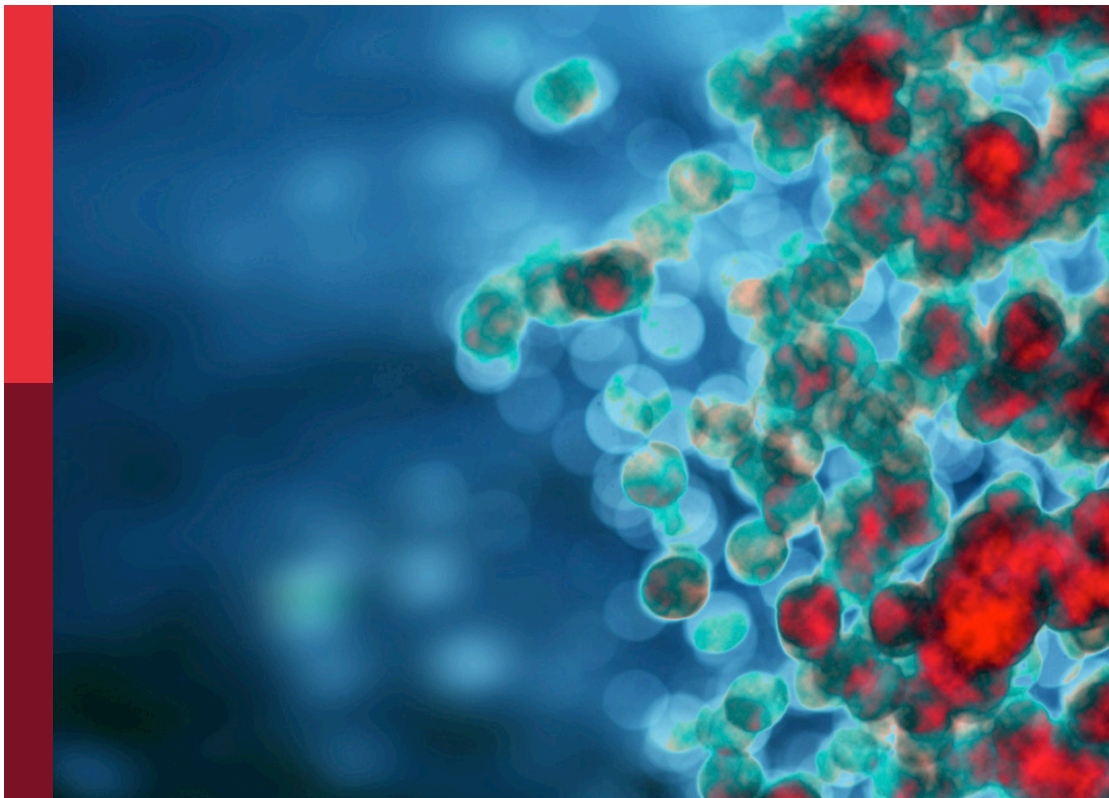

ISSN 1664-8714
ISBN 978-2-8325-7379-2
DOI 10.3389/978-2-8325-7379-2

Generative AI statement
Any alternative text (Alt text) provided alongside figures in the articles in this ebook has been generated by Frontiers with the support of artificial intelligence and reasonable efforts have been made to ensure accuracy, including review by the authors wherever possible. If you identify any issues, please contact us.

About Frontiers

Frontiers is more than just an open access publisher of scholarly articles: it is a pioneering approach to the world of academia, radically improving the way scholarly research is managed. The grand vision of Frontiers is a world where all people have an equal opportunity to seek, share and generate knowledge. Frontiers provides immediate and permanent online open access to all its publications, but this alone is not enough to realize our grand goals.

Frontiers journal series

The Frontiers journal series is a multi-tier and interdisciplinary set of open-access, online journals, promising a paradigm shift from the current review, selection and dissemination processes in academic publishing. All Frontiers journals are driven by researchers for researchers; therefore, they constitute a service to the scholarly community. At the same time, the *Frontiers journal series* operates on a revolutionary invention, the tiered publishing system, initially addressing specific communities of scholars, and gradually climbing up to broader public understanding, thus serving the interests of the lay society, too.

Dedication to quality

Each Frontiers article is a landmark of the highest quality, thanks to genuinely collaborative interactions between authors and review editors, who include some of the world's best academicians. Research must be certified by peers before entering a stream of knowledge that may eventually reach the public - and shape society; therefore, Frontiers only applies the most rigorous and unbiased reviews. Frontiers revolutionizes research publishing by freely delivering the most outstanding research, evaluated with no bias from both the academic and social point of view. By applying the most advanced information technologies, Frontiers is catapulting scholarly publishing into a new generation.

What are Frontiers Research Topics?

Frontiers Research Topics are very popular trademarks of the *Frontiers journals series*: they are collections of at least ten articles, all centered on a particular subject. With their unique mix of varied contributions from Original Research to Review Articles, Frontiers Research Topics unify the most influential researchers, the latest key findings and historical advances in a hot research area.

Find out more on how to host your own Frontiers Research Topic or contribute to one as an author by contacting the Frontiers editorial office: frontiersin.org/about/contact

Vaccines and breakthrough infections

Topic editors

Sonia Jangra — The Rockefeller University, United States

Donald James Alcendor — Meharry Medical College, United States

Fabio Fiorino — LUM Univesity "Giuseppe Degennaro", Italy

Citation

Jangra, S., Alcendor, D. J., Fiorino, F., eds. (2026). *Vaccines and breakthrough infections*. Lausanne: Frontiers Media SA. doi: 10.3389/978-2-8325-7379-2

Table of contents

frontiers | Frontiers in Immunology

TYPE Review
PUBLISHED 05 March 2025
DOI 10.3389/fimmu.2025.1520968

OPEN ACCESS

EDITED BY
Fabio Fiorino,
LUM University Giuseppe Degennaro, Italy

REVIEWED BY
Paulo J. G. Bettencourt,
Universidade Católica Portuguesa, Portugal
Sivaram Gunisetty,
Emory University, United States
Milad Zandi,
Lorestan University of Medical Sciences, Iran

*CORRESPONDENCE
Xiaoyang Liu
xliu263@jhmi.edu

RECEIVED 31 October 2024
ACCEPTED 12 February 2025
PUBLISHED 05 March 2025

CITATION
Liu X (2025) Opportunities and challenges of mRNA technologies in development of dengue virus vaccine.
Front. Immunol. 16:1520968.
doi: 10.3389/fimmu.2025.1520968

Opportunities and challenges of mRNA technologies in development of dengue virus vaccine

Xiaoyang Liu*

Department of International Health, Bloomberg School of Public Health, Johns Hopkins University, Baltimore, MD, United States

Dengue virus (DENV) is a mosquito-borne virus with a significant human health concern. With 390 million infections annually and 96 million showing clinical symptoms, severe dengue can lead to life-threatening conditions like dengue hemorrhagic fever (DHF) and dengue shock syndrome (DSS). The only FDA-approved vaccine, Dengvaxia, has limitations due to antibody-dependent enhancement (ADE), necessitating careful administration. The recent pre-approval of TAK-003 by WHO in 2024 highlights ongoing efforts to improve vaccine options. This review explores recent advancements in dengue vaccine development, emphasizing potential utility of mRNA-based vaccines. By examining current clinical trial data and innovations, we aim to identify promising strategies to address the limitations of existing vaccines and enhance global dengue prevention efforts.

KEYWORDS

dengue, ADE, mRNA vaccine, DENV vaccine, tropical disease, vaccine development

1 Introduction

Dengue virus, a mosquito-borne flavivirus, presents a serious global health challenge, especially in tropical regions across South America, the Caribbean (including Puerto Rico), the Western Pacific, Eastern Mediterranean, Africa, and the Americas (1). The World Health Organization (WHO) estimates that around 390 million dengue infections occur annually, with approximately 96 million cases showing clinical symptoms. While many infections are asymptomatic, severe cases can be life-threatening. Dengue fever ranges from mild flu-like symptoms to severe forms such as dengue hemorrhagic fever (DHF) and dengue shock syndrome (DSS) (2). DHF is marked by increased vascular permeability, leading to plasma leakage, bleeding, and low platelet counts; if untreated, it can progress to DSS, characterized by severe hypotension and circulatory collapse requiring intensive medical support. From 2000 to 2019, reported dengue cases rose tenfold, largely due to the expanding reach of *Aedes aegypti* and *Aedes albopictus* mosquitoes, driven by climate change. This environmental shift has introduced dengue to regions previously considered dengue-free (3).

Currently, the only FDA-approved dengue vaccine is Dengvaxia (CYD-TDV), a live-attenuated, tetravalent vaccine developed by Sanofi Pasteur in 2015 to protect against all four dengue virus serotypes (DENV-1 to DENV-4) (4). Despite its significance, Dengvaxia has limitations, notably the risk of antibody-dependent enhancement (ADE). ADE occurs when non-neutralizing antibodies from previous infection or vaccination facilitate viral uptake and replication in subsequent infections, potentially worsening symptoms. This risk is particularly concerning for flavivirus-naïve individuals, especially young children, so Dengvaxia is restricted to individuals with confirmed prior dengue exposure (5). In May 2024, WHO prequalified a new vaccine candidate, TAK-003, which avoids inducing ADE but has shown a lower antibody response against DENV-3 compared to other strains, underscoring the need for a comprehensive and safe dengue vaccine (6). Furthermore, global vaccine coverage remains limited, with only a small percentage of the population vaccinated, primarily in endemic areas. This limitation highlights the urgent need for vaccine strategies that can provide broad protection without ADE risks.

Given the existence of four distinct DENV serotypes, a universal DENV vaccine must elicit strong, balanced immunity against all strains to prevent ADE. Recent research has made promising strides towards this goal- the creation of a DENV envelope vaccine using computationally optimized broadly reactive antigen (COBRA) algorithms. This candidate elicited broadly neutralizing antibodies against all four serotypes in both mice and rhesus macaques, regardless of prior DENV exposure (7). Additionally, another research on a tetravalent DENV virus-like particles (VLPs) vaccine reported that high levels of neutralizing antibodies against all four strains were induced in non-human primates with a one-year immunity longevity and no observance of ADE (8). Unfortunately, none of these candidates has moved to clinical trials. Further evaluation of these vaccine constructs' safety and efficacy should be performed in clinical trials.

The success of mRNA technology in recent vaccines, notably COVID-19 vaccines, offers a promising platform for dengue vaccine development. mRNA vaccines are adaptable, cost-effective, and can be produced rapidly. They work by instructing cells to produce a harmless viral protein, which then stimulates the immune system to generate specific antibodies. As non-infectious vaccines, mRNA platforms provide a safe and potent immune response (9). This review examines recent advancements in dengue vaccine development, with a particular focus on mRNA vaccine candidates. By analyzing current clinical trial data and recent innovations, we aim to highlight promising strategies to overcome the limitations of existing vaccines and enhance global dengue prevention efforts.

2 Dengue epidemiology

The earliest documented dengue outbreak dates to 1779, with cases reported in Jakarta, Indonesia, and Egypt (10). In recent decades, dengue incidence has dramatically increased, putting nearly half the global population at risk. From 2000 to 2019, reported dengue cases surged from 505,430 to 0ver 5.2 million, with a corresponding rise in deaths from 960 to 4032 (11). Annual dengue infections are estimated at around 390 million, with 67-136 million cases exhibiting clinical symptoms, particularly in tropical and subtropical regions. In the United States, dengue fever incidence has historically been low, with recent spikes occurring between 2013 and 2016 (0.17-0.31 cases per 100,000) and peaking in 2019 (0.35 cases per 100,000). 94% of cases between 2010 and 2021 were travel related. Puerto Rico, however, has seen a higher incidence, with an average of 200 cases per 100,000 between 1980 and 2015, and almost all cases were locally acquired (12). The substantial increase in dengue infections is primarily attributed to the expanded distribution of its vectors, particularly *Aedes aegypti* and *Aedes albopictus* mosquitoes, driven by climate change. Rising temperatures, increased rainfall, flooding, and humidity extend mosquito breeding periods and reduce virus incubation times (13, 14). Additionally, social and environmental factors such as population density increase, population mobility, and inadequate water storage practices, are closely associated with dengue transmission, particularly in rural areas (15). A longitudinal study from 2007 to 2009 in Puerto Rico emphasized that water storage containers and discarded tries play critical roles in mosquito breeding, as most pupae were found in human-managed water containers, storage vessels, plant pots, and leaking water meters (16).

3 Clinically approved vaccines

3.1 Dengvaxia

Invented by Sanofi Pasteur, Dengvaxia (CYD-TDV) is a live-attenuated, tetravalent vaccine administered as a three-dose regimen. It was approved by the U.S. Food and Drug Administration (FDA) in 2019. Incorporating structural pre-membrane (prM) and envelope (E) genes of the four DENV strains with non-structural genes of the yellow fever 17D vaccine strain, Dengvaxia aims to provide tetravalent immunity to all strains of DENV by targeting the prM and E proteins (17). In individuals over 9 years old who had previously been infected with dengue, the vaccine efficacy (VE) achieved 91% (95%CI, 58-99%) and up to 93.2% efficacy against severe disease. However, in dengue-naïve children under 9, VE is around 45% (95%CI, -54-88%), limiting its suitability for this group (18, 19). Therefore, Dengvaxia works as a "fill-in" vaccine with patients' prior exposure served as the initial prime. In a phase-II clinical trial (NCT00880893), the safety of Dengvaxia was evaluated in subjects aged 2 to 45 years in Singapore. Throughout the whole study, there were only three (0.3%) recorded serious adverse events (SAEs) in the vaccination group- acute leukemia of ambiguous lineage, tuberculosis lymphadenitis, and tension headache- and three cases of adverse events (AEs)- fever, rash, and cervical spondylosis (20). On the other hand, due to concerns about ADE, Dengvaxia is recommended only for individuals with prior dengue exposure.

3.2 TAK-003

TAK-003 (Takeda) is a live-attenuated, tetravalent vaccine, comprising of four DENV strains with the attenuated DENV serotype 2 strain (DENV-2) as the vaccine backbone and three other recombinant strains, swapping the prM and E genes of DENV-2 with DENV-1, DENV-3, or DENV-4 (Table 1) (21). Previous phase I and II clinical trials for TAK-003 vaccine had addressed its capability of eliciting tetravalent neutralizing antibody responses and polyfunctional T-cell responses. In a Phase III trial (NCT02747927), two doses administered to children aged 4 to 16 showed a vaccine efficacy (VE) of 66.2% (95% CI, 44.9-77.5) for seronegative and 76.1% (95% CI, 68.5-81.9) for seropositive recipients (22). Cumulatively, VE was 90.4% (95% CI, 82.6-94.7) and 85.9% (95% CI, 31.9-97.1) against hospitalizations related to dengue and DHF. After three years, VE declined to 54.3% (95% CI, 41.9-64.1) for virologically confirmed dengue (VCD) and 77.1% (95% CI, 58.6-87.3) against hospitalized VCD in initially seronegative participants. Efficacy remained stable in seropositive groups, with VE at 65% (95% CI, 58.9-70.1) against VCD and 86% (95% CI, 78.4-91.0) against hospitalized cases. In another phase III trial evaluating safety of TAK-003 (NCT03771963), among 168 participants, there were only five participants experienced SAEs with two subjects reporting moderate hepatic failure and severe osteoarthritis and three reporting bradycardia, inguinal hernia, and sepsis (21). However, no efficacy was observed against DENV-3 in seronegative individuals, and VE against DENV-2 declined over time, raising concerns about potential antibody-dependent enhancement (ADE) in these cases.

4 Vaccines under evaluations in clinical trials

4.1 TV003/TV005

The National Institute of Allergy and Infectious Disease (NIAID) has spearheaded the development of a live-attenuated tetravalent dengue vaccine over the past 15 years, aiming to provide comprehensive protection against all four dengue virus serotypes while minimizing the risk of ADE. The initial candidate, TV003, utilized deletions of 30 and 31 nucleotides (Δ30 and Δ31) at the 3' UTR of each serotype to create four monovalent strains-rDEN1Δ30, rDEN2/4Δ30, and rDEN3Δ30/3Δ31 (23). To achieve a more balanced infectivity, in the TV005 formulation, the doses of rDENV2/4Δ30 were increased 10 fold (24). From previous phase I trials (NCT01072786 and NCT01436422), comparing to TV003, TV005 demonstrated a higher and more stable frequency of seroconversion and stronger antibody response (Table 1). Both candidates conferred sterilizing immunity against DENV infection for at least 12 months with a booster dose at 6 months. Mild dengue-related rash was the most common AE, occurring in 66% (27/41) of TV003 recipients and 26%(37/144) of TV004 recipients, with occasional reports of fever and arthralgia (25). Following a second dose, antibody titers to all serotypes roughly doubled, confirming the establishment of sterilizing immunity. TV003/TV005 are now undergoing Phase III trials (NCT02406729) in dengue-endemic areas, led by Brazil's Butantan Institute.

4.2 TDEN F17/F19

TDEN F17 vaccine is a tetravalent, live-attenuated vaccine that targets all four dengue virus serotypes. Derived from a natural viral isolate, it was attenuated through serial passages in primary dog kidney (PDK) cells. To enhance neutralizing antibody responses, the F17pre formulation adjusted attenuation levels by increasing PDK cell passages for DENV1 and reducing them for DENV4 (26). Clinical trial (NCT00350337) demonstrated that TDEN F17/F17Pre/F19 induced robust humoral responses with tetravalent response rates of 60%, 71.4%, and 66.7% after 2-dose administration. In a phase-II trial conducted in Puerto Rico (NCT00468858) achieved 100% seroconversion to tetravalent immunity in primed subjects (27, 28). In a pilot study on TDEN F17's VE in children, a 52.6% seroconversion was achieved, suggesting the vaccine might be safe and effective in children. Administered in a two-dose regimen, TDEN F17 has been shown to be safe across ages 12 months to 50 years, though 31% of F17pre recipients exhibited viremia after the first dose, which was absent after the second (29). A five-year Phase I/II study in Thai children aged 6-7 (NCT00384670), followed by a third-dose booster trial one year later (NCT01843621), demonstrated strong long-term immunity: 100% seroconversion to DENV-1, -2, and -3 and 83.3% to DENV-4. No mortality or serious adverse events were reported, indicating the safety of TDEN F17 (30).

4.3 DPIV

Invented at Walter Reed Army Institute of Research (WRAIR), the tetravalent dengue purified inactivated vaccine (DPIV) is administered with two-dose schedule 28 days apart. The DENV-2 S16803 strain was chosen as the initial vaccine prototype, which was successfully propagated in Vero cells and tested safe and immunogenic in mice and rhesus monkeys with a 100% seroconversion after the second dose administration (31). Adjuvanted with $AS01_E$(3-O-desacylcinomnophsphoryl lipid A) and $AS03_B$(oil-in-water) by GlaxoSmithKline, the formalin-inactivated viruses from DENV-1 Westpac 74, DENV-2 S16803, DENV-3 CH53489, and DENV-4 TVP360 were incorporated into the tetravalent formulation of DPIV. In a phase-I trial conducted in Puerto Rico (NCT01702857), DPIV adjuvanted by AS01E/AS03B elicited neutralizing antibody responses against all four DENV serotypes in flavivirus-naïve adults, but the response wanned in 6 months after the second dose (32). In addition, the inactivated nature of DPIV poses a potential limit on immune responses to non-neutralizing epitopes on target envelope and capsid proteins. Viral challenge studies in rhesus macaques revealed the vaccine failed to control DENV infection and inadvertently led to antibody-dependent enhancement of DENV infection with increased levels of viremia, AST, IL-10, and IL-18 in challenged animals (33).

TABLE 1 Current licensed or trialed dengue vaccines.

Name	Valency	Formulation	Evaluation	Manufacturer	Efficacy	Adverse events	Dose Schedule	Year
Dengvaxia	Tetravalence	Chimeric combination of YFV/ DENV1-4	Licensed	Sanofi Pasteur	The general VE[e] against all four serotypes was 65.6%	ADE response occurred in dengue naïve individuals was the major safety concern	3	2015
TAK-003	Tetravalence	Chimeric viruses with DENV-2 PDK35 as the backbone	Pre-licensed on May 2024 by WHO	Takeda	The cumulative VE against DENV1-4 was 66.2%	The most common adverse events were injection site pain and headache	2	2006
TV003/TV005	Tetravalence	Genetic attenuated viruses	Phase-III clinical trial	NIAID[a], Butantan, and Merck	Seroconversion rate[f] for TV003 was 74% and 97% for TV005	Headache, rash, fatigue, and myalgia were the most common observed adverse events	1	2003
TDEN F17/F19	Tetravalence	Virus combination attenuated by PDK cells	Phase II clinical trial	WRAIR[b] and GSK[c]	Seroconversion rate against DENV1-3 was 100% and 83.3% against DENV4	Arthralgia, fatigue, muscle aches, and pain behind eyes were observed in recipients	2	2017
DPIV	Tetravalence	Purified inactivated DENV1-4 with aluminum adjuvants	Phase I clinical trial	WRAIR and GSK	Tetravalent neutralizing antibodies were induced	There were few cases of moderate adverse events recorded during the trial	2	2012
TVDV	Tetravalence	DNA vaccine encoding prM and E proteins of DENV1-4 and adjuvanted with VAXFECTIN	Phase I clinical trial	WRAIR and U.S. NMRC[d]	Anti-DENV IFN-γ T cells response was stimulated	No severe adverse events were observed	3	2018
V180	Tetravalence	Recombinant prM and E proteins of DENV1-4 combined with multiple adjuvants	Phase I clinical trial	Merck & Co.	Seroconversion rate against all four serotypes was 85.7%	Injection site pain was the most common adverse event throughout the trial	3	2018

[a]National Institute of Allergy and Infectious Diseases; [b]Walter Reed Army Institute of Research; [c]GlaxoSmithKline; [d]U.S. Naval Medical Research Center;
[e]VE refers to vaccine efficacy, which is measured by comparing the number of disease cases in the vaccinated group to that of the placebo group;
[f]Seroconversion rate is the percentage of individuals who develop detectable specific antibodies to a pathogen in their blood post vaccination or infection. This rate is a common indicator of vaccine effectiveness in immunological research.

10.3389/fimmu.2025.1520968

4.4 TVDV

The U.S. Army Medical Research and Material Command developed the tetravalent DNA vaccine (TBDV) against dengue, using a VAXFECTIN-adjuvanted VR1012 plasmid encoding the prM and E proteins from each DENV serotype. TBDV combines equal amounts of four monovalent plasmids derived from distinct strains: DENV1 (West Pacific 74), a modified DENV2 strain, and low-passage Philippine strains for DENV3 and DENV4 (34). In New Zealand white rabbits, TBDV induced seroconversion across all four serotypes. A Phase I clinical trial (NCT01502358) with 40 flavivirus-naïve participants demonstrated TBDV's safety and its ability to elicit IFN-γ-producing T-cell responses without causing dengue-related rash or serious adverse events (SAEs) (34). The most common adverse events were mild, including fatigue (17/40), headache (18/40), and muscle aches (19/40). While neutralizing antibodies were not detected, T-cell responses were observed, with an average response rate of 66.3% across groups receiving either low-dose TBDV, low-dose TVDV adjuvanted with Vaxfectin, or high-dose TVDV adjuvanted with Vaxfection (34).

4.5 V180

Merck & Co. developed V180, a recombinant tetravalent dengue vaccine targeting DENV envelope and prM glycoproteins, administered in a three-dose regimen. In a Phase I randomized, placebo-controlled, double-blind study (NCT01477580), neither unadjuvanted nor aluminum-adjuvanted V180 formulations induced a strong immune response. However, six formulations with the ISCOMATRIX adjuvant achieved robust immunogenicity (GMT > 150) with seroconversion rates exceeding 85.7% for all DENV serotypes. Memory B cell responses for all serotypes were also observed in high-dose V180-ISCOMATRIX recipients, though increased adverse events, such as injection site pain and swelling, were noted (35). A subsequent Phase I trial (NCT02450838) evaluated V180, plain or adjuvanted with Alhydrogel, as booster in adults previously vaccinated with a live-attenuated tetravalent dengue vaccine. While V180 was well-tolerated and enhanced serum neutralization titers, it did not meet the predefined booster criteria (GMT > 150) for a positive immune response (36).

5 mRNA DENV vaccines

The remarkable success of COVID-19 mRNA vaccines has highlighted the potential for mRNA-based dengue (DENV) vaccines (Table 2). Unlike viral vectored vaccines, which carry risks of reversion to virulence and require complex culturing processes, mRNA vaccines are non-infectious and do not carry nucleic acids that can integrate into the host genome, eliminating the risks of mutagenesis and oncogenesis. Comparing to inactivated and protein subunit vaccines that usually require adjuvants to enhance immune responses, mRNA vaccines inherently stimulate both cellular and humoral immunity through antigen expression within host cells, as seen with COVID mRNA vaccines (37). Furthermore, comparing to other novel platforms, like VLPs vaccines that mimic the structure of viruses and rely on complex bioprocessing, mRNA vaccines' cell-free manufacturing nature accelerates the production process and makes them highly scalable (9). Their modular and flexible designs not only allow for precise targeting of antigens but also ensure the adaptability to new serotypes, making them a versatile platform for global vaccine development (38).

In 2019, Claude Roth and colleagues conducted a preclinical study in transgenic HLA Class-I (HLA-A0201, -A2402, B3501) mice to evaluate a modified mRNA vaccine against DENV-1 strain KDH0026A (Figure 1A) (39). This vaccine encoded immunodominant non-structural (NS) epitopes from NS3, NS4B, and NS5, designed to enhance CD4+ and CD8+ T-cell responses (40, 41). Encapsulated in lipid nanoparticles (LNPs) for delivery, the vaccine induced strong CD8+ T-cell responses, with 26% of CD8+ T-cells producing IFN-γ and TNF-α against HLA-B3501 peptide p49. The design intentionally avoided inducing

TABLE 2 Summary of mRNA DENV vaccine candidates.

Name	Target Serotype(s)	Development Stage	Preliminary effect	Safety Data	Year
Modified mRNA Vaccine	DENV-1 (NS3, NS4B, NS5) [c]	Preclinical (Mouse Model)	Strong CD8+ T-cell responses were elicited	Vaccine design reduced the risk of ADE [f] by avoiding inducing Nab [g]	2019
mRNA-LNP [a] Vaccine	DENV-2 (prME, E80, NS1) [d]	Preclinical (Mouse Model)	Sterilizing immunity was induced in immunocompetent mice; reduced spleen viral load was also observed	Heterologous ADE was observed with E80-mRNA vaccinated mice	2020
DENV1 prM/E [b] mRNA-LNP Vaccine	DENV-1 (prM, E)	Preclinical (Mouse Model)	Robust humoral and cellular responses were elicited; vaccinated immunocompromised mice were protected from lethal DENV challenge	No morbidity and mortality cases were observed among those vaccinated mice	2021
Multi-target mRNA-LNP Vaccine	All four serotypes (NS1, E-DIII) [e]	Preclinical (Mouse Model)	Neutralizing antibody against all four serotypes was elicited along with strong T-cell responses	ADE potential was minimized with only 5% of cell enhancement detected [h]	2022

[a]Lipid nanoparticle; [b]Pre-membrane protein/Envelope protein; [c]Modified mRNA vaccine encoded DENV-1's non-structural epitopes from NS3, NS4B, and NS5; [d]mRNA-LNP vaccine targeted structural proteins- prM/E and E80- and one non-structural protein, NS-1; [e]Multi-target mRNA-LNP vaccine encoded NS-1 protein and envelope domain III to target all four serotypes; [f]Antibody enhancement effect; [g]Neutralizing antibody; [h]Enhancement effect was measured by antibody-dependent analysis of DENV1-4 infection in K562 cells.

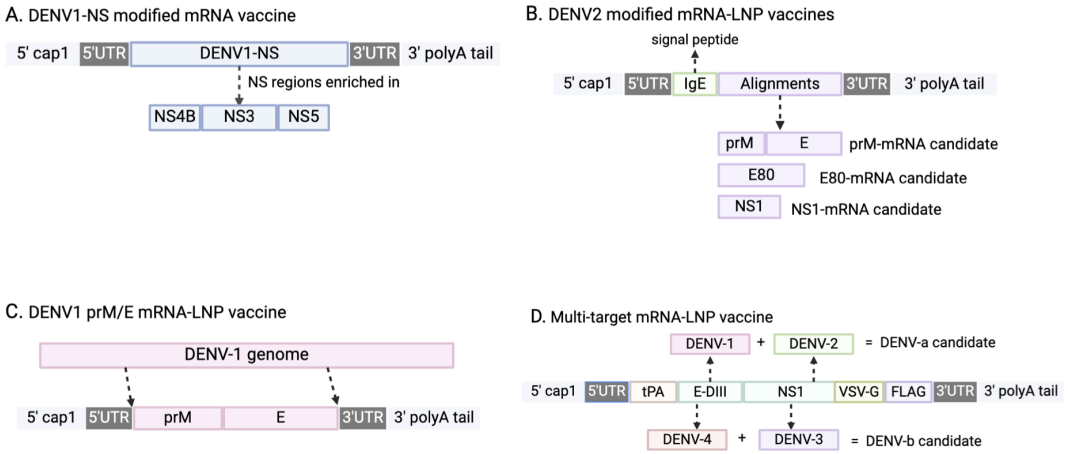

FIGURE 1
Schematic illustrations of mRNA DENV vaccine designs. **(A)** The major component of DENV1-NS modified mRNA vaccine is non-structural (NS) protein from DENV1 strain, and is enriched in NS4B, NS3, and NS5. **(B)** DENV2 modified mRNA-LNP vaccines incorporate a sequence of human IgE as a signal peptide to prompt alignments translocation. **(C)** The major component of this vaccine are sequences of pre-membrane(prM) and envelope (E) proteins extracted from DENV-1 genome. **(D)** The design incorporated tissue-type plasminogen activator (tPA) as the signal peptide, transmembrane and cytoplasmic domain of vesicular stomatitis virus G (VSV-G), and FLAG tag to aid the identification of target protein expression.

neutralizing antibodies to minimize the risk of antibody-dependent enhancement (ADE) (39). However, the study did not explore responses to other DENV serotypes or test vaccine efficacy in a challenge model.

In 2020, another modified mRNA-LNP vaccine against DENV-2 strain 16681 was tested in mice (by Mengling Zhang et al), targeting two structural proteins, prME and E80, and one non-structural protein (NS1) (Figure 1B). Immunization generated high levels of DENV-2-specific IgG and strong T-cell responses, achieving sterilizing immunity against DENV-2 in immunocompetent BALB/c mice. E80-mRNA induced high titers of neutralizing antibodies (average PRNT50 titer of 13,000), while NS1-mRNA elicited a significant antibody response (PRNT50 titer of 12,000) and reduced viral loads in the spleen. However, NS1-mRNA alone did not induce neutralizing antibodies, limiting its utility as a primary vaccine component (42). Although E80-mRNA showed promise, it also induced high levels of heterologous ADE and cross-reactive immune responses, constraining its application.

In the following year, another similar mRNA-LNP vaccine against serotype 1, the DENV1 prM/E mRNA-LNP vaccine, was developed (by Clayton J. Wollner et al) (Figure 1C), targeting DENV-1 (strain 16007) with prM and E proteins with T7 promoter sequences and 5'/3' URTs based on a ZIKV mRNA platform (43, 44). A two-dose regimen generated robust humoral and cellular responses, with antibody titers reaching 120,000 and neutralizing antibody titers of 420 measured by FRNT. This vaccine protected immunocompromised AG129 mice from lethal DENV-1 challenge without morbidity or mortality, indicating its potential effectiveness in immunocompromised populations (45). After vaccination, there was no morbidity or mortality signs shown among these mice, demonstrating a successful protection. Although it effectively elicited CD4+ and CD8+ T cell responses against DENV-1, it did not generate cross-reactive responses to other DENV serotypes.

Previous DENV mRNA vaccines only targeted one serotype; fortunately, in 2022, a multi-target mRNA-LNP vaccine formulation was designed and tested in mice (by Lihong He et al.) (Figure 1D) (46). The multivalent vaccines encoded NS1 and envelope domain III (E-DIII) to target all four DENV serotypes. The DENV-a candidate combined DENV-1 and DENV-2 antigens, while DENV-b combined DENV-3 and DENV-4. The efficacy of DENV-a, DENV-b, and DENV-ab was tested separately in mice. DENV-a elicited E-DIII specific IgG against DENV1 with an average antibody titer of 15,264 with a 20 μg dose. DENV-b immunized mice generated an E-DIII mean titer of 4608 in the 20 μg group. For NS-1, both DENV-a and DENV-b induced slightly higher titers than those of E-DIII, with mean titers of 61,440 and 32,768 (46). DENV-ab, a combination of DENV-a and DENV-b, produced the highest levels of neutralizing antibodies across all serotypes, and induced strong T-cell responses with high IFN-γ production. Additionally, ADE assays indicated minimal ADE potential (<5% of cells), underscoring the vaccine's safety profile (46). The success of DENV-ab in mice suggests it as a promising candidate for further evaluation in larger animal models prior to clinical trials.

Comparing to traditional vaccine platforms, mRNA vaccines can mitigate ADE risks either through mutating fusion loop epitope of the E protein or by eliciting serotype-specific neutralizing antibodies. Previous research on DENV E protein has revealed three distinct domains, and domain II containing with an internal fusion loop was found to participate in membrane fusion and dimerization (47). By single point mutations of three fusion loop residues, tryptophan at position 101, leucine at position 107, and phenylalanine at position 108, the binding activity of cross-reactive anti-E antibodies, which were responsible for ADE, was greatly reduced (48). In addition, DENV1 prM/E mRNA-LNP vaccine did not induce cross-reactive antibodies that elicit heterotypic enhancement. In a focus reduction neutralization test (FRNT), DENV1 mRNA-vaccinated mice did not elicit neutralizing antibody against DENV2, and only a mild

enhancement, around 1.2-fold, at 1/100 serum dilution was discovered (43). mRNA platform allows rapid development of vaccines, however global implementation of mRNA vaccines in dengue-endemic areas remains challenging. Vaccine stability is one of the greatest impediments, as mRNA formulations require ultra-cold storage, which is difficult to maintain in tropical climates with limited health infrastructures (49). Therefore, future efforts to advance LNP technology and thermostable mRNA formulations are essential to overcome this barrier.

Future research on DENV mRNA vaccines should focus on developing tetravalent vaccines that safely elicit both cellular and humoral immunity against all four serotypes. In addition to improving current LNPs formulation, lumazine synthase (LuS), can also be incorporated into future development of DENV mRNA vaccines (50). LuS oligomers, displaying as an efficient platform for antigen presentation, have already been successfully employed in other vaccine studies against infectious diseases, such as HIV, influenza, and rotavirus. When utilized as a scaffold, LuS was able to display spike glycoprotein from SARS-CoV-2 with decent yield and antigenicity in mice (51). Multimerization nature of LuS contributes to assembling antigens in a highly ordered fashion and promoting the activation of B cells receptors; thereby, potent and long-lasting immune responses in the germinal centers will be generated (52). When utilized as a protein cage, LuS carrying ovalbumin peptides OT-1 and OT-2 efficiently delivered and successfully stimulated Dendritic Cells (DCs) to produce OT-1 specific CD8+ T cells and OT-2 specific CD4+ T cells in mice (53). Immunity longevity of mRNA DENV vaccines is another aspect should be focused on. Though currently there is no published results on protection longevity, according to previous studies on SARS-CoV2 mRNA vaccine's durability, it could infer that immunity provided by DENV mRNA vaccines might also last around one year (54). Moreover, further clinical studies and targeted research, which tailor dosing regimens, should be conducted to achieve consistent immunity in diverse populations, including children under five, the elderly, and immunodeficient people. The success of the DENV-1 prM/E mRNA-LNP vaccine in immunocompetent mice builds a promising foundation on the potential optimization of mRNA vaccines for immunocompromised population who has heightened risk of serve dengue. To further enhance efficacy, future strategies could include modifying LNP formulations to improve delivery, ensuring a controlled and sustained release of the mRNA payload. Additionally, incorporating adjuvants such as CpG oligonucleotides (55) or TLR7/8 (56) agonists may help boost innate and adaptive immune responses. Leveraging advanced antigen designs, such as self-assembling nanoparticles, could also ensure safety and efficacy in vulnerable populations. By addressing all aspects mentioned above, we will be one step closer to the successful deployment of mRNA vaccines in dengue-prevalent areas.

6 Conclusion

Currently, Dengvaxia is the only WHO-approved dengue vaccine, with global administration. However, in May 2024, WHO prequalified TAK-003, increasing global access to dengue vaccination. Among advanced candidates, TV003/TV005 has shown the strongest immune response in flavivirus-naïve recipients, with TV005 inducing fewer side effects like vaccine-related rash than TV003. TV003/TV005 provide 1-2 years of protection with a single dose, while Dengvaxia and TAK-003 offer protection for at least 6 and 4.5 years, respectively (57). Across all candidates, fewer than 1% of participants experienced serious adverse events, with rash as the most common side effect. Antibody-dependent enhancement (ADE) remains a concern, particularly for Dengvaxia, which poses an increased risk of severe dengue in seronegative individuals due to ADE. To reduce this risk, Dengvaxia is limited to those with prior dengue infection, confirmed by serology (58). Other vaccines show a lower ADE risk based on current trial data.

mRNA dengue vaccines offer significant advantages, including rapid development, scalability, and precise immune targeting Unlike live-attenuated vaccines, mRNA vaccines can be developed quickly without growing pathogens. mRNA vaccines can be engineered to encode antigens for all four dengue serotypes, ensuring balanced immune responses. Early preclinical trials indicate that mRNA vaccines effectively stimulate neutralizing antibodies and T-cell responses. Multi-target mRNA-LNP vaccines, targeting all four serotypes, show particular promise and may be advanced to clinical trials following safety and immunogenicity evaluations in non-human primates, such as rhesus macaques, cynomolgus macaques, or common marmosets (42). Once the candidate showed safety utilization in NHPs and was able to elicit strong immune responses, it could be advanced to clinical trials and eventually be brought to the market.

Future efforts in dengue vaccine development should focus on boosting efficacy and safety. Broadening immune responses could involve adding adjuvants like aluminum-based MF59 or AS01 to enhance Th2 responses in live-attenuated vaccines (59). Another promising approach involves specialized designs, such as self-assembling nanoparticles that mimic virus structure, enhancing antigen presentation and immune response. Nanoparticles can present multiple dengue antigens, while VLPs and multiepitope designs allow antigen presentation in a native conformation, increasing immune responses without viral replication risk (60–62). For mRNA vaccines, future work could refine lipid nanoparticle (LNP) formulations and nucleotide modifications, alongside novel antigen presentation platforms to optimize immune efficacy. Refining dosing regimens for diverse age groups, particularly under 4 and over 60 years old, will also be essential for broadening coverage and achieving herd immunity in dengue-endemic regions. It is pivotal to broaden the protection scope to achieve the goal of herd immunity in dengue-endemic areas.

In addition to scientific innovations, future directions in dengue vaccine development should also prioritize strategies for global accessibility. Overcoming logistical and economic barriers will require collaborative efforts, especially the international partnerships between local governments, non-governmental organizations (NGOs), and private industry to fund research, streamline regulatory approval, and subsidize vaccine costs in resource-limited settings. The success of TV003 highlights the

potential of collaborative efforts in advancing dengue vaccine development. TV003 was developed by NIH but produced in partnership with a local company, Butantan Institute, in Brazil (63). This partnership not only facilitated the local production of TV003 but also underscored the importance of leveraging regional expertise to enhance vaccine accessibility and affordability in endemic areas. Such collaborations serve as a valuable model for advancing mRNA dengue vaccines, which could similarly benefit from partnerships with regional manufacturers to ensure scalability and cost-effectiveness. Innovative approaches like combining vaccination programs with mosquito control initiatives, such as Wolbachia-infected mosquito releases (64) or sterile insect techniques (65), could significantly enhance disease control efforts. To deepen understanding of dengue pathogenesis and vaccine-induced immunity, experimental methodologies like metabolomics and proteomics could identify biomarkers for vaccine efficacy, immune correlates of protection, and mechanisms of antibody-dependent enhancement. These insights would guide the optimization of vaccine designs and dosing regimens, ensuring more effective and accessible solutions for global dengue control.

Author contributions

XL: Writing – original draft, Writing – review & editing.

Funding

The author(s) declare that no financial support was received for the research, authorship, and/or publication of this article.

Conflict of interest

The author declares that the research was conducted in the absence of any commercial or financial relationships that could be construed as a potential conflict of interest.

Generative AI statement

The author(s) declare that no Generative AI was used in the creation of this manuscript.

Publisher's note

References

1. Bhatt S, Gething P, Brady O, Messina JP, Farlow AW, Moyes CL, et al. The global distribution and burden of dengue. *Nature*. (2013) 496:504–7. doi: 10.1038/nature12060

2. Pintado Silva J, Fernandez-Sesma A. Challenges on the development of a dengue vaccine: a comprehensive review of the state of the art. *J Gen Virol*. (2023) 104:1831. doi: 10.1099/jgv.0.001831

3. World Health Organization (WHO). Dengue and severe dengue(2024). Available online at: https://www.who.int/news-room/fact-sheets/detail/dengue-and-severe-dengue (Accessed May 26, 2024).

4. Administration FaD. DENGVAXIA(2020). Available online at: www.fda.gov/vaccines-blood-biologics/dengvaxia (Accessed May 26, 2024).

5. Teo A, Tan HD, Loy T, Chia PY, Chua CLL. Understanding antibody-dependent enhancement in dengue: Are afucosylated IgG1s a concern? *PloS Pathog*. (2023) 19:e1011223. doi: 10.1371/journal.ppat.1011223

6. Takeda. Takeda's dengue vaccine candidate provides continued protection against dengue fever through 4.5 years in pivotal clinical trial(2022). Available online at: www.takeda.com/newsroom/newsreleases/2022/takedas-dengue-vaccine-candidate-provides-continued-protection-against-dengue-fever-through-4.5-years-in-pivotal-clinical-trial/ (Accessed May 26, 2024).

7. Uno N, Ross TM. Universal dengue vaccine elicits neutralizing antibodies against strains from all four dengue virus serotypes. *J Virol*. (2021) 95:e00658–20. doi: 10.1128/JVI.00658-20

8. Thoresen D, Matsuda K, Urakami A, Ngwe Tun MM, Nomura T, Moi ML, et al. A tetravalent dengue virus-like particle vaccine induces high levels of neutralizing antibodies and reduces dengue replication in non-human primates. *J Virol*. (2024) 98:e0023924. doi: 10.1128/jvi.00239-24

9. Pardi N, Hogan MJ, Porter FW, Weissman D. mRNA vaccines - a new era in vaccinology. *Nat Rev Drug Discovery*. (2018) 17:261–79. doi: 10.1038/nrd.2017.243

10. Wu W, Bai Z, Zhou H, Tu Z, Fang M, Tang B, et al. Molecular epidemiology of dengue viruses in southern China from 1978 to 2006. *Virol J*. (2011) 8:322. doi: 10.1186/1743-422X-8-322

11. World Health Organization (WHO). Dengue: Global situation(2023). Available online at: https://www.who.int/emergencies/disease-outbreak-news/item/2023-DON498 (Accessed May 26, 2024).

12. Chen LH, Marti C, Diaz Perez C, Jackson BM, Simon AM, Lu M. Epidemiology and burden of dengue fever in the United States: a systematic review. *J Travel Med*. (2023) 30:taad127. doi: 10.1093/jtm/taad127

13. Hawley WA. The biology of Aedes albopictus. *J Am Mosq Control Assoc Supplement*. (1988) 1:1–39. doi: 10.2149/tmh.2011-S04

14. Higa Y. Dengue vectors and their spatial distribution. *Trop Med Health*. (2011) 39:17–27. doi: 10.2149/tmh.2011-S04

15. Schmidt WP, Suzuki M, Thiem VD, White RG, Tsuzuki A, Yoshida LM, et al. Population density, water supply, and the risk of dengue fever in Vietnam: cohort study and spatial analysis. *PloS Med*. (2011) 8:e1001082. doi: 10.1371/journal.pmed.1001082

16. Barrera R, Amador M, MacKay AJ. Population dynamics of Aedes aEgypti and dengue as influenced by weather and human behavior in San Juan, Puerto Rico. *PloS Negl Trop Dis*. (2011) 5:e1378. doi: 10.1371/journal.pntd.0001378

17. Guy B, Briand O, Lang J, Saville M, Jackson N. Development of the Sanofi Pasteur tetravalent dengue vaccine: One more step forward. *Vaccine*. (2015) 33:7100–11. doi: 10.1016/j.vaccine.2015.09.108

18. Paz-Bailey G, Adams L, Wong JM, Poehling KA, Chen WH, McNally V, et al. Dengue Vaccine: Recommendations of the Advisory Committee on Immunization Practices, United States, 2021. MMWR. Recommendations and reports: Morbidity and mortality weekly report. *Recommendations Rep*. (2021) 70:1–16. doi: 10.15585/mmwr.rr7006a1

19. Hadinegoro SR, Arredondo-García JL, Capeding MR, Deseda C, Chotpitayasunondh T, Dietze R, et al. Efficacy and long-term safety of a dengue vaccine in regions of endemic disease. *New Engl J Med*. (2015) 373:1195–206. doi: 10.1056/NEJMoa1506223

20. Capeding RZ, Luna IA, Bomasang E, Lupisan S, Lang J, Forrat R, et al. Live-attenuated, tetravalent dengue vaccine in children, adolescents and adults in a dengue endemic country: randomized controlled phase I trial in the Philippines. *Vaccine*. (2011) 29:3863–72. doi: 10.1016/j.vaccine.2011.03.057

21. Patel SS, Winkle P, Faccin A, Nordio F, LeFevre I, Tsoukas CG. An open-label, Phase 3 trial of TAK-003, a live attenuated dengue tetravalent vaccine, in healthy US adults: immunogenicity and safety when administered during the second half of a 24-month shelf-life. *Hum Vaccines Immunother*. (2023) 19:2254964. doi: 10.1080/21645515.2023.2254964

22. Rivera L, Biswal S, Sáez-Llorens X, Reynales H, López-Medina E, Borja-Tabora C, et al. Three-year efficacy and safety of Takeda's dengue vaccine candidate (TAK-003). *Clin Infect Dis: an Off Publ Infect Dis Soc America*. (2022) 75:107–17. doi: 10.1093/cid/ciab864

23. Pintado Silva J, Fenutria R, Bernal-Rubio D, Sanchez-Martin I, Hunziker A, Chebishev E, et al. The dengue virus 4 component of NIAID's tetravalent TV003 vaccine drives its innate immune signature. *Exp Biol Med (Maywood NJ)*. (2022) 247:2201–12. doi: 10.1177/15353702231151241

24. Durbin AP. Historical discourse on the development of the live attenuated tetravalent dengue vaccine candidate TV003/TV005. *Curr Opin Virol*. (2020) 43:79–87. doi: 10.1016/j.coviro.2020.09.005

25. Whitehead SS, Durbin AP, Pierce KK, Elwood D, McElvany BD, Fraser EA, et al. In a randomized trial, the live attenuated tetravalent dengue vaccine TV003 is well-tolerated and highly immunogenic in subjects with flavivirus exposure prior to vaccination. *PloS Negl Trop Dis*. (2017) 11:e0005584. doi: 10.1371/journal.pntd.0005584

26. Sun W, Cunningham D, Wasserman SS, Perry J, Putnak JR, Eckels KH, et al. Phase 2 clinical trial of three formulations of tetravalent live-attenuated dengue vaccine in flavivirus-naïve adults. *Hum Vaccines*. (2009) 5:33–40. doi: 10.4161/hv.5.1.6348

27. Thomas SJ, Eckels KH, Carletti I, de la Barrera R, Dessy F, Fernandez S, et al. A phase II, randomized, safety and immunogenicity study of a re-derived, live-attenuated dengue virus vaccine in healthy adults. *Am J Trop Med Hyg*. (2013) 88:73–88. doi: 10.4269/ajtmh.2012.12-0361

28. Bauer K, Esquilin IO, Cornier AS, Thomas SJ, Quintero Del Rio AI, Bertran-Pasarell J, et al. A phase II, randomized, safety and immunogenicity trial of a re-derived, live-attenuated dengue virus vaccine in healthy children and adults living in Puerto Rico. *Am J Trop Med Hyg*. (2015) 93:441–53. doi: 10.4269/ajtmh.14-0625

29. Watanaveeradej V, Gibbons RV, Simasathien S, Nisalak A, Jarman RG, Kerdpanich A, et al. Safety and immunogenicity of a rederived, live-attenuated dengue virus vaccine in healthy adults living in Thailand: a randomized trial. *Am J Trop Med Hyg*. (2014) 91:119–28. doi: 10.4269/ajtmh.13-0452

30. Simasathien S, Thomas SJ, Watanaveeradej V, Nisalak A, Barberousse C, Innis BL, et al. Safety and immunogenicity of a tetravalent live-attenuated dengue vaccine in flavivirus naive children. *Am J Trop Med Hyg*. (2008) 78:426–33. doi: 10.4269/ajtmh.2008.78.426

31. Putnak R, Barvir DA, Burrous JM, Dubois DR, D'Andrea VM, Hoke CH, et al. Development of a purified, inactivated, dengue-2 virus vaccine prototype in Vero cells: immunogenicity and protection in mice and rhesus monkeys. *J Infect Dis*. (1996) 174:1176–84. doi: 10.1093/infdis/174.6.1176

32. Diaz C, Lin L, Martinez LJ, Eckels KH, Campos M, Jarman RG, et al. Phase I randomized study of a tetravalent dengue purified inactivated vaccine in healthy adults from Puerto Rico. *Am J Trop Med Hyg*. (2018) 98:1435–43. doi: 10.4269/ajtmh.17-0627

33. Fernandez S, Thomas SJ, de la Barrera R, Im-Erbsin R, Jarman RG, Baras B, et al. An adjuvanted, tetravalent dengue virus purified inactivated vaccine candidate induces long-lasting and protective antibody responses against dengue challenge in rhesus macaques. *Am J Trop Med Hyg*. (2015) 92:698–708. doi: 10.4269/ajtmh.14-0268

34. Danko JR, Kochel T, Teneza-Mora N, Luke TC, Raviprakash K, Sun P, et al. Safety and immunogenicity of a tetravalent dengue DNA vaccine administered with a cationic lipid-based adjuvant in a phase 1 clinical trial. *Am J Trop Med Hyg*. (2018) 98:849–56. doi: 10.4269/ajtmh.17-0416

35. Manoff SB, Sausser M, Falk Russell A, Martin J, Radley D, Hyatt D, et al. Immunogenicity and safety of an investigational tetravalent recombinant subunit vaccine for dengue: results of a Phase I randomized clinical trial in flavivirus-naïve adults. *Hum Vaccines Immunother*. (2019) 15:2195–204. doi: 10.1080/21645515.2018.1546523

36. Durbin AP, Pierce KK, Kirkpatrick BD, Grier P, Sabundayo BP, He H, et al. Immunogenicity and safety of a tetravalent recombinant subunit dengue vaccine in adults previously vaccinated with a live attenuated tetravalent dengue vaccine: results of a phase-I randomized clinical trial. *Am J Trop Med Hyg*. (2020) 103:855–63. doi: 10.4269/ajtmh.20-0042

37. Gote V, Bolla PK, Kommineni N, Butreddy A, Nukala PK, Palakurthi SS, et al. A comprehensive review of mRNA vaccines. *Int J Mol Sci*. (2023) 24:2700. doi: 10.3390/ijms24032700

38. Rosa SS, Prazeres DMF, Azevedo AM, Marques MPC. mRNA vaccines manufacturing: Challenges and bottlenecks. *Vaccine*. (2021) 39:2190–200. doi: 10.1016/j.vaccine.2021.03.038

39. Roth C, Cantaert T, Colas C, Prot M, Casadémont I, Levillayer L, et al. A modified mRNA vaccine targeting immunodominant NS epitopes protects against dengue virus infection in HLA class I transgenic mice. *Front Immunol*. (2019) 10:1424. doi: 10.3389/fimmu.2019.01424

40. Kurane I, Zeng L, Brinton MA, Ennis FA. Definition of an epitope on NS3 recognized by human CD4+ cytotoxic T lymphocyte clones cross-reactive for dengue virus types 2, 3, and 4. *Virology*. (1998) 240:169–74. doi: 10.1006/viro.1997.8925

41. Livingston PG, Kurane I, Dai LC, Okamoto Y, Lai CJ, Men R, et al. Dengue virus-specific, HLA-B35-restricted, human CD8+ cytotoxic T lymphocyte (CTL) clones. Recognition of NS3 amino acids 500 to 508 by CTL clones of two different serotype specificities. *J Immunol (Baltimore Md: 1950)*. (1995) 154:1287–95. doi: 10.4049/jimmunol.154.3.1287

42. Zhang M, Sun J, Li M, Jin X. Modified mRNA-LNP Vaccines Confer Protection against Experimental DENV-2 Infection in Mice. *Mol Ther Methods Clin Dev*. (2020) 18:702–12. doi: 10.1016/j.omtm.2020.07.013

43. Wollner CJ, Richner M, Hassert MA, Pinto AK, Brien JD, Richner JM. A dengue virus serotype 1 mRNA-LNP vaccine elicits protective immune responses. *J Virol*. (2021) 95:e02482–20. doi: 10.1128/JVI.02482-20

44. Richner JM, Himansu S, Dowd KA, Butler SL, Salazar V, Fox JM, et al. Modified mRNA Vaccines Protect against Zika Virus Infection. *Cell*. (2017) 169:176. doi: 10.1016/j.cell.2017.03.016

45. Baldon LVR, de Mendonça SF, Ferreira FV, Rezende FO, Amadou SCG, Leite THJF, et al. AG129 mice as a comprehensive model for the experimental assessment of mosquito vector competence for arboviruses. *Pathog (Basel Switzerland)*. (2022) 11:879. doi: 10.3390/pathogens11080879

46. He L, Sun W, Yang L, Liu W, Li J. A multiple-target mRNA-LNP vaccine induces protective immunity against experimental multi-serotype DENV in mice. *Virol Sin*. (2022) 37:746–57. doi: 10.1016/j.virs.2022.07.003

47. Modis Y, Ogata S, Clements D, Harrison SC. A ligand-binding pocket in the dengue virus envelope glycoprotein. *Proc Natl Acad Sci USA*. (2003) 100:6986–91. doi: 10.1073/pnas.0832193100

48. Lai CTsai WLin S, Kao C, Hu H, King C, Wu H, Chang G, et al. Antibodies to Envelope Glycoprotein of Dengue Virus during the Natural Course of Infection Are Predominantly Cross-Reactive and Recognize Epitopes Containing Highly Conserved Residues at the Fusion Loop of Domain II. *Cell*. (2008) 169(1):176. doi: 10.1128/jvi.00316-08

49. Uddin MN, Roni MA. Challenges of storage and stability of mRNA-based COVID-19 vaccines. *Vaccines*. (2021) 9:1033. doi: 10.3390/vaccines9091033

50. Ladenstein R, Morgunova E. Second career of a biosynthetic enzyme: Lumazine synthase as a virus-like nanoparticle in vaccine development. *Biotechnol Rep (Amsterdam Netherlands)*. (2020) 27:e00494. doi: 10.1016/j.btre.2020.e00494

51. Zhang B, Chao CW, Tsybovsky Y, Abiona OM, Hutchinson GB, Moliva JI, et al. A platform incorporating trimeric antigens into self-assembling nanoparticles reveals SARS-CoV-2-spike nanoparticles to elicit substantially higher neutralizing responses than spike alone. *Sci Rep*. (2020) 10:18149. doi: 10.1038/s41598-020-74949-2

52. Roier S, Mangala Prasad V, McNeal MM, Lee KK, Petsch B, Rauch S. mRNA-based VP8* nanoparticle vaccines against rotavirus are highly immunogenic in rodents. *NPJ Vaccines*. (2023) 8:190. doi: 10.1038/s41541-023-00790-z

53. Ra JS, Shin HH, Kang S, Do Y. Lumazine synthase protein cage nanoparticles as antigen delivery nanoplatforms for dendritic cell-based vaccine development. *Clin Exp Vaccine Res*. (2014) 3:227–34. doi: 10.7774/cevr.2014.3.2.227

54. Figueroa AL, Ali K, Berman G, Zhou H, Deng W, Xu W, et al. Safety and durability of mRNA-1273-induced SARS-CoV-2 immune responses in adolescents: results from the phase 2/3 TeenCOVE trial. *EClinicalMedicine*. (2024) 74:102720. doi: 10.1016/j.eclinm.2024.102720

55. Klinman DM. Immunotherapeutic uses of CpG oligodeoxynucleotides. Nature reviews. *Immunology*. (2004) 4:249–58. doi: 10.1038/nri1329

56. Dowling JK, Mansell A. Toll-like receptors: the swiss army knife of immunity and vaccine development. *Clin Trans Immunol*. (2016) 5:e85. doi: 10.1038/cti.2016.22

57. Wilder-Smith A. Controlled human infection study underpins efficacy of the tetravalent live-attenuated dengue vaccine TV005. *J Clin Invest*. (2024) 134:e177610. doi: 10.1172/JCI177610

58. Center of Disease Control and Prevention (CDC). Dengue vaccination: What Everyone Should Know. Vaccines and Preventable Diseases. Available online at: https://www.cdc.gov/vaccines/vpd/dengue/index.html (Accessed June 1, 2024).

59. Zhao T, Cai Y, Jiang Y, He X, Wei Y, Yu Y, et al. Vaccine adjuvants: mechanisms and platforms. *Signal Transduct Target Ther*. (2023) 8:283. doi: 10.1038/s41392-023-01557-7

60. López-Sagaseta J, Malito E, Rappuoli R, Bottomley MJ. Self-assembling protein nanoparticles in the design of vaccines. *Comput Struct Biotechnol J*. (2015) 14:58–68. doi: 10.1016/j.csbj.2015.11.001

61. Mohsen MO, Bachmann MF. Virus-like particle vaccinology, from bench to bedside. *Cell Mol Immunol*. (2022) 19:993–1011. doi: 10.1038/s41423-022-00897-8

62. Donaldson B, Lateef Z, Walker GF, Young SL, Ward VK. Virus-like particle vaccines: immunology and formulation for clinical translation. *Expert Rev Vaccines*. (2018) 17:833–49. doi: 10.1080/14760584.2018.1516552

63. Whitehead SS. Development of TV003/TV005, a single dose, highly immunogenic live attenuated dengue vaccine; what makes this vaccine different from the Sanofi-Pasteur CYD™ vaccine? *Expert Rev Vaccines*. (2016) 15:509–17. doi: 10.1586/14760584.2016.1115727

64. Pinto SB, Riback TIS, Sylvestre G, Costa G, Peixoto J, Dias FBS, et al. Effectiveness of Wolbachia-infected mosquito deployments in reducing the incidence of dengue and other Aedes-borne diseases in Niterói, Brazil: A quasi-experimental study. *PloS Negl Trop Dis*. (2021) 15:e0009556. doi: 10.1371/journal.pntd.0009556

65. Alphey L, Benedict M, Bellini R, Clark GG, Dame DA, Service MW, et al. Sterile-insect methods for control of mosquito-borne diseases: an analysis. *Vector Borne Zoonotic Dis (Larchmont NY)*. (2010) 10:295–311. doi: 10.1089/vbz.2009.0014

frontiers | Frontiers in Immunology

TYPE Original Research
PUBLISHED 20 March 2025
DOI 10.3389/fimmu.2025.1539492

OPEN ACCESS

EDITED BY
Sonia Jangra,
The Rockefeller University, United States

REVIEWED BY
Gagandeep Singh,
Icahn School of Medicine at Mount Sinai, United States
Sara S. El Zahed,
Icahn School of Medicine at Mount Sinai, United States

*CORRESPONDENCE
Kaissar Tabynov
ktabynov@gmail.com

RECEIVED 04 December 2024
ACCEPTED 19 February 2025
PUBLISHED 20 March 2025

CITATION
Tabynov K, Kuanyshbek A, Yelchibayeva L, Zharmambet K, Zhumadilova Z, Fomin G, Petrovsky N, Shekoni OC, Renukaradhya GJ and Tabynov K (2025) Evaluation of safety, immunogenicity, and efficacy of inactivated reverse-genetics-based H5N8 highly pathogenic avian influenza virus vaccine with various adjuvants via parenteral and mucosal routes in chickens.
Front. Immunol. 16:1539492.
doi: 10.3389/fimmu.2025.1539492

Evaluation of safety, immunogenicity, and efficacy of inactivated reverse-genetics-based H5N8 highly pathogenic avian influenza virus vaccine with various adjuvants via parenteral and mucosal routes in chickens

Kairat Tabynov[1,2,3], Aidana Kuanyshbek[1,4], Leila Yelchibayeva[1], Kuantay Zharmambet[1], Zauresh Zhumadilova[2], Gleb Fomin[2], Nikolai Petrovsky[5], Olaitan C. Shekoni[6], Gourapura J. Renukaradhya[6] and Kaissar Tabynov[1,2,3]*

[1]International Center for Vaccinology, Kazakh National Agrarian Research University, Almaty, Kazakhstan, [2]Central Reference Laboratory, M. Aikimbayev National Scientific Center for Especially Dangerous Infections, Almaty, Kazakhstan, [3]T&TvaX LLC, Almaty, Kazakhstan, [4]National Collection of Deposited Strains, Almaty Branch of National Reference Veterinary Center, Almaty, Kazakhstan, [5]Vaxine Pty Ltd, Adelaide, SA, Australia, [6]Center for Food Animal Health, Department of Animal Sciences, College of Food Agricultural and Environmental Sciences, The Ohio State University (OSU), Wooster, OH, United States

Background: Highly pathogenic H5Nx avian influenza (HPAI) poses a significant threat to poultry health globally, necessitating the development of effective vaccination strategies.

Methods: This study assessed the immunogenicity and efficacy of a reverse-genetics-derived, Differentiating Infected from Vaccinated Animals (DIVA)-compatible inactivated H5N8 vaccine based on the IDCDC-RG71A strain. The vaccine was formulated with different adjuvants, including Montanide ISA 78 VG, ISA 71 R VG, GEL P PR, and mannose-conjugated chitosan nanoparticles, and administered via either the subcutaneous (SC) or intranasal (IN) route. To evaluate safety, the vaccine was tested in specific antibody negative (SAN) chickens, showing no adverse effects. Immunogenicity was assessed by measuring hemagglutination inhibition (HI) antibody titers, antigen-specific IgA and IgY levels, and CD4+ and CD8+ T cell proliferation. Vaccine efficacy was determined through a challenge study using a field isolate of H5N1.

Results: This showed that a single SC dose of vaccine containing ISA 78 VG or ISA 71 R VG provided the best efficacy against infection, with high survival rates, control of abnormally high temperature incidence, reduced virus shedding, and reduced lung and liver lesions. The ISA 78 VG-adjuvanted SC vaccine induced the highest HI titers and CD4+ T cell proliferation, while ISA 71 R VG and GEL P PR elicited the strongest IgY responses. In contrast, IN formulations induced IgA in the lungs and trachea however, even after two doses, failed to generate high HI

titers and provided poor, if any, protection against infection. This highlights the superior efficacy of the SC over the IN route of vaccination for reducing H5N1 viral shedding.

Conclusion: These results underscore the importance of both the adjuvants and delivery route to maximize HPAI vaccine efficacy. This presented system could thereby be used to develop potent and DIVA-compatible vaccines to enhance biosecurity and disease management in regions affected by endemic HPAI.

KEYWORDS

avian influenza, vaccine, H5N8, reverse genetics; efficacy, adjuvants, nanoparticles

1 Introduction

Outbreaks of novel H5N1, H5N6, and H5N8 highly pathogenic avian influenza (HPAI) viruses of the A/Goose/Guangdong/1/96 (Gs/GD) lineage have been extensively spreading across Asia, Europe, Africa, and North America (1–4). These epidemics pose a serious global threat to the poultry industry, ecosystems, and endangered wild bird species and represent a zoonotic risk to human health (5).

Beginning in late 2020, there have been ongoing reports of outbreaks of the HPAI H5N1 virus (clade 2.3.4.4b) worldwide, affecting both wild birds and, on several occasions, domestic poultry. During this period, significant genetic evolution and reassortment have occurred, leading to the emergence of multiple variants (6). Since the fall of 2020, Kazakhstan (KZ) has experienced a series of large outbreaks of HPAI poultry outbreaks among domestic birds that turned out to be the H5N8 subtype of HPAI clade 2.3.4.4b virus (7, 8). The first reported outbreaks occurred in populated areas along the KZ–Russian border. By the end of 2023, outbreaks had been reported in 11 regions of KZ. The Veterinary Service of Kazakhstan made efforts to slow down the spread of the disease through strict quarantines in the affected settlements, imposed export restrictions on poultry and poultry products, and organized prompt vaccination of poultry (9). The recent outbreak of HPAI in KZ (around Lake Karakol near the Caspian Sea coast in Mangistau Oblast) in wild birds was registered between December 28, 2023, and January 9, 2024, wherein 228 mute swans died (2), and a total of 1,132 swans were reported dead until January 25, 2024 (10). During the HPAI outbreak, our research group isolated and characterized a genetically distinct strain of avian influenza virus, A/mute swan/Mangystau/1-S24R-2/2024 (1-S24R-2), subtype H5N1 (clade 2.3.4.4b), from the lung of a deceased mute swan. The highly pathogenic nature of this strain was confirmed based on the presence of the PLREKRRRRKRGLF polybasic cleavage site in the hemagglutinin (HA) gene (2).

Vaccination remains a cornerstone in controlling the spread of HPAI viruses, with the choice of adjuvant and delivery route playing a critical role in determining vaccine efficacy. Adjuvants enhance vaccine protection by optimizing antigen presentation and recognition and prolonging immune memory. Commonly used adjuvants in birds include oil-based emulsions, aqueous formulations, and nanoparticles, each tailored to specific parenteral or mucosal delivery routes. For example, mineral oil-based adjuvants like Montanide ISA 71 R VG and ISA 78 VG elicit strong humoral and cellular responses, while aqueous-based adjuvants such as Montanide GEL P PR are optimized for ease of administration and reduced reactogenicity (11). Recent advances, including mannose-conjugated chitosan nanoparticles (mCS-NPs), provide targeted mucosal delivery and enhance antigen uptake by dendritic cells, potentially improving adaptive immunity (12).

Vaccination is used to control the spread of H5Nx HPAI virus in bird populations in the Republic of Kazakhstan (KZ). According to the national strategy for control of HPAI in KZ beginning 2019, vaccination of parent stock of birds in poultry farms and in households located within a 20-km zone from the hotspot farms as well as poultry in farms located in areas close to migration of wild birds and high-risk areas was carried out (13). Similar vaccination strategies have been adopted in other countries heavily affected by H5Nx HPAI outbreaks. For instance, China has implemented widespread vaccination programs to control HPAI in domestic poultry, which has significantly reduced virus circulation. Egypt, Mexico, and Vietnam have also utilized targeted vaccination campaigns to manage endemic HPAI outbreaks in high-risk regions (14). These strategies emphasize the importance of vaccination as a global tool to mitigate the economic and ecological impact of HPAI in poultry industries and to reduce the zoonotic risk to humans.

Despite the ongoing mass immunization of flocks against HPAI in KZ poultry farms, cases of mortality and reduced productivity of poultry from HPAI vaccine breakthrough infections still continue to occur (personal communication with veterinarians of poultry farms). The effectiveness of poultry vaccines is influenced by many factors, including the match between the vaccine strain and the antigenic variations in the circulating virus strains (15). According to our analysis (2), the genetic similarity in the nucleotide sequence of the hemagglutinin (HA) gene of vaccine strains widely used in

commercial HPAI vaccines in Eurasian Economic Union (EEU) countries and the circulating KZ strain 1-S24R-2 of HPAI virus (clade 2.3.4.4b) is only 90%–92%. However, HPAI vaccine efficacy is not only associated with HA similarity between the vaccine and the virus strain but also depends on any adjuvant used, antigen dose, and immunization route (16).

Previous studies have demonstrated that reverse-genetics-based H5N8 vaccines offer a promising approach for combating HPAI viruses due to their ability to incorporate precise genetic modifications for improved safety and immunogenicity. A study by Gao et al. (2022) highlighted the robust immune responses elicited by an inactivated reverse-genetics-based H5N8 vaccine derived from the A/Astrakhan/3212/2020 strain. This vaccine, formulated with squalene-based adjuvant, induced strong humoral immunity and cross-reactivity across multiple H5 clades in animal models, emphasizing the critical role of adjuvant selection (17). Similarly, the rgH5N2 vaccine provided broad protection in avian H5Nx models. Studies, including those by Panickan et al. (2022), have shown that rgH5N2, either alone or combined with HA stalk antigens, elicits strong hemagglutination inhibiting (HI) activity and neutralizing antibody responses against H5N1, H5N8, and H9N2, reduces viral shedding, and provides protection against lethal H5N1 and H5N8 challenges. However, HA stalk antigens alone proved inadequate against H5N1 and H5N8, highlighting the critical need for strategic antigen selection and optimized vaccine design for broader protection (18). Despite these advances, challenges remain in optimizing the efficacy of these vaccines against evolving clade 2.3.4.4b viruses and ensuring compatibility with diverse immunization strategies. For this study, we assessed a panel of veterinary adjuvants supplied by Seppic. This included Montanide ISA 71 R VG, a water-in-mineral-oil adjuvant based on a mannide-oleate-based surfactant system that can be used at flexible ratios in the vaccine, Montanide ISA 78 VG, a water-in-oil emulsion specifically designed for use in chickens, and Montanide GEL P PR, based on a dispersion of highly stable gel particles of sodium polyacrylate in water that induces a depot effect with slow release due to polymer adsorption properties. In addition, we tested an in-house mannose-conjugated chitosan nanoparticle (mCS-NP) adjuvant as previously described (12).

Our aim in this study was to develop and evaluate different HPAI vaccine formulations using a WHO candidate vaccine virus, IDCDC-RG71A (H5N8; clade 2.3.4.4b; reverse genetics derived reassortant) (19), with a range of injectable and mucosal adjuvants. The safety, immunogenicity, and efficacy of candidate HPAI vaccines (clade 2.3.4.4b) administered via parenteral and mucosal routes were compared to a commercial vaccine available in the EEU countries. The intranasal (IN) route of inoculation was chosen to evaluate its potential to induce localized immunity in the upper respiratory tract, particularly in the nasal and airway mucosa, which are primary sites of avian influenza virus entry and replication. The vaccines were assessed for their ability to protect specific antibody negative (SAN) chickens against H5N1 infection. The study results will facilitate the development of improved vaccines effective against current HPAI threats in KZ, thereby assisting to mitigate the impact of HPAI outbreaks on poultry industries, wildlife, and public health.

2 Materials and methods

2.1 Facility and biosafety statement

All experiments involving the infectious HPAI virus were conducted in biosafety level 3 (BSL-3) and animal biosafety level 3 (ABSL-3) facilities within the Central Reference Laboratory (CRL) at the M. Aikimbayev National Scientific Center for Especially Dangerous Infections (NSCEDI) under the Ministry of Health of the Republic of Kazakhstan (MoH RK). These facilities are accredited according to ISO 35001:2019, which outlines biorisk management for laboratories and other related organizations. The facility's security is maintained through procedures approved by the NSCEDI institutional biosafety officers. All aspects of the facilities, including procedures, training records, safety drills, and inventory logs, undergo regular inspections and continuous oversight by the institutional biosafety officers, who work closely with the facility managers. Experienced personnel worked indoors in pairs (following the two-person rule). Staff wore powered air-purifying respirators (PAPRs) that filtered the air when they worked with HPAI in the lab and birds. Researchers were decontaminated before leaving the facility and then showered upon exiting the facility. The research program, including procedures, occupational health plans, security, and facilities, is subject to an annual review by an official from the MoH RK (20). At the conclusion of the experiments, all waste and infected animal carcasses were autoclaved and incinerated to ensure the elimination of biohazards.

2.2 Ethics statement

All animal experiments were conducted in full compliance with the ARRIVE guidelines, adhering strictly to the UK Animals (Scientific Procedures) Act of 1986 and associated guidelines as well as the EU Directive 2010/63/EU. The sex of the animals was indicated, and any influence or association of sex on the study's results was appropriately analyzed and reported. The protocol was approved by the Institutional Animal Care and Use Committee (IACUC) of the NSCEDI (Protocol No. 17, dated November 1, 2022). The birds were kept in specialized cages (three pullets/m^2) in a facility with 35%–45% humidity at 22°C –23°C, with air exchange occurring at least 16 times per hour. They were housed on deep bedding with drinkers, which were monitored and changed frequently, and feed was provided *ad libitum*. All birds were kept separately in groups (i.e., one group per room) in the ABSL-3 laboratory of the CRL. The birds received daily veterinary supervision, conditions were maintained to ensure a normal state of health, opportunities were provided to meet their physiological and behavioral needs, and factors that could cause stress and distress were rapidly eliminated. Following the challenge with

HPAI infection, all surviving pullets were euthanized by administering sodium pentobarbital (5 g/mL). Humane endpoint criteria for birds after infection comprised of greater than or equal to 35% body weight loss or inability to remain upright.

2.3 Viruses, cells, and birds

The influenza virus strain A/mute swan/Mangystau/1-S24R-2/2024 (H5N1; clade 2.3.4.4b; 1-S24R-2; GISAID accession number: EPI_ISL_18898050; GenBank accession numbers: PP267962, PP267963, PP267964, PP267965, PP267966, PP267967, PP267968, and PP267969) was isolated in 10-day-old SAN embryonated chicken eggs (ECEs) from the lung of a dead mute swan found in Lake Karakol (Kazakhstan) during a HPAI outbreak in 2024 (2).

The influenza virus IDCDC-RG71A (H5N8; clade 2.3.4.4b; RG71A; Lot A2021JUL06) is a reverse-genetics-derived reassortant (19). The RG71A virus is composed of six gene segments (PB2, PB1, PA, NP, M, and NS) that encode A/Puerto Rico/8/1934 (H1N1) proteins. The HA gene segment and neuraminidase (NA) gene segment of RG71A were derived from A/Astrakhan/3212/2020 (H5N8; GenBank HA: OM403993; GenBank NA: OM403994) with HA protein modified to contain a protease cleavage site characteristic of low pathogenic AI viruses. RG71A influenza virus was generated under a quality system using qualified Vero cells per WHO guidance and excluded from the select agent list by the United States Department of Agriculture on August 12, 2021 to enable use under USDA APHIS BSL-2 permit for candidate vaccine virus. The virus RG71A was kindly provided by the Centers for Disease Control and Prevention (CDC, USA) as part of the WHO's Pandemic Influenza Preparedness Framework. The 50% egg infective dose (EID_{50}) of the virus was measured, and aliquots of allantoic fluid were stored at −80°C until use.

Madin-Darby Canine Kidney (MDCK) cells (ATCC® CCL-34™, NBL-2) were grown in Dulbecco's modified Eagle's medium (DMEM; Gibco, UK) supplemented with heat-inactivated 10% fetal bovine serum (FBS; Gibco, UK) and antibiotics (100 units/mL penicillin and 100 µg/mL streptomycin; Gibco, UK) at 37°C in a 5%-CO_2 incubator. MDCK cells in 96-well tissue culture plates were used to measure viral titers in tracheal and cloacal swab samples after challenge infection using the Reed and Mench method (21) expressed in $\log_{10}$ $TCID_{50}$/0.2 mL.

Four-week-old SAN White Leghorn pullets (*G. gallus domesticus*) purchased from a commercial poultry farm in Almaty, Kazakhstan, were used in this experiment. The pullets had not been vaccinated in the poultry farm and were subjected to serological testing upon arrival at the ABSL-3 facility using the hemagglutination inhibition (HI) assay with 1% chicken red blood cells (RBCs). All pullets tested seronegative for H5 AIV.

2.4 Preparation of experimental vaccine formulations

The candidate vaccine strain RG71A was inoculated containing 10^4 EID_{50} of virus in 0.1 mL into the allantoic cavity of 10-day-old SAN embryonated chicken eggs (ECEs) and incubated at 34°C. The allantoic fluids were harvested at 48 h post-infection and clarified by centrifugation at 1,800 × *g* for 30 min at 4°C, and the titer was determined using EID_{50} and hemagglutination (HA) assays. The clarified allantoic fluid of RG71A virus was inactivated with 0.1% formaldehyde (Sigma, Germany) for 30 h at 37°C, and neutralization of formaldehyde was carried out with sodium

TABLE 1 Vaccine formulations and routes of administration.

Group	Description of the adjuvant/ vaccine/controls	Antigen HAU in HA assay	Adjuvant to antigen ratio, wt.%	Method of administration
1	Montanide ISA 78 VG + antigen*	128	70:30	SC
2	Montanide ISA 71 R VG + antigen*	128	70:30	SC
3	Montanide GEL P PR + antigen*	128	10:90	SC
4	Commercial vaccine VOLVAC® B.E.S.T AI+ND (oil-based adjuvant + antigen**)	256	70:30	SC
5	PBS + antigen*	128	70:30***	SC
6	Mannose-conjugated chitosan nanoparticles + antigen*	128	N/A	IN
7	Montanide GEL P PR + antigen*	128	10:90	IN
8	PBS + antigen*	128	10:90***	IN
9	PBS alone	–	–	SC, IN

HA, hemagglutination; HAU, hemagglutination units; IN, intranasal; SC, subcutaneous; PBS, phosphate-buffered saline; N/A, not applicable.
*Candidate vaccine strain IDCDC-RG71A (H5N8) inactivated with 0.1% formaldehyde.
**Recombinant baculovirus recH5 encoding HA of the A/dk/China/E319-2/2003 (H5N1) strain of HPAI virus belonging to clade 2.3.2 (Genbank accession AY518362.1).
***PBS to antigen ratio.

bisulfite ($NaHSO_3$) at a final concentration of 0.4%. Complete inactivation of the candidate vaccine virus was confirmed by inoculating the virus into the allantoic fluid of 10-day-old ECEs, followed by the hemagglutination (HA) assay using 1% chicken red blood cells (RBCs). We used HA units to measure the functional activity of the hemagglutinin (HA) protein rather than the HA mass in micrograms (μg). This approach reflects the functional capacity of the HA antigen and is used for standardization of influenza vaccine doses. The inactivated candidate vaccine strain "antigen" was mixed with Montanide ISA 71 R VG, Montanide ISA 78 VG, and Montanide GEL P PR (Seppic, France) for parenteral administration, and for mucosal IN delivery, mannose-conjugated chitosan nanoparticles (mCS-NPs) and Montanide GEL P PR adjuvants were used according to the vaccine preparation protocols from the manufacturer (Table 1). Commercial vaccine VOLVAC®B.E.S.T AI+ND (Table 1; Group 4) produced by Boehringer Ingelheim Vetmedica, S.A. DEC.V (Guadalajara, Mexico), registered in the State Register of Veterinary Drugs and Feed Additives of the Ministry of Agriculture of the Republic of Kazakhstan, was used for comparison. The commercial vaccine contained at least 256 HA units (HAU) of recH5 recombinant antigen (strain A/duck/China/E319-2/03, subtype H5N1, clade 2.3.2) and 128 HA units of NDV antigen (strain LaSota) per dose (0.5 mL), obtained in ECEs. Both viral antigens (AI+ND) were produced as an oil-based adjuvant vaccine (70:30 by weight).

The detailed information on preparing the vaccine formulations is given in Table 1.

2.4.1 Vaccine formulations with Montanide ISA 78 VG or Montanide ISA 71 R VG adjuvants

To prepare the experimental vaccine formulations (groups 1 and 2), adjuvants Montanide ISA 78 VG and Montanide ISA 71 R VG (Seppic, France) and vaccine candidate virus antigen (aqueous phase; 128 HAU) were mixed in a 70:30 ratio by wt.% by stirring at 4,000 rpm using an IKA Ultra Turrax® Tube Drive Basic high shear stirrer (Ref. 3646000; IKA, Germany) with a DT-20 rotor–stator insert tube (Ref. 3703100; IKA, Germany) working with a volume of 2–15 mL. The adjuvant was placed in the DT-20 rotor–stator tube, and the aqueous phase was carefully added to the same tube without stirring, ensuring that the emulsion temperature was below 20°C before initiating the mixing process. Preemulsification step: The tube was connected to the docking station, and the mixing speed was set to 1,100 rpm (speed level "3"). The mixing process was then carried out for 2 min. Emulsification step: The stirring speed was set to 4,000 rpm (speed level "9"), and the mixing process was carried out for 10 min. The prepared formulations are poured into sterile 10-mL vials, sealed, and stored at 4°C until testing.

2.4.2 Vaccine formulation with Montanide GEL P PR adjuvant

To prepare the experimental vaccine formulation (groups 3 and 7), the Montanide GEL P PR adjuvant and the candidate vaccine antigen (aqueous phase; 128 HAU) were mixed in a ratio of 10:90 by wt.% by stirring at 200 rpm using the Stegler HS-Pro DT magnetic stirrer (Stegler, China) for 5–10 min at RT. The prepared formulation is poured into 10-mL sterile vials, sealed, and stored at 4°C until testing.

2.4.3 Antigen and negative control

After confirming complete inactivation, antigen, 128 HAU/dose in PBS, was diluted in ratios of 70:30 (group 5) and 10:90 (group 8). PBS alone (group 9) was used as a negative control.

2.4.4 Vaccine formulation with mannose-conjugated chitosan nanoparticles

The vaccine antigen (128 HAU) and mannose-conjugated chitosan nanoparticles (mCS NPs) formulation (group 6) was prepared by using a standard ionic gelation method as described previously (22). The mCS NPs morphology, antigen loading efficiency, and size distribution were determined using appropriate methods. The vaccine formulation was lyophilized and stored at −20°C until use. Resuspension of the mCS NP-vaccine was carried out with PBS to the desired volume. All vaccine formulations were kept sterile and contained <2 EU/dose endotoxin.

2.5 Safety, immunogenicity, and efficacy of experimental HPAI (clade 2.3.4.4b) vaccines administered via parenteral and mucosal routes in a single and double immunization regimen in chickens

Ninety White Leghorn pullets, negative for specific antibodies (SAN), were used to assess the safety, immunogenicity, and efficacy of the experimental HPAI (clade 2.3.4.4b) vaccines administered via parenteral or mucosal routes in a single and double immunization regimen in chickens according to the study design (Table 2).

The pullets at the age of 4 weeks were divided into nine experimental groups by randomization with 10 White Leghorns in each group on single (groups 1–5) and double (groups 6–8) immunization regimens. In groups 1–3, experimental vaccine formulations containing ISA-78, ISA-71-R, and GEL-P adjuvants were administered subcutaneously; in group 4, a commercial-oil-adjuvanted recH5 vaccine was administered subcutaneously for comparison; in groups 6 and 7, the vaccine with mCS-NPs and GEL-P adjuvant was administered intranasally; in groups 5 and 8, the vaccine without adjuvant was administered subcutaneously and intranasally, respectively; and in group 9 (negative control), PBS was administered instead of the vaccine, both subcutaneously and intranasally simultaneously.

2.5.1 Sample collection

Blood samples were collected from the wing vein for antibody analysis at 7, 14, 21, and 28 days post-vaccination in the vaccinated and control groups. After blood clotting, the samples were centrifuged at 5,000 × *g* for 10 min at 4°C to collect serum, which was stored in aliquots at −80°C until tested. The tracheal and cloacal swab samples were collected at 2, 4, and 6 days post-challenge in all groups (Table 2). The swab samples were resuspended in 1 mL of

TABLE 2 Study design of safety, immunogenicity, and efficacy of the experimental HPAI (clade 2.3.4.4b) vaccines via parenteral and mucosal routes in a single and double immunization regimen in chickens.

Vaccine Antigen: RG-H5N8 Adjuvant: ISA-78	Vaccine Antigen: RG-H5N8 Adjuvant: ISA-71-R	Vaccine Antigen: RG-H5N8 Adjuvant: GEL-P	Vaccine Antigen: recH5 Adjuvant: Oil-based	Vaccine Antigen: RG-H5N8 Adjuvant: None	Nanovaccine Antigen: RG-H5N8 Adjuvant: mCS-NPs*	Vaccine Antigen: RG-H5N8 Adjuvant: GEL-P*	Vaccine Antigen: RG-H5N8 Adjuvant: None	Negative control: PBS alone
Group 1	Group 2	Group 3	Group 4	Group 5	Group 6*	Group 7*	Group 8*	Group 9
Volume of vaccine or negative control administered								
0.5 mL	0.5 mL	0.5 mL	0.5 mL	0.5 mL	0.5 mL	0.5 mL	0.5 mL	0.5 mL
Single or double immunization schedule								
SC	SC	SC	SC	SC	IN*	IN*	IN*	SC and IN**
Number of pullets per group (Leghorn)								
N = 10	N = 10	N = 10	N = 10	N = 10	N = 10	N = 10	N = 10	N = 10
A 35-day clinical follow-up with weekly weight monitoring								
N = 10	N = 10	N = 10	N = 10	N = 10	N = 10	N = 10	N = 10	N = 10
Blood tests for IgY, IgA, and anti-hemagglutinin antibodies 0, 7, 14, 21, and 28 days after vaccination (immunogenicity)								
N = 10	N = 10	N = 10	N = 10	N = 10	N = 10	N = 10	N = 10	N = 10
Intranasal challenge of pullets with virulent strain A/mute swan/Mangystau/1-S24R-2/2024 (H5N1; clade 2.3.4.4b) at 35 days after vaccination and 10 days of clinical observation with daily body temperature monitoring								
N = 5	N = 5	N = 5	N = 5	N = 5	N = 5	N = 5	N = 5	N = 5
Collection of tracheal and cloacal swabs on days 2, 4, and 6 after challenge								
N = 5	N = 5	N = 5	N = 5	N = 5	N = 5	N = 5	N = 5	N = 5
Euthanasia and collection of respiratory, intestinal, lymphoreticular, and nervous system tissues for histologic studies 10 days after challenge								
N = 5	N = 5	N = 5	N = 5	N = 5	N = 5	N = 5	N = 5	N = 5

PBS, phosphate-buffered saline; SC, subcutaneous; IN, intranasal; RG-H5N8, reverse genetics, candidate vaccine strain IDCDC-RG71A (H5N8) inactivated with 0.1% formaldehyde; mCS-NPs, mannose-conjugated chitosan nanoparticles; ISA-78 VG, Montanide ISA 78 VG; ISA-71-R, Montanide ISA 71 R VG; GEL-P, Montanide GEL P PR; recH5, recombinant baculovirus recH5 encoding HA of the A/dk/China/E319-2/2003 (H5N1) strain of HPAI virus belonging to clade 2.3.2 (Genbank accession AY518362.1); IgY, Immunoglobulin Y.
*Vaccine was administered in a double regimen intranasally with an interval of 14 days.
**Administration of PBS via two routes (SC and IN) at the same time.

DMEM (Gibco, UK) supplemented with 2,000 mg/mL streptomycin and 2,000 IU/mL penicillin. The suspensions were centrifuged at 3,000 × *g* for 10 min, and 0.2 mL of the supernatants from the tracheal or cloacal swabs was used to inoculate the MDCK cells.

2.5.2 Safety

The chickens were examined daily for 35 days for clinical symptoms (activity, appetite, and respiratory and digestive status) and the presence or absence of other abnormalities. All chickens were weighed weekly to monitor their growth dynamics.

2.5.3 Immunogenicity

The immunogenicity of the experimental vaccine in chickens was determined by indirect enzyme-linked immunosorbent assay (iELISA) to measure influenza-specific immunoglobulin Y (IgY) and immunoglobulin A (IgA) antibody levels and by hemagglutination inhibition (HI) assay. Peripheral blood mononuclear cells (PBMCs) were used for the analysis of CD4 + and CD8 + T cell proliferation.

Detection of anti-H5 influenza IgY or IgA antibodies was performed by iELISA using Jet Biofil plates (#FEP-101-896; Guangzhou, China) precoated overnight at 2°C–8°C with inactivated candidate vaccine strain RG71A (128 HAU) diluted 1:10 in a commercial coating buffer (#B288159, BioLegend). The coated plates were blocked using an ELISA Assay Diluent (#421203, BioLegend) at 200 µL per well and incubated under constant shaking (300–330 rpm on a PST-60HL thermal shaker, Biosan) for 1 h at RT. Sera from vaccinated and non-vaccinated chickens were individually titrated (IgY only) twofold from dilutions 1:500–1:2,048,000, and 100-µL samples were added from each dilution to the wells and incubated under constant shaking (300–330 rpm) for 1.5–2 h at RT. After washing (×4), secondary goat anti-chicken IgY H&L (HRP; 1:50,000, #ab6877, Abcam, MA, USA) or goat anti-chicken IgA H&L (HRP; 1:10,000, #ab112817, Abcam, MA, USA) antibodies were added, and the plates were incubated (1 h at RT with shaking). After additional washing (×4), the plates were incubated with streptavidin–HRP conjugate [1:10,000 final dilution for IgY or 1:20,000 final dilution for IgA (Pierce #21130)] for 30 min at RT

with shaking. Finally, the plates were washed (five times) and added with a ready-to-use TMB substrate (#N301, Thermo Fisher Scientific, 100 µL per well). The color reaction was stopped by adding a stop solution (#B308260, BioLegend, 100 µL per well), and the optical density (OD) was measured (measuring wavelength 450 nm, reference wavelength 630 nm) on a ChroMate 4300 analyzer (Awareness Technology, Inc.). The cutoff value for determining seropositivity was the average OD value of the negative sample + three times the standard deviation (23).

The HI assay was performed using the following standard protocol (24). Briefly, cholera filtrate was used as a receptor-destroying enzyme (RDE) according to the WHO protocol (25) to remove innate inhibitors from the serum that could interfere with the assay. The serum was then heated to 56°C for 30 min to remove nonspecific hemagglutination inhibition factors and to inactivate the cholera filtrate. The RDE-treated serum samples (25 µL) were diluted twofold with PBS (25 µL) in 96-well V-bottom plates and incubated with 4 HA units (HAU) of the candidate vaccine strain RG71A for 30 min at RT. Then, 50 µL of a 1% suspension of RBCs was added to each well and incubated at RT for 30 min for the readout. The HI titer was expressed as the reciprocal ($\log_2$ titers) of the highest serum dilution that completely inhibited hemagglutination. Serum HI titers equal to or >1:16 (>4 $\log_2$) were considered positive, while sera with titers in between 1:10 and 1:16 (3.3 to 4 $\log_2$) or with undetectable antibodies were considered negative. The limit of detection was at dilution 1:5 (2.3 $\log_2$), and samples with undetectable titers were assigned a dilution value of 1:5 (2.3 $\log_2$) for statistical purposes.

PBMCs were isolated from chicken blood. Approximately 3 mL of peripheral blood was collected from the subclavian vein of each bird following a sterile procedure and immediately transferred to tubes containing EDTA. The leukothrombocytic layer (750 µL) was separated by centrifugation at 1,800 rpm for 40 min. Subsequently, 750 µL of Histopaque R-1077 was placed into a 2-mL microcentrifuge tube, and 750 µL of the leukothrombocytic layer was gently layered on top of it. Centrifugation was performed for 30 min at 1,800 rpm at RT. Mononuclear cells were aspirated from the opaque surface of the top layer. The cells were washed three times with sterile PBS and then once with RPMI 1640 medium by centrifugation at 1,000 rpm for 10 min. The cells were resuspended in 1 mL of RPMI 1640 and counted using an automated cell counter (Countess II FL; Thermo Fisher Scientific Inc.). The PBMCs were used for lymphocyte proliferation assay study. The CellTrace™ Violet Cell Proliferation Kit for flow cytometry (Thermo Fisher Scientific) was used according to the manufacturer's instructions. Labeled lymphocytes were cultured for 5 days at 37 °C in 5% CO2, both in the presence of the vaccine antigen at a HA titer of 1:128 and in its absence. Flow cytometry analysis of PBMCs from post-immunized chickens was performed using monoclonal antibodies (MAbs) against chicken CD8 alpha (CT-8), PECyanine5 (#MA528727, Invitrogen, USA), and CD4 (CT-4), fluorescein isothiocyanate (FITC; #MA528685, Invitrogen, USA). Briefly, 100 µL of PBMCs (10^5–10^6 cells) in PBS was mixed with 5 µL of MAbs (0.5 µg/µL) in separate tubes, each with an isotype control for individual birds. The cells were gently mixed and incubated at 37°C for 1 h. The tubes were then washed three times with a washing/blocking buffer containing PBS, 1% bovine serum albumin (BSA), and 0.1% sodium azide (SA) and centrifuged at 4,000 rpm for 5 min. The cells were then resuspended, fixed with 0.5% paraformaldehyde (PFA) for 30 min at RT, and analyzed on an Attune™ NxT Flow Cytometer (Thermo Fisher Scientific, USA) using Attune NxT Software (Thermo Fisher Scientific, USA). Analysis of lymphocyte proliferation was performed as previously described by us (26) in the FCS/SSC dot-plot lymphocyte isolate. CD4+ and CD8+ T-cell frequency was calculated as the difference (Δ) between antigen-stimulated and unstimulated samples from the total number of live proliferating lymphocytes and expressed as a percentage.

2.5.4 Efficacy

To test the efficacy of the vaccine formulations at 35 days after immunization, five chickens from each group were transferred to the ABSL-3 facility and challenged with a dose of 10^6 EID_{50} (embryonic infectious dose 50%) of the A/mute swan/Mangystau/1-S24R-2/2024 (H5N1) strain of HPAI in a volume of 500 µL by the intranasal route. Virus back-titration was performed in ECEs immediately following inoculation, confirming that birds received 10^6 EID_{50}. The birds were then monitored daily for 10 days for clinical signs and mortality with daily weighing and body temperature measurement. We considered rectal temperatures greater than or equal to 42.3°C as abnormally high temperatures based on this threshold for potential disease severity (27). The efficacy (protection) of the vaccine was calculated according to the following equation (6):

$$\text{Protection}\,(\%) = \frac{\text{Number of survivors}}{\text{Total number of challenged birds}} \times 100$$

Tracheal and cloacal swabs were collected from each bird on days 2, 4, and 6 after challenge to measure the level of viral shedding across the different groups by calculating the tissue culture infectious dose 50% ($TCID_{50}$) per 1 mL of swab sample in 96-well plates of MDCK cells. After incubation at 37°C for 120 h, the plates were observed daily for the presence of cytopathic effect (CPE) by means of an inverted optical microscope. Then, the cell supernatants were harvested and transferred to V-bottom 96-well plates. The presence of the virus was detected using a hemagglutination assay (16). The endpoint titers were calculated according to the Reed and Muench method (21) based on six replicates for titration. Virus titers are expressed as $\log_{10}$ $TCID_{50}$/mL.

2.5.5 Histological analysis

Dead and euthanized chickens after the challenge were necropsied, and tissues from the respiratory (lung, trachea), digestive (liver, pancreas), intestinal (large and small intestine), lymphoreticular (spleen and bursa of Fabricius), and nervous system (brain) were collected for histological studies. Necropsy and histopathological studies were evaluated as previously described (23, 28) using the following five-level histological scale: 0 (no changes; 0%), 1 (mild inflammation; <25%), 2 (moderate inflammation; 26%–50%), 3 (pronounced inflammation; 51%–75%), and 4 (severe inflammation;

76%–100%) (29). Briefly, the chicken tissues were fixed in 10% buffered formaldehyde, washed in water, and treated with four portions of 100% isopropyl alcohol and two portions of xylene. Subsequently, the tissues were soaked in four portions of paraffin to create paraffin blocks, which were then used to prepare 5-µm sections using a microprocessor-controlled microtome (MZP-01, KB Technom, Russia). The tissue sections were deparaffinized in two portions of xylene and three portions of ethyl alcohol with decreasing concentrations (96%, 80%, and 70%) and stained with hematoxylin (BioVitrum, Russia) and eosin (DiaPath, Italy). Following clarification in ascending ethyl alcohol concentrations (70%, 80%, and 96%) and two portions of xylene, the sections were covered with coverslips using Bio Mount synthetic medium (Bio Optica, Italy). The slides were observed under an Mshot microscope (model MF52-N, China), and photographs were taken at ×100 and ×400 magnification using an Mshot MS23 camera with the Mshot Image Analysis System program. Also, using this program, a measuring scale of 100 and 500 µm was placed on the photographs. A standardized scale was used for calibration, and all measurements were made in micrometers.

2.6 Statistical analysis

GraphPad Prism 9.0.0 (GraphPad Software, San Diego, CA, USA) was used for preparing graphs and for the statistical analysis of the experimental data. Differences in hematological parameters, antibody titers, viral load in swabs, and tissues between animal groups were assessed using Tukey's multiple comparisons test or Dunnett's multiple comparisons tests or Holm–Šídák's multiple comparisons test. The detection limit of the infectivity titer was 0.7 $\log_{10}$ $TCID_{50}$/mL. The detection limit of IgY titers was 1:500 (9.0 $\log_2$). The limit of detection of HI titers was at dilution 1:5 (2.3 $\log_2$), and samples with undetectable titers were assigned a dilution value of 1:5 (2.3 $\log_2$) for statistical purposes. For all comparisons, P <0.05 was considered a significant difference.

3 Results

3.1 Experimental vaccine preparation, safety, and potency

The candidate vaccine strain IDCDC-RG71A (H5N8; clade 2.3.4.4b) was propagated in embryonated chicken eggs, and the virus was harvested from allantoic fluids after 48 h. The fluid containing 128 HAU/50 µL was inactivated using 0.1% formaldehyde, with complete inactivation confirmed by the absence of viral growth in ECEs after three consecutive passages. Various vaccine formulations were prepared using different adjuvants: (1) ISA-78 and ISA-71-R mixed with the antigen at a 70:30 ratio, (2) GEL-P mixed at a 10:90 ratio, (3) mCS-NPs prepared using ionic gelation, lyophilized, and stored at −20°C, and (4) controls that included PBS alone and PBS with antigen at 70:30 and 10:90 ratios.

The safety of the experimental vaccines was evaluated by administering them to SAN chickens and monitoring for any adverse reactions over a 5-week period prior to challenge. The chickens were examined daily for 35 days for clinical signs

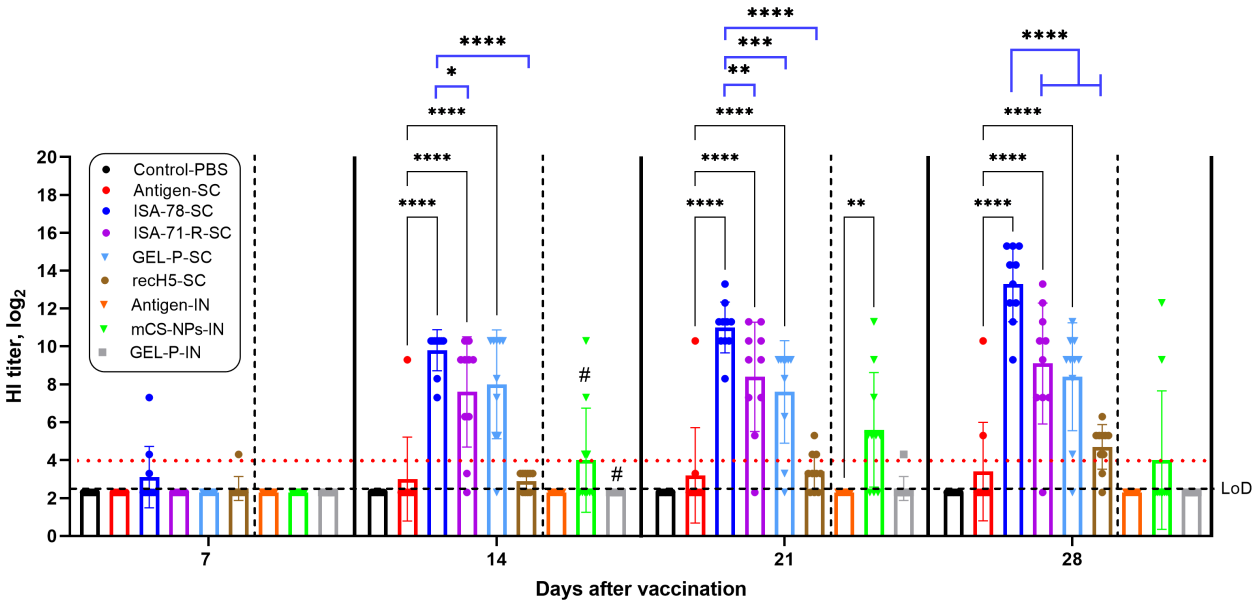

FIGURE 1
Detection of anti-hemagglutinin antibodies in chickens vaccinated with experimental and commercial recH5-SC vaccines by HI assay. Serum HI titers equal to or >4 $\log_2$ were considered positive (horizontal red dotted line), while sera with titers in between 3.3 and 4 $\log_2$ or with undetectable antibodies were considered negative. The limit of detection (LoD) was at dilution 2.3 $\log_2$ (horizontal dotted line). #, second intranasal vaccination for groups GEL-P-IN and mCS-NPs-IN. Data are mean ± SD titer of 10 chickens in each group. Statistical differences between groups were assessed using Tukey's and Dunnett's multiple comparisons tests. For all comparisons, P < 0.05 was considered a significant difference. *P = 0.0354; **P = 0.0010, and 0.0075; ***P = 0.0002; ****P < 0.0001.

including activity, appetite, and respiratory and digestive status as well as the presence or absence of abnormalities. All chickens were weighed weekly to monitor their growth dynamics (Supplementary Table S1). All vaccinated chickens, including those in groups ISA-78-SC, ISA-71-R-SC, GEL-P-SC, mCS-NPs-IN, and GEL-P-IN, showed no local or systemic reactions to the vaccine, with the vaccine formulations all being well tolerated (data not shown) in a similar manner to the commercial vaccine recH5-SC. In conclusion, the experimental vaccines all demonstrated effective inactivation, safety, and tolerance in SAN chickens, validating their potential as vaccine candidates for further evaluation.

3.2 Immunogenicity of the experimental and commercial vaccines in chickens

The immunogenicity of the experimental and commercial vaccines in chickens was assessed by measuring HI antibody levels at 7, 14, 21, and 28 days post-immunization (Figure 1). By day 7, HI antibody responses were detected in groups ISA-78-SC and recH5-SC with seropositivity rates of 20% and 10%, respectively. By day 14, HI seropositivity reached 100% in ISA-78-SC, 90% in GEL-P-SC, 80% in ISA-71-R-SC, and 30% in mCS-NPs-IN. At day 21, seropositivity remained at 100% in group ISA-78-SC, while groups ISA-71-R-SC, GEL-P-SC, mCS-NPs-IN, recH5-SC, GEL-P-IN, and antigen-SC exhibited rates of 90%, 80%, 70%, 30%, 10%, and 10%, respectively. By day 28, group ISA-78-SC maintained 100% seropositivity, with groups GEL-P-SC, ISA-71-R-SC, recH5-SC, mCS-NPs-IN, and antigen-SC showing 90%, 90%, 80%, 20%, and 20% seropositivity, respectively.

On days 14, 21, and 28 post-vaccination, HI antibodies in groups ISA-78-SC, GEL-P-SC, and ISA-71-R-SC were significantly higher ($P < 0.0001$) compared to those in antigen-SC. In group mCS-NPs-IN, the HI antibody levels were significantly elevated ($P = 0.0010$) compared to the antigen-IN group only at 21 days post-vaccination. Group ISA-78-SC exhibited significantly higher HI antibody levels on days 21 and 28 post-vaccination compared to groups GEL-P-SC ($P = 0.0002$; $P < 0.0001$), ISA-71-R-SC ($P = 0.0075$; $P < 0.0001$), and recH5-SC ($P < 0.0001$). At day 14 post-vaccination, a similarly significant difference was observed only with groups ISA-71-R-SC ($P = 0.0354$) and recH5-SC ($P < 0.0001$).

Overall, the adjuvanted SC formulations GEL-P-SC and ISA-71-R-SC showed robust HI responses and were not significantly different among each other. However, the ISA-78-SC group demonstrated superior immunogenicity, achieving 100% seropositivity and significantly higher antibody levels compared to other SC groups. These findings suggest that ISA-78-SC formulation is more effective in inducing a strong and sustained immune response.

The immunogenicity of both experimental and commercial vaccines in chickens was evaluated by measuring the levels of serum immunoglobulin Y (IgY) 28 days after immunization (Figure 2). IgY is the primary serum antibody in birds, functioning similarly to mammalian IgG, and serves as a key marker of vaccine-induced immunity in avian models. Groups ISA-71-RS-C and Gel-P-SC showed the highest anti-influenza IgY levels, followed by group ISA-78-SC, which had intermediate levels and not significantly different to the commercial recH5-SC vaccine, and interestingly it was significantly lower ($P = 0.0274$) compared to ISA-71-R-SC. While most chickens that received antigen alone via

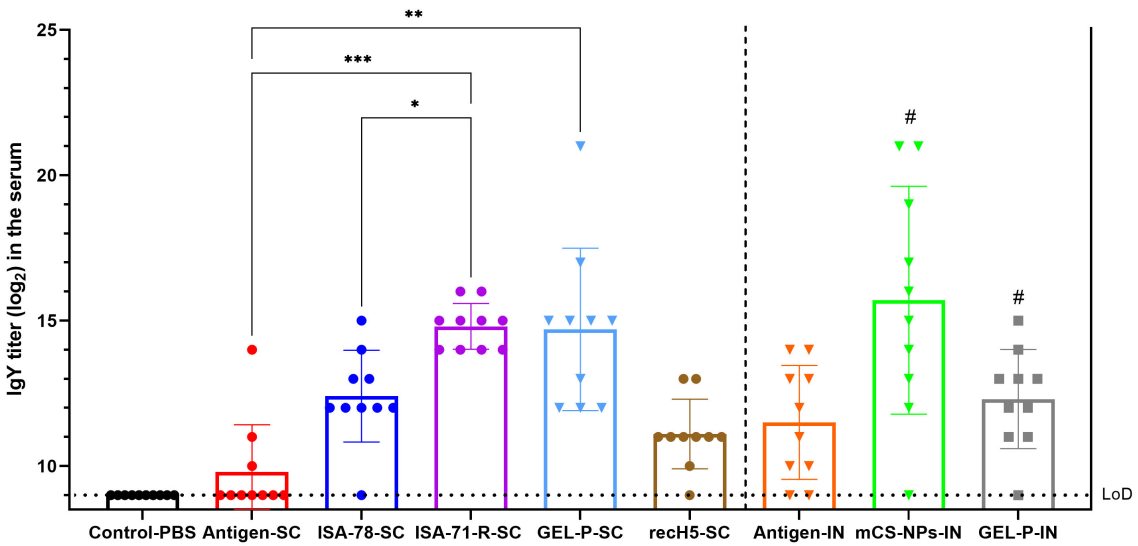

FIGURE 2
Detection of IgY antibodies in chickens vaccinated with experimental and commercial vaccines by iELISA. IgY is the primary immunoglobulin in birds, reptiles, and amphibians, functionally equivalent to mammalian IgG. It plays a critical role in humoral immune response by neutralizing pathogens and providing immunity. The limit of detection (LoD) was at titer 9.0 $\log_2$ (horizontal dotted line). #—A second intranasal immunization was administered to groups GEL-P-IN and mCS-NPs-IN at 14 days after prime vaccination. Data are mean ± SD titer of 10 chickens in each group. Statistical differences between groups were assessed using Tukey's multiple comparisons test. For all comparisons, $P < 0.05$ was considered a significant difference. *$P = 0.0274$; **$P = 0.0015$; ***$P = 0.0008$.

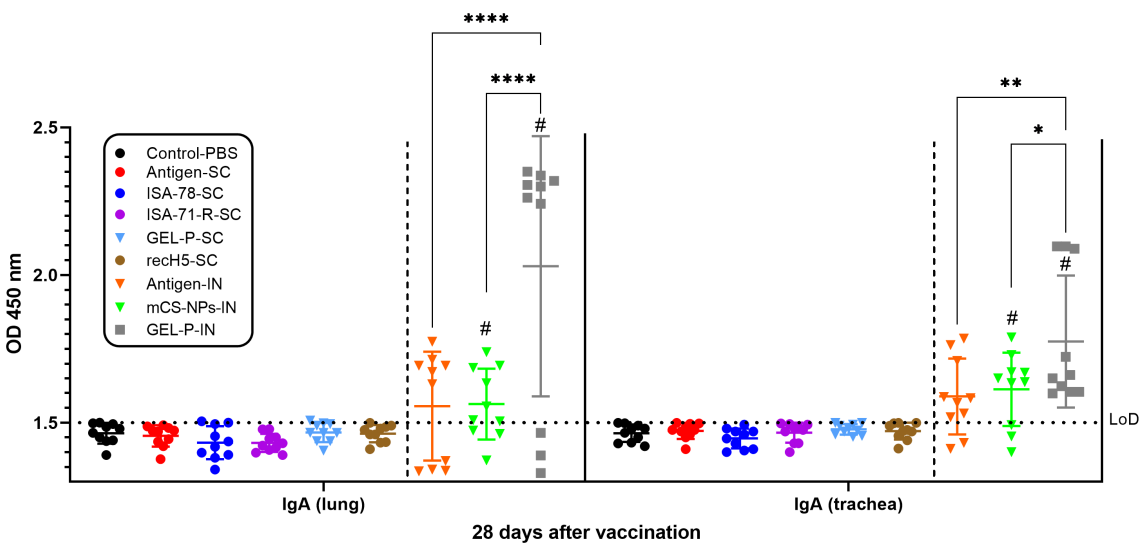

FIGURE 3
Detection of IgA antibodies in chickens vaccinated with experimental and commercial vaccine formulations by iELISA. The limit of detection (LoD) was 1.5 at an optical density (OD) with a wavelength of 450 nm (horizontal dotted line). #A second intranasal immunization was administered to groups GEL-P-IN and mCS-NPs-IN at 14 days after prime vaccination. Data are presented as mean ± SD titers from 10 chickens in each group. Statistical differences between groups were assessed using Šídák's multiple-comparison test. For all comparisons, $P < 0.05$ was considered a significant difference. *$P = 0.0144$; **$P = 0.0019$; ****$P < 0.0001$.

SC route did not induce any IgY response, most of those that received antigen alone via IN route made serum IgY responses equivalent to the high and intermediate IgY responses of SC groups Gel-P-SC and ISA-78-SC, respectively. No significant difference in IgY was observed when comparing the mCS-NPs-IN and GEL-P-IN groups with the antigen-IN group.

Immunogenicity was further assessed using iELISA by measuring influenza-binding IgA levels in lung and trachea on day 28 post-vaccination (Figure 3). Influenza-specific IgA in the lung and trachea was only detected in the IN groups (antigen-IN, and mCS-NPs-IN, and GEL-P-IN), with high influenza-binding IgA levels only seen in group GEL-P-IN.

We assessed antigen-stimulated CD4+ and CD8+ T cell proliferation in PBMCs from chickens vaccinated with both experimental and commercial vaccines on day 28 post-vaccination (Figure 4). Only in group ISA-78-SC were the levels of CD4+ T cell

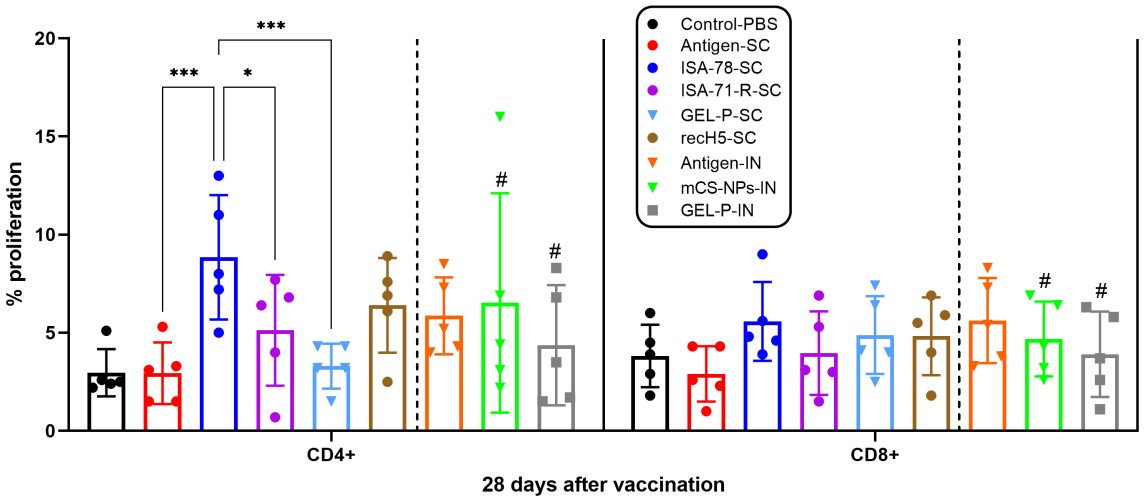

FIGURE 4
Antigen-stimulated CD4 + and CD8 + T cell proliferation in PBMCs from chickens vaccinated with experimental and commercial vaccines. #A second intranasal immunization was administered to groups GEL-P-IN and mCS-NPs-IN at 14 days after prime vaccination. CD4+ and CD8+ T cell proliferation was calculated as the difference (Δ) in the number of proliferating lymphocytes between stimulated vs. non-stimulated cells. Data are mean ± SD titer of five chickens in each group. Statistical differences between groups were assessed using the Tukey's multiple comparisons test. For all comparisons, $P < 0.05$ was considered a significant difference. *$P = 0.0420$; ***$P = 0.0001$ and $P = 0.0003$.

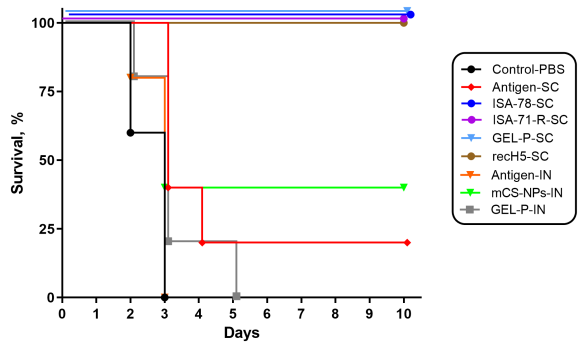

FIGURE 5
Kaplan–Meier survival curve of vaccinated and control chickens.

proliferation significantly higher (P = 0.0001) compared to the SC antigen alone group. In addition, group ISA-78-SC showed significantly higher CD4+ T cell proliferation compared to groups ISA-71-RS-SC (P = 0.0420) and Gel-P-SC (P = 0.0003). There were no significant differences in CD8+ T cell proliferation levels between groups. Overall, ISA-78-SC exhibited the highest CD4+ T cell response.

3.3 Efficacy of the experimental and commercial vaccines in chickens

To assess the efficacy of vaccine formulations, chickens at 35 days post-immunization were transferred to our ABSL-3 facility and challenged with 10^6 EID_{50} of the A/mute swan/Mangystau/1-S24R-2/2024 (H5N1) strain of HPAI via the IN route. The birds were monitored for 10 days for clinical signs (rectal temperature) and mortality, and efficacy was calculated based on survival rates (Supplementary Table S2; Figure 5).

High efficacy group (100% protection): The SC immunization groups, ISA-78-SC, ISA-71-R-SC, GEL-P-SC, and recH5-SC all demonstrated 100% protection. Moderate efficacy group (40% protection): The mCS-NPs-IN group exhibited 40% protection, consistent with the overall poor systemic immunogenicity responses in all of the IN groups despite receiving two vaccine doses. Low efficacy group (20% protection): The antigen alone SC group administered subcutaneously showed 20% protection, indicating that the SC route of vaccination provided better protection than the IN route. No efficacy group (0% protection): The IN groups GEL-P-IN and antigen-IN showed no protection, with all birds dying after the challenge. As expected, the control group, which received PBS via both subcutaneous and intranasal routes, exhibited 0% protection, with all birds dying after the challenge.

The body temperature of the chickens was recorded daily for 10 days following the H5N1 challenge (Supplementary Table S3; Figure 6). High efficacy group: Groups ISA-78-SC, ISA-71-R-SC, GEL-P-SC, and recH5-SC had high temperature incidences, ranging from 0% (ISA-78-SC, ISA-71-R-SC, and recH5-SC) to 20% (GEL-P-SC). Despite some abnormally high temperature occurrences, all of these groups achieved 100% protection, showing that these vaccines prevented mortality even when some chickens still exhibited a high temperature in response to the infection.

Moderate and low efficacy groups: The moderate efficacy group (40% protection) and the low efficacy group (20% protection) both exhibited an abnormally high temperature incidence of 60%. This suggests that, while the mCS-NPs-IN formulation provides some immune response, it may not be potent enough to offer substantial protection, and the antigen-SC formulation appears relatively ineffective. In both cases, the observed febrile reactions may

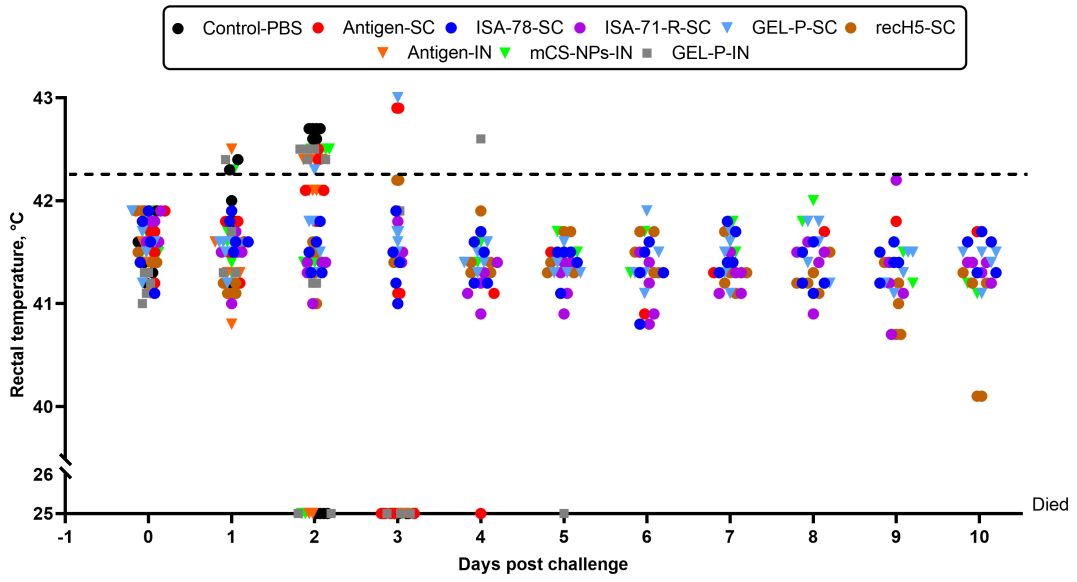

FIGURE 6
Daily body temperatures (°C) of chickens post-challenge. The horizontal dotted line indicates an abnormally high temperature (≥42.3°C) for White Leghorns.

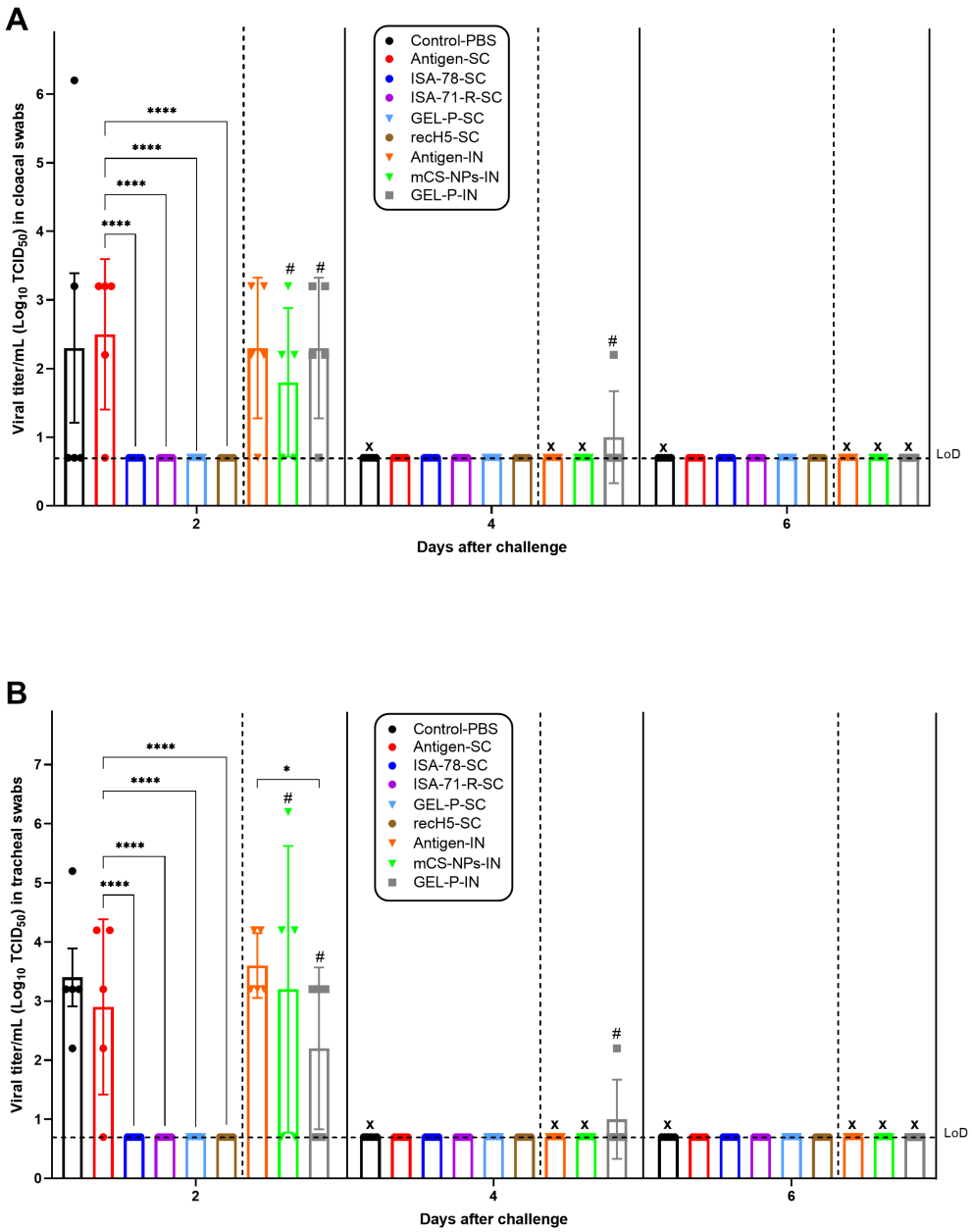

FIGURE 7
Viral shedding of the immunized chickens at 2, 4, and 6 days post-challenge. **(A)** Cloacal swabs and **(B)** tracheal swabs. The immunized chickens with experimental and commercial vaccine formulations were subjected to a challenge with 10^6 EID_{50} of the A/mute swan/Mangystau/1-S24R-2/2024 (H5N1) strain of HPAI via the intranasal route. The limit of detection (LoD) was at titer 0.7 log_{10} $TCID_{50}$ (horizontal dotted line). X, dead chickens. In graphs A and B, in the antigen-SC group at 4 days post-challenge, the X sign was omitted because one bird in this group remained alive until 10 days post-infection. Data are mean ± SD titer of five chickens in each group. Statistical differences between groups were assessed using Tukey's multiple comparisons test. For all comparisons, $P < 0.05$ was considered a significant difference. *$P = 0.0142$; ****$P < 0.0001$. A second intranasal immunization was administered to groups GEL-P-IN and mCS-NPs-IN at 14 days after prime vaccination.

indicate poor immunogenicity or an insufficiently balanced immune response, failing to provide robust protection while still inducing temperature elevations in some individuals.

No efficacy group: Groups control-PBS and GEL-P-IN provided no protection and had the highest abnormally high temperature incidence (100%), whereas group antigen-IN also showed an abnormally high temperature incidence (60%).

This categorization highlights the relationship between protective efficacy and an abnormally high temperature incidence, with higher protection groups generally showing a lower abnormally high temperature incidence, while groups with minimal to no protection have higher temperature rates. This suggests that optimal adjuvant and delivery strategies are key to achieving high protection and low adverse reactions.

To investigate the capability of different vaccine formulations to control viral shedding after challenge with the A/mute swan/Mangystau/1-S24R-2/2024 (H5N1) strain, virus shedding in cloacal (Figure 7A) and tracheal (Figure 7B) swabs was measured at days 2, 4,

and 6 post-infection. Adjuvanted SC groups ISA-78-SC, ISA-71-R-SC, GEL-P-SC, and recH5-SC demonstrated undetectable viral titers in cloacal and tracheal swabs on days 2, 4, and 6 post-challenge, indicating effective protection against viral shedding. In contrast, groups antigen-IN, mCS-NPs-IN, and GEL-P-IN, which received IN vaccines, as well as groups control-PBS and antigen-SC, exhibited viral titers in both cloacal and tracheal swabs on day 2 post-challenge. In the GEL-P-IN group, compared with the antigen-IN group, the viral titer in the trachea was lower on day 2 post-challenge; however, it remained detectable up to day 4 following the infection. This shows that SC vaccines were more effective in reducing viral replication and shedding compared to IN vaccines.

3.4 Histological analysis

The ability of the vaccines to prevent lung and liver tissue lesions caused by H5N1 virus infection was evaluated by a histological analysis of dead and euthanized chickens. It is worth noting that histological examination revealed no pathological changes in the trachea, pancreas, large and small intestine, spleen, bursa of Fabricius, or brain of the challenged chickens (data not shown).

Control infected birds showed notable pathological changes near the parabronchi, including necrosis of the atrial epithelium, transudate accumulation in the parabronchial cavity, erythrostasis within vessels, and low-grade lymphocytic infiltration (Figure 8), indicating localized tissue damage and inflammatory responses associated with infection. The histopathological analysis of liver specimens of control infected birds also revealed significant changes, including enlargement of sinusoidal spaces, focal necrosis in the parenchyma, particularly in the periportal region and near the centrilobular vein, as well as areas of hemorrhage and erythrostasis within vessels (Figure 9).

SC vaccines, particularly ISA-78-SC, GEL-P-SC, ISA-71-R-SC, and the commercial vaccine rec-H5-SC, reduced the pathology caused by H5N1 infection (Figure 10A) as evidenced by significantly lower lesion scores ($P < 0.0001$) compared to the group that received antigen alone SC, which displayed the highest lesion scores after the SC and IN PBS control groups. In the IN groups, including GEL-P-IN and mCS-NPs-IN, the lesion scores were not significantly different from those of the group that received antigen alone via the IN route.

For liver lesions, only the SC groups ISA-78-SC and ISA-71-R-SC showed effective protection ($P < 0.0001$) (Figure 10B). IN administration of GEL-P-IN or mCS-NPs-IN provided no protection against liver lesions.

This confirmed that the SC route of administration was superior to IN for preventing lung and liver damage following H5N1 infection, with ISA-78-SC and ISA-71-R-SC formulations showing the greatest protection.

4 Discussion

H5Nx HPAI is a devastating infection of poultry in Asian, European, North African, and Central and Northern American countries. An increasing number of HPAI outbreaks and the establishment of endemicity in many countries have resulted in an increased use of vaccination as a tool in control programs (30). According to the World Organisation for Animal Health (WOAH), more than 30 countries have resorted to vaccination against HPAI since 2005, including Mexico, China, Guatemala, Honduras, El Salvador, Egypt, and European Union (31). Among the various techniques for vaccine strain development, reverse genetics is the most extensively utilized for creating non-pathogenic DIVA (differentiation of infected from vaccinated animals) marker vaccines (32, 33).

The present study was aimed at evaluating different adjuvants (oil-based, aqueous, and nanoparticles) and delivery routes (parenteral and mucosal) for a reverse-genetics-based vaccine based on IDCDC-RG71A (H5N8; clade 2.3.4.4b), developed as part of the WHO's Pandemic Influenza Preparedness Framework (19). The selection of the IDCDC-RG71A (H5N8) strain for vaccine development is supported by its high genetic homology in the HA gene with the circulating H5N1 field virus in KZ (clade 2.3.4.4b), sharing 97% identity, as reported in our previous studies (2). This high level of HA gene similarity ensures that the HA of the vaccine strain closely resembles the circulating virus, thereby conferring the high chance of protection against local H5N1 strains. Additionally, the inclusion of a neuraminidase (NA) gene from a different subtype than the target H5N1 field virus confers DIVA compatibility to the H5N8 vaccine. This design allows for the serological differentiation of H5N8-vaccinated birds from those naturally infected with H5N1 by using N1-based serological assays (30), which is in line with the heterologous NA DIVA strategy (32).

These study results confirm the successful inactivation, safety, and tolerability of the formaldehyde-inactivated H5N8 vaccine in SAN chickens. The absence of adverse effects alongside consistent growth metrics underscores the tolerability and safety of the tested adjuvant formulations, which were comparable to the commercial recH5-SC (VOLVAC® B.E.S.T AI+ND) vaccine (33). Notably, the experimental adjuvanted vaccine formulations induced much higher HI activity than the commercial recH5-SC vaccine which induced very little HI activity, highlighting the importance of the adjuvants that we used to maximize vaccine immunogenicity. This result is consistent with the findings reported by Kandeil et al. (2018) showing low HI titers induced by commercial HPAI vaccines (34).

The study demonstrated that the single-dose SC H5N8 formulations, particularly those containing Montanide mineral oil adjuvants (ISA-78, ISA-71-R) or aqueous adjuvant (GEL-P-SC), provided the most robust protection against H5N1 infection and clinical disease, alongside the commercial oil-based recH5-SC vaccine, while also significantly reducing virus shedding via the respiratory and digestive tracts by day 2 post-challenge compared to the antigen-SC group (antigen administered subcutaneously without adjuvant). These findings align with data from Kuruppuarachchi et al. (2022) (35), which showed that an oil-adjuvanted inactivated H5N6 vaccine completely protected the chickens from the lethal infection with homologous H5N6 and

10.3389/fimmu.2025.1539492

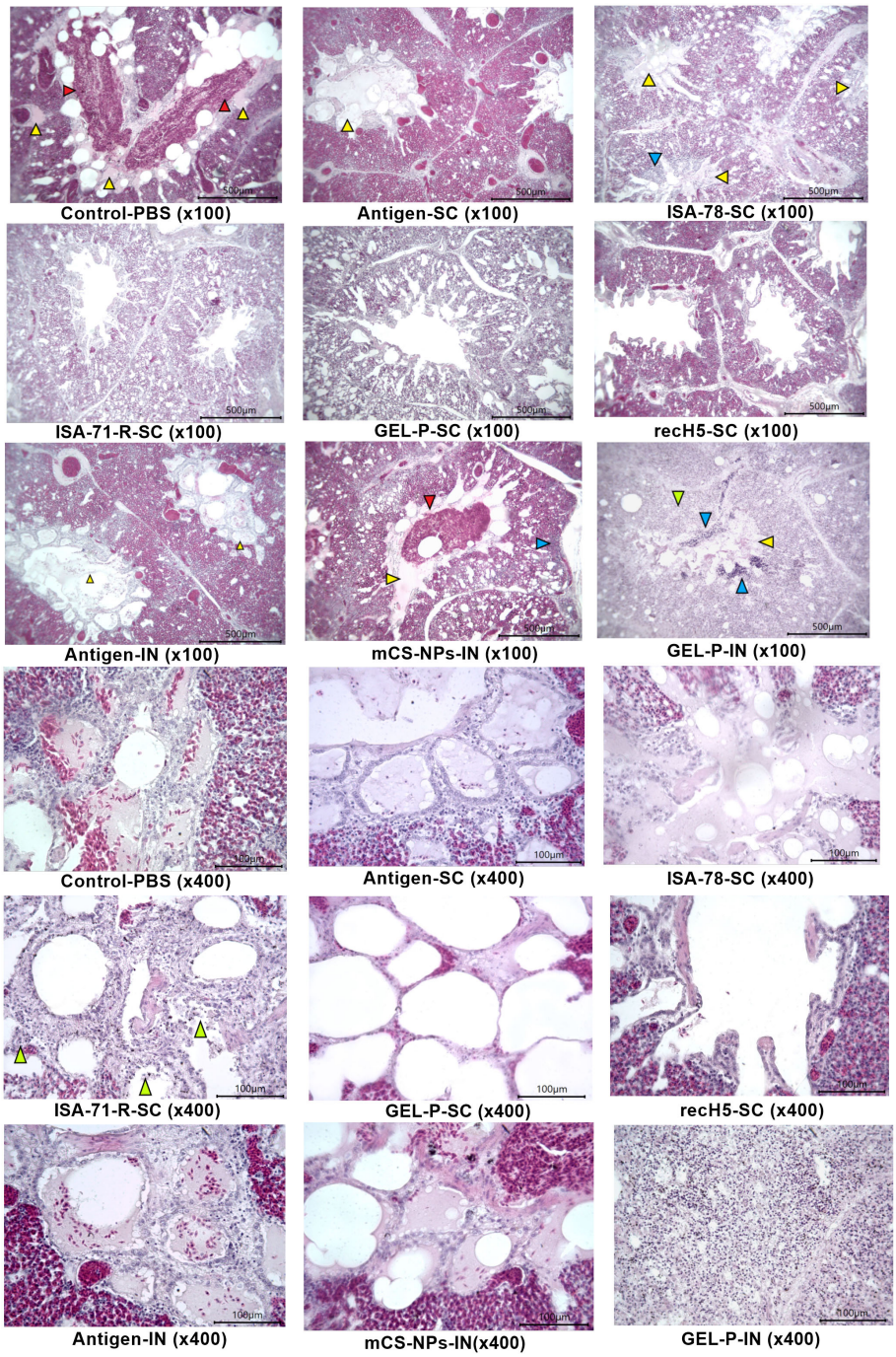

FIGURE 8
Histological analysis of lung tissue. Control-PBS (x100): transudate (yellow arrow) and mass accumulation of erythrocytes (red arrow) in the parabronchus cavity; antigen-SC (x100): transudate in parabronchus cavity (yellow arrow), erythrostasis in vessels; ISA-78-SC (x100): edematous fluid in the lumen of parabronchi (yellow arrows) and lymphocytic infiltrate in the atrial wall [blue arrow; ISA-71-R-SC (x100)]: parabronchial structure; GEL-P-SC (x100): structure of parabronchi; recH5-SC (x100): structure of parabronchi; antigen-IN (x100): transudate in parabronchus cavity (yellow arrow), erythrostasis in vessels; mCS-NPs-IN (x100): transudate (yellow arrow) and erythrocyte accumulation (red arrow) in the parabronchus cavity, as well as lymphocytic infiltrate in the walls of atria (blue arrow); GEL-P-IN (x100): necrosis of atria (green arrow), lymphocytic infiltration (blue arrow), and transudate in the parabronchus cavity (yellow arrow); control-PBS (x400): atria filled with transudate and erythrocytes, necrosis of atrial wall epithelium; antigen-SC (x400): atria filled with transudate and necrosis of atrial wall epithelium. ISA-78-SC (x400): transudate in atrial cavities and necrotized atrial walls; ISA-71-R-SC (x400): weak necrosis of atria epithelium (green arrow); GEL-P-SC (x400): structure of the atria; recH5-SC (x400): structure of the atria; antigen-IN (x400): atria filled with transudate and necrosis of atrial wall epithelium; mCS-NPs-IN (x400): atria filled with transudate and erythrocytes, necrosis of atrial wall epithelium; GEL-P-IN (x400): massive necrosis of atria; hematoxylin–eosin staining.

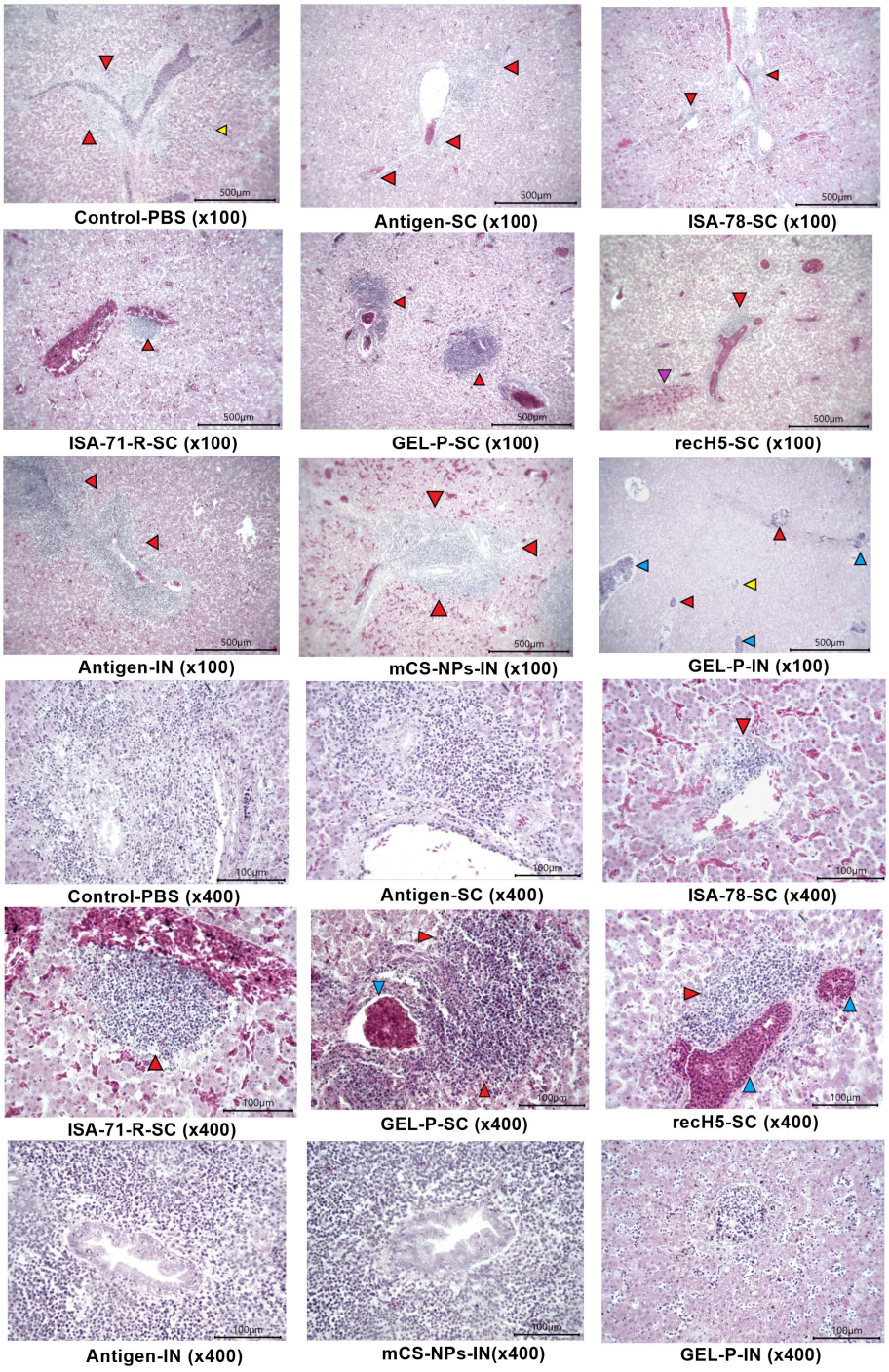

FIGURE 9
Histological analysis of liver tissue. Control-PBS (×100): severe foci of periportal necrosis (red arrows) and parenchyma hepatocyte necrosis (yellow arrow); antigen-SC (×100): severe periportal necrosis; ISA-78-SC (×100): diffuse hemorrhage and foci of necrosis with lymphocytic infiltration near the portal tract (red arrows); ISA-71-R-SC (×100): focal moderate foci of periportal necrosis (red arrow) and diffuse hemorrhages in the parenchyma; GEL-P-SC (×100): foci of centrilobular and periportal necrosis (red arrows); recH5-SC (×100): focal hemorrhage in the parenchyma (purple arrow) and periportal necrosis (red arrow) of hepatocytes; antigen-IN (×100): foci of periportal necrosis; mCS-NPs-IN (×100): strongly marked focus of periportal necrosis (red arrow) and diffuse hemorrhages in the parenchyma; GEL-P-IN (×100): hepatocyte necrosis in the parenchyma (yellow arrow), periportal and centrilobular foci of necrosis (red arrows), and vessels filled with lymphocytes and macrophages (blue arrow); control-PBS (×400): severe foci of periportal hepatocyte necrosis; antigen-SC (×400): severe foci of necrosis at the bile duct; ISA-78-SC (×400): mild centrilobular necrosis of hepatocytes with lymphoid cells (red arrow). GEL-P-SC (×400): foci of marked centrilobular necrosis (red arrows) and erythrostasis (blue arrow) in the vessel. GEL-P-IN (×400): hepatocyte necrosis and lymphocytes in sinusoidal spaces. ISA-71-R-SC (×400): focal moderate foci of periportal necrosis (red arrow) and diffuse hemorrhages in the parenchyma; recH5-SC (×400): moderate periportal necrosis of hepatocytes (red arrow) and erythrostasis in the vessel (blue arrow). Antigen-IN (×400): a pronounced focus of periportal necrosis; mCS-NPs-IN (×400): strongly marked focus of necrosis at the bile duct; hematoxylin–eosin staining.

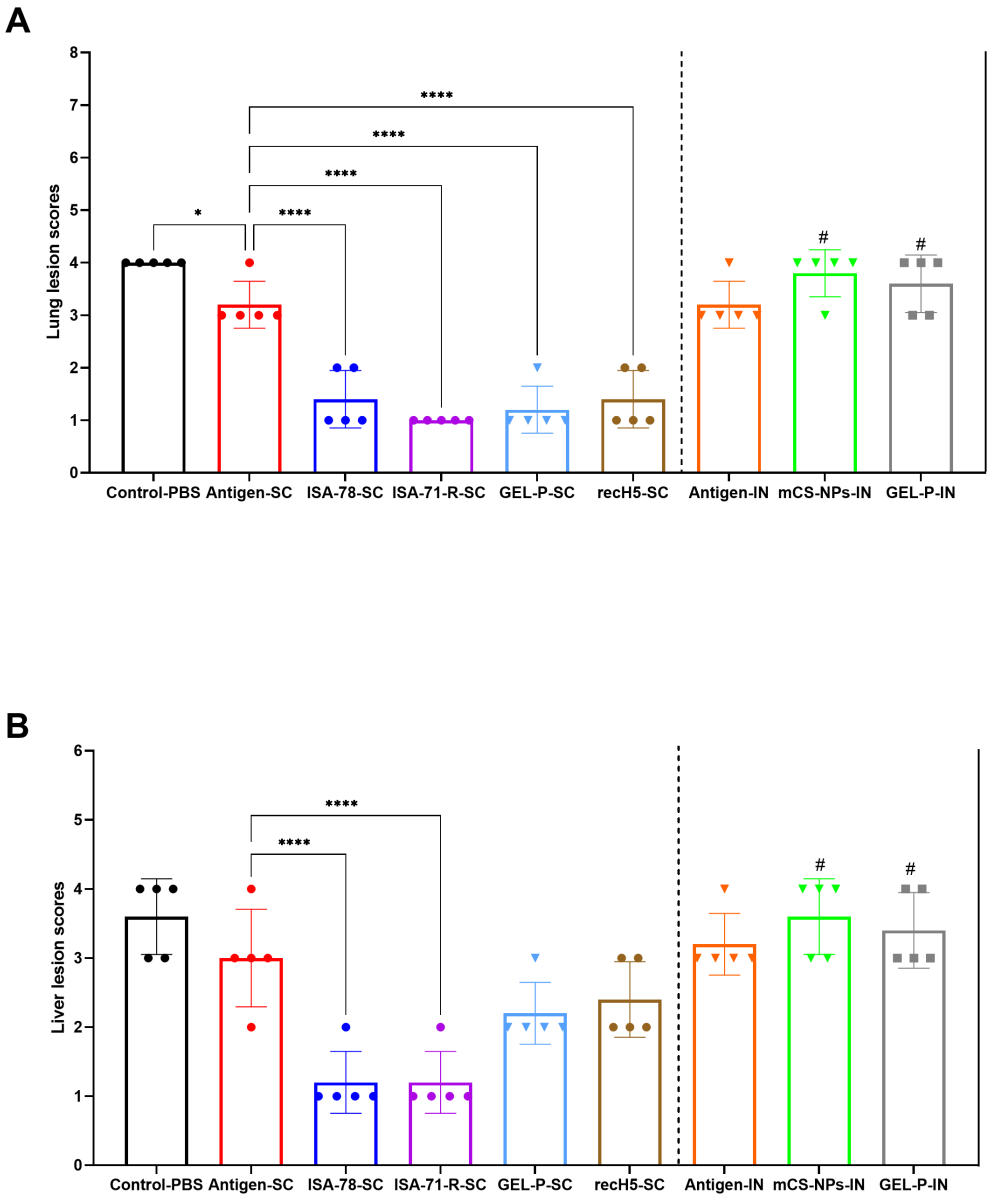

FIGURE 10
Histopathological scoring of lung and liver lesions in H5N1-infected chickens. **(A)** Lung lesion scores. **(B)** Liver lesion scores. The histological scale used was as follows: 0 (no changes; 0%), 1 (mild inflammation; <25%), 2 (moderate inflammation; 26%–50%), 3 (pronounced inflammation; 51%–75%), and 4 (severe inflammation; 76%–100%). Data are mean ± SD titer of five chickens in each group. Statistical differences between groups were assessed using Holm–Šídák's multiple comparisons test. For all comparisons, $P < 0.05$ was considered a significant difference. *$P = 0.0233$; ****$P < 0.0001$. A second intranasal immunization was administered to groups GEL-P-IN and mCS-NPs-IN at 14 days after prime vaccination.

heterologous H5N1 HPAI viruses. In their study, no viral shedding was observed from either the trachea or cloaca on day 3 post-challenge with the H5N6 vaccine, whereas our H5N8 vaccine achieved similar results by day 2 post-challenge. The histological analysis further confirmed the effectiveness of SC-adjuvanted vaccine formulations, especially those with ISA-78 and ISA-71-R, in protecting chickens from lung and liver lesions caused by H5N1 infection, whereas all of the IN H5N8 vaccine formulations (mCS-NPs-IN and GEL-P-IN) provided minimal protection even after two doses.

The ISA-71-R SC formulation achieved the highest serum anti-influenza IgY levels, whereas only the IN groups, particularly GEL-P-IN, induced anti-influenza IgA production in the lung and trachea. While a positive correlation was observed between serum influenza-binding IgY, HI activity, and protection, the mucosal IgA responses showed no correlation with protection. It is generally suggested that IgA antibody subtype is the primary isotype induced at the mucosal surfaces and could be involved in protecting animals from infections by influenza viruses (36). In studies by Hwang et al. (2011) (37), it was shown that in chickens immunized with a single dose of an oil-adjuvanted inactivated H5N1 vaccine, IgG was predominantly induced over IgA in the sera, with the authors suggesting that IgG plays the most important role in protecting the immunized chickens against the lethal H5N1 infections.

There were no significant differences in CD8+ T cell responses between any groups. CD4+ T cell responses showed high variability and were only significantly increased in group ISA-78-SC compared to the SC antigen alone group, showing a correlation with protection in this group only. These results partially confirm other reports (38) showing that the major correlate of H5N1 protection in animals is systemic HI activity and Th1-cytokine-secreting CD4+ T cells.

These findings underscore the importance of adjuvants and SC delivery to maximize HPAI vaccine efficacy.

The limitations of this study include several factors that may affect the generalizability and robustness of the findings. One primary limitation is the challenge model itself, as only a single H5N1 strain was used for the post-vaccination challenge, which may not fully represent the broad diversity of H5 avian influenza strains. This approach may limit the generalizability of the findings to other clades. The DIVA capability of this vaccine may be limited in regions with extensive H5Nx circulation, as cross-reactive antibodies could reduce assay specificity. Further validation is needed to ensure effectiveness in diverse settings. Furthermore,antigen-specific cytokine production, such as IFN-gamma, was not assessed in this study. The absence of an IFN-gamma ELISPOT assay limits the understanding of the functional T-cell responses elicited by the vaccines. Future studies will incorporate this assay to provide a more comprehensive evaluation of T-cell activation and its role in protective immunity. An additional limitation is the lackof IgG assessment, which could further clarify the protective mechanisms of our vaccine. While IgY is the primary immunoglobulin in birds, future studies will evaluate IgG responses to enhance our understanding of immunity against HPAI virus. Another limitation involves the reliance on IN delivery in certain groups, which showed lower efficacy compared to SC routes. This outcome suggests a need for optimization in adjuvant selection and administration routes for mucosal vaccines to enhance immune responses. Additionally, the study was conducted with SAN chickens, which may exhibit different immune responses than poultry populations with prior exposures to low pathogenic avian influenza viruses. This factor should be considered when interpreting the real-world applicability of the vaccine efficacy results. The study also employed relatively small group sizes, potentially impacting the statistical power and robustness of the findings. Furthermore, the study was not repeated, necessitating independent replication to confirm the efficacy and consistency of the results. Another limitation is thelack of assessment for the durability of protection, as the study focused on short-term outcomes post-vaccination. This leaves open questions about the long-term immunity provided by the vaccine formulations. Although safety and immunogenicity were rigorously assessed over a 35-day period, longer-term studies are warranted to evaluate sustained immunity and potential impacts on poultry production metrics. An additional limitation is the lack of mucosal immune response evaluation in IN vaccination groups, which restricts understanding of localized immunity. This experiment will be repeated in future studies with nasal secretion sampling to assess mucosal antibody responses. Finally, apart from HI activity, the study did not measure functional antibodies, such as neutralizing antibodies (MN) or neuraminidase inhibition (NI) activity. These assays are crucial to assess the quality of immune responses and understand the protective mechanisms of the vaccines. Future studies will incorporate MN and NI assays to comprehensively evaluate the functional antibody responses elicited by the vaccine formulations. These limitations together highlight the need for future studies with larger sample sizes, repeat trials, and extended observation periods to assess the durability of protection,which would provide a more comprehensive understanding of vaccine efficacy.

In conclusion, this study demonstrates the promise of H5N8 strain IDCDC-RG71A, developed using reverse genetics, to protect against H5N1 infection in poultry. When combined with ISA-78 or ISA-71-R mineral oil adjuvants, these SC vaccines demonstrated robust efficacy with high survival rates and control of clinical signs (abnormally high temperature), reduced the virus shedding, and prevented the lung and liver lesions caused by HPAI H5N1. These results underscore the importance of adjuvants and SC delivery to maximize avian influenza vaccine efficacy and offer valuable insights for the development of potent, DIVA-compatible vaccines that could significantly enhance biosecurity and disease management in regions affected by endemic HPAI.

Data availability statement

The raw data supporting the conclusions of this article will be made available by the authors, without undue reservation.

Ethics statement

The animal study was approved by Institutional Animal Care and Use Committee (IACUC) of the NSCEDI (Protocol No. 17, dated November 1, 2022). The study was conducted in accordance with the local legislation and institutional requirements.

Author contributions

KairT: Data curation, Investigation, Methodology, Software, Validation, Writing – original draft, Writing – review & editing. AK: Investigation, Writing – review & editing. LY: Investigation, Writing – review & editing. KZ: Investigation, Writing – review & editing. ZZ: Investigation, Project administration, Writing – review & editing. GF: Investigation, Writing – review & editing. NP: Formal analysis, Visualization, Writing – review & editing. OS: Investigation, Writing – review & editing. GR: Formal analysis, Visualization, Writing – review & editing. KaisT: Conceptualization, Formal analysis, Funding acquisition, Methodology, Project administration, Resources, Software, Supervision, Visualization, Writing – review & editing.

Funding

The author(s) declare that financial support was received for the research and/or publication of this article. This research was funded by the Science Committee of the Ministry of Science and Higher Education of the Republic of Kazakhstan (Grant No. AP19675939). Partial funding was also provided by the startup company T&TvaX LLC (Kazakhstan). The funders had no role in the study design, data collection, analysis, or interpretation, nor in the writing of the manuscript or the decision to submit it for publication.

Acknowledgments

The authors express their gratitude to L. Zhambyrbayeva and A. Mukhambetova for their dedicated care and maintenance of the laboratory animals. Special thanks are extended to Dr. N. Turebekov for providing valuable guidance on biosafety and biosecurity during experiments involving highly pathogenic avian influenza.

Conflict of interest

Authors KaisT and KairT were employed by the company T&TvaX LLC. Author NP was employed by the company Vaxine Pty Ltd.

The remaining authors declare that the research was conducted in the absence of any commercial or financial relationships that could be construed as a potential conflict of interest.

Generative AI statement

The author(s) declare that no Generative AI was used in the creation of this manuscript.

Publisher's note

All claims expressed in this article are solely those of the authors and do not necessarily represent those of their affiliated organizations, or those of the publisher, the editors and the reviewers. Any product that may be evaluated in this article, or claim that may be made by its manufacturer, is not guaranteed or endorsed by the publisher.

Supplementary material

The Supplementary Material for this article can be found online at: https://www.frontiersin.org/articles/10.3389/fimmu.2025.1539492/full#supplementary-material

References

1. Lin S, Chen J, Li K, Liu Y, Fu S, Xie S, et al. Evolutionary dynamics and comparative pathogenicity of clade 2.3.4.4b H5 subtype avian influenza viruses, China, 2021-2022. *Virol Sin*. (2024) 39:358–68. doi: 10.1016/j.virs.2024.04.004

2. Tabynov K, Strochkov V, Sandybayev N, Karibayev T, Berdikulov M, Yelchibayeva L, et al. Detection and genomic characterization of an avian influenza virus A/mute swan/Mangystau/1-S24R-2/2024 (H5N1; clade 2.3.4.4b) strain isolated from the lung of a dead swan in Kazakhstan. *Microbiol Resour Announc*. (2024) 22: e0026024. doi: 10.1128/mra.00260-24

3. Chen J, Xu L, Liu T, Xie S, Li K, Li X, et al. Novel reassortant avian influenza A (H5N6) virus, China, 2021. *Emerg Infect Dis*. (2022) 28:1703–7. doi: 10.3201/eid2808.212241

4. Shi W, Gao GF. Emerging H5N8 avian influenza viruses. *Science*. (2021) 372:784–6. doi: 10.1126/science.abg6302

5. Bui CHT, Kuok DIT, Yeung HW, Ng KC, Chu DKW, Webby RJ, et al. Risk assessment for highly pathogenic avian influenza A(H5N6/H5N8) clade 2.3.4.4 viruses. *Emerg Infect Dis*. (2021) 27:2619–27. doi: 10.3201/eid2710.210297

6. Mahmoud SH, Khalil AA, Abo Shama NM, El Sayed MF, Soliman RA, Hagag NM, et al. Immunogenicity and cross-protective efficacy induced by an inactivated recombinant avian influenza A/H5N1 (Clade 2.3.4.4b) vaccine against co-circulating influenza A/H5Nx viruses. *Vaccines (Basel)*. (2023) 11:1397. doi: 10.3390/vaccines11091397

7. Lewis NS, Banyard AC, Whittard E, Karibayev T, Al Kafagi T, Chvala I, et al. Emergence and spread of novel H5N8, H5N5 and H5N1 clade 2.3.4.4 highly pathogenic avian influenza in 2020. *Emerg Microbes Infect*. (2021) 10:148–51. doi: 10.1080/22221751.2021.1872355

8. Baikara B, Seidallina A, Baimakhanova B, Kasymbekov Y, Sabyrzhan T, Daulbaeva K, et al. Genome sequence of highly pathogenic avian influenza virus A/chicken/north Kazakhstan/184/2020 (H5N8). *Microbiol Resour Announc*. (2023) 12: e0115122. doi: 10.1128/mra.01151-22

9. Amirgazin A, Shevtsov A, Karibayev T, Berdikulov M, Kozhakhmetova T, Syzdykova L, et al. Highly pathogenic avian influenza virus of the A/H5N8 subtype, clade 2.3.4.4b, caused outbreaks in Kazakhstan in 2020. *PeerJ*. (2022) 10:e13038. doi: 10.7717/peerj.13038

10. Before the mass death of swans, sewage water was discharged into the Karakol. What will happen next? Radio Azattyk(2024). Available online at: https://rus.azattyq.org/a/Kazakhstan-mangystau-region-lake-of-karakol-and-mass-death-of-swans/32811734.html (Accessed February 9, 2024).

11. He Y, Wang J, Chi L, Dong Y, Chen H, Meng X, et al. Combination adjuvants enhance recombinant H5 hemagglutinin vaccine protection against high-dose viral challenge in chickens. *Vaccines (Basel)*. (2024) 12:1448. doi: 10.3390/vaccines12121448

12. Bugybayeva D, Dumkliang E, Patil V, Yadagiri G, Suresh R, Singh M, et al. Evaluation of efficacy of surface coated versus encapsulated influenza antigens in mannose-chitosan nanoparticle-based intranasal vaccine in swine. *Vaccines (Basel)*. (2024) 12:647. doi: 10.3390/vaccines12060647

13. Avian influenza prevention: how many birds are vaccinated in Kazakhstan (2020). Available online at: https://forbes.kz/news/newsid_239318 (Accessed December 8, 2020).

14. Swayne DE. Impact of vaccines and vaccination on global control of avian influenza. *Avian Dis*. (2012) 56:818–28. doi: 10.1637/10183-041012-Review.1

15. Wong SS, Webby RJ. Traditional and new influenza vaccines. *Clin Microbiol Rev*. (2013) 26:476–92. doi: 10.1128/CMR.00097-12

16. Kong D, He Y, Wang J, Chi L, Ao X, Ye H, et al. A single immunization with H5N1 virus-like particle vaccine protects chickens against divergent H5N1 influenza viruses and vaccine efficacy is determined by adjuvant and dosage. *Emerg Microbes Infect*. (2024) 13:2287682. doi: 10.1080/22221751.2023.2287682

17. Gao F, Liu X, Dang Y, Duan P, Xu W, Zhang X, et al. AddaVax-adjuvanted H5N8 inactivated vaccine induces robust humoral immune response against different clades of H5 viruses. *Vaccines (Basel)*. (2022) 10:1683. doi: 10.3390/vaccines10101683

18. Panickan S, Bhatia S, Bhat S, Bhandari N, Pateriya AK, Kalaiyarasu S, et al. Reverse genetics based H5N2 vaccine provides clinical protection against H5N1, H5N8 and H9N2 avian influenza infection in chickens. *Vaccine*. (2022) 40:6998–7008. doi: 10.1016/j.vaccine.2022.10.018

19. World Health Organization. Summary of status of development and availability of A(H5) non–A(H5N1) candidate vaccine viruses and potency testing reagents (2024). Available online at: https://cdn.who.int/media/docs/default-source/influenza/cvvs/cvv-zoonotic—southern-hemisphere-2024/summary_a_h5_cvv_sh24.pdf?sfvrsn=a3dc6046_4&download=true (Accessed January 25, 2024).

20. Tabynov K, Orynbassar M, Yelchibayeva L, Turebekov N, Yerubayev T, Matikhan N, et al. A spike protein-based subunit SARS-coV-2 vaccine for pets:

safety, immunogenicity, and protective efficacy in juvenile cats. *Front Vet Sci*. (2022) 9:815978. doi: 10.3389/fvets.2022.815978

21. Reed LJ, Muench H. A simple method for estimating fifty percent endpoints. *Am J Hyg*. (1938) 27:493–7.

22. Tabynov K, Solomadin M, Turebekov N, Babayeva M, Fomin G, Yadagiri G, et al. Author Correction: An intranasal vaccine comprising SARS–CoV–2 spike receptor–binding domain protein entrapped in mannose–conjugated chitosan nanoparticle provides protection in hamsters. *Sci Rep*. (2023) 13:12485. doi: 10.1038/s41598-023-39818-8

23. Tabynov K, Babayeva M, Nurpeisov T, Fomin G, Nurpeisov T, Saltabayeva U, et al. Evaluation of a novel adjuvanted vaccine for ultrashort regimen therapy of artemisia pollen-induced allergic bronchial asthma in a mouse model. *Front Immunol*. (2022) 13:828690. doi: 10.3389/fimmu.2022.828690

24. Kaufmann L, Syedbasha M, Vogt D, Hollenstein Y, Hartmann J, Linnik JE, et al. An optimized hemagglutination inhibition (HI) assay to quantify influenza-specific antibody titers. *J Vis Exp*. (2017) 130):55833. doi: 10.3791/55833

25. Webster R, Cox N, Stöhr K. WHO animal influenza manual. *WHO/CDS/CSR/NCS*. (2002) 2002:5:1–99.

26. Tabynov K, Turebekov N, Babayeva M, Fomin G, Yerubayev T, Yespolov T, et al. An adjuvanted subunit SARS-CoV-2 spike protein vaccine provides protection against Covid-19 infection and transmission. *NPJ Vaccines*. (2022) 7:24. doi: 10.1038/s41541-022-00450-8

27. Squibb RL. Body temperatures of immature White Leghorn cockerels infected with Newcastle disease virus. *Avian Dis*. (1961) 5:292–6. doi: 10.2307/1587638

28. Vreman S, Bergervoet SA, Zwart R, Stockhofe-Zurwieden N, Beerens N. Tissue tropism and pathology of highly pathogenic avian influenza H5N6 virus in chickens and Pekin ducks. *Res Vet Sci*. (2022) :146:1–4. doi: 10.1016/j.rvsc.2022.03.010

29. Gibson-Corley KN, Olivier AK, Meyerholz DK. Principles for valid histopathologic scoring in research. *Vet Pathol*. (2013) 50:1007–15. doi: 10.1177/0300985813485099

30. Bhatia S, Khandia R, Sood R, Bhat S, Siddiqui A, Jahagirdhar G, et al. Reverse genetics based rgH5N2 vaccine provides protection against high dose challenge of H5N1 avian influenza virus in chicken. *Microb Pathog*. (2016) 97:172–7. doi: 10.1016/j.micpath.2016.06.011

31. Reuters. Healthcare & Pharmaceuticals Public Health. Bird flu vaccination policies by country(2023). Available online at: https://www.reuters.com/business/healthcare-pharmaceuticals/bird-flu-vaccination-policies-by-country-2023-02-17/ (Accessed February 17, 2023).

32. Suarez DL. Overview of avian influenza DIVA test strategies. *Biologicals*. (2005) 33:221–6. doi: 10.1016/j.biologicals.2005.08.003

33. Martinez-Sobrido L, DeDiego ML, Nogales A. Reverse genetics approaches for the development of new vaccines against influenza A virus infections. *Curr Opin Virol*. (2020) 44:26–34. doi: 10.1016/j.coviro.2020.06.001

34. Kandeil A, Sabir JSM, Abdelaal A, Mattar EH, El-Taweel AN, Sabir MJ, et al. Efficacy of commercial vaccines against newly emerging avian influenza H5N8 virus in Egypt. *Sci Rep*. (2018) 8:9697. doi: 10.1038/s41598-018-28057-x

35. Kuruppuarachchi KAPP, Jang Y, Seo SH. Evaluation of efficacy of oil adjuvanted H5N6 inactivated vaccine against highly pathogenic H5N6 and H5N1 influenza viruses infected chickens. *Front Biosci (Landmark Ed)*. (2022) 27:268. doi: 10.31083/j.fbl2709268

36. Lamm ME. Interaction of antigens and antibodies at mucosal surfaces. *Annu Rev Microbiol*. (1997) 51:311–40. doi: 10.1146/annurev.micro.51.1.311

37. Hwang SD, Kim HS, Cho SW, Seo SH. Single dose of oil-adjuvanted inactivated vaccine protects chickens from lethal infections of highly pathogenic H5N1 influenza virus. *Vaccine*. (2011) 29:2178–86. doi: 10.1016/j.vaccine.2010.12.013

38. Honda-Okubo Y, Bart Tarbet E, Hurst BL, Petrovsky N. An Advax-CpG adjuvanted recombinant H5 hemagglutinin vaccine protects mice against lethal influenza infection. *Vaccine*. (2023) 41:5730–41. doi: 10.1016/j.vaccine.2023.08.009

frontiers | Frontiers in Immunology

TYPE Original Research
PUBLISHED 27 March 2025
DOI 10.3389/fimmu.2025.1557426

OPEN ACCESS

EDITED BY
Sonia Jangra,
The Rockefeller University, United States

REVIEWED BY
Sivaram Gunisetty,
Emory University, United States
Emily Coates,
National Institute of Allergy and Infectious Diseases (NIH), United States

*CORRESPONDENCE
Julie Decock
jdecock@hbku.edu.qa

†PRESENT ADDRESS
Adviti Naik,
Biological Sciences, Carnegie Mellon University- Qatar, Doha, Qatar

‡These authors share first authorship

RECEIVED 08 January 2025
ACCEPTED 11 March 2025
PUBLISHED 27 March 2025

CITATION
Thomas R, Zaqout A, Meqbel B, Jafar U, Vaikath NN, Aldushain A, Naik A, Shaath H, Al-Akl NS, Adam A, Moussa HYA, Shin KC, Taha RZ, Abukhattab M, Almaslamani MA, Alajez NM, Arredouani A, Park Y, Abdulla SA, El-Agnaf OMA, Omrani AS and Decock J (2025) Longitudinal cellular and humoral immune responses following COVID-19 BNT162b2-mRNA-based booster vaccination of craft and manual workers in Qatar. *Front. Immunol.* 16:1557426. doi: 10.3389/fimmu.2025.1557426

Longitudinal cellular and humoral immune responses following COVID-19 BNT162b2-mRNA-based booster vaccination of craft and manual workers in Qatar

Remy Thomas[1‡], Ahmed Zaqout[2‡], Bakhita Meqbel[1‡], Umar Jafar[1,3], Nishant N. Vaikath[4], Abdullah Aldushain[2], Adviti Naik[1†], Hibah Shaath[1], Neyla S. Al-Akl[5], Abdi Adam[6], Houda Y. A. Moussa[4], Kyung C. Shin[4], Rowaida Z. Taha[4], Mohammed Abukhattab[2], Muna A. Almaslamani[2], Nehad M. Alajez[1,3], Abdelilah Arredouani[3,5], Yongsoo Park[3,4], Sara A. Abdulla[3,4], Omar M. A. El-Agnaf[3,4], Ali S. Omrani[2,7] and Julie Decock[1,3*]

[1]Translational Oncology Research Center, Qatar Biomedical Research Institute (QBRI), Hamad Bin Khalifa University (HBKU), Qatar Foundation (QF), Doha, Qatar, [2]Communicable Disease Center, Hamad Medical Corporation (HMC), Doha, Qatar, [3]College of Health and Life Sciences (CHLS), Hamad Bin Khalifa University (HBKU), Qatar Foundation (QF), Doha, Qatar, [4]Neurological Disorders Research Center, Qatar Biomedical Research Institute (QBRI), Hamad Bin Khalifa University (HBKU), Qatar Foundation (QF), Doha, Qatar, [5]Diabetes Research Center, Qatar Biomedical Research Institute (QBRI), Hamad Bin Khalifa University (HBKU), Qatar Foundation (QF), Doha, Qatar, [6]Clinical Core, Qatar Biomedical Research Institute (QBRI), Hamad Bin Khalifa University (HBKU), Qatar Foundation (QF), Doha, Qatar, [7]College of Medicine, Qatar University, Doha, Qatar

Background: In March 2020, the rapid spread of SARS-CoV-2 prompted global vaccination campaigns to mitigate COVID-19 disease severity and mortality. The 2-dose BNT162b2-mRNA vaccine effectively reduced infection and mortality rates, however, waning vaccine effectiveness necessitated the introduction of a third vaccine dose or booster.

Aim: To assess the magnitude and longevity of booster-induced immunity, we conducted a longitudinal study of SARS-CoV-2 specific cellular and humoral immune responses among Qatar's vulnerable craft and manual worker community. We also investigated the impact of prior naturally acquired immunity on booster vaccination efficacy.

Methods: Seventy healthy participants were enrolled in the study, of whom half had prior SARS-CoV-2 infection. Blood samples were collected before and after booster vaccination to evaluate immune responses through SARS-CoV-2 specific ELISpots, IgG ELISA, neutralization assays, and flow cytometric immunophenotyping.

Results: T cell analysis revealed increased Th1 cytokine responses, marked by enhanced IFN-γ release, in recently infected participants, which was further

enhanced by booster vaccination for up to 6-months. Furthermore, booster vaccination stimulated cytotoxic responses in infection-naïve participants, characterized by granzyme B production. Both natural SARS-CoV-2 infection and booster vaccination induced robust and durable SARS-CoV-2 specific humoral immune responses, with high neutralizing antibody levels. Prior natural infection was also linked to an increased number of class-switched B cells prior to booster vaccination.

Conclusions: These findings underscore the importance of booster vaccination in enhancing anti-viral immunity across both infection-naïve and previously infected individuals, enhancing distinct arms of the anti-viral immune response and prolonging naturally acquired immunity.

KEYWORDS

SARS-CoV-2, BNT162b2, booster, immune response, immunological memory

Introduction

The emergence of severe acute respiratory syndrome coronavirus 2 (SARS-CoV-2) in 2019 led to a global pandemic. SARS-CoV-2, believed to have originated from bats in Wuhan, China, rapidly spread to humans through zoonotic and human-to-human transmission (1). The virus causes Coronavirus Disease 19 (COVID-19), a highly infectious disease with a range of clinical manifestations from asymptomatic infections to severe respiratory failures. Among infected individuals, 10-15% required hospitalization, with 15-20% of those needing intensive care (2, 3). Similar to other coronaviruses, SARS-CoV-2 is a single-stranded, positive-sense RNA that encodes structural proteins that are essential for viral entry, replication and assembly including the spike (S), envelope (E), membrane (M) and nucleocapsid (N) proteins (4). The spike protein in particular plays a critical role in the virus' pathogenesis by binding the angiotensin-converting enzyme 2 (ACE2) receptor on host cells, facilitating viral entry (5). Mutations in the spike protein can greatly impact virus transmissibility, as observed with the Alpha, Delta and Omicron variants of concern (VOCs) (6). As SARS-CoV-2 evolved, distinct genetic variants emerged, displaying altered transmission rates, disease severity and ability to escape immunosurveillance. Moreover, the duration of infectiousness evolved, with individuals infected with Omicron exhibiting an earlier onset of infectiousness compared to those infected with the Delta variant, accelerating viral transmission (7).

To reduce the global health burden of COVID-19, public health measures and global vaccination campaigns were rapidly implemented. The World Health Organization (WHO) approved 21 vaccines, including vaccines based on inactivated viruses, protein, recombinant adenovirus, DNA, and messenger RNA (mRNA) (8). Among all vaccines, the Pfizer/BioNTech (BNT162b2) and Moderna (mRNA-1273) mRNA vaccines were widely administered. While a single dose provided only limited protection (9–11), a two-dose regimen significantly improved vaccine effectiveness (VE), with Pfizer achieving > 90% effectiveness shortly after the second dose and Moderna over 80% (12–16). Nevertheless, a meta-analysis of 18 studies revealed a decline in pooled VE from 83% at one month post-vaccination to 22% at five months, with a sharp drop after 100 days following two-dose vaccination with BNT162b2 (Pfizer-BioNTech), mRNA-1273 (Moderna) and Ad26.COV2.S (Janssen) (17, 18). A large study of 10.6M individuals further demonstrated a decline in BNT162b2 VE from 94.5% at two months after the first dose to 66.6% at seven months, while mRNA-1273 VE declined from 95.9% to 80.3% over the same timespan (18). It has been postulated that the waning protection of the two-dose vaccination regimen may be attributable to both a decline in immunity and the emergence of VOCs. For instance, in a period during which the Alpha VOC was the most prevalent the two-dose VE reached 85.7% for BNT162b2 and 93.7% for mRNA-1273, whereas in a period dominated by the Delta VOC the BNT162b2 and mRNA-1273 VE values declined to 63.5% and 75.6% (19). Notably, one study investigating the effect of pre-vaccination natural immunity on two-dose BNT162b2 and mRNA-1273 VE reported that vaccine-mediated protection declines independently of prior natural infection (20). Without bias correction, they found a pooled VE of 91.3% at 14 days post second-dose which declined to 50.8% at 7 months post vaccination. Similarly, bias-corrected VE at 7 months post-vaccination reached 53.2%. In line with declining vaccine effectiveness, two doses of the BNT162b2 vaccine were shown to elicit humoral and adaptive immune responses for up to five months after the first dose (21). Analysis of six healthy, adult vaccine recipients showed an early increase in anti-spike antibody responses after the first dose (day 20), followed by a second increase after the second dose (day 34) and subsequent decline at 150 days. Anti S1-specific T cell responses mirrored this pattern, with the second dose enhancing T cell responses in all six recipients, four of whom exhibited detectable

10.3389/fimmu.2025.1557426

responses up to five months after the first dose. Thus, the waning of vaccine-induced immunity and emergence of VOCs prompted the need for booster vaccination to restore protection. In Qatar, BNT162b2 VE sharply dropped to below 40% at 181-270 days following the second dose, whereas administration of a third dose or booster increased VE to approximately 80% (22). Similarly, three-dose BNT162b2 and mRNA-1273 VE values at 4-11 months post second dose were comparable to two-dose VE values at 1 to 2 months post second dose in a predominantly white, non-Hispanic population (23). Notably, anti-spike antibody levels have been found to peak at 90 days after the first mRNA vaccine dose (BNT162b2, mRNA-1273), drop by day 180, and increase 2.5-fold compared to day 90 following vaccination with the third dose before gradually declining from day 251 to day 535 (24). Overall, administering a third dose of either BNT162b2 or mRNA-1273 enhanced antibody level persistence with a slower decline compared to two-dose regimens. Booster vaccination with BNT162b2 also enhanced antibody avidity, with higher levels at 6 months post-third dose compared to mRNA-1273 (25).

In this study, we examined the effects of a third dose of the BNT162b2 vaccine on cellular and humoral immune responses in craft and manual workers (CMWs) in Qatar. Previous studies highlighted that this community, comprising approximately 80% of Qatar's population, experiences higher infection rates due to overcrowded living and working conditions and educational barriers (26–28). Given their higher vulnerability, we sought to investigate how a third vaccine dose impacts immune responses in this population and whether prior natural Sars-CoV-2 infection influences vaccine-induced immunity. Using diverse approaches, we observed that administering a third dose of the BNT162b2 vaccine effectively induced both cellular and humoral immune responses in our CMW population, while also enhancing pre-existing immunity in previously infected participants.

Materials and methods

Study population

A total of 70 healthy adults from the CMW community in Qatar were included in the study. All participants were enrolled in our study when they presented at the Communicable Disease Center, Qatar between May 25, 2022 and July 4, 2022 for their third BNT162b2 vaccine dose as part of the national vaccination program. We only included individuals who received two prior doses of the BNT162b2 mRNA vaccine, as verified through Qatar's centralized electronic medical system. Demographic data and information on prior PCR-confirmed Sars-CoV-2 infection (Feb 1, 2020 onwards) were also extracted from the centralized electronic medical records (Table 1). As part of the Qatar national testing framework, all suspected Sars-CoV-2 infections were tested by PCR and automatically updated in the electronic medical records. None of the individuals tested positive for SARS-CoV-2 infection within 4 weeks prior to the scheduled booster dose, were immunocompromised due to underlying disease or medical treatment, or were pregnant.

Sample collection and processing

Peripheral blood was collected in 10ml EDTA blood tubes at three timepoints; at the time of the third dose (timepoint 1), 3-months after the third dose (timepoint 2) and 6-months post third dose (timepoint 3). Serum was collected after centrifugation at 3000 rpm for 10 minutes and stored at -80°C. Peripheral blood mononuclear cells (PBMCs) were isolated from freshly collected blood samples using SepMate™ density gradient centrifugation (85460; Stem Cell Technologies) according to the manufacturer's guidelines. Next, isolated PBMCs were resuspended in freezing media (50% FBS, 40% serum-free Roswell Park Memorial Institute 1640 medium (RPMI), 10% Dimethyl sulfoxide) and stored in liquid nitrogen until further use.

TABLE 1 Study cohort demographics.

	n	(%)
Age		
18-49	64	(91)
50+	6	(9)
sex		
female	6	(9)
male	64	(91)
race		
Asian	65	(93)
White	4	(6)
African	1	(1)
nationality		
Bangladesh	9	(13)
Egypt	2	(3)
India	48	(69)
Lebanon	1	(1)
Nigeria	1	(1)
Pakistan	1	(1)
Philippines	3	(4)
Sri Lanka	4	(6)
United Kingdom	1	(1)
co-morbidities		
diabetes mellitus	1	(1)
high blood pressure	3	(4)
prior SARS-CoV-2 infection		
infection-naïve	35	(50)
earlier infection	18	(26)
recent infection	17	(24)

Enzyme-linked immunosorbent spot

We used two distinct ELISpot assays to quantify the number of immune cells that secrete either IFN-γ (3420-4AST-P1-1; Mabtech, Nacka Strand, Sweden) or granzyme B (3486n-4APW-P1-1; Mabtech, Nacka Strand, Sweden) in response to a pool of SARS-CoV-2 peptides. Immune cell reactivity was measured against 166 peptides derived from the S1 domain of the spike protein (amino acids 13-685, divided into two peptide pools S1 and S2) and 47 synthetic peptides, covering the spike, nucleoprotein, membrane protein, ORF3a and ORF7a (SNMO peptide pool). ELISpot assays were conducted according to the manufacturer's guidelines using 2.5x10e5 PBMCs/well in duplicate with a final concentration of 2 ug/ml of each peptide. In addition, wells with PBMCs alone (unstimulated) were used as negative control, and PBMCs treated with an anti-human anti-CD3 antibody (mAb CD3-2, #3420-4HST-10, Mabtech, Nacka Strand, Sweden) overnight served as positive control. After 48 hours of incubation with the peptides at 37°C, PBMCs were removed, the plates were washed, and spots were developed. For each individual, the number of spot forming units (SFUs) obtained for the negative controls were subtracted from the sample values at the respective timepoints. To enable detection of secreted IFN-γ, plates were incubated with 7-B6-1-biotin detection antibody for 2 hours, followed by 1 hour incubation with Streptavidin-HRP and addition of TMB substrate. Detection of granzyme B SFUs was obtained using the MT8610-biotin detection antibody, Streptavidin-ALP and BCIP/NBT-Plus substrate according to the manufacturer's instructions. In addition to the IFN-γ and granzyme B ELISpot assays, we also performed an IgG ELISpot assay to enumerate B cells that are secreting human IgG in response to the Sars-CoV-2 receptor binding domain (RBD) (3850-4HPW-R1-1; Mabtech, Nacka Strand, Sweden). Moreover, to gain insight into the magnitude and longevity of the humoral SARS-CoV-2 immune response of vaccinated individuals, PBMCs were pre-stimulated with R848 (1 µg/ml) and recombinant human IL-2 (10 ng/ml) for 3 days to promote the differentiation of memory B cells into antibody-secreting cells, enabling their quantification through measurement of IgG secretion. Next, pre-stimulated and unstimulated cells were seeded in duplicate at 2.5x10e5 cells/well in the ELISpot plate which was pre-coated with anti-human IgG monoclonal antibodies. After 48 hours at 37°C, RBD-specific IgG spots were detected using a WASP-tagged RBD protein, followed by anti-WASP-HRP and TMB substrate. Finally, for each ELISpot assay the number of SFUs were determined using the AID iSpot ELISpot reader (Autoimmun Diagnostika GmbH, Strasburg, Germany). Representative images are depicted in Supplementary Figure S1-S3.

SARS-CoV-2 IgG/IgM enzyme-linked immunosorbent assay

In addition to the IgG ELISpot assay, secretion of SARS-CoV-2 specific IgG/IgM antibodies was determined using an in-house developed ELISA. In short, 96-well plates (Nunc, Maxisorp) were coated overnight at 4°C with 1µg/ml SARS-Cov-2 spike protein or Nucleoprotein in 0.2M $NaHCO_3$ (pH 9.6). Plates were washed three times with PBST (0.05% Tween-20) and blocked for 1 hour at room temperature using PBST-2.25% gelatin. Next, diluted serum samples (1:800) were added to washed plates for 2 hours (room temperature, 100 rpm), followed by incubation with either goat anti-human IgG-HRP or goat anti-human IgM-HRP for 1 hour at room temperature. Finally, TMB substrate was added for 20min, and absorbance values were measured at 450nm using the EnVision® Multilabel Plate Reader (PerkinElmer).

SARS-CoV-2 neutralizing antibody assay

To assess the presence of SARS-CoV-2 antibodies with neutralizing abilities, we utilized an in-house neutralization antibody (NAb) assay. Briefly, recombinant hACE2 protein (1µg/ml in 0.2 M $NaHCO_3$, pH 9.6) was coated on 96-well ELISA plates (Maxisorp, Nunc) at 4°C overnight. Plates were washed three times with PBST (0.05% Tween-20) and blocked with 2.25% gelatin in PBST for 1 hour at room temperature. Serum samples were diluted (1:10) and preincubated with 100 ng/ml RBDmFc (Genscript) in blocking buffer for 1 hour at room temperature, after which they were added to the pre-coated ELISA plate for 1 hour. In parallel, anti-SARS nanobody NbS72-Biv (500 ng/ml) was preincubated with RBDmFc (Genscript) to serve as neutralization control. Next, wells were incubated with goat anti-mouse Fc-HRP (1:10,000) for 1 hour, followed by TMB substrate for 20min. Absorbance values were measured at 450nm using the EnVision® Multilabel Plate Reader (PerkinElmer).

Immune cell phenotyping by flow cytometry

We characterized the presence of T and B cell subpopulations using DuraClone IM T cells (Beckman Coulter; #B53328) and DuraClone IM B cell tubes (#B53318, Beckman Coulter) respectively. A total of 3.0x10e5 PBMCs were resuspended in stain buffer (#554656, BD Pharmingen™) and added to the DuraClone tubes, which were vortexed for 5 seconds and incubated for 15 min in the dark at room temperature. Next, the cells were washed in DPBS (#14190-144, Gibco) and resuspended in PBS prior to analysis on the LSRFortessaTM X-20 flow cytometer (BD Biosciences) using FACS Diva Software (BD Biosciences). For each sample, 30,000 events were recorded, and further analysis was performed using FlowJo™ Software (BD Biosciences, version 10.8). Representative gating strategies are provided in Supplementary Figure S4 and Supplementary Figure S5.

Statistical analysis

Statistical analyses were performed using GraphPad PRISM V9.5.1 (GraphPad Software, CA, USA). Data normality was assessed by Shapiro-Wilk test and differences between groups

were analyzed using the unpaired t-test or one-way ANOVA test with Tukey correction. A p value ≤ 0.05 was considered significant.

Results

Natural infection and booster vaccination differentially stimulate SARS-Cov-2 specific cellular immune responses

A total of 70 participants were enrolled in the study. For 45 study participants (group 1), we collected blood samples at all three timepoints; immediately prior to the third vaccine dose (Day-0, D0), three months post-booster (Month-3, M3) and six months post-booster (Month-6, M6). Among these 45 participants, 27 had a documented SARS-CoV-2 infection before their booster dose, as verified through their electronic medical records, while 18 had no prior PCR-confirmed infection (Figure 1). These blood samples were used to assess cellular and humoral immune responses through ELISpot and flow cytometry analyses. In addition to the 45 participants, we included 25 participants from whom less than three blood samples were obtained (group 2) to evaluate anti-SARS-CoV-2 specific antibody levels, including the level of antibodies with neutralizing activity (Figure 1).

Previously infected participants exhibited increased anti-spike T cell responses (S1 and S2 peptide pools) at three- and six-months post-booster (M3, M6) compared to infection-naïve participants, as measured by IFN-γ secretion of peripheral blood lymphocytes following incubation with SARS-CoV-2 peptides (Figure 2A). This is likely the combined result of an, albeit non-significant, elevated baseline (D0) response and the boosting effect from the third vaccine dose. No significant differences in anti-SNMO IFN-γ responses were observed in relation to previous infection or booster vaccination. Next, we stratified the previously infected participants based on the timing of infection: earlier infection (infection before second dose), and recent infection (infection between second and third dose). Upon stratification, we observed higher pre-booster anti-spike IFN-γ responses (D0 - S1 and S2) in individuals with a recent infection as compared to infection-naïve individuals or those with earlier infections (Figure 2B). However, booster vaccination did not significantly increase anti-spike responses within each participant group (infection-naïve, earlier infection, recent infection). In addition to elevated pre-booster anti-spike responses, recently infected participants exhibited higher baseline IFN-γ responses against the SNMO peptide pool, although these responses declined post-booster to similar levels as observed in infection-naïve and earlier infected participants. This suggests that more recent infections induce stronger anti-spike and anti-SNMO T cell responses, which naturally taper off with time and are not further enhanced or sustained by booster vaccination.

To assess the effect of booster vaccination and pre-booster Sars-CoV-2 infection on cytotoxic cellular responses, we measured granzyme B release by peripheral blood lymphocytes in response to SARS-CoV-2 peptide pools. Pre-booster (D0), no significant

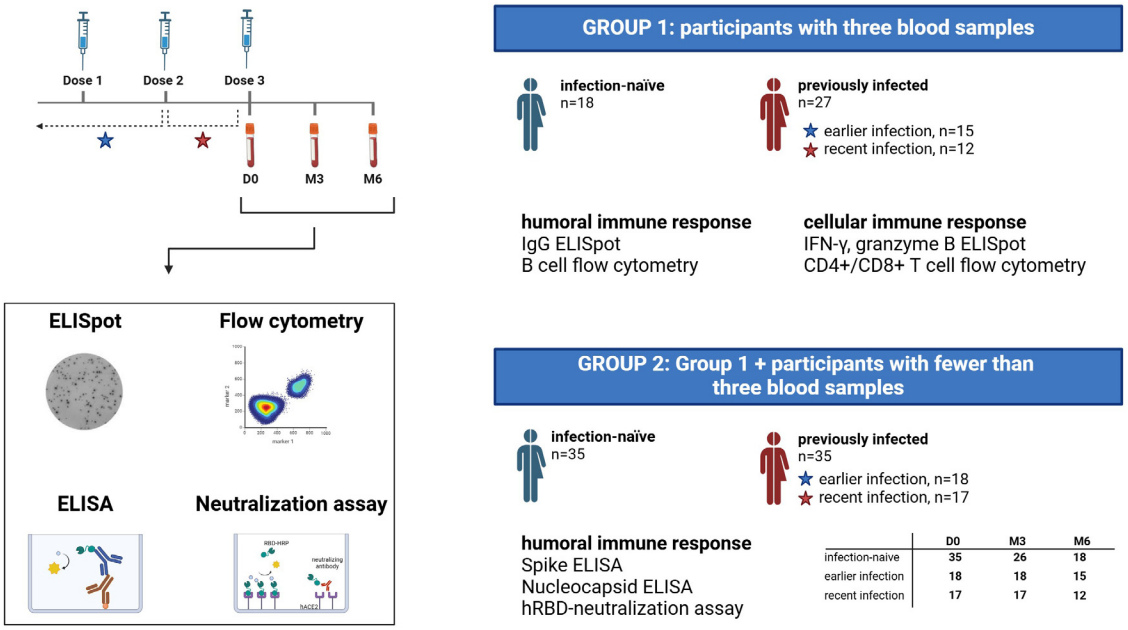

FIGURE 1
Study design diagram. Flowchart depicting the study cohort, blood sample collection and assays performed. A total of 70 participants were enrolled in the study, of whom 45 participants had blood samples collected at three timepoints (group 1), while the remaining 25 participants had fewer than 3 blood samples available (constituting group 2 together with participants from group 1). PCR-confirmed Sars-CoV-2 infection status was extracted from electronic medical records, and previously infected participants were subdivided into two groups based on the time of infection; earlier infection and recent infection. D0, Day 0; M3, 3-month post-booster; M6, 6-months post-booster.

differences in the number of granzyme B-producing cells were observed between infection-naïve and previously infected participants (Figure 3A, B). Following booster vaccination, we found a borderline significant (p=0.06) increase in anti-spike granzyme B responses, in particular anti-S1, in infection-naïve participants (S1 – M3 versus M6) (Figure 3A). Furthermore, booster vaccination enhanced late anti-SNMO responses in previously infected participants (SNMO – M6 versus D0 and M3). No differences were found when previously infected participants were stratified by the time of infection, except for a 3-months post-booster significant increase in SNMO-responses in earlier infected participants compared to infection-naïve participants (SNMO – M3) (Figure 3B). These findings suggest that natural SARS-CoV-2 infection primarily primes memory Th1 cytokine responses, characterized by IFN-γ release, whereas booster vaccination induces granzyme B-mediated cytotoxic responses, which primarily involve CD8+ T cell and NK cell activity, particularly in infection-naïve participants.

Natural infection induces robust SARS-CoV-2 specific humoral responses with neutralizing abilities, which can be enhanced by booster vaccination

Based on our observations that SARS-CoV-2 natural infection and booster vaccination likely prime different components of the antiviral cellular immune response – specifically Th1 cytokine and

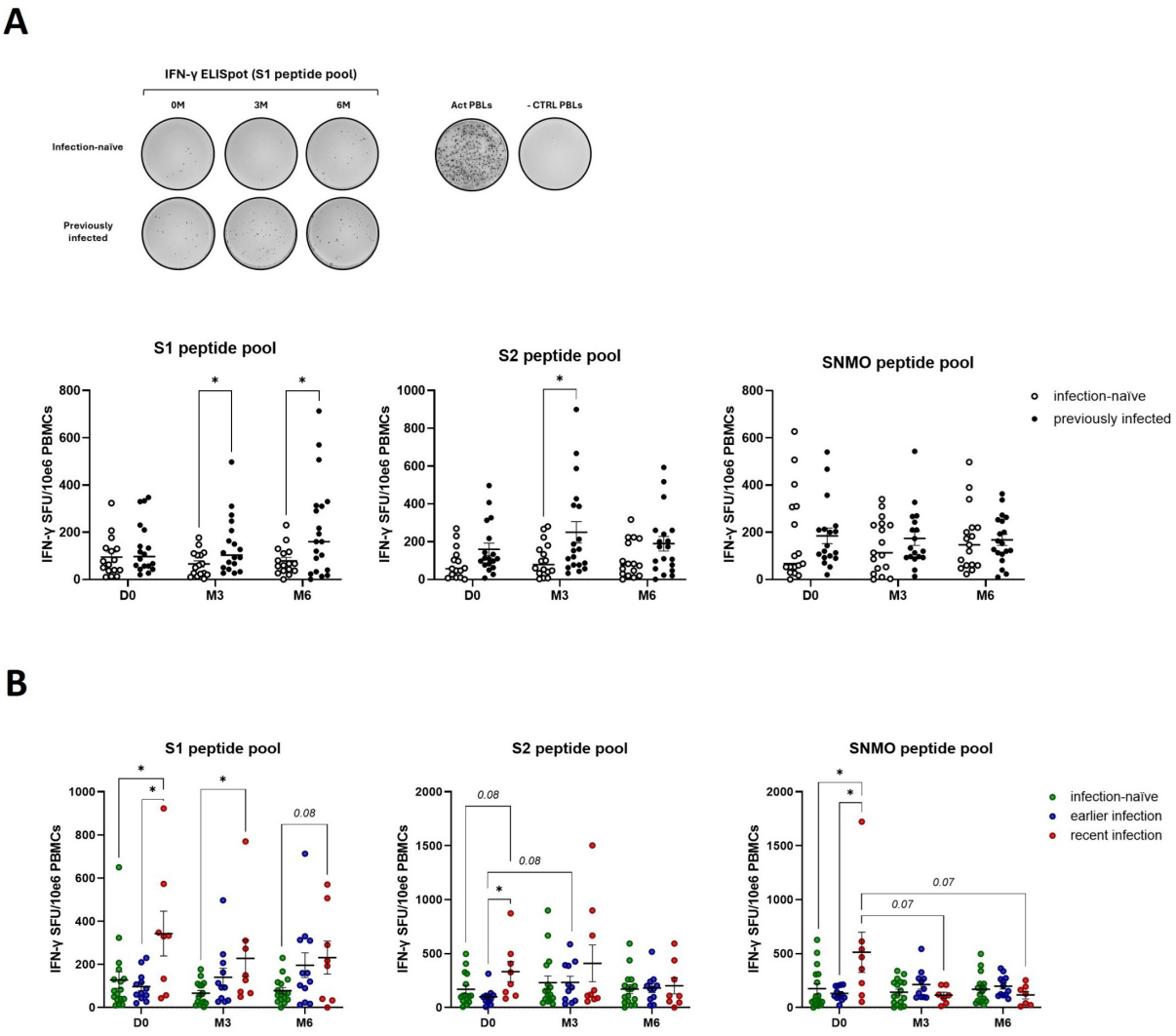

FIGURE 2
Natural exposure to SARS-CoV-2 enhances IFN-γ cellular immune responses. **(A)** Quantification of anti-spike and anti-SNMO specific IFN-γ responses in infection-naïve and previously infected participants before and after booster vaccination, as determined by IFN-γ ELISpot analysis. Representative ELISpot image for anti-S1 responses in infection-naïve and previously infected participants, with CD3-activated PBLs and unstimulated PBLs (-CTRL PBLs) as positive and negative control respectively. **(B)** Quantification of anti-spike and anti-SNMO specific IFN-γ responses in infection-naïve and previously infected participants, stratified by the time of infection. Scatter dot plots represent mean with standard error of mean (± SEM). Statistical analysis performed using unpaired Student's t-test or one-way ANOVA with Tukey correction. *p ≤ 0.05. D0, Day 0; M3, 3-month post-booster; M6, 6-months post-booster; PBLs, peripheral blood lymphocytes; Act PBLs, activated PBLs.

granzyme B-mediated cytotoxic responses - we next investigated their impact on SARS-CoV-2 specific humoral immune responses. Prior to booster vaccination, previously infected participants displayed a higher number of IgG-secreting memory B cells (Figure 4A), particularly those with recent infections (Figure 4B). Furthermore, booster vaccination induced a transient increase in IgG-positive memory B cells in infection-naïve participants, with a peak at 3-months before declining at 6-months, while in participants with earlier infections the number of IgG-positive memory B cells peaked at 6-months (Figure 4A, B). This suggests that previously infected participants display a robust and durable humoral memory response which can be activated upon antigen re-exposure, while booster vaccination can further enhance B cell responses. To confirm these findings, we developed an ELISA to detect IgGs against the full-length spike protein. In accordance with our IgG ELISpot results, previously infected individuals, particularly those with recent infections, exhibited higher baseline IgG-secreting memory B cell responses (Figure 4C, D). Furthermore, we confirmed that booster vaccination enhanced those responses across all participants, including infection-naïve participants. Looking at anti-nucleocapsid IgG levels specifically, we observed a post-booster steady increase in previously infected participants, particularly those with recent infections (Figure 5A, B), further indicating that both natural infection and booster vaccination contribute to memory B cell responses. To further assess the functional abilities of these humoral responses, we used an in-house neutralization assay that demonstrated a post-booster increase in neutralizing antibody activity in infection-naïve and previously infected participants, particularly in recently infected participants, underscoring the role of booster vaccination in enhancing functional memory B cell responses (Figure 5C-D).

Phenotyping analysis of cellular and humoral immune responses

Given the presence of a cytotoxic cellular and neutralizing humoral immune response in participants with previous natural infection and following booster vaccination, we further investigated the immune cell phenotypes that may contribute to this

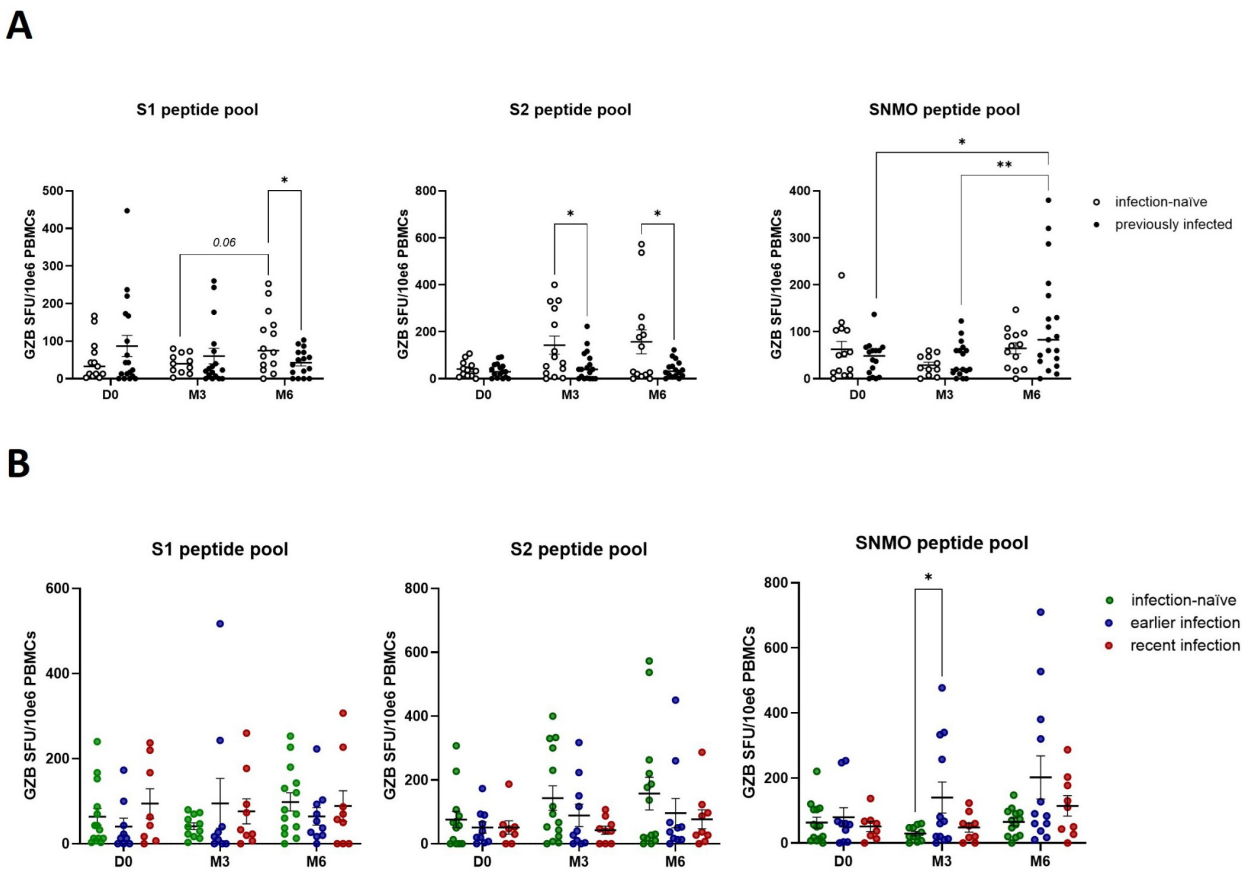

FIGURE 3
SARS-CoV-2 specific cytotoxic immune responses are enhanced by booster vaccination in the absence of prior natural infection. **(A)** Quantification of anti-spike and anti-SNMO specific granzyme B responses in infection-naïve and previously infected participants pre- and post-booster vaccination, as determined by granzyme B ELISpot analysis. **(B)** Quantification of anti-spike and anti-SNMO specific granzyme B responses in infection-naïve and previously infected participants, stratified by the time of infection. Scatter dot plots represent mean with standard error of mean (± SEM). Statistical analysis performed using unpaired Student's t-test or one-way ANOVA with Tukey correction. *p ≤ 0.05, **p ≤ 0.01. D0, Day 0; M3, 3-month post-booster; M6, 6-months post-booster.

immunological memory. We did not observe any differences in CD8+ T cell phenotypes that may complement the increased cytotoxic activity following natural infection and booster vaccination (Figure 6A). In line with our observations demonstrating the presence of an enhanced Th1 cytokine response in previously infected participants, we observed a decrease in the number of naïve CD4+ T cells (TN) following booster vaccination of recently infected participants (Figure 6B). In addition, they exhibited a trend (p=0.08) towards a higher number of CD4+ effector memory cells (TEM) at baseline compared to those with earlier infections. Of note, we did not find any significant changes in the number of CD4+ or CD8+ T cells expressing PD-1, suggesting that neither CD4+ nor CD8+ T cells exhibited an exhausted phenotype through PD-1/PD-L1 signaling (Figure 6C). Moreover, we observed a higher pre-booster number of class-switched B cells in recently infected individuals, which was sustained for up to 6 months post-booster (Figure 6D), underscoring the impact of natural infection in the development of a robust and durable memory B cell response which can be re-activated in response to booster vaccination.

Discussion

In March 2020, the WHO declared COVID-19 a pandemic, making it the first pandemic caused by a coronavirus. Given its high infection and mortality rate, global efforts focused on limiting the spread of the SARS-CoV-2 virus through implementation of nation-wide vaccination campaigns. According to data from Our World in Data (updated August 14th, 2024), 64.8% of the global population (approximately 5.18 billion people) has completed the initial COVID-19 vaccination protocol, which consists out of two doses for most vaccines (29). Following the success of the initial vaccine approaches, vaccine effectiveness waned over time, raising the question whether a booster dose could mitigate the decline in protection. Worldwide, 54% of individuals who completed the

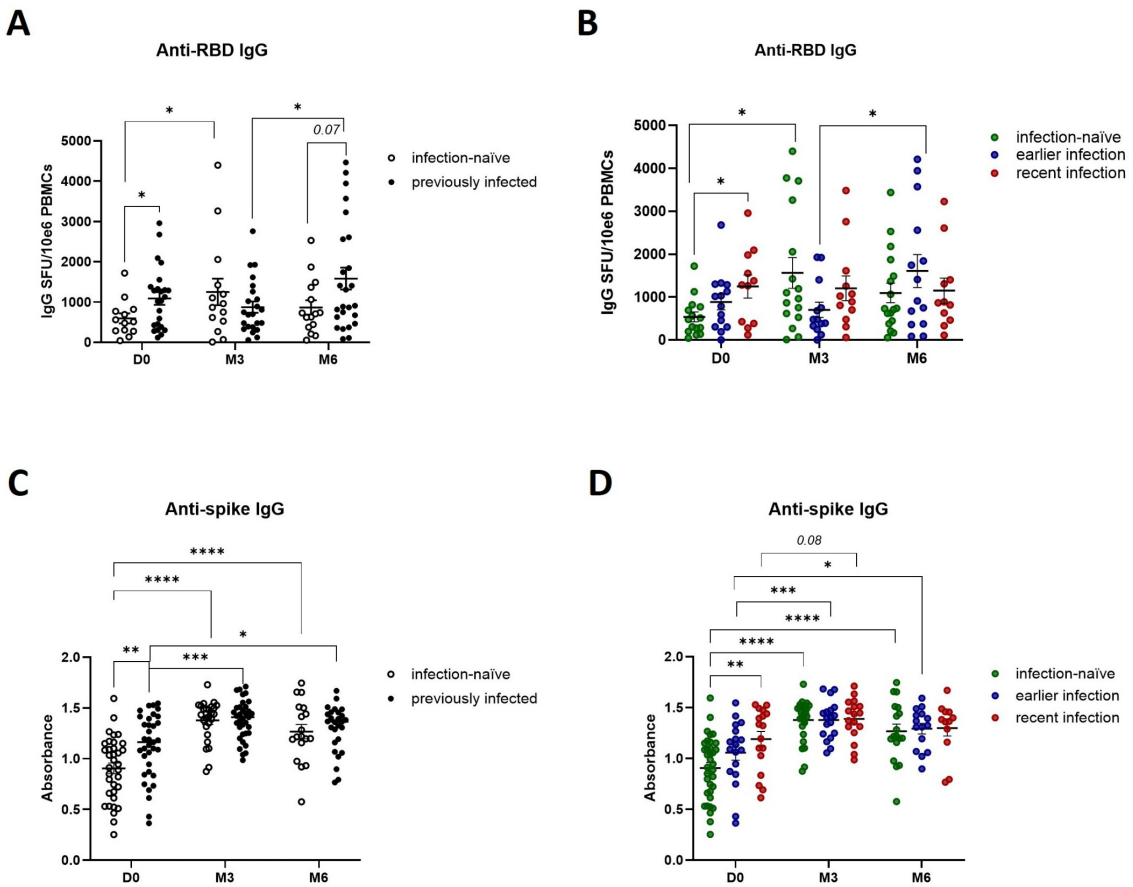

FIGURE 4
Effect of prior natural infection and booster vaccination on anti-SARS-CoV-2 RBD and spike IgG levels. **(A)** Quantification of anti-RBD IgG producing memory B cells in infection-naïve and previously infected participants before and after booster vaccination, as determined by anti-RBD IgG ELISpot analysis. **(B)** Quantification of anti-RBD IgG producing memory B cells in infection-naïve and previously infected participants, stratified by the time of infection. **(C)** Quantification of anti-spike IgG levels in infection-naive and previously infected participants, as determined by in-house ELISA of pre- and post-booster samples. **(D)** Quantification of anti-spike IgG levels in infection-naive and previously infected participants, stratified by time of infection. Scatter dot plots represent mean with standard error of mean (± SEM). Statistical analysis performed using unpaired Student's t-test or one-way ANOVA with Tukey correction. *p ≤ 0.05, **p ≤ 0.01, ***p ≤ 0.001, ****p ≤ 0.0001. D0, Day 0; M3, 3-month post-booster; M6, 6-months post-booster.

initial vaccination protocol (approximately 2.82 billion people) also received a booster dose (29). Here, we present a comprehensive longitudinal analysis of cellular and humoral immune responses against SARS-CoV-2 pre- and post-booster vaccination and provide insights into the role of prior natural infection in establishing immunological memory (Figure 7).

In our study, we demonstrate that previously infected participants exhibit robust humoral immune responses, characterized by higher pre-booster anti-spike antibody levels, including those of neutralizing antibodies. Those responses were further enhanced by booster vaccination. In addition, the recently infected participants showed an increased number of class-switched B cells before receiving the third vaccine dose, indicative of a durable B cell memory response. In infection-naïve participants, booster vaccination resulted in a sustained increase in the number of anti-spike neutralizing antibodies, reaching levels comparable to those observed in previously infected individuals. These findings are in line with a Danish study that reported prolonged anti-spike antibody persistence following vaccination with a third vaccine dose of BNT162b2 or mRNA-1273 (24). Furthermore, although previously infected participants showed a stronger baseline anti-spike humoral response than infection-naïve participants, we found similar responses following the booster vaccination, corroborating the previous study by Andrejko et al. that reported comparable vaccine effectiveness at 7-months post-vaccination, regardless of pre-vaccination naturally acquired immunity (20).

To further characterize the anti-viral immune response, we assessed any changes in the cellular immune response and found that different arms of the cellular immune response were preferentially induced by either naturally acquired or vaccination-induced immunity. Recent exposure to SARS-CoV-2 primarily induced a durable Th1 cytokine response with increased IFN-γ production, and a non-significant trend towards an increased number of CD4+ T effector memory cells. In contrast, booster vaccination more readily induced granzyme-B mediated cytotoxic immune responses, predominantly involving both T and NK cell activity, in infection-naïve participants for up to 6-months post-booster. We did not find any increase in the number of PD-1 positive CD4+ or CD8+ T cells, suggesting a lack of PD-1 mediated T cell exhaustion up to 6-months following the third vaccine dose. This raises the question whether cellular immune responses could be sustained for more than 6-months post-booster. Future studies should further assess the magnitude, longevity and exhaustion status of immunological memory beyond 6-months post-booster. Moreover, it would be of interest to study additional immune checkpoint markers and specific exhaustion markers (TOX, TCF1

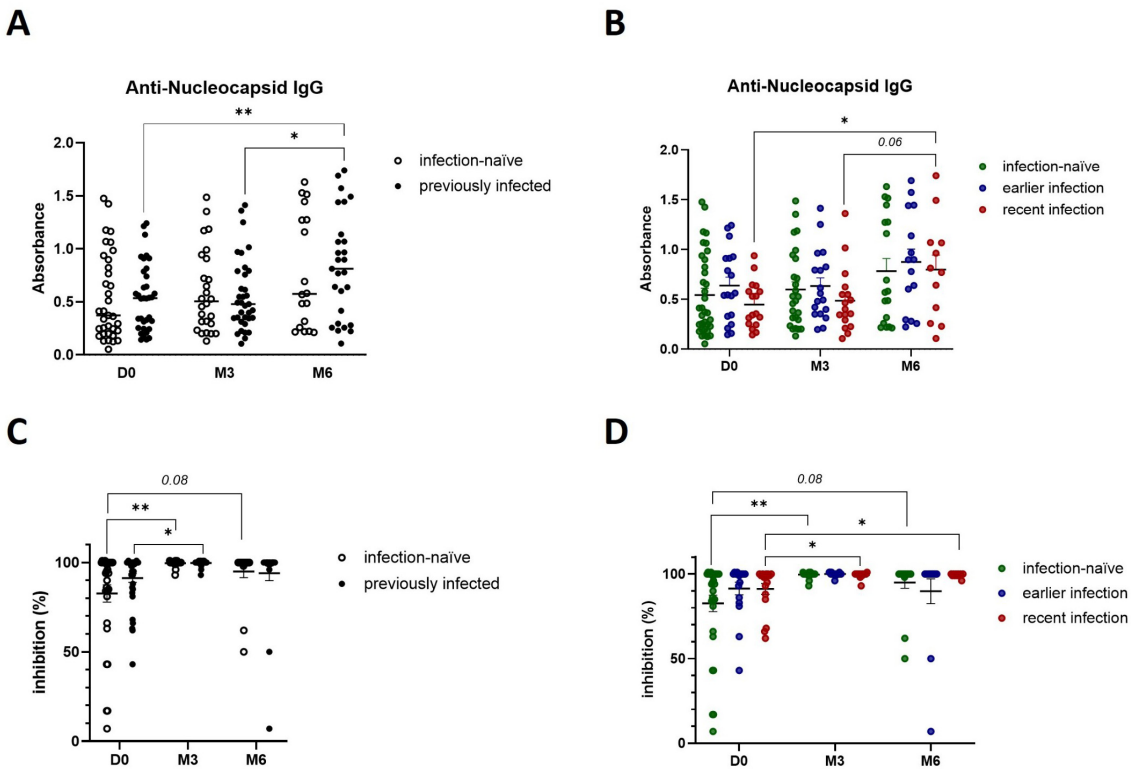

FIGURE 5
Booster vaccination increases the presence of SARS-CoV-2 neutralizing antibodies. **(A)** Anti-nucleocapsid IgG levels in infection-naïve and previously infected participants pre- and post-booster vaccination, as determined by in-house ELISA. **(B)** Anti-nucleocapsid IgG production in infection-naïve and infected participants, stratified by the time of infection. **(C)** Quantification of SARS-CoV-2 IgG with neutralizing ability in infection-naïve and previously infected participants pre- and post-booster vaccination, as determined by in-house neutralization assay. **(D)** Analysis of SARS-CoV-2 neutralizing IgG antibodies in infection-naïve and infected participants, stratified by the time of infection. Scatter dot plots represent mean with standard error of mean (± SEM). Statistical analysis performed using unpaired Student's t-test or one-way ANOVA with Tukey correction. *p ≤ 0.05, **p ≤ 0.01. D0, Day 0; M3, 3-month post-booster; M6, 6-months post-booster.

and CXCL13) across CD4+ and CD8+ T cell subpopulations including T effector memory cells and tissue-resident memory T cells. Collectively, our findings indicate that prior natural SARS-CoV-2 infection and booster vaccination both stimulate the humoral immune response while activating different aspects of the cellular immune response, and that these responses can persist for at least 6-months after receiving the third vaccine dose of BNT162b2.

In conclusion, we demonstrate that booster vaccination plays a critical role in enhancing the anti-viral humoral and cellular immune responses regardless of infection history, likely providing broader protection in the population. However, it remains to be determined whether booster-induced immune responses and/or naturally acquired immunity confer protection against emerging Sars-CoV-2 variants. A recent epidemiological study identified two distinct protection patterns against reinfection based on VOC

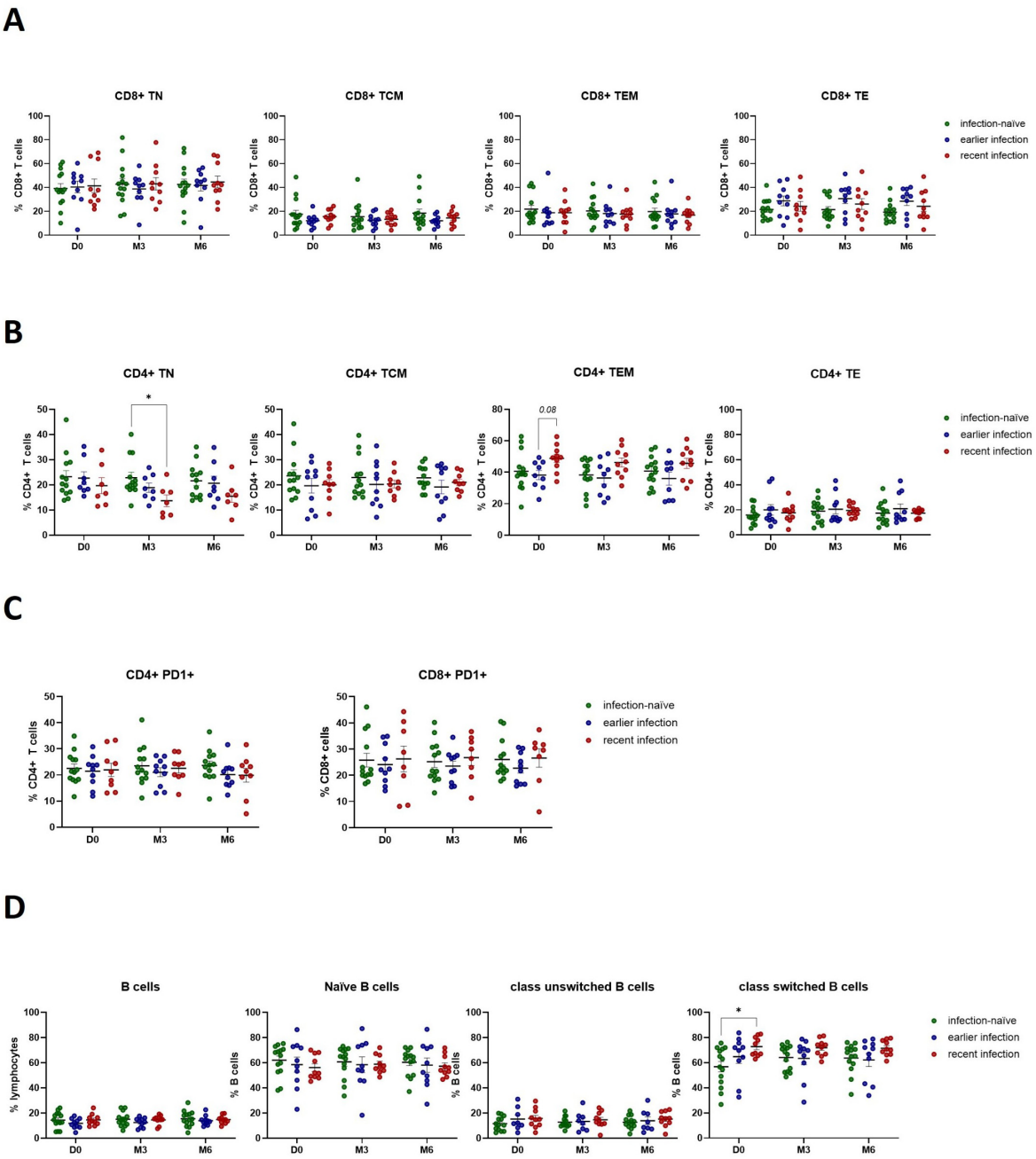

FIGURE 6
SARS-CoV-2 infection activates the anti-viral immune response by promoting CD4+ T effector memory and inducing class-switched B cell responses. **(A)** Flow cytometry analysis of CD8+ T cell phenotypes. **(B)** Flow cytometry analysis of CD4+ T cell phenotypes. **(C)** Flow cytometry analysis of PD1 expression on CD4+ and CD8+ T cells. **(D)** Flow cytometry analysis of B cell phenotypes. Scatter dot plots represent mean with standard error of mean (± SEM). Statistical analysis performed using unpaired Student's t-test or one-way ANOVA with Tukey correction. *$p \leq 0.05$. TN, naïve; TCM, central memory; TEM, effector memory; TE, effector T cells. D0, Day 0; M3, 3-month post-booster; M6, 6-months post-booster.

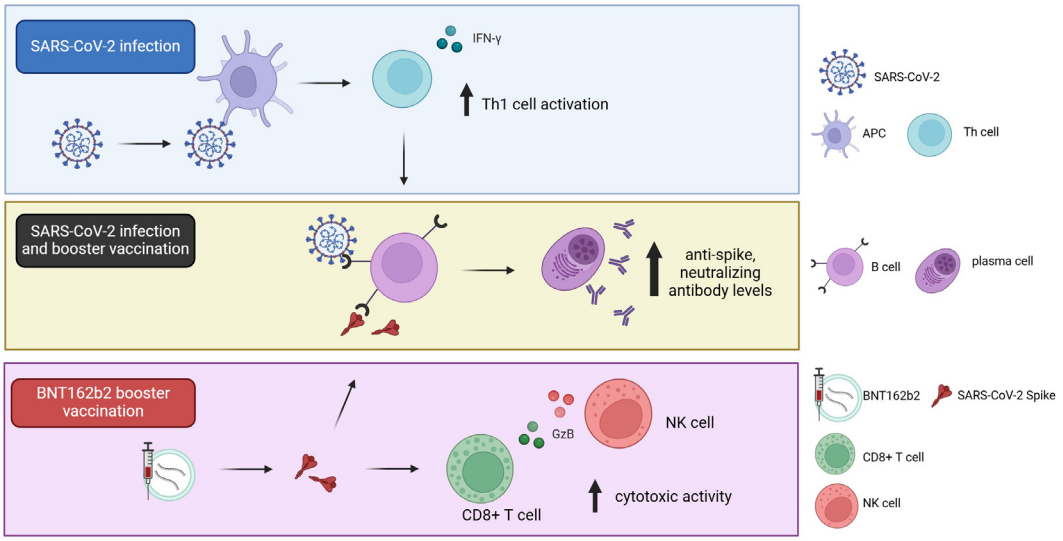

FIGURE 7
Diagram depicting the effect of SARS-CoV-2 natural infection and BNT162b2 third dose vaccination on cellular and humoral immune responses. Prior natural infection induces Th1 cytokine and humoral immune responses. Booster vaccination with BNT162b2 further enhances humoral immune responses, and promotes a cytotoxic cellular response in infection-naïve individuals.

dominance. While pre-Omicron infections provided strong and durable protection against reinfection, infections during the time when Omicron was dominant more effectively prevented reinfection within the first 3 to 6 months post-infection (30). These recent findings highlight the importance of continuous monitoring of Sars-CoV-2 viral spread and evolution to better inform vaccination strategies.

Data availability statement

The original contributions presented in the study are included in the article/supplementary material. Further inquiries can be directed to the corresponding author.

Ethics statement

The studies involving humans were approved by Institutional Review Board, Qatar Biomedical Research Institute (study ID 2022-52) and Institutional Review Board, Hamad Medical Corporation (study ID MRC-01-21-1063). The studies were conducted in accordance with the local legislation and institutional requirements. The participants provided their written informed consent to participate in this study.

Author contributions

RT: Formal Analysis, Investigation, Methodology, Writing – original draft, Writing – review & editing. AZ: Data curation, Resources, Writing – review & editing. BM: Investigation, Resources, Writing – review & editing, Writing – original draft. UJ: Formal Analysis, Investigation, Writing – review & editing, Visualization. NV: Investigation, Methodology, Writing – review & editing. AAl: Data curation, Resources, Writing – review & editing. AN: Resources, Writing – review & editing. HS: Resources, Writing – review & editing. NA: Resources, Writing – review & editing. AAd: Resources, Writing – review & editing. HM: Resources, Writing – review & editing. KS: Resources, Writing – review & editing. RT: Resources, Writing – review & editing. MA: Resources, Writing – review & editing. MAA: Resources, Writing – review & editing. NAl: Writing – review & editing. AAr: Writing – review & editing. YP: Writing – review & editing. SA: Writing – review & editing. OE: Writing – review & editing. AO: Conceptualization, Writing – review & editing. JD: Conceptualization, Formal Analysis, Funding acquisition, Project administration, Supervision, Visualization, Writing – original draft, Writing – review & editing.

Funding

The author(s) declare that financial support was received for the research and/or publication of this article. This work was supported by funding from the Qatar Biomedical Research Institute (QB10-IDRP-2021), Qatar Foundation and the Hamad Medical Corporation (MRC-01-21-1063).

Acknowledgments

The manuscript has been deposited as preprint (BIORXIV/2024/627725).

Conflict of interest

All authors declare that the research was conducted in the absence of any commercial or financial relationships that could be construed as a potential conflict of interest.

The author(s) declared that they were an editorial board member of Frontiers, at the time of submission. This had no impact on the peer review process and the final decision.

Generative AI statement

The author(s) declare that no Generative AI was used in the creation of this manuscript.

Publisher's note

All claims expressed in this article are solely those of the authors and do not necessarily represent those of their affiliated organizations, or those of the publisher, the editors and the reviewers. Any product that may be evaluated in this article, or claim that may be made by its manufacturer, is not guaranteed or endorsed by the publisher.

Supplementary material

The Supplementary Material for this article can be found online at: https://www.frontiersin.org/articles/10.3389/fimmu.2025.1557426/full#supplementary-material

References

1. Coronaviridae Study Group of the International Committee on Taxonomy of Viruses. The species Severe acute respiratory syndrome-related coronavirus: classifying 2019-nCoV and naming it SARS-CoV-2. *Nat Microbiol.* (2020) 5:536–44. doi: 10.1038/s41564-020-0695-z

2. Nachtigall I, Lenga P, Jóźwiak K, Thürmann P, Meier-Hellmann A, Kuhlen R, et al. Clinical course and factors associated with outcomes among 1904 patients hospitalized with COVID-19 in Germany: an observational study. *Clin Microbiol Infect Off Publ Eur Soc Clin Microbiol Infect Dis.* (2020) 26:1663–9. doi: 10.1016/j.cmi.2020.08.011

3. Kwasniewski M, Korotko U, Chwialkowska K, Niemira M, Jaroszewicz J, Sobala-Szczygiel B, et al. Implementation of the web-based calculator estimating odds ratio of severe COVID-19 for unvaccinated individuals in a country with high coronavirus-related death toll. *Allergy.* (2023) 78:311–4. doi: 10.1111/all.15524

4. Lu R, Zhao X, Li J, Niu P, Yang B, Wu H, et al. Genomic characterisation and epidemiology of 2019 novel coronavirus: implications for virus origins and receptor binding. *Lancet Lond Engl.* (2020) 395:565–74. doi: 10.1016/S0140-6736(20)30251-8

5. Jackson CB, Farzan M, Chen B, Choe H. Mechanisms of SARS-CoV-2 entry into cells. *Nat Rev Mol Cell Biol.* (2022) 23:3–20. doi: 10.1038/s41580-021-00418-x

6. Markov PV, Ghafari M, Beer M, Lythgoe K, Simmonds P, Stilianakis NI, et al. The evolution of SARS-coV-2. *Nat Rev Microbiol.* (2023) 21:361–79. doi: 10.1038/s41579-023-00878-2

7. Backer JA, Eggink D, Andeweg SP, Veldhuijzen IK, van Maarseveen N, Vermaas K, et al. Shorter serial intervals in SARS-CoV-2 cases with Omicron BA.1 variant compared with Delta variant, the Netherlands, 13 to 26 December 2021. *Euro Surveill Bull Eur Sur Mal Transm. Eur Commun Dis Bull.* (2022) 27:2200042. doi: 10.2807/1560-7917.ES.2022.27.6.2200042

8. Pascolo S. Vaccines against COVID-19: Priority to mRNA-Based Formulations. *Cells.* (2021) 10:2716. doi: 10.3390/cells10102716

9. Mohammed I, Nauman A, Paul P, Ganesan S, Chen K-H, Jalil SMS, et al. The efficacy and effectiveness of the COVID-19 vaccines in reducing infection, severity, hospitalization, and mortality: a systematic review. *Hum Vaccines Immunother.* (2022) 18:2027160. doi: 10.1080/21645515.2022.2027160

10. Lopez Bernal J, Andrews N, Gower C, Robertson C, Stowe J, Tessier E, et al. Effectiveness of the Pfizer-BioNTech and Oxford-AstraZeneca vaccines on covid-19 related symptoms, hospital admissions, and mortality in older adults in England: test negative case-control study. *BMJ.* (2021) 373:n1088. doi: 10.1136/bmj.n1088

11. Syed MA, AQotba HA, Alnuaimi AS. Effectiveness of COVID-19 vaccines. *J Infect.* (2022) 84:e118–9. doi: 10.1016/j.jinf.2022.02.034

12. Chemaitelly H, Yassine HM, Benslimane FM, Al Khatib HA, Tang P, Hasan MR, et al. mRNA-1273 COVID-19 vaccine effectiveness against the B.1.1.7 and B.1.351 variants and severe COVID-19 disease in Qatar. *Nat Med.* (2021) 27:1614–21. doi: 10.1038/s41591-021-01446-y

13. Polack FP, Thomas SJ, Kitchin N, Absalon J, Gurtman A, Lockhart S, et al. Safety and efficacy of the BNT162b2 mRNA covid-19 vaccine. *N Engl J Med.* (2020) 383:2603–15. doi: 10.1056/NEJMoa2034577

14. Dagan N, Barda N, Kepten E, Miron O, Perchik S, Katz MA, et al. BNT162b2 mRNA covid-19 vaccine in a nationwide mass vaccination setting. *N Engl J Med.* (2021) 384:1412–23. doi: 10.1056/NEJMoa2101765

15. Baden LR, El Sahly HM, Essink B, Kotloff K, Frey S, Novak R, et al. Efficacy and safety of the mRNA-1273 SARS-coV-2 vaccine. *N Engl J Med.* (2021) 384:403–16. doi: 10.1056/NEJMoa2035389

16. Thompson MG, Stenehjem E, Grannis S, Ball SW, Naleway AL, Ong TC, et al. Effectiveness of covid-19 vaccines in ambulatory and inpatient care settings. *N Engl J Med.* (2021) 385:1355–71. doi: 10.1056/NEJMoa2110362

17. Ssentongo P, Ssentongo AE, Voleti N, Groff D, Sun A, Ba DM, et al. SARS-CoV-2 vaccine effectiveness against infection, symptomatic and severe COVID-19: a systematic review and meta-analysis. *BMC Infect Dis.* (2022) 22:439. doi: 10.1186/s12879-022-07418-y

18. Lin D-Y, Gu Y, Wheeler B, Young H, Holloway S, Sunny S-K, et al. Effectiveness of covid-19 vaccines over a 9-month period in north carolina. *N Engl J Med.* (2022) 386:933–41. doi: 10.1056/NEJMoa2117128

19. Puranik A, Lenehan PJ, Silvert E, Niesen MJM, CorChado-Garcia J, O'Horo JC, et al. Comparative effectiveness of mRNA-1273 and BNT162b2 against symptomatic SARS-CoV-2 infection. *Med N Y N.* (2022) 3:28–41.e8. doi: 10.1016/j.medj.2021.12.002

20. Andrejko KL, Pry JM, Myers JF, Mehrotra M, Lamba K, Lim E, et al. Waning of 2-dose BNT162b2 and mRNA-1273 vaccine effectiveness against symptomatic SARS-coV-2 infection accounting for depletion-of-susceptibles bias. *Am J Epidemiol.* (2023) 192:895–907. doi: 10.1093/aje/kwad017

21. Mestiri S, Merhi M, Inchakalody VP, Taib N, Smatti MK, Ahmad F, et al. Persistence of spike-specific immune responses in BNT162b2-vaccinated donors and generation of rapid ex-vivo T cells expansion protocol for adoptive immunotherapy: A pilot study. *Front Immunol.* (2023) 14:1061255. doi: 10.3389/fimmu.2023.1061255

22. Sukik L, Chemaitelly H, Ayoub HH, Coyle P, Tang P, Yassine HM, et al. Effectiveness of two and three doses of COVID-19 mRNA vaccines against infection, symptoms, and severity in the pre-omicron era: A time-dependent gradient. *Vaccine.* (2024) 42:3307–20. doi: 10.1016/j.vaccine.2024.04.026

23. Niesen MJM, Matson R, Puranik A, O'Horo JC, Pawlowski C, Vachon C, et al. Third dose vaccination with mRNA-1273 or BNT162b2 vaccines improves protection against SARS-CoV-2 infection. *PNAS Nexus.* (2022) 1:pgac042. doi: 10.1093/pnasnexus/pgac042

24. Reekie J, Stovring H, Nielsen H, Johansen IS, Benfield T, Wiese L, et al. Development of antibody levels and subsequent decline in individuals with vaccine induced and hybrid immunity to SARS-CoV-2. *Int J Infect Dis.* (2024) 146:107111. doi: 10.1016/j.ijid.2024.107111

25. Bullock JL, Hickey TE, Kemp TJ, Metz J, Loftus S, Haynesworth K, et al. Longitudinal assessment of BNT162b2- and mRNA-1273-induced anti-SARS-coV-2 spike igG levels and avidity following three doses of vaccination. *Vaccines.* (2024) 12:516. doi: 10.3390/vaccines12050516

26. Al-Thani MH, Farag E, Bertollini R, Al Romaihi HE, Abdeen S, Abdelkarim A, et al. SARS-coV-2 infection is at herd immunity in the majority segment of the population of Qatar. *Open Forum Infect Dis.* (2021) 8:ofab221. doi: 10.1093/ofid/ofab221

27. Al-Kuwari MG, Al-Nuaimi AA, Abdulmajeed J, Semaan S, Al-Romaihi HE, Kandy MC, et al. COVID-19 infection across workplace settings in Qatar: a comparison of COVID-19 positivity rates of screened workers from March 1st until July 31st, 2020. *J Occup Med Toxicol Lond Engl.* (2021) 16:21. doi: 10.1186/s12995-021-00311-5

28. van Teijlingen E, Sathian B, Simkhada P, Banerjee I. COVID-19 in Qatar: Ways forward in public health and treatment. *Qatar Med J.* (2020) 2020:38. doi: 10.5339/qmj.2020.38

29. Mathieu E, Ritchie H, Rodés-Guirao L, Appel C, Gavrilov D, Giattino C, et al. Coronavirus (COVID-19) vaccinations. *Our World Data.* (2020).

30. Chemaitelly H, Ayoub HH, Coyle P, Tang P, Hasan MR, Yassine HM, et al. Differential protection against SARS-CoV-2 reinfection pre- and post-Omicron. *Nature.* (2025). doi: 10.1038/s41586-024-08511-9

frontiers | Frontiers in Immunology

TYPE Perspective
PUBLISHED 03 April 2025
DOI 10.3389/fimmu.2025.1569251

OPEN ACCESS

EDITED BY
Sonia Jangra,
The Rockefeller University, United States

REVIEWED BY
Willy A. Valdivia-Granda,
Orion Integrated Biosciences, United States

*CORRESPONDENCE
Ali Azizi
ali.azizi@cepi.net

RECEIVED 31 January 2025
ACCEPTED 18 March 2025
PUBLISHED 03 April 2025

CITATION
Schwartz LM, Vila-Belda J, Carless J, Dhakal S, Hostyn K, Gorman T, Ogbeni D, Kamuyu G, Manak M, Bernasconi V and Azizi A (2025) Monitoring immunological COVID-19 vaccine clinical testing across the CEPI Centralized Laboratory Network. *Front. Immunol.* 16:1569251. doi: 10.3389/fimmu.2025.1569251

Monitoring immunological COVID-19 vaccine clinical testing across the CEPI Centralized Laboratory Network

Lauren M. Schwartz[1], Jose Vila-Belda[1], Jerome Carless[1], Sadish Dhakal[1], Koen Hostyn[1], Trina Gorman[1], Deborah Ogbeni[2], Gathoni Kamuyu[2], Mark Manak[3], Valentina Bernasconi[4] and Ali Azizi[5]*

[1]Gorman Consulting, Edmonds, WA, United States, [2]Coalition for Epidemic Preparedness Innovations (CEPI), London, United Kingdom, [3]Turesol Consulting, King of Prussia, PA, United States, [4]Coalition for Epidemic Preparedness Innovations (CEPI), Oslo, Norway, [5]Coalition for Epidemic Preparedness Innovations (CEPI), Washington, DC, United States

The CEPI-Centralized Laboratory Network (CLN) has significantly contributed to the development of several approved SARS-CoV-2 vaccines by conducting over 70,000 clinical samples for testing from various vaccine developers. A centralized data management system was developed to track, review, store and share immunological clinical results generated from sample testing. The data system ensures the completeness and accuracy of submitted results and checks the set criteria in controls for each assay. Each testing facility within the network submits their results to a secure storage system using report forms with embedded data quality checks. Upon submission, a statistical program runs additional checks to identify errors in completeness and uniqueness. Any discrepancies or errors are shared with the testing facility to rectify. Reports are further reviewed by CEPI-CLN experts before releasing to the vaccine developer. Study results are then consolidated into an internal relational database management system, enabling CEPI to analyze the data through an interactive dashboard that visualizes control trends and sample results across all studies. This analysis facilitates the harmonization of immunological data and helps to inform CEPI's programmatic and strategic decision making. Given the success of this approach with SARS-CoV-2 vaccines, the system will be adopted for new pathogens and assay types currently under development at CEPI-CLN.

KEYWORDS

vaccine results, data management, quality, trial monitoring, database

Background

As of May 2024, the CEPI-Centralized Laboratory Network (CLN) has significantly contributed to the development of several approved SARS-CoV-2 vaccines by conducting over 120,000 assay runs (over 70,000 clinical samples) for testing from various vaccine developers worldwide (1–4). In summary six SARS-CoV-2 immunological assays have been developed, validated or qualified, and transferred to the network using the same materials, key reagents, and protocols: three binding assays (S-, RBD, and N-ELISA), a microneutralization assay (MNA), a pseudotyped virus-based neutralization assay (PNA), and an IFN-γ T-cell ELISpot assay. Inter-lab studies using replicate assays, as well as revalidation in receiving facilities, have shown that results are highly reproducible, allowing for direct comparison of different vaccines throughout the network (2). Reliability of clinical sample testing is assured through the implementation of an internal centralized system designed to store sensitive and proprietary data and perform data quality checks on the immunological clinical results, ensuring the integrity and consistency of data collected. Additionally, the system enables trend analysis of reference standards and controls, generated by the Medicines and Healthcare Products Regulatory Agency (MHRA, formerly NIBSC), allowing CEPI-CLN to harmonize results across laboratories and to identify any potential issues or anomalies in the data that indicate of loss of consistency between facilities. This centralized system plays a crucial role in maintaining the quality and integrity of clinical sample testing processes.

Data pipeline

The automated process by which submitted clinical data is checked for consistency, consolidated, cleaned, and stored in a database to enable analysis, is called the data pipeline (Figure 1). All steps in the data pipeline were developed by CEPI-CLN and for internal use only. The data pipeline is managed by Apache Airflow (5), an open-source platform that initiates and tracks each dependent step. Further, isolated and encrypted environments on both Amazon Web Services (AWS) and Heroku are used to house Apache Airflow and the database, respectively. Compliance with international data privacy laws (General Data Protection Regulation [GDPR]) (6) and ISO 27001 is achieved through multiple technical and organizational measures that have been deployed throughout the data pipeline including: pseudonymized specimen identifiers, regulated and restricted data access to all software and database storage systems through the principle of least privilege, weekly database and systems backups, and the use of isolated and encrypted cloud environments. The data pipeline was first built within a testing space to ensure a valid and secure pipeline before moving to a production space where regular audits and vulnerability assessments are conducted.

Step 1: Submission of report forms

Testing facilities within the network have quality management systems in place, employing quality control procedures throughout the analytical process. From sample receipt through to reporting, facilities are responsible for assuring the integrity of the results they generate.

Assay results are entered into a standardized report form at each facility. All facilities participate in virtual training sessions to review consistent data entry protocols. Each report may contain all or a subset of sample testing results for each clinical study with only information relevant for immunologic testing including sample and participant unique identifiers, study time point, data of collection, plate control identifier, and assay result. Additional information collected during the course of a clinical trial, such as participant-level demographic variables, is not shared with the facilities. The report form contains data validation rules, drop down menus, formulas, and conditional formatting (Table 1) as a first step in ensuring the completeness and consistency of results. For example, cells change color if any information related to a test sample or plate control is missing. This allows facility staff and reviewers to scan the report to identify missing critical data before submission. Additionally, to complement facility quality control procedures, warnings appear when plate control values fall outside of pre-defined acceptance ranges, signaling samples that need to be retested. The report form is locked, and password protected so that the facility staff cannot accidentally change the embedded functionality. Within each facility, all report forms are approved by a quality control manager or designated expert before being uploaded onto a central encrypted file storage system that is compliant with GDPR (6).

Step 2: Detection of submitted report forms

Following data submission, sample and control immunological results enter CEPI's automated data pipeline, where each subsequent step is initiated by Apache Airflow (5). The file storage system is automatically checked every hour to detect if new report forms have been submitted. Once a new report form is detected, a python program downloads the file to a temporary directory, triggering a series of automated data quality checks, as described in Step 3.

Step 3: Data quality checks for report forms

A statistical program designed in Stata is run to ensure each report form retains embedded functionality and calculations, is complete, and passes a series of other quality checks, such as that dates are valid and that plate control acceptance criteria, based on the reagent lot, is calculated correctly (Table 1). Results of these

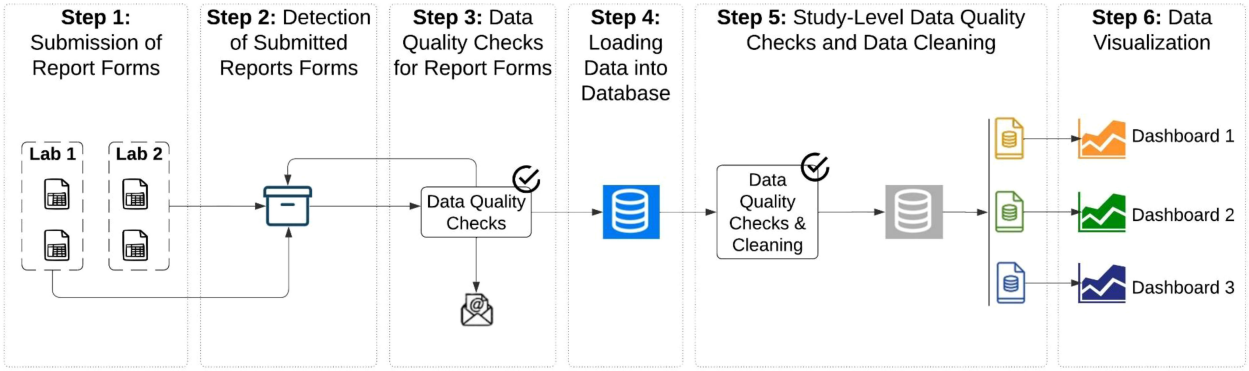

FIGURE 1
Design of the data pipeline from report submission to visualization. Image shows the different steps of the data pipeline including labs submitting report forms (Step 1), detection of report forms in the centralized storage repository (Step 2), automated data quality checks on the report forms (Step 3), loading (Step 4) and further cleaning of the data in the database (Step 5) and finally visualizations in dashboards (Step 6).

checks are saved in a spreadsheet that is uploaded to the central file storage system. An email is sent to relevant CEPI-CLN staff informing them of the result of these checks. The CEPI-CLN team reviews the spreadsheet, identifying and communicating any data quality errors to the facility if needed. Subsequently, the facility may submit a revised report form, which supersedes the previous version, thereby avoiding duplicates in the central file storage system. Report forms approved by CEPI are shared with vaccine developers through the central file storage system. Interpretation of clinical testing results and their relevance to efficacy of the vaccine are the responsibility of the vaccine developer.

Step 4: Loading data into the database

All rows from the submitted report form with complete sample and plate control data are bulk inserted into a single relational PostgreSQL database. The database is located in a dedicated and

TABLE 1 Data quality checks conducted throughout the data pipeline.

Step	Data Quality Check	Method
Data Collection (Report Form) – Step 1	For key variables (lab name, report status, study ID) only selected list possible	Excel dropdown menu
	Consistent dates across reports and labs	Data format requirement in excel
	Non-missing data on key variables	Color conditioning so that cells with missing data turn orange
	Plate control acceptance criteria calculated correctly according to reagent lot	Excel formula to calculate if controls fall between acceptance criteria, based on lot number
Report-Level Data Quality Checks (Stata Program) – Step 3	For key variables (lab name, report status, study ID) only selected list possible	Program checks for selected known list for each variable
	Consistent dates across reports and labs	Program checks for correct format
	Non-missing data on key variables	Program checks all required fields are filled in
	Unique laboratory specimen IDs and client sample IDs	Program checks for duplicate values by ID and assay date in one report
	Consistent time points	Program checks for consistent time point within a report (Day v Month)
	All accepted sample results come from accepted plates	Program checks that each sample aligns with a run, plate, and assay date from an accepted plate control
	Plate control acceptance criteria calculated correctly according to reagent lot	Program re-calculates formula to ensure users have no user error
Study -Level Data Quality Checks (Database) – Step 5	Unique laboratory specimen IDs and client sample IDs	Program checks for duplicate values by ID and assay date across all reports within a study
	Consistent time points	Program checks for consistent time point across all reports within a study (Day v Month)

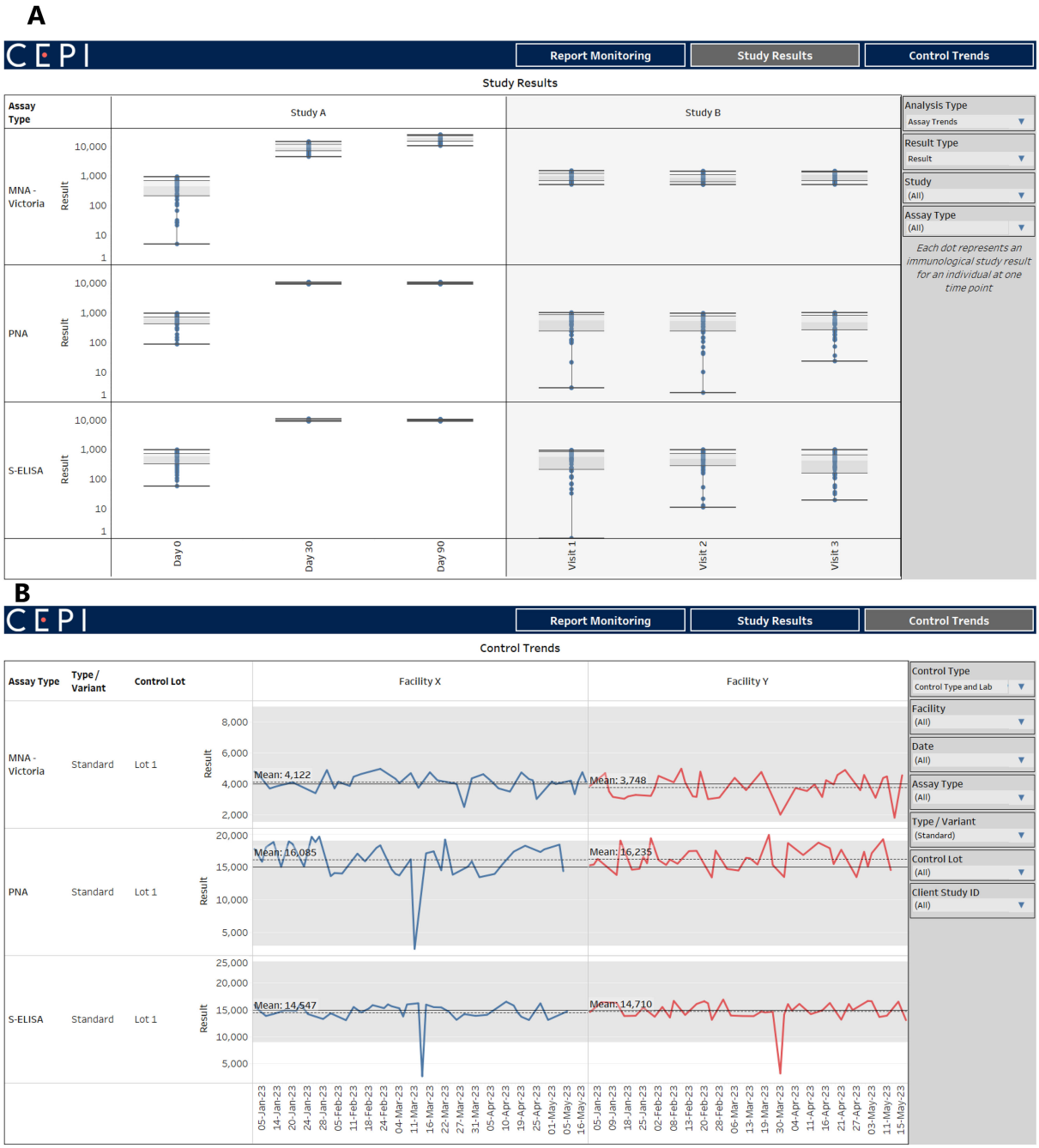

FIGURE 2
Tableau dashboard with with assay results and control trends. **(A)** shows example clinical trials results on a dashboard connected to CEPI-CLN database. **(B)** shows example control results which can be used to track trends by facility and across time to ensure consistency and identify any possible quality issues.

isolated environment designed for storing sensitive data. PostgresSQL is inherently ACID compliant. Specifically, the psycopg2 package (7, 8) handles Atomicity and Isolation by managing transactions using connection objects, commits, and rollbacks. Consistency is maintained by enforcing unique constraints across all tables in the database. Durability is achieved through a combination of postgres' internal Write-Ahead Logging (9) and hourly backup snapshots managed by Heroku (10).

Data is first moved to staging tables which contain all pre-processed data. This provides a historical snapshot of the clinical trial data across each batch. Data are loaded into separate tables for clinical sample results, plate control results, and data quality check summaries. Key identifiers are maintained across all tables and include facility name, assay type, report name, study ID and load date. To maintain idempotency, records matching the bulk insert load date are removed before each insert, ensuring no unexpected duplication.

Step 5: Study-level data quality checks and data cleaning

A second round of data quality checks are performed within the database across all reports submitted for each study, to ensure all key indicators (sample identifiers, assay type, facility name, study ID, dates) are complete and properly recorded and time points are consistent and valid (Table 1). Discrepant results are again reviewed by the CEPI team and, if needed, the facility resubmits revised reports to correct issues. The quality checks are run automatically as each new report is submitted, but it may take weeks until all samples are tested and for final data quality checks to be performed. In the final production tables, version control for revised report forms is maintained through tracking the submission time of each report form and upsert queries ensure that only unique data are inserted. Various data cleaning processes are performed including calculating international standard unit conversions and aligning study visit time point variables across studies (e.g. 'day1' and 'D01' cleaned to 'Day 1'). Materialized views are created from the final production tables that aggregate, combine, or reshape data as needed for the visualizations.

Step 6: Data visualization

Using an encrypted connection to the materialized views in the database, an interactive dashboard of data visualizations enables CEPI to continually analyze and monitor submitted results. The dashboard visualizes aspects such as 1) the number and status of reports that have been submitted to support scheduling and inventory control, 2) trends in immunological results by assay and study (Figure 2A), and 3) plate control trends by assay, lot, and lab over time (Figure 2B). As of May 2024, over 300 reports have been uploaded and quality checked since the start of the data pipeline in 2022. Importantly, control results are used to track trends by facility and across time to ensure consistency and identify any possible quality issues.

Discussion

The CEPI-CLN currently includes 18 facilities across the world. This network relies on a series of processes to ensure the consistency, completeness, and reliability of vaccine test sample results across all facilities. These processes include standardized and harmonized assay procedures, regular proficiency testing after the post-technology transfer, data quality checks, and ongoing communication and collaboration among the network. By implementing these rigorous processes, the CEPI-CLN aims to maintain high standards of quality assurance and control, ultimately contributing to the development of safe and effective vaccines against emerging infectious diseases. The data quality checks and ongoing analysis provide additional confidence in the data, which is both shared with vaccine developers and used to inform CEPI's programmatic and strategic decisions. Using the resulting data and visualizations, CEPI can facilitate rapid evaluation and dissemination of the most effective vaccine candidates. Additionally, CEPI can also obtain a better understanding of aspects such as the correlation and duration of protection across multiple SARS-CoV-2 vaccine clinical trials, as well as identifying which vaccine platforms require support towards licensure. Given the success of this approach with COVID-19 vaccines, the system is currently being adopted for new pathogens and assay types currently under development at CEPI-CLN (11). The database may also start to leverage machine learning or Artificial Intelligence (AI) tools to supplement quality control systems. Since 2023, CEPI has made significant investments and partnered with several private companies and recognized academic institutions to incorporate AI-driven tools in various areas to support CEPI's 100 Days Mission: to quickly make safe and effective vaccines against any viral pandemic threat. Additionally, we plan to incorporate study-level demographic information in the database to support high-level analyses related to vaccine response in different populations. In summary, these processes not only maintain high-quality standards but also strengthen global preparedness, reinforcing CEPI's commitment to equitable access to vaccines against rare pathogens.

Data availability statement

The datasets presented in this article are not readily available because of privacy concerns. Requests to access the datasets should be directed to author AA, ali.azizi@cepi.net.

Author contributions

LS: Conceptualization, Data Curation, Formal analysis, Investigation, Methodology, Project administration, Software, Supervision, Validation, Visualization, Writing – original draft, Writing – review & editing. JV-B: Data curation, Formal analysis, Investigation, Methodology, Software, Validation, Writing – original draft, Writing – review & editing. JC: Data curation, Formal analysis, Investigation, Software, Writing – original draft, Writing – review & editing. SD: Data curation, Formal analysis, Investigation, Software, Writing – original draft, Writing – review & editing. KH: Methodology, Software, Writing – original draft, Writing – review & editing. TG: Methodology, Writing – original draft, Writing – review & editing. DO: Investigation, Writing – original draft, Writing – review & editing. GK: Investigation, Writing – original draft, Writing – review & editing. MM: Conceptualization, Funding acquisition, Investigation, Methodology, Resources, Supervision, Validation, Writing – original draft, Writing – review & editing. VB: Conceptualization, Funding acquisition, Investigation, Methodology, Resources, Supervision, Validation, Writing – original draft, Writing – review & editing. AA: Conceptualization, Funding acquisition, Investigation, Methodology, Resources, Supervision, Validation, Writing – original draft, Writing – review & editing.

Funding

The author(s) declare that financial support was received for the research and/or publication of this article. All work discussed here in was funded by CEPI under contractual agreements with the respective laboratories. The authors do not receive any royalties, licenses, stock options, or other financial benefit.

Acknowledgments

We would like to thank CEPI-CLN facilities for their support during the development of the database.

Conflict of interest

Authors LS, JV-B, JC, SD, KH and TG were employed by company Gorman Consulting. Author MM was employed by company Turesol Consulting.

The remaining authors declare that the research was conducted in the absence of any commercial or financial relationships that could be construed as a potential conflict of interest.

Generative AI statement

The author(s) declare that no Generative AI was used in the creation of this manuscript.

Publisher's note

All claims expressed in this article are solely those of the authors and do not necessarily represent those of their affiliated organizations, or those of the publisher, the editors and the reviewers. Any product that may be evaluated in this article, or claim that may be made by its manufacturer, is not guaranteed or endorsed by the publisher.

References

1. Azizi A, Manak M, Bernasconi V. The CEPI centralized laboratory network for COVID-19 will help prepare for future outbreaks. *Nat Med*. (2023) 29:2684–5. doi: 10.1038/s41591-023-02534-x

2. Manak M, Gagnon L, Phay-Tran S, Levesque-Damphousse P, Fabie A, Daugan M, et al. Standardised quantitative assays for anti-SARS-CoV-2 immune response used in vaccine clinical trials by the CEPI Centralized Laboratory Network: a qualification analysis. *Lancet Microbe*. (2024) 5:e216–25. doi: 10.1016/S2666-5247(23)00324-5

3. Azizi A, Bernasconi V. Unifying global efforts by CEPI's centralized laboratory network. *Front Immunol*. (2024) 15:1404309. doi: 10.3389/fimmu.2024.1404309

4. Azizi A, Kamuyu G, Ogbeni D, Levesque-Damphousse P, Knott D, Gagnon L, et al. Driving consistency: CEPI-Centralized Laboratory Network's conversion factor initiative for SARS-CoV-2 clinical assays used for efficacy assessment of COVID vaccines. *Hum Vaccines Immunother*. (2024) 20:2344249. doi: 10.1080/21645515.2024.2344249

5. Apache Airflow. Home (2024). Available online at: https://airflow.apache.org/ (Accessed June 24, 2024).

6. GDPR.eu. GDPR compliance checklist (2024). Available online at: https://gdpr.eu/checklist/ (Accessed June 24, 2024).

7. The connection class — Psycopg 2.9.10 documentation (2024). Available online at: https://www.psycopg.org/docs/connection.html (Accessed June 24, 2024).

8. Basic module usage — Psycopg 2.9.10 documentation (2024). Available online at: https://www.psycopg.org/docs/usage.html (Accessed June 24, 2024).

9. PostgreSQL Documentation. 28.3. Write-Ahead Logging (WAL) (2024). Available online at: https://www.postgresql.org/docs/17/wal-intro.html (Accessed June 24, 2024).

10. Heroku PGBackups | Heroku Dev Center . Available online at: https://devcenter.heroku.com/articles/heroku-postgres-backups (Accessed June 24, 2024).

11. Azizi A, Rose K, Kamuyu G, Ogbeni D, Bernasconi V. Preparedness and priority research to tackle the mpox outbreak response. *Nat Med*. (2025) 31:14–5. doi: 10.1038/s41591-024-03367-y

frontiers | Frontiers in Immunology

TYPE Original Research
PUBLISHED 16 April 2025
DOI 10.3389/fimmu.2025.1565862

OPEN ACCESS

EDITED BY
Fabio Fiorino,
LUM University Giuseppe Degennaro, Italy

REVIEWED BY
Paola Massari,
Tufts University, United States
David S. Stephens,
Emory University, United States

*CORRESPONDENCE
Elisabetta Frigimelica
elisabetta.x.frigimelica@gsk.com
Isabel Delany
isabel.x.delany@gsk.com

†PRESENT ADDRESS
Giacomo Vezzani,
GSK Vaccines Institute for Global Health,
Siena, Italy

RECEIVED 23 January 2025
ACCEPTED 24 March 2025
PUBLISHED 16 April 2025

CITATION
Vezzani G, Viviani V, Audagnotto M, Rossi A, Cinelli P, Pacchiani N, Limongi C, Santini L, Giusti F, Tomei S, Torricelli G, Faenzi E, Sammicheli C, Tavarini S, Efron A, Biolchi A, Finco O, Delany I and Frigimelica E (2025) Isolation of human monoclonal antibodies from 4CMenB vaccinees reveals PorB and LOS as the main OMV components inducing cross-strain protection. *Front. Immunol.* 16:1565862. doi: 10.3389/fimmu.2025.1565862

Isolation of human monoclonal antibodies from 4CMenB vaccinees reveals PorB and LOS as the main OMV components inducing cross-strain protection

Giacomo Vezzani[1,2†], Viola Viviani[1], Martina Audagnotto[1], Alessandro Rossi[1], Paolo Cinelli[1], Nicola Pacchiani[1], Chiara Limongi[1], Laura Santini[1], Fabiola Giusti[1], Sara Tomei[1], Giulia Torricelli[1], Elisa Faenzi[1], Chiara Sammicheli[1], Simona Tavarini[1], Adriana Efron[3], Alessia Biolchi[1], Oretta Finco[1], Isabel Delany[1*] and Elisabetta Frigimelica[1*]

[1]GSK Vaccines, Siena, Italy, [2]Department of Pharmacy and Biotechnology (FABIT), University of Bologna, Bologna, Italy, [3]Departamento de Bacteriología, Instituto Nacional de Enfermedades Infecciosas-ANLIS "Dr. Carlos G. Malbrán", Buenos Aires, Argentina

Introduction: The 4CMenB vaccine licensed against serogroup B Neisseria meningitidis (MenB) contains three recombinant proteins and Outer Membrane Vesicles (OMV) from a New Zealand epidemic strain. The protective response mediated on differentmeningococcal strains has been historically ascribed to one of the four main vaccine antigens fHbp, NHBA, NadA, and PorA nominated as the immunodominant antigen of the OMV component. It is however accepted that the extensive cross-protection observed after vaccination may be attributed to other proteins in the OMV. Here we interrogate the B cell responses elicited in humans to the OMV component after 4CMenB vaccination to elucidate the contribution of additional OMV antigens to meningococcal cross-protection.

Methods: Following the isolation of plasmablasts from vaccinees, the OMV-specific human monoclonal antibodies (HumAbs) were recombinantly expressed and characterized for their binding and functional activity on a panel of MenB strains. Their target specificity was assessed through a tailor-made protein array and Western blot.

Results: We found that 18 HumAbs showing bactericidal activity were PorB-specific, 1 was LOS-specific and 4 functional HumAbs remain with unknown targets. We identified three functional classes within the PorB HumAbs, through binding and in silico docking experiments, likely to be elicited from distinct epitopes on PorB and highlighting this antigen as a multi-epitope immunogenic OMV component responsible for distinct cross-protection across multiple MenB strains. Interestingly three of the PorB HumAbs and the LOS-specific HumAb showed bactericidal activity also against gonococcus.

10.3389/fimmu.2025.1565862

Discussion: We identified PorB and LOS as antigens on the OMV that may be implicated in the real-world observations of moderate protection against gonorrhea infection after OMV-based vaccinations.

KEYWORDS

4CMenB, outer membrane vesicles, PorB, lipooligosaccharides (LOS), cross-strain protection, human monoclonal antibodies

Introduction

Over the last three decades, several outer membrane vesicle (OMV)-based vaccines have been used to control infection from outbreaks of *Neisseria meningitidis* serogroup B (MenB) causing meningococcal disease in Cuba (1), Norway (2), Chile (3), and New Zealand (4). Furthermore, one of the two broadly cross-protective MenB vaccines, currently licensed for all age groups, is the 4-component multivalent 4CMenB vaccine comprising detergent extracted OMV from the New Zealand 98/254 epidemic strain and three recombinant proteins (fHbp, NadA and NHBA), identified with the reverse vaccinology approach (5). The main OMV antigen contributing to protection has been historically recognized to be the Porin A (PorA), which is one of the most abundant proteins in the OMV (6) however non-PorA antigens are thought to contribute to the full extent of cross protection. Clinical studies have shown added value of inclusion of the OMV component with the three recombinant antigens in 4CMenB vaccine formulations for broad protection across MenB strains (7–9). Moreover, studies performed in infants showed that 4CMenB was able to induce immunogenicity and bactericidal activity against strains bearing heterologous PorA, suggesting that additional, non-PorA, antigens in the OMV could generate functional antibodies (8).

Due to the diversity of disease-causing isolates, the Meningococcal Antigen Typing System (MATS) was developed in an attempt to predict which strains would be covered by the multicomponent vaccine-induced responses. MATS combines conventional genotyping of PorA with a specialized sandwich ELISA that measures the levels of expression of fHbp, NadA, and NHBA proteins in a given meningococcal isolate and their immunological cross reactivity with the corresponding vaccine antigen (10). The effectiveness of 4CMenB vaccine measured after widespread implementation revealed that vaccine efficacy of 4CMenB in infants, measured as bactericidal activity elicited in infant sera, was usually higher than the strain coverage rates predicted using MATS (11, 12). Several non-exclusive explanations have been proposed to support the observed protection (1): synergy among antibodies targeting the multiple components included in the vaccine; (2) an intrinsic adjuvating effect of OMV and its components; or (3) the role of non-PorA antigens within the OMV component which act as additional protective antigens (13). Preclinical evidence on the importance of other OMV components in eliciting protective immune responses came from the work of Matthias and co-workers, which showed that OMV derived from bacteria depleted of PorA still conferred cross-strain protection in immunized mice and rabbits (14). Furthermore, after the MenZB immunization program in New Zealand, a vaccine that consists solely of the OMV component of 4CMenB, effectiveness against non-strain specific group B demonstrated protection beyond the PorA subtype (15). Finally, a recent publication from Viviani and collaborators identified OpcA and PorB as antigens involved in the broad cross-protection induced by the 4CMenB vaccine in mice and humans (16).

Besides the coverage of different MenB strains, 4CMenB elicits immune responses effective against non-B meningococcal serogroups that can be mainly attributed to antibodies targeting one or more antigens acting alone or synergistically (17–19). In particular, the potential coverage of 4CMenB on meningococcal serogroups A (20), C, W, X (21) and Y has been evaluated by testing a large number of clinical isolates from different countries in human serum bactericidal assay (hSBA). In addition, real world data suggest an effective role of 4CMenB vaccination in the prevention of infections from MenW strains (22–25).

Interestingly, a moderate effectiveness against gonorrhea infection has been reported recently in a number of observational retrospective studies after vaccination with OMV-containing meningococcal vaccines (26–33). Meningococcus and gonococcus, although etiological agents of very different human diseases, share greater than 85% of sequence conservation in their genomes (34) and it has been shown that OMV-induced antibodies recognized gonococcal proteins (35, 36) and human 4CmenB vaccinees have antibodies that recognize both gonococcal proteins and LOS (37, 38).

Overall, in the last decade the protective role played by different antigens contained in the OMV component of 4CMenB vaccine has been demonstrated, but their exact identity and contribution still need to be fully understood and characterized. Interrogating vaccine-induced B cell responses in humans is a powerful approach to identify protective antigens and epitopes included in a vaccine formulation. The approach, named Reverse Vaccinology 2.0, is based on the isolation of the variable regions of heavy (VH) and light (VL) chain genes of vaccine-specific immunoglobulins and on their recombinant expression and functional

characterization (39, 40). This approach has been previously applied to isolate and characterize human monoclonal antibodies (HumAbs) elicited by the three recombinant proteins of 4CMenB in adult subjects after vaccination (5). Very recently the isolation of gonococcal -specific HumAbs from memory B cells from 4CMenB vaccinees has been reported (Troisi, Fabbrini et al., 2023, bioRxiv, https://www.biorxiv.org/content/10.1101/2023.12.07.570438v1). Here we selected vaccinees that after 4CMenB immunization are highly responsive to the OMV component and recovered the Ig sequences from single sorted B cells, to clone HumAbs from vaccine-responsive plasmablast mononucleate cells (PBs). By characterizing the OMV-specific HumAbs, we determined the antibody targets and hence immunogenic antigens contained in the OMV preparation. We characterized their bactericidal killing against a panel of meningococcal strains as well as their cross-functionality on *N.gonorrhoeae*.

Methods

Ethics statement

Human samples obtained from adults immunization in a Phase I clinical study conducted in Krakow, Poland and sponsored by Novartis Vaccine, now part of the GSK group of Companies, using two doses of multicomponent serogroup B meningococcal vaccine 4CMenB formulations. In this study vaccinated subjects were immunized with formulations with 2 different doses of OMV component: rMenB + 25 µg OMV, and rMenB + 6.25 µg OMV. The Clinical trial protocol was approved by the Bioethics Committee of the District Medical Doctors' Chamber in Krakow (authorization number: 87/KBL/OIL/2010; approval date: September 15th 2010) and the study was conducted in accordance with the Declaration of Helsinki. Written informed consent was obtained from each of the subjects.

Elispot assay

Plasmablasts were collected from subjects 1 week after the second immunization and were tested for specificity and quantity using a standard ELISpot protocol. Ninety-six well ELISpot plates (Millipore MultiScreenHTS HA Filter Plate) were coated with 100 µL/well of phosphate-buffered saline (PBS), OMV (5 µg/mL) or 2.5 µg/mL goat anti-human IgG +5 µg/mL goat anti-human IgM (BD Pharmingen). Coated plates were incubated at 4°C overnight and then washed 3 times with 200 µl per well of sterile PBS. Wells were blocked with 200 ul of PBS containing 1% dried skimmed milk for 2 h at room temperature prior to the addition of cells, which were diluted in complete medium (RPMI, Invitrogen 12633012, supplemented with 5% FBS, HyClone, Cytiva SH30070.01HI). Suspensions of 4 – 8 × 10^6 thawed PBMC were seeded in duplicate wells and serially diluted 2-fold in a final volume of 100 µl/well and plates were incubated at 37°C, 5% CO2 for 2 h before stopping the assay by extensive washing with PBS 0.05% - Tween 20 (Sigma–Aldrich). Secondary antibodies anti human IgG FITC (Jackson ImmunoResearch 609-095-213), and anti-human IgM biotinylated (BD Biosciences 314504) were then added for detection in 100 µl/well of PBS containing 4% bovine serum albumin and incubated ON at 4°C. After the incubation, plates were washed and further incubated for 40 min with 100 µl/well of PBS - 0.05% Tween20 containing horseradish peroxidase (HRP)-conjugated streptavidin (MERCK GERPN1231) and an alkaline phosphatase (AP)-conjugated mouse anti-FITC antibody (Roche 11426338910). Spots of antibody secreting cells were revealed by adding in the dark the HRP substrate AEC kit (Vectro Laboratories SK4200) for 40 min and, after extensive washings with deionized water, the AP substrate kit III for 40 min (Vector Laboratories SK5300). Antigen-specific and total IgG and IgM Ab-secreting cells were enumerated using the CTL immunospot S5 UV analyzer (CTL Europe, Bonn, Germany).

Flow cytometry sorting of human B cells

Plasmablasts (PBs) were isolated from human peripheral blood cells. PB cells were stained with anti-human CD27-PE (BD Biosciences, 340425), CD38-Cy7 (BD Biosciences 335825), CD19-V421 (BD Biosciences 562440), CD20-FITC (BD Biosciences 345792) and IgD-A700 (BD Biosciences 561302) for 30' at 4°C. After washing with 1% FBS in PBS, cells have been centrifuged and resuspended in PBS/EDTA 2.5 mM. PB subset has been identified as CD19+CD20dmIgD-CD27++CD38++ and single-cell sorted using a FACS sorter (BD Biosciences, FACSAria III Cell Sorter) into 96w plates containing lysis buffer (RNAse OUT, Invitrogen 10777019; BSA, AMBION AM2616 1 mg/ml in DEPC water, AMBION AM9915G) and immediately frozen for storage at -80° until use.

Cloning of variable region genes and HumAb recombinant expression

Heavy and light chain variable (VH and VL, respectively) region genes of single plasmablasts isolated from peripheral blood were retrotranscribed with gene-specific primers and amplified separately by 2 nested PCR reaction, performed with a mix of primers designed to amplify the highest number of V families (Supplementary Table 1), and then ligated by Polymerase Incomplete Primer Extension (PIPE) into mammalian expression plasmids (pcDNA 3.1, Thermofisher V79020) containing the leader sequence for secretion and the constant region fragment of IgG1 heavy or k-light chain, respectively. The plasmid carries, within the coding sequence of the human IgG1 constant region of heavy chain, the hexabody mutations E345R/E430G or E345R/E430G/S440Y to enhance functionality of obtained mAbs (41). For transient expression of mAbs, two separate linear Transcriptionally Active PCR (TAP) products were generated for each paired VH-VL ligation product. TAP fragments were amplified from the plasmid ligation reactions of the variable regions with primers annealing on the plasmid and included the HCMV promoter, the full antibody

sequence and the plasmid poly-adenylation signal (protocol adapted from (42)). The paired TAP products were then used for co-transfection and transient expression in Expi293F cells (Thermofisher A14527), using Expifectamine (Thermofisher A14525) according to manufacturers' instructions.

HumAb purification from culture supernatants

The sequences corresponding to VH and VL of desired human monoclonal antibodies were obtained by Sanger and Illumina sequencing of the TAP products, codon-optimized for mammalian expression and synthetized either by GeneArt (Thermofisher) or Twist and cloned into expression vectors containing the human IgG1 hexabody, Igκ or Igλ constant regions. Transient recombinant expression of antibodies was achieved by co-transfecting paired heavy and light chain expression plasmids into suspension cultures of Expi293F cells according to manufacturer's protocol. Supernatants were collected 6 days after transfection. Culture supernatants were recovered after centrifugation at 900×g for 10 min and filtered through a 0.22 µm pore size filter (Millipore P1313), and recombinant antibodies were purified by affinity chromatography with Protein G (GE Healthcare 17061802) according to the manufacturer's instructions. Antibodies were eluted with 0.1 M glycine (pH 2.1), neutralized in 1 M Tris (pH 8.0) and then the buffer was exchanged to PBS. Purified antibodies were quantified by absorbance at 280 nm and their purity was assessed by SDS-page electrophoresis and ProBlue safe staining (Giotto Biotech, G00PB005).

Luminex binding screening of HumAbs in culture supernatants

For IgG quantification and binding specificity of the raw supernatants from TAP-transfected Expi293 cells, a Luminex assay was developed. The vaccine components fHBP-GNA2091, GNA1030-NHBA, and NadA recombinant antigens, and OMV from NZ98/254 (43), and the recombinantly expressed PorA (16) and Protein A were individually coupled to 6 distinct luminex beads (MC12XXX; MagPlex) according to the manufacturers' instructions. Coated beads were incubated for 1 hour with 5 µl of raw supernatant diluted (1:2) in PBS with 0.05% Tween 20 (Sigma-Aldrich 28320) and 1% bovine serum albumin (BSA, A3294 Merck). After washing in PBS with 0.05% Tween 20, the beads were incubated for 45 min with R-Phycoerythrin-AffiniPure F(ab')2 Fragment Goat Anti-Human IgG, Fcγ Fragment Specific (109-116-098 Jackson Immunoresearch) and signals were acquired with BioPlex200 (BIO-RAD) (Subjects 1 and 2) or with BioPlex 3D suspension array system (BIO-RAD) (Subject 3). All fluorescence intensities were subtracted of background signals, represented by the signal of the beads incubated with a transfection supernatant of an unrelated mAb or a supernatant of non-transfected cells. A standard curve with human IgG was made to extrapolate the mAbs concentration in the supernatants with a dynamic range between 1 ng/ml and 50 ng/ml. All signals were analyzed with Bio-Plex manager software (BIO-RAD). Supernatants with estimated IgG concentration ranging between 10 and 20 ng/µl and with an antigen-specific MFI greater than 5000, or with estimated IgG concentration greater than 20 ng/µl and an antigen-specific MFI greater than 10000, were deemed positive for that antigen. All supernatants analyzed with BioPlex 3D instrument showing antigen-specific MFI greater than 1000 were deemed positive for that antigen. With both instruments, in case of MFI < 1000, supernatants were deemed positive if relative concentration was <10 ng/µl (Supplementary Table 2).

Bacterial strains and growth conditions

The meningococcal and gonococcal strains used in this study are listed in Supplementary Tables 3 and 4 respectively. Bacteria were routinely grown overnight at 37°C on plates containing GC media with CO_2 for meningococcus strains, or on plates containing GC with 1% IsoVitaleX (BD Biosciences, 11798163) for gonococcal strains. Unless differently stated, the liquid growth conditions were the following: meningococcal bacteria were grown in Mueller-Hinton Broth (MHB) containing 0.25% (w/v) glucose until early log phase (OD_{600} of ~ 0.25). *N.gonorrhoeae* (*Ng*) strain FA1090 bacteria were grown at 37 °C in GC liquid medium supplemented with 1% IsoVitaleX and 1 µg/mL of CMP-NANA (Cytidine-5′-MonoPhospho-N-Acetyl NeurAminic acid sodium salt, Merck C8271) until mid-exponential phase.

OMV production and purification

N.meningitidis and *N.gonorrhoeae* strains were plated on GC agar plates or GC +1% IsoVitaleX, respectively. Plates were incubated overnight at 37°C in 5% CO_2. The following day, *N. gonorrhoeae* colonies were inoculated in 5 ml of GC + 1% IsoVitaleX + lactate and the growth was maintained for 28 h in 24 deep-well plate at 37°C with shaking at 350 rpm. *N.meningitidis* colonies were instead inoculated in 10 ml of Mueller-Hinton Broth at a starting optical density at 600 nm (OD_{600}) of ~0.05 and grown until OD_{600} of ~1.0-1.5 at 37°C. Then 10 ml were transferred in 50 ml of prewarmed slightly modified MCDMI medium and incubated at 37°C in 5% CO_2. OD_{600} was constantly monitored, and the growth was stopped when OD_{600} remained stable for 1.5 hours. Bacteria cultures were clarified by centrifugation for 60 min at 4000xg and the supernatants were subjected to high-speed centrifugation at 119000xg for 2 h at 4°C (Beckman Coulter Optima Ultracentrifuge). The pellets containing the OMV were washed with phosphate buffer saline (PBS), ultracentrifuged again as above and finally resuspended in PBS. OMV total protein content was quantified through the Lowry assay (DC Protein Assay, BioRad) following manufacturer's instructions.

Protein array design, generation, validation and hybridization

All the HumAbs produced and purified were tested for antigen identification on protein microarrays previously generated (16). In particular, the recombinant protein microarray encompassed 12 recombinant proteins spotted at 0.5 mg/ml in 40% glycerol along with the three recombinant meningococcal antigens of the 4CMenB vaccine (NHBA-GNA1030; GNA2091-fHbp and NadA at 0.5 mg/ml in 40% glycerol) while the vesicles protein chip contained 26 recombinant *E.coli* Generalized Modules for Membrane Antigens (GMMA) expressing meningococcal antigens and two GMMA empty (16) (Supplementary Figure 3A). The species-specific *N.meningitidis* and *N.gonorrhoeae* OMV array were printed with 18 different meningococcal (at 1.0 mg/ml or 0.5 mg/ml in 20% glycerol) and 23 gonococcal OMV (at 0.25 mg/ml in 20% glycerol). Controls consisted of 8 serial two-fold dilutions of human IgG (from 0.5 mg/ml to 0.004 mg/ml in 40% glycerol), unrelated proteins expressed and purified from *E. coli* following the same expression and purification protocol but originating from pathogens other than MenB (0.5 mg/ml in 40% glycerol), and PBS + 40% glycerol spots. Each sample was spotted randomly in replicates per array onto ultra-thin nitrocellulose coated glass slides (FAST slides; Maine Manufacturing Z721158). Printing was performed with the ink-jet spotter Marathon Argus (Arrayjet) (200 pl each spot) in a cabinet with controlled temperature and humidity (18 °C and 50–55%, respectively). To ensure efficient and reproducible protein immobilization a preliminary array validation was carried out. Preliminary experiments with mAbs showed that a range of 0.5-1 µg/ml corresponded to the best signal to noise ratio. For mAbs hybridization experiments, nonspecific binding was minimized by preincubating the slides with a blocking solution (BlockIt, ArrayIt BKT) for 1 hour. Purified mAbs were then diluted in Block-It buffer and overlaid for 1 h at room temperature prior to undergoing two washes with Tween 0.1% in PBS (TPBS). AlexaFluor 647-conjugated anti-human IgG secondary antibody (Jackson Immunoresearch, 115-605-174) diluted 1:800 was incubated for another hour, before proceeding with slide scanning. Fluorescence images were obtained using InnoScan 710 AL (Innopsys) and the images were generated with Mapix software at 10 µm/pixel resolution. ImaGene 9.0 software (Biodiscovery Inc.) was used to calculate spot fluorescence intensities while the microarray data analysis step was carried out with an in-house developed R script. For each protein the Mean Fluorescence Intensity (MFI) of replicates was obtained after the subtraction of local background values surrounding each spot. MFI greater than 5000, corresponding to the MFI of control protein spots after detection with fluorescent-labelled antibodies, plus ten times the standard deviation, were considered positive. MFI scores were ranked in four categories (1): high reactivity; MFI ≥ 30000; (2) medium reactivity; 15000 ≤ MFI < 30000; (3) low reactivity; 5000 ≤ MFI < 15000; (4) no reactivity; MFI < 5000.

Bactericidal activity assay

The bactericidal activity of the HumAbs against *N.meningitidis* strains was evaluated in a bactericidal assay with rabbit complement as previously reported (5). Briefly, meningococcal bacteria were grown in MHB containing 0.25% (w/v) glucose until early log phase (OD_{600} of ~ 0.25) and diluted in Dulbecco's Phosphate Buffered Saline (DPBS) containing 0.25% glucose and 0.1% BSA to the working dilution of 10^5 CFU/ml and incubated with serial two-fold dilutions of test monoclonal antibodies starting from either raw supernatants from TAP transfections diluted 1:4, or purified HumAbs at a concentration of 125 µg/ml with the addition of 25% baby rabbit complement (Cedarlane CL3441-R). Bactericidal activity of mAbs against *Ng* strain FA1090 was assessed with a similar approach. Bacteria were grown at 37 °C in GC liquid medium supplemented with 1% IsoVitaleX and 1 µg/mL of CMP-NANA until mid-exponential phase. Then bacteria were diluted in Dulbecco's Phosphate-Buffered Saline (DPBS, Sigma) containing 0.1% glucose and 1% BSA, to the working dilution of $1x10^3$ CFU/ml and incubated for 1h at 37°C with serial two-fold dilutions of test monoclonal antibodies and exogenous human complement, obtained from volunteer donors under informed consent, at 10% final concentration. After the incubation, 100 µl of GC medium plus 0.5% of Bacto Agar was added to the reaction mixture and incubated overnight at 37C° with 5% CO2. The day after, the plate well images were automatically acquired with a high throughput image analysis system and the Colony Forming Units (CFUs) were automatically counted for each well by an internally customized colony counting software. Bactericidal titers were defined as the monoclonal antibody concentration giving 50% decrease in CFU number compared to the reaction mixture, in the absence of antibodies.

LOS and protein immunostaining

To analyze LOS, meningococcal strains were grown in the same conditions utilized to perform bactericidal assay experiments. Once OD_{600} of ~0.25 was reached, 30 ml of culture were centrifuged at 2500xg for 15 minutes, washed with sterile-filtered PBS, and pelleted again. Bacterial pellets were boiled for 10 minutes at 100° C in reducing conditions (1x 1,4-dithioreitol, Sigma Aldrich 15508013) and equilibrated in LDS sample buffer 1x (ThermoFisher J61894) and 10 µl were loaded into 4-12% Bis Tris gel that was run at 120 V for 90 minutes. To analyze the proteins, the same preparation and running procedures were applied to 10 µg of each protein of interest loaded in the wells. Proteins and polysaccharides were transferred on a nitrocellulose membrane with iBlot (Invitrogen IB23001) and membranes, after 1h saturation in PBS - 10% BSA, were incubated overnight at 4°C with the antibodies for which the target was to assess. After 3 washes with PBS - 0.5% Tween20 (PBST) membranes were incubated with anti-human HRP conjugated polyclonal antibody (Invitrogen

A18817) for 1 hour at room temperature, washed three times with PBST and incubated for 5 minutes with Super signal west pico PLUS (ThermoFisher 34579). Chemiluminescent signals were acquired by ChemiDoc instrument (BIORAD) with auto optimal option.

Electron microscopy immunogold experiments

Meningococcal strains were grown in the same conditions utilized to perform bactericidal assay experiments. Once OD_{600} of ~0.25 was reached, 5 ml of culture were centrifuged at 2500xg for 15 minutes, washed with sterile-filtered PBS, and centrifuged again. Pelleted bacteria were then resuspended in 4% paraformaldehyde for 5 minutes at room temperature for fixation. The fixation buffer was then removed, and bacteria resuspended in PBS to a final OD_{600} of 1. Five µl of bacteria suspension were adsorbed to 300-mesh nickel grids, blocked in PBS containing 1% bovine serum albumin (BSA) and incubated with HumAbs at a concentration of 0.5 µg/ml in PBS, for 1 h. Grids were washed several times and incubated with 12-nm gold-labeled anti-human secondary antibody diluted 1:40 in PBS for 1 h. After several washes with distilled water the grids were air dried and analyzed using a TEM FEI Tecnai G2 spirit microscope operating at 120kV. The micrographs were acquired using a Tvips TemCam-F216.

FACS staining

Bacteria were pelleted at 2500xg for 15 minutes, washed and resuspended in an equal amount of sterile-filtered PBS. 50 µl of bacterial suspension were incubated for 1h at RT with 50 µl of each HumAb at a final concentration of 10 µg/ml. Bacteria were pelleted at 4000xg for 5 minutes, washed 2 times and resuspended in 100 µl of anti-Human IgG-FITC conjugated antibody (Invitrogen, cat. 31529) at the final concentration of 10 µg/ml diluted in PBS - 1% BSA - 0.5% Tween20. After 30 minutes incubation at room temperature, bacteria were washed twice, and fluorescent intensity was acquired by CANTOII Flow cytometer (Becton Dickinson). Signals were analyzed by FlowJo software (BD Biosciences), considering as positive bacteria with fluorescence intensity higher than the negative control, i.e. bacteria incubated only with secondary anti-Human IgG-FITC conjugated antibody.

Functional data clustering

The mAbs clustering, based on functional data, was performed using *ad-hoc* code developed in Python (v3.9.12) by using the *AgglomerativeClustering* function from the Scikit-learn (v0.24.1) package (https://scikit-learn.org/). To express a global measure of similarity for the functional activity of the 18 tested anti-PorB mAbs, binding and killing activity data were combined. Since the two data sources presented very different scales, they were pre-processed separately to transform data in the same range. MFI values from binding activity were scaled by computing the logarithm (base 10) and then normalized in the range by the Min-Max normalization. To describe the bactericidal activity, we started from the last detected value of positivity from the serial two-fold dilutions of the assay. We applied a logarithmic scale, with base 2, to get the number of dilution steps and, again, we normalized data in the range by the Min-Max scaling. The two datasets (binding and killing activity) were then merged to create a unique set of normalized features for each mAb. The distance matrix was computed by the Euclidean distance and the threshold for the hierarchical clustering was set to fall in the largest interval where the number of clusters remains constant when varying the threshold itself.

Sequence analysis and clustering

Sequence level properties of acquired HumAbs were analyzed after alignment against human Ig germlines downloaded from IMGT (https://www.imgt.org/) germline database (v202038-1). A first alignment of nucleotide sequences was performed by NCBI IgBLAST (v1.17.1) suite (44) to get V(D)J gene labeling and CDRs/FWRs regions annotation, together with the corresponding aminoacidic sequence translation. ANARCI (https://opig.stats.ox.ac.uk/webapps/newsabdab/sabpred/anarci/) was used to annotate equivalent antibody residue positions enabling the comparison of conserved amino acid residues in the hyper-variable CDRs loops following the canonical IMGT numbering scheme (45). Obtained annotations were used to cluster mAbs sequences in clonotypes having identical V-J genes and maximum 1 aa mismatch over 12 residues in CDR3 (46). We grouped sequences based on the heavy chain only, this one being usually assumed to contribute more to the epitope binding. All the data processing and clustering was performed in Python (v3.9.12) with the Scikit-learn (v0.24.1) package (https://doi.org/10.48550/arXiv.1201.0490). The Plotly (v5.9.0) package (https://plotly.com/) was used for visualization, while the clonotype network was realized with the NetworkX (v.2.6.3) package (https://networkx.org/).

Computational structure modeling and docking experiments

PorB forms trimer on the bacterial surface as well as in the available X-ray structure (PDB: 3VZT). The whole trimeric organization was used in the docking set up but only the monomer unit was considered as binding partner. Similarly, only the variable domain of the antibody was docked. The New Zealand 98/254 MenB PorB 3D structure was modeled with AlphaFold2 multimer protocol showing an RMSD of 2.68 Å compared to the experimental structure

publicly available (PDB: 3VZT) and highlighting the conformational variability of the loop regions. The HumAbs were modeled with DeepAb (47) by applying the default protocol.

We docked the 18 selected mAbs to the modeled trimeric PorB with version 2.4 of the HADDOCK software (48). The binding site on PorB was defined as the solvent-exposed loop regions with respect to the embedded transmembrane part. The paratope region of the selected mAbs was identified with Paragraph (49) and defined in HADDOCK as "active" while the epitope regions on PorB as "passive", meaning the paratope region needed to make contact with at least one of the PorB residues and there was no penalty if it didn't contact them all, allowing the HumAb to freely explore the binding loops. All three docking iterations (namely it0, it1, and water) were performed generating 1000, 400, and 200 poses respectively using the default values and scoring function. Clustering was performed based on backbone RMSD with a distance cutoff of 5 Å on the latest 200 generated poses. Finally, the lowest score was used to select the "best cluster" as the most antigen/antibody interaction representative.

Results

Isolation of plasmablasts from blood of 4CMenB vaccinees identifies 100 OMV-specific HumAbs

To interrogate the human B cell responses to the OMV component of 4CMenB, we screened Peripheral Blood Mononuclear Cells (PBMCs) from multiple subjects after vaccination with 4CMenB formulations for OMV-specific Plasmablasts (PBs). PBMCs from 56 adult subjects immunized with the 4CMenB vaccine formulations were collected 1 week after the last vaccine dose. The percentage of OMV-specific PBs in the total population of PBMCs from each subject was measured by ELISpot analysis. We observed some heterogeneity in the frequency of OMV-specific PBs among the different subjects, which ranged from more than 20% in a few subjects to less than 5% in half of the individuals (Supplementary Figure S1). We selected three subjects (Sbj 1-3) among those with the highest

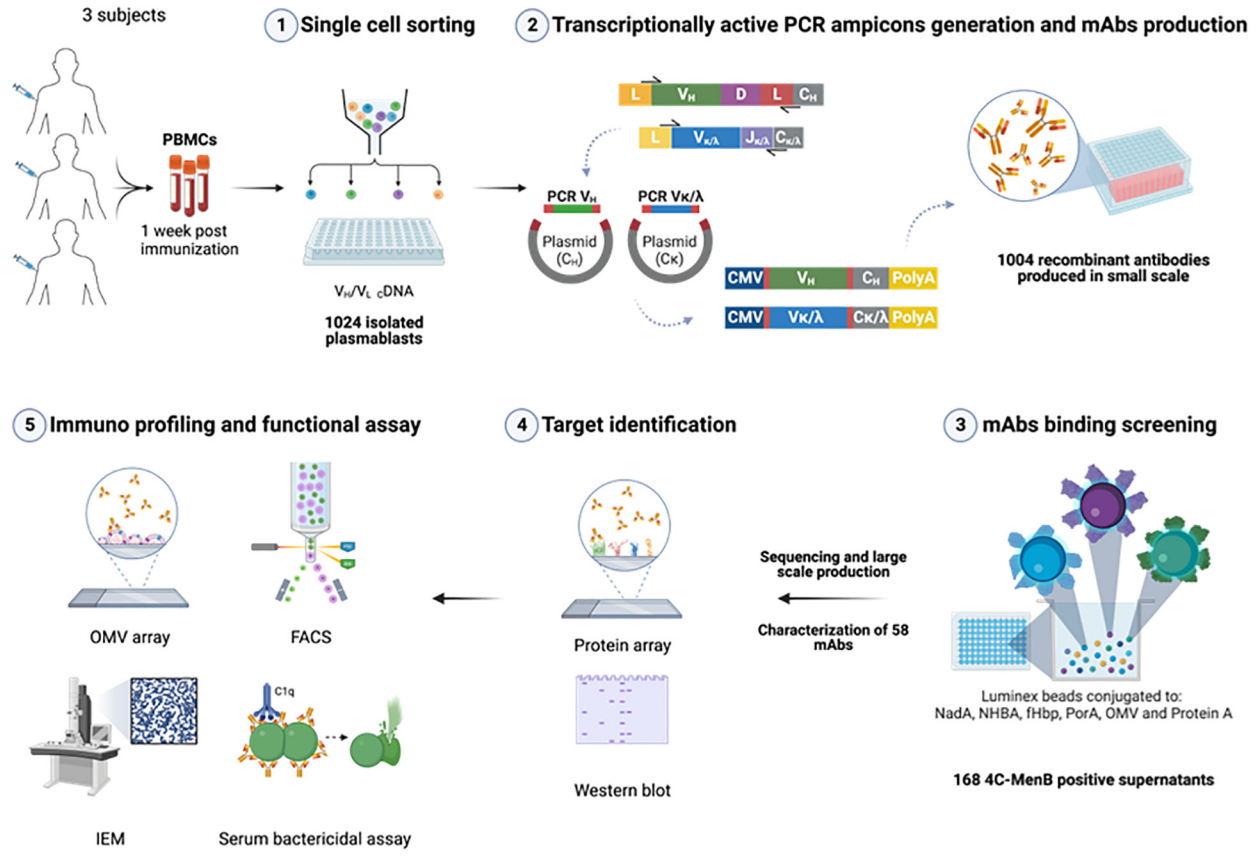

FIGURE 1
Exploitation of the human antibody repertoire induced by 4CMenB vaccination to elucidate the contribution of OMV component to cross-protection. Plasmablasts (PBs) isolated from blood of selected subjects 1 week after the last immunization were single cell sorted (1), retrotranscribed and IgG variable region of Heavy (VH) and Light (VL) chains were amplified and cloned into IgG1 expression plasmids. Minimal gene fragments to allow recombinant mAbs expression (transcriptionally active PCR amplicons, TAP) were amplified and used to co-transfect mammalian cell line Expi293 for small scale expression in 96w plates (2). Raw supernatants were tested in Luminex assay for IgG quantification and binding specificity of the expressed HumAbs (3). 100 OMV-specific HumAbs were sequenced and unique HumAbs were expressed at larger scale and 58 purified HumAbs were then tested on protein microarray and Western blot for target identification (4). HumAbs were further characterized and assessed for functionality with different approaches (5). Created in BioRender. Cinelli, P. (2025) https://BioRender.com/vbcb0d5.

frequency of OMV-specific PBs for which adequate PMBCs were recovered for the following analyses. Interestingly, Sbj1 and Sbj3 were immunized with the complete formulation of 4CMenB vaccine (rMenB + 25 μg OMV), while Sbj2 received the formulation containing ¼ of the OMV dose (rMenB + 6.25 μg OMV).

For the identification of 4CMenB-specific PBs and OMV-specific HumAbs we used the approach depicted in Figure 1. PBs were stained and sorted by flow cytometry, from PBMCs of each of the three subjects, as positive for CD27, CD38 and CD19 markers and negative for CD20 and IgD receptor and were isolated as single cells. The variable regions of paired heavy and light chains (VH and VL, respectively) were amplified from single PBs and ligated into linearized plasmids containing the constant chain of a human IgG1 and the constant chain of human Igk, respectively. The IgG1 constant chain included an Fc modification (E345R/E430G or E345R/E430G/S440Y, Hexabody) to enhance complement activation capability of mAbs (41) to increase the possibility of identifying functional HumAbs in our screening. In a second step, ligation products of paired VH/VL were further amplified to produce Transcriptionally Active PCR (TAP) fragments which were then used to transiently transfect the mammalian cell line Expi293 for small-scale expression of the recombinant HumAbs. Raw supernatants containing secreted antibodies were tested in two different Luminex binding assays: a mono-plex assay with Protein A beads, to quantify the total IgG content, and a multiplex assay with beads coated with fHbp, NHBA, NadA vaccine antigens, the OMV component and the PorA recombinant protein, to evaluate HumAb specificity for the different 4CMenB components. A total of 1024 PBs were sorted and their corresponding recombinant HumAbs were expressed with a success rate of 98%, as revealed by a concentration of IgG > 1 ng/ml measured in the supernatant of 1004 transfected cells. Among the 1004 IgG-positive supernatants screened, a total of 168, corresponding approximately to 16%, were positive for one of the 4CMenB components as determined by the multiplex 4CMenB component Luminex assay. The distribution of the overall and subject-related HumAb antigen specificity is depicted in Figure 2. Overall, 100 out of the 168 HumAbs (representing approximately 60% of 4CMenB-specific antibodies) resulted positive for OMV (Figure 2, green) and, quite surprisingly, only 11 of these recognized the recombinant PorA protein, commonly considered as the immunodominant antigen in the OMV (Figure 2, dashed green). The specificity of the remaining HumAbs was distributed among the recombinant

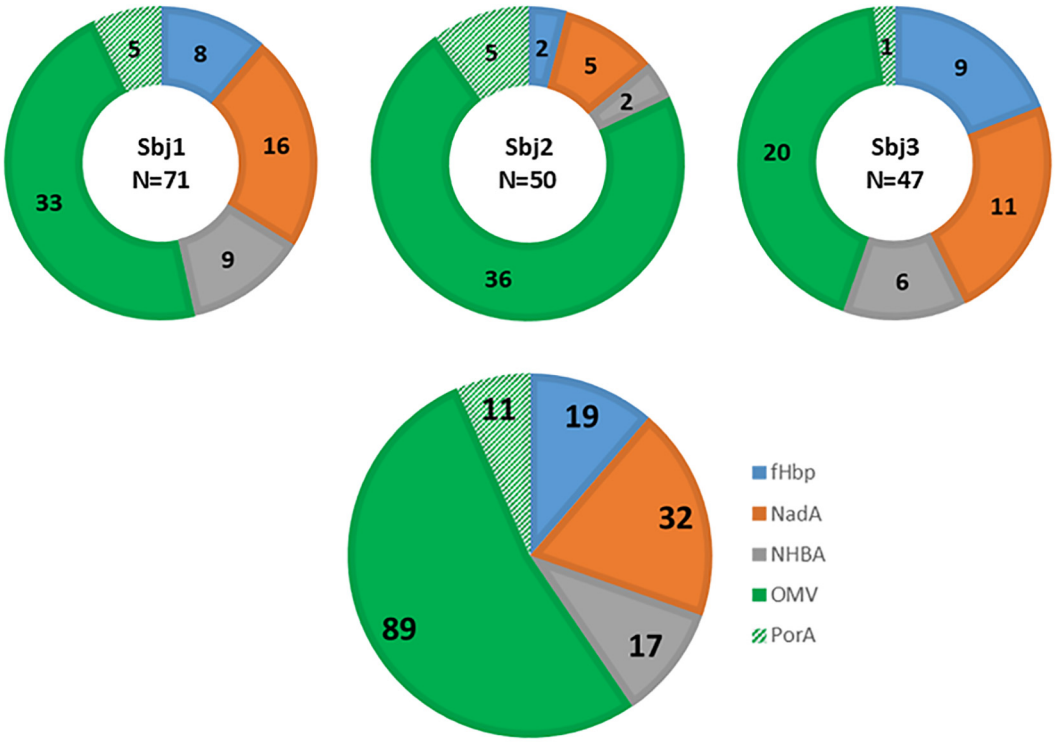

FIGURE 2
Luminex analysis of binding specificity of TAP-expressed recombinant HumAbs derived from PBs isolated from three subjects immunized with 4CMenB. Representation of specificity distribution of recombinant HumAbs for the 4 main antigen components as well as PorA (NadA, NHBA-GNA1030, GNA2091-fHbp, OMV, and recombinant PorA_P1.7 2.4), highlighted with different colors. Luminex beads were conjugated with each component (GNA2091-fHBP, blue; NHBA-GNA1030, grey; NadA; red, and OMV from NZ98/254, green; and the recombinantly expressed PorA, hashed green). Doughnut pies represent distribution and absolute numbers for each subject (N reported in the center of doughnut pies represents the total number of 4CMenB-specific mAbs identified for the subject). Pie chart represents the overall distribution and absolute numbers of the 168 4CMenB-specific HumAbs identified.

antigens present in 4CMenB, with a slight prevalence for anti-NadA mAbs (Figure 2, orange), in line with previous findings (5).

The entire set of OMV-positive supernatants, including those specific for PorA, was tested for functionality in a bactericidal assay, which measures the ability of the HumAbs to engage the complement on the surface of the bacterium resulting in bacterial lysis. The bactericidal assay was performed with two different meningococcal strains: NZ98/254, the isolate from which the OMV of 4CMenB are produced and which is the reference strain for the vaccine PorA protein (P1.7 - 2.4), and the strain M07576, mismatched for the PorA antigen (P1.22-2.14) and selected because of its high susceptibility to the OMV-mediated killing from human sera (16). These two strains were used to discriminate the PorA contribution to bacterial killing. Out of 100 raw supernatants tested, 29 showed bactericidal activity at a dilution ≥ 2 on the selected strains, including 6 of the 11 PorA-positive HumAb supernatants and 23 of the 89 OMV-specific supernatants (Supplementary Figure S2). In general, all the PorA-specific HumAbs with killing ability (Sbj1_mAb1, Sbj1_mAb23, Sbj1_mAb30, Sbj2_mAb9, Sbj2_mAb29 and Sbj3_mAb3) exhibited higher bactericidal activity towards NZ98/254 than M07576. The other non-bactericidal 5 supernatants were estimated at Luminex to have low levels of expressed IgG (Supplementary Table 2). On the contrary, all the other functional OMV-specific supernatants surprisingly showed no or low activity against the NZ98/254 strain, with the exception of Sbj1_mAb16, and higher bactericidal activity towards the M07576 strain, in line with the observation that these HumAbs recognize a non-PorA meningococcal antigen. We considered of lower interest HumAbs with high concentration in the supernatant (>10 ng/mL), low signal in the Luminex binding assay (<1000 MFI) and no bactericidal activity as raw supernatant. Based on this assumption, we prioritized a subset of 66 HumAbs for large-scale expression and purification, based on their positive activity in the bactericidal assay in supernatants and/or their relative binding signal on the vaccine OMV in the Luminex assay.

Specificity of 4CMenB-induced HumAbs revealed that PorB is a highly immunogenic OMV antigen able to induce bactericidal activity

To further investigate the specificity and functionality of the selected HumAbs, we cloned codon optimized gene fragments into expression vectors and attempted their production at larger scale. We successfully obtained 58 HumAbs in the recombinant form, including two out of the eight PorA-specific HumAbs. The specificity of the purified HumAbs was determined using a protein microarray previously described (16), encompassing approximately 30 of the most abundant proteins found in OMV vaccine lots. All the purified HumAbs were tested at a normalized concentration and results are summarized in Figure 3A and Supplementary Figure 3. A total of 26 out of the 58 HumAbs tested were able to recognize at least one antigen present on the protein microarray. In particular, the most recognized antigen was PorB, for which 18 antibodies resulted specific. The 2 HumAbs previously defined as anti-PorA were confirmed by microarray analysis able to recognize the PorA antigen either as recombinant or when expressed in GMMA. Finally, the antigens RmpM (NEIS1783), BamE (NEIS0196), PilW (NEIS1264), ComL (NEIS0653) and the hypothetical protein NEIS1065 were recognized by one single HumAb each, namely Sbj3_mAb16, Sbj3_mAb9, Sbj1_mAb22, Sbj3_mAb6 and Sbj3_mAb4 respectively (Figure 3A, Supplementary Figure 3). Interestingly, 12 HumAbs reacted positively only with the NZ98/254 OMV suggesting that the target antigen was not represented in the protein microarray, preventing its identification. Surprisingly, 22 of the tested HumAbs, almost 1/3, did not react with any specific antigen nor with the NZ98/254 OMV on the array, conflicting with the Luminex results (Supplementary Figure 2). We hypothesized, given the higher sensitivity of Luminex technique with respect to the protein array, that these 20 HumAbs might have a target with

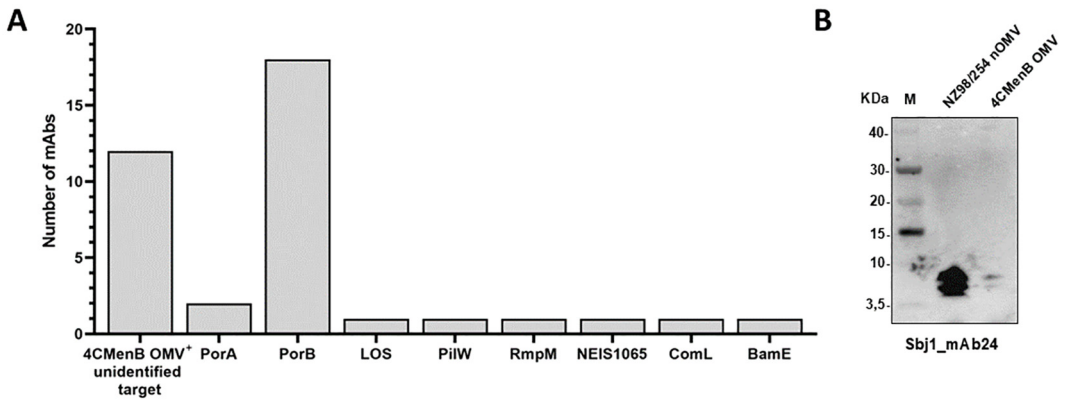

FIGURE 3
Identification of HumAbs cognate target by protein microarray and Western blot. **(A)** Representation of the targets identified by protein microarray and western blot analysis for 38 of the 58 tested HumAbs. Each bar represents the number of antibodies reactive for the specific antigen reported in the horizontal axis (numbers reported in **(A)** are derived from data described in Supplementary Figure S3). **(B)** Western blot analysis of the only LOS-specific identified HumAb, Sbj1_mAb24. The analysis has been performed on extracts from NZ98/254 nOMV and 4CMenB OMV, numbers on the left report the molecular weight of the Novex sharp pre-stained protein standard (M) represented in the first lane of the gel.

very low abundance in the OMV bacterial membrane and we did not investigate them any further.

When multiple positive signals were obtained for the same HumAb according to protein microarray screening, the specific target was confirmed by Western blot analysis performed with specific recombinant proteins, vaccine OMV (detergent extracted) and/or OMV naturally released in culture supernatants during bacteria growth and hereafter called nOMV (native outer membrane vesicles) (Supplementary Figure 3B). Interestingly, when the Sbj1_mAb24 was probed by Western blot it reacted with two low molecular weight bands in both OMV preparations (Figure 3B). This profile was compatible with the recognition of the meningococcal lipooligosaccharide (LOS), that normally run in SDS-page with apparent molecular weight between 3.5 and 10 kDa. In line with this, the bands were clearly visible in the nOMV preparation and barely detectable in the OMV sample, in which the LOS is largely lost due to the detergent extraction of the preparation.

In conclusion, the protein microarray and Western blot screening were instrumental in discovering the targets of 26 HumAbs identifying highly immunogenic antigens of the OMV able to trigger potentially protective immune responses.

PorB- and LOS-specific mAbs show bactericidal activity against a panel of MenB strains

In order to investigate the functional activity of 36 cloned recombinant antibodies, including the 12 OMV+ mAbs with unknown targets and the 24 mAbs with known non-PorA targets, a panel of 18 different meningococcal strains were selected (Supplementary Table 3). The 18 MenB strains have been previously shown to be susceptible to killing mediated by sera from 4CMenB vaccinees but the bactericidal activity was largely not expected to be mediated by the major antigenic vaccine components (fHbp, NHBA, NadA and PorA) as these strains are largely mismatched in the strain panel. In particular, 7 of the 18 strains (namely M07 0241084, M07576, M09929, M08389, M14569, M12898, and LNP24651) had previously shown susceptibility in SBA to sera from infants vaccinated with 4CMenB formulation but not with the rMenB formulation (fHbp, NHBA, and NadA only) and were recently reported to be suitable OMV-indicator strains (16). They include the PorB reference strains M07576 and M09929. Five strains from Argentina that were MATS negative but showed susceptibility to 4CMenB infant sera were included (50). In addition, NZ98/254 as PorA indicator strain and M13520 and M07463, M13547, M08129 and M18717 were included as they resulted susceptible in the serum bactericidal assay performed with sera from 4CMenB vaccinated subjects.

In order to test the reactivity of the 36 HumAbs to surface antigens across the entire panel of meningococcal isolates, we generated a multi-strain OMV microarray from the panel for high throughput simultaneous binding analysis with low amount of HumAb. Native OMV (nOMV) were purified from supernatants after bacterial growth and, following quality assessment, nOMV were spotted onto nitrocellulose-coated glass slides along with the NZ98/254 OMV component from 4CMenB as positive control. All the HumAbs were then tested for binding on this multi-strain microarray and their reactivity was assessed as mean fluorescence intensity (MFI) values on each OMV sample. Hybridization results are summarized in the heatmap of Figure 4A where almost all the tested mAbs showed a signal higher than the cut-off on at least one of the 18 nOMVs spotted on the array, exhibiting strain-specific binding profiles. Around 50% of HumAbs were highly cross-reactive, showing binding on most of the tested strains, even if with different intensities. Only the PilW- and ComL-specific mAb did not react with any OMV on the array.

Based on the results of the OMV array, the 36 mAbs with positive signals were tested for functionality in a bactericidal assay in presence of a rabbit complement source on the strains for which they showed recognition (Figure 4B). Six of the 12 mAbs with unidentified target showed no bactericidal activity on any of the tested strains, while the remaining 6 were able to kill at least 3 strains. The highest bactericidal activity across the panel of strains was observed with Sbj1_mAb16, exhibiting cross-killing on all of the 17 tested strains. The 5 HumAbs with known protein target (i.e. PilW, RmpM, BamE, ComL, and NEIS1065) did not show any bactericidal activity on the tested strains, while the LOS-specific HumAb Sbj1_mAb24 was able to mediate bactericidal killing on four of the five Argentinian strains tested. Interestingly, our analysis revealed that all the anti-PorB mAbs were able to kill at least one of the MenB strains tested, with the majority of HumAbs (12 out of 18) being cross-functional on more than 3 strains. Hierarchical clustering of the PorB-specific mAbs based on their binding and killing features revealed three major groups, as shown in Figure 4. Cluster 1, constituted by a single HumAb (Sbj2_mAb13) was able to kill all the MenB strains recognized on the OMV array. Cluster 2 included 6 HumAbs from Sbj1 and 1 HumAb from Sbj2, and while these mAbs recognized the majority of the strains on the OMV array they were able to kill only a subgroup of them which included most of the Argentinian strains tested. Cluster 3, composed of 10 HumAbs from subjects 2 and 3, whose mAbs were able to recognize a reduced number of strains on the array and to kill mainly the PorB reference strains M07576 and M09929. Overall, we observed that PorB HumAbs with similar cross-binding and cross-killing behaviors isolated from different subjects could be grouped by these features.

From this analysis, the correlation between OMV binding and the bactericidal activity on the corresponding strain of our HumAbs existed only for cluster 1 mAb, Sbj2_mAb13. The strains M07576 and M09929, that are considered reference strains for PorB-mediated killing were indeed recognized and killed by almost all the PorB-specific mAbs tested (except for Sbj3_mAb5, that did not show functional activity on M09929). However, we identified strains that were recognized by almost all HumAbs on the OMV array (such as M14569, M07 241084 and LNP24651) but were only killed by one HumAb in bactericidal assay. On the other hand, we identified some highly cross reactive mAbs (such as the mAbs in Cluster 2 and the Sbj3_mAb14 in Cluster 3) that were able to kill

10.3389/fimmu.2025.1565862

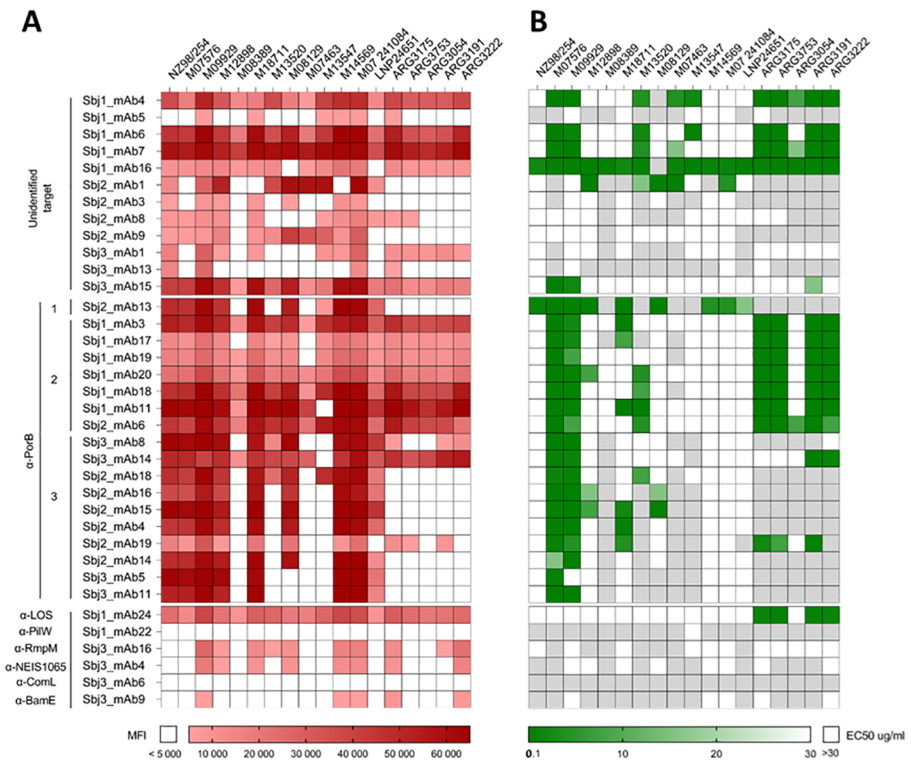

FIGURE 4
Binding and functional characterization of HumAbs on a panel of nOMV purified from 18 MenB strains. **(A)** Heatmap representing the reactivity (Mean Fluorescence Intensity, MFI) of the 36 purified HumAbs (12 OMV-specific with unknown target, 18 PorB-specific and 6 mAbs directed against OMV subdominant antigens) against native OMVs purified from the supernatant of 18 selected MenB strains. White boxes represent values below cut-off of positivity (MFI < 5000). **(B)** Heatmap representing the EC50 of each HumAb against the tested strain. White boxes indicate absence of bactericidal activity at the highest mAb concentration tested (30μg/ml) while light grey boxes indicate that mAbs were not tested on the relative strain.

only a subset of the recognized strains. This lack of consistency between binding to the OMV and killing of the corresponding strain for the PorB-specific mAbs could be ascribed to a low accessibility or density of the mAbs to PorB on the bacterial surface, suggesting that PorB *per se* might be accessible on the bacterial surface but in an epitope-dependent manner.

Characterization of PorB-specific mAbs binding on meningococcal strains

To further characterize the accessibility of the PorB protein on the bacterial surface of different meningococcal strains, we selected a subset of 13 PorB-specific mAbs, representative of the different behaviors observed, and analyzed 5 strains with different susceptibility to PorB-mediated killing by FACS surface staining experiments. Bacteria were collected in early exponential phase and incubated with the monoclonal antibodies. The binding of the mAbs to the different strains was then revealed using fluorescently labelled secondary antibodies. Secondary antibody alone, as well as an unrelated mAbs, were used as negative controls. As shown in Figure 5A, FACS experiments revealed not only that the accessibility of PorB is different among different strains, as we might expect, but also that the bacterial population in the same preparation is not homogeneous for the accessibility of this antigen. The strain M09929 was recently shown to be sensitive to PorB-dependent killing and, in line with this finding, all the mAbs but one (Sbj3_mAb5, not bactericidal on this strain) were able to bind the surface of this strain. On the contrary, the NZ98/254 strain, that shared an identical PorB (variant 3.42), was negative for the majority of the tested mAbs, in line with the already described low accessibility of PorB on this strain (16). The only HumAb tested able to bind more than 50% of the bacterial population for this strain was Sbj2_mAb13 (cluster 1), that resulted also the only one bactericidal on this strain. Interestingly, another 4 weakly FACS-positive mAbs on NZ98/254 were able to recognize less than 50% of bacteria after staining. The LNP24651 strain, that carried a different PorB variant (PorB 3.63) and was a strain resistant to PorB-mediated bactericidal killing with the mAbs identified in this study, was also poorly recognized by the HumAbs except for Sbj2_mAb13 (Cluster 1) which kills this strain. As for the strains M12898 (bearing a similar PorB3.63 to LNP24651), and M18711 (bearing a different PorB3 variant) the binding pattern observed in FACS with the panel of mAbs was more heterogeneous:

10.3389/fimmu.2025.1565862

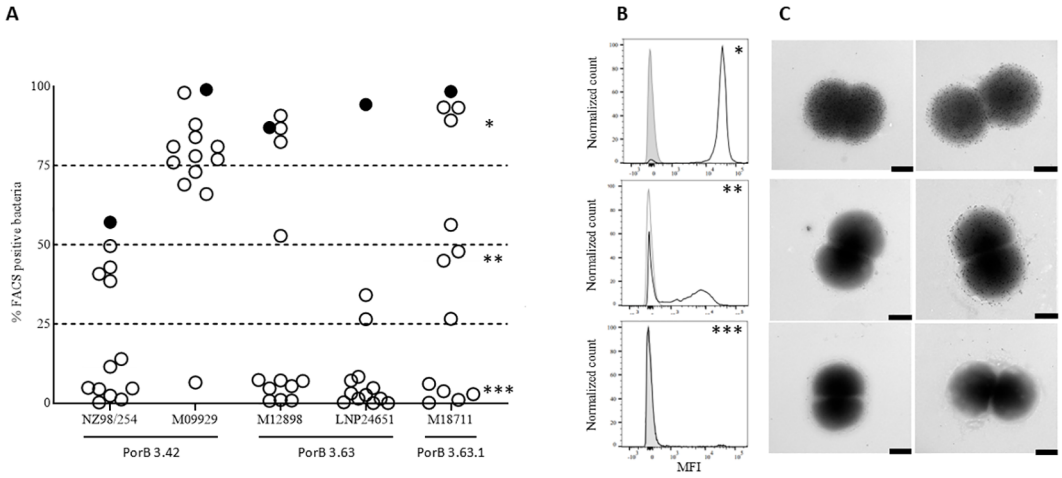

FIGURE 5
Accessibility of HumAbs epitopes on different MenB strains: **(A)** FACS analysis of 13 PorB-specific HumAbs binding to the surface of 5 MenB strains. On the X axis are reported the 5 different MenB strains and the PorB variant expressed. On the Y axis is reported, for each strain, the percentage of bacteria showing a fluorescence intensity superior to the secondary mAb alone when incubated with the different strains. Full circle represents the only HumAb belonging to Cluster 1 (Sbj2_mAb13). **(B)** Histograms showing the binding profile of 3 representative HumAbs on the MenB strain M18711 and identified by asterisks in panel A: the upper panel (*) shows the binding profile of a HumAb binding the surface of the whole bacterial population (Sbj2_mAb4); the central panel (**) shows the binding profile of a HumAb able to bind the surface of almost 50% of the bacterial population with good intensity, while the remaining 50% of the population is almost completely negative (Sbj3_mAb5); the lower panel (***) shows the binding profile of a HumAb not binding the selected strain (Sbj1_mAb19). **(C)** Immunogold analysis of the binding profile of 3 representative HumAbs on the MenB strain M18711: the upper panels shows the binding profile of a HumAb binding the surface of the whole bacterial population; the central panel shows the binding profile of a HumAb able to bind the surface of almost 50% of the bacterial population with good intensity, while the remaining 50% of the population is almost completely negative; the lower panel shows the binding profile of a HumAb not binding the selected strain. Two representative images are reported for each HumAb, black bar represents 100nm.

we observed the three representative binding patterns, 1) mAbs able to bind the entire bacterial population (*), 2) mAbs able to bind only a sub-population of bacteria, around 50% or less (**), and 3) mAbs that were largely negative (***) (Figure 5A). Figure 5B shows the MFI per count FACS scan for 3 mAbs with representative binding patterns on the strain M18711, highlighting the diverse FACS-positive subpopulation patterns. This different binding behavior of HumAbs was confirmed by immunoelectron microscopy (IEM) analysis (Figure 5C), in which we clearly see a mixed population of gold-particle coated or negative bacteria for the weakly FACS positive mAb with intermediate binding around 50% or less (**). This is indicative of a bi-phasic behavior in which bacterial subpopulations within the same strain exhibit binding or no-binding and interestingly this bi-phasic behavior is measured only for the cluster 2 and cluster 3 mAbs, and not for cluster 1 which binds highly and kills all strains tested. We interpret this biphasic behavior of the PorB mAbs to suggest that the accessibility of PorB epitopes on the surface of different meningococcal strains could be masked by other membrane components that seem subjected to phase variation.

VH4 and VH3 gene families dominate the PorB-specific mAbs repertoires

We analyzed the PorB mAbs of the three clusters identified by functional data clustering in terms of gene usage and sequence heterogeneity (Supplementary Table 5). To shed light on their sequence characteristics, we performed multiple sequence alignments of CDR3 regions (Figure 6A) and clonotype analysis of mutations and the variety of V-J genes pairing were sufficient to segregate the sequences into multiple clonotypes (Figure 6B). The 10 mAbs in cluster 3 showed high diversity both in terms of CDR3H aminoacidic sequence length and identity (Figure 6A) as well as diversity in VH gene usage (Figure 6B) since sequences are spread across VH1, VH3 and VH4 gene families. Three mAbs shared the same VH1-69 gene, one mAb used a different VH1 family gene (VH1-18) while the rest of members mainly used different VH3 family genes and one of VH4 family (VH4-30-4). Conversely, cluster 2 mAbs showed highly polarized VH usage and were all rearranged with the VH4-34 germline, often pairing with same light chain V gene (VL1-51) (Supplementary Table 5). Furthermore cluster 2 exhibit high CDR3H sequence similarity (Figure 6A). This may be related back to the origin of the monoclonals, with 6 out of the 7 sequences coming from the same donor Sbj1 and being identified by clonotype analysis as one large clonal family within the VH4-34 germline (Figure 6B).

In silico docking of PorB-specific HumAbs on NZ98/254 PorB model reveals different loops preferentially bound by the 3 clusters

To better understand the possible implications, in terms of physico-chemical and structural properties, of the observed

mutations, we decided to further investigate them through computational structure modeling and docking experiments. Given the results described before, we were interested in better defining the epitopes recognized by the diverse clusters of mAbs on PorB. With this aim, the 18 PorB-specific mAbs were further analyzed with an *in-silico* docking approach to the immunogen PorB protein of the NZ98/254 strain. The foundation for each docking analysis requires the molecular structures and as diverse PorB allele structures have been solved and characterized as trimeric (51–53), we employed AlphaFold2 Multimer to computationally predict a trimeric conformation of the NZ98/254 PorB allele. As shown in Figure 7A, the resulting model is a trimeric complex with 6 out of 8 loops located in the outward facing portion while loop2 and loop3 remain inside the ß-barrel, with the first located at the interface between the monomers. A total of eight regions were identified as potential binding sites, defined by the following aminoacidic positions: 39-46 (loop1), 81-95 (loop2), 113-143 (loop3), 164-176 (loop4), 197-210 (loop5), 234-249 (loop6), 270-284 (loop7) and 309-319 (loop8) (Figure 7A). For the structural prediction of the paratope region from each of the HumAb sequences, DeepAb, an AI algorithm specific for antibody modeling that provides a highly confident estimation of the CDR3 region, was used while the paratope region was predicted with Paragraph (54) on the generated models. Each of the 18 PorB mAbs paratope structures were docked to the modeled trimeric PorB with multiple iterations of the HADDOCK software, and the docking interface for each HumAb/PorB pair was identified as the functional cluster giving rise to the lowest energy pose and therefore the most representative antigen/antibody interaction. Figures 7B–D shows the docking analysis with individual histograms for the highest relative number of poses (Y axis) on each aminoacidic position of PorB (X axis) for the each HumAb from cluster 1 (Figure 7B),

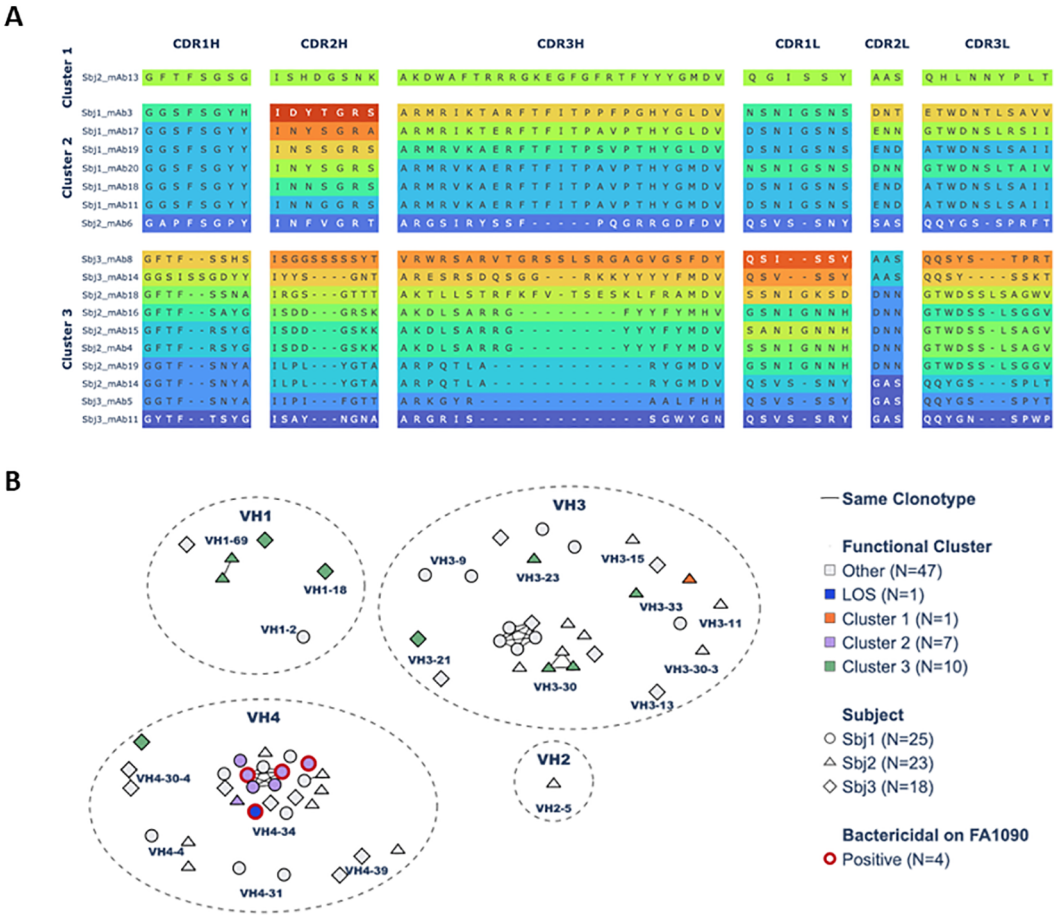

FIGURE 6
Sequence analysis of PorB-specific HumAbs: **(A)** Heavy and Light chain CDRs sequence alignment of PorB-specific HumAbs. Sequences are grouped according to the 3 identified functional clusters of the HumAbs and vertically ordered, inside the same cluster, according to length and similarity of the Heavy chain CDR3 (CDR3H). Different colors within each box differentiate CDRs with at least one mutation at residue level. Gap positions (-) are inserted according to ANARCI alignment at cluster level following IMGT numbering scheme. **(B)** Clonotypes network of HumAbs identified in this study in a 2D map representing Heavy chain sequences properties. HumAbs, each represented by an individual symbol, are closer in the map if they share the V family, V gene and J gene, as well as if they have similar CDR3 sequence. Symbols connected by a solid black line are assigned to the same clonotype. Groups of mAbs using the same Heavy chain V gene family are surrounded by a dashed circle reporting the corresponding family label. Orange, lilac and green color of each symbol indicates the functional cluster of the PorB-specific mAbs while blue identifies the LOS-specific mAb and grey identifies mAbs with other specificity. The shape indicates the subject from which each mAb has been isolated while the red edge line identifies mAbs resulted bactericidal against Gonococcus FA1090 strain.

cluster 2 (Figure 7C), and cluster 3 (Figure 7D), highlighting the loops with which they interact and the likely epitopes for each. The Sbj2_mAb13 HumAb (cluster 1) showed a preferential binding on the NZ98/254 PorB loop5 (Figure 7B) and the epitope is highlighted in Figure 7E (left panel). Binding profile analysis conducted on the best docking pose from mAbs from cluster 2, composed of mAbs that showed high sequence similarity for both heavy and light chain CDRs (Figure 6A), revealed a preferential interaction with the PorB loop7, that was bound by all HumAbs mostly as single loop (5/7 tested mAbs) or in combination with PorB loop3 (2/7 tested mAbs) (Figures 7C, E, central panel). The third cluster (Cluster 3) includes HumAbs exhibiting high sequence heterogeneity for both heavy and light chain CDRs (Figure 6A), and, not surprisingly, in silico docking revealed a mixed PorB binding profile (Figure 7D): the most representative group of mAbs (5/10) interacted with PorB loop8 alone or in combination with loop7; another group of mAbs (4/10) that interact with PorB loop7 alone or in interaction with loop6; and one that interacts with loop6 only. While the docking highlights

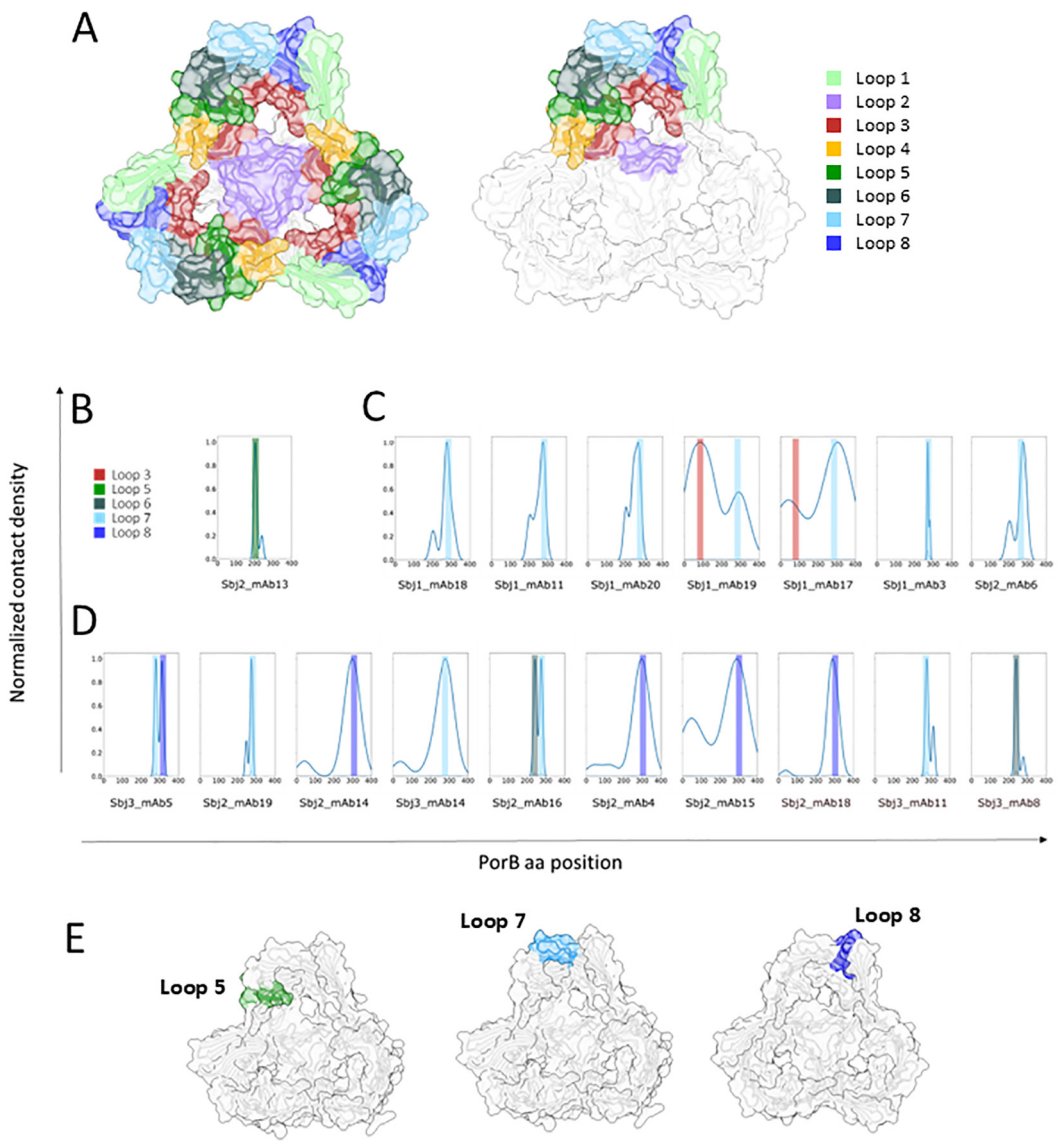

FIGURE 7
Representation of AF model of trimeric PorB NZ98/254 and in silico binding profile analysis of anti PorB HumAbs: **(A)** AF2 multimer model of PorB forming a trimer. The whole model is represented in white cartoon and surface while the 8 loops facing outwards the OM are highlighted with different colors on all the three monomers (left) or only on one monomer (right) to highlight the trimeric assembly of PorB. Loops are colored as follows: loop1 in light green, loop2 in medium purple, loop3 in brown, loop4 in orange, loop5 in green, loop6 in dark slate gray, loop7 in light blue and loop8 in dark blue. Binding profile analysis conducted on the best docking pose of each HumAb (reported below in the histogram) for each of the PorB HumAbs functional clusters: **(B)** cluster 1, **(C)** cluster 2, and **(D)** cluster 3. Histograms represent the relative number of poses (Y axis) for the individual HumAbs on each aminoacidic position (X axis), color bars highlight the interacting loop. **(E)** Structural models with the loops preferentially interacting with each HumAb cluster highlighted (loop5 for cluster 1 on the left, loop7 for cluster 2 in the middle and loop 8 for cluster 3 on the right).

10.3389/fimmu.2025.1565862

heterogeneity of the epitopes from this cluster, in line with the heterogeneity of the functional responses observed, the most representative epitope from this cluster, loop 8, is highlighted in Figure 7E (right panel).

PorB and LOS HumAbs are able to bind multiple gonococcal strains and are bactericidal against *Neisseriae gonorrhoeae* FA1090 strain

Our results suggest that HumAbs elicited by 4CMenB against PorB and LOS may enhance the breadth of coverage of this vaccine on meningococcal strains. To investigate whether HumAbs identified in our study against these antigens may be involved in the cross-protection against Gonococcus induced by 4CMenB vaccination in humans, we investigated binding and functional activity of the HumAbs against gonococcal strains. An OMV array printed with native OMVs purified from 23 different gonococcal strains, representative of both laboratory and circulating strains, was used to screen gonococcal surface antigen binding of a subset of 13 PorB-specific mAbs belonging to all the 3 clusters, together with the only LOS-specific mAb identified in this study. Five PorB mAbs belonging to clusters 1 and 2, and the LOS-specific HumAb, were able to recognize OMV derived from the selected *N.gonorrhoeae* strains (Figure 8A, red heatmap), with different binding profiles. Interestingly, cluster 1 did not show binding to OMV from the PorB1A strains in the panel (SK92-679, WHO-N and BG11), while some cluster 2 mAbs bound both PorB1B and PorB1A, and cluster 3 did not bind gonococcus OMV at all. We tested the ability of the 6 mAbs to kill the gonococcal strain FA1090 through a bactericidal assay performed with human serum as complement source. Three PorB-specific mAbs (from cluster 2) and the LOS-specific mAb showed bactericidal activity on FA1090 (Figure 8A, green heatmap), suggesting that PorB and LOS antibodies may cross-bind and kill gonococcal strains with cross-recognized epitopes adequately presented on their surface.

Identification of the LOS epitope bound by the 4CMenB-elicited by the Sbj1_mAb24 cross-functional mAb

LOS from meningococcus and gonococcus share partial similarity (55, 56) and consist of a lipid An anchor connected by a heptose (Hep) and KDO containing inner core to the outer oligosaccharide extensions. The biosynthesis of LOS in *Neisseria* spp is under the control of phase variable *lgt* genes (57) and can be synthesized with diverse oligosaccharide structures, depending on the complement of LOS biosynthetic genes expressed in each single bacterium (Figure 8B). While the γ-chain is constant, the *lgtG* phase-variable (PV) gene controls the β-chain glycan extension from the Hep2 core heptose and the PV *lgtA*, *lgtC* and *lgtD* genes control α-chain glycan extensions from the Hep1 core heptose and

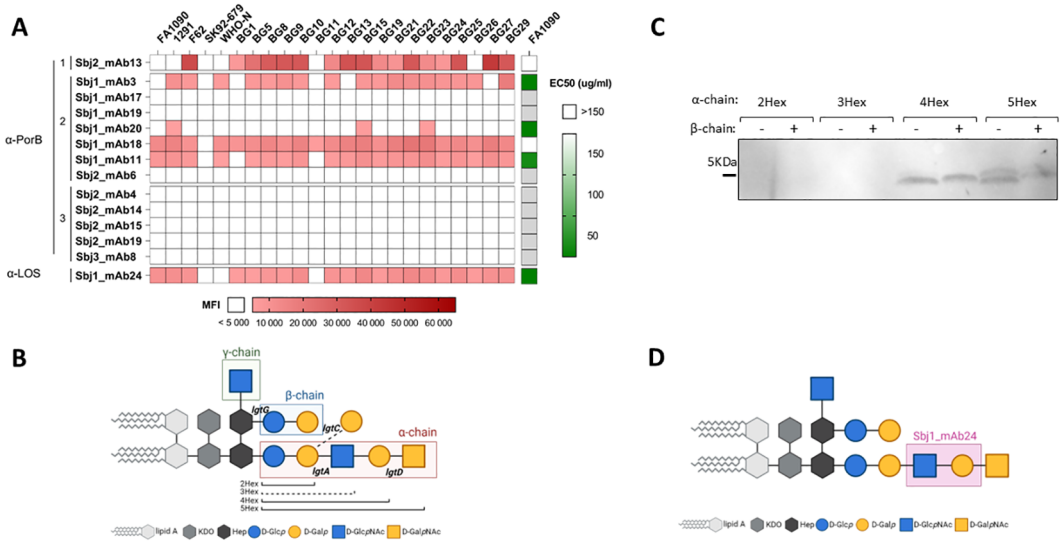

FIGURE 8
Characterization of HumAbs on *N.gonorrhoeae*: **(A)** Binding and functionality of PorB- and LOS-specific mAbs on gonococcus: red heatmap on the left represents the reactivity (MFI) of the 14 HumAbs (13 PorB specific and 1 mAb directed against LOS) against OMV from the 23 selected gonococcal strains. White boxes represent values below cut-off of positivity (MFI < 5000). Green heatmap on the right shows the EC50 of each mAb against FA1090 gonococcal strain. White boxes represent EC50 higher than the cut-off of 150 μg/ml, while light grey boxes indicate mAbs not tested in SBA. **(B)** Schematic representation of gonococcal LOS structures, with the 3 chains boxed with different colors and the relevant *lgt* genes involved in its biosynthesis reported in the respective attachment sites. The alternative α-chain, through activity of the *lgtC* gene, is highlighted by dotted line and nominated the 3Hex structure. **(C)** Binding profile of LOS-specific mAb Sbj1_mAb24 on a panel of 8 different gonococcal mutant strains on the MS11 genetic background, each one exposing largely a single LOS structures reported in the legend. **(D)** Identification of the putative epitope recognized by the LOS-specific mAb Sbj1_mAb24 based on the Western blot results. Created in BioRender. Cinelli, P. (2025) https://BioRender.com/9k43x2j.

depending on which *lgt* genes are expressed may be of variable length or consist of an alternate α-chain structure. As a result of PV *lgt* genes LOS structures expressed by *Neisserial* strains may vary considerably. In order to define the putative LOS epitope recognized by the specific Sbj1_mAb24 antibody, we performed Western blot analysis on 8 different MS11 gonococcal strains genetically engineered to express only one LOS structure (58). In each MS11 mutant strain, the phase variable *lgt* loci (*lgtA, C, D* and *G*) were genetically fixed either 'ON' or 'OFF' in different combinations giving rise to 8 possible glycan structures characterized by different number of hexose (Hex) sugars in the α-chain (2Hex, 3Hex, 4Hex and 5Hex), with or without the β-chain (β+ or β-, respectively) as represented in Figure 8B. Western blot analysis showed that the Sbj1_mAb24 HumAb was able to recognize LOS structures characterized by 4 or 5 hexoses in the α-chain (4Hex and 5Hex), regardless of the presence of the β-chain, while it did not cross-react with the shorter 2Hex and 3Hex structures (Figure 8C). This binding profile was consistent with the LOS structure present on the 4CMenB OMV component as the NZ98/254 MenB strain expresses mainly L1 and L3,7,9 LOS, the latter of which consists of the extended α-chain (7). We conclude that the specific epitope recognized by the Sbj1_mAb24 HumAb is likely contained in the extended α-chain mAb between the 2Hex and 4Hex structures and consisting of the GlcNAc–Gal sugar moiety, as highlighted in Figure 8D.

Discussion

Real world evidence from different countries have demonstrated that OMV-based vaccines can provide broader than expected protection against meningococcal disease (27) and moderate protection against gonorrhoeae (59). To assess the breadth of coverage of the OMV-based MenB vaccines, the immunogenicity profile of different OMV formulations have been analyzed and many OMV components other than PorA have been previously identified as immunogenic (16, 60, 61). Recent studies have focused on identifying the contribution of the OMV component of 4CMenB to the full extent of protection against different *N.meningitidis* strains (13, 16) as well as cross-reacting proteins in gonococcal strains (38). In this study, we isolated 36 OMV-specific HumAbs from sorted plasmablasts of three 4CMenB vaccinees in order to identify the target OMV antigens of antibodies that may be responsible for cross protection in humans. The dissection of their target specificity allowed us to identify, in addition to PorA, seven OMV immunogenic antigens, and among those already known - PorB, RmpM, BamE and LOS - we identified the novel immunogenic antigens NEIS1065, PilW and ComL proteins. Interestingly, while the target antigens of one third of the mAbs remain still unidentified, half of the characterized antibodies resulted specific to the Porin B, confirming that this antigen elicits strong responses in humans, unsurprisingly as it is the most abundant OMV antigen estimated around 40% of the total protein, as opposed to 25-30% measured for PorA of the OMV protein content (62). All 18 PorB HumAbs were bactericidal for at least one MenB strain in our OMV-indicator strain panel and, in addition, a single LOS HumAb was also identified as bactericidal. Therefore, through B cell cloning of HumAbs from plasmablasts collected 1 week after 4CMenB vaccination we identified PorB and LOS as antigens in the OMV that elicit functional bactericidal responses and likely contribute to cross protection across MenB strains. The identification of PorB as a bactericidal antigen of the OMV is in agreement with recent work by Viviani and co-authors, where both PorB and OpcA were identified as antigens eliciting responses contributing to the 4CMenB cross-coverage in humans, while NspA was able to mediate bactericidal killing in immunized mice. We did not however identify any HumAb specific for OpcA or NspA. The identification of 6 bactericidal HumAbs with unknown targets suggests that there may be other minor antigens contributing to 4CMenB protective responses in humans and in particular the highly cross-reactive Sbj1_mAb16 HumAb appears very interesting as it targets a common antigen across diverse MenB strains. However, we cannot exclude that these mAbs may recognize conformational epitopes that are not faithfully maintained in recombinantly produced proteins of the microarray or Western blot and these will be the focus of future studies.

The lack of functionality of the RmpM, BamE, NEIS1065, PilW or ComL specific mAbs, despite complement activation mutations included in the Fc portion of the recombinant antibodies, suggests that, although these OMV antigens are immunogenic in humans, their expression levels on bacterial surface may be insufficient to trigger, at least alone, the complement cascade leading to bacteriolysis. However, these antigens may contribute to cooperativity or synergy occurring in polyclonal responses following 4CMenB vaccination (13). We know indeed that the combination of multiple HumAbs, targeting the distinct fHbp and NHBA antigens, while not bactericidal alone, act synergistically in the killing when combined (5, 63).

Through hierarchical clustering of binding and functional behavior and *in silico* docking experiments of the 18 PorB HumAbs, we show that PorB in the OMV may have multiple immunodominant epitopes driving distinct antibody features. *In silico* docking analysis of the binding profile of each mAb suggested loop5, loop7 and loop8 on PorB as the prevalent targets of mAbs belonging to cluster 1, 2 and 3, respectively. Only the unique HumAb belonging to cluster 1 (Sbj2_mAb13) showed bactericidal activity for each of the strains to which it bound suggesting that its predicted epitope, loop5, is highly accessible on the bacterial surface of these strains. Conversely, FACS and EM data showed that the accessibility of epitopes bound by HumAbs belonging to clusters 2 and 3 was variable among different strains, even bearing the same allele of PorB, but also within the same bacterial population. These PorB HumAbs demonstrated biphasic behavior, either binding or not binding to distinct subpopulations within each strain, and as PorB itself is not phase variable the data suggest that loop7 and loop8 accessibility may be masked by another membrane component subject to phase-variation. This different accessibility of PorB on distinct strains has been reported previously (16, 64) and

the lack of epitope exposure has been hypothesized to be a shielding effect of the carbohydrate chains of LOS possibly combined with short extra-cellular loops in the PorB protein. Our data demonstrate that the shielding is phase variable and as such may be dependent on phase variable nature of LOS or indeed decorations such as phosphoethanolamine which is also known to be under phase variation (65). Importantly, different loops showed different accessibility in our experiments and the unique HumAb Sbj2_mAb13 from cluster 1 does not appear to exhibit this behavior, suggesting that not all epitopes of PorB may be susceptible to phase variable masking.

Interestingly, all the PorB-specific HumAbs belonging to cluster 2 and two of those belonging to cluster 3 were able to recognize and kill the Argentinian strains tested in this study, together with the LOS-specific mAb, suggesting that multiple non-PorA components of the OMV of 4CMenB contribute together to the cross-coverage of the vaccine on these strains. These strains belong to the ST-865 complex, which was reported by Efron and co-authors as susceptible to 4CMenB-induced killing despite the lack of coverage predicted by MATS (50). The MATS assay predicts the potential coverage of a strain based on the presence and sero-conservation of the 4 main vaccine antigens expressed in the strain and here we revealed that PorB and LOS responses elicited by the OMV may be responsible for the 4CMenB coverage of these strains. Real world evidence showed that protection conferred by 4CMenB is broader than what is predicted by current typing methods for circulating strains (11, 12) and has the potential to provide some protection beyond MenB disease (19) and cross-protecting responses to OMV antigens such as PorB and LOS may be responsible for some of this.

Multiple post-implementation surveillance studies revealed a decline in gonorrhea rates in subjects immunized with OMV-based meningococcal vaccines, such as 4CMenB and MeNZB, possibly due to cross-protection induced by similar components on the surface of meningococci and gonococci (19, 27, 30–33). Preclinical studies showed that antibodies induced by the OMV-based vaccine recognized gonococcal surface antigens (37) and 4CMenB immunization of mice accelerated clearance of the infection after gonococcal challenge (38). Our results show that despite only moderate homology (67% identity) between PorB3 of the OMV and gonococcus PorB1B, anti-PorB mAbs belonging to Cluster 2, together with the LOS-specific HumAb, could recognize several laboratory and circulating gonococcal strains (both PorB1A and PorB1B) and effect bactericidal activity against FA1090 gonococcus strain. While the serum bactericidal antibody assay is the "gold standard" for measuring serologic protection against *Neisseria meningitidis* (66), there is no such correlate of protection for gonococcus. However, the cross functional activity of these 4CMenB HumAbs suggests that these antigens could be implicated in the cross protection observed after vaccination with 4CMenB or indeed MeNZB against gonococcal infections. Complement-mediated killing has been implicated as important for protection against gonococcus, and the 2C7 mAb to LOS is bactericidal *in vitro* and has been shown to be protective in mouse models (67). The cross functional PorB HumAbs that result bactericidal against gonococcus were all members of a VH4-34 clonal family in cluster 2, all elicited from Sbj1. In a parallel study isolating OMV-specific HumAbs from memory B cells from 4CMenB vaccinees and selecting specifically for gonococcal-specific HumAbs, intriguingly the same 2 antigens PorB and LOS have been identified as the target antigens and all of the functional PorB HumAbs were from the VH4-34 germline (Troisi, Fabbrini et al., 2023, bioRxiv, https://www.biorxiv.org/content/10.1101/2023.12.07.570438v1). Therefore, despite interrogating a distinct B cell set (memory B cells as opposed to plasmablasts) from different subjects and using a distinct screening pipeline (gonococcal-specific mAbs instead of meningococcal-specific) both studies converged on similar results. Interestingly the LOS mAbs isolated from both studies appear to recognize distinct epitopes on the α-chain extended from the Hep1 core, which is within the L3,7,9 LOS immunotype expressed on the meningococcal 4CMenB OMV component. Both LOS and PorB antigens contribute to the ability of gonococci to resist complement-mediated killing through complement negative regulator engagement in gonococcus (68) and therefore targeting immune evasion mechanisms may be an important strategy in cross protection of 4CMenB and future gonococcal interventions.

The LOS HumAb isolated here with cross-functional bactericidal activity binds an epitope consisting of the third and fourth sugars on the α-chain extended from the Hep1 core. Interestingly, this epitope is distinct from the epitope recognized by the bactericidal and protective 2C7 mAb (69), which was isolated from hybridomas after immunization of mice with gonococcus. This epitope has been reported to be commonly present on gonococcus during human infection (8). 2C7 recognizes an epitope engaging the first 2 sugars of both the α-chain and β-chain (58). This suggests that the 4CMenB OMV may elicit cross-functional LOS antibodies and may be distinct from those that are induced by the gonococcus, that can cross react with gonococcal strains expressing similar LOS structures. Furthermore, we show here that the PorB HumAbs responses are multiple and predicted to have been elicited from multiple distinct epitopes, however only the polarized VH4-34 response in individuals leads to cross reactivity with gonococcus. There are some evidence from the literature that anti-LOS and anti-PorB responses in humans may be protective against gonococcus. In a study of human experimental gonococcal infection, male volunteers who mounted an anti-LOS response after gonococcal challenge were relatively resistant to re-infection with the homologous strain supporting a protective role for LOS antibodies (70). In a study in women with recurring gonococcal infections, women subsequently infected with a strain of the same PorB serotype were less likely to develop salpingitis, suggesting that PorB responses may provide serotype-specific protection against ascending gonococcal disease (71). Finally, retrospective analysis on a failed vaccine human challenge trial showed that the ratio of the concentration of PorB and LOS antibodies to that of Rmp antibody (PorB-Ab + LOS-Ab/Rmp-Ab) in the sera of the subjects was positively correlated with protection in both vaccine and placebo recipients (72).

In summary, this study along with others of its type are revealing interesting results on antigens and epitopes elicited by current vaccines such as 4CMenB, towards understanding the full potential for OMV-based meningococcal vaccines to confer broad protection against meningococcal disease and also against *N.gonorrhoeae* infection. Given the lack of correlates of protection against gonorrhea infection and slow progress in vaccine candidates, these findings were both reminiscent of early studies where anti PorB and LOS responses were investigated and intriguing for future gonococcal vaccine design.

Data availability statement

The data presented in this study are deposited in the NCBI's Gene Expression Omnibus repository, accession numbers GSE291727, GSE291733, GSE291737, GSE291739.

Ethics statement

The studies involving humans were approved by Bioethics Committee of the District Medical Doctors' Chamber in Krakow. The studies were conducted in accordance with the local legislation and institutional requirements. The participants provided their written informed consent to participate in this study.

Author contributions

GV: Conceptualization, Investigation, Writing – original draft, Writing – review & editing. VV: Investigation, Writing – original draft, Writing – review & editing. MA: Investigation, Writing – original draft, Writing – review & editing. AR: Investigation, Writing – original draft, Writing – review & editing. PC: Investigation, Writing – review & editing. NP: Investigation, Writing – review & editing. CL: Investigation, Writing – review & editing. LS: Investigation, Writing – review & editing. FG: Investigation, Writing – review & editing. SaT: Investigation, Writing – review & editing. GT: Investigation, Writing – review & editing. EFa: Investigation, Writing – review & editing. CS: Investigation, Writing – review & editing. SiT: Investigation, Writing – review & editing. AE: Writing – review & editing. AB: Writing – review & editing. OF: Writing – review & editing. ID: Conceptualization, Writing – review & editing. EFr: Conceptualization, Supervision, Writing – original draft, Writing – review & editing.

Funding

The author(s) declare that no financial support was received for the research and/or publication of this article.

Acknowledgments

The authors are grateful to Xin Wang and Henju Marjuki from the Centers for Disease Control and Prevention for providing the U.S. meningococcal serogroup B strains (M13520, M07576, M07463, M13547, M09929, M08389, M14569, M08129, M12898, M18711), Ray Borrow (Public Health England) for M07 0241084; E. Richard Moxon (University of Oxford, Oxford) for MC58; D.R. Martin (Institute of Environmental Science and Research, Porirua) for NZ98/254, and Dr. Darryl Hill (University of Bristol, United Kingdom) for providing BG strains and Dr. Sanjay Ram (University of Massachusetts, US) for providing MS11 LOS mutants. The authors also wish to thank Maria Teresa Curri and Francesca Papi (GSK, Italy) for their support in recombinant mAbs expression.

Conflict of interest

GV, VV, MA, AR, PC, NP, LS, FG, SiT, GT, EFa, CS, SaT, AB, ID, EFr are currently employees of the GSK group of companies. At the time of the study, GV was a PhD student at the University of Bologna funded by GSK. Authors NP, ID, OF and EFr hold shares in the GSK group of companies and declare no other financial and non-financial relationships and activities.

The remaining authors declare that the research was conducted in the absence of any commercial or financial relationships that could be construed as a potential conflict of interest.

The author(s) declared that they were an editorial board member of Frontiers, at the time of submission. This had no impact on the peer review process and the final decision.

Generative AI statement

The author(s) declare that no Generative AI was used in the creation of this manuscript.

Publisher's note

Supplementary material

The Supplementary Material for this article can be found online at: https://www.frontiersin.org/articles/10.3389/fimmu.2025.1565862/full#supplementary-material

References

1. Sierra GV, Campa HC, Varcacel NM, Garcia IL, Izquierdo PL, Sotolongo PF, et al. Vaccine against group B Neisseria meningitidis: protection trial and mass vaccination results in Cuba. *NIPH Ann*. (1991) 14:195–207.

2. Fredriksen JH, Rosenqvist E, Wedege E, Bryn K, Bjune G, Frøholm LO, et al. Production, characterization and control of MenB-vaccine "Folkehelsa": an outer membrane vesicle vaccine against group B meningococcal disease. *NIPH Ann*. (1991) 14:67–79.

3. Boslego J, Garcia J, Cruz R, Zollinger W, Brandt B, Ruiz S, et al. Efficacy, safety, and immunogenicity of a meningococcal group B (15:P1.3) outer membrane protein vaccine in Iquique, Chile. Chilean National Committee for Meningococcal Disease. *Vaccine*. (1995) 13:821–9. doi: 10.1016/0264-410X(94)00037-N

4. Holst J, Feiring B, Fuglesang E, Høiby EA, Nøkleby H, Aaberge IS, et al. Serum bactericidal activity correlates with the vaccine efficacy of outer membrane vesicle vaccines against Neisseria meningitidis serogroup B disease. *Vaccine*. (2003) 21:734–7. doi: 10.1016/S0264-410X(02)00591-1

5. Giuliani M, Bartolini E, Galli B, Santini L, Lo Surdo P, Buricchi F, et al. Human protective response induced by meningococcus B vaccine is mediated by the synergy of multiple bactericidal epitopes. *Sci Rep*. (2018) 8:3700. doi: 10.1038/s41598-018-22057-7

6. Martin DR, Ruijne N, McCallum L, O'Hallahan J, Oster P. The VR2 epitope on the PorA P1.7-2,4 protein is the major target for the immune response elicited by the strain-specific group B meningococcal vaccine MeNZB. *Clin Vaccine Immunol*. (2006) 13:486–91. doi: 10.1128/CVI.13.4.486-491.2006

7. Findlow J, Borrow R, Snape MD, Dawson T, Holland A, Tessa MJ, et al. Multicenter, open-label, randomized phase II controlled trial of an investigational recombinant Meningococcal serogroup B vaccine with and without outer membrane vesicles, administered in infancy. *Clin Infect Dis*. (2010) 51:1127–37. doi: 10.1086/656741

8. Snape MD, Dawson T, Evans A, Terssa MJ, Ohene-Kena B, Findlow J, et al. Immunogenicity of two investigational serogroup B meningococcal vaccines in the first year of life: a randomized comparative trial. *Pediatr Infect Dis J*. (2010) 29:e71–79. doi: 10.1097/INF.0b013e3181f59f6d

9. Esposito S, Prymula R, Zuccotti GV, Xie F, Barone M, Dull PM, et al. A phase 2 randomized controlled trial of a multicomponent meningococcal serogroup B vaccine, 4CMenB, in infants (II). *Hum Vaccin Immunother*. (2014) 10:2005–14. doi: 10.4161/hv.29218

10. Donnelly J, Medini D, Boccadifuoco G, Biolchi A, Ward J, Frasch C, et al. Qualitative and quantitative assessment of meningococcal antigens to evaluate the potential strain coverage of protein-based vaccines. *Proc Natl Acad Sci U.S.A*. (2010) 107:19490–5. doi: 10.1073/pnas.1013758107

11. Frosi G, Biolchi A, Lo Sapio M, Rigat F, Gilchrist S, Lucidarme J, et al. Bactericidal antibody against a representative epidemiological meningococcal serogroup B panel confirms that MATS underestimates 4CMenB vaccine strain coverage. *Vaccine*. (2013) 31:4968–74. doi: 10.1016/j.vaccine.2013.08.006

12. Martinón-Torres F, Banzhoff A, Azzari C, De Wals P, Marlow R, Marshall H, et al. Recent advances in meningococcal B disease prevention: real-world evidence from 4CMenB vaccination. *J Infect*. (2021) 83:17–26. doi: 10.1016/j.jinf.2021.04.031

13. Viviani V, Biolchi A, Pizza M. Synergistic activity of antibodies in the multicomponent 4CMenB vaccine. *Expert Rev Vaccines*. (2022) 21:645–58. doi: 10.1080/14760584.2022.2050697

14. Matthias KA, Reveille A, Connolly KL, Jerse AE, Gao YS, Bash MC. Deletion of major porins from meningococcal outer membrane vesicle vaccines enhances reactivity against heterologous serogroup B Neisseria meningitidis strains. *Vaccine*. (2020) 38:2396–405. doi: 10.1016/j.vaccine.2020.01.038

15. Arnold R, Galloway Y, McNicholas A, O'Hallahan J. Effectiveness of a vaccination programme for an epidemic of meningococcal B in New Zealand. *Vaccine*. (2011) 29:7100–6. doi: 10.1016/j.vaccine.2011.06.120

16. Viviani V, Fantoni A, Tomei S, Marchi S, Luzzi E, Bodini M, et al. OpcA and PorB are novel bactericidal antigens of the 4CMenB vaccine in mice and humans. *NPJ Vaccines*. (2023) 8:54. doi: 10.1038/s41541-023-00651-9

17. Biolchi A, De Angelis A, Moschioni M, Tomei S, Brunelli B, Giuliani M, et al. Multicomponent meningococcal serogroup B vaccination elicits cross-reactive immunity in infants against genetically diverse serogroup C, W and Y invasive disease isolates. *Vaccine*. (2020) 38:7542–50. doi: 10.1016/j.vaccine.2020.09.050

18. Biolchi A, Tomei S, Brunelli B, Giuliani M, bambini S, Borrow R, et al. 4CMenB immunization induces serum bactericidal antibodies against non-serogroup B meningococcal strains in adolescents. *Infect Dis Ther*. (2021) 10:307–16. doi: 10.1007/s40121-020-00370-x

19. Ruiz García Y, Sohn WY, Seib KL, Taha MK, Vázquez JA, de Lemos APS, et al. Looking beyond meningococcal B with the 4CMenB vaccine: the Neisseria effect. *NPJ Vaccines*. (2021) 6:130. doi: 10.1038/s41541-021-00388-3

20. Carter NJ. Multicomponent meningococcal serogroup B vaccine (4CMenB; Bexsero(®)): a review of its use in primary and booster vaccination. *BioDrugs*. (2013) 27:263–74. doi: 10.1007/s40259-013-0029-2

21. Hong E, Giuliani MM, Deghmane AE, Comanducci M, Brunelli B, Dull P, et al. Could the multicomponent meningococcal serogroup B vaccine (4CMenB) control Neisseria meningitidis capsular group X outbreaks in Africa? *Vaccine*. (2013) 31:1113–6. doi: 10.1016/j.vaccine.2012.12.022

22. Rivero-Calle I, Raguindin PF, Gómez-Rial J, Rodriguez-Tenreiro C, Martinón-Torres F. Meningococcal group B vaccine for the prevention of invasive meningococcal disease caused by neisseria meningitidis serogroup B. *Infect Drug Resist*. (2019) 12:3169–88. doi: 10.2147/IDR.S159952

23. Marshall HS, Andraweera PH, Wang B, McMillan M, Koehler AP, Lally N, et al. Evaluating the effectiveness of the 4CMenB vaccine against invasive meningococcal disease and gonorrhoea in an infant, child and adolescent program: protocol. *Hum Vaccin Immunother*. (2021) 17:1450–4. doi: 10.1080/21645515.2020.1827614

24. McMillan M, Wang B, Koehler AP, Sullivan TR, Marshall HS. Impact of meningococcal B vaccine on invasive meningococcal disease in adolescents. *Clin Infect Dis*. (2021) 73:e233–7. doi: 10.1093/cid/ciaa1636

25. Efron A, Biolchi A, Pereira CS, Tomei S, Campos J, De Belder D, et al. Bactericidal killing of meningococcal W strains isolated in Argentina by the sera of adolescents and infants immunized with 4-component meningococcal serogroup B vaccine (4CMenB). *Hum Vaccin Immunother*. (2023) 19:2288389. doi: 10.1080/21645515.2023.2288389

26. Whelan J, Kløvstad H, Haugen IL, Holle MR, Storsaeter J. Ecologic study of meningococcal B vaccine and neisseria gonorrhoeae infection, Norway. *Emerg Infect Dis*. (2016) 22:1137–9. doi: 10.3201/eid2206.151093

27. Petousis-Harris H, Paynter J, Morgan J, Saxton P, McArdle B, Goodyear-Smith F, et al. Effectiveness of a group B outer membrane vesicle meningococcal vaccine against gonorrhoea in New Zealand: a retrospective case-control study. *Lancet*. (2017) 390:1603–10. doi: 10.1016/S0140-6736(17)31449-6

28. Reyes Díaz LM, Lastre González MSJB, Cuello M, Sierra-González VG, Pupo RR, Lantero MI, et al. VA-MENGOC-BC vaccination induces serum and mucosal anti neisseria gonorrhoeae immune responses and reduces the incidence of gonorrhea. *Pediatr Infect Dis J*. (2021) 40:375–81. doi: 10.1097/INF.0000000000003047

29. Raccagni AR, Diotallevi S, Lolatto R, Bruzzesi E, Martearena Garcia MC, Mainardi I, et al. Breakthrough rectal neisseria gonorrhoeae infections after meningococcal B vaccination: microbiological and clinical features. *Open Forum Infect Dis*. (2024) 11:ofae562. doi: 10.1093/ofid/ofae562

30. Wang B, Giles L, Andraweera P, McMillan M, Almond S, Beazley R, et al. Effectiveness and impact of the 4CMenB vaccine against invasive serogroup B meningococcal disease and gonorrhoea in an infant, child, and adolescent programme: an observational cohort and case-control study. *Lancet Infect Dis*. (2022) 22:1011–20. doi: 10.1016/S1473-3099(21)00754-4

31. Abara WE, Bernstein KT, Lewis FMT, Schillinger JA, Feemster K, Pathela P, et al. Effectiveness of a serogroup B outer membrane vesicle meningococcal vaccine against gonorrhoea: a retrospective observational study. *Lancet Infect Dis*. (2022) 22:1021–9. doi: 10.1016/S1473-3099(21)00812-4

32. Bruxvoort KJ, lewnard JA, Cheng LH, Tseng HF, Chang J, Veltman J, et al. Prevention of neisseria gonorrhoeae with meningococcal B vaccine: A matched cohort study in southern california. *Clin Infect Dis*. (2023) 76:e1341–9. doi: 10.1093/cid/ciac436

33. Raccagni AR, Galli L, Spagnuolo V, Bruzzesi E, Muccini C, Bossolasco S, et al. Meningococcus B vaccination effectiveness against neisseria gonorrhoeae infection in people living with HIV: A case-control study. *Sex Transm Dis*. (2023) 50:247–51. doi: 10.1097/OLQ.0000000000001771

34. Marjuki H, Topaz N, Joseph SJ, Gernert KM, Kersh EN. Genetic similarity of gonococcal homologs to meningococcal outer membrane proteins of serogroup B vaccine. *mBio*. (2019) 10. doi: 10.1128/mBio.01668-19

35. Semchenko EA, Tan A, Borrow R, Seib KL. The serogroup B meningococcal vaccine bexsero elicits antibodies to neisseria gonorrhoeae. *Clin Infect Dis*. (2019) 69:1101–11. doi: 10.1093/cid/ciy1061

36. Leduc I, Connolly KL, Begum A, Underwood K, Darnnell S, Shafer WM, et al. The serogroup B meningococcal outer membrane vesicle-based vaccine 4CMenB induces cross-species protection against Neisseria gonorrhoeae. *PLoS Pathog*. (2020) 16:e1008602. doi: 10.1371/journal.ppat.1008602

37. Stejskal L, Thistlethwaite A, Ramirez-Bencomo F, Rashmi S, Harrison O, Feavers IM, et al. Profiling IgG and IgA antibody responses during vaccination and infection in a high-risk gonorrhoea population. *Nat Commun*. (2024) 15:6712. doi: 10.1038/s41467-024-51053-x

38. Tzeng YL, Sannigrahi S, Borrow R, Stephens DS. Neisseria gonorrhoeae lipooligosaccharide glycan epitopes recognized by bactericidal IgG antibodies elicited by the meningococcal group B-directed vaccine, MenB-4C. *Front Immunol*. (2024) 15:1350344. doi: 10.3389/fimmu.2024.1350344

39. Rappuoli R, Bottomley MJ, D'Oro U, Finco O, De Gregorio E. Reverse vaccinology 2.0: Human immunology instructs vaccine antigen design. *J Exp Med*. (2016) 213:469–81. doi: 10.1084/jem.20151960

40. Bidmos FA, Siris S, Gladstone CA, Langford PR. Bacterial vaccine antigen discovery in the reverse vaccinology 2.0 era: progress and challenges. *Front Immunol*. (2018) 9:2315. doi: 10.3389/fimmu.2018.02315

41. De Jong RN, Beurskens FJ, Verploegen S, Strumane K, Van Kampen MD, Voorhorst M, et al. A novel platform for the potentiation of therapeutic antibodies based on antigen-dependent formation of igG hexamers at the cell surface. *PLoS Biol*. (2016) 14:e1002344. doi: 10.1371/journal.pbio.1002344

42. Clargo AM, Hudson AR, Ndlovu W, Wootton RJ, Cremin LA, O'Dowd VL, et al. The rapid generation of recombinant functional monoclonal antibodies from individual, antigen-specific bone marrow-derived plasma cells isolated using a novel fluorescence-based method. *MAbs*. (2014) 6:143–59. doi: 10.4161/mabs.27044

43. Giuliani MM, Adu-Bobie J, Comanducci M, Aricò B, Savino S, Santini L, et al. A universal vaccine for serogroup B meningococcus. *Proc Natl Acad Sci U S A*. (2006) 103:10834–9. doi: 10.1073/pnas.0603940103

44. Ye J, Ma N, Madden TL, Ostell JM. IgBLAST: an immunoglobulin variable domain sequence analysis tool. *Nucleic Acids Res*. (2013) 41:W34–40. doi: 10.1093/nar/gkt382

45. Lefranc M-P, Pommié C, Ruiz M, Giudicelli V, Foulquier E, Truong L, et al. IMGT unique numbering for immunoglobulin and T cell receptor variable domains and Ig superfamily V-like domains. *Dev Comp Immunol*. (2003) 27:55–77. doi: 10.1016/S0145-305X(02)00039-3

46. Galson JD, Clutterbuck EA, Trück J, Ramasamy MN, Münz M, Fowler A, et al. BCR repertoire sequencing: different patterns of B-cell activation after two Meningococcal vaccines. *Immunol Cell Biol*. (2015) 93:885–95. doi: 10.1038/icb.2015.57

47. Ruffolo JA, Sulam J, Gray JJ. Antibody structure prediction using interpretable deep learning. *Patterns (N Y)*. (2022) 3:100406. doi: 10.1016/j.patter.2021.100406

48. Dominguez C, Boelens R, Bonvin AM. HADDOCK: a protein-protein docking approach based on biochemical or biophysical information. *J Am Chem Soc*. (2003) 125:1731–7. doi: 10.1021/ja026939x

49. Chinery L, Wahome N, Moal I, Deane CM. Paragraph—antibody paratope prediction using graph neural networks with minimal feature vectors. *Bioinformatics*. (2022) 39. doi: 10.1021/ja026939x

50. Efron A, Brozzi A, Biolchi A, Bodini M, Giuliani M, Guidotti S, et al. Genetic characterization and estimated 4CMenB vaccine strain coverage of 284 Neisseria meningitidis isolates causing invasive meningococcal disease in Argentina in 2010-2014. *Hum Vaccin Immunother*. (2024) 20:2378537. doi: 10.1080/21645515.2024.2378537

51. Massari P, King CA, MacLeod H, Wetzler LM. Improved purification of native meningococcal porin PorB and studies on its structure/function. *Protein Expression Purification*. (2005) 44:136–46. doi: 10.1016/j.pep.2005.04.021

52. Tanabe M, Nimigean CM, Iverson TM. Structural basis for solute transport, nucleotide regulation, and immunological recognition of *Neisseria meningitidis* PorB. *Proc Natl Acad Sci*. (2010) 107:6811–6. doi: 10.1073/pnas.0912115107

53. Bartsch A, Ives CM, Kattner C, Pein F, Diehn M, Tanabue M, et al. An antibiotic-resistance conferring mutation in a neisserial porin: Structure, ion flux, and ampicillin binding. *Biochim Biophys Acta Biomembr*. (2021) 1863:183601. doi: 10.1016/j.bbamem.2021.183601

54. Chinery L, Wahome N, Moal I, Deane CM. Paragraph-antibody paratope prediction using graph neural networks with minimal feature vectors. *Bioinformatics*. (2023) 39. doi: 10.1093/bioinformatics/btac732

55. Mandrell RE, Griffiss JM, Macher BA. Lipooligosaccharides (LOS) of Neisseria gonorrhoeae and Neisseria meningitidis have components that are immunochemically similar to precursors of human blood group antigens. Carbohydrate sequence specificity of the mouse monoclonal antibodies that recognize crossreacting antigens on LOS and human erythrocytes. *J Exp Med*. (1988) 168:107–26. doi: 10.1084/jem.168.1.107

56. Mubaiwa TD, Hartley-Tassell LE, Semchenko EA, Jen ECF, Srikhanta TN, Day CJ, et al. The glycointeractome of serogroup B Neisseria meningitidis strain MC58. *Sci Rep*. (2017) 7:5693. doi: 10.1038/s41598-017-05894-w

57. Jennings MP, Srikhanta YN, Moxon ER, Kramer M, Poolman JT, Kuipers B, et al. The genetic basis of the phase variation repertoire of lipopolysaccharide immunotypes in Neisseria meningitidis. *Microbiol (Reading)*. (1999) 145:3013–21. doi: 10.1099/00221287-145-11-3013

58. Chakraborti S, Lewis LA, Cox AD, St Michael F, Li J, Rice PA, et al. Phase-Variable Heptose I Glycan Extensions Modulate Efficacy of 2C7 Vaccine Antibody Directed against Neisseria gonorrhoeae Lipooligosaccharide. *J Immunol*. (2016) 196:4576–86. doi: 10.4049/jimmunol.1600374

59. Waltmann A, Chen JS, Duncan JA. Promising developments in gonococcal vaccines. *Curr Opin Infect Dis*. (2024) 37:63–9. doi: 10.1097/QCO.0000000000000992

60. Awanye AM, Chang CM, Wheeler JX, Chan H, Marsay L, Dold C, et al. Immunogenicity profiling of protein antigens from capsular group B Neisseria meningitidis. *Sci Rep*. (2019) 9:6843. doi: 10.1038/s41598-019-43139-0

61. Findlow J, Lucidarme J, Taha MK, Burman C, Balmer P. Correlates of protection for meningococcal surface protein vaccines: lessons from the past. *Expert Rev Vaccines*. (2022) 21:739–51. doi: 10.1080/14760584.2021.1940144

62. Tani C, Stella M, Donnarumma D, Biagini M, Parente P, Vada A, et al. Quantification by LC-MS(E) of outer membrane vesicle proteins of the Bexsero® vaccine. *Vaccine*. (2014) 32:1273–9. doi: 10.1016/j.vaccine.2014.01.011

63. Natali EN, Principato S, Ferlicca F, Bianchi F, Fontana LE, Faleri A, et al. Synergic complement-mediated bactericidal activity of monoclonal antibodies with distinct specificity. *FASEB J*. (2020) 34:10329–41. doi: 10.1096/fj.201902795R

64. Michaelsen TE, Aase A, Kolberg J, Wedge E, Rosenqvist E. PorB3 outer membrane protein on Neisseria meningitidis is poorly accessible for antibody binding on live bacteria. *Vaccine*. (2001) 19:1526–33. doi: 10.1016/S0264-410X(00)00324-8

65. Kandler JL, Holley CL, Reimche JL, Dhulipala V, Balthazar JT, Muszyński A, et al. The misR response regulator is necessary for intrinsic cationic antimicrobial peptide and aminoglycoside resistance in neisseria gonorrhoeae. *Antimicrob Agents Chemother*. (2016) 60:4690–700. doi: 10.1128/AAC.00823-16

66. Goldschneider I, Gotschlich EC, Artenstein MS. Human immunity to the meningococcus. II. Development of natural immunity. *J Exp Med*. (1969) 129:1327–48. doi: 10.1084/jem.129.6.1327

67. Gulati S, Beurskens FJ, De Kreuk B-J, Roza M, Zheng B, DeOliveira RB, et al. Complement alone drives efficacy of a chimeric antigonococcal monoclonal antibody. *PLoS Biol*. (2019) 17:e3000323. doi: 10.1371/journal.pbio.3000323

68. Lewis LA and Ram S. Complement interactions with the pathogenic Neisseriae: clinical features, deficiency states, and evasion mechanisms. *FEBS Lett*. (2020) 594:2670–94. doi: 10.1002/1873-3468.13760

69. Gulati S, McQuillen DP, Mandrell RE, Jani DB, Rice PA. Immunogenicity of Neisseria gonorrhoeae lipooligosaccharide epitope 2C7, widely expressed *in vivo* with no immunochemical similarity to human glycosphingolipids. *J Infect Dis*. (1996) 174:1223–37. doi: 10.1093/infdis/174.6.1223

70. Schmidt KA, Schneider H, Lindstrom JA, Boslego JW, Warren R, Van De Verg L, et al. Experimental gonococcal urethritis and reinfection with homologous gonococci in male volunteers. *Sex Transm Dis*. (2001) 28:555–64. doi: 10.1097/00007435-200110000-00001

71. Buchanan TM, Eschenbach DA, Knapp JS, Holmes KK. Gonococcal salpingitis is less likely to recur with Neisseria gonorrhoeae of the same principal outer membrane protein antigenic type. *Am J Obstet Gynecol*. (1980) 138:978–80. doi: 10.1016/0002-9378(80)91091-1

72. Rice PA, Shafer WM, Ram S, Jerse AE. Neisseria gonorrhoeae: drug resistance, mouse models, and vaccine development. *Annu Rev Microbiol*. (2017) 71:665–86. doi: 10.1146/annurev-micro-090816-093530

frontiers | Frontiers in Immunology

TYPE Original Research
PUBLISHED 02 May 2025
DOI 10.3389/fimmu.2025.1579163

OPEN ACCESS

EDITED BY
Fabio Fiorino,
LUM University Giuseppe Degennaro, Italy

REVIEWED BY
Patrícia Cc Neves,
Oswaldo Cruz Foundation, Brazil
Ritthideach Yorsaeng,
Chulalongkorn University, Thailand

*CORRESPONDENCE
Anna Casabianca
anna.casabianca@uniurb.it
Giuseppe Stefanetti
giuseppe.stefanetti@uniurb.it

†These authors have contributed equally to this work

RECEIVED 18 February 2025
ACCEPTED 08 April 2025
PUBLISHED 02 May 2025

CITATION
Torre D, Orlandi C, Conti I, Barocci S, Carlotti E, Magnani M, Casabianca A and Stefanetti G (2025) Analysis of humoral and cellular immune activation up to 21 months after heterologous and homologous COVID-19 vaccination.
Front. Immunol. 16:1579163.
doi: 10.3389/fimmu.2025.1579163

Analysis of humoral and cellular immune activation up to 21 months after heterologous and homologous COVID-19 vaccination

Davide Torre[1†], Chiara Orlandi[2,3†], Ilaria Conti[1], Simone Barocci[4], Eugenio Carlotti[5], Mauro Magnani[1,3], Anna Casabianca[2,3*†] and Giuseppe Stefanetti[1,2*†]

[1]Department of Biomolecular Sciences, University of Urbino Carlo Bo, Urbino, Italy, [2]Department of Biomolecular Sciences, Section of Biochemistry and Biotechnology, University of Urbino Carlo Bo, Fano, Italy, [3]Laboratorio Covid, University of Urbino Carlo Bo, Fano, Italy, [4]Department of Clinical Pathology, Azienda Sanitaria Territoriale (AST) di Pesaro-Urbino, Urbino, Italy, [5]Department of Prevention, Azienda Sanitaria Territoriale (AST) di Pesaro-Urbino, Urbino, Italy

To address the COVID-19 pandemic, diverse vaccination strategies, including homologous and heterologous schedules, were employed to enhance immune protection. This study evaluates the long-term humoral and cellular immune responses in individuals vaccinated with homologous (ChAdOx1-S/ChAdOx1-S [ChAd/ChAd]) and heterologous (ChAdOx1-S/BNT162b2 [ChAd/BNT]) schedules, followed by a third-dose mRNA booster (BNT162b2 [BNT] or mRNA-1273). Anti-Spike IgG titers were measured at 9-, 12-, and 21-months post-primary vaccination (corresponding to 3-, 6-, and 15-months post-booster), while SARS-CoV-2-specific B- and T-cell responses were assessed at 21-months post-booster. Antibody titers declined by 12-months post-primary vaccination, regardless of the third dose administered, and increased significantly by 21-months, potentially due to a fourth dose (BNT or mRNA-1273) or natural SARS-CoV-2 infection. The heterologous ChAd/BNT schedule elicited a stronger and more durable immune response than the homologous ChAd/ChAd, as evidenced by higher anti-Spike IgG titers, increased IgM-/IgG+ memory B-cell activation, and enhanced cytotoxic CD8+ T-cell cytokine expression in infected individuals. SARS-CoV-2 infection further boosted humoral and cellular responses, with infected individuals showing higher anti-Spike IgG titers and greater CD8+ T-cell activation compared to uninfected individuals. These findings highlight the benefits of heterologous vaccination schedules and the role of infection-driven immune activation, providing valuable insights for optimizing vaccination strategies to improve long-term immunity against SARS-CoV-2.

KEYWORDS

SARS-CoV-2, COVID-19, heterologous vaccine, anti-spike IgG response, T-cell response, B-cell response, long-term immunity, hybrid immunity

1 Introduction

The coronavirus disease 2019 [COVID-19] pandemic fundamentally transformed both the vaccine development process and global vaccination strategies to combat the rapid spread of Severe Acute Respiratory Syndrome Coronavirus 2 [SARS-CoV-2] and its associated mortality (1). Within less than a year, several vaccine platforms—including mRNA-based vaccines (e.g., Pfizer-BioNTech BNT162b2 [BNT] and Moderna [mRNA-1273]), viral vector vaccines (e.g., Oxford-AstraZeneca ChAdOx1-S nCoV-19 [ChAd]), and protein subunit vaccines (e.g., Novavax Nuvavoxid [NVX-CoV2373]) —were developed and received emergency use authorization, an unprecedented achievement in medical science (2). To address increasing public health concerns and supply chain constraints, novel vaccination strategies were adopted, based on current available vaccines. While many individuals received homologous vaccination schedules—using the same vaccine for both doses—others received heterologous schedules, combining different vaccine platforms (3, 4). Notably, heterologous vaccination has also been employed for booster doses, demonstrating improved neutralizing antibody titers and enhanced T-cell responses compared to homologous regimens (5). Despite these promising outcomes, the effectiveness and safety of different vaccine strategies continue to be closely monitored in real-time to evaluate immune response durability and identify adverse effects, such as vaccine-induced thrombosis with thrombocytopenia [VITT], which briefly halted the use of adenoviral vector vaccines like Janssen's COVID-19 vaccine (6, 7).

Previously, we conducted both cross-sectional and longitudinal analyses of humoral responses from a voluntary cohort in the northern Marche region of Italy (8, 9). In these studies, antibody levels against the SARS-CoV-2 spike [S] protein were compared among individuals who received homologous adenoviral-vector (ChAd/ChAd) or mRNA-based (BNT/BNT) vaccinations and those who received heterologous ChAd/BNT vaccinations. At two months post-primary vaccination, heterologous ChAd/BNT schedules elicited significantly higher anti-spike IgG titers than either homologous schedule (8). Follow-up analyses at four and six months confirmed the robustness of the immune response induced by heterologous schedules, in terms of both higher level and longer-lasting anti-S IgG response; despite a decline in IgG titers over time, which eventually resulted in comparable antibody levels between ChAd/BNT and BNT/BNT groups. Finally, focusing on clinical variables such as sex, age, smoking and body mass index, we observed that only the vaccine schedule influenced anti-S IgG titers at all time points (9).

Building on this foundation, the current study shifts focus on the impact of third dose (booster) mRNA vaccinations and long-term immunity. Approximately six months after primary immunization, participants received a booster dose (BNT or mRNA-1273). This study evaluates the long-term humoral and cellular responses following booster administration, measuring anti-S IgG levels at 9-, 12-, and 21-months post-primary vaccination (corresponding to 3-, 6-, and 15-months post-booster). Cellular immune responses, including T- and B-cell activation, were assessed at 21-months post-primary vaccination (15 months post-booster) to understand the role of vaccination schedules and infection-driven immune activation. The study also investigates the impact of natural SARS-CoV-2 infection on immune system activation. These analyses aim to provide a comprehensive understanding of how different vaccination strategies shape both humoral and cellular immunity over an extended period and contribute to the growing body of evidence informing optimal COVID-19 vaccination strategies.

2 Materials and methods

2.1 Recruitment and study cohort characteristics

The study participants (n = 203) were recruited among personnel from the University of Urbino, Carlo Bo (Urbino (PU), Italy), vaccinated against COVID-19 between December 2020 and June 2021, and that subsequently received a third (booster) dose administration (BNT162b2 or mRNA-1273) between October 2021 and January 2022. These individuals were a subset of a larger cohort previously studied for their humoral response to COVID-19 vaccination (8, 9). Follow up evaluations were conducted at 3 months (n = 195), 6 months (n = 173) and 15 months (n = 99) after booster immunization. These time points corresponded to approximately 9, 12 and 21 months after the primary immunizations (Table 1, Supplementary Table S1, Supplementary Figure S1). Overall, 87 individuals completed assessments at all three time points (9, 12 and 21 months after the primary immunizations), 90 participants attended two time points, and 26 individuals provided samples at a single time point (Supplementary Figure S2, Supplementary Table S2). In addition, a small subset of the cohort (20/203), between August 2021 and January 2023, also received a fourth vaccine dose, with differences observed based on vaccination schedules (Supplementary Table S3). Serological samples were obtained at each time point for humoral response analysis (Table 1A), while cellular response analyses (antigen-specific B- and T-cells) were conducted using samples collected at 21 months after the primary immunizations (Table 1B).

Additional subgrouping included participants with a confirmed SARS-CoV-2 infection during the study period (Supplementary Figure S3). Participants were classified as N+ (nucleocapsid-positive) if they tested positive for SARS-CoV-2 nucleocapsid-specific IgG and/or IgM antibodies, or N-(nucleocapsid-negative). Infection rates increased significantly from 9 to 21 months, with variations observed based both on vaccination schedules and booster types, particularly at both 12 and 21 months, where the group ChAd/BNT/mRNA-1273 showed the highest percentage of infected individuals (63.6% and 83.3%, respectively) (Supplementary Figure S3, Supplementary Table S4). None of the participants declared reinfection during the study period.

10.3389/fimmu.2025.1579163

TABLE 1 Demographic characteristics of participants in humoral and cellular analyses.

A. Subjects involved for humoral analysis						
Vaccine schedule				9 months	12 months	21 months
Primary	Booster					
All	Total	Gender Age BMI	Male Years, median (IQR) Median (IQR)	*n* = 195 88/195 (45.1%) 55.0 (26.0-72.0) 24.1 (16.2-37.6)	*n* = 173 74/173 (42.8%) 55 (31-72) 24.1 (37.6-16.2)	*n* = 99 39/99 (39.4%) 56.0 (32.0-72.0) 24.2 (16.2-37.3)
	mRNA-1273	Gender Age BMI	Male Years, median (IQR) Median (IQR)	*n* = 127 (65.1%) 59/127 (46.5%) 55.0 (26.0-71.0) 24.1 (16.2-37.6)	*n* = 116 (67.1%) 51/116 (44.0%) 55.0 (31.0-70.0) 24.0 (16.2-37.6)	*n* = 62 (62.6%) 26/62 (41.9%) 57.0 (32.0-69.0) 24.4 (16.2-37.3)
	BNT	Gender Age BMI	Male Years, median (IQR) Median (IQR)	*n* = 68 (34.9%) 29/68 (42.6%) 53.0 (32.0-72.0) 24.2 (19.0-36.7)	*n* =57 (32.9%) 23/57 (40.4%) 54.0 (32.0-72.0) 24.4 (19.0-36.7)	*n* = 37 (37.4%) 13/37 (35.1%) 55.0 (32.0-72.0) 24.0 (19.0-36.7)
ChAd/ChAd	Total	Gender Age BMI	Male Years, median (IQR) Median (IQR)	*n* = 134 (68.7%) 88/134 (65.7%) 55.0 (30.0-72.0) 24.0 (16.2-37.6)	*n* = 124 (71.7%) 57/124 (46.0%) 55.0 (31.0-72.0) 24.1 (16.2-37.6)	*n* = 69 (69.7%) 29/69 (42.0%) 57.0 (32.0-72.0) 24.5 (16.2-37.3)
	mRNA-1273	Gender Age BMI	Male Years, median (IQR) Median (IQR)	*n* = 111 (65.1%) 52/111 (46.8%) 56.0 (30.0-71.0) 24.0 (16.2-37.6)	*n* = 105 (67.1%) 48/105 (45.7%) 55.0 (31.0-70.0) 23.8 (16.2-37.6)	*n* = 56 (62.6%) 24/56 (42.9%) 57.0 (32.0-69.0) 24.4 (16.2-37.3)
	BNT	Gender Age BMI	Male Years, median (IQR) Median (IQR)	*n* = 23 (34.9%) 9/23 (39.1%) 55.0 (32.0-72.0) 24.5 (19.5-36.2)	*n* = 19 (32.9%) 9/19 (47.4%) 55.0 (37.0-72.0) 25.1 (20.5-36.2)	*n* = 13 (37.4%) 5/13 (38.5%) 60.0 (36.0-72.0) 25.3 (19.5-36.2)
ChAd/BNT	Total	Gender Age BMI	Male Years, median (IQR) Median (IQR)	*n* = 61 (31.3%) 27/61 (44.3%) 53.0 (26.0-62.0) 24.3 (18.7-36.7)	*n* = 49 (28.3%) 17/49 (34.7%) 54.0 (32.0-61.0) 24.1 (18.7-36.7)	*n* = 30 (30.3%) 10/30 (33.3%) 54.5 (32.0-61.0) 23.4 (18.7-36.7)
	mRNA-1273	Gender Age BMI	Male Years, median (IQR) Median (IQR)	*n* = 16 (65.1%) 7/16 (43.8%) 54.5 (26.0-61.0) 25.5 (18.7-35.6)	*n* = 11 (67.1%) 3/11 (27.3%) 55.0 (45.0-61.0) 25.4 (18.7-35.6)	*n* = 6 (62.6%) 2/6 (33.3%) 56.5 (45.0-61.0) 23.8 (18.7-33.5)
	BNT	Gender Age BMI	Male Years, median (IQR) Median (IQR)	*n* = 45 (34.9%) 20/45 (44.4%) 52.0 (32.0-62.0) 24.0 (19.0-36.7)	*n* = 38 (32.9%) 14/38 (36.8%) 53.0 (32.0-60.0) 23.8 (19.0-36.7)	*n* = 24 (37.4%) 8/24 (33.3%) 53.5 (32.0-60.0) 23.4 (19.0-36.7)

B. Subjects involved for cellular analysis					
Vaccine schedule				B-cells	T-cells
Primary	Booster				
All	Total	N. of individuals (% on total)		*n* = 23 (23.2%)	*n* =24 (24.2%)
		Gender	Male	10/23 (43.5%)	11/24 (45.8%)
		Age	Years, median (IQR)	55.0 (32.0-67.0)	54.5 (32.0-67.0)
		BMI	Median (IQR)	24.0 (18.1-30.2)	23.8 (18.1-30.2)
	mRNA-1273	N. of individuals (% on total)		*n* = 10 (10.1%)	*n* = 11 (11.1%)
		Gender	Male	5/10 (50.0%)	6/11 (54.5%)
		Age	Years, median (IQR)	54.5 (32.0-67.0)	54.0 (32.0-67.0)

(Continued)

10.3389/fimmu.2025.1579163

TABLE 1 Continued

B. Subjects involved for cellular analysis					
Vaccine schedule				B-cells	T-cells
Primary	Booster				
		BMI	Median (IQR)	25.1 (18.1-30.2)	24.8 (18.1-30.2)
	BNT	N. of individuals (% on total)		*n* = 12 (12.1%)	*n* = 12 (12.1%)
		Gender	Male	4/12 (33.3%)	4/12 (33.3%)
		Age	Years, median (IQR)	55.5 (36.0-66.6)	55.5 (36.0-66.6)
		BMI	Median (IQR)	23.6 (19.0-28.3)	23.6 (19.0-28.3)
ChAd/ChAd	Total	N. of individuals (% on total)		*n* = 12 (12.1%)	*n* = 12 (12.1%)
		Gender	Male	7/12 (58.3%)	7/12 (58.3%)
		Age	Years, median (IQR)	53.0 (32.0-67.0)	53.0 (32.0-67.0)
		BMI	Median (IQR)	24.3 (18.1-30.2)	24.3 (18.1-30.2)
	mRNA-1273	N. of individuals (% on total)		*n* = 7 (7.1%)	*n* = 7 (7.1%)
		Gender	Male	4/7 (57.1%)	4/7 (57.1%)
		Age	Years, median (IQR)	52.0 (32.0-67.0)	52.0 (32.0-67.0)
		BMI	Median (IQR)	26.3 (18.1-30.2)	26.3 (18.1-30.2)
	BNT	N. of individuals (% on total)		*n* = 4 (4.0%)	*n* = 4 (4.0%)
		Gender	Male	2/4 (50.0%)	2/4 (50.0%)
		Age	Years, median (IQR)	58.0 (36.0-66.0)	58.0 (36.0-66.0)
		BMI	Median (IQR)	22.3 (19.5-24.5)	22.3 (19.5-24.5)
ChAd/BNT	Total	N. of individuals (% on total)		*n* = 11 (11.1%)	*n* = 12 (12.1%)
		Gender	Male	3/11 (27.3%)	4/12 (33.3%)
		Age	Years, median (IQR)	55.0 (51.0-58.0)	55.0 (51.0-58.0)
		BMI	Median (IQR)	23.1 (18.7-28.3)	22.7 (18.7-28.3)
	mRNA-1273	N. of individuals (% on total)		*n* = 3 (3.0%)	*n* = 4 (4.0%)
		Gender	Male	1/3 (33.3%)	2/4 (50.0%)
		Age	Years, median (IQR)	58.0 (55.0-58.0)	56.5 (52.0-58.0)
		BMI	Median (IQR)	20.2 (18.7-25.4)	21.2 (20.2-25.4)
	BNT	N. of individuals (% on total)		*n* = 8 (8.1%)	*n* = 8 (8.1%)
		Gender	Male	2/8 (25.0%)	2/8 (25.0%)
		Age	Years, median (IQR)	54.5 (51.0-58.0)	54.5 (51.0-58.0)
		BMI	Median (IQR)	24.2 (19.0-28.3)	24.2 (19.0-28.3)

ChAd/ChAd refers to the ChAdOx1 COVID-19 vaccine [ChAd] administered as both the first and second doses (primary immunization), while ChAd/BNT refers to ChAd as the first dose and the BNT162b2 COVID-19 vaccine [BNT] as the second dose (primary immunization), IQR: interquartile range (25^{th}-75^{th} IQR within brackets).

2.2 Blood collection and serum separation and mononuclear cell isolation

Whole blood samples were collected at the Laboratory of Clinical Pathology (with certified quality management UNI EN ISO 9001:2015) of Urbino Hospital (AST Azienda Sanitaria Territoriale Pesaro - Urbino) using serum separator tubes (SST) with a gel barrier. The samples were allowed to clot at room temperature for 30 minutes before being centrifuged at 1,500 × g for 10 minutes. This procedure yielded clear serum, separated from blood cells by the gel barrier. Serum was then aliquoted within a few hours and stored at -80°C until further analysis. To avoid potential alterations of immunological readouts, no heat treatment of serum samples was performed.

For PBMC isolation, blood samples collected in EDTA vacuettes were processed within 96 hours of collection. PBMCs were separated using Lymphoprep™ density gradient medium. following a standard density gradient centrifugation protocol. The isolated PBMCs were cultured overnight at 37°C in humified atmosphere containing 5% CO_2 in Roswell Park Memorial Institute 1640 [RPMI-1640] complete medium supplemented with 25 mM HEPES, 2 mM L-glutamine. 1% penicillin-streptomycin and 10% fetal bovine serum [FBS]. Alternatively, PBMCs were cryopreserved at -80°C in FBS supplemented with 10% dimethyl sulfoxide [DMSO] for subsequent analyses.

2.3 Determination of antibody levels

Serum samples were analyzed for SARS-CoV-2 IgG antibodies using the "LIAISON® SARS-CoV-2 TrimericS IgG" Chemiluminescent Immunoassay (CLIA) kit, as previously described (8), at the Clinical Pathology Laboratory of the Urbino Hospital (AST Azienda Sanitaria Territoriale Pesaro – Urbino). Serum storage prior to testing was limited to less than 4 days to maintain sample integrity. The assay has high sensitivity (98.7%) and specificity (99.5%) for detecting anti-trimeric SARS-CoV-2 Spike protein IgG antibodies.

The method demonstrates a strong positive percent agreement (95% CI: 97.8–100.0%) and a negative percent agreement of 96.9% (95% CI: 92.9–98.7%) when compared with neutralizing IgG antibodies. The quantification range is 4.81–2080 BAU/mL, with a cut-off value of 33.8 BAU/mL for positivity. Results were expressed in binding antibody units per milliliter (BAU/mL) using a conversion factor of 2.6 (1 BAU/mL = 2.6 AU/mL) (10, 11).

For samples with IgG titers exceeding 2080 BAU/mL, the LIAISON® TrimericS IgG Diluent Accessory was used for dilution according to the manufacturer's recommendations (1:20 or 1:5 dilution factor, as appropriate) before re-testing to ensure accurate quantification. All the serum samples were assayed for the nucleocapsid-specific IgM and/or IgG antibodies (COVID-19 ELISA IgM and COVID-19 ELISA IgG kits, Diatheva srl, Cartoceto, PU, Italy), following the manufacturer's instructions, and were classified as N+-(nucleocapsid-positive) or N- (nucleocapsid-negative) based on the presence or absence of SARS-CoV-2 nucleocapsid-specific IgG and/or IgM antibodies.

2.4 Activation marker and intracellular cytokine assays

The analysis of SARS-CoV-2-specific T cell responses was performed using the SARS-CoV-2 Prot_S T Cell Analysis Kit (Miltenyi Biotec). Approximately 1 × 10^6 thawed or freshly isolated PBMCs were rested overnight at 37°C. Subsequently, the PBMCs were cultured in 96-well plates for 6 hours in the presence of 15-mer peptides with an 11-amino-acid overlap spanning the complete coding sequence (amino acids 5–1273) of the SARS-CoV-2 spike (S) glycoprotein (GenBank MN908947.3, Protein QHD43416.1), as provided in the PepTivator® SARS-CoV-2 Prot_S Complete, premium grade (Miltenyi Biotech). After 2 hours of stimulation, Brefeldin A was added at a final concentration of 1 µg/mL to block cytokine secretion.

Following stimulation, cells were washed with phosphate buffer supplemented with 2 mM EDTA and 0.5% bovine serum albumin (BSA) [PEB buffer]. The cells were then fixed and permeabilized before staining for 20 minutes with an antibody mix containing the following markers: CD3-APC, CD4-Vio® Bright B515, CD8-VioGreen™, IFN-γ-PE, TNF-α-PE-Vio770, CD14-VioBlue®, CD20-VioBlue®, and CD154-APC-Vio770, Viability 405/452 Fixable Dye was used to identify and exclude dead cells.

Sample acquisition was performed on a BD FACS Canto II flow cytometer. The gating strategy to identify activation markers and intracellular cytokine production in $CD4^+$ and $CD8^+$ T cell populations was as follows: Lymphocyte gate > DEAD/CD14-/CD20- > CD3+ > CD4+ or CD8+ > mean fluorescence intensity [MFI]of TNF-α, IFN-γ, or CD154, and percentage of positive cells (Supplementary Figure S4A).

2.5 Quantification of SARS-CoV-2 specific B-cells

The analysis of SARS-CoV-2-specific B-cells was performed using the SARS-CoV-2 Spike B Cell Analysis Kit, anti-human (Miltenyi Biotec). Approximately 5–10 × 10^6 thawed PBMCs were rested overnight at 37°C in complete RPMI-1640 medium. Following incubation, PBMCs were washed in PEB buffer and stained with an antibody cocktail containing the following reagents: Recombinant SARS-CoV-2 Spike-Protein (HEK)-Biotin-Streptavidin-PE, Recombinant SARS-CoV-2 Spike-Protein (HEK)-Biotin-Streptavidin-PE-Vio® 770, CD19-APC-Vio® 770, CD27-Vio Bright FITC. IgG-VioBlue® and IgM-APC. Live/dead cell discrimination was performed using 7-AAD staining.

Samples were acquired on a BD FACS Canto II flow cytometer. The gating strategy to identify SARS-CoV-2-specific memory B-cells was as follows: Lymphocyte gate > Single cells > Live/Dead- > CD19+ > CD27+ > IgG+/IgM- or IgG-/IgM+ > Spike-Protein-PE +/PE-Vio® 770+ (Supplementary Figure S4B).

2.6 Statistical analysis

To compare IgG levels between two independent vaccination groups, the Mann-Whitney U test was employed. For comparisons of IgG levels involving three or more vaccination groups, or for repeated measures within the same group across different time points, the Kruskal-Wallis test followed by Dunn's multiple comparisons post-test was applied.

The relationship between vaccination groups and clinical or demographic variables was assessed using the chi-square test for categorical variables and the Kruskal-Wallis test followed by Dunn's multiple comparisons post-test for continuous variables.

For the analysis of cellular responses, the Kruskal-Wallis test followed by Dunn's multiple comparisons post-test was used for comparisons involving three or more groups. The Mann-Whitney U test was used for comparisons between two independent groups.

A p-value of less than 0.05 was considered statistically significant. All analyses and visualizations, including box-and-whisker plots, were performed using GraphPad Prism software (version 8.4.2; GraphPad Software, San Diego, CA, USA). The specific statistical test used for each comparison is indicated in the legends.

3 Results

3.1 Longitudinal analysis of SARS-CoV-2 anti-trimeric Spike IgG levels at 9-, 12- and 21-months post-vaccination

A positive SARS-CoV-2 anti-trimeric Spike IgG antibody response was observed across all vaccination groups throughout the study period. The longitudinal analysis of antibody titers at 9, 12, and 21 months post-primary vaccination revealed significant temporal variations, particularly when comparing homologous and heterologous vaccination strategies. In the ChAd/ChAd/mRNA-1273 group, a significant decrease in IgG titers was observed from month 9 to 12 ($p < 0.001$), followed by a statistically significant increase between months 12 and 21 ($p < 0.01$) (Table 2, Figure 1A). In contrast, participants in the ChAd/ChAd/BNT, ChAd/BNT/mRNA-1273 and ChAd/BNT/BNT groups showed a similar pattern of antibody decline at month 12 followed by recovery at month 21; however, these changes were not statistically significant.

Inter-group comparisons demonstrated that the heterologous ChAd/BNT/mRNA-1273 prime-boost regimen elicited the highest anti-Spike IgG levels at both 9 and 21 months post-primary vaccination compared to homologous immunization schedules (ChAd/ChAd/mRNA-1273 and ChAd/ChAd/BNT). Specifically, median titers for the ChAd/BNT/mRNA-1273 group were 3070 BAU/mL at month 9, declined to 1148 BAU/mL at month 12 and rebounded to 4647.5 BAU/mL by month 21. Similarly, the heterologous ChAd/BNT/BNT group maintained comparable IgG levels at months 9 and 12 (2020 BAU/mL and 2035 BAU/mL, respectively) but displayed a marked increase at month 21 (3915 BAU/mL) that surpassed titers observed in the homologous groups (~2400 BAU/mL). Notably, although not statistically significant ($p = 0.0521$), the ChAd/BNT/mRNA-1273 group demonstrated higher IgG levels compared to ChAd/ChAd/mRNA-1273 at the 21-month time point (Table 2, Figure 1A).

These results demonstrate the enhanced and more sustained humoral response elicited by heterologous vaccination schedules. particularly ChAd/BNT/mRNA-1273, compared to homologous regimens.

3.2 Impact of SARS-CoV-2 infection on humoral immunity

To evaluate the impact of viral infection on humoral immunity, anti-trimeric Spike IgG levels were compared between N+ and N– participants within each vaccination group. Notably, N+ individuals displayed significantly higher anti-Spike IgG titers compared to N– individuals across all time points, consistent with an infection-driven immune boost. For instance, within the ChAd/ChAd/mRNA-1273 group, IgG levels significantly decreased in N– individuals between 9 and 12 months ($p < 0.0001$) but increased between 12 and 21 months ($p < 0.001$) post-primary vaccination, likely due to the administration of a fourth vaccine dose in some participants or late natural infections (Figure 1B, Table 3, Supplementary Table S5). Similar trends were observed in the ChAd/BNT/BNT group, where N+ individuals consistently

TABLE 2 SARS-CoV-2 anti-trimeric Spike IgG titers by vaccination schedule and time points.

IgG titer (BAU/mL)	ChAd/ChAd/ mRNA-1273	ChAd/ChAd/ BNT	ChAd/BNT/ mRNA-1273	ChAd/BNT/ BNT
9 months Median (IQR)	n = 111 (56.9%) 2100 (39.3-41400)	n = 23 (11.8%) 1944 (395-13160)	n = 16 (8.2%) 3070 (711-17540)	n = 45 (23.1%) 2020 (605-40000)
12 months Median (IQR)	n = 105 (60.7%) 1470 (39.2-17600)	n = 19 (11%) 1800 (102-7460)	n = 11 (6.3%) 1148 (670-10340)	n = 38 (22.0%) 2035 (237-20600)
21 months Median (IQR)	n = 56 (56.6%) 2332.5 (333-15260)	n = 13 (13.1%) 2480 (117-12240)	n = 6 (6.1%) 4647.5 (1515-6050)	n = 24 (24.2%) 3915 (165-14500)

Median and interquartile range [IQR] of SARS-CoV-2 anti-trimeric Spike IgG levels (BAU/mL) at 9, 12 and 21 months post-primary vaccination among the groups of recruited vaccinated subjects. Sample size (*n*) and relative percentages are reported for each group at each time point.

10.3389/fimmu.2025.1579163

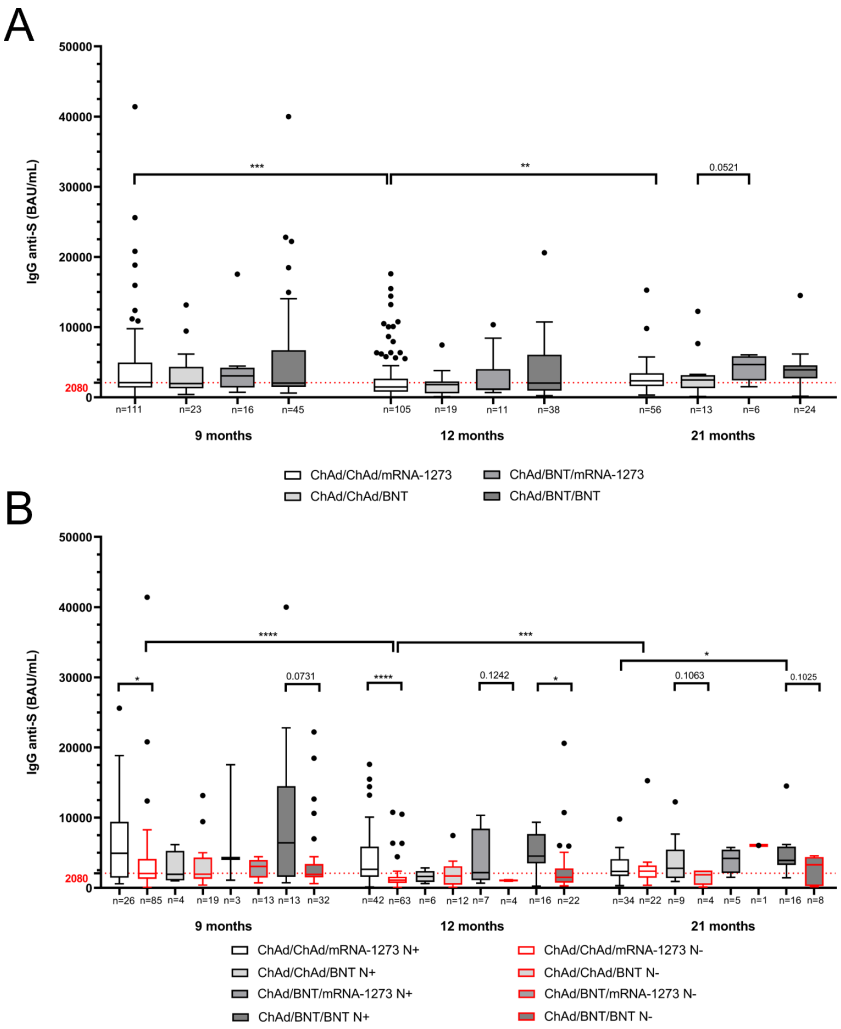

FIGURE 1
Inter-group comparison of SARS-CoV-2 anti-trimeric Spike protein IgG levels (BAU/mL) among the four vaccination groups at 9, 12 and 21 months post-primary vaccination. **(A)** IgG levels across all vaccinated subjects. **(B)** Comparison of IgG titers between anti-Nucleocapsid-positive [N+] and anti-Nucleocapsid-negative [N–] subjects within each vaccination group. Boxplots show the median and interquartile range [IQR], with whiskers representing the lowest and highest values (Tukey-style). Outliers are displayed as individual points. Statistical comparisons were performed using the Kruskal-Wallis test with Dunn's *post hoc* multiple comparisons and the Mann-Whitney U test for pairwise comparisons. *$p < 0.05$; **$p < 0.01$; ***$p < 0.001$; ****$p < 0.0001$. Results for the ChAd/BNT/mRNA-1273 N– group at 21 months are not shown due to the presence of only a single subject, precluding meaningful statistical comparisons.

exhibited higher IgG titers than N– individuals, particularly at 21 months ($p < 0.05$).

Intra-group analysis revealed a statistically significant difference ($p < 0.0001$) in anti-trimeric Spike IgG titers between N+ and N– individuals immunized with ChAd/ChAd/mRNA-1273 at the 12-month time point, with higher IgG titers observed in N+ subjects. Smaller but statistically significant differences ($p < 0.05$) were also detected at i) month 9 within the same group, ii) month 12 between N+ and N– individuals in the ChAd/BNT/BNT group, and iii) month 21 for the ChAd/BNT/mRNA-1273 group (Figure 1B). Non-significant trends in IgG differences between N+ and N– individuals were observed in the ChAd/BNT/BNT group at month 9 ($p = 0.0731$), ChAd/BNT/mRNA-1273 at month 12 ($p = 0.1242$), ChAd/ChAd/BNT at month 21 ($p = 0.1063$), and ChAd/BNT/BNT at month 21 ($p = 0.1025$).

When focusing on the magnitude of anti-trimeric Spike IgG responses, higher median antibody levels were consistently observed in N+ compared to N– individuals across both homologous and heterologous vaccination schedules (ChAd/ChAd/mRNA-1273, ChAd/BNT/mRNA-1273 and ChAd/BNT/BNT) at all study time points, with one exception. At 21 months, IgG levels in the ChAd/ChAd/mRNA-1273 group were comparable between N+ and N– individuals (Supplementary Table S5). In contrast, for the ChAd/ChAd/BNT group, anti-trimeric Spike IgG median levels remained comparable between N+ and N– subjects at 9 and 12 months, but an increased response was evident in N+ subjects at 21 months. These findings suggest that while infection significantly boosts antibody responses across all vaccination groups, the magnitude and duration of this boost may vary

depending on the specific vaccination regimen and time since vaccination or infection.

3.3 Influence of fourth dose on humoral immunity

To assess the potential impact of a fourth vaccine dose on SARS-CoV-2 anti-trimeric Spike IgG titers, subjects were grouped based on their vaccination schedule and infection status. Although no statistical comparisons were performed due to the small number of participants receiving a fourth dose, descriptive analysis was provided. At 21 months, 20 individuals (20.2% of the cohort) received a fourth vaccine dose with variations depending on their vaccination schedule and infection status (Supplementary Table S3, Table 3). Among participants in the ChAd/ChAd/mRNA-1273 group, 2.9% of infected [N+] individuals received BNT, while 8.8% received mRNA-1273. Conversely, 27.3% of uninfected [N–] individuals in the same group received either BNT or mRNA-1273. Similarly, in the ChAd/ChAd/BNT group, fourth-dose administration was more frequent among uninfected subjects (50% for BNT), whereas 44.4% of infected individuals received BNT. In contrast, the ChAd/BNT/mRNA-1273 and ChAd/BNT/BNT groups showed limited fourth-dose uptake, with mRNA-1273 administered exclusively in uninfected individuals of the ChAd/BNT/mRNA-1273 group and BNT being the predominant choice in ChAd/BNT/BNT recipients.

3.4 Impact of homologous and heterologous priming on long-term anti-trimeric Spike IgG responses

To evaluate the impact of primary vaccination schedules (ChAd/ChAd vs ChAd/BNT) on long-term immune responses, we analyzed anti-trimeric Spike IgG levels at 9, 12, and 21 months post-primary vaccination. While this analysis focuses on the priming effect of homologous versus heterologous schedules, it is important to note that by month 21, participants had also received additional doses (third and, in some cases, fourth). These subsequent doses likely contributed to the observed recovery in IgG levels, as discussed in earlier sections. However, isolating the impact of the primary schedule provides valuable insights into the foundational immune response. Longitudinal analysis of the anti-trimeric Spike IgG response revealed a similar trend between homologous and heterologous primary vaccination schedules, characterized by a decline in antibody titers between months 9 and 12, followed by a recovery at month 21. In the homologous ChAd/ChAd schedule, IgG titers decreased significantly between months 9 and 12 ($p < 0.001$), from a median of 2050 BAU/mL (IQR: 39.3–41400) to 1495 BAU/mL (IQR: 39.2–17600), and then increased significantly at month 21 ($p < 0.01$) to a median of 2420 BAU/mL (IQR: 117–15260) (Supplementary Figure S5A, Supplementary Table S6). A similar, non-statistically significant decline was observed in the heterologous ChAd/BNT schedule, where IgG levels decreased from a median of 2280 BAU/mL (IQR: 605–40000) at month 9 to 1952 BAU/mL (IQR: 237–20600) at month 12 ($p = 0.0679$). By month 21, IgG levels in the ChAd/BNT group reached a median of 3920 BAU/mL (IQR: 165–14500), significantly higher than those observed in the ChAd/ChAd group ($p < 0.01$).

3.5 Longitudinal analysis of SARS-CoV-2 anti-Nucleocapsid at 9 12 and 21 months post-vaccination between homologous and heterologous schedule

Evaluation of IgM and IgG anti-Nucleocapsid (anti-N) antibodies in subjects vaccinated with ChAd/ChAd (homologous)

TABLE 3 Distribution of subjects receiving BNT or mRNA-1273 as the fourth dose.

Vaccine Schedule	Subjects	4th dose				
		BNT		mRNA-1273		Total 4th dose
		N+	N-	N+	N-	
ChAd/ChAd/mRNA-1273	N+ = 34 N- = 22 Tot = 56	1/34 (2.9%) - 1/56 (1.8%)	- 3/22 (13.6%) 3/56 (5.4%)	3/34 (8.8%) - 3/56 (5.4%)	- 3/22 (13.6%) 3/56 (5.4%)	N+ = 4/34 (11.8%) N- = 6/22 (27.3%) Tot = 10/56'(17.9%)
ChAd/ChAd/BNT	N+ = 9 N- = 4 Tot = 13	4/9 (44.4%) - 4/13 (30.8%)	- 2/4 (50.0%) 2/13 (15.4%)	1/9 (11.1%) - 1/13 (7.7%)	- 0/4 (0.0%) 0/13 (0.0%)	N+ = 5/9 (55.6%) N- = 2/4 (50.0%) Tot = 7/13 (53.8%)
ChAd/BNT/mRNA-1273	N+ = 5 N- = 1 Tot = 6	0/5 (0.0%) - 0/6 (0.0%)	- 0/1 (0.0%) 0/6 (0.0%)	0/5 (0.0%) - 0/6 (0.0%)	- 1/1 (100.0%) 1/6 (16.7%)	N+ = 0/5 (0.0%) N- = 1/1 (100.0%) Tot = 1/6 (16.7%)
ChAd/BNT/BNT	N+ = 16 N- = 8 n = 24	1/16 (6.3%) - 1/24 (4.2%)	- 1/8 (12.5%) 1/24 (4.2%)	0/16 (0.0%) - 0/24 (0.0%)	- 0/8 (0.0%) 0/24 (0.0%)	N+ = 1/16 (6.3%) N- = 1/8 (12.5%) Tot = 2/24 (8.3%)

Distribution of subjects receiving BNT or mRNA-1273 as the fourth dose at 21 months post-primary vaccination, stratified by vaccination schedule and infection status (N+ = infected, N– = uninfected). Data are presented as the number of subjects over the total within each subgroup, with relative percentages provided in parentheses.

and ChAd/BNT (heterologous) schedules revealed a comparable increase in the percentage of SARS-CoV-2 positive individuals over the study period. Specifically, positivity rates increased from 22.4% to 62.3% in the ChAd/ChAd group and from 26.3% to 70.0% in the ChAd/BNT group between months 9, 12, and 21 (Supplementary Figure S6).

Longitudinal analysis of anti-trimeric Spike IgG titers among infected [N+] and uninfected [N−] individuals within the ChAd/ChAd and ChAd/BNT groups highlighted statistically significant differences, particularly in N− participants (Supplementary Figure S5B). In the ChAd/ChAd group, anti-trimeric Spike IgG titers in N− individuals showed a significant decrease between months 9 and 12 ($p < 0.0001$), followed by a significant increase at month 21 ($p < 0.01$). In contrast. N− individuals in the ChAd/BNT group exhibited a smaller, non-significant decrease in IgG titers between months 9 and 12 ($p = 0.0535$).

Intra-group comparisons revealed significant differences in IgG titers between N+ and N− individuals at months 9 and 12 for both vaccination schedules. At month 12, the differences were more pronounced in the ChAd/ChAd group ($p < 0.0001$) compared to the ChAd/BNT group ($p < 0.01$). At month 9, smaller but significant differences ($p < 0.05$) were observed between N+ and N− individuals for both schedules. By month 21, N+ participants in the ChAd/BNT group had significantly higher IgG titers compared to N+ individuals in the ChAd/ChAd group ($p < 0.01$).

Focusing on IgG levels, the highest median titers across all time points were consistently observed in N+ individuals vaccinated with ChAd/BNT, with values of 6195 BAU/mL at month 9, 4220 BAU/mL at month 12, and 3925 BAU/mL at month 21 (Supplementary Figure S5B, Table 4). In contrast, N− individuals in both vaccination groups had the lowest median antibody titers, ranging from 1144 BAU/mL (ChAd/ChAd at month 12) to 3480 BAU/mL (ChAd/BNT at month 21). Notably, at month 21, N− participants in the ChAd/BNT group showed a median IgG titer (3480 BAU/mL) comparable to that of N+ participants (3925 BAU/mL), suggesting a robust recovery of antibody levels in this subgroup.

3.6 Spike-specific memory B-cells induction at 21 months post-vaccination

To investigate the cellular response induced by different vaccination strategies, the percentages of Spike-specific memory B-cells [MBCs] were analyzed in PBMCs collected 21 months post-primary vaccination. Although not statistically significant, participants who received heterologous vaccination schedules (ChAd/BNT/mRNA-1273 and ChAd/BNT/BNT) displayed higher percentages of IgM−/IgG+ MBCs compared to those vaccinated with homologous schedules (ChAd/ChAd/mRNA-1273 and ChAd/ChAd/BNT) (Figure 2A). Notably, the largest difference was observed between ChAd/ChAd/mRNA-1273 and ChAd/BNT/BNT ($p = 0.1699$). For IgM+/IgG− MBCs, a significant increase ($p < 0.05$) was detected in ChAd/ChAd/BNT subjects compared to ChAd/ChAd/mRNA-1273 participants (Figure 2B). A similar but non-significant trend was observed when comparing ChAd/ChAd/mRNA-1273 to ChAd/BNT/BNT ($p = 0.1395$) (Figure 2B). Overall, IgM−/IgG+ MBCs were more prevalent than IgM+/IgG− MBCs across all vaccination strategies. Despite the variability among groups, heterologous vaccination schedules demonstrated a tendency to elicit stronger memory B-cell responses compared to homologous immunization.

3.7 Spike-specific memory B-cells induction at 21 months following homologous or heterologous primary vaccination

Comparison of Spike-specific IgM−/IgG+ memory B-cells [MBCs] responses between subjects receiving homologous (ChAd/ChAd) and heterologous (ChAd/BNT) primary vaccination schedules revealed a higher, though not statistically significant response in the heterologous group ($p = 0.1133$) (Figure 3A). In contrast, comparable levels of IgM+/IgG− MBCs

TABLE 4 SARS-CoV-2 anti-trimeric Spike IgG titers by primary vaccination schedule, time points and infection status.

		ChAd/ChAd		ChAd/BNT	
		N+	N-	N+	N-
IgG titer (BAU/mL)	9 months Median (IQR)	n = 30 (15.4%) 3420 (579-25600)	n = 104 (53.3%) 2040 (39.3-41400)	n = 16 (8.2%) 6195 (725-40000)	n = 45 (23.1%) 1930 (605-22200)
	12 months Median (IQR)	n = 48 (27.9%) 2500 (123-17600)	n = 75 (43.6%) 1144 (39.2-10760)	n = 23 (13.4%) 4220 (237-10340)	n = 26 (15.1%) 1275 (287-20600)
	21 months Median (IQR)	n = 43 (43.4%) 2650 (333-12240)	n = 26 (26.3%) 2345 (117-15260)	n = 21 (21.2%) 3925 (1440-14500)	n = 9 (9.1%) 3480 (165-6050)

Median and interquartile range (IQR) of SARS-CoV-2 anti-trimeric Spike IgG levels in ChAd/ChAd and ChAd/BNT immunized subjects at 9, 12, and 21 months post-vaccination. stratified by infection status (N+ = infected. N− = uninfected). Data are presented as median IgG titers (BAU/mL) with IQR (25^{th}-75^{th}) in parentheses, alongside the number and percentage of subjects within each group.

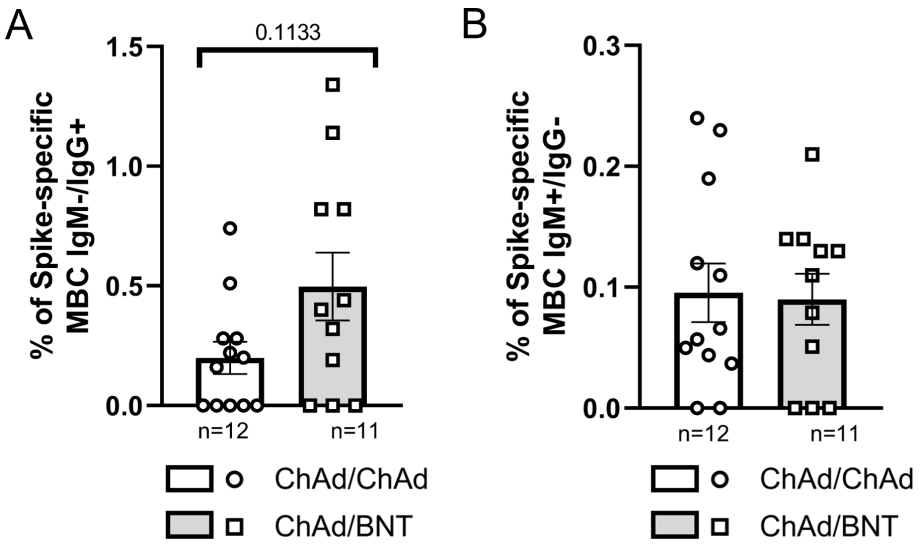

FIGURE 2
Inter-group comparison of the percentage of Spike-specific memory B-cells [MBCs] among four vaccinated groups at 21 months post-vaccination. **(A)** Percentages of IgM−/IgG+ MBCs. **(B)** Percentages of IgM+/IgG− MBCs. Bars represent the mean with standard error of the mean [SEM]. The number of subjects analyzed in each group is reported below the x-axis. Statistical significance was assessed using the Kruskal-Wallis test with Dunn's *post hoc* comparison and Mann-Whitney U-test ($p < 0.05$).

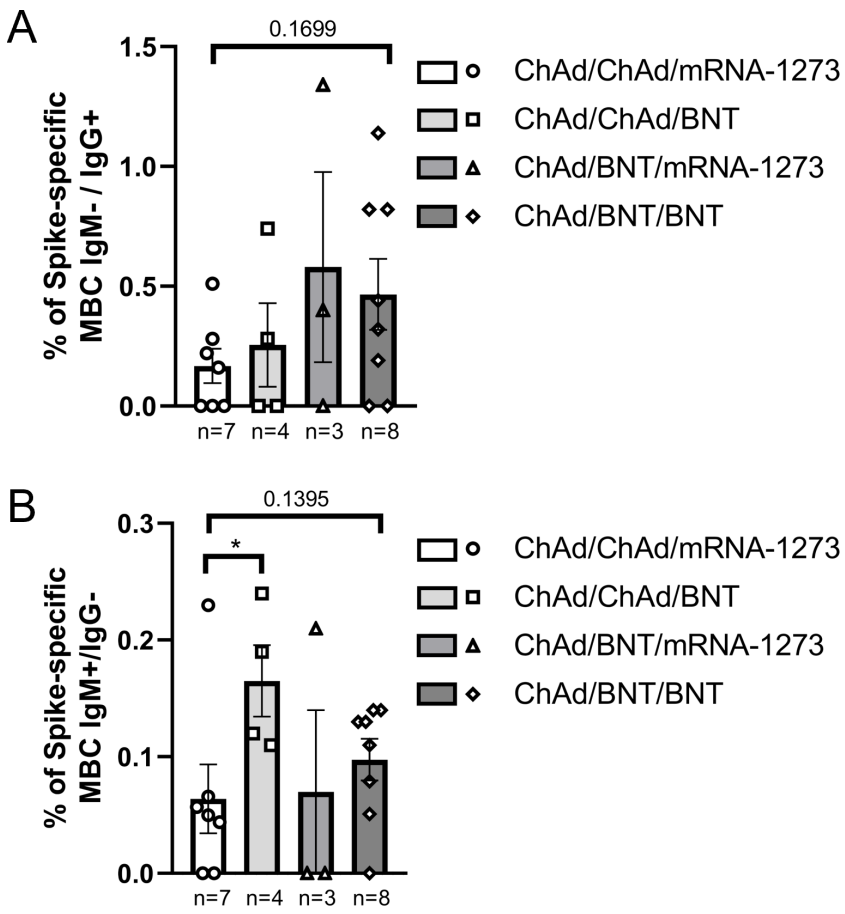

FIGURE 3
Inter-group comparison of the percentage of Spike-specific memory B-cells [MBCs] between subjects receiving homologous (ChAd/ChAd) and heterologous (ChAd/BNT) primary vaccination schedules at 21 months post-vaccination. **(A)** Percentages of IgM−/IgG+ MBCs. **(B)** Percentages of IgM+/IgG− MBCs. Bars represent the mean with standard error of the mean [SEM]. The number of subjects analyzed in each group is reported below the x-axis. Statistical significance was assessed using the Mann-Whitney U-test. *$p < 0.05$.

were observed between the two groups (Figure 3B). Notably, the percentages of IgM−/IgG+ MBCs were consistently higher than those of IgM+/IgG− MBCs across both vaccination strategies. The mean values were 0.2% (ChAd/ChAd) and 0.5% (ChAd/BNT) for IgM−/IgG+ MBCs, compared to 0.1% (ChAd/ChAd) and 0.09% (ChAd/BNT) for IgM+/IgG− MBCs.

Further intra-group analysis at 21 months stratified by infection status (N+ = infected, N− = uninfected) showed a trend toward higher IgM−/IgG+ MBCs induction in infected [N+] subjects compared to uninfected [N−] within the ChAd/BNT group, though this difference did not reach statistical significance (p = 0.0563) (Supplementary Figure S7A). Moreover, within infected participants, the ChAd/BNT group exhibited an increased IgM −/IgG+ MBC response compared to the ChAd/ChAd group (p = 0.1212). Conversely, levels of IgM+/IgG− MBCs were similar across infection statuses and vaccination strategies (Supplementary Figure S7B).

3.8 Spike-specific T-cells induction at 21 months post-vaccination

Intracellular cytokine expression by T-cells isolated from PBMCs of vaccinated subjects was evaluated at 21 months post-immunization. Comparable levels of IFNγ, TNFα, and CD154 expression by CD4+ T-cells, as well as IFNγ and TNFα expression by CD8+ T-cells, were observed across the four vaccination groups: ChAd/ChAd/mRNA-1273, ChAd/ChAd/BNT, ChAd/BNT/mRNA-1273 and ChAd/BNT/BNT (Figures 4A, B). When subjects were grouped according to their homologous or heterologous primary vaccination schedules, no statistically significant differences were detected in the expression of the same T-cell cytokines (i.e. IFNγ, TNFα and CD154 for CD4+ T-cells and IFNγ and TNFα for CD8+ T-cells) (Figures 5A, B). Intra-group analysis based on infection status (N+ = infected; N− = uninfected) within the ChAd/ChAd and ChAd/BNT groups showed no significant differences in CD4+ T-cell cytokine expression (IFNγ, TNFα and CD154) between infected [N+] and uninfected [N−] individuals (Supplementary Figure S8A). However, a trend toward higher mean cytokine expression, particularly IFNγ and TNFα, was observed in infected individuals compared to uninfected participants within the same vaccination group. For CD8+ T-cells, a statistically significant difference in TNFα expression was identified between infected [N+] and uninfected [N−] subjects within the ChAd/BNT group ($p < 0.05$) (Supplementary Figure S8B). Additionally, although not statistically significant, higher TNFα expression was observed in N+ heterologous primary vaccinated subjects compared to N+ homologous immunized individuals (p = 0.1717). Similarly, increased IFNγ expression in CD8+ T-cells was noted in N+ ChAd/BNT subjects compared to other groups, but this difference did not reach statistical significance (p = 0.1490), (Supplementary Figure S9). While the overall trend of activation across vaccination groups were similar, MFI-based analysis highlighted differences in cytokine expression intensity that were not evident when analyzing only the percentage of cytokine-positive cells. This discrepancy likely reflects the increased expression level per cell, rather than an increased frequency of positive cells, and suggests that MFI better captures the magnitude of T-cell activation, particularly in the context of previous infection (Figures 4C, D, 5C, D, Supplementary Figure S8C, D). Polyfunctionality analysis of cytokine-expressing T cells revealed no statistically significant differences among the four vaccine groups (Supplementary Figure S9), between homologous (ChAd/ChAd) and heterologous (ChAd/BNT) primary regimens (Supplementary Figure S10), or between infected and uninfected individuals within these groups (Supplementary Figure S11). Overall, these results indicate that both homologous and heterologous vaccination regimens induced persistent T-cell responses, with a notable enhancement of TNFα production in CD8+ T-cells among SARS-CoV-2 infected individuals who received a heterologous primary vaccination schedule

4 Discussion

The COVID-19 pandemic has necessitated rapid vaccine development and the implementation of diverse immunization strategies, including homologous and heterologous schedules, as well as additional booster doses (5, 12–15). Notwithstanding the interest on the development of increasingly new SARS-CoV-2 vaccines able to adapt and respond to the emerging variants of concerns, there remains limited research on the long-term durability of immune responses induced by different vaccination strategies (16–18).

Our previous studies focused on the evaluation of heterologous and homologous COVID-19 vaccination up to six months after primary immunization (8, 9). Analysis of the humoral response highlighted a stronger anti-viral immune induction for the heterologous ChAd/BNT vaccination compared to the homologous ChAd/ChAd at 2-, 4- and 6-months after the primary immunization. Additional studies have further highlighted the efficacy of heterologous vaccination schedules. For example, highest titers of SARS-CoV-2 anti-S IgG levels and increased T-cell responses were reported in BNT/ChAd and ChAd/BNT vaccinated healthy adults compared to the homologous ChAd/ChAd group (3). Similarly, higher and longer-lasting anti-RBD antibody levels were observed in heterologous ChAd/Coronavac vaccination schedules when compared to homologous ChAd/ChAd regimens (19).

In this study, we extended the observation period to 21 months post-primary vaccination, providing a long-term analysis of both humoral and cellular immune responses following SARS-CoV-2 vaccination. We compared homologous (ChAd/ChAd) and heterologous (ChAd/BNT) vaccination schedules in participants who also received a third mRNA booster dose (BNT or mRNA-1273). Moreover, due to the extended duration of this study, participants were exposed to SARS-CoV-2 variants of concern circulating during the study period, likely including Delta, which was dominant at the start of the study, and Omicron which emerged and became the prevailing variant by late 2021 and early 2022. Also,

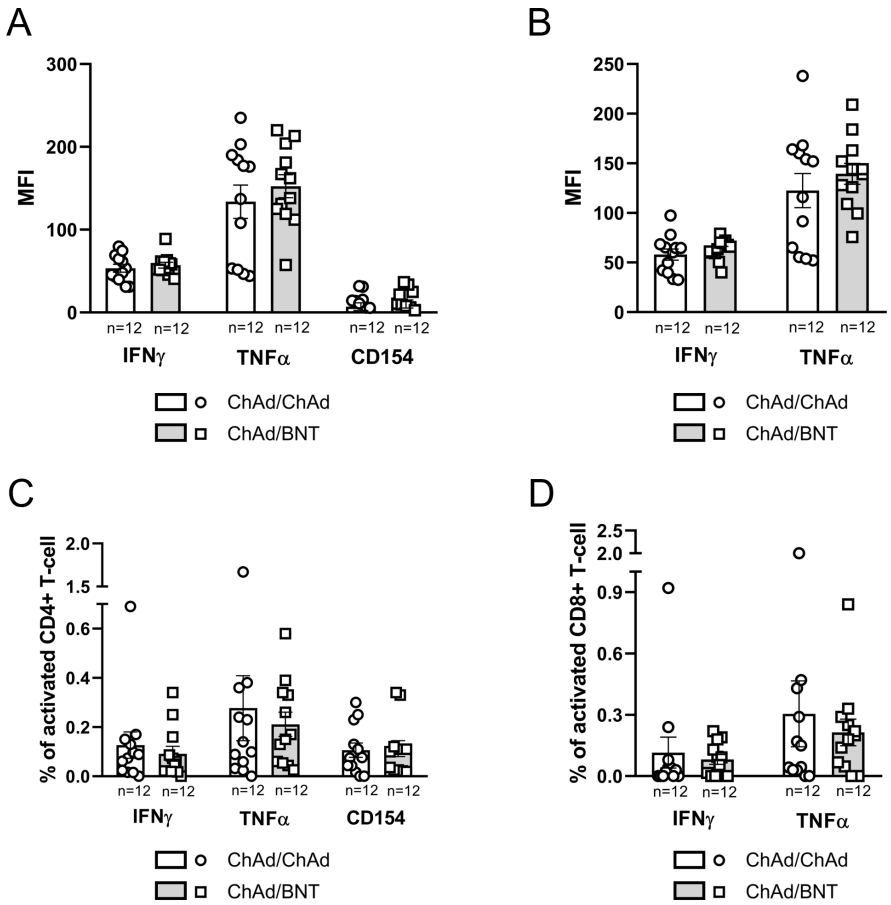

FIGURE 4
Inter-group comparison of the intracellular cytokine expression in CD4+ and CD8+ T-cells across four vaccination groups at 21 months post-vaccination. **(A)** Mean fluorescence intensity [MFI] of IFNγ, TNFα, and CD154 expression in CD4+ T-cells. **(B)** MFI of IFNγ and TNFα expression in CD8 + T-cells. **(C)** Percentage of CD4+ T cells expressing IFNγ, TNFα, or CD154. **(D)** Percentage of CD8+ T cells expressing IFNγ or TNFα. Bars represent the mean with standard error of the mean [SEM]. Sample sizes for each group are reported below the x-axis. Statistical significance was assessed using the Kruskal-Wallis test with Dunn's *post hoc* multiple comparisons.

some participants were already SARS-CoV-2 positive at the first time point (9 months after primary vaccination), suggesting earlier encounters with the virus. This prior exposure may have included other variants, such as Beta or Gamma, potentially influencing the baseline immune responses and contributing to the observed variability over time. It is also important to note that the vaccines used in this study—Pfizer-BioNTech (BNT162b2), AstraZeneca (ChAdOx1-S), and Moderna (mRNA-1273)—were all based on the spike protein of the original Wuhan-Hu-1 strain, which may further influence immune recognition and responses to emerging variants (20). The longitudinal analysis of anti-S IgG titers revealed a general trend across all groups: antibody levels peaked at 9 months (three months post-booster), declined by 12 months and increased again by 21 months. The elevated antiviral antibody concentration observed at 9 months can be attributed to immune system activation following the third dose of SARS-CoV-2 vaccine, as samples were collected approximately three months post-booster (21, 22). Booster vaccination is known to robustly enhance antibody levels, peaking within the first 1–3 months after administration, before gradually declining over time due to the natural waning of plasma cell activity (23, 24). Finally, the increase in anti-S IgG observed at 21 months is likely a result of natural SARS-CoV-2 infections acting as immune boosters, alongside the administration of a fourth vaccine dose at approximately month 16, which further stimulated humoral immune responses (25, 26).

Our findings demonstrate that heterologous vaccination with ChAd/BNT, followed by an mRNA booster, elicits a more robust and sustained humoral response compared to homologous ChAd/ChAd vaccination. This is evident in the higher anti-S IgG titers observed in the heterologous groups, particularly at the 21-month time point. These results align with previous studies that have shown the benefits of heterologous prime-boost strategies for COVID-19 and other infectious diseases (3, 27, 28). In contrast, the homologous ChAd/ChAd/mRNA-1273 group was the only group to show a significant increase in anti-S IgG levels between months 9 and 12, followed by a significant decrease from months 12 to 21. These findings highlight a differential impact of homologous and heterologous primary vaccination schedules on the durability

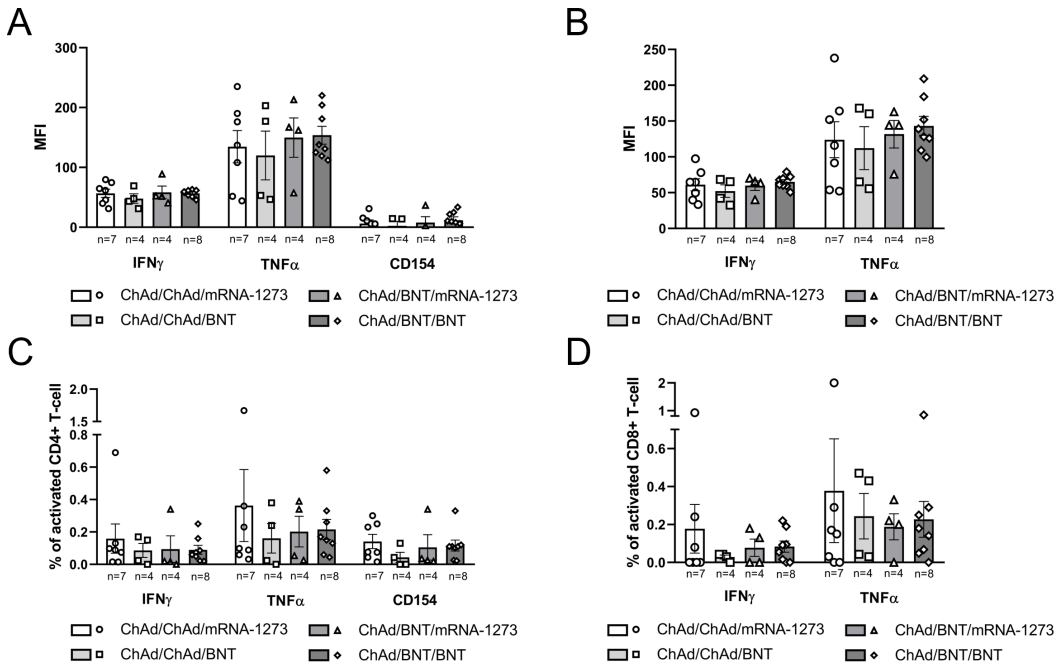

FIGURE 5
Inter-group comparison of the intracellular cytokine expression in CD4+ and CD8+ T-cells between homologous (ChAd/ChAd) and heterologous (ChAd/BNT) primary vaccination schedules at 21 months post-vaccination. **(A)** Mean fluorescence intensity [MFI] of IFNγ, TNFα and CD154 expression in CD4+ T-cells. **(B)** MFI of IFNγ and TNFα expression in CD8+ T-cells. **(C)** Percentage of CD4+ T cells expressing IFNγ, TNFα, or CD154. **(D)** Percentage of CD8+ T cells expressing IFNγ or TNFα. Bars represent the mean with standard error of the mean [SEM]. Sample sizes for each group are reported below the x-axis. Statistical significance was assessed using the Mann-Whitney U test.

and dynamics of the immune response, consistent with previous observations (5).

Given the extended study period, we analyzed additional variables that could influence anti-viral antibody production, such as SARS-CoV-2 infection and the administration of a fourth vaccine dose. When evaluating the percentage of SARS-CoV-2 infected [N+] and uninfected [N−] individuals, we observed a general increase in the number of infected participants from month 9 to month 21, independently of the vaccination schedule., This trend indicates that infection rates increased across all groups over time, with the ChAd/BNT/mRNA-1273 group showing the highest percentages of infected individuals at both 12 and 21 months. While this observation may suggest differences in exposure or other external factors, all vaccination schedules contributed to a sustained level of immune protection over the study period.

When comparing anti-S IgG titers between N+ and N− subjects within each vaccination group, notable differences emerged. At all-time points, N+ individuals exhibited higher anti-S IgG levels compared to N− individuals, likely due to a 'booster effect' induced by SARS-CoV-2 infection (29). In addition, we observed significant differences within specific vaccination groups at later time points. For instance, in the ChAd/ChAd/mRNA-1273 group, a significant increase in anti-S IgG titers was seen in N− individuals between months 12 and 21, likely driven by the fourth vaccine dose administered at month 16 (approximately 30% of N− individuals in this group received BNT or mRNA-1273 as a fourth dose). Similarly. in the ChAd/ChAd/BNT group, the higher anti-S IgG titers observed in N+ individuals compared to N− participants at month 21 may reflect a 'double booster effect' resulting from both SARS-CoV-2 infection and the fourth vaccine dose. Notably, around 50% of participants in this group—regardless of infection status—received a fourth dose (BNT or mRNA-1273) at month 16.

A significant variability in anti-S IgG titers was observed over the study period, particularly in the ChAd/ChAd/mRNA-1273 group. Specifically: i) a significant decrease in antibody levels occurred between months 9 and 12, followed by an increase between months 12 and 21; ii) at month 21, anti-S IgG titers in this group were lower compared to those in the ChAd/BNT/BNT group; and iii) significant differences between N+ and N− individuals were noted at months 9 and 12, but these differences were no longer observed at month 21. Conversely, in the ChAd/BNT/BNT group, higher anti-S IgG titers were observed for N+ subjects compared to N− subjects, but only at the 12-month time point.

To further clarify the impact of primary vaccination on the immune response, we grouped participants based on homologous (ChAd/ChAd) or heterologous (ChAd/BNT) regimens, increasing the statistical power of the analysis. Significant fluctuations were observed in the homologous schedule, with a marked decrease in IgG levels from 9 to 12 months followed by a rebound at 21 months, a pattern particularly evident in N− individuals and likely influenced by the ChAd/ChAd/mRNA-1273 group. In contrast, the heterologous schedule showed more stable IgG levels over time, with consistently higher antibody titers compared to the homologous group, especially at the later time points.

Despite these variations, both the ChAd/ChAd and ChAd/BNT schedules demonstrated comparable trends in infection rates over time, as indicated by similar increases in the percentage of N+ subjects. While these findings suggest that the overall immunization capacity of both schedules is similar in preventing SARS-CoV-2 infection, homologous vaccination may result in a lower production of long-lived plasma cells compared to heterologous vaccination, potentially explaining the observed differences in antibody persistence (25, 30).

Finally, we further investigated the cellular immune response to the different vaccination schedules in a subgroup of participants equally distributed between N+ and N− individuals who had received either homologous or heterologous primary vaccination. At 21-month post-primary immunization, analysis of both B- and T-cell populations revealed the persistence of anti-S specific memory B cells [MBCs] and T-cells. This persistence extends beyond the 6–8 months typically reported following COVID-19 vaccination or natural infection (31–33). Higher percentages of anti-S specific IgM^-/IgG^+ MBCs were observed in participants who received the heterologous primary ChAd/BNT vaccination schedule compared to those who received the homologous ChAd/ChAd schedule, in both two-dose and three-dose groups. Additionally, an increased proportion of anti-viral IgM^-/IgG^+ MBCs was detected in SARS-CoV-2 infected [N+] individuals within both ChAd/ChAd and ChAd/BNT groups, underscoring the 'booster effect' of natural viral infection in reactivating the immune system (26). In contrast, low and variable percentages of IgM^+/IgG^- MBCs were observed across the vaccinated groups. This is likely due to their early emergence during the initial months following immunization, followed by a gradual class-switching to IgM^-/IgG^+ MBCs over the course of the study period (31). Regarding $CD4^+$ and $CD8^+$ T-cell responses, comparable levels of anti-S specific cytokine production were observed across the vaccinated groups, regardless of the number of doses administered. However, higher mean expression of IFN-γ and TNF-α by $CD8^+$ T-cells was particularly evident in SARS-CoV-2 infected [N+] individuals within the ChAd/BNT group compared to uninfected [N-] subjects. This finding suggests a preferential cytotoxic activation of the immune system as a consequence of natural SARS-CoV-2 infection (34) While this study provides valuable insights into the long-term immune responses following different COVID-19 vaccination strategies, certain limitations should be acknowledged. The sample size, while sufficient for the primary analyses, could be expanded in future studies to enhance the statistical power, especially when analyzing subgroups based on infection status (N+ and N-) or the administration of a fourth vaccine dose. Additionally, the reliance on anti-nucleocapsid antibody testing at specific time points to determine infection status may have resulted in some misclassification of individuals with prior asymptomatic infections. Incorporating more frequent testing and exploring other markers of infection could improve the accuracy of infection status determination in future investigations. Furthermore, the predominantly young to middle-aged adult cohort from a single region in Italy may not fully represent the broader population. Therefore, caution should be exercised when generalizing these findings to other age groups or geographical locations. Despite these limitations, the study's longitudinal design, detailed immunological assessments, and inclusion of both homologous and heterologous vaccination schedules provide valuable data on the persistence and nature of immune responses following COVID-19 vaccination and infection.

5 Conclusions

This study provides a comprehensive, real-world assessment of long-term immune responses following homologous and heterologous COVID-19 vaccination, analyzing data from an Italian cohort up to 21 months post-primary immunization. Our results demonstrate that both homologous (ChAd/ChAd) and heterologous (ChAd/BNT) vaccination strategies, particularly when followed by an mRNA booster, induce robust and persistent humoral and cellular immunity, including anti-Spike IgG, memory B cells, and T cells. Notably, the heterologous ChAd/BNT regimen, boosted with an mRNA vaccine, elicited a significantly stronger and more durable immune response compared to the homologous ChAd/ChAd schedule, particularly in terms of long-term antibody persistence and cellular immune activation. Furthermore, we found that natural SARS-CoV-2 infection significantly enhanced both humoral and cellular immune responses, acting as a natural booster and potentially broadening protection. These findings underscore the effectiveness of heterologous vaccination in achieving robust long-term immunity and highlight the significant impact of hybrid immunity. Future studies should focus on larger, more diverse cohorts to further validate these findings and investigate the durability of responses beyond 21 months. Moreover, further research is needed to elucidate the optimal timing and frequency of booster doses, particularly in the context of emerging variants and varying infection histories. Such studies will be crucial to inform future vaccine development and refine immunization policies for achieving long-term population protection against COVID-19.

Data availability statement

The original contributions presented in the study are included in the article/Supplementary Material. Further inquiries can be directed to the corresponding author/s.

Ethics statement

The studies involving humans were approved by the Ethics Committee (Comitato Etico per la Sperimentazione Umana) of the

University of Urbino Carlo Bo on 24 June 2021 (protocol code n. 46/2021). The studies were conducted in accordance with the local legislation and institutional requirements. The participants provided their written informed consent to participate in this study.

Author contributions

DT: Data curation, Formal analysis, Investigation, Writing – original draft. CO: Data curation, Formal analysis, Investigation, Writing – review & editing. IC: Data curation, Formal analysis, Writing – original draft, Writing – review & editing. SB: Conceptualization, Project administration, Writing – review & editing. EC: Project administration, Resources, Writing – review & editing. MM: Conceptualization, Project administration, Writing – review & editing. AC: Conceptualization, Formal analysis, Funding acquisition, Methodology, Resources, Supervision, Writing – review & editing. GS: Conceptualization, Data curation, Formal analysis, Investigation, Methodology, Resources, Supervision, Writing – original draft, Writing – review & editing.

Funding

The author(s) declare that financial support was received for the research and/or publication of this article. This research was funded by Fondo sanzioni SPSAL (Servizio di Prevenzione e Sicurezza Ambienti di Lavoro) art.42 L.R. 11/2001 (Centro di Costo 0210399) and Fondi d'Ateneo Covid-Lab. This work has been funded by the European Union - NextGenerationEU, Mission 4, Component 2, under the Italian Ministry of University and Research (MUR) National Innovation Ecosystem grant ECS00000041 - VITALITY - CUP H33C22000430006.

Acknowledgments

The authors wish to thank Susanna Piergiovanni (University of Urbino Carlo Bo) for the administrative support provided, and they also extend their gratitude to all of the volunteers enrolled in the study.

Conflict of interest

The authors declare that the research was conducted in the absence of any commercial or financial relationships that could be construed as a potential conflict of interest.

The author(s) declared that they were an editorial board member of Frontiers, at the time of submission. This had no impact on the peer review process and the final decision.

Publisher's note

Supplementary material

The Supplementary Material for this article can be found online at: https://www.frontiersin.org/articles/10.3389/fimmu.2025.1579163/full#supplementary-material

References

1. Thanh Le T, Andreadakis Z, Kumar A, Gómez Román R, Tollefsen S, Saville M, et al. The COVID-19 vaccine development landscape. *Nat Rev Drug Discov*. (2020) 19:305–6. doi: 10.1038/d41573-020-00073-5

2. Kaur SP, Gupta V. COVID-19 Vaccine: A comprehensive status report. *Virus Res*. (2020) 288:198114. doi: 10.1016/j.virusres.2020.198114

3. Liu X, Shaw RH, Stuart ASV, Greenland M, Aley PK, Andrews NJ, et al. Safety and immunogenicity of heterologous versus homologous prime-boost schedules with an adenoviral vectored and mRNA COVID-19 vaccine (Com-COV): a single-blind, randomised, non-inferiority trial. *Lancet*. (2021) 398:856–69. doi: 10.1016/S0140-6736(21)01694-9

4. Hillus D, Schwarz T, Tober-Lau P, Vanshylla K, Hastor H, Thibeault C, et al. Safety, reactogenicity, and immunogenicity of homologous and heterologous prime-boost immunisation with ChAdOx1 nCoV-19 and BNT162b2: a prospective cohort study. *Lancet Respiratory Med*. (2021) 9:1255–65. doi: 10.1016/S2213-2600(21)00357-X

5. Atmar RL, Lyke KE, Deming ME, Jackson LA, Branche AR, El Sahly HM, et al. Homologous and heterologous covid-19 booster vaccinations. *New Engl J Med*. (2022) 386:1046–57. doi: 10.1056/NEJMoa2116414

6. Johnson & Johnson Prepares to Resume Phase 3 ENSEMBLE Trial of its Janssen COVID-19 Vaccine Candidate in the U.S (2020). Available online at: https://www.jnj.com/media-center/press-releases/our-company/johnson-johnson-prepares-to-resume-phase-3-ensemble-trial-of-its-janssen-covid-19-vaccine-candidate-in-the-us (Accessed April 22, 2025).

7. Bok K, Sitar S, Graham BS, Mascola JR. Accelerated COVID-19 vaccine development: milestones, lessons, and prospects. *Immunity*. (2021) 54:1636–51. doi: 10.1016/j.immuni.2021.07.017

8. Barocci S, Orlandi C, Diotallevi A, Buffi G, Ceccarelli M, Vandini D, et al. Evaluation of two-month antibody levels after heterologous chAdOx1-S/BNT162b2 vaccination compared to homologous chAdOx1-S or BNT162b2 vaccination. *Vaccines (Basel)*. (2022) 10:491. doi: 10.3390/vaccines10040491

9. Orlandi C, Stefanetti G, Barocci S, Buffi G, Diotallevi A, Rocchi E, et al. Comparing heterologous and homologous COVID-19 vaccination: A longitudinal study of antibody decay. *Viruses*. (2023) 15:1162. doi: 10.3390/v15051162

10. LIAISON® SARS-coV-2 trimericS igG. Available online at: https://www.diasorin.com/sites/default/files/allegati_prodotti/liaisonr_sars-cov-2_trimerics_igg_assay_m0870004408_a_lr_0.pdf (Accessed April 22, 2025).

11. Swadźba J, Anyszek T, Panek A, Martin E. Anti-Spike SARS-CoV-2 IgG Assessment with a Commercial Assay during a 4-Month Course after COVID-19 Vaccination. *Vaccines (Basel)*. (2021) 9:1367. doi: 10.3390/vaccines9111367

12. Jeyanathan M, Afkhami S, Smaill F, Miller MS, Lichty BD, Xing Z. Immunological considerations for COVID-19 vaccine strategies. *Nat Rev Immunol*. (2020) 20:615–32. doi: 10.1038/s41577-020-00434-6

13. Moghadas SM, Vilches TN, Zhang K, Nourbakhsh S, Sah P, Fitzpatrick MC, et al. Evaluation of COVID-19 vaccination strategies with a delayed second dose. *PLoS Biol*. (2021) 19:e3001211. doi: 10.1371/journal.pbio.3001211

14. Moreira ED, Kitchin N, Xu X, Dychter SS, Lockhart S, Gurtman A, et al. Safety and efficacy of a third dose of BNT162b2 covid-19 vaccine. *New Engl J Med*. (2022) 386:1910–21. doi: 10.1056/NEJMoa2200674

15. Biganzoli G, Mendola M, Perrone PM, Antonangeli LM, Longo ABE, Carrer P, et al. The effectiveness of the third dose of COVID-19 vaccine: when should it be performed? *Vaccines*. (2024) 12:315. doi: 10.3390/vaccines12030315

16. Hogan AB, Doohan P, Wu SL, Mesa DO, Toor J, Watson OJ, et al. Estimating long-term vaccine effectiveness against SARS-CoV-2 variants: a model-based approach. *Nat Commun*. (2023) 14:4325. doi: 10.1038/s41467-023-39736-3

17. Wu N, Joyal-Desmarais K, Ribeiro PAB, Vieira AM, Stojanovic J, Sanuade C, et al. Long-term effectiveness of COVID-19 vaccines against infections, hospitalisations, and mortality in adults: findings from a rapid living systematic evidence synthesis and meta-analysis up to December, 2022. *Lancet Respiratory Med*. (2023) 11:439–52. doi: 10.1016/S2213-2600(23)00015-2

18. Lin D-Y, Gu Y, Wheeler B, Young H, Holloway S, Sunny S-K, et al. Effectiveness of covid-19 vaccines over a 9-month period in north carolina. *New Engl J Med*. (2022) 386:933–41. doi: 10.1056/NEJMoa2117128

19. Phuensan P, Sirimongkolkasem J, Tantawichien T, Phannajit J, Kerr SJ, Hansasuta P, et al. Immunogenicity and safety of heterologous versus homologous prime-boost schedules with inactivated and adenoviral vectored SARS-CoV-2 vaccines – A prospective multi-center study. *Heliyon*. (2024) 10:e23246. doi: 10.1016/j.heliyon.2023.e23246

20. Carabelli AM, Peacock TP, Thorne LG, Harvey WT, Hughes J, de Silva TI, et al. SARS-CoV-2 variant biology: immune escape, transmission and fitness. *Nat Rev Microbiol*. (2023) 21:162–77. doi: 10.1038/s41579-022-00841-7

21. Hartley GE, Fryer HA, Gill PA, Boo I, Bornheimer SJ, Hogarth PM, et al. Homologous but not heterologous COVID-19 vaccine booster elicits IgG4+ B-cells and enhanced Omicron subvariant binding. *NPJ Vaccines*. (2024) 9:1–11. doi: 10.1038/s41541-024-00919-8

22. Riefolo F, Castillo-Cano B, Martín-Pérez M, Messina D, Elbers R, Brink-Kwakkel D, et al. Effectiveness of homologous/heterologous booster COVID-19 vaccination schedules against severe illness in general population and clinical subgroups in three European countries. *Vaccine*. (2023) 41:7007–18. doi: 10.1016/j.vaccine.2023.10.011

23. Haq MA, Roy AK, Ahmed R, Kuddusi RU, Sinha M, Hossain MS, et al. Antibody longevity and waning following COVID-19 vaccination in a 1-year longitudinal cohort in Bangladesh. *Sci Rep*. (2024) 14:11467. doi: 10.1038/s41598-024-61922-6

24. Terreri S, Piano Mortari E, Vinci MR, Russo C, Alteri C, Albano C, et al. Persistent B cell memory after SARS-CoV-2 vaccination is functional during breakthrough infections. *Cell Host Microbe*. (2022) 30:400–408.e4. doi: 10.1016/j.chom.2022.01.003

25. Wietschel KA, Fechtner K, Antileo E, Abdurrahman G, Drechsler CA, Makuvise MK, et al. Non-cross-reactive epitopes dominate the humoral immune response to COVID-19 vaccination – kinetics of plasma antibodies, plasmablasts and memory B cells. *Front Immunol*. (2024) 15:1382911. doi: 10.3389/fimmu.2024.1382911

26. Palm A-KE, Henry C. Remembrance of things past: long-term B cell memory after infection and vaccination. *Front Immunol*. (2019) 10:1787. doi: 10.3389/fimmu.2019.01787

27. Spencer AJ, McKay PF, Belij-Rammerstorfer S, Ulaszewska M, Bissett CD, Hu K, et al. Heterologous vaccination regimens with self-amplifying RNA and adenoviral COVID vaccines induce robust immune responses in mice. *Nat Commun*. (2021) 12:2893. doi: 10.1038/s41467-021-23173-1

28. Barros-Martins J, Hammerschmidt SI, Cossmann A, Odak I, Stankov MV, Morillas Ramos G, et al. Immune responses against SARS-CoV-2 variants after heterologous and homologous ChAdOx1 nCoV-19/BNT162b2 vaccination. *Nat Med*. (2021) 27:1525–9. doi: 10.1038/s41591-021-01449-9

29. Murphy EA, Guzman-Cardozo C, Sukhu AC, Parks DJ, Prabhu M, Mohammed I, et al. SARS-CoV-2 vaccination, booster, and infection in pregnant population enhances passive immunity in neonates. *Nat Commun*. (2023) 14:4598. doi: 10.1038/s41467-023-39989-y

30. Vogel E, Kocher K, Priller A, Cheng C-C, Steininger P, Liao B-H, et al. Dynamics of humoral and cellular immune responses after homologous and heterologous SARS-CoV-2 vaccination with ChAdOx1 nCoV-19 and BNT162b2. *eBioMedicine*. (2022) 85:104294. doi: 10.1016/j.ebiom.2022.104294

31. Cohen KW, Linderman SL, Moodie Z, Czartoski J, Lai L, Mantus G, et al. Longitudinal analysis shows durable and broad immune memory after SARS-CoV-2 infection with persisting antibody responses and memory B and T cells. *Cell Rep Med*. (2021) 2:100354. doi: 10.1016/j.xcrm.2021.100354

32. Ciabattini A, Pastore G, Fiorino F, Polvere J, Lucchesi S, Pettini E, et al. Evidence of SARS-coV-2-specific memory B cells six months after vaccination with the BNT162b2 mRNA vaccine. *Front Immunol*. (2021) 12:740708. doi: 10.3389/fimmu.2021.740708

33. Winklmeier S, Eisenhut K, Taskin D, Rübsamen H, Gerhards R, Schneider C, et al. Persistence of functional memory B cells recognizing SARS-CoV-2 variants despite loss of specific IgG. *iScience*. (2022) 25:103659. doi: 10.1016/j.isci.2021.103659

34. Ganji A, Farahani I, Khansarinejad B, Ghazavi A, Mosayebi G. Increased expression of CD8 marker on T-cells in COVID-19 patients. *Blood Cells Molecules Dis*. (2020) 83:102437. doi: 10.1016/j.bcmd.2020.102437

frontiers | Frontiers in Immunology

TYPE Original Research
PUBLISHED 22 May 2025
DOI 10.3389/fimmu.2025.1569151

OPEN ACCESS

EDITED BY
Sonia Jangra,
The Rockefeller University, United States

REVIEWED BY
Alex-Mikael Barkoff,
University of Turku, Finland
Aapo Knuutila,
University of Turku, Finland

*CORRESPONDENCE
Anita H. J. van den Biggelaar
anita@bionet.one
Wassana Wijagkanalan
wassana.w@bionet-asia.com

RECEIVED 31 January 2025
ACCEPTED 23 April 2025
PUBLISHED 22 May 2025

CITATION
Abu-Raya B, Del Giudice G, van den Biggelaar AHJ, Tang Y, Bhat N, Pham HT and Wijagkanalan W (2025) Avidity of pertussis toxin antibodies following vaccination with genetically versus chemically detoxified pertussis toxin-containing vaccines during pregnancy. *Front. Immunol.* 16:1569151. doi: 10.3389/fimmu.2025.1569151

Avidity of pertussis toxin antibodies following vaccination with genetically versus chemically detoxified pertussis toxin-containing vaccines during pregnancy

Bahaa Abu-Raya[1,2,3], Giuseppe Del Giudice[4], Anita H. J. van den Biggelaar[4*], Yuxiao Tang[5], Niranjan Bhat[5], Hong Thai Pham[4] and Wassana Wijagkanalan[4*]

[1]Canadian Center for Vaccinology, Dalhousie University, Izaak Walton Killam (IWK) Health Centre and the Nova Scotia Health Authority, Halifax, NS, Canada, [2]Department of Pediatrics, Dalhousie University, Halifax, NS, Canada, [3]Department of Microbiology and Immunology, Dalhousie University, Halifax, NS, Canada, [4]BioNet-Asia, Bangkok, Thailand, [5]Center for Vaccine Innovation and Access, Seattle, WA, United States

Background: Both the quantity and quality of circulating anti-pertussis toxin antibodies are important for protection against severe pertussis. We compared the avidity of PT-IgG antibodies in pregnant women and their infants following vaccination during pregnancy with pertussis vaccines containing genetically-detoxified pertussis toxin (PT_{gen}) or chemically-detoxified PT (PT_{chem}).

Methods: We analyzed serum samples collected earlier from pregnant women (at delivery) and their infants (at birth and 2 months of age) participating in a clinical trial where pregnant women had been vaccinated during pregnancy with recombinant acellular pertussis vaccine containing 1 µg PT_{gen} (standalone, $ap1_{gen}$, [n=37], or combined to tetanus and diphtheria, $Tdap1_{gen}$ [n=34]), 2 µg PT_{gen} ($Tdap2_{gen}$, n=35), or 5 µg PT_{gen} ($TdaP5_{gen}$, n=34), or acellular pertussis vaccine containing 8 µg PT_{chem} ($Tdap8_{chem}$, n=35). Avidity was assessed by adding increasing concentrations (0.25, 0.5, 1, 1.5, 2, and 3 M) of NH_4SCN as a bond-breaking agent and measuring PT-IgG levels by ELISA.

Findings: Compared with $Tdap8_{chem}$, $TdaP5_{gen}$ vaccination was associated with significantly higher total absolute avidity ($p<0.001$) and medium-high to very-high avidity PT-IgG levels ($p\leq0.02$) in mothers at delivery, infants at birth and infants at 2 months of age. Avidity was comparable to $Tdap8_{chem}$ after vaccination with the low-dose PT_{gen} formulations ($ap1_{gen}$, $Tdap1_{gen}$ or $Tdap2_{gen}$). There were no differences for vaccination during the 2nd or 3rd trimester of pregnancy.

Interpretation: Compared with chemically detoxified vaccines, vaccination during pregnancy with recombinant genetically detoxified acellular pertussis vaccine at lower PT concentration provides infants with at least similar or higher quality PT-IgG antibodies. Consequently, recombinant pertussis vaccines may offer comparable or better protection against pertussis.

KEYWORDS

pertussis, avidity, pertussis toxin, genetically inactivated, recombinant vaccine, maternal immunization, vaccination during pregnancy

1 Introduction

Pertussis is a highly contagious human respiratory infection caused by the bacterium *Bordetella pertussis*. Despite high vaccination coverage, the incidence of pertussis has been increasing globally with cyclic epidemics occurring every 2 to 5 years (1). In 2024, many countries reported the largest pertussis outbreaks since decades (2–5). Pertussis is most severe in young infants who are too young to be vaccinated (6, 7). Pertussis vaccination during pregnancy is a safe and effective strategy to protect vulnerable young infants from severe pertussis (8–11).

Pertussis toxin (PT) plays a fundamental role in the pathogenesis of pertussis (12–14) and is a component of all acellular pertussis vaccines (15–17). Especially in young infants, anti-PT antibodies are an important mechanism of protection against severe disease, which depends on both the quantity and quality of the antibody response (18–21).

Pertussis toxin must be inactivated before it can be safely administered to humans. In most acellular pertussis vaccines, PT has been chemically detoxified; however, chemical treatment can cause conformational changes that lead to dominant immunity against nonprotective epitopes (22–26). Recombinant acellular pertussis vaccines using DNA technologies introducing substitutions in the S1 subunit of wild type PT to inactivate PT were successfully developed and used in childhood immunization programs (27, 28). Genetically detoxified PT (PT_{gen}) retains an antigenic conformation similar to native PT with preservation of epitopes involved in toxin-neutralization (26, 27, 29). In recent years several programs for the development of recombinant acellular pertussis booster vaccines have been initiated (30–33). Results from various clinical trials involving adolescents, adults, and pregnant women and their infants, consistently show that vaccination with PT_{gen} elicits higher PT-IgG antibody titers compared with chemically detoxified PT (PT_{chem}) (30, 31, 34–37).

Avidity, which is a measure of the binding strength between an epitope and an antibody's binding site, is an important parameter of the functionality of antibodies. Higher PT-IgG avidity may contribute to a higher capacity to neutralize pertussis toxin and protect against severe disease (38, 39). PT-IgG avidity following vaccination with chemically inactivated acellular pertussis vaccines has been studied in different populations including in infants born to mothers who were vaccinated during pregnancy (40–42), but to our knowledge has never been studied for recombinant pertussis vaccines containing PT_{gen}.

In this study we compared PT-IgG avidity in pregnant women and their infants following vaccination during pregnancy (20–33 weeks gestation) with one of four different formulations of a recombinant acellular pertussis vaccine containing variable amounts of PT_{gen} compared with chemically inactivated acellular pertussis booster vaccine. A wide range of concentrations of chaotropic (bond-breaking) agent was used to allow a comprehensive analysis of PT-IgG avidity (43).

2 Materials and methods

2.1 Study design

As an exploratory objective of a phase 2 randomized controlled trial of pertussis vaccination during pregnancy, the avidity of PT-IgG antibodies was assessed in serum samples collected from a pre-selected subset of participating maternal-infant pairs. The study design, safety and immunogenicity outcomes have been reported previously (Thai Clinical Trials Registry, TCTR20180725004) (36, 37). Briefly, a total of 400 healthy pregnant women (18–40 years old) living in Bangkok, Thailand, were enrolled between February and October 2019. Participating pregnant women were randomized 1:1:1:1:1 to receive during pregnancy (at 20–33 weeks gestation) one dose of one of five study vaccines, including four recombinant acellular pertussis vaccine formulations (see: Study vaccines). Individual vaccination histories were not available, but assuming participants followed the Thai national immunization program that has had a 99% coverage for 3 childhood doses since 1996, participants likely received 3 doses of whole cell pertussis containing vaccine during childhood (44). Women who had received diphtheria, tetanus or pertussis-containing vaccine(s) within 1 year prior to enrolment were excluded.

2.2 Study vaccines

Recombinant pertussis vaccines were produced by BioNet-Asia (Thailand). PT_{gen} was produced from a recombinant *B. pertussis* strain containing a substitution of two amino acids (R9K and E129G) at the enzymatic active site in sub-unit S1 in the PT operon (29). Formulations included: $ap1_{gen}$ containing 1 µg PT_{gen} and 1 µg filamentous hemagglutinin (FHA); $Tdap1_{gen}$ containing tetanus toxoid (7.5 Lf) and reduced-dose diphtheria toxoid (2 Lf) (Td) combined with $ap1_{gen}$; $Tdap2_{gen}$ ($Boostagen_{RED}$®) containing 2 µg PT_{gen} and 5 µg FHA combined with Td; a licensed $TdaP5_{gen}$ (Boostagen®) 5 µg PT_{gen} and 5 µg FHA combined with Td. The licensed $Tdap8_{chem}$ comparator (Boostrix™, GlaxoSmithKline) contained 8 µg PT_{chem}, 8 µg FHA and 2.5 µg pertactin combined with 5 Lf tetanus toxoid and 2.5 Lf diphtheria toxoid.

2.3 Ethical consideration

The clinical study was conducted in compliance with the International Council for Harmonisation of Technical Requirements for Pharmaceuticals for Human Use (ICH) and Good Clinical Practice (GCP), the Declaration of Helsinki, and local ethical guidelines. Ethical approval was obtained from the Institutional Review Boards of the Faculty of Medicine Siriraj Hospital at Mahidol University, Faculty of Medicine at Chulalongkorn University, Bangkok, Thailand and Western Institutional Review Board (now known as WIRB-Copernicus Group), Washington, USA. Written informed consent was obtained from all pregnant women before recruitment, including consent for follow-up of their newborns.

2.4 Samples collection and processing

Venous blood samples were randomly selected as a subpopulation of cohort samples obtained from pregnant women at the time of delivery, and from their infants at the time of birth (cord blood or from newborn within 72 hours after birth) and at 2 months of age. Avidity was assessed for a randomly selected subset of mother-infant pairs: $ap1_{gen}$, n=37, $Tdap1_{gen}$, n=34, $Tdap2_{gen}$, n=35, $TdaP5_{gen}$, n=34 (n=33 for infants at 2 months), and $Tdap8_{chem}$, n=35 (n=34 for infants at 2 months). Sera were stored at ≤ -20 °C before being shipped on dry ice to the University of British Columbia (Vancouver, British Columbia, Canada) for avidity testing.

2.5 Measurement of total PT-IgG, PT-IgG avidity, avidity indices and calculations

Avidity of PT-IgG antibodies was assessed by measuring PT-specific IgG antibody binding in the presence of a range of chaotrope concentrations (NH_4SCN at 0.25 molar (M), 0.5M, 1M, 1.5M, 2M, 3M]) using a commercial ELISA kit (EURIMMUN) coated with native highly purified *Bordetella pertussis* toxin, as published previously (41, 43). Total PT-IgG was measured in PBS (0M NH_4SCN) in the same ELISA kit at the same time for avidity assay. PT-IgG levels were calculated against the calibration serums quantified based on the WHO International Standard Pertussis Antiserum, human (1st IS NIBSC code 06/140) according to the instruction. Different avidity indices for PT-IgG were calculated as published previously (41, 43) and as described in 2.5.1, 2.5.2 and 2.5.3, and summarized in Table 1.

TABLE 1 Calculation of relative avidity index, fractional relative avidity index, total relative avidity index and quantification of fractional and absolute avidity levels of anti-PT IgG.

Avidity indices	NH_4SCN concentration							
	3 M	2 M	1.5 M	1 M	0.5 M	0.25 M	0 M	<0.25M **
PT-IgG levels (IU/mL)	T_{3M}	T_{2M}	$T_{1.5M}$	T_{1M}	$T_{0.5M}$	$T_{0.25M}$	T_{0M}	N/A
Relative avidity index (RAI)* (%)	$RAI_{3M} = T_{3M}/T_{0M}*100$	$RAI_{2M} = T_{2M}/T_{0M}*100$	$RAI_{1.5M} = T_{1.5M}/T_{0M}*100$	$RAI_1 = T_{1M}/T_{0M}*100$	$RAI_{0.5} = T_{0.5M}/T_{0M}*100$	$RAI_{0.25M} = T_{0.25M}/T_{0M}*100$	N/A	N/A
Fractional RAI (%)	$F\ RAI_{3M} = RAI_{3M}$	$F\ RAI_{2M} = RAI_{2M}-RAI_{3M}$	$F\ RAI_{1.5M} = RAI_{1.5M}-RAI_{2M}$	$F\ RAI_{1M} = RAI_{1M}-RAI_{1.5M}$	$F\ RAI_{0.5M} = RAI_{0.5M}-RAI_{1M}$	$F\ RAI_{0.25M} = RAI_{0.25M}-RAI_{0.5M}$	N/A	$F\ RAI_{<0.25M} = 100\% - RAI_{0.25M}$
Total RAI (AU)	$(F\ RAI_{3M}*3) + (F\ RAI_{2M}*2) + (F\ RAI_{1.5M}*1.5) + (F\ RAI_{1M}*1) + (F\ RAI_{0.5M}*0.5) + (F\ RAI_{0.25M}*0.25) + (F\ RAI_{<0.25M}*0.125)$							
Fractional absolute avidity levels (IU/mL)	$F\ abs_{3M} = F\ RAI_{3M}*T_{0M}$	$F\ abs_{2M} = F\ RAI_{2M}*T_{0M}$	$F\ abs_{1.5M} = F\ RAI_{1.5M}*T_{0M}$	$F\ abs_{1M} = F\ RAI_{1M}*T_{0M}$	$F\ abs_{0.5M} = F\ RAI_{0.5M}*T_{0M}$	$F\ abs_{0.25M} = FRAI_{0.25M}*T_{0M}$	N/A	$F\ abs <_{0.25M} = FRAI_{<0.25M}*T_{0M}$
Total absolute avidity levels (AAU/mL)	$(F\ abs_{3M}*3) + (F\ abs_{2M}*2) + (F\ abs_{1.5M}*1.5) + (F\ abs_{1M}*1) + (F\ abs_{0.5M}*0.5) + (F\ abs_{0.25M}*0.25) + (F\ abs_{<0.25M}*0.125)$							

PT, pertussis toxin; IgG, immunoglobulin G; M, molar; N/A, not applicable; IU/mL, international unit/ml; T, total; RAI, relative avidity index; F, fractional; AU, Avidity Unit; AAU/mL, Absolute Avidity Unit/mL; abs, absolute.

*Samples treated with 0.25M, 0.5M, 1M, 1.5M, 2M, 3M concentrations of NH_4SCN and with optic density values lower than LLOQ in ELISA were assigned an arbitrary RAI value of 15%, 12.5%, 10%, 7.5%, 5%, 2.5% for each NH_4SCN concentrations, respectively. The fractional absolute levels of antibodies quantified at 0.25 M, 0.5 M, 1M, 1.5 M, 2M, and 3M of chaotrope were classified as low, low-medium, medium, medium–high, high and very-high avidity antibodies, respectively. The levels of antibodies eluted by the lowest chaotrope concentration (0.25 M) were classified as very-low avidity antibodies.

**This column includes the Fractional (F) RAI and Fractional (F) absolute (abs) avidity levels of PT-IgG antibodies eluted at the lowest NH_4SCN concentration (Reproduced with minimal changes from Abu-Raya et al, Front. Immunol. 2019).

2.5.1 Total relative avidity index

The total relative avidity index (total RAI) of PT-IgG antibodies was calculated for each sample. First, a relative avidity index (RAI) was calculated for each NH_4SCN concentration as the proportion (%) of PT-IgG concentration in samples treated versus not treated with NH_4SCN (for example, $RAI_{3M}=T_{3M}/T_{0M}*100$ where T_{3M} is PT-IgG concentrations in the presence of 3M NH_4SCN and T_{0M} is PT-IgG concentrations in the absence of NH_4SCN). Next, a fractional RAI (F RAI) (%), defined as the RAI achieved at a specific NH_4SCN concentration, was calculated as the RAI at a specific concentration minus the RAI achieved at the next higher concentration of NH_4SCN (for example, $RAI_{1M}=RAI_{1M}-RAI_{1.5M}=70\%-30\%=40\%$, where 1M and 1.5M represent increasing NH_4SCN concentrations). Finally, for each sample the total RAI (AU), reflecting the weighted contribution of the fractional RAIs achieved at different NH_4SCN concentrations, was calculated by applying a factor to each fractional RAI corresponding to the respective concentration of NH_4SCN giving higher weight to antibodies with higher avidity (e.g. fractional RAI at 2M given a weight of 2): (F RAI_{3M}*3) + (F RAI_{2M}*2) + (F $RAI_{1.5M}$*1.5) + (F RAI_{1M}*1) + (F $RAI_{0.5M}$*0.5) + (F $RAI_{0.25M}$*0.25) + (F $RAI_{<0.25M}$*0.125) as published previously (41, 43).

2.5.2 Fractional absolute avidity levels

As indices involving RAI are relative measures, fractional and total absolute avidity levels were calculated. The fractional absolute avidity level (F abs) of PT-IgG (IU/mL) reflects the level of PT-IgG that is still bound to the antigen at a specific NH_4SCN concentration and calculated as the fractional RAI at a specific NH_4SCN concentration multiplied by the anti-PT IgG concentration in the absence of NH_4SCN (for example, F abs_{3M} = F RAI_{3M}*T_{0M}). F abs quantified (bound to PT) at 0.25M, 0.5M, 1M, 1.5M, 2M, and 3M of NH_4SCN were classified as low, low-medium, medium, medium-high, high and very-high avidity antibodies, respectively. The levels of antibodies eluted (i.e. not bound to the plate) at the lowest NH_4SCN concentration (0.25M) were classified as 'very-low' avidity antibodies.

2.5.3 Total absolute avidity levels

Total absolute avidity levels (AAU/mL) reflect the weighted contribution of the F abs, and higher weight was given to antibodies with higher avidity by applying a factor to each fractional absolute avidity levels corresponding to the respective concentration of NH_4SCN: (F abs_{3M}*3) + (F abs_{2M}*2) + (F $abs_{1.5M}$*1.5) + (F abs_{1M}*1)+ (F $abs_{0.5M}$*0.5) + (F $abs_{0.25M}$*0.25) + (F $abs_{<0.25M}$*0.125) as published previously (41, 43).

2.6 Statistical analysis

Statistical analyses were performed by the Center of Excellence for Biomedical and Public Health Informatics (BIOPHICS), Bangkok, Thailand, using Statistical Analysis System (SAS) version 9.4. Data was analyzed *per protocol*. As this was an exploratory analysis of the main clinical study, no formal hypothesis was generated for this study.

Samples treated with 0.25M, 0.5M, 1M, 1.5M, 2M, 3M concentrations of NH_4SCN and with optic density values lower than LLOQ were assigned an arbitrary RAI value of 15%, 12.5%, 10%, 7.5%, 5%, 2.5% for each NH_4SCN concentrations, respectively. Total PT-IgG levels, total absolute avidity levels of PT-IgG, and F abs levels of PT-IgG did not follow a normal distribution and were log-transformed to calculate geometric mean concentrations (GMCs) and 95% confidence intervals (95% CI). Total RAI of PT-IgG followed a normal distribution and means with 95% CI were calculated. Outcomes were compared for statistical differences between the five different vaccine groups using the Kruskal-Wallis test. In addition, differences between an individual recombinant vaccine group and $Tdap8_{chem}$ were compared using an Independent t-test. Correlations between total PT-IgG and total RAI were assessed by calculating the Spearman correlation coefficient rho. A p-value of ≤ 0.05 was considered statistically significant.

3 Results

3.1 Study population

Demographics and baseline characteristics of pregnant women and their infants included in the avidity analysis are presented in Supplementary Table S1. Vaccination during the 2nd (13–26 weeks gestation) vs. 3rd trimester of pregnancy (≥ 27 weeks gestation) was evenly distributed amongst the vaccine groups.

3.2 Correlation between avidity and PT-IgG levels

Overall correlations between PT-IgG levels and total RAI across (for all vaccine groups combined) were moderate in pregnant women at delivery (Spearman rho = 0.620, p<0.0001), in infants at birth (rho = 0.526, p < 0.0001) and at 2 months of age, rho = 0.724, p<0.0001) (Supplementary Figure S1). This indicates that the avidity of anti-PT IgG measures a function that is not entirely dependent on anti-PT IgG levels.

3.3 Total relative avidity index

PT-IgG total RAIs were comparable in pregnant women at delivery and in infants at birth for each of the recombinant pertussis vaccine formulations compared with $Tdap8_{chem}$ (Figure 1A) (Table 2). However, at 2 months of age, PT-IgG total RAI was significantly higher in infants whose mothers had received $TdaP5_{gen}$ as compared with $Tdap8_{chem}$ (p < 0.001) (Figure 1A; Table 2).

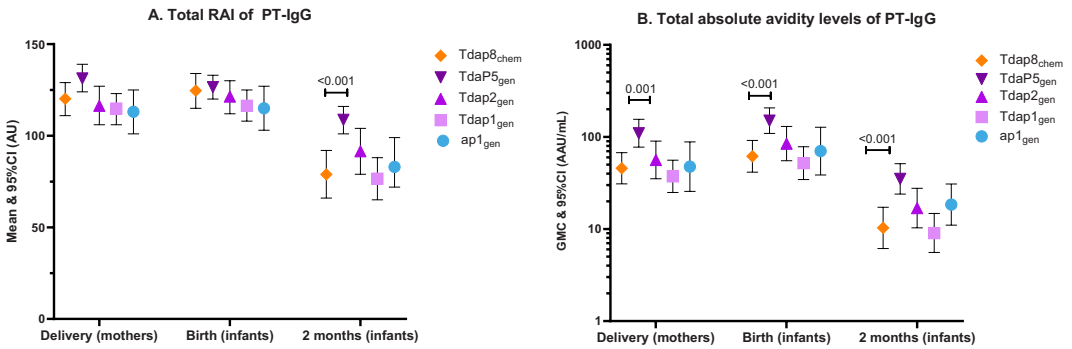

FIGURE 1
PT-IgG total relative avidity index and total absolute avidity in women at delivery, newborns at birth and infants at 2 months of age. The figure shows **(A)** means and 95% confidence intervals (CI) of PT-IgG total relative avidity (total RAI), and **(B)** geometric mean concentrations (GMC) and 95% CI of PT-IgG total absolute avidity levels in pregnant women at delivery and their infants at birth and 2 months of age after vaccination during pregnancy with $Tdap8_{chem}$ (orange; diamond);$TdaP5_{gen}$ (dark purple; downward triangle); $Tdap2_{gen}$ (purple; upward triangle); $Tdap1_{gen}$ (pink; square); or $ap1_{gen}$ (blue; circle). For each individual recombinant vaccine group responses were compared with responses for $Tdap8_{chem}$ using an Independent t-test: when significant (p-value ≤ 0.05), the p-value is noted.

3.4 Total absolute avidity levels

PT-IgG total absolute avidity was significantly higher for $TdaP5_{gen}$ compared with $Tdap8_{chem}$ in pregnant women at the time of delivery (p = 0.0011), in infants at the time of birth (p = 0.0006), and in infants at 2 months of age (p = 0.0002) (Figure 1B) (Table 2). PT-IgG total absolute avidity after vaccination with the lower-dose recombinant pertussis vaccines ($ap1_{gen}$, $Tdap1_{gen}$ or $Tdap2_{gen}$) was comparable with $Tdap8_{chem}$ (Figure 1B; Table 2).

3.5 Fractional absolute avidity (very-low to very-high avidity)

PT-IgG antibodies of absolute very-low to very-high avidity were comparable at the time of delivery in women vaccinated with $ap1_{gen}$, $Tdap1_{gen}$ or $Tdap2_{gen}$ as compared with $Tdap8_{chem}$, except for significantly higher levels of very-low avidity antibodies in infants at birth after vaccination in pregnancy with $Tdap2_{gen}$ versus $Tdap8_{chem}$ (Figures 2A-C; Table 2). Vaccination with $TdaP5_{gen}$ was associated with significantly higher fractional absolute avidity of PT-IgG of all strengths including medium-high, high and very-high binding strength, in pregnant women at delivery, infants at birth, and infants at 2 months of age as compared with $Tdap8_{chem}$ vaccination, with the exception of PT-IgG of low avidity which was comparable in women at delivery and infants at 2 months of age (Figures 2A-C; Table 2).

3.6 Effect of gestation age at the time vaccination on PT-IgG avidity

No differences in PT-IgG avidity were observed in any of the vaccine groups when comparing vaccination in the 2nd versus 3rd trimester of pregnancy. This includes total RAI, total absolute avidity levels, and fractional absolute PT-IgG levels at delivery, in infants at birth and 2 months of age (Figures 3A-C; Supplementary Table S2).

4 Discussion

To our best knowledge, this is the first study describing avidity for PT-IgG antibodies induced by recombinant acellular pertussis vaccine containing genetically inactivated PT. $TdaP5_{gen}$, a licensed recombinant acellular pertussis vaccine containing 5 µg genetically inactivated PT, induced significantly higher PT-IgG avidity in pregnant women and transferred to their infants than a widely used Tdap booster containing 8 µg chemically detoxified PT. Vaccination with lower-dose recombinant acellular pertussis vaccines induced comparable PT-IgG avidity in pregnant women and infants than the comparator $Tdap_{chem}$ vaccine while containing 4- or 8- times less PT.

Several studies have reported on PT-IgG avidity after vaccination with conventional chemically detoxified acellular pertussis vaccines, including three studies analysing cord blood samples from cohorts following vaccination during pregnancy (40, 41, 45). These studies did not follow infants prospectively to investigate the persistence of PT-IgG avidity during the first months of life. In our study, we assessed PT-IgG avidity in cord but also in corresponding samples of mothers at the time of delivery, and longitudinally in infants at 2 months of age. We demonstrated the effective transplacental transfer of PT-IgG avidity from vaccinated mothers to newborns for all pertussis vaccines. Subsequent follow-up of infants at 2 months of age demonstrated that PT-IgG avidity remained significantly higher when mothers had been vaccinated with recombinant $TdaP5_{gen}$.

A plausible explanation why genetically inactivated PT is associated with higher PT-IgG avidity is that in contrast to chemical detoxification of PT that leads to varying degrees of denaturation and loss of important protective conformational

10.3389/fimmu.2025.1569151

TABLE 2 Levels of total PT-IgG, and PT-IgG total relative avidity index, total absolute avidity, and fractional absolute avidity levels of very low to very high avidities in pregnant women at the time of delivery, and infants at the time of birth and at 2 months of age after vaccination during pregnancy with different formulations of recombinant pertussis vaccines or chemically detoxified pertussis vaccine.

Pregnant women at delivery						
	ap1$_{gen}$ (n=37)	**Tdap1$_{gen}$ (n=34)**	**Tdap2$_{gen}$ (n=35)**	**TdaP5$_{gen}$ (n=34)**	**Tdap8$_{chem}$ (n=35)**	**P-value**
PT-IgG, IU/mL GMC (95% CI)	46.88 (29.44-74.66)	33.85 (24.65-46.48)	50.96 (35.05-74.07)	85.06 (61.70-117.25)	39.58 (29.47-53.17)	0.0018
Total RAI, AU Mean (SD)	113.09 (36.48)	114.82 (25.08)	116.36 (31.45)	131.25 (21.96)	120.20 (27.40)	0.0468
Total absolute avidity, AAU/mL GMC (95% CI)	47.62 (25.65-88.42)	37.38 (24.96-55.99)	56.31 (35.18-90.15)	109.72 (77.49-155.34)	45.64 (30.90-67.42)	0.0009
F absolute avidity, IU/mL GMC (95% CI)						
Very low (<0.25 M) Low (0.25 M) Low-medium (0.5 M) Medium (1.0 M) Medium-high (1.5 M) High (2.0 M) Very high (3.0 M)	4.21 (2.47-7.16) 2.59 (1.44-4.67) 5.69 (3.12-10.36) 5.68 (3.03-10.64) 7.29 (3.91-13.59) 6.91 (3.24-14.74) 2.69 (1.37-5.30)	3.58 (2.48-5.17) 1.75 (1.03-2.98) 4.90 (3.31-7.27) 5.37 (3.62-7.97) 5.06 (3.37-7.58) 5.34 (2.92-9.76) 1.26 (0.75-2.11)	4.62 (3.11-6.86) 3.57 (2.55-5.00) 8.18 (5.07-13.18) 6.18 (3.69-10.35) 5.97 (3.45-10.35) 9.19 (5.06-16.67) 2.81 (1.59-4.96)	7.19 (5.25-9.85) 4.08 (2.53-6.58) 12.67 (8.68-18.51) 12.66 (8.68-18.46) 11.20 (7.42-16.91) 19.60 (13.42-28.63) 7.43 (4.68-11.77)	3.68 (2.59-5.22) 2.46 (1.66-3.64) 6.74 (4.70-9.66) 5.35 (3.65-7.84) 5.96 (4.21-8.44) 6.40 (3.66-11.19) 2.21(1.27-3.85)	0.0446 0.0818 0.0314 0.0019 0.0087 0.0020 0.0011
Infants at the time of birth						
	ap1$_{gen}$ (n=37)	**Tdap1$_{gen}$ (n=34)**	**Tdap2$_{gen}$ (n=35)**	**TdaP5$_{gen}$ (n=34)**	**Tdap8$_{chem}$ (n=35)**	**P-value**
PT-IgG, IU/mL GMC (95% CI)	67.39 (42.77-106.19)	46.33 (33.72-63.65)	72.10 (50.45-103.06)	120.17 (88.85-162.52)	51.58 (38.30-69.47)	0.0010
Total RAI, AU Mean (SD)	115.00 (37.91)	116.40 (24.16)	121.40 (27.21)	126.53 (18.46)	124.65 (29.02)	0.4630
Total absolute avidity, AAU/mL GMC (95% CI)	70.23 (38.67-127.57)	51.92 (34.46-78.23)	84.61 (55.10-129.94)	150.31 (109.38-206.55)	61.58 (41.42-91.55)	0.0014
F absolute avidity, IU/mL GMC (95% CI)						
Very low (<0.25 M) Low (0.25 M) Low-medium (0.5 M) Medium (1.0 M) Medium-high (1.5 M) High (2.0 M) Very high (3.0 M)	4.85 (2.74-8.58) 3.84 (2.09-7.06) 9.61 (5.37-17.19) 7.67 (4.31-13.63) 6.88 (3.68-12.86) 12.28 (6.00-25.14) 4.51 (2.37-8.60)	5.33 (3.76-7.57) 2.43 (1.56-3.79) 6.87 (4.30-10.96) 6.93 (4.73-10.17) 5.78 (3.61-9.24) 9.05 (5.35-15.30) 2.17 (1.29-3.66)	7.43 (5.56-9.92) 4.68 (3.12-7.03) 10.26 (7.02-15.01) 9.00 (5.59-14.49) 11.22 (6.89-18.28) 13.22 (7.81-22.36) 4.50 (2.54-7.97)	11.18 (7.69-16.27) 7.33 (4.89-10.99) 18.72 (13.82-25.34) 16.47 (11.96-22.68) 18.29 (12.67-26.42) 27.57 (18.98-40.05) 9.32 (6.17-14.06)	4.39 (3.04-6.33) 3.73 (2.62-5.32) 7.31 (4.98-10.73) 6.98 (4.78-10.18) 7.28 (4.91-10.80) 9.67 (5.87-15.95) 3.69 (2.14-6.34)	0.0092 0.0332 0.0015 0.0167 0.0009 0.0006 0.0037
Infants at 2 months of age						
	ap1$_{gen}$ (n=37)	**Tdap1$_{gen}$ (n=34)**	**Tdap2$_{gen}$ (n=35)**	**TdaP5$_{gen}$ (n=33)**	**Tdap8$_{chem}$ (n=34)**	**P-value**
PT-IgG, IU/mL GMC (95% CI)	24.96 (17.55-35.49)	13.63 (10.01-18.55)	20.95 (15.08-29.10)	33.34 (24.30-45.74)	15.30 (11.09-21.10)	0.0012
Total RAI, AU Mean (SD)	82.98 (33.43)	76.57 (34.79)	91.53 (37.57)	108.73 (21.46)	78.88 (38.81)	0.0011
Total absolute avidity, AAU/mL GMC (95% CI)	18.42 (11.02-30.79)	9.05 (5.56-14.74)	16.87 (10.29-27.67)	35.04 (23.97-51.23)	10.29 (6.13-17.26)	0.0010
F absolute avidity, IU/mL GMC (95% CI)						
Very low (<0.25 M) Low (0.25 M)	3.35 (2.08-5.40) 1.87 (1.07-3.25)	1.84 (1.09-3.11) 0.68 (0.40-1.16)	2.72 (1.73-4.29) 0.96 (0.59-1.57)	3.84 (2.77-5.32) 1.97 (1.25-3.10)	1.89 (1.13-3.18) 1.09 (0.66-1.81)	0.0547 0.0124

(Continued)

10.3389/fimmu.2025.1569151

TABLE 2 Continued

Infants at 2 months of age						
	$ap1_{gen}$ (n=37)	$Tdap1_{gen}$ (n=34)	$Tdap2_{gen}$ (n=35)	$TdaP5_{gen}$ (n=33)	$Tdap8_{chem}$ (n=34)	P-value
Low-medium (0.5 M)	3.86 (2.29-6.50)	2.03 (1.15-3.59)	2.87 (1.71-4.84)	5.19 (3.60-7.48)	1.91 (1.06-3.47)	0.0550
Medium (1.0 M)	2.57 (1.41-4.68)	1.23 (0.67-2.25)	2.07 (1.18-3.65)	4.87 (3.30-7.18)	1.22 (0.67-2.25)	0.0125
Medium-high (1.5 M)	1.85 (1.01-3.38)	1.03 (0.56-1.90)	2.17 (1.22-3.88)	5.73 (4.08-8.06)	1.04 (0.56-1.95)	0.0003
High (2.0 M)	1.90 (0.96-3.78)	0.67 (0.36-1.23)	1.76 (0.91-3.42)	4.78 (2.69-8.48)	0.95 (0.49-1.83)	0.0005
Very high (3.0 M)	0.73 (0.47-1.14)	0.37 (0.25-0.55)	0.64 (0.40-1.03)	1.11 (0.68-1.81)	0.43 (0.29-0.64)	0.0024

RAI, relative avidity index; F, Fractional; SD, standard deviation; AU, Avidity Unit; AAU/mL, Absolute Avidity Unit/mL; $ap1_{gen}$, acellular-pertussis vaccine containing 1 µg of pertussis toxin genetically detoxified (PT_{gen}); $Tdap1_{gen}$, tetanus, reduced-dose diphtheria [Td] combined with $ap1_{gen}$; $Tdap2_{gen}$, Td combined with 2 µg PT_{gen}; $TdaP5_{gen}$, Td combined with 5 µg PT_{gen}; $Tdap8_{chem}$ Td combined with 8 µg of pertussis toxin chemically-detoxified; PT, Pertussis toxin; IgG, immunoglobulin G; IU, international unit; GMC, Geometric mean concentration; CI, Confidence interval. P-values are based on comparison of outcomes for all vaccine groups using Kruskal-Wallis Test. A p-value of ≤ 0.05 is considered statistically significant.

epitopes, site-specific genetic detoxification maintains the three-dimensional structure of the toxin (22, 26, 33). The crystal structure of PT_{gen} R9K/E129G (included in the recombinant pertussis vaccines studied here) is nearly identical to that of native PT and antigen stimulation of human whole blood indicated broader immunogenicity of PT_{gen} R9K/E129G compared with PT_{chem} (33). Furthermore, using cryo-electron microscopy it was recently shown that two potently neutralizing anti-PT antibodies with complementary mechanisms, hu11E6 and hu1B7, bind to PT_{gen} R9K/E129G, thereby confirming the preservation of these neutralizing binding sites in PT_{gen} (26).

Analysis of epitope binding, PT-neutralizing antibodies, memory-B cells, and avidity are all parameters of the quality of the anti-PT immune response. It has been demonstrated in multiple clinical trials that vaccination with genetically detoxified PT induces higher PT-neutralizing antibody titers compared with licensed $Tdap_{chem}$ vaccines (31, 34, 35, 46). Longitudinal follow-up studies of participants vaccinated with recombinant acellular pertussis vaccine containing 5 µg PT_{gen} have shown that PT-neutralizing antibody levels remain elevated for at least 5 years (47, 48), and following vaccination during pregnancy PT-neutralizing antibodies are effectively transferred to infants in whom they remain elevated for at least 2 months at significantly higher levels compared with $Tdap_{chem}$ (36, 37). Vaccination with PT_{gen} but not PT_{chem} also elicits robust memory B-cell responses to PT as demonstrated in a clinical trial of booster vaccination in adolescents (34). The current observations of higher PT-IgG avidity add further evidence to the higher quality of the immune response induced by genetically as compared with chemically detoxified PT (38, 49, 50).

This study further showed that recombinant vaccine containing lower quantities of PT_{gen} (1 µg and 2 µg) elicited PT-IgG avidity comparable to $Tdap_{chem}$ containing 4- or 8- fold more PT. This provides further evidence that the inactivation process of PT is a critical determinant of PT-IgG avidity and that genetic versus chemical detoxification leads to higher avidity.

We also studied whether vaccination at various stages of gestation of pregnancy might affect the avidity of antibodies transferred to infants. No differences in PT-IgG avidity were observed when mothers were vaccinated during the 2^{nd} or 3^{rd} trimester of pregnancy for any of the studied vaccines. This is consistent with a Swiss study that analyzed cord blood samples from infants born to mothers vaccinated with $Tdap_{chem}$ during pregnancy, and did not find PT-IgG avidity when comparing second versus third trimester vaccination, or different intervals between vaccination and birth (51). A difference with our study is that in the Swiss study PT-IgG avidity was assessed using three concentrations of NH_4SCN (1M, 2M and 3M) as compared with six in our study (0.25M, 0.5M, 1M, 1.5M, 2M and 3M) and results were presented in relative avidity indices that do not incorporate absolute antibody levels. In another study using a series of chaotropic concentrations similar to our study, PT-IgG avidity was found to be higher in newborns when mothers had been vaccinated with $Tdap_{chem}$ during 28–32 weeks of gestation as compared with 33–36 weeks of gestation, or when vaccinated 5–12 weeks before delivery versus within 4 weeks before delivery (41). It is plausible that using a broader range of chaotropic concentrations provides deeper insights into avidity development, thereby increasing the likelihood of detecting differential avidity responses. Other factors that may explain discrepancies in reported results include but are not limited to differences in pertussis epidemiology and vaccination history and the small sample size in this study.

Although there is no direct evidence confirming the clinical relevance of PT-IgG avidity, there is evidence from other respiratory bacterial infections supporting the notion that higher avidity provides higher protection. For example, in mice the levels of anti-pneumococcal serotype 6B-specific antibodies needed to prevent lethal bacteremia from the same serotype were found to be lower for high avidity antibodies (38). For *Haemophilus influenzae* type b (Hib) the avidity of antibodies induced following vaccination with Hib conjugate vaccine was shown to be a surrogate for protective immunity (49). Therefore, it may be assumed that the higher PT-IgG avidity response induced by vaccination with PT_{gen} containing vaccine contributes to improved protection compared to PT_{chem}. While there are no efficacy trials for the current new generation of recombinant acellular pertussis vaccines, it has previously been reported that the efficacy of a former pediatric

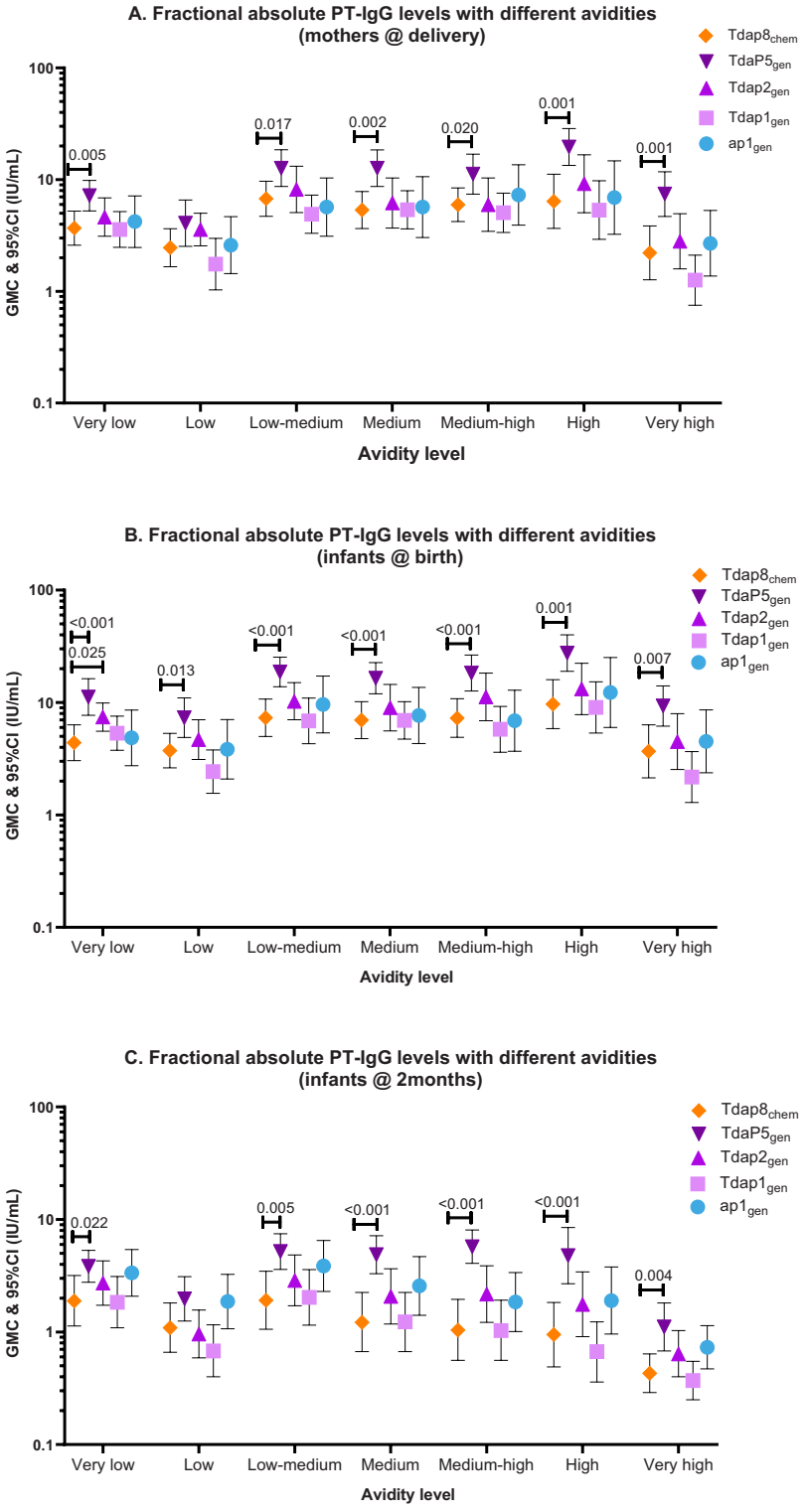

FIGURE 2
PT-IgG fractional absolute avidity (F abs) levels in women at delivery, newborns at birth and infants at 2 months of age. The figure shows geometric mean concentrations (GMC) and 95% confidence intervals (CI) for PT-IgG fractional absolute levels (F abs) with different avidities in **(A)** pregnant women at delivery, and **(B)** their infants at birth and **(C)** 2 months of age after vaccination during pregnancy with $Tdap8_{chem}$ (orange; diamond); $TdaP5_{gen}$ (dark purple; downward triangle); $Tdap2_{gen}$ (purple; upward triangle); $Tdap1_{gen}$ (pink; square)); or $ap1_{gen}$ (blue; circle). F abs quantified at 0.25M, 0.5M, 1M, 1.5M, 2M, and 3M of NH_4SCN were classified as low, low-medium, medium, medium-high, high and very-high avidity, respectively. Responses were compared For each individual recombinant vaccine group with responses for $Tdap8_{chem}$ using an Independent t-test: when significant (p-value $\leq$ 0.05), the p-value is noted.

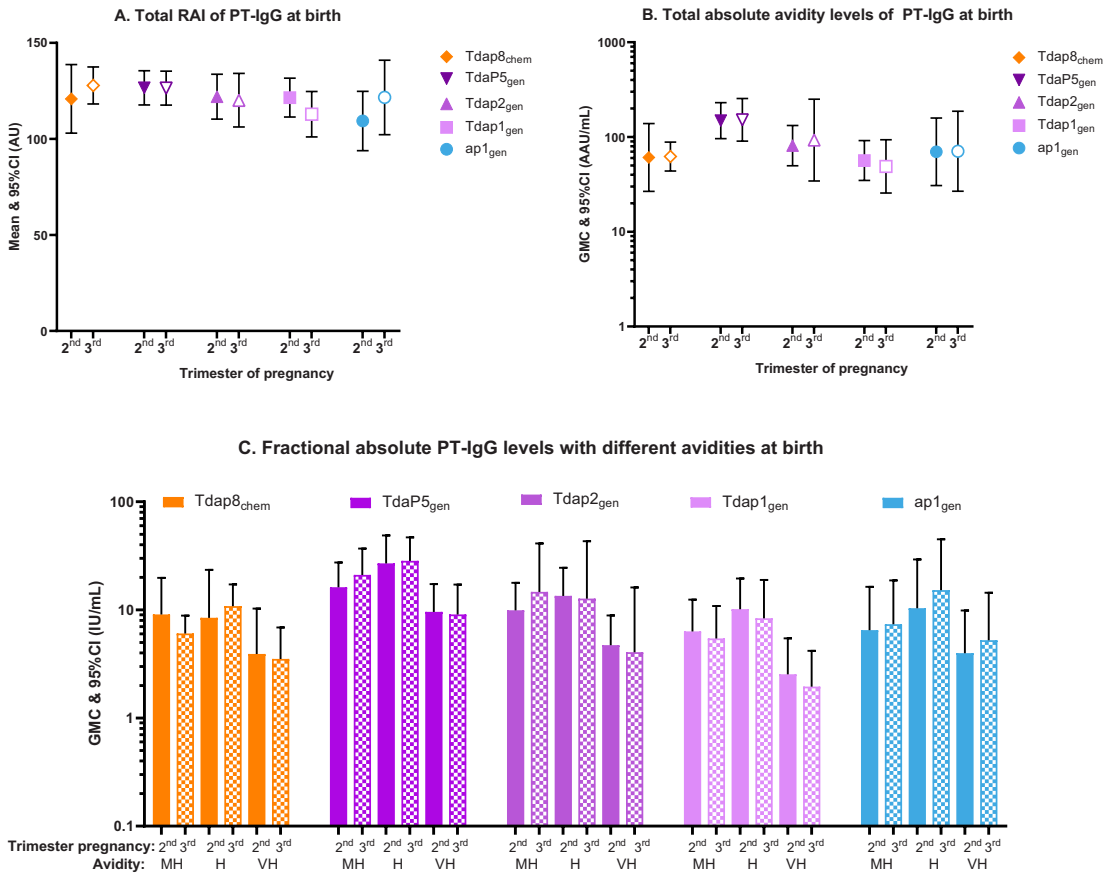

FIGURE 3
Total relative avidity index (Total RAI), total absolute avidity levels, and fractional absolute PT-IgG levels measured in newborns at the time of birth according to vaccination in the 2nd or 3rd trimester of pregnancy. The figure shows **(A)** means and 95% confidence intervals (CI) of PT-IgG total relative avidity (total RAI), **(B)** geometric mean concentrations (GMC) and 95% CI of PT-IgG total absolute levels, and **(C)** GMCs and 95% CI of fractional absolute levels (F abs) in infants at the time of birth after vaccination with $Tdap8_{chem}$ (orange; diamond); $TdaP5_{gen}$ (dark purple; downward triangle); $Tdap2_{gen}$ (purple; upward triangle); $Tdap1_{gen}$ (pink; square); or $ap1_{gen}$ (blue; circle) during the 2nd trimester (closed symbols and bars) or 3rd trimester (open symbols and pattern bars). Only F abs quantified at 1.5M, 2M, and 3M of NH_4SCN and classified as medium-high (MH), high (H) and very-high (VH) avidity, are presented. Responses were compared for vaccination during the 2nd versus. 3rd trimester using an Independent t-test, but no statistical differences were found.

recombinant acellular pertussis vaccine was comparable to that of chemically detoxified acellular pertussis vaccine whilst containing 5-times less PT (50). In our study, formulations of recombinant pertussis vaccine with 4-to-8-times less PT content than the chemically detoxified comparator induced similar PT-IgG avidity, which may translate into similar efficacy.

Our study has strengths and limitations. Our study is unique in that it provides detailed characterization of a full spectrum of avidity of PT-IgG for different PT_{gen} doses and formulations of recombinant acellular pertussis vaccine. Using a dilution series of NH_4SCN to provide the whole spectrum of avidity is essential considering the lack of knowledge of a clinically relevant levels avidity (42). In addition, antibody avidity was not only assessed in infants at birth, but also at 2 months old, and in the vaccinated mothers. This makes it one of the most comprehensive studies on PT-IgG antibody avidity following pertussis vaccination in pregnancy. Longer follow-up of infants beyond 2 months of age would have enabled demonstrating the persistence of elevated PT-IgG avidity and potential longer-lasting protection offered by maternal $Tdap5_{gen}$ vaccination in infants; however, infants received childhood DTP vaccines starting at 2 months of age and assessing PT-IgG avidity in children following primary immunization was out of the scope of this study. In the main clinical trial, however, it was demonstrated that at 5 months of age (1 month after infants had completed the 2nd priming dose), PT-IgG levels remained significantly higher in infants whose mothers had received $TdaP5_{gen}$ versus $Tdap8_{chem}$: a difference that may be explained by the persistence of higher maternal PT-IgG levels in the maternal recombinant $TdaP5_{gen}$ vaccine group (52).Assessing PT-IgG avidity in infants where the local recommendation is to start the first priming dose at 3 months of age or older, may be something to consider for a future study. Other limitations include the relatively small sample size which could affect the generalizability of the results and limit statistical power, and that we did not analyze PT-IgG avidity in baseline samples in pregnant women before vaccination. Pre-vaccination PT-IgG levels had been assessed earlier and found to be low in all study groups (36): measurement of avidity would not have yielded quantifiable levels that can be

analyzed. It is also yet to be studied how vaccination history may impact avidity responses. Like most pregnant women worldwide, including in countries that changed to priming with acellular pertussis vaccines, pregnant women participating in our study were vaccinated in childhood with whole cell pertussis vaccines and are unlikely to have received pertussis booster vaccines after priming in infancy (44). Studies in forthcoming years, when relatively more pregnant women will have vaccinated exclusively with acellular pertussis vaccines, may show how this affects PT-IgG antibody avidity in infants of mothers vaccinated in pregnancy.

In conclusion, the method that is used to inactivate PT for immunization influences PT-IgG avidity. Vaccination during pregnancy with recombinant acellular pertussis vaccines containing genetically detoxified PT at lower content than acellular pertussis vaccines containing chemically detoxified PT results in efficient transplacental transfer of at least similar or higher quantity and quality anti-PT antibodies. Vaccination with recombinant acellular pertussis vaccine may therefore provide infants with highly efficient and longer-lasting immune protection during the first most vulnerable months in life, but this remains to be studied.

Data availability statement

The data that support the findings of this study are available from the corresponding author upon request.

Ethics statement

The studies involving humans were approved by the Institutional Review Boards of the Faculty of Medicine Siriraj Hospital at Mahidol University, Faculty of Medicine at Chulalongkorn University, Bangkok, Thailand and Western Institutional Review Board (now known as WIRB-Copernicus Group), Washington, USA. The studies were conducted in accordance with the local legislation and institutional requirements. Written informed consent for participation in this study was provided by the participants' legal guardians/next of kin.

Author contributions

BA-R: Formal analysis, Writing – original draft, Writing – review & editing, Conceptualization, Investigation, Methodology, Supervision. GG: Formal analysis, Investigation, Methodology, Writing – original draft, Writing – review & editing. AB: Formal analysis, Investigation, Writing – original draft, Writing – review & editing, Visualization. YT: Formal analysis, Writing – original draft, Writing – review & editing. NB: Investigation, Methodology, Project administration, Writing – original draft, Writing – review & editing. HTP: Funding acquisition, Investigation, Resources, Supervision, Writing – original draft, Writing – review & editing. WW: Conceptualization, Formal analysis, Investigation, Methodology, Project administration, Writing – original draft, Writing – review & editing.

Funding

The author(s) declare that financial support was received for the research and/or publication of this article. This work was funded by a grant from the Bill & Melinda Gates Foundation Seattle, USA (grant number OPP1120084). The findings and conclusions contained within are those of the authors and do not necessarily reflect the positions or policies of the Bill & Melinda Gates Foundation.

Acknowledgments

We thank all study participants (pregnant women and their infants), study investigators, and clinical staff at the Faculty of Medicine Siriraj Hospital, Mahidol University and Center of Excellence in Pediatric Infectious Diseases and Vaccines, Chulalongkorn University, for their valuable contributions to the clinical trial that provided the serum samples of this analysis. We also thank BioNet-Asia's clinical operations team for their significant contributions to the clinical trials, and ethical approval and sample arrangement for this supply chain team for sample shipment, and the members of BioNet scientific advisory board for their advice. We also thank BIOPHICS for data management and statistical analysis, and the PATH team.

Conflict of interest

Author BA-R received honoraria for participation in live meetings from Sanofi Pasteur France and Canada related to pertussis and RSV. BA-R received nominal payment as a reviewer for ELSEVIER and as a member of a data and safety monitoring board for a study conducted by Chulalongkorn University (Bangkok, Thailand). BA-R is co-investigator on studies funded by GSK, Pfizer, Merck, Moderna, Vaccitech and Inventprise. All funds have been paid to his institute, and he has not received any personal payments. Authors GG and AB received consultancy honoraria from BioNet-Asia including for the published work. Authors WW and HTP are employees of BioNet-Asia.

The remaining authors declare that the research was conducted in the absence of any commercial or financial relationships that could be construed as a potential conflict of interest.

Generative AI statement

The author(s) declare that no Generative AI was used in the creation of this manuscript.

Publisher's note

Supplementary material

The Supplementary Material for this article can be found online at: https://www.frontiersin.org/articles/10.3389/fimmu.2025.1569151/full#supplementary-material

References

1. Decker MD, Edwards KM. Pertussis (Whooping cough). *J Infect Dis*. (2021) 224: S310–s20. doi: 10.1093/infdis/jiaa469

2. European Centre for Disease Prevention and Control E. *Increase of pertussis cases in the EU/EEA*. Stockholm: ECDC (2024).

3. Nordholm AC, Emborg HD, Nørgaard SK, Nygaard U, Ronayne A, Nielsen LB, et al. Pertussis epidemic in Denmark, August 2023 to February 2024. *Euro Surveill*. (2024) 29. doi: 10.2807/1560-7917.es.2024.29.14.2400160

4. UK Health Security Agency. Confirmed cases of pertussis in England by month . Available online at: https://www.gov.uk/government/publications/pertussis-epidemiology-in-england-2024/confirmed-cases-of-pertussis-in-england-by-month (Accessed December 1, 2024).

5. Holt E. Pertussis outbreak in Czech Republic. *Lancet Infect Dis*. (2024) 24:e359. doi: 10.1016/s1473-3099(24)00291-3

6. Winter K, Zipprich J, Harriman K, Murray EL, Gornbein J, Hammer SJ, et al. Risk factors associated with infant deaths from pertussis: A case-control study. *Clin Infect Dis*. (2015) 61:1099–106. doi: 10.1093/cid/civ472

7. Abu-Raya B, Bettinger JA, Vanderkooi OG, Vaudry W, Halperin SA, Sadarangani M, et al. Burden of children hospitalized with pertussis in Canada in the acellular pertussis vaccine era, 1999-2015. *J Pediatr Infect Dis Soc*. (2020) 9:118–27. doi: 10.1093/jpids/piy128

8. Amirthalingam G, Andrews N, Campbell H, Ribeiro S, Kara E, Donegan K, et al. Effectiveness of maternal pertussis vaccination in England: an observational study. *Lancet*. (2014) 384:1521–8. doi: 10.1016/s0140-6736(14)60686-3

9. Baxter R, Bartlett J, Fireman B, Lewis E, Klein NP. Effectiveness of vaccination during pregnancy to prevent infant pertussis. *Pediatrics*. (2017) 139. doi: 10.1542/peds.2016-4091

10. Fernandes EG, Sato APS, Vaz-de-Lima LRA, Rodrigues M, Leite D, de Brito CA, et al. The effectiveness of maternal pertussis vaccination in protecting newborn infants in Brazil: A case-control study. *Vaccine*. (2019) 37:5481–4. doi: 10.1016/j.vaccine.2019.03.049

11. Kandeil W, van den Ende C, Bunge EM, Jenkins VA, Ceregido MA, Guignard A. A systematic review of the burden of pertussis disease in infants and the effectiveness of maternal immunization against pertussis. *Expert Rev Vaccines*. (2020) 19:621–38. doi: 10.1080/14760584.2020.1791092

12. Paddock CD, Sanden GN, Cherry JD, Gal AA, Langston C, Tatti KM, et al. Pathology and pathogenesis of fatal Bordetella pertussis infection in infants. *Clin Infect Dis*. (2008) 47:328–38. doi: 10.1086/589753

13. Halasa NB, Barr FE, Johnson JE, Edwards KM. Fatal pulmonary hypertension associated with pertussis in infants: does extracorporeal membrane oxygenation have a role? *Pediatrics*. (2003) 112:1274–8. doi: 10.1542/peds.112.6.1274

14. Scanlon K, Skerry C, Carbonetti N. Association of pertussis toxin with severe pertussis disease. *Toxins (Basel)*. (2019) 11. doi: 10.3390/toxins11070373

15. Taranger J, Trollfors B, Lagergard T, Sundh V, Bryla DA, Schneerson R, et al. Correlation between pertussis toxin IgG antibodies in postvaccination sera and subsequent protection against pertussis. *J Infect Dis*. (2000) 181:1010–3. doi: 10.1086/315318

16. Dalby T, Andersen PH, Hoffmann S. Epidemiology of pertussis in Denmark, 1995 to 2013. *Euro Surveill*. (2016) 21:30334. doi: 10.2807/1560-7917.es.2016.21.36.30334

17. Gregg KA, Merkel TJ. Pertussis toxin: a key component in pertussis vaccines? *Toxins (Basel)*. (2019) 11:557. doi: 10.3390/toxins11100557

18. Nguyen AW, DiVenere AM, Papin JF, Connelly S, Kaleko M, Maynard JA. Neutralization of pertussis toxin by a single antibody prevents clinical pertussis in neonatal baboons. *Sci Adv*. (2020) 6:eaay9258. doi: 10.1126/sciadv.aay9258

19. Healy CM, Rench MA, Swaim LS, Timmins A, Vyas A, Sangi-Haghpeykar H, et al. Kinetics of maternal pertussis-specific antibodies in infants of mothers vaccinated with tetanus, diphtheria and acellular pertussis (Tdap) during pregnancy. *Vaccine*. (2020) 38:5955–61. doi: 10.1016/j.vaccine.2020.06.050

20. Abu-Raya B, Forsyth K, Halperin SA, Maertens K, Jones CE, Heininger U, et al. Vaccination in pregnancy against pertussis: a consensus statement on behalf of the global pertussis initiative. *Vaccines (Basel)*. (2022) 10:1990. doi: 10.3390/vaccines10121990

21. Barkoff AM, Knuutila A, Mertsola J, He Q. Evaluation of anti-PT antibody response after pertussis vaccination and infection: the importance of both quantity and quality. *Toxins (Basel)*. (2021) 13. doi: 10.3390/toxins13080508

22. Ibsen PH. The effect of formaldehyde, hydrogen peroxide and genetic detoxification of pertussis toxin on epitope recognition by murine monoclonal antibodies. *Vaccine*. (1996) 14:359–68. doi: 10.1016/0264-410x(95)00230-x

23. Sutherland JN, Chang C, Yoder SM, Rock MT, Maynard JA. Antibodies recognizing protective pertussis toxin epitopes are preferentially elicited by natural infection versus acellular immunization. *Clin Vaccine Immunol*. (2011) 18:954–62. doi: 10.1128/cvi.00561-10

24. Van den Biggelaar AHJ, Poolman JT. Predicting future trends in the burden of pertussis in the 21st century: implications for infant pertussis and the success of maternal immunization. *Expert Rev Vaccines*. (2016) 15:69–80. doi: 10.1586/14760584.2016.1105136

25. Eberhardt CS, Siegrist CA. What is wrong with pertussis vaccine immunity? Inducing and recalling vaccine-specific immunity. *Cold Spring Harb Perspect Biol*. (2017) 9. doi: 10.1101/cshperspect.a029629

26. Goldsmith JA, Nguyen AW, Wilen RE, Wijagkanalan W, McLellan JS, Maynard JA. Structural basis for antibody neutralization of pertussis toxin. *PNAS*. (2025) 122: e2419457122. doi: 10.1073/pnas.2419457122

27. Rappuoli R. Rational design of vaccines. *Nat Med*. (1997) 3:374–6. doi: 10.1038/nm0497-374

28. Del Giudice G, Rappuoli R. Genetically derived toxoids for use as vaccines and adjuvants. *Vaccine*. (1999) 17 Suppl 2:S44–52. doi: 10.1016/s0264-410x(99)00234-0

29. Buasri W, Impoolsup A, Boonchird C, Luengchaichawange A, Prompiboon P, Petre J, et al. Construction of Bordetella pertussis strains with enhanced production of genetically-inactivated Pertussis Toxin and Pertactin by unmarked allelic exchange. *BMC Microbiol*. (2012) 12:61. doi: 10.1186/1471-2180-12-61

30. Leroux-Roels G, Lattanzi M, Solis CD, Contorni M, Costantini M, Moraschini L, et al. randomized, controlled, dose-ranging study of investigational acellular pertussis (aP) and reduced tetanus-diphtheria-acellular pertussis (TdaP) booster vaccines in adults. *Hum Vaccin Immunother*. (2017) 14:45–58. doi: 10.1080/21645515.2017.1385686

31. Sricharoenchai S, Sirivichayakul C, Chokephaibulkit K, Pitisuttithum P, Dhitavat J, Pitisuthitham A, et al. A genetically inactivated two-component acellular pertussis vaccine, alone or combined with tetanus and reduced-dose diphtheria vaccines, in adolescents: a phase 2/3, randomised controlled non-inferiority trial. *Lancet Infect Dis*. (2018) 18:58–67. doi: 10.1016/s1473-3099(17)30612-6

32. Auderset F, Ballester M, Mastelic-Gavillet B, Fontannaz P, Chabaud-Riou M, Reveneau N, et al. Reactivating immunity primed by acellular pertussis vaccines in the absence of circulating antibodies: enhanced bacterial control by TLR9 rather than TLR4 agonist-including formulation. *Front Immunol*. (2019) 10:1520. doi: 10.3389/fimmu.2019.01520

33. Ausar SF, Zhu S, Duprez J, Cohen M, Bertrand T, Steier V, et al. Genetically detoxified pertussis toxin displays near identical structure to its wild-type and exhibits robust immunogenicity. *Commun Biol*. (2020) 3:427. doi: 10.1038/s42003-020-01153-3

34. Blanchard Rohner G, Chatzis O, Chinwangso P, Rohr M, Grillet S, Salomon C, et al. Boosting teenagers with acellular pertussis vaccines containing recombinant or chemically inactivated pertussis toxin: a randomized clinical trial. *Clin Infect Dis*. (2018) 68:1213–22. doi: 10.1093/cid/ciy594

35. Chokephaibulkit K, Puthanakit T, Bhat N, Mansouri S, Tang Y, Lapphra K, et al. A phase 2 randomized controlled dose-ranging trial of recombinant pertussis booster

vaccines containing genetically inactivated pertussis toxin in women of childbearing age. *Vaccine*. (2022) 40:2352–61. doi: 10.1016/j.vaccine.2021.10.076

36. Puthanakit T, Chokephaibulkit K, Chaithongwongwatthana S, Bhat N, Tang Y, Anugulruengkitt S, et al. A phase 2 randomized controlled dose-ranging trial of recombinant pertussis booster vaccines containing genetically inactivated pertussis toxin in pregnant women. *Vaccine*. (2023) 31:4541–53. doi: 10.1016/j.vaccine.2023.06.001

37. Chokephaibulkit K, Puthanakit T, Chaithongwongwatthana S, Bhat N, Tang Y, Anugulruengkitt S, et al. Effective and safe transfer of maternal antibodies persisting two months postpartum following maternal immunization with different doses of recombinant pertussis-containing vaccines. *Vaccine*. (2024) 42:383–95. doi: 10.1016/j.vaccine.2023.11.042

38. Usinger WR, Lucas AH. Avidity as a determinant of the protective efficacy of human antibodies to pneumococcal capsular polysaccharides. *Infect Immun*. (1999) 67:2366–70. doi: 10.1128/iai.67.5.2366-2370.1999

39. Oostindie SC, Lazar GA, Schuurman J, Parren P. Avidity in antibody effector functions and biotherapeutic drug design. *Nat Rev Drug Discov*. (2022) 21:715–35. doi: 10.1038/s41573-022-00501-8

40. Abu Raya B, Bamberger E, Almog M, Peri R, Srugo I, Kessel A. Immunization of pregnant women against pertussis: the effect of timing on antibody avidity. *Vaccine*. (2015) 33:1948–52. doi: 10.1016/j.vaccine.2015.02.059

41. Abu-Raya B, Giles ML, Kollmann TR, Sadarangani M. The effect of timing of tetanus-diphtheria-acellular pertussis vaccine administration in pregnancy on the avidity of pertussis antibodies. *Front Immunol*. (2019) 10:2423. doi: 10.3389/fimmu.2019.02423

42. Knuutila A, Dalby T, Ahvenainen N, Barkoff AM, Jørgensen CS, Fuursted K, et al. Antibody avidity to pertussis toxin after acellular pertussis vaccination and infection. *Emerg Microbes Infect*. (2023) 12:e2174782. doi: 10.1080/22221751.2023.2174782

43. Abu-Raya B, Giles ML, Kollmann TR, Sadarangani M. Profiling avidity of antibodies elicited by vaccination using enzyme-linked immunosorbent assay-based elution - Insights into a novel experimental and analytical approach. *Vaccine*. (2020) 38:5389–92. doi: 10.1016/j.vaccine.2020.06.060

44. Blackwood JC, Cummings DA, Broutin H, Iamsirithaworn S, Rohani P. Deciphering the impacts of vaccination and immunity on pertussis epidemiology in Thailand. *Proc Natl Acad Sci U S A*. (2013) 110:9595–600. doi: 10.1073/pnas.1220908110

45. Cabore RN, Maertens K, Dobly A, Leuridan E, Van Damme P, Huygen K. Influence of maternal vaccination against diphtheria, tetanus, and pertussis on the avidity of infant antibody responses to a pertussis containing vaccine in Belgium. *Virulence*. (2017) 8:1245–54. doi: 10.1080/21505594.2017.1296998

46. Puthanakit T, Tangsathapornpong A, Anugulruengkitt S, Nantanee R, Bunjoungmanee P, Mansouri S, et al. A reduced-dose recombinant pertussis vaccine booster in Thai adolescents: a phase 2/3, observer-blinded, randomised controlled, non-inferiority trial. *Lancet Child Adolesc Health*. (2024) 8:900–9. doi: 10.1016/s2352-4642(24)00173-1

47. Pitisuttithum P, Dhitavat J, Sirivichayakul C, Pitisuthitham A, Sabmee Y, Chinwangso P, et al. Antibody persistence 2 and 3 years after booster vaccination of adolescents with recombinant acellular pertussis monovalent aP(gen) or combined TdaP(gen) vaccines. *EClinicalMedicine*. (2021) 37:100976. doi: 10.1016/j.eclinm.2021.100976

48. Pitisuttithum P, Sirivichayakul C, Dhitavat J, Pitisuthitham A, Mansouri S, Pham HT. Pertussis immunity 5 years after booster vaccination with recombinant pertussis vaccines. *JAMA Netw Open*. (2024) 7:e2449182. doi: 10.1001/jamanetworkopen.2024.49182

49. Goldblatt D, Vaz AR, Miller E. Antibody avidity as a surrogate marker of successful priming by Haemophilus influenzae type b conjugate vaccines following infant immunization. *J Infect Dis*. (1998) 177:1112–5. doi: 10.1086/517407

50. Rappuoli R. The vaccine containing recombinant pertussis toxin induces early and long-lasting protection. *Biologicals*. (1999) 27:99–102. doi: 10.1006/biol.1999.0189

51. Sartoretti J, Fontannaz P, Martinez de Tejada B, Othenin-Girard V, Chilin A, Lemaître B, et al. Influence of timing of maternal pertussis immunization on the avidity of transferred antibodies in term and preterm neonates. *Clin Infect Dis*. (2023) 77:645–8. doi: 10.1093/cid/ciad227

52. Puthanakit T, Chokephaibulkit K, Anugulruengkitt S, Chaithongwongwatthana S, Phongsamart W, Wittawatmongkol O, et al. Infant responses to primary immunization following vaccination in pregnancy with varying doses of recombinant acellular pertussis vaccine alone or combined with tetanus-diphtheria. *Pediatr Infect Dis J*. (2025) 44:S56–s60. doi: 10.1097/inf.0000000000004609

frontiers | Frontiers in Immunology

TYPE Original Research
PUBLISHED 15 July 2025
DOI 10.3389/fimmu.2025.1589733

OPEN ACCESS

EDITED BY
Fabio Fiorino,
LUM University Giuseppe Degennaro, Italy

REVIEWED BY
Piergiuseppe De Berardinis,
Consiglio Nazionale delle Ricerche (Napoli), Italy
Even Fossum,
Norwegian Institute of Public Health (NIPH), Norway

*CORRESPONDENCE
Maurício Lacerda Nogueira
mauricio.nogueira@edu.famerp.br
Rafaella Fortini Queiroz e Grenfell
rafaella.queiroz@fiocruz.br

†These authors share first authorship

‡These authors share senior authorship

RECEIVED 07 March 2025
ACCEPTED 14 May 2025
PUBLISHED 15 July 2025

CITATION
Corsini CA, Campos GRF, Martins PFdS, Filgueiras PS, Lima AEdS, Gomes SVC, Curimbaba CDAL, Lorencini DA, Morandi Junior E, da Silva VM, Cervi MC, Borges MdC, de Lima PR, Nascimento JPRd, Correa PRL, Castilho LdR, de Oliveira JG, Filho OAM, Nogueira ML, Immunita team and Grenfell RFQe (2025) Neutralizing antibody response to Omicron subvariants BA.1 and BA.5 in children and adolescents following the two-dose CoronaVac protocol (Immunita-002, Brazil): a 12-month longitudinal study. *Front. Immunol.* 16:1589733. doi: 10.3389/fimmu.2025.1589733

Neutralizing antibody response to Omicron subvariants BA.1 and BA.5 in children and adolescents following the two-dose CoronaVac protocol (Immunita-002, Brazil): a 12-month longitudinal study

Camila Amormino Corsini[1†], Guilherme Rodrigues Fernandes Campos[2†], Priscila Fernanda da Silva Martins[1], Priscilla Soares Filgueiras[1], Ana Esther de Souza Lima[1], Sarah Vieira Contin Gomes[1], Caroline De Almeida Leitao Curimbaba[3], Daniela Aparecida Lorencini[3], Eolo Morandi Junior[3], Victor Mattos da Silva[3], Maria Célia Cervi[4], Marcos de Carvalho Borges[4,5], Poliana Remundini de Lima[5], João Paulo Resende do Nascimento[5], Paulo Roberto Lopes Correa[6], Leda dos Reis Castilho[7], Jaquelline Germano de Oliveira[1], Olindo Assis Martins Filho[1], Maurício Lacerda Nogueira[2,8,9*‡], Immunita team and Rafaella Fortini Queiroz e Grenfell[1,10,11*‡]

[1]Instituto René Rachou, Oswaldo Cruz Foundation (FIOCRUZ), Belo Horizonte, Minas Gerais, Brazil, [2]Faculty of Medicine of São José do Rio Preto (FAMERP), São José do Rio Preto, São Paulo, Brazil, [3]Instituto Butantan, São Paulo, São Paulo, Brazil, [4]Faculty of Medicine, University of São Paulo (USP), São Paulo, São Paulo, Brazil, [5]Serrana Clinical Research Center, Serrana, São Paulo, Brazil, [6]Belo Horizonte Municipal Health Department (SMS), Belo Horizonte, Brazil, [7]Cell Culture Engineering Laboratory (COPPE), Federal University of Rio de Janeiro (UFRJ), Rio de Janeiro, Rio de Janeiro, Brazil, [8]Hospital de Base, São José do Rio Preto, São Paulo, Brazil, [9]Department of Pathology, University of Texas Medical Branch, Galveston, TX, United States, [10]Federal University of Minas Gerais (UFMG), Belo Horizonte, Minas Gerais, Brazil, [11]Department of Infectious Diseases, College of Veterinary Medicine, University of Georgia (UGA), Athens, GA, United States

Introduction: The covid-19 pandemic prompted an unprecedented global effort to develop and deploy vaccines, including CoronaVac, an inactivated virus-based vaccine. While these vaccines effectively reduced severe cases and hospitalizations, limited data exists on their immunogenicity in younger populations, particularly children and adolescents. Understanding the immune response in these groups is essential to guide vaccination strategies and assess protection against emerging variants of concern, such as Omicron subvariants BA.1 and BA.5. This study evaluated the neutralizing antibody response in children

and adolescents aged 3–17 years over 12 months following the two-dose CoronaVac protocol in Brazil.

Methods: A cohort of 108 children (3–11 years) and adolescents (12–17 years) from Serrana, Brazil, received two doses of CoronaVac. Peripheral blood samples were collected at baseline, and at 1, 3, 6, and 12 months after the second dose. Participants were stratified by serostatus prior to vaccination. Neutralizing antibodies against Omicron BA.1 and BA.5 were assessed using microneutralization assays.

Results: Neutralizing antibody titers increased significantly after vaccination in both seronegative and seropositive individuals. For seronegative participants, seroconversion rates for BA.5 rose from 16.6% pre-vaccination to 93.3% one month after the second dose in children, and from 50% to 92% in adolescents, with sustained levels for 12 months. Seropositive participants also showed enhanced antibody titers, particularly against BA.5. No significant differences in neutralization between BA.1 and BA.5 were observed post-vaccination, contrary to prior literature, suggesting uniform effectiveness against these subvariants.

Discussion: This study demonstrates that CoronaVac significantly enhances and sustains neutralizing antibody titers in children and adolescents for up to one year, including against immune-evading subvariants like BA.5. The robust response highlights the vaccine's potential as a critical tool for reducing SARS-CoV-2 transmission and preventing severe disease, particularly in regions with limited access to updated vaccines. Further studies with larger cohorts are needed to validate these findings and inform vaccination strategies for immunoresistant variants.

KEYWORDS

vaccine, covid-19, SARS-CoV-2, neutralizing antibody, Omicron, children and adolescents

1 Introduction

For According to the World Health Organization (WHO), as of January 5, 2025, more than 777 million cases of COVID-19 had been confirmed worldwide. In Brazil, the number of confirmed cases surpassed 37 million, with approximately 702,000 deaths recorded by that date, making it the second country in terms of deaths from the disease, behind only the United States (1). In an unprecedented effort, covid-19 vaccines were rapidly developed and approved for emergency use, with notable examples including vaccines based on inactivated viruses, mRNA, and non-replicating adenoviral vectors (2). These vaccines demonstrated efficacy in reducing cases and deaths. However, the pandemic persisted due to the emergence and spread of SARS-CoV-2 variants characterized by higher transmissibility, infectivity, and the ability to evade both immunity induced by previous infections and immunity provided by available vaccines (3–5).

The inactivated virus vaccine platform used by CoronaVac has been shown to induce a robust immune response against various viral proteins, including the S (Spike), N (Nucleocapsid), and M (Membrane) proteins (6). Furthermore, CoronaVac has proven to be effective and safe, inducing high levels of neutralizing antibodies, with good tolerability and no severe adverse events or vaccine-related fatalities reported during clinical trials (7, 8). Its efficacy was reported as 83.5% against symptomatic COVID-19 among volunteers aged 18 to 59 years (7, 8).

By January 2022, approximately 85 million doses of this vaccine had been administered to the Brazilian population (9). In the same year, Anvisa (Brazil's National Health Surveillance Agency) expanded the vaccination protocol to include children and adolescents nationwide (10). Although CoronaVac is no longer the primary vaccine used in Brazil, data from its widespread application continues to contribute to public health strategies worldwide (11). The immune response induced by COVID-19 vaccines remains under investigation, particularly in children and adolescents. In this age group, the duration and intensity of immune protection, as well as its efficacy against different variants of concern (VOCs), are not yet fully defined (11). These aspects are essential for determining the

need for booster doses and supporting evidence-based decisions by healthcare managers (12). Based on this, the objective of the present study was to comprehensively evaluate the neutralizing antibody response in children and adolescents aged 3 to 17 years over 12 months following the administration of the primary two-dose CoronaVac protocol in Brazil against the Omicron subvariants BA.1 and BA.5 circulating in the country during 2022.

2 Methods

2.1 Ethics statement and participants

This study was approved by the Research Ethics Committee involving Human Subjects at the Oswaldo Cruz Foundation, the Ethics Committee of the Hospital das Clínicas of the Faculty of Medicine of Ribeirão Preto, University of São Paulo, and the National Council of Ethics in Research (CAAE 55183322.6.0000.5091). The study was supervised by the National Health Surveillance Agency.

Inclusion criteria included children and adolescents aged 3 to 17 years who were unvaccinated for covid-19 and who voluntarily participated in the study with the agreement of their parents or legal guardians, signing the informed consent and assent forms (ICF/IAF). Exclusion criteria included children and adolescents aged 6 to 17 years with immunosuppression, who were not eligible for participation. Additionally, children and adolescents who reported COVID-19 infection during the study were not included in the statistical analyses.

2.2 Participant recruitment, sample collection, and follow-up

Participants were invited to join the research at a public healthcare center located in Serrana, São Paulo, Brazil. A total of 108 participants who met the inclusion criteria were followed for twelve months after completing the two-dose primary protocol of the CoronaVac vaccine (Sinovac, Butantan Institute), administered with a 28-day interval between doses.

Peripheral blood samples were collected at multiple time points: prior to vaccination, on the day of the second dose administration, and at one, three, six, and twelve months post-second dose, relative to the date of administering the second dose of the CoronaVac vaccine (Sinovac, Butantan Institute). A 10 mL whole blood sample was obtained via venous puncture from each participant following biosafety standards and subsequently centrifuged at 3,000 g for 5 min to obtain serum for immunogenicity analyses. Samples were collected from March 2022 to July 2023.

2.3 Assessment of anti-S and anti-N IgG antibodies via ELISA for defining baseline seroreactivity

To assess baseline seroreactivity, enzyme-linked immunosorbent assays (ELISAs) were performed to detect IgG antibodies specific to the SARS-CoV-2 Spike (anti-S) and Nucleocapsid (anti-N) proteins. All serum samples obtained from the study participants were tested for total IgG antibodies specific to the Spike (S) and Nucleocapsid (N) proteins of SARS-CoV-2. Participants who tested reactive in both ELISA assays at the first time point of the study (detection of anti-S and anti-N IgG antibodies), before receiving the first dose of the vaccine, were classified as seropositive, while those who were non-reactive in both ELISA assays were classified as seronegative. These proteins, used as antigens, were derived from the Wuhan reference strain (B.1), and were generated in stable recombinant HEK293 cells, as described by Alvim et al. (2022) (13). Antibody detection was performed using standardized ELISA assays, following the methodology established by GRENFELL et al. (2022), which had been validated by the National Institute of Health Quality Control of the Oswaldo Cruz Foundation (INCQS/Fiocruz) (14). The cutoff value adopted for the determination of positivity was 0.1508. This cutoff value was previously established based on validated positive and negative controls. These controls were derived from samples of individuals with SARS-CoV-2 infection confirmed by RT-PCR, ensuring adequate sensitivity and specificity for the detection of IgG antibodies in the assay (14).

2.4 Viral neutralization assays to SARS-CoV-2 variants (BA.1 and BA.5)

All serum samples across all time points were subjected to neutralizing antibody assays (VNT50) to detect antibodies against the Omicron variant, subvariants BA.1 (HIAE –W.A) and BA.5 (EPI_ISL_18277186), as outlined by CAMPOS et al. (2022) (9). VNT50 was performed as published before (9, 11). Serum samples from children and adolescents were collected before and after vaccination, inactivated at 56°C for 30 minutes, and serially diluted two-fold (1:20 to 1:2560). Diluted samples were incubated for 1 hour at 37°C with 50 TCID50 of SARS-CoV-2 subvariants BA.1 and BA.5. After incubation, 100 µl of these solutions were transferred to Vero cell-seeded 96-well plates and incubated in supplemented DMEM for 72 hours at 37°C with 5% CO_2. The median neutralization titer (VNT50) was determined as the reciprocal dilution providing 50% protection against cytopathic effects, calculated using the Spearman-Karber method. Each sample was tested in triplicate (15, 16). A dilution of 1:20 was established as the cutoff point for seroconversion.

2.5 Statistical analysis

Data analyses were performed using GraphPad Prism® software version 8.0. The median neutralization titer (VNT50) was determined as the reciprocal of the dilution that provided 50% protection against cytopathic effects, calculated using the Spearman-Karber method. Antibody titer quantification results were analyzed statistically using the Kruskal-Wallis test, while pairwise comparisons were conducted using the Mann-Whitney test. A significance level of $p < 0.05$ was applied for all analyses. The

correlation between neutralizing antibodies against BA.1 and BA.5 subvariants was evaluated using Spearman's rank correlation coefficient, with statistical significance set at $p < 0.05$.

3 Results

3.1 Baseline characteristics of participants

In total, 108 individuals were included in this study, 60 (55.56%) children aged 3 to 11 years, and 48 adolescents aged 12 to 17 years (44.44%). For the seronegative group, 60 participants were included, and for the seropositive group, 48 participants were included, covering both age ranges. The remaining characteristics of the cohort, such as biological gender and comorbidities, are presented in Table 1.

3.2 Neutralization levels against BA.1 and BA.5 variants before and after vaccination

The viral microneutralization assay enabled the evaluation of seroconversion rates and the determination of mean neutralizing antibody titers against the Omicron subvariants BA.1 and BA.5 in children and adolescents over 12 months following the primary CoronaVac vaccination protocol.

In the evaluation of neutralizing antibodies in seronegative individuals, a significant increase in antibody titers was observed after the primary CoronaVac vaccination protocol, both for the BA.1 and BA.5 subvariants, in children aged 3 to 11 years (Figure 1A). Notably, seropositivity for the BA.5 subvariant increased from 16.6% prior to vaccination to 93.3% one month after the second vaccine dose and remained high up to the last follow-up point (12 months post-second dose).

In the evaluation of seronegative adolescents (aged 12–17; Figure 1B), no significant difference in neutralizing antibody titers against the BA.1 subvariant was observed after the primary vaccination protocol. However, for the BA.5 subvariant, seropositivity increased significantly from 50% to 92% after vaccination, remaining elevated until the study's last follow-up point.

When comparing neutralizing antibody titers against BA.1 and BA.5 separately by age group (Figures 2A, B) and by subvariant (Figures 2C, D) in seronegative individuals, higher antibody titers against BA.1 were observed in adolescents before receiving the first dose of CoronaVac (V1). This finding may indicate prior infection with this subvariant in this group.

In the evaluation of neutralizing antibodies in seropositive individuals prior to receiving the primary protocol, a significant increase in neutralizing antibody titers post-CoronaVac vaccination was observed only for the BA.5 subvariant. Seropositivity increased from 86.6% to 100% in children aged 3 to 11 years (Figure 3A) and from 93.3% to 100% in adolescents aged 12 to 17 years (Figure 3B).

When comparing neutralizing antibody titers against BA.1 and BA.5 separately by age group (Figures 4A, B) and by subvariant (Figures 4C, D) in seropositive individuals, higher neutralizing antibody titers against the BA.1 subvariant were observed in both children and adolescents before receiving the first dose of CoronaVac (V1). This finding may also suggest prior infection with this subvariant in these groups.

3.3 Correlation between neutralizing antibodies against BA.1 and BA.5 variants

When evaluating the correlation between neutralizing antibodies against BA.1 and BA.5 in seronegative children by ELISA, a moderate and statistically significant positive correlation

TABLE 1 General characteristics of the included participants.

Epidemiological data	Seronegative before vaccination[1] (n,%)	Soropositive before vaccination[2] (n,%)	Total (n=108)
Age, years			
3-11	30, 27.78	30, 27.78	60, 55.56
12-17	30, 27.78	18, 16.67	48, 44.44
Biological gender			
Male	32, 29.63	18, 16.67	50, 46.30
Female	28, 25.93	30, 27.78	58, 53.70
Comorbidities			
Allergic rhinitis	3, 2.78	6, 5.56	9, 8.33
Asthma	1, 0.93	1, 0.93	2, 1.85
Obesity	0, 0	2, 1.85	2, 1.85
Hypothyroidism	0, 0	1, 0.93	1, 0.93
No comorbidities	56, 51.85	38, 35.19	94, 87.04

[1]Seronegative for SARS-CoV-2 anti-S and anti-N IgG antibodies by ELISA prior to the CoronaVac primary vaccination protocol.
[2]Soropositive for SARS-CoV-2 anti-S and anti-N IgG antibodies by ELISA prior to the CoronaVac primary vaccination protocol.

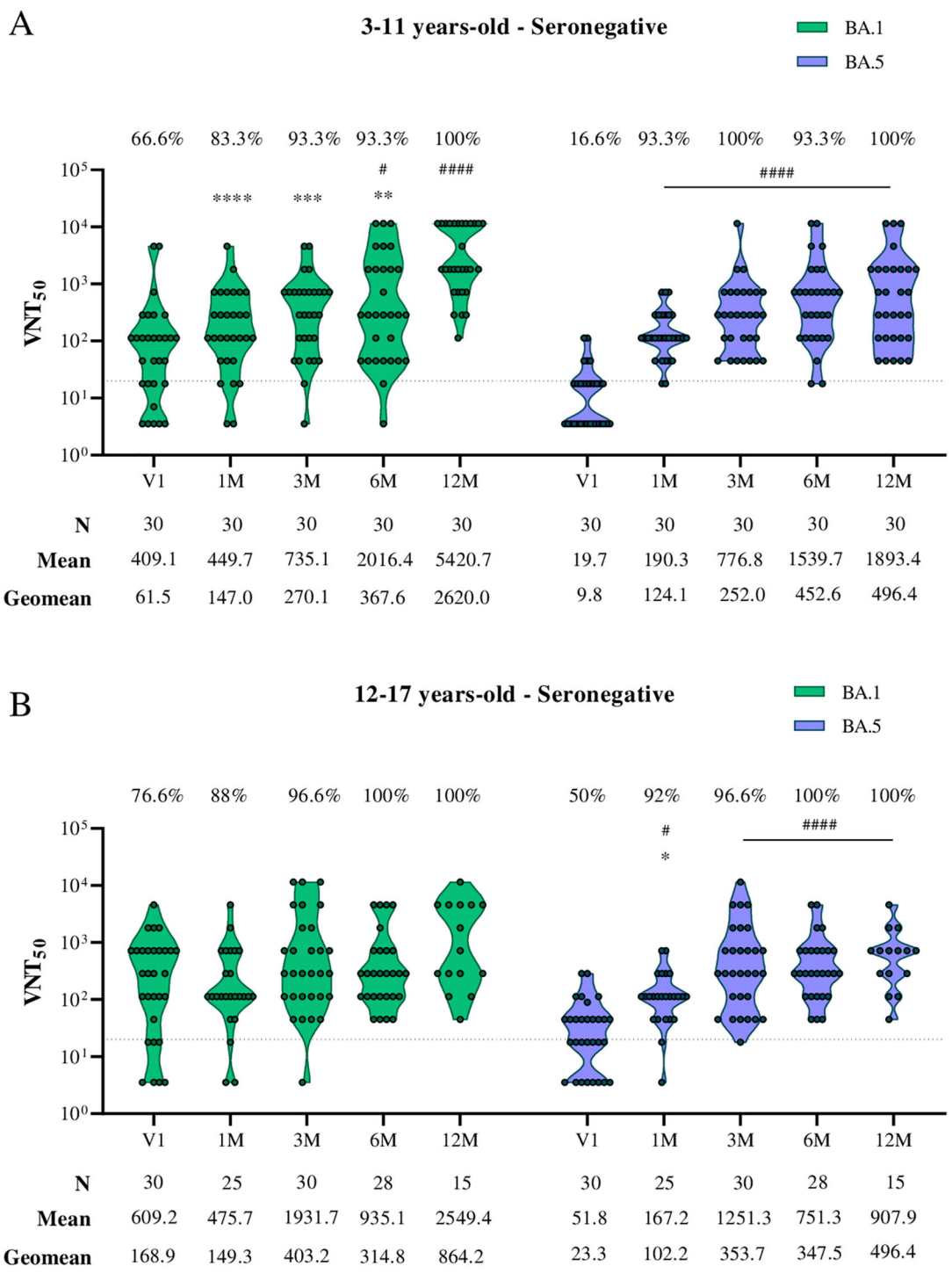

FIGURE 1
Viral microneutralization assay against Omicron subvariants to evaluate neutralization titers (VNT50) and seroconversion rates over 12 months in children and adolescents vaccinated with the CoronaVac primary protocol. The Omicron subvariants BA.1 and BA.5 are represented in green and purple, respectively. **(A)** Neutralizing antibodies in children aged 3 to 11 years seronegative for SARS-CoV-2 S and N antibodies before the CoronaVac primary protocol. **(B)** Neutralizing antibodies in adolescents aged 12 to 17 years seronegative for SARS-CoV-2 S and N antibodies before the CoronaVac primary protocol. The sample size (n), VNT50 means, and geometric mean titers for each group are highlighted below the graphs. Dashed lines represent the seroconversion dilution cutoff (1:20), while seroconversion rates are expressed as percentages. Significance lines indicate differences among the mean neutralization titers of the groups. P-values lower than 0.05 were considered significant.

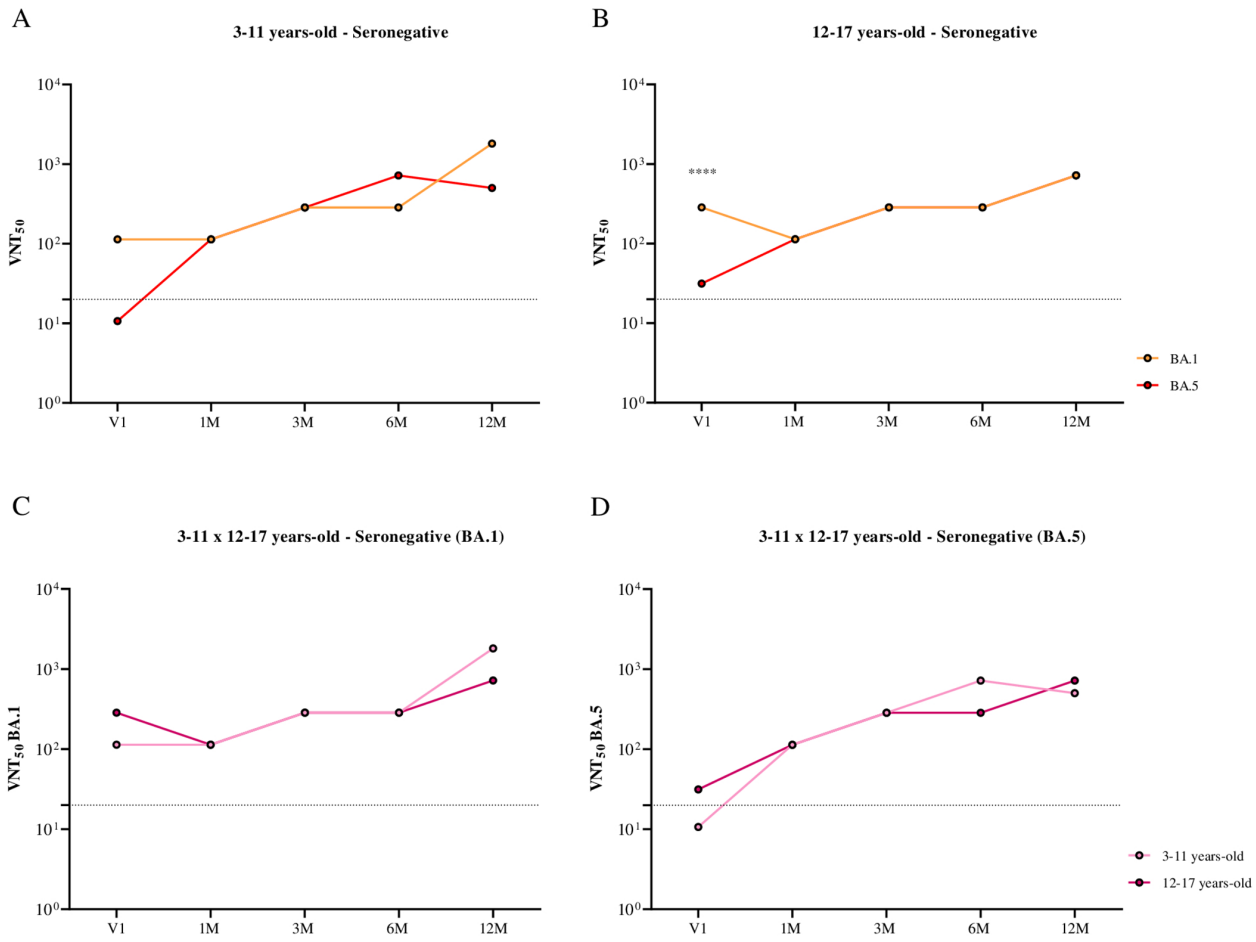

FIGURE 2
Comparison of the kinetics of neutralizing antibodies against BA.1 and BA.5, stratified by age group and subvariant, in children and adolescents seronegative for SARS-CoV-2 S and N antibodies before the CoronaVac primary protocol, over 12 months following the administration of two doses of the CoronaVac vaccine. **(A)** Comparison of the kinetics of neutralizing antibodies against BA.1 and BA.5 in children aged 3 to 11 years. **(B)** Comparison of the kinetics of neutralizing antibodies against BA.1 and BA.5 in adolescents aged 12 to 17 years. **(C)** Comparison of the kinetics of neutralizing antibodies against the BA.1 subvariant in children and adolescents aged 3 to 17 years. **(D)** Comparison of the kinetics of neutralizing antibodies against the BA.5 subvariant in children and adolescents aged 3 to 17 years. Dashed lines represent the seroconversion dilution cutoff (1:20), while seroconversion rates are expressed as percentages. Significance lines indicate differences among the mean neutralization titers of the groups. P-values lower than 0.05 were considered significant.

was observed in most time points analyzed after vaccination (Figure 5). In adolescents, a strong positive correlation was identified at the first pre-vaccination time point (Spearman r = 0.6381, p = 0.0001) and further intensified three months after receiving the second dose of CoronaVac (Spearman r = 0.7551, p < 0.0001), suggesting a consistent association between these parameters (Figure 6).

Conversely, among seropositive individuals, only a moderate correlation between these neutralizing antibodies was observed before the administration of the first dose (Spearman r = 0.4569, p = 0.0111) in children aged 3 to 11 years (Figure 7). In adolescents, however, no significant correlation was found between BA.1 and BA.5 neutralizing antibodies at pre- and post-vaccination time points, indicating a weak or nonexistent association within this group across the evaluated periods (Figure 8).

4 Discussion

The COVID-19 pandemic reshaped immunization strategies, accelerating vaccine development and distribution to curb viral spread and new variants. Global collaboration among institutions, scientists, and regulatory agencies enabled the rapid rollout of safe and effective vaccines, allowing mass immunization within a year of the pandemic's onset, significantly reducing cases, hospitalizations, and deaths (7, 17–25).

Initially, phase II and III clinical trials prioritized adults and the elderly, as they were the most affected (18, 21). Consequently, vaccines were first approved for adults, while children and adolescents relied on non-pharmacological measures during early waves of infection (26–28). Clinical trials for younger populations began later, following safety and efficacy data from adult studies

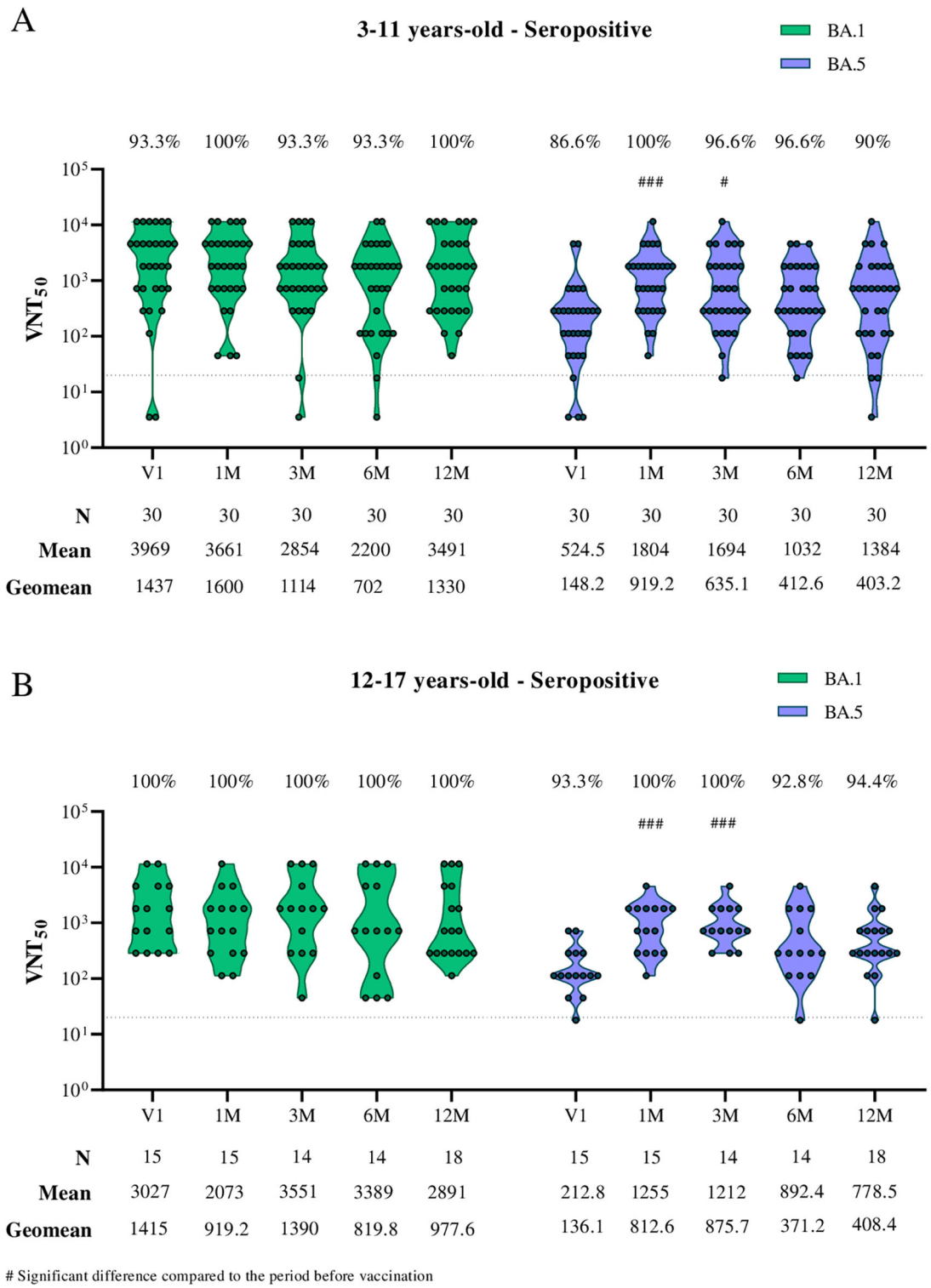

FIGURE 3
Viral microneutralization assay against Omicron subvariants to evaluate neutralization titers (VNT50) and seroconversion rates over 12 months in children and adolescents vaccinated with the CoronaVac primary protocol. The Omicron subvariants BA.1 and BA.5 are represented in green and purple, respectively. **(A)** Neutralizing antibodies in children aged 3 to 11 years seropositive for SARS-CoV-2 S and N antibodies before the CoronaVac primary protocol. **(B)** Neutralizing antibodies in adolescents aged 12 to 17 years seropositive for SARS-CoV-2 S and N antibodies before the CoronaVac primary protocol. The sample size (n), VNT50 means, and geometric mean titers for each group are highlighted below the graphs. Dashed lines represent the seroconversion dilution cutoff (1:20), while seroconversion rates are expressed as percentages. Significance lines indicate differences among the mean neutralization titers of the groups. P-values lower than 0.05 were considered significant.

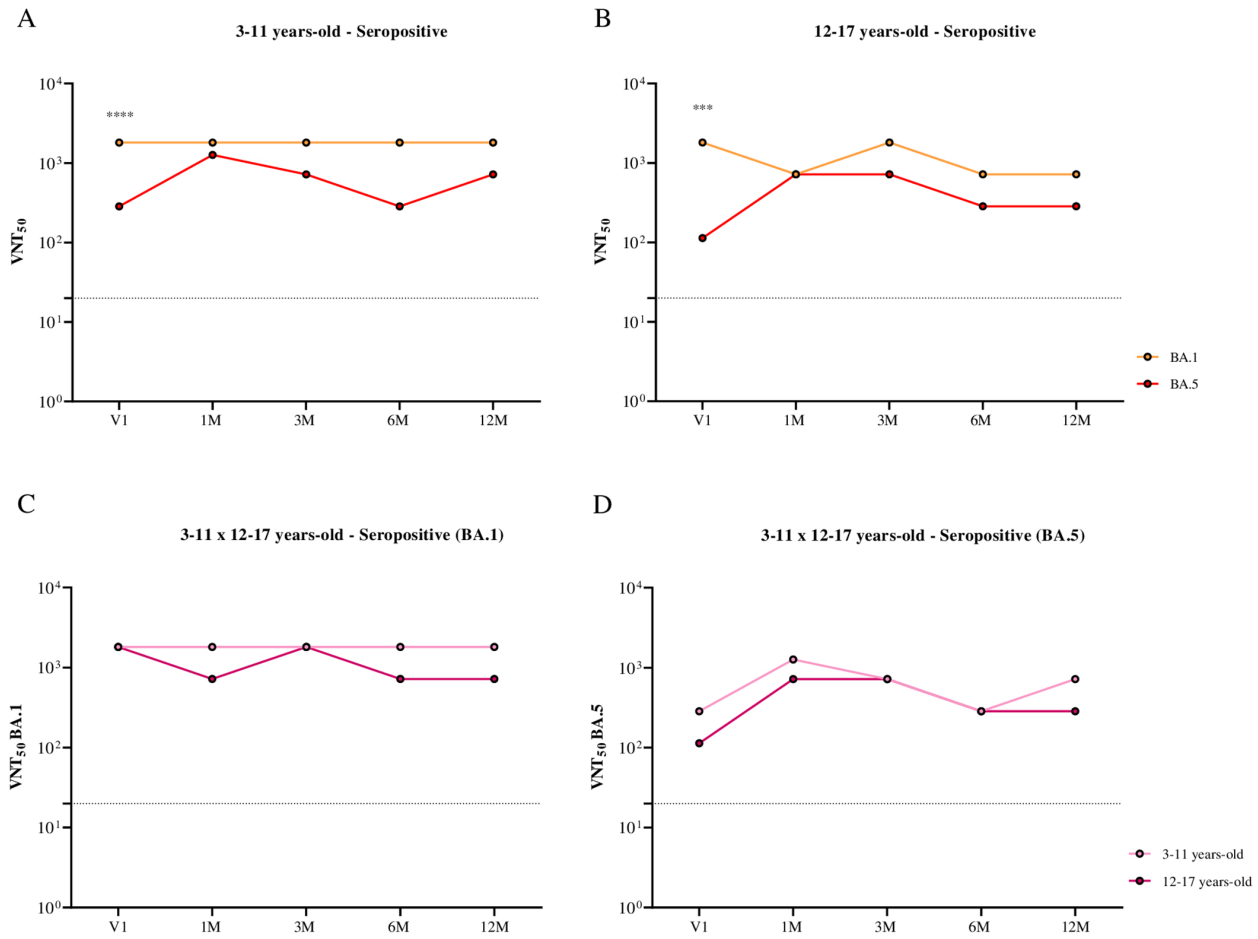

FIGURE 4
Comparison of the kinetics of neutralizing antibodies against BA.1 and BA.5, stratified by age group and subvariant, in children and adolescents seropositive for SARS-CoV-2 S and N antibodies before the CoronaVac primary protocol, over 12 months following the administration of two doses of the CoronaVac vaccine. **(A)** Comparison of the kinetics of neutralizing antibodies against BA.1 and BA.5 in children aged 3 to 11 years. **(B)** Comparison of the kinetics of neutralizing antibodies against BA.1 and BA.5 in adolescents aged 12 to 17 years. **(C)** Comparison of the kinetics of neutralizing antibodies against the BA.1 subvariant in children and adolescents aged 3 to 17 years. **(D)** Comparison of the kinetics of neutralizing antibodies against the BA.5 subvariant in children and adolescents aged 3 to 17 years. Dashed lines represent the seroconversion dilution cutoff (1:20), while seroconversion rates are expressed as percentages. Significance lines indicate differences among the mean neutralization titers of the groups. P-values lower than 0.05 were considered significant.

(29–31). As mass vaccination advanced, younger age groups gained attention, particularly during the Delta variant surge, when adults and the elderly were fully immunized, leaving individuals under 18 as the most exposed group (32, 33). Beyond direct clinical impacts, their lack of immunization sustained viral transmission, potentially contributing to new variant emergence (34).

This shift in vaccination priority diverged from traditional immunization programs, such as in Brazil, where most vaccines are administered within the first 15 months of life to ensure early protection (35, 36). However, prioritizing high-risk groups—elderly individuals with immune senescence and middle-aged adults with frequent exposure—was a logical and effective approach, demonstrating success in controlling the pandemic (23, 37–40).

A key concern regarding childhood and adolescent immunization was the potential herd immunity from prior SARS-CoV-2 exposure. The delayed vaccination in this group led to increased infections, resulting in a significant number of individuals with prior virus contact. This background informed the study's design, distinguishing groups based on confirmed previous infection.

Our data shows that neutralizing antibodies against Omicron variants, especially BA.1, were also detected prior vaccination in children and adolescents without history of previous infection, indicating the occurrence of asymptomatic cases. Some studies highlight that youngsters, when compared to adults and elderly people, are more likely to develop asymptomatic infections (41, 42), and this scenario represents a great challenge in determining the real infectiousness of this age group since these infections are mostly under-reported (43, 44).

On the other hand, despite neutralizing antibodies being detected in seropositive and seronegative groups prior vaccination, our results suggest an important contribution of immunization in the improvement of serological response. When compared to V1 (time-point before immunization), neutralization

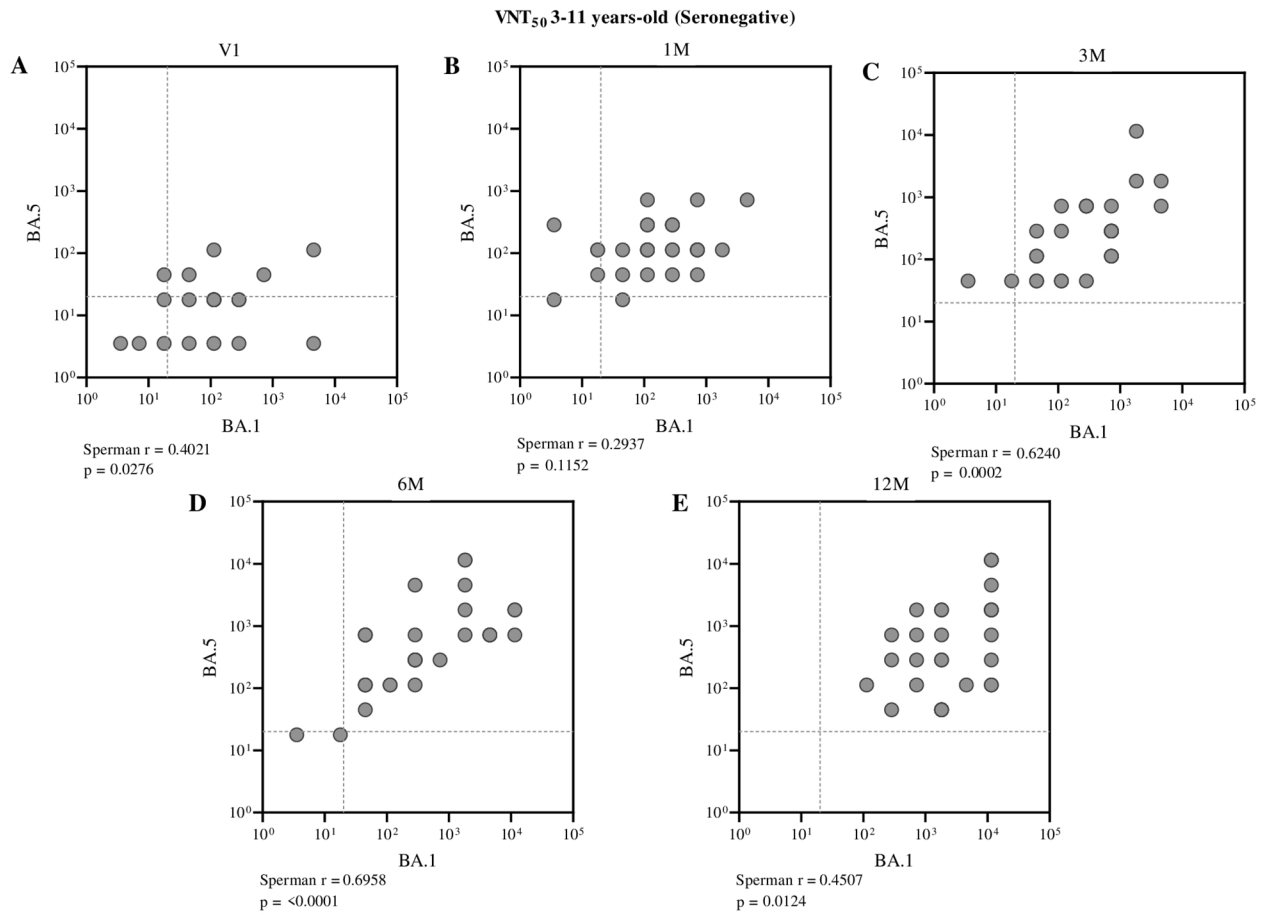

FIGURE 5
Correlation between neutralizing antibody titers against BA.1 and BA.5 in seronegative children (aged 3 to 11 years), assessed at different time points: before vaccination **(A)**, one month **(B)**, three months **(C)**, six months **(D)**, and twelve months **(E)** after receiving the second dose of CoronaVac. Each point represents an individual sample from a participant. The assay cutoff value of 20 is indicated by the dashed lines on the x and y axes. Spearman's correlation coefficient was used, with statistical significance set at $p < 0.05$.

titers were significantly enhanced in children and adolescents by CoronaVac vaccination, especially against BA.5 subvariant. These data corroborate with some studies in the literature, where COVID-19 vaccination significantly improved the antibody response in individuals previously infected by SARS-CoV-2 when compared to vaccinated naïve individuals (45–47). Additionally, it is described that this hybrid immunity also showed higher serological protection in the respiratory tract, the main infection route of SARS-CoV-2, especially due to elevated levels of IgA antibody response in the mucosa after vaccination (48, 49).

A similar pattern was observed in individuals vaccinated with CoronaVac, the same immunizing platform used in this study. A study performed by Niyomnaitham et al., in 2022, evaluated the impact of different vaccines in naïve and previously infected participants. As expected, CoronaVac showed lower responses when compared to other vaccines, but using a SARS-CoV-2 pseudo virus neutralization assay, the authors observed that a single dose of CoronaVac was able to induce the same neutralization titer, against Omicron variant, as naïve individuals vaccinated with two doses of BNT162b2 (50). Our results corroborate and reinforce this observation, since we performed all neutralization assays using infectious particles instead of pseudo virus platform, showing that a two doses immunization with CoronaVac was capable to enhance and maintain high levels of antibody response against Omicron subvariants, independently of previous contact with SARS-CoV-2.

Other vaccination platforms, using attenuated adenoviral vector or mRNA as the immunizing agent, presented the same trend on improving immune protection (51, 52). A study performed in the United Kingdom, conducted with more than 35 thousand asymptomatic healthcare workers, showed that both serological and cellular immunity acquired only by previous infection decay after 1 year. However, after full vaccination of these seropositive individuals with ChAdOx1 nCoV-19 or BNT162b2 vaccines, protection levels remained high and consistent over time (90% of effectiveness on preventing subsequent infections) (53).

From the serological response perspective, our findings highlight that vaccination of children and adolescents, with CoronaVac, induced high levels of neutralizing antibodies against BA.1 and BA.5, two Omicron subvariants with different

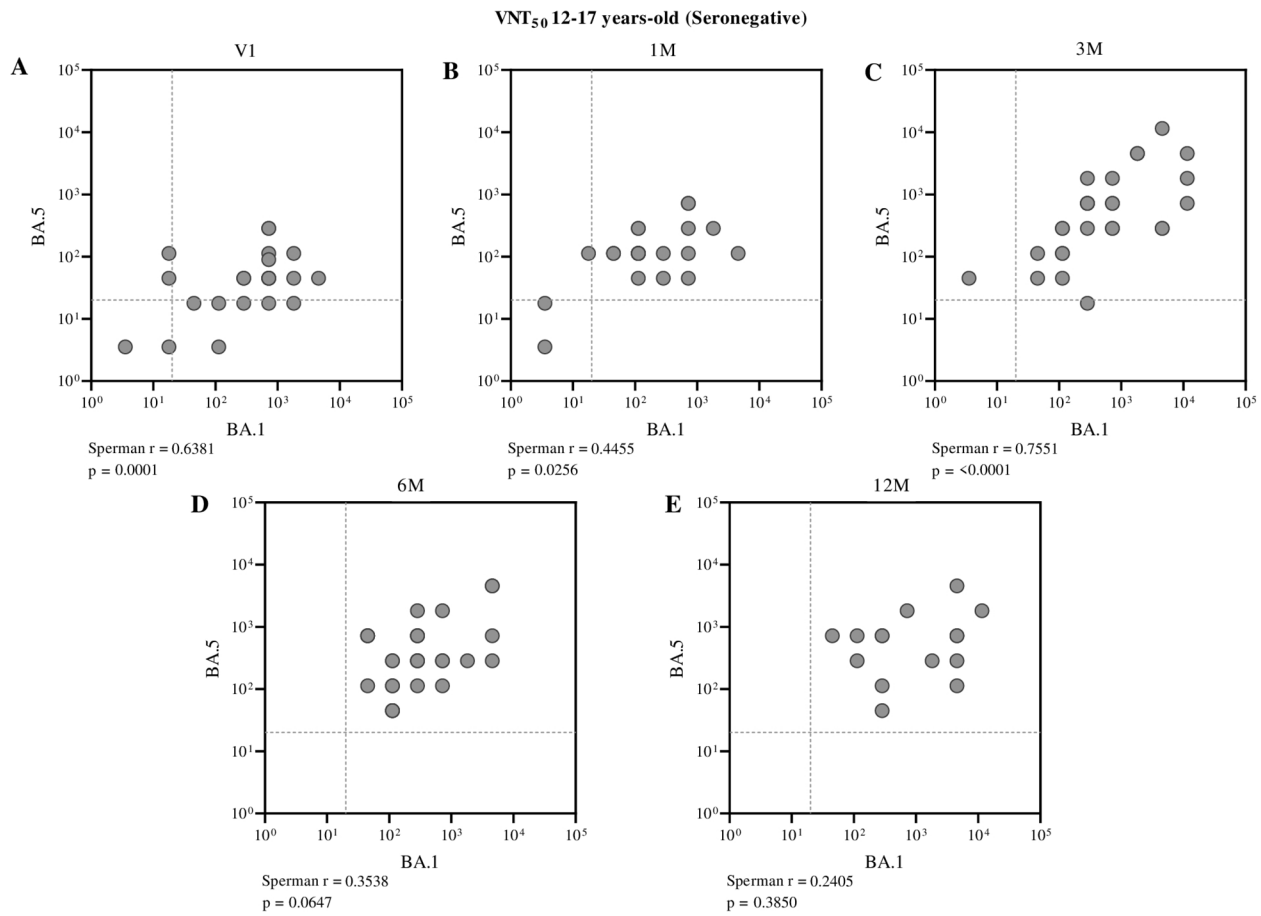

FIGURE 6
Correlation between neutralizing antibody titers against BA.1 and BA.5 in seronegative adolescents (aged 12 to 17 years), assessed at different time points: before vaccination **(A)**, one month **(B)**, three months **(C)**, six months **(D)**, and twelve months **(E)** after receiving the second dose of CoronaVac. Each point represents an individual sample from a participant. The assay cutoff value of 20 is indicated by the dashed lines on the x and y axes. Spearman's correlation coefficient was used, with statistical significance set at $p < 0.05$.

immunological features that influence on neutralization escape (54). Some studies, including a previous one from our group, showed that BA.5 is less neutralized by previous infection (55) and vaccination induced antibodies (11, 56, 57) than BA.1, the first omicron subvariant that emerged.

In this study, the correlation between neutralizing antibodies against BA.1 and BA.5 in seronegative children and adolescents, revealing a moderate and statistically significant positive correlation at most time points analyzed post-vaccination. Additionally, interestingly, the data presented here showed that, when comparing neutralization levels against BA.1 and BA.5 in children and adolescents, no significant differences were observed after CoronaVac administration, and this response was maintained over time. This finding contrasts with previous reports from *in vitro* and cohort studies, which suggest differential neutralization efficacy against these subvariants (58, 59). As an example, a study conducted in Japan with 13 thousand individuals, during BA.1/BA.2 and BA.5 infection waves, showed that vaccination protection against BA.5 was short-lasting and probably contributed to BA.5 infection peak (60).

This induction and maintenance of considerable titers of neutralizing antibodies in both age groups, independently of infection history, could suggest new perspectives on vaccination protocols for immunoresistant subvariants such as BA.5.

In a scenario where SARS-CoV-2 continues to circulate and evolve, updated monovalent vaccines, specifically targeting currently circulating variants, have replaced the previous bivalent Wuhan/BA.5 vaccines and are now considered essential tools. Some of these updated vaccines have already been tested and approved (61–65). Although CoronaVac is no longer the primary vaccine used in Brazil, the accumulated data from its widespread application continue to inform public health strategies globally. Moreover, CoronaVac, as a safe and effective inactivated virus vaccine, remains a valuable tool for controlling SARS-CoV-2 infection and preventing progression to severe disease, particularly in countries where updated vaccines are not yet readily available (11).

As a limitation of our study, since our data showed no difference on neutralization titers, after immunization, between subvariants, and this opposes the literature regarding BA.5 immune escape, an

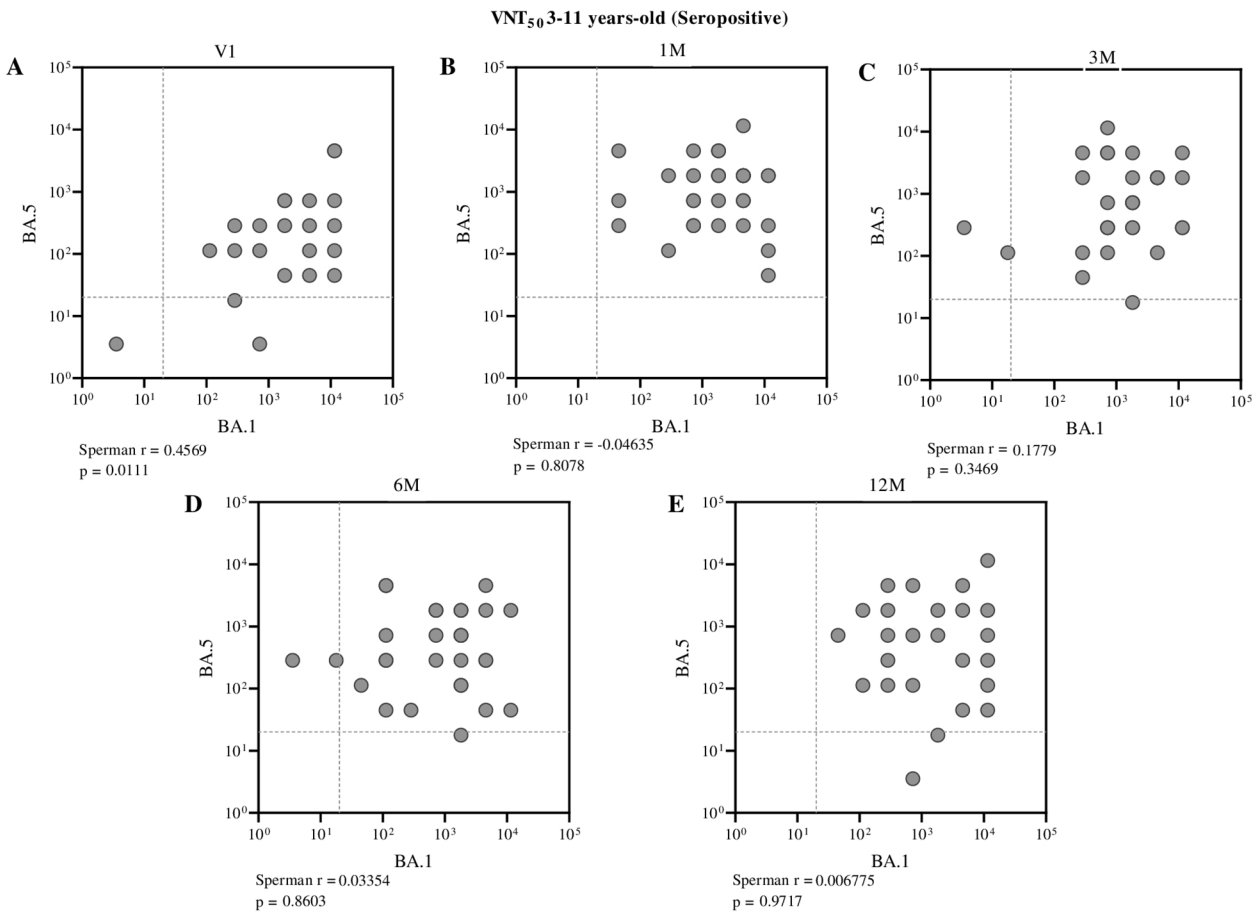

FIGURE 7
Correlation between neutralizing antibody titers against BA.1 and BA.5 in seropositive children (aged 3 to 11 years), assessed at different time points: before vaccination **(A)**, one month **(B)**, three months **(C)**, six months **(D)**, and twelve months **(E)** after receiving the second dose of CoronaVac. Each point represents an individual sample from a participant. The assay cutoff value of 20 is indicated by the dashed lines on the x and y axes. Spearman's correlation coefficient was used, with statistical significance set at $p < 0.05$.

increase in the number of samples could strengthen even more the findings about vaccination and protection of youth population. As a methodological limitation of the study, regarding the criterion adopted to define prior SARS-CoV-2 infection, based on simultaneous positivity for anti-S and anti-N IgG antibodies detected by ELISA using antigens from the Wuhan reference strain, although this approach was chosen to ensure greater specificity, it is possible that it led to the misclassification of some previously infected individuals as seronegative. This misclassification may result from both the natural waning of total antibody levels over time and the attenuated immune response induced by variants such as Omicron, which may elicit antibodies with low affinity for ancestral strain antigens, thus hindering their detection by ELISA-based assays. The presence of relatively high neutralizing antibody titers in some participants classified as seronegative prior to vaccination reinforces this possibility, suggesting the occurrence of asymptomatic infections that were not serologically detected. Therefore, we acknowledge that this approach may have underestimated the proportion of individuals with prior infection, which should be considered when interpreting the immunological results observed after vaccination. In addition, it is important to consider that the neutralization assays performed in this study used total serum samples, without prior separation by immunoglobulin isotype. Therefore, it is not possible to attribute the observed neutralizing activity exclusively to the IgG fraction. Other isotypes, such as IgM and especially IgA, the latter particularly relevant in mucosal immune responses, may have contributed to the detected neutralization titers, particularly during the early stages of the immune response following vaccination. This potential interference should be considered when interpreting the data, as the total neutralizing activity measured does not necessarily reflect only the long-term humoral memory response mediated by IgG.

The results presented here highlight important and necessary information regarding vaccination of children and adolescents. A full immunization protocol with CoronaVac contributed to a significant enhancement of serological response for naïve and previous infected individuals, including against immunoresistant subvariants such as BA.5, and this robust antibody neutralization is stable for one year after vaccination. This positive response, in a

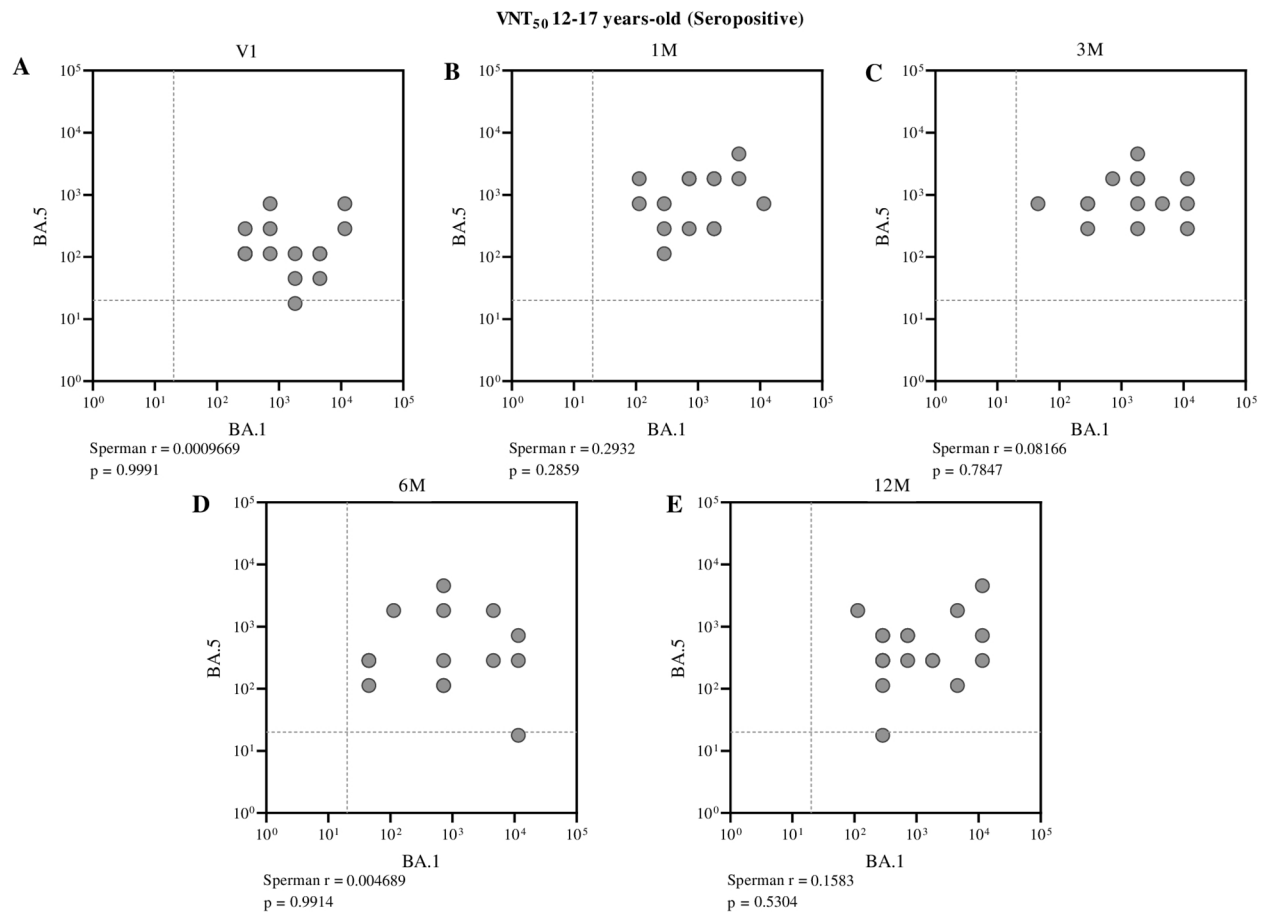

FIGURE 8
Correlation between neutralizing antibody titers against BA.1 and BA.5 in seropositive adolescents (aged 12 to 17 years), assessed at different time points: before vaccination **(A)**, one month **(B)**, three months **(C)**, six months **(D)**, and twelve months **(E)** after receiving the second dose of CoronaVac. Each point represents an individual sample from a participant. The assay cutoff value of 20 is indicated by the dashed lines on the x and y axes. Spearman's correlation coefficient was used, with statistical significance set at $p < 0.05$.

population that was vaccinated later, could be crucial to deaccelerate SARS-CoV-2 circulation and reduce the emergence of new subvariants. In addition, an inactivated viral vaccine showed to be an interesting tool to increase immunity of less protected individuals, especially in regions where new and updated vaccines are not available yet.

Data availability statement

The raw data supporting the conclusions of this article will be made available by the authors, without undue reservation.

Ethics statement

The studies involving humans were approved by Research Ethics Committee involving Human Subjects at the Oswaldo Cruz Foundation, the Ethics Committee of the Hospital das Clínicas of the Faculty of Medicine of Ribeirão Preto, University of São Paulo, and the National Council of Ethics in Research. The studies were conducted in accordance with the local legislation and institutional requirements. Written informed consent for participation in this study was provided by the participants' legal guardians/next of kin.

Author contributions

CCo: Data curation, Formal Analysis, Investigation, Methodology, Writing – original draft. GC: Data curation, Formal Analysis, Investigation, Methodology, Writing – original draft. PM: Conceptualization, Formal Analysis, Investigation, Methodology, Writing – original draft. PF: Data curation, Formal Analysis, Investigation, Writing – original draft. AL: Data curation, Formal Analysis, Investigation, Methodology, Writing – original draft. SG: Investigation, Methodology, Writing – original draft. CCu: Conceptualization, Data curation, Supervision, Validation, Writing – review & editing. DL: Conceptualization, Data curation, Supervision, Validation, Writing – review & editing. EM: Conceptualization, Data curation, Supervision, Validation, Writing – review & editing. VS: Data curation, Supervision,

Validation, Writing – review & editing. MC: Data curation, Formal Analysis, Investigation, Methodology, Supervision, Validation, Writing – review & editing. MB: Data curation, Formal Analysis, Investigation, Methodology, Supervision, Validation, Writing – review & editing. PL: Data curation, Investigation, Methodology, Writing – review & editing. JN: Data curation, Investigation, Methodology, Writing – review & editing. PC: Conceptualization, Supervision, Validation, Writing – review & editing. LC: Methodology, Writing – review & editing. JD: Conceptualization, Data curation, Funding acquisition, Investigation, Writing – review & editing. OM: Data curation, Formal Analysis, Methodology, Validation, Writing – review & editing. MN: Data curation, Formal Analysis, Methodology, Writing – review & editing. IT: Data curation, Formal Analysis, Investigation, Methodology, Writing – review & editing. RG: Conceptualization, Data curation, Formal Analysis, Funding acquisition, Investigation, Methodology, Project administration, Resources, Supervision, Validation, Visualization, Writing – review & editing.

Group members of Immunita team

Ana Clara Almeida[1], Daniel Alvim Pena de Miranda[1], Isabela Camargos[1], Raquel Amorim[1], Érica Louback de Oliveira[1], Clara Raíssa do Prado Pêgo[1], Viviane Cristina Fernandes dos Santos[1].

Funding

The author(s) declare that financial support was received for the research and/or publication of this article. Oswaldo Cruz Foundation (FIOCRUZ) (to RG and scholarship to CC, PF), The Brazilian National Council for Scientific and Technological Development (CNPq) (scholarships to DM and SG), funds through parliamentary amendment administered by The Minas Gerais Research Funding Foundation (FAPEMIG) (to RG), FAPEMIG (scholarship to PF), and the Butantan Institute (to RG). MN is supported by FAPESP grant # 2022/03645-1, INCT Dengue Program grant 465425/2014-3, and by INCT Viral Genomic Surveillance and One Health grant 405786/2022-0. MN is a Brazilian National Council for Scientific and Technological Development (CNPq) Research Fellow. MN is partly funded by the Centers for Research in Emerging Infectious Diseases (CREID), "The Coordinating Research on Emerging Arboviral Threats Encompassing the Neotropics (CREATE-NEO)" grant U01AI151807 by the National Institutes of Health (NIH/USA).

Acknowledgments

The authors thank the participants and their parents and Serrana, São Paulo, Brazil (SMS-Serrana), Dr. Simone Kashima from the Blood Center of Ribeirão Preto, Ribeirão Preto, São Paulo, Dr. Glenda R. Moraes for the Epidemic Service in Serrana, São Paulo and CPC-S (Clinical Research Center – S) in Serrana, São Paulo and, all the investigators. The authors would like to acknowledge the generous donation of trimeric spike protein of SARS-COV-2 from the Cell Culture Engineering Laboratory of COPPE/UFRJ - Federal University of Rio de Janeiro.

Conflict of interest

All MN has received research grants from Instituto Butantan, Janssen Vaccines and Prevention B.V., Medicago R&D Inc, and Pfizer/BioNTech SE. RG has received grants from Instituto Butantan.

The remaining authors declare that the research was conducted in the absence of any commercial or financial relationships that could be construed as a potential conflict of interest.

Generative AI statement

The author(s) declare that no Generative AI was used in the creation of this manuscript.

Publisher's note

References

1. WHO. WHO Coronavirus (COVID-19) Dashboard (2024). Available online at: https://covid19.who.int/ (Accessed February 2025).

2. WHO. *COVID-19 Vaccines with WHO Emergency Use Listing*. (2022) Geneva, Switzerland: World Health Organization (WHO).

3. Jiang Y, Wu Q, Song P, You C. The variation of SARS-coV-2 and advanced research on current vaccines. *Front Med (Lausanne)*. (2021) 8:806641. doi: 10.3389/fmed.2021.806641

4. Tartof SY, Slezak JM, Fischer H, Hong V, Ackerson BK, Ranasinghe ON, et al. Effectiveness of mRNA BNT162b2 COVID-19 vaccine up to 6 months in a large integrated health system in the USA: a retrospective cohort study. *Lancet*. (2021) 398:1407–16. doi: 10.1016/S0140-6736(21)02183-8

5. Goldberg Y, Mandel M, Bar-On YM, Bodenheimer O, Freedman L, Haas EJ, et al. Waning immunity after the BNT162b2 vaccine in Israel. *N Engl J Med*. (2021) 385:e85. doi: 10.1056/NEJMoa2114228

6. Krammer F. SARS-CoV-2 vaccines in development. *Nature*. (2020) 586:516–27. doi: 10.1038/s41586-020-2798-3

7. Tanriover MD, Doganay HL, Akova M, Guner HR, Azap A, Akhan S, et al. Efficacy and safety of an inactivated whole-virion SARS-CoV-2 vaccine (CoronaVac):

interim results of a double-blind, randomised, placebo-controlled, phase 3 trial in Turkey. *Lancet*. (2021) 398:213–22. doi: 10.1016/S0140-6736(21)01429-X

8. Hu L, Sun J, Wang Y, Tan D, Cao Z, Gao L, et al. A review of inactivated COVID-19 vaccine development in China: focusing on safety and efficacy in special populations. *Vaccines (Basel)*. (2023) 11. doi: 10.3390/vaccines11061045

9. Campos GRF, Almeida NBF, Filgueiras PS, Corsini CA, Gomes SVC, de Miranda DAP, et al. Booster dose of BNT162b2 after two doses of CoronaVac improves neutralization of SARS-CoV-2 Omicron variant. *Commun Med (Lond)*. (2022) 2:76. doi: 10.1038/s43856-022-00141-4

10. BRASIL. Agência Nacional de Vigilância Sanitária. Anvisa aprova uso emergencial da CoronaVac para crianças de 3 a 5 anos (2022). Available online at: https://www.gov.br/anvisa/pt-br/assuntos/noticias-anvisa/2022/anvisa-aprova-uso-emergencial-da-coronavac-para-criancas-de-3-a-5-anos (Accessed February 2025).

11. Campos GRF, Almeida NBF, Filgueiras PS, Corsini CA, Gomes SVC, de Miranda DAP, et al. Second booster dose improves antibody neutralization against BA.1, BA.5 and BQ.1.1 in individuals previously immunized with CoronaVac plus BNT162B2 booster protocol. *Front Cell Infect Microbiol*. (2024) 14:1371695. doi: 10.3389/fcimb.2024.1371695

12. Walter EB, Talaat KR, Sabharwal C, Gurtman A, Lockhart S, Paulsen GC, et al. Evaluation of the BNT162b2 covid-19 vaccine in children 5 to 11 years of age. *N Engl J Med*. (2022) 386:35–46. doi: 10.1056/NEJMoa2116298

13. Alvim RGF, Lima TM, Rodrigues DAS, Marsili FF, Bozza VBT, Higa LM, et al. From a recombinant key antigen to an accurate, affordable serological test: Lessons learnt from COVID-19 for future pandemics. *Biochem Eng J*. (2022) 186:108537. doi: 10.1016/j.bej.2022.108537

14. Grenfell RFQ, Almeida NBF, Filgueiras PS, Corsini CA, Gomes SVC, de Miranda DAP, et al. Immunogenicity, effectiveness, and safety of inactivated virus (CoronaVac) vaccine in a two-dose primary protocol and BNT162b2 heterologous booster in Brazil (Immunita-001): A one year period follow up phase 4 study. *Front Immunol*. (2022) 13:918896. doi: 10.3389/fimmu.2022.918896

15. Spearman C. The method of "Right and wrong cases" (Constant stimuli) without gauss's formula. *Br J Psychol*. (1908) 1908:15. doi: 10.1037/h0063767

16. Kärber G. Beitrag zur kollektiven Behandlung pharmakologischer Reihenversuche. *Archiv f experiment Pathol u Pharmakol*. (1931) 1931:4. doi: 10.1007/BF01863914

17. Ella R, Reddy S, Jogdand H, Sarangi V, Ganneru B, Prasad S, et al. Safety and immunogenicity of an inactivated SARS-CoV-2 vaccine, BBV152: interim results from a double-blind, randomised, multicentre, phase 2 trial, and 3-month follow-up of a double-blind, randomised phase 1 trial. *Lancet Infect Dis*. (2021) 21:950–61. doi: 10.1016/S1473-3099(21)00070-0

18. Zhang Y, Zeng G, Pan H, Li C, Hu Y, Chu K, et al. Safety, tolerability, and immunogenicity of an inactivated SARS-CoV-2 vaccine in healthy adults aged 18–59 years: a randomised, double-blind, placebo-controlled, phase 1/2 clinical trial. *Lancet Infect Dis*. (2021) 21:181–92. doi: 10.1016/S1473-3099(20)30843-4

19. Oh S, Purja S, Shin H, Kim MS, Park S, Kronbichler A, et al. Efficacy, immunogenicity, and safety of COVID-19 vaccines in randomized control trials in the pre-delta era: A systematic review and network meta-analysis. *Vaccines (Basel)*. (2022) 10. doi: 10.3390/vaccines10101572

20. Polack FP, Thomas SJ, Kitchin N, Absalon J, Gurtman A, Lockhart S, et al. Safety and efficacy of the BNT162b2 mRNA covid-19 vaccine. *N Engl J Med*. (2020) 383:2603–15. doi: 10.1056/NEJMoa2034577

21. Wu Z, Hu Y, Xu M, Chen Z, Yang W, Jiang Z, et al. Safety, tolerability, and immunogenicity of an inactivated SARS-CoV-2 vaccine (CoronaVac) in healthy adults aged 60 years and older: a randomised, double-blind, placebo-controlled, phase 1/2 clinical trial. *Lancet Infect Dis*. (2021) 21:803–12. doi: 10.1016/S1473-3099(20)30987-7

22. Falsey AR, Sobieszczyk ME, Hirsch I, Sproule S, Robb ML, Corey L, et al. Phase 3 safety and efficacy of AZD1222 (ChAdOx1 nCoV-19) covid-19 vaccine. *N Engl J Med*. (2021) 385:2348–60. doi: 10.1056/NEJMoa2105290

23. Banho CA, Sacchetto L, Campos GRF, Bittar C, Possebon FS, Ullmann LS, et al. Impact of SARS-CoV-2 Gamma lineage introduction and COVID-19 vaccination on the epidemiological landscape of a Brazilian city. *Commun Med (Lond)*. (2022) 2:41. doi: 10.1038/s43856-022-00108-5

24. Moghadas SM, Vilches TN, Zhang K, Wells CR, Shoukat A, Singer BH, et al. The impact of vaccination on coronavirus disease 2019 (COVID-19) outbreaks in the United States. *Clin Infect Dis*. (2021) 73:2257–64. doi: 10.1093/cid/ciab079

25. Lopez Bernal J, Andrews N, Gower C, Robertson C, Stowe J, Tessier E, et al. Effectiveness of the Pfizer-BioNTech and Oxford-AstraZeneca vaccines on covid-19 related symptoms, hospital admissions, and mortality in older adults in England: test negative case-control study. *BMJ*. (2021) 373:n1088. doi: 10.1136/bmj.n1088

26. Chiapinotto S, Sarria EE, Mocelin HT, Lima JAB, Mattiello R, Fischer GB. Impact of non-pharmacological initiatives for COVID-19 on hospital admissions due to pediatric acute respiratory illnesses. *Paediatr Respir Rev*. (2021) 39:3–8. doi: 10.1016/j.prrv.2021.04.003

27. Maglietta G, Puntoni M, Caminiti C, Pession A, Lanari M, Caramelli F, et al. Effects of COVID-19-targeted non-pharmaceutical interventions on pediatric hospital admissions in North Italian hospitals, 2017 to 2022: a quasi-experimental study interrupted time-series analysis. *Front Public Health*. (2024) 12:1393677. doi: 10.3389/fpubh.2024.1393677

28. Armero G, Guitart C, Soler-Garcia A, Mele M, Esteva C, Brotons P, et al. Non-pharmacological interventions during SARS-coV-2 pandemic: effects on pediatric viral respiratory infections. *Arch Bronconeumol*. (2024) 60:612–8. doi: 10.1016/j.arbres.2024.05.019

29. Han B, Song Y, Li C, Yang W, Ma Q, Jiang Z, et al. Safety, tolerability, and immunogenicity of an inactivated SARS-CoV-2 vaccine (CoronaVac) in healthy children and adolescents: a double-blind, randomised, controlled, phase 1/2 clinical trial. *Lancet Infect Dis*. (2021) 21:1645–53. doi: 10.1016/S1473-3099(21)00319-4

30. Frenck RW Jr., Klein NP, Kitchin N, Gurtman A, Absalon J, Lockhart S, et al. Safety, immunogenicity, and efficacy of the BNT162b2 covid-19 vaccine in adolescents. *N Engl J Med*. (2021) 385:239–50. doi: 10.1056/NEJMoa2107456

31. Li G, Cappuccini F, Marchevsky NG, Aley PK, Aley R, Anslow R, et al. Safety and immunogenicity of the ChAdOx1 nCoV-19 (AZD1222) vaccine in children aged 6–17 years: a preliminary report of COV006, a phase 2 single-blind, randomised, controlled trial. *Lancet*. (2022) 399:2212–25. doi: 10.1016/S0140-6736(22)00770-X

32. Siegel DA, Reses HE, Cool AJ, Shapiro CN, Hsu J, Boehmer TK, et al. Trends in COVID-19 cases, emergency department visits, and hospital admissions among children and adolescents aged 0–17 years - United States, august 2020-august 2021. *MMWR Morb Mortal Wkly Rep*. (2021) 70:1249–54. doi: 10.15585/mmwr.mm7036e1

33. Kim L, Whitaker M, O'Halloran A, Kambhampati A, Chai SJ, Reingold A, et al. Hospitalization rates and characteristics of children aged <18 years hospitalized with laboratory-confirmed COVID-19 - COVID-NET, 14 states, march 1-july 25, 2020. *MMWR Morb Mortal Wkly Rep*. (2020) 69:1081–8. doi: 10.15585/mmwr.mm6932e3

34. DeBiasi RL, Delaney M. Symptomatic and asymptomatic viral shedding in pediatric patients infected with severe acute respiratory syndrome coronavirus 2 (SARS-coV-2): under the surface. *JAMA Pediatr*. (2021) 175:16–8. doi: 10.1001/jamapediatrics.2020.3996

35. Domingues C, Maranhao AGK, Teixeira AM, Fantinato FFS, Domingues RAS. The Brazilian National Immunization Program: 46 years of achievements and challenges. *Cad Saude Publica*. (2020) 36Suppl 2:e00222919. doi: 10.1590/0102-311X00222919

36. Calendário de Vacinação (2025). Available online at: https://www.gov.br/saude/pt-br/vacinacao/calendario (Accessed February 2025).

37. Zheng C, Shao W, Chen X, Zhang B, Wang G, Zhang W. Real-world effectiveness of COVID-19 vaccines: a literature review and meta-analysis. *Int J Infect Dis*. (2022) 114:252–60. doi: 10.1016/j.ijid.2021.11.009

38. Link-Gelles R, Weber ZA, Reese SE, Payne AB, Gaglani M, Adams K, et al. Estimates of bivalent mRNA vaccine durability in preventing COVID-19-associated hospitalization and critical illness among adults with and without immunocompromising conditions - VISION network, september 2022-april 2023. *MMWR Morb Mortal Wkly Rep*. (2023) 72:579–88. doi: 10.15585/mmwr.mm7221a3

39. Saied AA, Metwally AA, Madkhali NAB, Haque S, Dhama K, et al. Egypt's COVID-19 recent happenings and perspectives: A mini-review. *Front Public Health*. (2021) 9:696082. doi: 10.3389/fpubh.2021.696082

40. Nham E, Noh JY, Park O, Choi WS, Song JY, Cheong HJ, et al. COVID-19 vaccination strategies in the endemic period: lessons from influenza. *Vaccines (Basel)*. (2024) 12. doi: 10.3390/vaccines12050514

41. Gotzinger F, Santiago-Garcia B, Noguera-Julian A, Lanaspa M, Lancella L, Calo Carducci FI, et al. COVID-19 in children and adolescents in Europe: a multinational, multicentre cohort study. *Lancet Child Adolesc Health*. (2020) 4:653–61. doi: 10.1016/S2352-4642(20)30177-2

42. Parri N, Lenge M, Buonsenso D, Coronavirus Infection in Pediatric Emergency Departments Research Group. Children with covid-19 in pediatric emergency departments in Italy. *N Engl J Med*. (2020) 383:187–90. doi: 10.1056/NEJMc2007617

43. Madewell ZJ, Yang Y, Longini IM Jr, Halloran ME, Dean NE. Household transmission of SARS-coV-2: A systematic review and meta-analysis. *JAMA Netw Open*. (2020) 3:e2031756. doi: 10.1001/jamanetworkopen.2020.31756

44. Nathanielsz J, Toh ZQ, Do LAH, Mulholland K, Licciardi PV. SARS-CoV-2 infection in children and implications for vaccination. *Pediatr Res*. (2023) 93:1177–87. doi: 10.1038/s41390-022-02254-x

45. Ntziora F, Kostaki EG, Karapanou A, Mylona M, Tseti I, Sipsas NV, et al. Protection of vaccination versus hybrid immunity against infection with COVID-19 Omicron variants among Health-Care Workers. *Vaccine*. (2022) 40:7195–200. doi: 10.1016/j.vaccine.2022.09.042

46. Bates TA, McBride SK, Leier HC, Guzman G, Lyski ZL, Schoen D, et al. Vaccination before or after SARS-CoV-2 infection leads to robust humoral response and antibodies that effectively neutralize variants. *Sci Immunol*. (2022) 7:eabn8014. doi: 10.1126/sciimmunol.abn8014

47. Altarawneh HN, Chemaitelly H, Ayoub HH, Tang P, Hasan MR, Yassine HM, et al. Effects of previous infection and vaccination on symptomatic omicron infections. *N Engl J Med*. (2022) 387:21–34. doi: 10.1056/NEJMoa2203965

48. Sano K, Bhavsar D, Singh G, Floda D, Srivastava K, Gleason C, et al. SARS-CoV-2 vaccination induces mucosal antibody responses in previously infected individuals. *Nat Commun*. (2022) 13:5135. doi: 10.1038/s41467-022-32389-8

49. Matuchansky C. Protection against SARS-CoV-2 after Vaccination and Previous Infection. *N Engl J Med*. (2022) 386:2534. doi: 10.1056/NEJMc2205618

50. Niyomnaitham S, Toh ZQ, Licciardi PV, Wongprompitak P, Srisutthisamphan K, Copeland KK, et al. Immunogenicity of a single dose of BNT162b2, ChAdOx1 nCoV-19, or CoronaVac against SARS-CoV-2 delta and omicron variants among

previously infected adults: A randomized trial. *J Infect*. (2022) 85:436–80. doi: 10.1016/j.jinf.2022.06.014

51. Bobrovitz N, Ware H, Ma X, Li Z, Hosseini R, Cao C, et al. Protective effectiveness of previous SARS-CoV-2 infection and hybrid immunity against the omicron variant and severe disease: a systematic review and meta-regression. *Lancet Infect Dis*. (2023) 23:556–67. doi: 10.1016/S1473-3099(22)00801-5

52. Jacobsen H, Cobos Jimenez V, Sitaras I, Bar-Zeev N, Cicin-Sain L, Higdon MM, et al. Post-vaccination T cell immunity to omicron. *Front Immunol*. (2022) 13:944713. doi: 10.3389/fimmu.2022.944713

53. Hall V, Foulkes S, Insalata F, Kirwan P, Saei A, Atti A, et al. Protection against SARS-CoV-2 after Covid-19 Vaccination and Previous Infection. *N Engl J Med*. (2022) 386:1207–20. doi: 10.1056/NEJMoa2118691

54. Rossler A, Netzl A, Knabl L, Schafer H, Wilks SH, Bante D, et al. BA.2 and BA.5 omicron differ immunologically from both BA.1 omicron and pre-omicron variants. *Nat Commun*. (2022) 13:7701. doi: 10.1038/s41467-022-35312-3

55. Cao Y, Yisimayi A, Jian F, Song W, Xiao T, Wang L, et al. BA.2.12.1, BA.4 and BA.5 escape antibodies elicited by Omicron infection. *Nature*. (2022) 608:593–602. doi: 10.1038/s41586-022-04980-y

56. Tuekprakhon A, Nutalai R, Dijokaite-Guraliuc A, Zhou D, Ginn HM, Selvaraj M, et al. Antibody escape of SARS-CoV-2 Omicron BA.4 and BA.5 from vaccine and BA.1 serum. *Cell*. (2022) 185:2422–2433 e13. doi: 10.1016/j.cell.2022.06.005

57. Hachmann NP, Miller J, Collier AY, Ventura JD, Yu J, Rowe M, et al. Neutralization escape by SARS-coV-2 omicron subvariants BA.2.12.1, BA.4, and BA.5. *N Engl J Med*. (2022) 387:86–8. doi: 10.1056/NEJMc2206576

58. Cheng SS, Mok CK, Li JK, Ng SS, Lam BH, Jeevan T, et al. Plaque-neutralizing antibody to BA.2.12.1, BA.4 and BA.5 in individuals with three doses of BioNTech or CoronaVac vaccines, natural infection and breakthrough infection. *J Clin Virol*. (2022) 156:105273. doi: 10.1016/j.jcv.2022.105273

59. Assawakosri S, Kanokudom S, Suntronwong N, Chansaenroj J, Auphimai C, Nilyanimit P, et al. Immunogenicity and durability against Omicron BA.1, BA.2 and BA.4/5 variants at 3–4 months after a heterologous COVID-19 booster vaccine in healthy adults with a two-doses CoronaVac vaccination. *Heliyon*. (2024) 10:e23892. doi: 10.1016/j.heliyon.2023.e23892

60. Arashiro T, Arima Y, Kuramochi J, Muraoka H, Sato A, Chubachi K, et al. Immune escape and waning immunity of COVID-19 monovalent mRNA vaccines against symptomatic infection with BA.1/BA.2 and BA.5 in Japan. *Vaccine*. (2023) 41:6969–79. doi: 10.1016/j.vaccine.2023.10.021

61. Usdan L, Patel S, Rodriguez H, Xu X, Lee DY, Finn D, et al. A bivalent omicron-BA.4/BA.5-adapted BNT162b2 booster in >/=12-year-olds. *Clin Infect Dis*. (2024) 78:1194–203. doi: 10.1093/cid/ciad718

62. Chalkias S, Whatley JL, Eder F, Essink B, Khetan S, Bradley P, et al. Original SARS-CoV-2 monovalent and Omicron BA.4/BA.5 bivalent COVID-19 mRNA vaccines: phase 2/3 trial interim results. *Nat Med*. (2023) 29:2325–33. doi: 10.1038/s41591-023-02517-y

63. Chalkias S, Harper C, Vrbicky K, Walsh SR, Essink B, Brosz A, et al. A bivalent omicron-containing booster vaccine against covid-19. *N Engl J Med*. (2022) 387:1279–91. doi: 10.1056/NEJMoa2208343

64. Bennett C, Woo W, Bloch M, Cheung K, Griffin P, Mohan R, et al. Immunogenicity and safety of a bivalent (omicron BA.5 plus ancestral) SARS-CoV-2 recombinant spike protein vaccine as a heterologous booster dose: interim analysis of a phase 3, non-inferiority, randomised, clinical trial. *Lancet Infect Dis*. (2024) 24:581–93. doi: 10.1016/S1473-3099(24)00077-X

65. Suzuki R, Suda M, Ishida K, Furihata K, Ota A, Takahashi K, et al. Booster vaccination using bivalent DS-5670a/b is safe and immunogenic against SARS-CoV-2 variants in children aged 5–11 years: a phase 2/3, randomized, active-controlled study. *Front Immunol*. (2024) 15:1445459. doi: 10.3389/fimmu.2024.1445459

frontiers | Frontiers in Immunology

TYPE Original Research
PUBLISHED 22 July 2025
DOI 10.3389/fimmu.2025.1629585

OPEN ACCESS

EDITED BY
Fabio Fiorino,
LUM University Giuseppe Degennaro, Italy

REVIEWED BY
Marcio Chaim Bajgelman,
National Center for Research in Energy and Materials, Brazil
Hyeran Won,
Korea National Institute of Health, Republic of Korea

*CORRESPONDENCE
Hongtao Liu
liuhongtao1@sinopharm.com
Yan Cai
caiyan3@sinopharm.com

RECEIVED 16 May 2025
ACCEPTED 07 July 2025
PUBLISHED 22 July 2025

CITATION
Liu H, Liu N, Sun Y, Li S, Li H, Wang M, Shuang H and Cai Y (2025) Development and characterization of the genotype F attenuated mumps candidate strains. *Front. Immunol.* 16:1629585. doi: 10.3389/fimmu.2025.1629585

Development and characterization of the genotype F attenuated mumps candidate strains

Hongtao Liu[1,2,3]*, Na Liu[1], Yueqiu Sun[1], Shuang Li[1], Hang Li[1], Menghan Wang[1], Hui Shuang[1] and Yan Cai[1,3]*

[1]Vaccines R&D Department, Changchun Keygen Biological Products Co., Ltd., Changchun, Jilin, China, [2]Vaccines R&D Department, Changchun Institute of Biological Products Co., Ltd., Changchun, Jilin, China, [3]State Key Laboratory of Novel Vaccines for Emerging Infectious Diseases, China National Biotec Group Company Limited, Beijing, China

Background: Mumps is an acute infectious disease caused by the mumps virus (MuV), primarily affecting the parotid glands, though it can also lead to systemic infections, including the nervous system. In China, the predominant circulating MuV genotype is F, while the vaccine strain (S79 or WM84) belongs to genotype A, raising concerns about immunization effectiveness.

Methods: A genotype F MuV strain was isolated from throat swabs of six suspected mumps patients. Through cell adaptation passage and plaque purification, two candidate vaccine strains QBB-2BS-3.2 and QBB-2BS-9.3 were prepared. Their immunogenicity was assessed by neutralizing antibody and cell-mediated immune responses in immunized mice. Additionally, neurotoxicity was evaluated in neonatal Lewis rats.

Results: Both QBB-2BS-3.2 and QBB-2BS-9.3 elicited strong neutralizing antibody responses and robust cell-mediated immune responses in mice. Notably, neurotoxicity testing revealed minimal neurotoxicity in QBB-2BS-3.2 and QBB-2BS-9.3 strains, comparable to the S79 vaccine strain.

Conclusions: This study successfully developed two attenuated genotype F MuV candidate strains with favorable immunogenicity and safety profiles, laying a critical foundation for the development of genotype F mumps live attenuated vaccines.

KEYWORDS

mumps virus, F genotype, QBB strain, immunogenicity, neurovirulence

1 Introduction

Mumps is an acute, self-limiting respiratory infection caused by the mumps virus (MuV), with the main clinical symptoms being fever, non-purulent swelling, and pain in the parotid glands (1, 2), which may also cause multi-organ damage, leading to serious complications such as pancreatitis, orchitis, deafness, aseptic meningitis, and encephalitis (3, 4). MuV belongs to the *Paramyxoviridae* family (*Paramyxoviridae*), whose viral genome is a non-segmented, single-stranded, negative-stranded RNA containing 15,384 nucleotides, encoding the transcriptional units of seven viral proteins, including nucleoprotein (N), phosphoprotein (P), matrix (M), fusion (F), small hydrophobic (SH), hemagglutinin-neuraminidase(HN), and large (L) proteins (5, 6). HN protein is a type II integral membrane protein. F and HN proteins work together on viral membrane proteins, play an important role in the binding and entry process of viruses into host cells, and are also the main antigens that elicit an immune response from the organism (7–9). The immunogenicity of the HN protein is closely associated with the spatial conformation of its surface-exposed antigenic epitopes. Studies indicate that three key regions (aa265–288, aa329–340, and aa352–360) on the HN protein surface exhibit strong antigenicity due to their exposure on the molecular surface. Among these, the aa329–340 region induces potent neutralizing antibodies in mouse models, confirming its role as a critical conformational epitope (9). Furthermore, experiments with the HN3 fragment (aa213–372) validate that this region simultaneously elicits both hemagglutination-inhibiting and neutralizing antibodies, highlighting its function as a core target for humoral immunity (10). Mumps virus consists of only one serotype, and the SH gene is highly variable and is often used as the basis for mumps virus genotyping. Based on the nucleotide sequence differences in the SH gene, mumps viruses are classified into 12 genotypes, including A, B, C, D, F, G, H, I, J, K, L, and N (11).

Vaccination is an effective means of preventing and controlling the spread of mumps (12). Since 1967, with the widespread use of live attenuated vaccine (LAV), especially the measles, mumps, and rubella vaccine (MMR), which has been incorporated into the national vaccination programs of many countries, the incidence of mumps has been significantly reduced. The most widely used live attenuated mumps vaccine is the Jeryl Lynn strain (genotype A), and its derivatives, such as RIT4385, S79, and Wm84, are also widely used. The live attenuated mumps vaccine strains mainly used in China are S79 and Wm84. Epidemiological data showed that the predominant genotype of MuV prevalent in China is the F genotype (13–15). MuV has only one serotype, and antigenic cross-protection exists between genotypes. Studies reported that cross-protection between genotypes is limited. Serum antibodies from the Jeryl Lynn strain could neutralize other genotypes of MuVs. However, the neutralizing antibody titers against other strains were significantly lower than its own (16, 17). It implied that the current genotype A vaccine may not provide sufficient protection against an epidemic of genotype F MuV, which may be the reason for the breakthrough mumps cases that have occurred even after vaccination (18–20).

Currently, the live attenuated mumps vaccine is mainly produced using primary chicken embryo cells (21, 22). A large number of chicken embryos were consumed, contrary to the 3R principles (Replacement, Reduction, and Optimization) advocated by the World Health Organization (WHO) for the use of animals (23). Moreover, chicken embryo cells as a heterologous cellular matrix may cause allergic reactions, and chicken embryo cells carry infectious avian retroviruses that can cause side effects (24–26). To improve the scale-up production efficiency of mumps-associated vaccine and improve product safety, there is an urgent need to develop new MuV-adapted cell lines to replace the traditional chicken embryo cell culture.

In this study, we successfully isolated one positive sample "MuV-QBB", which was identified as genotype F MuV by isolating clinical samples from throat swabs of mumps patients. Subsequently, several F-genotype MuV 2BS cell-adapted strains were prepared using passaging and plaque purification. Finally, the candidate strains were tested for genetic stability, immunogenicity, and neurotoxicity. These results provided a basis for the development of the F genotype live attenuated mumps vaccine and the prevention and control of mumps.

2 Materials and methods

2.1 Animals and ethics statement

The SPF female BALB/c mice (6–8 weeks old) were purchased from the Changchun Institute of Biological Products Co., Ltd. (Changchun, China), the SPF pregnant female Lewis rats were purchased from Beijing Vital River Laboratory Animal Technology Co., Ltd.(Beijing, China), which were maintained under SPF conditions with a 12 h/12 h light/dark cycle. All animal experiments were carried out under the guidelines of the Council on Animal Care and Use, with protocols approved by the Animal Ethics Committee of the Changchun Institute of Biological Products. Animals were monitored daily and received free access to water and food throughout the study. Mice were euthanized by cervical dislocation.

The only human materials used were collected from the clinical suspected mumps patients for the purpose of public health and disease control. The studies involving humans were approved by the Ethics Committee of the China-Japan Union Hospital of Jilin University. The studies were conducted in accordance with the local legislation and institutional requirements. Written informed consent for participation in this study was provided by the participants' legal guardians/next of kin.

2.2 Mumps clinic specimens collection and virus isolation

Six throat swab samples of children with mumps from an epidemic in Changchun City, Jilin Province, were collected and preserved after filtration and sterilization using a 0.22-micron filter. Within a biosafety level 2 (BSL-2) facility, clinical mumps specimens prescreened positive by reverse transcription polymerase chain reaction (RT-PCR) were inoculated onto confluent Vero cell monolayers in slant tubes for viral adsorption.

Post-adsorption, the inoculum was replaced with maintenance medium. Cultures were incubated at 35°C with daily monitoring for cytopathic effect (CPE). Viral harvest occurred when CPE exhibited >90% cellular degeneration or upon completion of 7-day incubation. The strain was purified and separated using limiting dilution in Vero cells by picking single-plaque with the double-layer agar method. And the resulting isolation was stored at 4°C. After two rounds of plaque purification, cultures that appeared CPE continued to be inoculated with Vero cells for viral passaging.

2.3 50% cell culture infective dose assay

Virus titration was carried out using the $CCID_{50}$ assay on Vero cells. The assay was performed in 96-well plates. Briefly, 10-fold serial dilutions (10^{-1}-10^{-7}) of viral samples were prepared in MEM (Gibco, 11095080) containing 2% FBS (RUNSUN, 200420100). Then, 100 µL of each virus dilution and 100 µL Vero cell suspension (1.6×10^5 cells/mL) were added to each well. Then, the plates were incubated at 37°C in 5% CO_2 for 7 days. After the incubation period, the cells were observed for cytopathic changes. The titer was calculated as the $CCID_{50}$/mL using the Reed-Muench method.

2.4 Western blotting assay

Cells cultured in 6-well plates were lysed using RIPA lysis buffer (Beyotime, P0013B). Samples were separated by SDS-PAGE (Beyotime, P0052B) and transferred to a nitrocellulose membrane. The membrane was blocked with 6% non-fat milk (Solarbio, D8340) for 1 h and incubated at 4°C overnight with appropriate primary antibodies: anti-HN (Detai, DT7988-1) and anti-NP (Eastcoast, HM400). Then, the membrane was washed and incubated with HRP-labeled secondary antibody (Abcam, ab205719) at room temperature for 1 h for subsequent detection using enhanced chemiluminescence.

2.5 TEM

TEM assays were performed as described. Briefly, viral particles were adsorbed onto glow-discharged carbon-coated copper grids (300 mesh) by incubating 7 µL of the sample suspension for 3 min at room temperature. Grids were treated with 2% phosphotungstic acid for 2 min (Solarbio, G1870). Stained grids were air-dried in a desiccator overnight to preserve structural integrity. All steps were performed using fresh staining solutions to minimize artifacts. Electron photomicrographs were taken from virus structures under a transmission electron microscope (Hitachi, HT7800).

2.6 Sequencing and phylogenetic analyses

Viral RNA was extracted from culture with cytopathic effect by using the TaKaRa MiniBEST Viral RNA/DNA Extraction Kit (TaKaRa, 9766). To obtain the complete SH gene sequences, RT-PCR was performed with the One-step RT-PCR kit (TaKaRa, RR096A) following the manufacturer's instructions. The primers of SH-1(5′-AATATCAAGTAGTGTCGATGA-3′) and SH-2 (5′-AGGTGCAAAGGTGGCATTGTC-3′) were used to amplify the entire SH gene. After purification of the PCR products with a QIA Gel Extraction Kit (Qiagen, 28704), the sequences were determined using the Sanger dideoxy terminator sequencing method with a BigDye Terminator Version 3.1 Cycle Sequencing kit (Life Technologies, 4337455) and ABI PRISMTM 3100 Genetic Analyzer (Life Technologies, Japan). Sequencher software version 5.0 (Gene Codes Corporation) was used to edit and assemble the raw sequence data to obtain the 316-nt complete SH gene sequences (2). Each dataset was used to build a neighbor joining phylogenetic tree with Mega5 using the maximum composite likelihood nucleotide substitution model. The topology of the phylogenetic tree was tested with 1000 bootstrap replications. Bootstrap values greater than 80% were indicated on the trees. Maximum likelihood tree was also generated with Mega. p-distances were computed in Mega. The number of synonymous nucleotide substitutions per synonymous site (dS) and the number of nonsynonymous substitutions per nonsynonymous site (dN) were estimated in Mega by Nei and Gojobori's method.

2.7 Vaccine immunization program

Female BALB/c mice aged 4–6 weeks were divided into three groups, the experimental group, the positive control, and the negative control. The experimental group (the QBB-Vero group, QBB-2BS-3.2 group, QBB-2BS-3.3 group, QBB-2BS-3.4 group, QBB-2BS-9.3 group) received an subcutaneous (SC) injection of 100 µL mumps virus at 1×10^6 $CCID_{50}$/mL. The virus was administered via two SC injections (a primer and a booster after a two-week interval). Using the same vaccination schedule, the positive and negative control groups were administered with live MuV (S79) and PBS, respectively. Blood and spleen samples were obtained at 2 weeks post the booster administration.

2.8 Enzyme-linked immunosorbent assay

MuV-specific total IgG antibody titers were determined using ELISA. 50 µL of MuV mixtures (1×10^5 $CCID_{50}$/mL of each genotype A and F) was added to each well and coated overnight in 96-well plates at 4°C, and plates were washed three times with PBST (0.05% v/v) and blocked with 1% BSA (Beyotime, ST023) in PBST for 2 h at 37°C. Mouse serum was serially diluted and incubated with these mixtures for 1 h at 37°C, following which, the mixtures were washed, probed with HRP-conjugated goat anti-mouse IgG secondary antibodies (1:2000) for 1 h at 37°C, and washed again with PBS/T (0.05% v/v). Tetramethylbenzidine (TMB) (Thermo, XB3498751) was then added as a substrate, and the reaction was quenched by adding the stop solution for TMB. For each sample, the optical density (OD) was measured at 450 nm using an ELISA

reader and correlated to values in the standard curve. MuV-specific total IgG antibody titers were tested in 3 wells per mouse, and the mean values were used for statistical analysis.

2.9 Mumps virus neutralization assay

The neutralizing antibody titers against the MuVs were determined using a microneutralization assay based on cytopathic effect (CPE) reduction. Briefly, heat-inactivated serum samples (56°C for 30 min) were serially diluted twofold in Modified Eagle Medium (MEM) supplemented with 2% fetal bovine serum (FBS), starting from an initial dilution of 1:4. Each serum dilution was mixed with an equal volume of MuVs strain (QBB or S79 MuVs, 500–2000 $CCID_{50}$/mL) and incubated at 37°C for 1 h for neutralization. The virus-serum mixtures (100 µL/well) were then transferred onto confluent Vero cell monolayers cultured in 96-well plates and further incubated at 37°C under 5% CO_2 for 7–10 days. Cells inoculated with virus-only (no serum) and cell-only (no virus) served as positive and negative controls, respectively. CPE was monitored daily under an inverted light microscope, and the neutralizing antibody titer was defined as the highest serum dilution that completely inhibited viral CPE in ≥50% of replicate wells. Statistical analysis was performed using GraphPad Prism v9.0, and geometric mean titers (GMT) with 95% confidence intervals were calculated.

2.10 Detection of IFN-γ and IL-2 secretion in vaccine-immunized mice

T-cell responses were determined by gamma interferon (IFN-γ) (MABTECH, 3321-4AST-2) and Interleukin-2 (IL-2) (MABTECH, 3441-4APW-2) enzyme-linked immunosorbent spot (ELISpot) assay according to the manufacturer's protocol. Spleens were harvested from immunized mice after booster immunization. Splenocytes were filtered through a 100 µm pore size nylon cell strainer (BD) and digested with red blood cell lysis buffer (Beyotime, C3702) to obtain a single-cell suspension. Splenocytes were seeded at 1×10^5 cells/well in RPMI-1640 supplemented with 10% FBS and 1× P/S, pre-incubated at 37°C under 5% CO_2 for 2 h, then stimulated with MuVs (1×10^5 $CCID_{50}$/mL each of genotypes A and F) and incubated for an additional 24 h under the same conditions. After stimulation, the cells were incubated with biotin-conjugated antibodies and streptavidin-HRP. Spots were developed using 3-amino-9 ethylcarbazole (AEC) substrate. The numbers of IFN-γ- and IL-2-secreting cells were counted using the automated ELISpot reader as described above. Data are presented as the number of spot-forming units (SFUs) per 10^5 splenocytes.

2.11 Mumps virus neurovirulence assessment

One-day-old Lewis rats were intracranially inoculated using a microsyringe (Thermo Fisher, T_7011481529) equipped with an ultra-fine dual-wall needle (internal diameter: 0.15 mm; outer diameter: 0.72 mm). The viral suspension (0.01 mL containing 10^3 $CCID_{50}$) was slowly injected perpendicularly through the skull (27). Tested viral strains included: S79 vaccine, QBB-Vero-P2, QBB-2BS-3.2-P20, QBB-2BS-3.2-P30, QBB-2BS-3.2-P40, QBB-2BS-9.3-P20, QBB-2BS-9.3-P30, QBB-2BS-9.3-P40. Rats were euthanized 30 days post-inoculation, and brains were removed and fixed in 4% fixative solution (Solarbio, P1110) for histological analysis. Two 3 to 4 mm-thick sagittal slices were selected at a standard distance from either side of the anatomical midline from a fixed brain, paraffin-embedded, sectioned, and stained with hematoxylin and eosin. The severity of hydrocephalus was determined as the percentage of the total brain cross-sectional area (excluding the cerebellum) occupied by the lateral ventricle on each of the two sections per rat using Image Pro Plus image analysis software (Media Cybernetics, Silver Spring, Md.). The mean percentage of hydrocephalus in each experimental group of rats was calculated and designated as the rat neurovirulence test (RNVT) score (28).

2.12 Statistical analysis

Graphing and analysis were performed using the GraphPad Prism 8 Software (San Diego, CA, USA). Statistical significance was analyzed by one-way ANOVA. Data represent mean ± SEM (n = 3). Statistical significance was represented by asterisks and was marked correspondingly in the Figures: (ns; not significant, * $p < 0.05$, ** $p < 0.01$, *** $p < 0.001$).

3 Results

3.1 Isolation and identification of F genotype mumps virus QBB strains

Viral isolation from clinical samples of suspected mumps patients was performed in Vero cells, and one positive adaptive growth strain was obtained by screening from six samples. According to the principle of mumps strain nomenclature, the strain was named MuV/JiLin.CHN/2022 (QBB strain) (27). The whole genome sequence of the QBB strain is shown in Supplementary Material S1. As shown in Figure 1A, the morphology of Vero cells showed aggregation, rounded morphology, cellular aging, and shedding on day 4 post-infection. The viral titers increased progressively through serial passaging, reaching 7.20 $lgCCID_{50}$/mL at passage 5 (P5) (Figure 1B). NP protein is the main structural protein of the MuV nucleocapsid, and HN protein is the main surface antigenic protein of MuV. As shown in Figure 1C, Western blot results showed that the amplicon bands of NP and HN proteins in MuV-QBB were consistent with S79 (positive control). Moreover, TEM revealed that the MuV-QBB virus exhibited a sphere-shaped morphology approximately 200 nm in diameter, which is in accordance with the structural characteristics of typical mumps

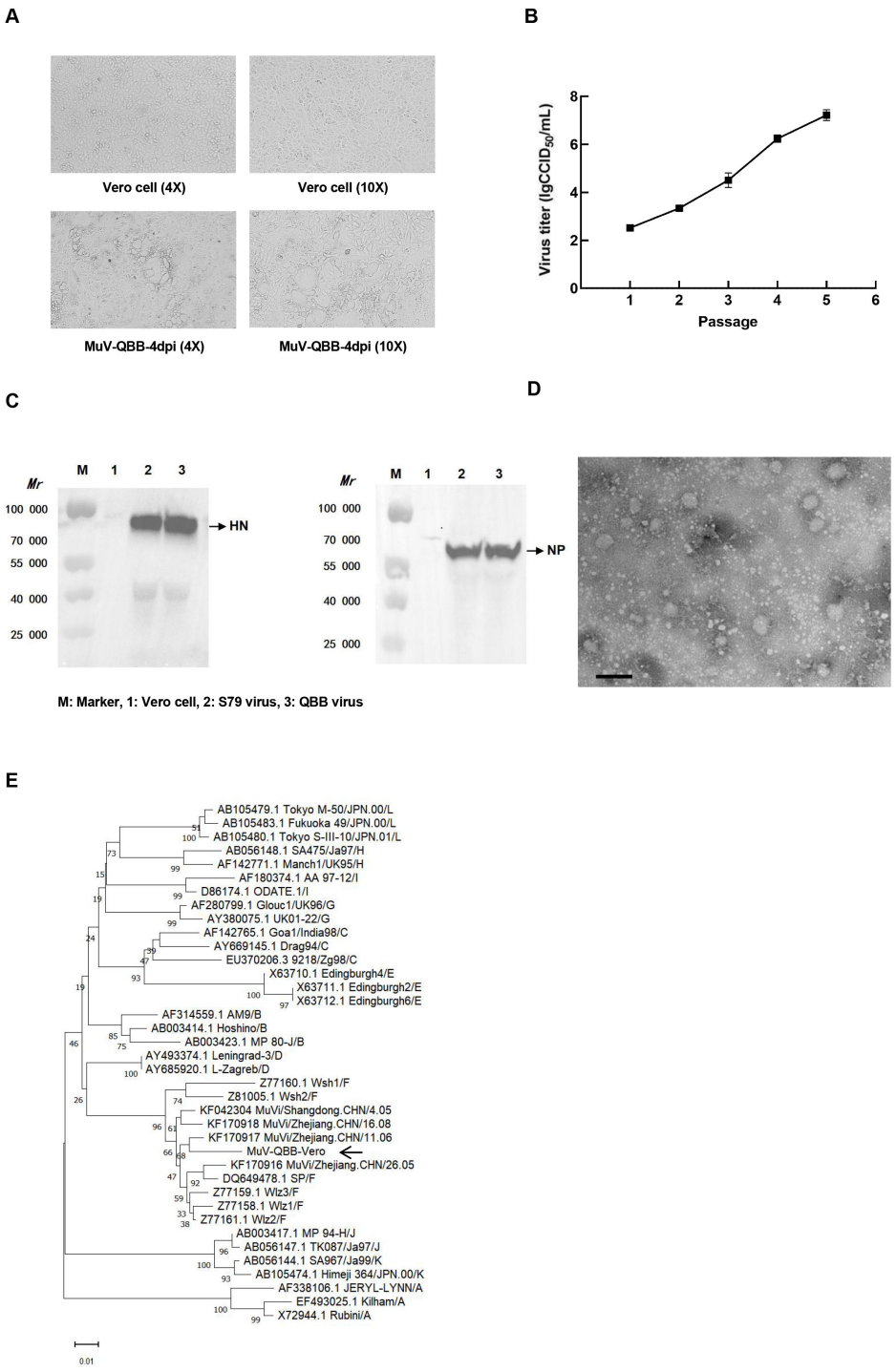

FIGURE 1
Isolation and identification of F genotype mumps virus QBB strains. **(A)** Cell morphology of Vero cells on day 4 post MuV-QBB infection. **(B)** Virus titer of different passages of MuV-QBB were detected in vero cells. **(C)** Western blot analysis of HN and NP proteins of the mumps. **(D)** Electron microscopy image of MuV- QBB. Scale bar: 500 nm. **(E)** Analysis and comparison the phylogenetic tree of SH and peripheral genes sequence of different genotypes mumps. Results are presented as means ± SD, n = 3.

virus (Figure 1D). The universal standard for MuV genotyping is based on the SH genesequences. To determine the genotypic classification of the MuV-QBB strain, we aligned the SH gene sequence with representative genotype F reference strains and constructed a neighbor-joining phylogenetic tree (2). As shown in Figure 1E, results of the evolutionary tree analysis showed that the MuV-QBB strain was located on the same branch as the Wshl, Wsh2, and Wlz1, Wlz2, Wlz3 and SP mumps strains (all F genotype mumps viruses), which indicated that MuV-QBB strains belonged to F genotype mumps viruses.

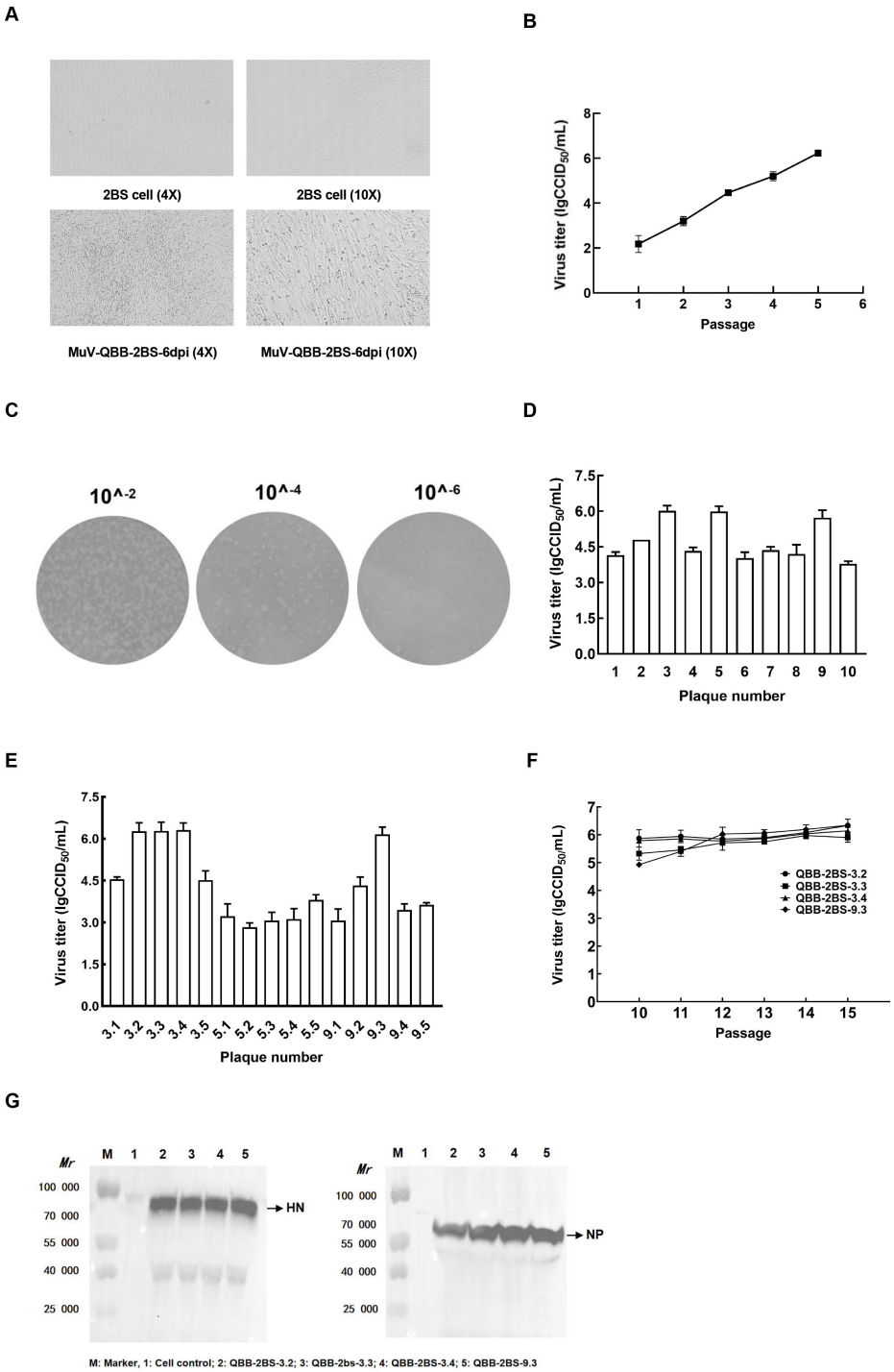

FIGURE 2
Generation of F genotype mumps virus 2BS cell-adapted strains. **(A)** Morphological changes in 2BS cells at 6 dpi with MuV-QBB. **(B)** Virus titer detection of MuV-QBB in 2BS cells at different passages. **(C)** Plaque clone of MuV-QBB mumps virus on 2BS cells. **(D)** Virus titer of the first round of plaque purification. **(E)** Virus titer of the second round of plaque purification. **(F)** Virus titer of four MuV-QBB 2BS cell-adapted strains from different passages. **(G)** Detection of HN and NP proteins by western blot in MuV-QBB 2BS-adapted strains. Results are presented as means ± SD, n = 3.

3.2 Preparation of MuVs 2BS cell adaptation strains

The MuV-QBB was passaged in 2BS cells up to P3, the cells exhibited typical cytopathic effects (CPE), whereas the negative control showed normal cell morphology (Figure 2A). As shown in Figure 2B, viral titer increased steadily, reaching 6.23 lgCCID$_{50}$/mL at P5 generation. Subsequently, two rounds of plaque purification followed by viral amplification were performed. As shown in Figure 2C, plaques appeared round with smooth surfaces and

well-defined edges at 7 days post-infection. The 3, 5, and 9 plaque numbers were selected from 10 plaques based on the viral titer after the first round of plaque purification (Figure 2D). In the second round, 5 plaques were screened respectively from the plaques obtained in the first round of screening (Figure 2E). The number of 3.2, 3.3, 3.4, and 9.3 plaques were taken based on the results of CPE and virus titers after passaging and inoculated on 2BS cells for culture. As shown in Figure 2F, the virus titers stabilized at 6.0 $lgCCID_{50}$/mL after passaging to P15. Western Blot assay showed that HN and NP proteins were detected in all four MuV-QBB 2BS cell-adapted strains (Figure 2G).

3.3 Evaluation of immunogenicity of the QBB strain of MuVs in mice

To evaluate the immunogenicity of the QBB candidate strains, BALB/c mice were immunized and tested for humoral and cellular immune responses. The immunization schedules are depicted in Figure 3A. As shown in Figure 3B, MuV-specific serum IgG levels, measured by ELISA, were significantly elevated in all immunized groups compared to the negative control group. Neutralization assay analysis of cross-protection conferred by the vaccine candidates revealed that mice vaccinated with QBB-2BS-3.2 developed significantly higher neutralizing antibody titers against the homologous QBB strain compared to those receiving the licensed S79 vaccine (Figure 3C), whereas neutralization titers against the heterologous S79 strain were comparable between both vaccine groups (Figure 3D). To explore the cellular immune response triggered by the QBB candidate strains, an ELISpot assay was performed to test IFN-γ and IL-2 using immunized BALB/c mice splenocytes stimulated with mixtures of MuVs. Immune responses indicate vaccine-induced responses detected in ELISpot IFN-γ and IL-2 assays. The levels of IL-2 were significantly higher in QBB-2BS-3.2 group compared to S79 group (Figure 3E), whereas the levels of IFN-γ were similar in QBB-2BS-9.3 and S79 group (Figure 3F).

3.4 Biological characteristics and genetic stability of the QBB strain of MuVs

To investigate the biological characteristics and genetic stability of the 2BS cell-adapted strain of F-genotype mumps virus (MuV). The QBB-2BS-3.2 and QBB-2BS-9.3 strains were serially passaged to P40 in 2BS cells, and virus titers were measured at P15, P20, P25, P30, P35, and P40. As shown in Figure 4A, the titers of the F genotype 2BS cell-adapted strains QBB-2BS-3.2 and QBB-2BS-9.3 gradually increased in the early generations and stabilized above 7.00 $lgCCID_{50}$/mL after P20. Western blot analysis revealed stable expression of HN and NP proteins remained consistent across P15 to P40 for both QBB-2BS-3.2 and QBB-2BS-9.3 strains (Figures 4B, C). Whole-genome sequencing showed that the QBB-2BS-3.2 strain had 8 non-synonymous mutations (Table 1), and the QBB-2BS-9.3 strain had 7 non-synonymous mutations during P5 to P40 generations (Table 2).

3.5 Evaluation of mumps virus neurovirulence in neonatal rat model

The neurovirulence of the candidate strains QBB-2BS-3.2 and QBB-2BS-9.3 was evaluated using the neonatal rat model. As shown in Figure 5, the left panel shows HE staining images of brain tissue from mice without hydrocephalus, and the right panel shows HE staining images of brain tissue from mice with hydrocephalus. The mean S/S0 ratio is the hydrocephalus neurotoxicity score. As shown in Figure 5B, there was no significant difference in cerebral neurotoxicity scores of QBB-2BS-3.2 and QBB-2BS-9.3 strains in all generations compared with the S79 vaccine group or the placebo group, and on the contrary, when compared with the QBB-Vero-P2 group. This indicates that the neurotoxicity of QBB-2BS-3.2 and QBB-2BS-9.3 was significantly weakened after adaptation, and there was no virulence reversion with the increase in the number of generations.

4 Discussion

Vaccines are an important means of preventing and controlling the spread of disease. Live attenuated vaccines are of great interest because of their long-lasting immunity and long duration of action, e.g., attenuated polio vaccine, attenuated chickenpox vaccine, and measles-mumps-rubella (MMR) vaccine, which have shown remarkable results in combating viral infections. The attenuated mumps vaccine was incorporated into China in the 1990s, and formally integrated into the National Expanded Programme on Immunization (EPI) in 2008. The most widely used vaccine strains in China are S79 and WM84, based on the JL strain (A genotype). There is only one serotype of the mumps virus, and virus strains of different genotypes have cross-protective effects. However, in the last decade, we have encountered repeated outbreaks of mumps in highly vaccinated populations, which call into question the effectiveness of available vaccines (29–33). Thus, vaccine strains and vaccination strategies may need to be further evaluated and optimized to ensure broader protection (34–36). Moreover, exploring the genetic characterization of mumps viruses and gaining insight into the immunogenicity differences between genotypes are essential to guide the design and use of mumps virus vaccines (37, 38).

In this study, six specimens of throat swabs were collected from clinical samples of mumps patients after decontamination and filtration and inoculated with Vero cells, of which one sample (MuV-QBB) was screened. Western blot bands showing NP and HN protein production in MuV-QBB and control S79 group (Figure 1C). Meanwhile, TEM results showed that MuV-QBB virus was a globular structure with a diameter of about 200 nm, a typical mumps virus morphological structure (Figure 1D). The SH gene sequences are usually used as mumps virus genotyping criteria. We analyzed the homology of the SH gene sequences of the MuV-QBB strain with the corresponding sequences of the representative strains of known genotypes, and constructed a gene kinship tree by using the neighbor-joining method, and the results of the

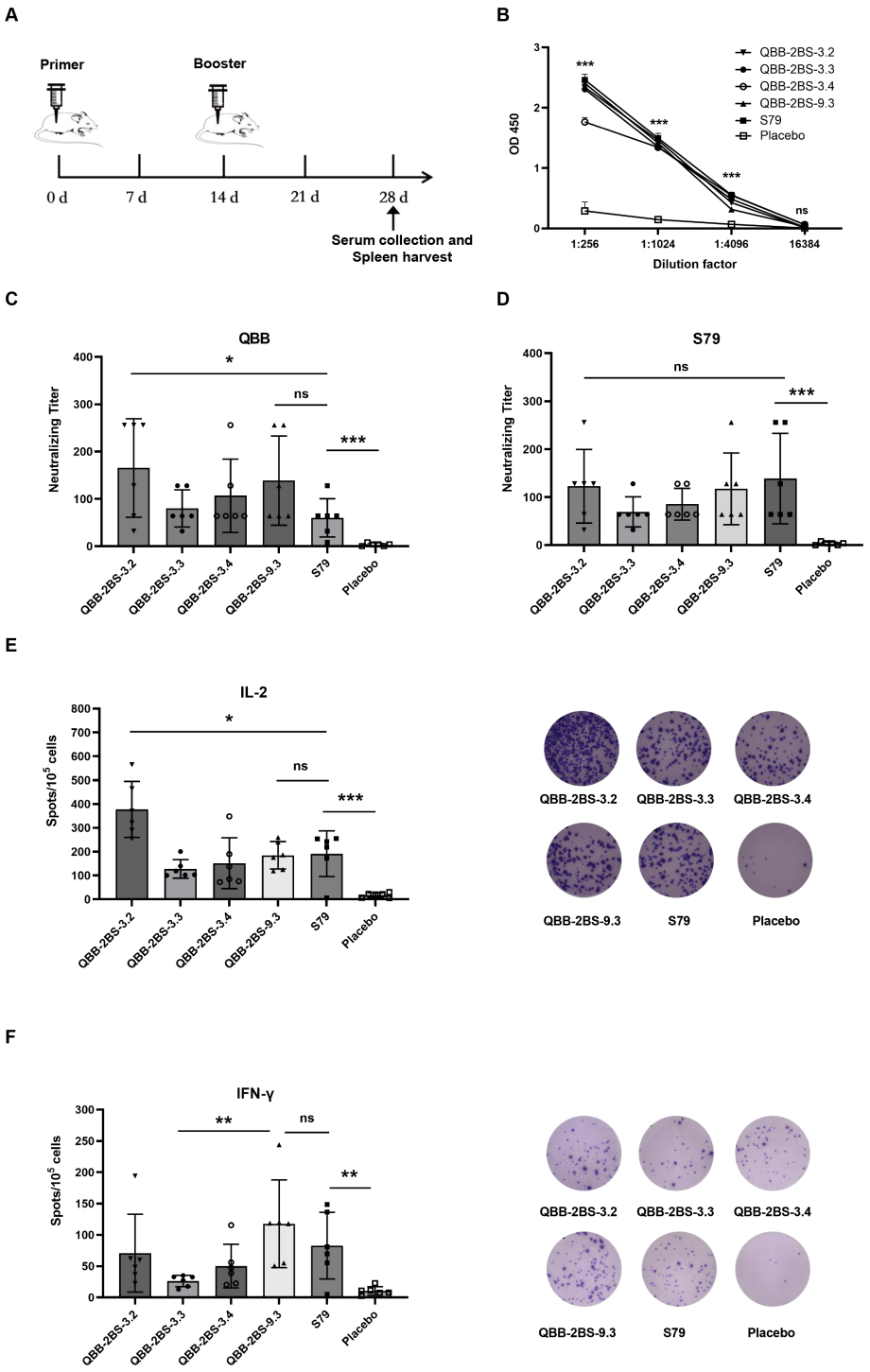

FIGURE 3
Evaluation of immunogenicity of the QBB strain of MuVs in mice. **(A)** Administration schedule of attenuated mumps vaccine candidates. **(B)** Total IgG elicited in BALB/c mice serum among different immune groups measured using ELISA. Results are presented as means ± SD, n = 3. ns; not significant, ***$p < 0.001$ (QBB-2BS-3.2 group compared to Placebo). **(C)** Serum neutralizing antibody titer against MuV-QBB. **(D)** Serum neutralizing antibody titer against S79. IL-2 **(E)** and IFN-γ **(F)** ELISpot analysis was performed and the spots were counted. ns; not significant, *$p < 0.05$, **$p < 0.01$, ***$p < 0.001$.

evolutionary tree analysis showed that the MuV-QBB strain was located on the same branch as Wshl, Wsh2, Wlz1, Wlz2, Wlz3, and SP. Wshl, Wlz1, Wlz2, Wlz3, SP, and other F genotype mumps strains were located in the same branch with high homology (Figure 1E), indicating that the MuV-QBB strain belongs to the F genotype mumps virus.

Cell lines used for vaccine production are increasingly becoming the focus of researchers. The WHO recommends

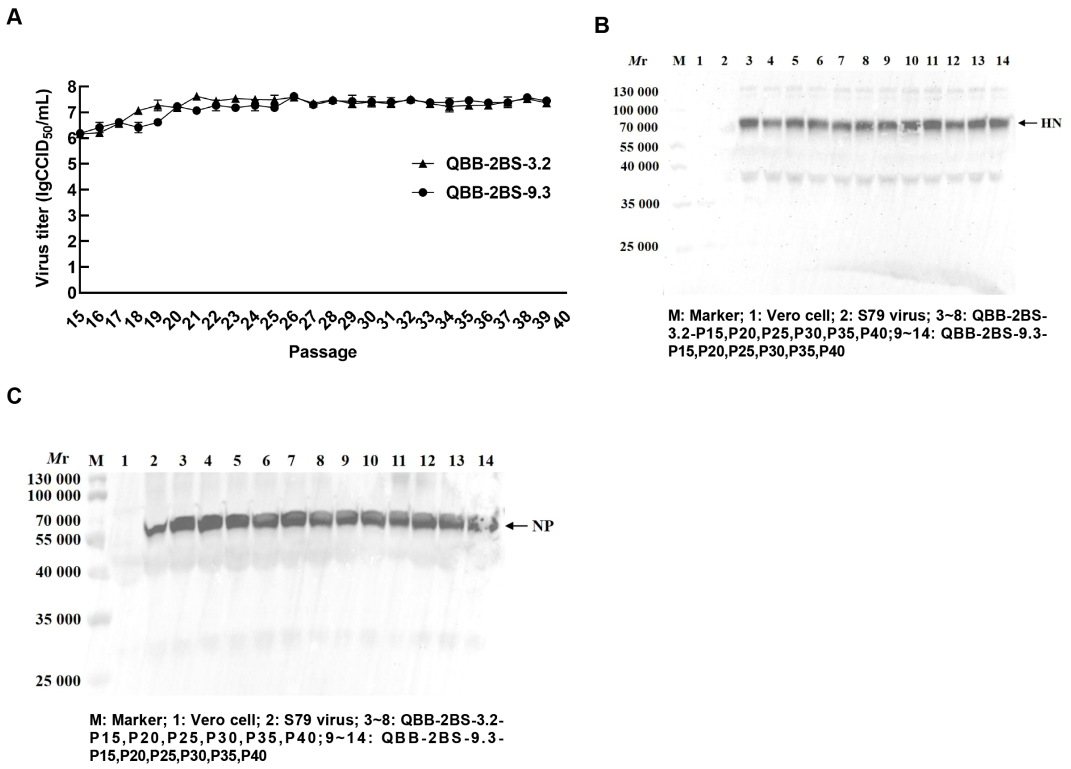

FIGURE 4
Biological characteristics and genetic stability of the QBB strain of MuVs. **(A)** The multiple growth curve of QBB-2BS-3.2 and QBB-2BS-9.3 strains from P15 to P40. Results are presented as means ± SD, n = 3. **(B)** Western blot of HN proteins in different passages of QBB strains. **(C)** Western blot of NP proteins in different passages of QBB strains.

Human diploid cell strains (HDCSs) as the safest cell culture substrate for the production of viral vaccines, and they have become the preferred cell substrate for vaccine production worldwide (39, 40). Mumps live attenuated vaccine is mainly produced using chicken embryo cells as a heterologous cellular lines, which may cause allergic reactions, and chicken embryo cells carrying infectious avian retroviruses may cause side effects. The human embryonic lung diploid cell 2BS strain is derived from healthy human embryonic lung tissue, which has the potential for large-scale culture and has a good safety profile (41). Currently, 2BS cells have been successfully produced in hepatitis A, polio, rubella, and varicella vaccines (42, 43). MuV-QBB virus was inoculated into 2BS cells, and after two rounds of plaque purification, four MuV-QBB adaptor strains were successfully screened. The viral titer was stabilized above 6.0 $lgCCID_{50}$/mL when the strains were passaged to P15 (Figure 2F). Western blot bands showing NP and HN protein production in four MuV-QBB-adapted strains (Figure 2G).

To evaluate the immunogenicity of the QBB candidate strains, BALB/c mice were immunized and tested for humoral and cellular immune responses. ELISA using the MuV-specific serum antibodies

TABLE 1 Comparison of whole genome sequences of different generations of QBB-2BS-3.2 strain.

Gene	Position	S79	QBB-2BS-3.2							Amino acids
			P5	P15	P20	P25	P30	P35	P40	
NP	74	T	T	C	C	C	C	C	C	I-T
M	200	G	G	A	A	A	A	A	A	V-I
F	194	A	A	G	G	G	G	G	G	T-A
	531	T	T	T	T	T	G	G	G	S-R
HN	347	T	T	C	C	C	C	C	C	T-H
	464	A	A	A	A	A	A	G	G	N-S
	526	A	G	A	A	A	A	A	A	K-E-K
L	1561	T	T	T	T	T	C	C	C	I-T

TABLE 2 Comparison of whole genome sequences of different generations of QBB-2BS-9.3 strain.

Gene	Position	S79	QBB-2BS-9.3							Amino acids
			P5	P15	P20	P25	P30	P35	P40	
M	171	G	G	G	G	A	A	A	A	C-Y
	200	G	G	G	G	A	A	A	A	V-I
F	194	A	A	G	G	G	G	G	G	T-A
HN	347	T	T	C	C	C	C	C	C	T-H
	466	A	G	G	G	G	A	A	A	N-S-N
	526	A	G	A	A	A	A	A	A	K-E-K
L	197	A	A	G	G	A	A	A	A	K-E

revealed that the total IgG levels was higher in all immunized groups than in the negative control group, but there was no significant difference among the six experimental groups (Figure 3B). Studies have shown that cross-protection between genotypes is limited. Consistent with reports of genotype-restricted cross-protection, our neutralization assays demonstrated that while QBB-2BS-3.2 induced significantly higher F-genotype-specific neutralizing titers than S79 (Figure 3C), both candidates maintained comparable neutralization against the homologous S79 strain (Figure 3D), mirroring the limited heterotypic immunity observed in Jeryl Lynn derived vaccines. To explore the cellular immune response triggered by the QBB candidate strains, an ELISpot assay was performed to test IFN-γ and IL-2 using immunized BALB/c mice splenocytes stimulated with mixtures of MuVs (44). IFN-γ serves as the central mediator of protective immunity against mumps virus by directly activating the viral clearance capacity of macrophages, enhancing antigen presentation, and inducing antiviral protein expression; whereas IL-2 primarily marks Th1 cell activation and indirectly supports immune responses by promoting T cell expansion (45). The levels of IFN-γ and IL-2 were significantly elevated in experimental groups compared to the placebo group. Moreover, the levels of IL-2 were significantly higher in QBB-2BS-3.2 groups compared to S79 group (Figure 3E), and the levels of IFN-γ were similar in QBB-2BS-9.3 and S79 groups (Figure 3F). Therefore, QBB-2BS-3.2 and QBB-2BS-9.3 were selected for subsequent genetic stability studies.

To investigate the biological characteristics and genetic stability of the 2BS cell-adapted strain of F-genotype mumps virus (MuV). The QBB-2BS-3.2 and QBB-2BS-9.3 strains were adapted to 40 passages in 2BS cells. The titers of the F-genotype 2BS cell-adapted strains QBB-2BS-3.2 and QBB-2BS-9.3 gradually increased from passage 15 to 40, and stabilized at 7.40 lgCCID$_{50}$/mL (Figure 4A). The expression levels of HN and NP proteins remained consistent across passages 15 to 40 for both QBB-2BS-3.2 and QBB-2BS-9.3 strains (Figures 4B, C). Whole-genome sequences showed that eight non-synonymous mutations occurred in QBB-2BS-3.2 and seven non-synonymous mutations occurred in QBB-2BS-3.2 during the passaging, compared with strain QBB-2BS-P5 (Tables 1, 2). It has been reported that the aa464 site of the HN protein was associated with viral neurotoxicity; Cui et al. showed that amino acids located at sites 329-340, 354, and 356 on the HN protein were associated with cross-neutralizing ability (46). Malik et al. confirmed that amino acid changes in the aa466 of the HN protein were associated with alterations in neurotoxicity (47, 48). Previous studies have confirmed that the aa464 (N-K) mutation in the HN protein of the Urabe AM9 vaccine strain enhances neurovirulence, whereas the aa466 (S-N) mutation in the 88–1961 strain reduces neurovirulence (46). Based on these findings, we will employ reverse

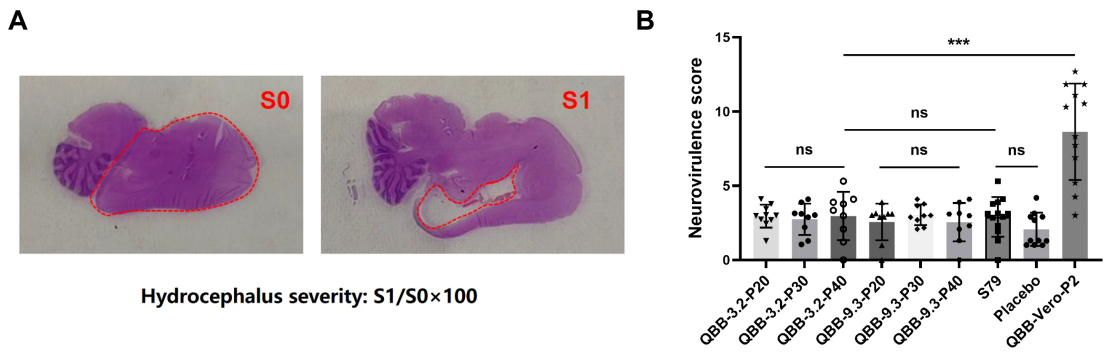

FIGURE 5
Evaluation of mumps virus neurovirulence in neonatal rat model. **(A)** HE staining of brain tissue of Lewis rats. **(B)** Neurovirulence score of rat hydrocephalus inoculated with MuVs candidates. ns; not significant, *$p < 0.05$, **$p < 0.01$, ***$p < 0.001$.

genetics techniques to generate infectious clones harboring these specific mutations and conduct neuroinvasive phenotype analysis in neuronal models. The correlation of amino acid mutations occurring during the transmission of the two candidate strains with the antigenicity and neurotoxicity of MuV remains to be investigated.

Neurotoxicity is one of the important indexes used to evaluate the safety of live attenuated MuV vaccines. Rhesus monkeys are commonly evaluated for MuV live attenuated vaccine neurotoxicity. However, it has been shown that mumps vaccine candidates assessed as safe by monkey neurotoxicity modeling can still cause meningitis and encephalitis in clinical trials (40). Rubin et al. proposed that neuropathology in neonatal rats inoculated with mumps virus could serve as a sensitive indicator of the neurovirulence potential of the human central nervous system, which could differentiate between wild-type (WT) virus strains and vaccine strains (23, 28, 49, 50). Subsequently, an international collaborative study conducted by the U.S. Food and Drug Administration (FDA) and the National Institute for Biological Standards and Control (NIBSC) evaluated the reliability, robustness, and reproducibility of the rat-based neurovirulence test (RNVT) in assessing the neurovirulence potential of MuV in humans (51). In this study, the neurotoxicity of QBB-2BS-3.2 and QBB-2BS-9.3 was evaluated using a neonatal Lewis suckling rat model. Results showed that no significant difference in RNVT score of QBB-2BS-3.2 and QBB-2BS-9.3 adapted strains in all generations compared with the vaccine group S79 or the placebo group (Figure 5B), indicating that the neurotoxicity of QBB-2BS-3.2 and QBB-2BS-9.3 was attenuated and can be used as candidate strains. Notably, the neurovirulence stability observed between p20 and p40, in contrast to the significant attenuation seen between p2 and p20, suggests that genetic adaptations leading to reduced neurovirulence are selected during early serial passaging, eventually reaching a stable plateau. In follow-up studies, we will analyze the whole genome sequencing results of key passaged virus populations to identify mutation sites associated with neurotoxicity attenuation, followed by functional validation using reverse genetics to characterize their specific effects on neurovirulence.

In conclusion, the F genotype mumps QBB strains were successfully isolated from clinical samples, and two MuV 2BS cell-adapted strains were screened by strain inoculation with 2BS cell-adapted cultures and plaque purification. In addition, the candidate strains were tested for genetic stability, immunogenicity, and neurotoxicity. These results provide a basis for the development of a live attenuated F genotype MuV vaccine.

Data availability statement

The datasets presented in this study can be found in online repositories. The names of the repository/repositories and accession number(s) can be found in the article/Supplementary Material.

Ethics statement

The studies involving humans were approved by the Ethics Committee of the China-Japan Union Hospital of Jilin University. The studies were conducted in accordance with the local legislation and institutional requirements. Written informed consent for participation in this study was provided by the participants' legal guardians/next of kin. The animal study was approved by the Animal Ethics Committee of the Changchun Institute of Biological Products. The study was conducted in accordance with the local legislation and institutional requirements. Written informed consent was obtained from the individual(s), and minor (s)' legal guardian/next of kin, for the publication of any potentially identifiable images or data included in this article.

Author contributions

HTL: Conceptualization, Data curation, Formal Analysis, Investigation, Software, Visualization, Writing – original draft, Writing – review & editing. NL: Conceptualization, Data curation, Investigation, Methodology, Supervision, Validation, Writing – review & editing. YS: Conceptualization, Data curation, Methodology, Validation, Writing – review & editing. SL: Methodology, Supervision, Validation, Writing – review & editing. HL: Methodology, Resources, Supervision, Validation, Writing – review & editing. MW: Formal Analysis, Investigation, Methodology, Software, Supervision, Visualization, Writing – original draft. HS: Funding acquisition, Project administration, Resources, Validation, Writing – original draft. YC: Funding acquisition, Investigation, Project administration, Resources, Validation, Writing – review & editing.

Funding

The author(s) declare that financial support was received for the research and/or publication of this article. This research was funded by the Science and Technology Development Project of Jilin Province (grant number 20200404191YY). The study sponsors had no role in the design and conduct of the study; collection, analysis, and interpretation of the data; preparation, review, or approval of the manuscript; or decision to submit the manuscript for publication.

Acknowledgments

We thank Dr. Tie Liu for providing the clinic mumps samples and gratefully appreciate the support from the Center of Laboratory Animal Science, Changchun Institute of Biological Products Co., Ltd., for providing the animal maintenance and testing site, and the experimental operation guidance.

Conflict of interest

Authors HTL, NL, YS, SL, HL, MW, HS, and YC were employed by Changchun Keygen Biological Products Co., Ltd. Author HTL was employed by Changchun Institute of Biological Products Co., Ltd. Authors HTL and YC were employed by China National Biotec Group Company Limited.

Generative AI statement

The author(s) declare that no Generative AI was used in the creation of this manuscript.

Publisher's note

Supplementary material

The Supplementary Material for this article can be found online at: https://www.frontiersin.org/articles/10.3389/fimmu.2025.1629585/full#supplementary-material

References

1. Hviid A, Rubin S, Mühlemann K. Mumps. *Lancet*. (2008) 371:932–44. doi: 10.1016/S0140-6736(08)60419-5

2. Mühlemann K. The molecular epidemiology of mumps virus. *Infect Genet Evol*. (2004) 4:215–9. doi: 10.1016/j.meegid.2004.02.003

3. Rubin S, Eckhaus M, Rennick LJ, Bamford CG, Duprex WP. Molecular biology, pathogenesis and pathology of mumps virus. *J Pathol*. (2015) 235:242–52. doi: 10.1002/path.4445

4. Wu H, Wang F, Tang D, Han D. Mumps orchitis: clinical aspects and mechanisms. *Front Immunol*. (2021) 12:582946. doi: 10.3389/fimmu.2021.582946

5. Deng X, Hu Y, Lu P, Wang Z, Guo H. Genetic characteristic of mumps virus from 2012 to 2016 and its serum antibody level among general healthy population during 2018–2020 in Jiangsu Province, China. *BMC Infect Dis*. (2024) 24:718. doi: 10.1186/s12879-024-09609-1

6. Bryant P, Caldwell H, Lamson DM, Yildirim T, St George K. Streamlined whole-genome sequencing of mumps virus for high-resolution outbreak analysis. *J Clin Microbiol*. (2022) 60:e0084121. doi: 10.1128/JCM.00841-21

7. Cox RM, Plemper RK. Structure and organization of paramyxovirus particles. *Curr Opin Virol*. (2017) 24:105–14. doi: 10.1016/j.coviro.2017.05.004

8. Li M, Schmitt PT, Li Z, McCrory TS, He B, Schmitt AP. Mumps virus matrix, fusion, and nucleocapsid proteins cooperate for efficient production of virus-like particles. *J Virol*. (2009) 83:7261–72. doi: 10.1128/JVI.00421-09

9. Frost JR, Shaikh S, Severini A. Exploring the mumps virus glycoproteins: A review. *Viruses*. (2022) 14:1335. doi: 10.3390/v14061335

10. Cusi MG, Fischer S, Sedlmeier R, Valassina M, Valensin PE, Donati M, et al. Localization of a new neutralizing epitope on the mumps virus hemagglutinin-neuraminidase protein. *Virus Res*. (2001) 74:133–7. doi: 10.1016/s0168-1702(00)00254-9

11. Jin L, Örvell C, Myers R, Rota PA, Nakayama T, Forcic D, et al. Genomic diversity of mumps virus and global distribution of the 12 genotypes. *Rev Med Virol*. (2015) 25:85–101. doi: 10.1002/rmv.1819

12. Di Pietrantonj C, Rivetti A, Marchione P, Debalini MG, Demicheli V. Vaccines for measles, mumps, rubella, and varicella in children. *Cochrane Database Syst Rev*. (2021) 11:Cd004407. doi: 10.1002/14651858.CD004407.pub5

13. Cui A, Zhu Z, Hu Y, Deng X, Sun Z, Zhang Y, et al. Mumps epidemiology and mumps virus genotypes circulating in Mainland China during 2013-2015. *PloS One*. (2017) 12:e0169561. doi: 10.1371/journal.pone.0169561

14. Ma J, Wang P, Tang J, Zheng L, Li S, Huo Y. Epidemiological and phylogenetic analysis of mumps virus isolated from 2016 to 2019 in Henan Province, China. *Jpn J Infect Dis*. (2021) 74:187–92. doi: 10.7883/yoken.JJID.2020.649

15. Wu R, Chen Z, Yang X, Chen Y, Chen D, Zhang H, et al. Investigating the characteristics of mumps outbreaks in Fujian Province, China. *Vaccine*. (2024) 42:126415. doi: 10.1016/j.vaccine.2024.126415

16. Shaikh S, Carpenter M, Lin L, Frost JR, McLachlan E, Stein D, et al. Serologic cross-reactivity between the mumps virus vaccine genotype A strain and the circulating genotype G strain. *Viruses*. (2024) 16:1434. doi: 10.3390/v16091434

17. Kim SY, Won H, Hwang YH, Kim SE, Lee JA, Kim D, et al. Immunogenicity and cross-protection efficacy of a genotype F-derived attenuated virus vaccine candidate against mumps virus in mice. *Vaccines*. (2024) 12:595. doi: 10.3390/vaccines12060595

18. Li D, Zhang H, You N, Chen Z, Yang X, Zhang H, et al. Mumps serological surveillance following 10 years of a one-dose mumps-containing-vaccine policy in Fujian Province, China. *Hum Vaccin Immunother*. (2022) 18:2096375. doi: 10.1080/21645515.2022.2096375

19. Šantak M, Lang-Balija M, Ivancic-Jelecki J, Košutić-Gulija T, Ljubin-Sternak S, Forcic D. Antigenic differences between vaccine and circulating wild-type mumps viruses decreases neutralization capacity of vaccine-induced antibodies. *Epidemiol Infect*. (2013) 141:1298–309. doi: 10.1017/S0950268812001896

20. Bockelman C, Frawley TC, Long B, Koyfman A. Mumps: an emergency medicine-focused update. *J Emerg Med*. (2018) 54:207–14. doi: 10.1016/j.jemermed.2017.08.037

21. Beck M, Welsz-Malecek R, Mesko-Prejac M, Radman V, Juzbasic M, Rajninger-Miholic M, et al. Mumps vaccine L-Zagreb, prepared in chick fibroblasts. I. Production and field trials. *J Biol Stand*. (1989) 17:85–90. doi: 10.1016/0092-1157(89)90031-0

22. Markusic M, Pavlović N, Santak M, Marić G, Kotarski L, Forcic D. Critical factors for the replication of mumps virus in primary chicken embryo fibroblasts defined by the use of design of experiments (DoE). *Appl Microbiol Biotechnol*. (2013) 97:1533–41. doi: 10.1007/s00253-012-4394-4

23. Lang Balija M, Jagušić M, Forčić D, Ivančić-Jelečki J, Košutić Gulija T. Mumps virus neurovirulence assessment-impact of viral doses, animal sex and age on results dispersion. *Vaccine*. (2025) 43:126487. doi: 10.1016/j.vaccine.2024.126487

24. Eseverri JL, Ranea S, Marin A. Adverse reactions to vaccines. *Allergol Immunopathol*. (2003) 31:125–38. doi: 10.1016/s0301-0546(03)79278-7

25. Chua GT, Li PH, Ho MH, Lai E, Ngai V, Yau FY, et al. Hong Kong Institute of Allergy and Hong Kong Society for Paediatric Immunology Allergy & Infectious Diseases joint consensus statement 2018 on vaccination in egg-allergic patients. *Hong Kong Med J*. (2018) 24:527–31. doi: 10.12809/hkmj177137

26. Hussain AI, Johnson JA, Da Silva Freire M, Heneine W. Identification and characterization of avian retroviruses in chicken embryo-derived yellow fever vaccines: investigation of transmission to vaccine recipients. *J Virol*. (2003) 77:1105–11. doi: 10.1128/jvi.77.2.1105-1111.2003

27. Jin L, Rima B, Brown D, Orvell C, Tecle T, Afzal M, et al. Proposal for genetic characterisation of wild-type mumps strains: preliminary standardisation of the nomenclature. *Arch Virol*. (2005) 150:1903–9. doi: 10.1007/s00705-005-0563-4

28. Rubin SA, Afzal MA. Neurovirulence safety testing of mumps vaccines–historical perspective and current status. *Vaccine*. (2011) 29:2850–5. doi: 10.1016/j.vaccine.2011.02.005

29. Qin W, Wang Y, Yang T, Xu XK, Meng XM, Zhao CJ, et al. Outbreak of mumps in a student population with high vaccination coverage in China: time for two-dose vaccination. *Hum Vaccin Immunother*. (2019) 15:2106–11. doi: 10.1080/21645515.2019.1581526

30. Ma C, Liu Y, Tang J, Jia H, Qin W, Su Y, et al. Assessment of mumps-containing vaccine effectiveness during an outbreak: Importance to introduce the 2-dose schedule for China. *Hum Vaccin Immunother*. (2018) 14:1392–7. doi: 10.1080/21645515.2018.1428508

31. Li M, Wang Z, Liu Z, Deng X, Wang L, Zhu Y, et al. Understanding mumps dynamics: epidemiological traits and breakthrough infections in the population under 15 years of age in Jiangsu Province, China, 2023. *Vaccines*. (2024) 12:986. doi: 10.3390/vaccines12090986

32. Connell AR, Connell J, Leahy TR, Hassan J. Mumps outbreaks in vaccinated populations-is it time to re-assess the clinical efficacy of vaccines? *Front Immunol*. (2020) 11:2089. doi: 10.3389/fimmu.2020.02089

33. Liu Y, Cai X, Yang D, Xiang Y, Wang Q, Yao N, et al. Epidemiological characteristics of breakthrough mumps infection cases from 2019 to 2023 in Chongqing, China. *Hum Vaccin Immunother*. (2024) 20:2426273. doi: 10.1080/21645515.2024.2426273

34. Gong X, Fang Q, Zheng W, Lai S, Xu W, Yin Z. Epidemiological characteristics and serological survey of mumps 15 years after MMR vaccine was included in the immunization program. *J Med Virol*. (2024) 96:e29856. doi: 10.1002/jmv.29856

35. Gao BG, Huang LF, Xie P. Effectiveness and safety of a mumps containing vaccine in preventing laboratory-confirmed mumps cases from 2002 to 2017: A meta-analysis. *Open Life Sci*. (2024) 19:20220820. doi: 10.1515/biol-2022-0820

36. Principi N, Esposito S. Mumps outbreaks: A problem in need of solutions. *J Infect*. (2018) 76:503–6. doi: 10.1016/j.jinf.2018.03.002

37. Almansour I. Mumps vaccines: current challenges and future prospects. *Front Microbiol*. (2020) 11:1999. doi: 10.3389/fmicb.2020.01999

38. Kauffmann F, Heffernan C, Meurice F, Ota MOC, Vetter V, Casabona G. Measles, mumps, rubella prevention: how can we do better? *Expert Rev Vaccines*. (2021) 20:811–26. doi: 10.1080/14760584.2021.1927722

39. Ma B, He L-F, Zhang Y-L, Chen M, Wang L-L, Yang H-W, et al. Characteristics and viral propagation properties of a new human diploid cell line, walvax-2, and its suitability as a candidate cell substrate for vaccine production. *Hum Vaccin Immunother*. (2015) 11:998–1009. doi: 10.1080/21645515.2015.1009811

40. Xu Y, Weng L, Wang X, Li M, Guo W, Liu Y, et al. Application prospects of the 2BS cell-adapted China fixed rabies virus vaccine strain 2aG4-B40. *Virol J*. (2024) 21:154. doi: 10.1186/s12985-024-02416-9

41. Barrett PN, Mundt W, Kistner O, Howard MK. Vero cell platform in vaccine production: moving towards cell culture-based viral vaccines. *Expert Rev Vaccines*. (2009) 8:607–18. doi: 10.1586/erv.09.19

42. Ma B, He LF, Zhang YL, Chen M, Wang LL, Yang HW, et al. Characteristics and viral propagation properties of a new human diploid cell line, Walvax-2, and its suitability as a candidate cell substrate for vaccine production. *Hum Vaccin Immunother*. (2015) 11:998–1009. doi: 10.1080/21645515.2015.1009811

43. Zhang W, Kong Y, Jiang Z, Li C, Wang L, Xia J. Comprehensive safety assessment of a human inactivated diploid enterovirus 71 vaccine based on a phase III clinical trial. *Hum Vaccin Immunother*. (2016) 12:922–30. doi: 10.1080/21645515.2015.1115934

44. Ovsyannikova IG, Haralambieva IH, Schaid DJ, Warner ND, Poland GA, Kennedy RB. Genome-wide determinants of cellular immune responses to mumps vaccine. *Vaccine*. (2023) 41:6579–88. doi: 10.1016/j.vaccine.2023.09.001

45. Ichiyama T, Maeba S, Suenaga N, Saito K, Matsubara T, Furukawa S. Analysis of cytokine levels in cerebrospinal fluid in mumps meningitis: comparison with echovirus type 30 meningitis. *Cytokine*. (2005) 30:243–7. doi: 10.1016/j.cyto.2005.01.022

46. Cui A, Brown DW, Xu W, Jin L. Genetic variation in the HN and SH genes of mumps viruses: a comparison of strains from mumps cases with and without neurological symptoms. *PloS One*. (2013) 8:e61791. doi: 10.1371/journal.pone.0061791

47. Tecle T, Mickiené A, Johansson B, Lindquist L, Orvell C. Molecular characterisation of two mumps virus genotypes circulating during an epidemic in Lithuania from 1998 to 2000. *Arch Virol*. (2002) 147:243–53. doi: 10.1007/s705-002-8317-y

48. Malik TH, Wolbert C, Nerret L, Sauder C, Rubin S. Single amino acid changes in the mumps virus haemagglutinin-neuraminidase and polymerase proteins are associated with neuroattenuation. *J Gen Virol*. (2009) 90:1741–7. doi: 10.1099/vir.0.009449-0

49. Rubin SA, Pletnikov M, Taffs R, Snoy PJ, Kobasa D, Brown EG, et al. Evaluation of a neonatal rat model for prediction of mumps virus neurovirulence in humans. *J Virol*. (2000) 74:5382–4. doi: 10.1128/jvi.74.11.5382-5384.2000

50. Rubin SA, Pletnikov M, Carbone KM. Comparison of the neurovirulence of a vaccine and a wild-type mumps virus strain in the developing rat brain. *J Virol*. (1998) 72:8037–42. doi: 10.1128/JVI.72.10.8037-8042.1998

51. Rubin SA, Afzal MA, Powell CL, Bentley ML, Auda GR, Taffs RE, et al. The rat-based neurovirulence safety test for the assessment of mumps virus neurovirulence in humans: an international collaborative study. *J Infect Dis*. (2005) 191:1123–8. doi: 10.1086/428098

frontiers | Frontiers in Immunology

TYPE Brief Research Report
PUBLISHED 28 July 2025
DOI 10.3389/fimmu.2025.1612205

OPEN ACCESS

EDITED BY
Sonia Jangra,
The Rockefeller University, United States

REVIEWED BY
Robet L. Drury,
ReThink Health, United States
Zhongshan Cheng,
St. Jude Children's Research Hospital, United States

*CORRESPONDENCE
Ren-He Xu
renhexu@um.edu.mo
Xiao Zhan Zhang
zxiao801@gmail.com
Chon Lok Lei
chonloklei@um.edu.mo

†These authors have contributed equally to this work

RECEIVED 15 April 2025
ACCEPTED 03 July 2025
PUBLISHED 28 July 2025

CITATION
Yuan Z, Wong IF, Xu R-H, Zhang XZ and Lei CL (2025) Hypertension attenuates COVID-19 vaccine protection in elderly patients: a retrospective cohort study. *Front. Immunol.* 16:1612205. doi: 10.3389/fimmu.2025.1612205

Hypertension attenuates COVID-19 vaccine protection in elderly patients: a retrospective cohort study

Zhen Yuan[1†], Iong Fong Wong[2†], Ren-He Xu[1*], Xiao Zhan Zhang[2*] and Chon Lok Lei[1*]

[1]Faculty of Health Sciences, University of Macau, Macao, Macao SAR, China, [2]Pneumology Department, Kiang Wu Hospital, Macao, Macao SAR, China

The COVID-19 pandemic has severely impacted elderly populations, particularly those with comorbidities. This study evaluated the effects of COVID-19 vaccination on 193 hospitalized elderly patients (≥ 60 years) in Macao. Vaccination was suggestively associated with a 2.3-fold higher likelihood of prognostic improvement (adjusted OR = 2.3, 95% CI: 0.980-5.940, P = 0.065), while hypertension significantly reduced the improvement rate by 67.5% (P = 0.039). Vaccinated patients also exhibited lower Modified Early Warning Scores and reduced mortality. These findings underscore the protective role of vaccination in improving prognosis among high-risk elderly patients and highlight the need for tailored strategies for those with comorbidities.

KEYWORDS

COVID-19, vaccination, prognosis, elderly patients, comorbidities

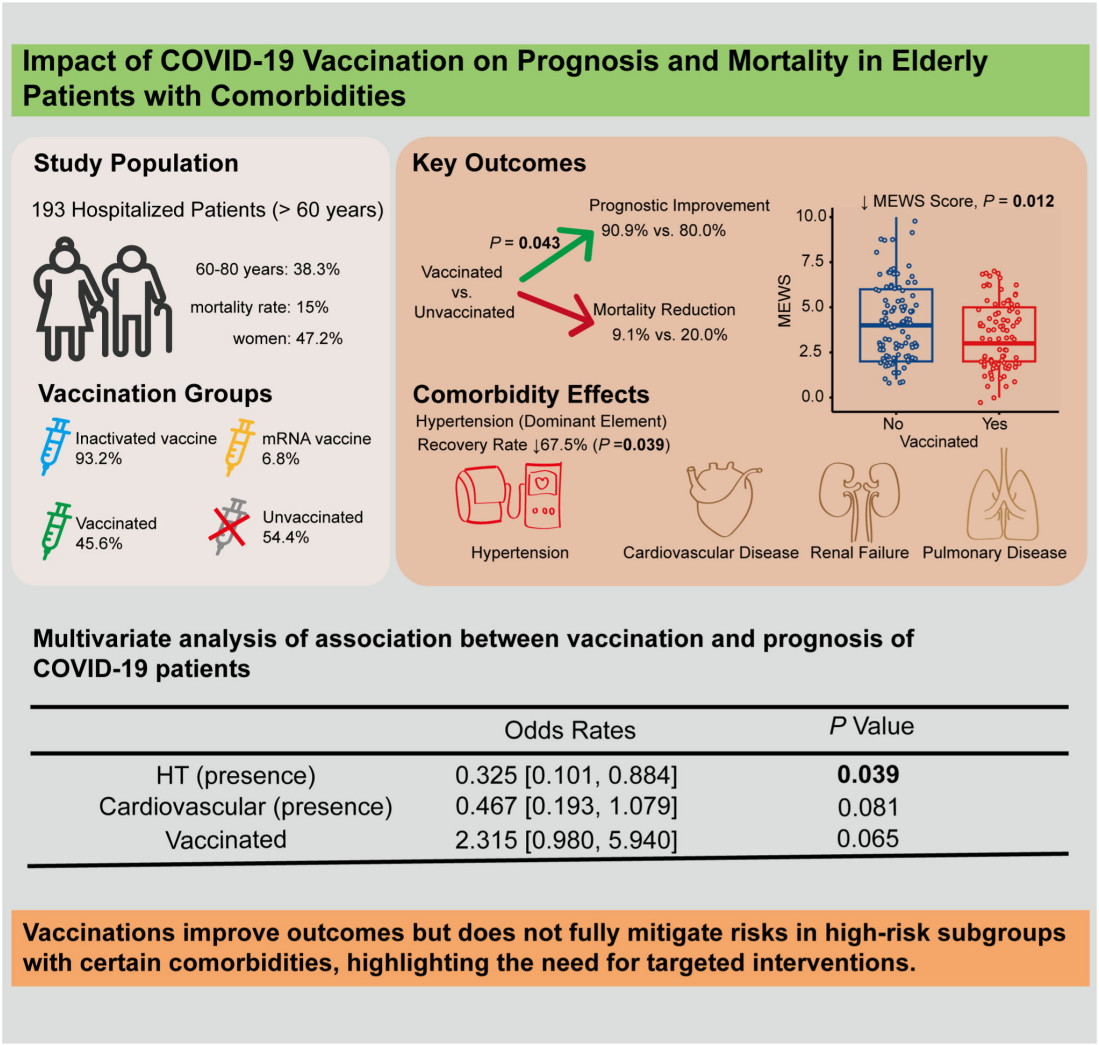

GRAPHICAL ABSTRACT

Introduction

The COVID-19 can affect individuals of all ages, especially those with weakened immune systems and comorbidities, increasing the risk of severe disease and mortality. Since the introduction of COVID-19 vaccines, vaccination has been shown to significantly reduce rates of infection, severe disease, and mortality (1).

Different types of vaccines, such as mRNA vaccines (Pfizer-BioNTech) and inactivated vaccines (Sinovac, Sinopharm) (2), have varying immunogenicity and efficacy, especially in older adults (3). Individuals aged 65 and older, as well as those with at least one underlying medical condition, remain at elevated risk for severe outcomes from COVID-19 even after completing primary vaccination (4). This study evaluates the clinical impact of vaccination on elderly hospitalized patients with comorbidities, focusing on prognosis improvement and mortality reduction to inform public health strategies.

Method

Study population

This retrospective study included patients aged 60 years and older who were hospitalized at Kiang Wu hospital in Macao between December 15, 2022, and March 15, 2023.

Inclusion criteria

(1) Residents of Macao who were aged 60 years or older. (2) Laboratory-confirmed COVID-19, defined as either a positive result from a nasopharyngeal swab rapid antigen test or a nucleic acid test with a cycle threshold value of less than 39. (3) Presence or absence of fever, respiratory symptoms, gastrointestinal symptoms, or other clinical manifestations of COVID-19.

Exclusion criteria

(1) Incomplete clinical data. (2) Hospitalization for less than 24 hours.

Diagnostic and treatment protocols

The diagnosis, severity classification, and treatment protocols followed the guidelines outlined in the Ninth Edition of the Chinese Medical Association COVID-19 Diagnosis and Treatment Protocol. Serum antibody for SARS-CoV-2 S (spike, RBD) was quantified using the Elecsys® Anti-SARS-CoV-2 S kit (Roche) via electrochemiluminescence immunoassay, following the manufacturer's instructions. Results were reported in U/mL, with< 0.80 U/mL considered negative and ≥ 0.80 U/mL positive.

Statistical analysis

The study population was stratified by age (60–80 years and >80 years) and vaccination status (unvaccinated or vaccinated). Patients with mixed vaccination types were excluded to minimize confounding. Vaccine type (e.g., mRNA, inactivated), dose count (1, 2, 3, 4), and concentrations of anti-S protein antibodies categorized into three levels (<0.8, 0.8–25000, >25000). The underlying medical conditions include hypertension (HT), diabetes mellitus (DM), tumors, renal failure, cardiovascular disease, and pulmonary disease. Prognosis categorized as either "improvement" or "mortality" alongside Modified Early Warning Score (MEWS) and chest X-ray (CXR) scores on hospital admission.

For the baseline analysis, categorical variables were described as counts and percentages. Fisher's Exact Test was used to calculate the *P*-value for each dichotomous variable. To enhance the reliability of the results, we further employed binomial logistic regression to adjust for confounders Equations 1, 2:

$$Y \sim B(m, p) \tag{1}$$

$$g(p) = \beta_0 + \beta_1 x_1 + \ \ldots + \beta_k x_k \tag{2}$$

$$logit(p) = In\left(\frac{p}{1-p}\right) \tag{3}$$

where m is the total patients, B is the binomial distribution, Y is the number of patients with improved prognosis or anti-S antibody levels out of m patients, $g(p)$ is improvement prognostic status, and p is the probability of patients with improved prognosis under the given conditions of $x_1,\ldots,x_k$, where x_i are different dichotomous variables: gender, age, vaccinated or not, cardiovascular disease, renal failure, HT, DM, tumor, other disease, and pulmonary disease, with k = 10. Some dichotomous variables (in the data) were not included in the construction of the model due to the assumption of independence of variables, e.g., the number of doses and "whether or not vaccinated" are related to the type of vaccine and the concentrations of anti-S protein antibodies. Using Equations 3 to perform a confounding factor analysis, $p/(1 - p)$ is the ratio of the probability of success to the probability of failure and is called the OR. We then chose the final independent variable (HT, DM and type of vaccine) by the Akaike information criterion (AIC) in a stepwise algorithm (the direction is both ways), and the maximum likelihood estimate is used to calculate the *P*-value.

We conducted a generalized linear model analysis using a Poisson distribution to evaluate CXR scores and MEWS, respectively.

$$Y \sim Poisson(\lambda)$$

$$g(\lambda) = \beta_0 + \beta_1 x_1 + \ \ldots \ + \beta_n x_n$$

Where Y is the CXR or MEWS, where x_i are different dichotomous variables: gender, age, vaccinated or not, cardiovascular disease, renal failure, HT, DM, tumor, other disease, and pulmonary disease, with n = 10. The subsequent steps are similar to prognostic analysis. All analyses were performed in R (version 4.4.1), and a *P*-value of< 0.05 was considered statistically significant.

Results

A total of 193 hospitalized COVID-19 elderly patients in Macao were included in this study (Tables 1, 2), comprising 91 women (47.2%). The median age was 83 years, with 119 patients (61.7%) aged > 80 years and 74 patients (38.3%) aged between 60 and 80 years. The overall mortality rate in this cohort was 15% (29/193). Among the participants, 45.6% (88/193) were vaccinated, including 82 patients (93.2%) who received inactivated vaccines and 6 patients (6.8%) who received mRNA vaccines. Vaccinated patients had a markedly lower mortality rate (9.1%, 8/88) compared to unvaccinated patients (20.0%, 21/105). Comorbidities were prevalent (Table 2): hypertension (65.3%, 126/193), cardiovascular disease (48.7%, 94/193), diabetes mellitus (34.2%, 66/193), renal failure (20.7%, 40/193), pulmonary disease (17.6%, 34/193), and tumors (16.1%, 31/193).

Vaccinated patients had significantly better prognostic outcomes compared to unvaccinated patients. Among the vaccinated group, 90.9% (80/88) showed improvement, compared to 80.0% (84/105) in the unvaccinated group (P = 0.043) (Table 1). Multivariate logistic regression analysis indicated that vaccination was suggestively associated with a 2.3-fold improvement in prognosis (95% CI: 0.980–5.940, P = 0.065) (graphical abstract table), whereas hypertensive patients were 67.5% less likely to improve than non-hypertensive patients (OR = 0.325, 95% CI: 0.101–0.884, P = 0.039) (Table 3).

Severe COVID-19 symptoms are correlated with higher adjusted Modified Early Warning Scores (MEWS) (5). The chest X-ray (CXR) scoring system has since been applied to quantify pulmonary damage in COVID-19 patient (6). Through multivariate

10.3389/fimmu.2025.1612205

TABLE 1 Baseline characteristics.

Subgroup	Mortality N=29	Improvement N=164	*P* value
Gender			0.549
Female	12 (41.4%)	79 (48.2%)	
Male	17 (58.6%)	85 (51.8%)	
Age			0.415
>80	20 (69.0%)	99 (60.4%)	
60-80	9 (31.0%)	65 (39.6%)	
Vaccine			0.043*
No	21 (72.4%)	84 (51.2%)	
Yes	8 (27.6%)	80 (48.8%)	
Vaccine type			0.067
inactivated	7 (24.1%)	75 (45.7%)	
mRNA	1 (3.4%)	5 (3.0%)	
none	21 (72.4%)	84 (51.2%)	
Concentrations of anti-S protein antibodies			0.276
>25000	1 (3.4%)	20 (12.2%)	
0.8-25000	19 (65.5%)	107 (65.2%)	
<0.8	9 (31.0%)	37 (22.6%)	
Number of doses			0.030*
0	21 (72.4%)	84 (51.2%)	
1	0 (0.00%)	28 (17.1%)	
2	4 (13.8%)	22 (13.4%)	
3	3 (10.3%)	28 (17.1%)	
4	1 (3.4%)	2 (1.2%)	

P-value is based on Fisher's Exact Test. *$P< 0.05$

TABLE 2 Baseline characteristics with underlying medical conditions.

Subgroup	Mortality N=29	Improvement N=164	*P* value
Pulmonary disease			0.604
No	23 (79.3%)	136 (82.9%)	
Yes	6 (20.7%)	28 (17.1%)	
Cardiovascular			0.069
No	10 (34.5%)	89 (54.3%)	
Yes	19 (65.5%)	75 (45.7%)	
Renal failure			1.000
No	23 (79.3%)	130 (79.3%)	
Yes	6 (20.7%)	34 (20.7%)	
Tumor			0.424
No	23 (79.3%)	139 (84.8%)	
Yes	6 (20.7%)	25 (15.2%)	
DM			0.833
No	20 (69.0%)	107 (65.2%)	
Yes	9 (31.0%)	57 (34.8%)	
Other disease			0.774
No	15 (51.7%)	75 (45.7%)	
Yes	14 (48.3%)	87 (53.0%)	
Unknown	0 (0%)	2 (1.3%)	
HT			0.035*
No	5 (17.2%)	62 (37.8%)	
Yes	24 (82.8%)	102 (62.2%)	

P-value is based on Fisher's Exact Test. *$P< 0.05$

logistic regression, vaccinated patients had significantly lower MEWS compared to unvaccinated patients (Adjusted Rate = 0.828, 95% CI: 0.715–0.958, $P = 0.012$). However, no significant difference was observed in CXR scores between the two groups (Table 4). Patients with renal failure and pulmonary disease exhibited significantly higher CXR scores (+17.6% and +16.8%, respectively; both $P< 0.01$), but no significant difference in mortality was observed.

Additionally, vaccinated patients had significantly higher concentrations of anti-S protein antibodies, which were associated with reduced mortality rates (Figure 1). We then analyzed the relationship between anti-S antibody levels and clinical outcomes. While anti-S antibody levels were not directly associated with prognosis, patients with antibody concentrations > 25,000 exhibited significantly lower MEWS scores (71.4%, $P = 0.025$) compared to those with lower antibody levels.

Discussion

This study demonstrates that COVID-19 vaccination, particularly with inactivated vaccines, significantly improves prognosis and reduces mortality in elderly hospitalized patients with comorbidities. Vaccinated patients exhibited a suggestive trend toward improved prognosis, with an adjusted odds ratio of 2.3 and significantly lower MEWS scores. However, comorbidities such as hypertension remained a critical risk factor, reducing the likelihood of recovery by 67.5%. These findings align with previous research (7) highlighting the protective effects of vaccination in high-risk populations while providing novel insights into its specific impact on clinical scores and mortality in elderly patients with multiple comorbidities.

Despite the well-documented protective effects of vaccination, our study highlights persistent challenges associated with comorbidities. Pulmonary disease and renal failure are correlated

TABLE 3 Multivariate logistic regression for prognostic improvement.

Subgroup	Rate	*P* value
Age 60-80	1.136 [0.462,2.944]	0.785
Vaccine (yes)	2.3 [0.980,5.940]	0.065
HT (presence)	0.325 [0.101,0.884]	0.039*

P-value is based on Wald Test. *, $P < 0.05$. Values in parentheses indicate 95% confidence intervals.

TABLE 4 Confounding factor analysis for CXR scores.

Subgroup	Rate	*P* value
Age 60-80	1.156 [1.066,1.254]	< 0.001***
Cardiovascular (presence)	0.927 [0.854,1.006]	0.071
Pulmonary Disease (presence)	1.168 [1.055,1.291]	0.0026**
Renal Failure (presence)	1.176 [1.069,1.292]	< 0.001***
Tumor (presence)	0.837 [0.743,0.941]	0.0032**
DM (presence)	1.097 [1.007,1.195]	0.034*

P-value is based on Wald Test. *$P< 0.05$; **$P< 0.01$; ***$P< 0.001$. Values in parentheses indicate 95% confidence intervals.

with worse clinical outcomes and are critical considerations in clinical decision-making. Notably, while vaccinated patients exhibited higher anti-S antibody levels, these levels were not directly correlated with prognosis, suggesting that antibody titers alone may not fully predict clinical outcomes. Instead, neutralizing antibodies play a more direct role in viral clearance and the Sinopharm vaccine, an inactivated whole-virus vaccine, induced a broader antigenic response and higher neutralizing antibody titers than mRNA vaccines, potentially contributing to the lower mortality observed in vaccinated patients (8, 9).

The study's retrospective design and limited sample size from a single center limit the generalizability of the findings. Future research should involve larger, multi-center cohorts to validate these associations and explore additional risk factors. Additionally, investigating the synergistic effects of vaccination and adjunctive therapies may further optimize treatment strategies for elderly patients with multiple comorbidities.

Our findings align with prior research (10) demonstrating the protective role of COVID-19 vaccines in elderly populations but offer new perspectives by incorporating detailed clinical severity assessments, where we further evaluated MEWS and CXR scores, providing a more granular assessment of disease severity. Vaccination improves outcomes but does not fully mitigate risks in high-risk subgroups with certain comorbidities, highlighting the need for targeted interventions.

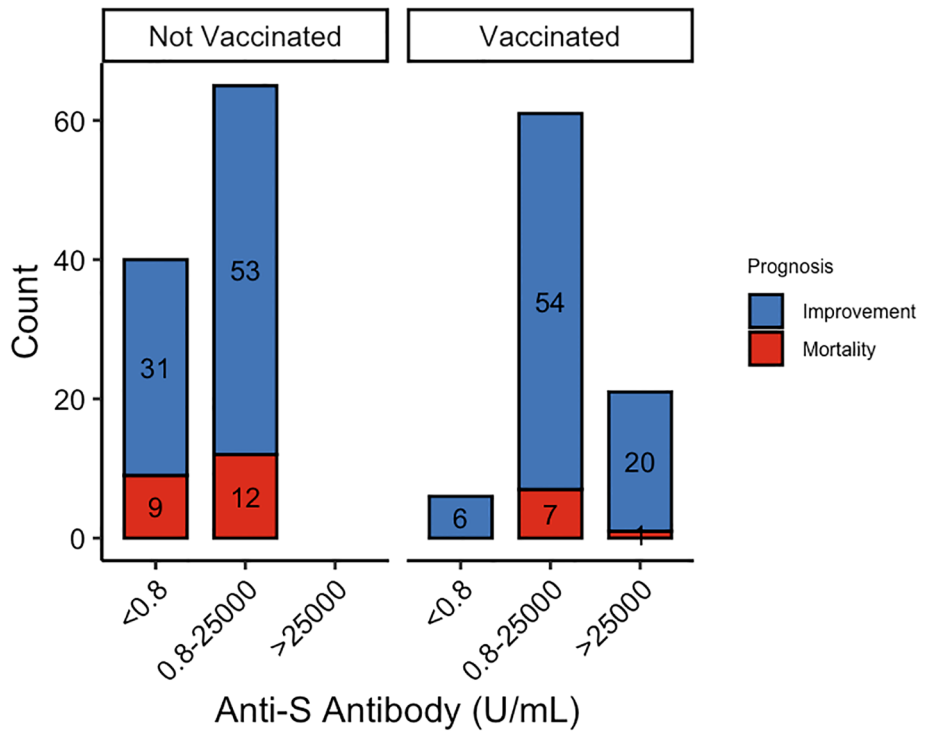

FIGURE 1
The number of patients with different immunity strength with or without vaccination.

Data availability statement

The original contributions presented in the study are included in the article/supplementary material. Further inquiries can be directed to the corresponding authors.

Ethics statement

This study was approved by the Ethics Committee of Kiang Wu Hospital (Approval ID: KWH 2024-020). All patient data were anonymized and securely stored to ensure confidentiality. The studies were conducted in accordance with the local legislation and institutional requirements. The participants provided their written informed consent to participate in this study. The animal study was approved by Ethics Committee of Kiang Wu Hospital. The study was conducted in accordance with the local legislation and institutional requirements. Written informed consent was obtained from the individual(s) for the publication of any potentially identifiable images or data included in this article.

Author contributions

ZY: Writing – original draft, Visualization, Formal Analysis. IFW: Writing – review & editing, Resources, Data curation, Investigation. R-HX: Supervision, Writing – review & editing, Conceptualization. XZZ: Writing – review & editing, Supervision, Investigation, Data curation, Resources, Conceptualization. CLL: Visualization, Conceptualization, Supervision, Formal Analysis, Writing – review & editing.

Funding

The author(s) declare that financial support was received for the research and/or publication of this article. C.L.L. acknowledges funding and support from the University of Macau (SRG2024-00014-FHS; UMDF-TISF/2025/005/FHS; MYRG-CRG2024-00046-FHS; and FHS Startup Grant), and from the Science and Technology Development Fund, Macao SAR (FDCT) under grant number 0155/2023/RIA3.

Conflict of interest

The authors declare that the research was conducted in the absence of any commercial or financial relationships that could be construed as a potential conflict of interest.

Generative AI statement

The author(s) declare that no Generative AI was used in the creation of this manuscript.

Publisher's note

All claims expressed in this article are solely those of the authors and do not necessarily represent those of their affiliated organizations, or those of the publisher, the editors and the reviewers. Any product that may be evaluated in this article, or claim that may be made by its manufacturer, is not guaranteed or endorsed by the publisher.

References

1. Whittaker R, Bråthen Kristofferson A, Valcarcel Salamanca B, Seppälä E, Golestani K, Kvåle R, et al. Length of Hospital Stay and Risk of Intensive Care Admission and in-Hospital Death among Covid-19 Patients in Norway: A Register-Based Cohort Study Comparing Patients Fully Vaccinated with an Mrna Vaccine to Unvaccinated Patients. *Clin Microbiol Infection*. (2022) 28:871–8. doi: 10.1016/j.cmi.2022.01.033

2. Baden LR, El Sahly HM, Essink B, Kotloff K, Frey S, Novak R, et al. Efficacy and safety of the mrna-1273 sars-cov-2 vaccine. *New Engl J Med*. (2021) 384:403–16. doi: 10.1056/nejmoa2035389

3. Haas EJ, Angulo FJ, McLaughlin JM, Anis E, Singer SR, Khan F, et al. Impact and effectiveness of mrna bnt162b2 vaccine against sars-cov-2 infections and covid-19 cases, hospitalisations, and deaths following a nationwide vaccination campaign in Israel: an observational study using national surveillance data. *Lancet*. (2021) 397:1819–29. doi: 10.1016/s0140-6736(21)00947-8

4. Yek C. Risk factors for severe covid-19 outcomes among persons aged≥ 18 years who completed a primary covid-19 vaccination series—465 health care facilities, United States, december 2020–october 2021. In: *MMWR Morbidity and mortality weekly report*, Atlanta, Georgia, USA: U.S. Centers for Disease Control and Prevention (CDC) vol. 71. (2022). Available online at: https://www.cdc.gov/mmwr/volumes/71/wr/mm7101a4.htm?s_cid=mm7101a4_w.

5. Al-Salman J, Alsabea ASS, Alkhawaja S, Al Balooshi AM, Alalawi M, Ebrahim BA, et al. Evaluation of an adjusted mews (Modified early warning score) for covid-19 patients to identify risk of icu admission or death in the kingdom of Bahrain. *J Infection Public Health*. (2023) 16:1773–7. doi: 10.1016/j.jiph.2023.09.002

6. Bernheim A, Mei X, Huang M, Yang Y, Fayad ZA, Zhang N, et al. Chest ct findings in coronavirus disease-19 (Covid-19): relationship to duration of infection. *Radiology*. (2020) 295:685–91. doi: 10.1148/radiol.2020200463

7. Pranata R, Lim MA, Huang I, Raharjo SB, Lukito AA. Hypertension is associated with increased mortality and severity of disease in covid-19 pneumonia: A systematic review, meta-analysis and meta-regression. *J renin-angiotensin-aldosterone system: JRAAS*. (2020) 21. doi: 10.1177/1470320320926899

8. Lei CL, Ng HM, Qin G, Yeung CK, Lei CL, Xu R-H. What we learned from lifting covid-19 restrictions in macao in december 2022. *Int J Biol Sci*. (2023) 19:5337–9. doi: 10.7150/ijbs.86875

9. Ng HM, Lei CL, Fu S, Li E, Leong SI, Nip CI, et al. Heterologous vaccination with inactivated vaccine and mrna vaccine augments antibodies against both spike and nucleocapsid proteins of sars-cov-2: A local study in macao. *Front Immunol*. (2023) 14:1131985. doi: 10.3389/fimmu.2023.1131985

10. McMenamin ME, Nealon J, Lin Y, Wong JY, Cheung JK, Lau EHY, et al. Vaccine effectiveness of one, two, and three doses of bnt162b2 and coronavac against covid-19 in hong kong: A population-based observational study. *Lancet Infect Dis*. (2022) 22:1435–43. doi: 10.1016/S1473-3099(22)00345-0

frontiers | Frontiers in Immunology

TYPE Original Research
PUBLISHED 04 August 2025
DOI 10.3389/fimmu.2025.1603612

OPEN ACCESS

EDITED BY
Sonia Jangra,
The Rockefeller University, United States

REVIEWED BY
Guilherme Campos,
Faculdade de Medicina de São José do Rio Preto, Brazil
Annapina Palmieri,
National Institute of Health (ISS), Italy
Ramu Subbramanian,
Cellular Technology Limited (CTL), United States

*CORRESPONDENCE
Ada M. B. Alves
ada@ioc.fiocruz.br

†These authors have contributed equally to this work and share first authorship

RECEIVED 31 March 2025
ACCEPTED 11 July 2025
PUBLISHED 04 August 2025

CITATION
Caetano BLL, Pinto PBA, Pacheco AR, Lage AR, Pereira ASG, Nascimento AVP, Machado TR, Paulino A, Medeiros TL, Fernandes-Siqueira LO, Da Poian AT, Horbach IS, Azevedo AS, Costa SM and Alves AMB (2025) Neutralizing antibody response to different COVID-19 vaccines in Brazil: the impact of previous infection and booster doses. *Front. Immunol.* 16:1603612. doi: 10.3389/fimmu.2025.1603612

Neutralizing antibody response to different COVID-19 vaccines in Brazil: the impact of previous infection and booster doses

Beatriz L. L. Caetano[1†], Paolla B. A. Pinto[1†], Agatha R. Pacheco[1], Agnes R. Lage[1], Aline S. G. Pereira[1], Amanda V. P. Nascimento[1], Thiago R. Machado[1], Anderson Paulino[1], Thiago L. Medeiros[1], Lorena O. Fernandes-Siqueira[2], Andrea T. Da Poian[2], Ingrid S. Horbach[3], Adriana S. Azevedo[3], Simone M. Costa[1] and Ada M. B. Alves[1*]

[1]Laboatório de Biotecnologia e Fisiologia de Infecções Virais, Instituto Oswaldo Cruz, Fundação Oswaldo Cruz, Rio de Janeiro, RJ, Brazil, [2]Instituto de Bioquímica Médica Leopoldo de Meis, Universidade Federal do Rio de Janeiro, Rio de Janeiro, RJ, Brazil, [3]Laboratório de Análise Imunomolecular, Instituto de Tecnologia em Imunobiológicos, Bio-Maguinhos, Fundação Oswaldo Cruz, Rio de Janeiro, RJ, Brazil

Introduction: In Brazil, three COVID-19 vaccines were among the first widely used (CoronaVac, ChAdOx1, and BNT162b2), which aimed to induce neutralizing antibodies (NAbs) against the original SARS-CoV-2 strain. Although effective against severe disease, they showed waning NAb levels and reduced efficacy against variants, prompting booster doses. Thus, it is important to investigate and compare the response induced by these vaccines and boosters.

Methods: In this study, we compare the magnitude, durability, and cross-reactivity of NAbs among vaccinated volunteers in Brazil using an enzyme-linked immunosorbent assay (ELISA)-based assay that measures Abs capable of blocking the interaction between the receptor binding domain (RBD) and human angiotensin-converting enzyme 2 (ACE2) receptor.

Results: The BNT162b2 two-dose regimen resulted in the highest and most durable NAb levels, followed by ChAdOx1, while those induced by CoronaVac significantly declined over time. Breakthrough infections boosted NAb levels, especially for CoronaVac and ChAdOx1. All vaccines showed reduced neutralizing capacity against Gamma, Delta, and Omicron variants. Booster doses, particularly the first one, significantly increased and maintained NAb levels, including those against Omicron.

Discussion: Our findings provide valuable population-based comparison of NAb levels elicited by different vaccines following primary inoculation and booster doses. Notably, the mRNA vaccine exhibited a strong primary and initial booster NAb response against SARS-CoV-2.

KEYWORDS

COVID-19, vaccine, neutralizing antibodies, booster dose, SARS-CoV-2

1 Introduction

In Brazil, three COVID-19 vaccines were initially widely used following approval by the National Health Surveillance Agency (ANVISA): CoronaVac, which was composed of the inactivated SARS-CoV-2 developed by the Sinovac Biotech Company (1) and produced by the Brazilian Butantan Institute; ChAdOx1 nCoV-19, which was based on an adenoviral vector developed by the Oxford University together with AstraZeneca Pharmaceutical (2) and produced in Brazil by the Oswaldo Cruz Foundation; and the mRNA-based BNT162b2 vaccine, developed by the BioNTech Company together with Pfizer Pharmaceutical (3). All these vaccines target the spike protein of the original SARS-CoV-2 strain as their main antigen aiming to reach a neutralizing antibody (NAb)-centered immunity. Unlike the other two platforms, CoronaVac may additionally induce antibodies against other structural viral proteins, although the spike protein remains the primary target for neutralization. Phase 3 clinical trials showed effectiveness against COVID-19, with CoronaVac at 50.7%–83.5% (4–6), ChAdOx1 at 70.4% (7), and BNT162b2 at 94%–95% (3). All three vaccines have shown seroconversion with neutralizing activity against SARS-CoV-2. However, follow-up studies revealed a decline in SARS-CoV-2 vaccine-induced antibody levels over time, along with lower vaccine efficacy against the constantly emerging SARS-CoV-2 viral variants (8–11). As a result, booster vaccinations using either the original or updated COVID-19 vaccines were recommended and remain in place today.

Although controlled clinical studies have confirmed the efficacy and safety of COVID-19 vaccines, direct comparisons are challenging due to variations in different populations and regions of the world, vaccination timing, and the prevalence of emerging viral variants. Population-based data offer a valuable and comprehensive source of tracking vaccination outcomes and should be considered when formulating future COVID-19 vaccination strategies (12).

The present study compares the magnitude, durability, and cross-reactivity of the NAb response among volunteers in Brazil who were vaccinated first with two doses of CoronaVac, ChAdOx1, or BNT162b2, followed by homologous or heterologous booster doses. The two-dose standard vaccination with BNT162b2 induced the strongest and most sustained responses, while CoronaVac showed the fastest decline. Prior infection enhanced responses across all groups. Boosters—especially the first—were essential to restore and maintain antibody levels, improve protection against variants like Omicron, and support long-term immunity up to 1 year post-vaccination. This study provides valuable insights into the dynamics and duration of vaccine-induced antibody responses, which are crucial for informing future guidelines on vaccine dosing regimens and heterologous dose combinations in combating the pandemic.

2 Materials and methods

2.1 Study population

The study included healthy volunteers residing in Rio de Janeiro, Brazil, who had received one or two doses of routine COVID-19 vaccination either with CoronaVac (Sinovac/Butantan), ChAdOx1 (Oxford/AstraZeneca), or BNT162b2 (Pfizer/BioNTech) and who were subsequently administered heterologous or homologous booster doses. Participants in the study were required to be over 18 years of age, sign an informed consent form, and provide detailed demographic information, including sex and date of birth, as well as data on previous SARS-CoV-2 infections identified through rapid tests and polymerase chain reaction (PCR). The study protocol was approved by the Ethics Committee of Oswaldo Cruz Institute (CEP-IOC) - Fiocruz (license numbers: CAAE 51345021.5.1001.5248 and CAAE 56246022.1.0000.5248) and of the Federal University of Rio de Janeiro (license number: 35.303.120.5.0000.5257).

A total of 506 individuals voluntarily participated in the study. The age distribution was categorized into two groups: 18 to 59 years old ($n = 425$), comprising 307 women and 118 men, and 60 years or older ($n = 81$), comprising 57 women and 24 men. Determination of previous SARS-CoV-2 infection was based on participants' self-reported positive results from PCR and/or rapid tests, as well as specific seroconversion to the viral nucleocapsid protein in the enzyme-linked immunosorbent assay (ELISA).

2.2 Sample collection and study design

Blood samples were collected by venipuncture in vacuum tubes (BD Vacutainer, BD Bioscience) containing sodium heparin anticoagulant by trained personnel. Each volunteer donated two tubes with 9 mL of blood. Plasma was obtained after centrifugation of heparinized blood at 1,000 × *g* for 10 min at room temperature (R.T.), aliquoted, and stored at −80°C until use.

Participants were vaccinated according to Brazil's national immunization campaign, which began in January 2021, with prioritization based on age, comorbidities, and occupational exposure. The sample collection occurred between mid-2021 and late 2023, depending on volunteer availability, and was not restricted to specific variant of concern (VOC) waves or vaccine batches. There was no active control over participants' vaccination timing, beyond their self-reported vaccination status and willingness to participate in this study. It is worth mentioning that between early 2021 and 2023, Brazil experienced distinct SARS-CoV-2 waves driven by variants like Gamma (early 2021), Delta (mid- to late 2021), and Omicron (December 2021 through 2023 with sub-lineages), each significantly impacting public health.

The study design included the collection of plasma samples after each dose of the COVID-19 vaccine at different time intervals. Groups were stratified according to their initial vaccination regimen of first and second homologous doses with either CoronaVac, ChAdOx1, or BNT162b2. Sample collections after the third and fourth vaccine doses were adopted as subsequent heterologous or homologous booster doses. In Brazil, the CoronaVac vaccine fell into disuse during the COVID-19 booster vaccination, leading to a preference for heterologous booster regimens involving either the ChAdOx1nCoV-19 or BNT162b2 vaccines. The sample collection timing intervals varied by each vaccine-recommended protocol and

volunteer willingness and availability. Sample times were designated as follows: T1, average time according to each vaccine stipulated regimen, varying from 15 to 86 days; T2, 15 to 75 days after the second dose; T3, 90 to 365 days after the second dose; T4, 15 to 75 days after the third dose; T5, 90 to 365 days after the third dose; T6, 15 to 75 days after the fourth dose; and T7, 90 to 365 days after the fourth dose. The average time of T1 collection varied according to the vaccine due to different vaccination regimens in Brazil: 23 days for CoronaVac, 71 days for ChAdOx1, and 66 days for BNT162b2. We clarify that the data presented in this study are predominantly treated as a cross-sectional cohort, with statistical treatment of individual samples as independent observations. While a limited subset of participants provided samples at multiple time points, it was not possible to monitor and collect samples from all participants at all designated time points throughout the study period (withdrawal from vaccination or participation in the study).

2.3 Quantification of SARS-CoV-2-specific neutralizing activity

Detection of NAb was performed using the cPass™ SARS-CoV-2 Neutralization Antibody kit (GenScript, cat# L00847), according to the manufacturer's instructions. The assay utilizes a recombinant receptor binding domain (RBD) of the SARS-CoV-2 spike protein. It quantifies Abs that block the interaction between the RBD and the human angiotensin-converting enzyme 2 (ACE2) receptor. The cPASS assay has received regulatory validation from the U.S. Food and Drug Administration as a reliable tool for SARS-CoV-2 neutralization, since, as stated by the agency document, "the test mimics the virus neutralization process" (13).

Briefly, plasma samples along with positive and negative controls provided with the kit were diluted in the sample dilution buffer and incubated with RBD conjugated to horseradish peroxidase (RBD-HRP) for 30 min at 37°C. Following incubation, the reaction mixtures were transferred to microplates pre-coated with ACE2 protein for 15 min at 37°C. The RBD-HRP bound to ACE2 was detected using tetramethylbenzidine (TMB, Sigma) substrate for 15 min at R.T. followed by a stopping solution. Optical density (O.D.) was measured at 450 nm using a GloMax Explorer GM3500 microplate reader (Promega). Plasma samples were incubated in single replicates, while controls were incubated in duplicates.

The NAb data were expressed in percentage or concentration in international units/mL (IU/mL).

For the percentage representation, the binding inhibition was calculated as follows:

$$\text{Inhibition}\,(\%) = \left(1 - \left(\frac{\text{sample O.D. value}}{\text{negative control O.D. value}}\right) \times 100\right)$$

As standardized by the manufacturer, the ≥30% cutoff was adopted for interpretation of positive SARS-CoV-2 neutralization activity. An inhibition percentage of ≥30% indicates the presence of Abs interacting with SARS-CoV-2 RBD and blocking the RBD–hACE2 interaction. The percentage of inhibition in plasma samples was assessed against original SARS-CoV-2 RBD (Wuhan isolate) as well as against its variants Gamma (GenScript, cat# Z03601), Delta (GenScript, cat# Z03614), and Omicron BA.1 (GenScript, cat# Z03730).

For the concentration representation as IU/mL, a semiquantitative analysis was also conducted, especially those collected after the third and fourth vaccine doses, using commercially provided SARS-CoV-2 Neutralizing Antibody Standard curves (GenScript, cat# A02087). This methodological shift was necessary due to the higher antibody levels, which approached the percentage detection threshold. Results were also expressed as antibody concentrations in IU, facilitating comparison with other assays that quantify SARS-CoV-2 NAbs (14).

2.4 Quantification of neutralizing antibodies against SARS-CoV-2 using classical PRNT

The Plaque Reduction Neutralization Test (PRNT), considered the gold standard for assessing NAbs against various viruses, including SARS-CoV-2, was also used in this study. Its results were compared with the cPass™ SARS-CoV-2 Neutralization Antibody kit as a way to validate our findings on viral neutralization inhibition. This comparison was performed with a total of 114 plasma samples, including CoronaVac (n = 38), ChAdOx1 (n = 37), and BNT162b2 (n = 40).

The PRNT protocol was previously described in detail (15). In summary, Vero cells (CCL81, ATCC) were seeded into 24-well plates (2×10^5 cells/well) in 199 media with Earle salts (E199, Sigma) supplemented with 5% fetal bovine serum (FBS, Invitrogen) 1 day before the assay. Plasma samples were heat-inactivated at 56°C for 30 min, serially diluted in culture medium (1:10 to 1:31,250), and incubated with approximately 60 plaque-forming units (PFU) of the ancestral strain of SARS-CoV-2 (SISGEN A994A37—donation from the Laboratory of Respiratory Viruses, Exanthematics, Enteroviruses and Viral Emergencies at IOC/Fiocruz) for 1 h at 37°C in a 5% CO_2 atmosphere. The plasma–virus mixture was added to Vero cell monolayers and incubated for 1 h at 37°C in 5% CO_2. After this incubation, the supernatants were discarded, and cells were covered with 199 media supplemented with 5% FBS and 1.5% carboxymethylcellulose (CMC, Sigma), incubated for 3 days at 37°C in 5% CO_2, followed by fixation and inactivation with 1.25% (v/v) formalin solution and stained with 0.04% (w/v) crystal violet dye. Plaques were counted manually. Finally, NAb titers were expressed as the highest serum dilution that resulted in 50% plaque reduction (PRNT50), considering samples with titers ≥ 1:14 seropositive to SARS-CoV-2. This threshold was established based on a receiver operating characteristic (ROC) curve analysis, which used 46 negative and 378 positive samples. The analysis identified 1.64 $\log_5$ as the optimal cutoff, corresponding to a dilution of 1:14. This point achieved the best balance between sensitivity and specificity, maximizing the assay's discriminatory power between positive and negative samples. PRNT assays were handled in a BSL-3 laboratory Multi-user Research Facility of

Biosafety Platform BSL3-HPP, Oswaldo Cruz Institute, Oswaldo Cruz Foundation, Rio de Janeiro, Brazil, following the approved international laboratory biosafety guidelines (CDC, Interim Laboratory Biosafety Guidelines for Handling and Processing Specimens Associated with Coronavirus Disease 2019).

2.5 Quantification of SARS-CoV-2-specific N antibody response

Plasma samples from all time points were evaluated for specific nucleocapsid (N) seroconversion as an indicator of previous SARS-CoV-2 infections. We quantified specific IgG Abs against the N protein from the original SARS-CoV-2 strain (Wuhan isolate) using a previously developed and validated ELISA protocol (16).

In summary, 96-well plates (Corning) were coated with the recombinant N protein (0.2 μg/mL) produced in human embryonic kidney (HEK) 293 cells and incubated overnight at 4°C. The following day, plates were washed with PBST [0.1% Tween in phosphate-buffered saline (PBS)] and blocked with 3% bovine serum albumin (BSA) in PBST for 1 h at R.T. The blocking solution was removed, and samples diluted 50-fold were added to the plates and incubated for 2 h at room temperature. After washing, the plates were incubated with secondary antibody (anti-IgG-HRP) diluted 1:5,000 in PBST for 1 h at 4°C. Plates were washed again and reactions were developed with TMB (50 μL per well) for 16 min at room temperature and then stopped with 3M HCl (50 μL per well). Absorbances were read at 450 nm on a spectrophotometer (Glomax Discover, Promega).

In this study, 15 samples collected prior to the COVID-19 pandemic (from individuals who had never been exposed to SARS-CoV-2) were used to determine the seroconversion positivity threshold for the N protein. The mean O.D. values plus three times the standard deviation was calculated and set as the cutoff for positivity. A pool of these samples was used as a control on all ELISA plates. Volunteers' samples with O.D. higher than the stablished threshold were considered positive for previous SARS-CoV-2 infection.

2.6 Statistics

Results were statistically analyzed using GraphPad Prism software, version 9.0 (La Jolla, USA). All graphical data are presented as the median and interquartile range (IQR). Statistical differences were assessed using the non-parametric Mann–Whitney test for two groups; non-parametric Kruskal–Wallis test with *post hoc* Dunn's correction for multiple comparisons was used for more than two groups. Correlation analyses were performed by computing Spearman's rank correlation coefficient and significance in GraphPad Prism. A p-value< 0.05 was considered statistically significant. Statistical comparisons involving very small sample sizes ($n< 5$) should be interpreted with caution.

3 Results

3.1 Study population characteristics

The study cohort comprises 452 volunteers initially vaccinated with two homologous doses of CoronaVac, ChAdOx1, or BNT162b2, including a total of 321 female and 131 male participants. Participants were categorized by age: 354 individuals were between 18 and 59 years old (272 women and 82 men), and 98 were aged 60 and above (49 women and 49 men).

Among those vaccinated with CoronaVac ($n = 108$), there were 81 women (75%) and 27 men (24%), with median ages of 47 and 45 years, respectively. In this group, 59 women (54.6%) and 18 men (16.6%) were aged 18 to 59 years, while 22 women (20.4%) and 9 men (8.4%) were ≥60 years. The ChAdOx1 group ($n = 285$) was the most representative cohort, consisting of 206 women (72.2%) and 79 men (27.8%), with median ages of 40 and 47 years, respectively. Within this group, 180 female (63.2%) and 40 male participants (14%) were aged 18 to 60 years, and 26 women (9.1%) and 39 men (13.7%) were 60 years or older. The BNT162b2 vaccine was used later in Brazil; thus, this group is smaller and with young volunteers, with 33 women (55.9%) and 24 men (40.7%), with median ages of 28 and 31 years, respectively. Of these, 33 women (55.9%) and 24 men (40.7%) were aged 18 to 59 years, and 1 woman (1.7%) and 1 man (1.7%) were ≥60 years (Table 1). The impact of sex and age groups was assessed during the data analysis in this study.

The distribution of the total samples for each vaccine group collected at the different time points (T1 to T7) is detailed in Table 2. Specifically, 183 samples were collected from volunteers vaccinated with CoronaVac, 630 samples were collected from volunteers vaccinated with ChAdOx1, and 129 samples were collected from volunteers vaccinated with BNT162b2, totaling 942 samples at different times throughout the study (Table 2**, top**). The distribution of samples across time points was not uniform because participant recruitment occurred continuously throughout the study period. The increased number of participants at T3 is likely attributable to a rise in public interest regarding vaccine effectiveness, together with the relaxation of social distancing measures. In general, participation in the study decreased over time as the COVID-19 pandemic progressed and booster doses were administered, affecting the number of samples of all vaccine groups.

Previous SARS-CoV-2 infection was determined either by self-reported positive results from PCR and/or rapid tests from volunteers up to 6 months prior to sample collection or by specific seroconversion to the viral nucleocapsid protein. The number of samples considered positive for previous SARS-CoV-2 infection is detailed in Table 2 (bottom). The impact of prior infection on the vaccine-induced antibody response was evaluated in the study.

TABLE 1 Demographic data for the COVID-19 vaccinated volunteers.

	All volunteers (*n* = 452)		CoronaVac (*n* = 108)		ChAdOx1 (*n* = 285)		BNT162b2 (*n* = 59)	
	Female	Male	Female	Male	Female	Male	Female	Male
Total, *n* (%)	321 (71.0)	131 (29.0)	81 (75.0)	27 (25.0)	206 (72.2)	79 (27.8)	34 (57.6)	25 (42.3)
Median age (range)	40 (15-92)	44 (18-84)	47 (19-86)	45 (21-62)	40 (20-83)	47 (19-84)	28 (18-61)	31 (18-60)
***n* (%) of Age group: 18 to 59**	272 (60.2)	82 (18.2)	59 (54.6)	18 (16.6)	180 (63.2)	40 (14.0)	33 (55.9)	24 (40.7)
***n* (%) of Age group: ≥ 60**	49 (10.8)	49 (10.8)	22 (20.4)	9 (8.4)	26 (9.1)	39 (13.7)	1 (1.7)	1 (1.7)

The demographic data for the volunteer cohort were stratified based on the initial vaccination regimen, which included two homologous doses from the CoronaVac, ChAdOx1, and BNT162B2 vaccine groups, followed by sex and age of each group. Age is represented in years.

3.2 Variation in the SARS-CoV-2 NAb response induced by CoronaVac, ChAdOx1, and BNT162b2 vaccination

The dynamics of NAb induced by vaccination were evaluated in samples from volunteers who received two homologous doses of CoronaVac, ChAdOx1, or BNT162b2 at three time points: collection after the first dose (T1: average time according to each vaccine stipulated regimen, varying from 19 to 84 days), short-term collection after the second dose (T2: 15 to 75 days), and long-term collection after the second dose (T3: 90 to 365 days). The average time of T1 collection varied according to the vaccine due to different vaccination regimens in Brazil: 23 days for CoronaVac, 71 days for ChAdOx1, and 66 days for BNT162b2. The total number of volunteers per group and the average time intervals for each time point are summarized in Figure 1A.

The NAb response against SARS-CoV-2 was measured using the cPass™ SARS-CoV-2 Neutralization Antibody ELISA kit (GenScript). Results were expressed as percentage inhibition, with 30% considered the positive threshold. CoronaVac induced the lowest NAb response (median: 24%), followed by ChAdOx1 (median: 47%) and BNT162b2 (median: 51%) after the first dose (T1), with the respective seroconversion rates of 45%, 67%, and 71%. All vaccinated groups showed a significant increase in the percentage

TABLE 2 Total number of collected samples by time point.

	All samples (*n* = 937)	CoronaVac (*n* =183)	ChAdOx1 (*n* = 626)	BNT162b2 (*n* = 128)
Total of collected samples, *n* (%)				
T1	197 (21.0)	22 (12.0)	141 (22.5)	34 (26.6)
T2	149 (15.9)	26 (14.2)	94 (15.0)	29 (22.7)
T3	217 (23.2)	65 (35.5)	127 (20.3)	25 (19.5)
T4	112 (12.0)	25 (13.7)	73 (11.7)	14 (10.9)
T5	149 (15.9)	30 (16.4)	108 (17.3)	11 (8.6)
T6	31 (3.3)	4 (2.2)	24 (3.8)	3 (2.3)
T7	82 (8.7)	11 (6.0)	59 (9.4)	12 (9.4)
*#Previous SARS-CoV-2 infection, *n* (%)				
T1	27 (13.7)	3 (13.6)	20 (14.2)	4 (11.8)
T2	34 (22.8)	10 (38.5)	18 (19.1)	6 (20.7)
T3	39 (18.0)	16 (24.6)	18 (14.2)	5 (20.0)
T4	39 (34.8)	5 (20.0)	27 (37.0)	7 (50.0)
T5	73 (49.0)	17 (56.7)	52 (48.1)	4 (36.4)
T6	12 (38.7)	1 (25.0)	9 (37.5)	2 (66.7)
T7	51 (62.2)	7 (63.6)	38 (64.4)	6 (50.0)

*Previous SARS-CoV-2 infection was determined through self-reported information from volunteers up to 6 months before sample collection, and/or by detecting seropositivity for the viral N protein.

#The numbers and percentages shown represent the proportion of positive samples out of the total samples collected at each time point.

Collection time intervals: T1—average time according to each vaccine stipulated regimen, varying from 15 to 86 days; T2—15 to 75 days after the second dose; T3—90 to 365 days after the second dose; T4—15 to 75 days after the third dose; T5—90 to 365 days after the third dose; T6—15 to 75 days after the fourth dose; T7—90 to 365 days after the fourth dose.

of NAb shortly after the second dose (T2), with 67% for CoronaVac, 89% for ChAdOx1, and 93% for BNT162b2. The second dose was crucial (T2), also evidenced by the high seroconversion rates 48 days after vaccination with CoronaVac (92%; 24 out of 26 individuals), 43 days after vaccination with ChAdOx1 (97%; 91 out of 94 individuals), and 42 days after vaccination with BNT162b2 (100%; 29 out of 29 individuals). Antibody persistence was assessed at T3 (90 to 365 days after the second dose). Individuals vaccinated with CoronaVac showed a significant decline in neutralizing capacity in T3 compared to T2, approximately 179 days after the second dose, with an average of 24% of NAb and 27 out of 65 individuals considered positive for seroconversion. ChAdOx1 and BNT162b2 groups showed a slight decline in NAb levels, with an average of 129 and 127 days after the second dose of each, although no statistically significant difference was observed comparing T2 and T3. Both groups maintained high seroconversion rates of 88% (112 out of 127 individuals) and 100% (25 out of 25 individuals), respectively (Figure 1B).

Longitudinal analysis of ChAdOx1 and CoronaVac vaccinees showed an initial increase in NAb levels shortly after the second dose (T2) followed by a decline long after the second dose (T3). However, BNT162b2 consistently maintained high and uniform NAb levels (Figure 1C). Comparative analysis of NAb levels shortly (T2) and long (T3) after the second dose demonstrated significant differences between vaccine strategies, with BNT162b2 showing a more homogeneous and higher NAb response compared to the other two. Notably, the standard two-dose CoronaVac regimen consistently induced lower percentages of NAb than ChAdOx1 and BNT162b2 at the two time points evaluated (T2 and T3) (Figure 1D). Our findings indicate that the standard two-dose regimen induces varying NAb responses against the original SARS-CoV-2 virus. CoronaVac elicited lower and less durable NAb, while ChAdOx1 produced a robust but also less durable response. In contrast, BNT162b2 generated a significantly stronger NAb response, characterized by higher levels, greater persistence, and overall robustness.

To validate the use of the cPass SARS-CoV-2 Neutralization Antibody ELISA kit with our cohort, we performed the gold standard plaque reduction neutralization titer assay (PRNT50) using plasma samples previously characterized as low, medium, and high neutralizing. A significant correlation was observed between the two assays, with a Spearman's rank correlation coefficient of $r = 0.74$ ($p< 0.0001$) (Supplementary Figure S1A). Individually, the correlations were as follows: $r = 0.72$ ($p< 0.0001$) for CoronaVac (Supplementary Figure S1B), $r = 0.73$ ($p< 0.0001$) for ChAdOx1 (Supplementary Figure S1C), and $r = 0.69$ ($p< 0.0001$) for BNT162B2 (Supplementary Figure S1D).

3.3 Previous infection with SARS-CoV-2 impacts the vaccine-induced NAb response after CoronaVac, ChAdOx1, and BNT162b2 vaccination

To assess the impact of previous SARS-CoV-2 infection on the vaccine-induced NAb response, we considered self-reported information from volunteers up to 6 months before the sample collection and/or detection of seropositivity for the viral N protein.

Previous SARS-CoV-2 infection significantly increased NAb levels against the original SARS-CoV-2 strain (Wuhan isolate) after the first dose (T1) in all vaccinated groups (Figure 2). In the CoronaVac and ChAdOx1 groups, individuals with previous infection exhibited higher average NAb levels shortly after the second dose (T2) and, more notably, at a later time point (T3), when these differences were statistically significant for both vaccines (Figures 2A, B). In contrast, individuals vaccinated with BNT162b2, regardless of having a previous SARS-CoV-2 infection, achieved high levels of NAb shortly and long after the second dose (T2 and T3), approaching the assay's limit of detection (Figure 2C). Because of the limited number of samples at certain time points in the vaccinated and infected groups, we combined the results from the three vaccinated groups (CoronaVac, ChAdOx1, and BNT162b2) and assessed the impact of prior infection, irrespective of the vaccination regimen. The average NAb values were higher in the group with prior SARS-CoV-2 exposure, both after the first dose (T1) and long-term follow-up after the second dose (T3) (Figure 2D).

These results indicate that prior infection with SARS-CoV-2 enhanced the specific NAb induced by two-dose vaccinations with CoronaVac and ChAdOx1, including the durability of these neutralizing responses. However, this prior infection had a minimal impact on the BNT162b2 regimen.

3.4 Dynamic comparison of NAb induced by CoronaVac, ChAdOx1, or BNT162b2 vaccination and their respective booster doses in individuals with and without previous SARS-CoV-2 infection

As the COVID-19 pandemic evolved with the emergence of new variants, booster vaccine dose regimens were implemented. To better quantify high-level NAb responses that may exceed the limits of percentage-based measurements following booster doses, we expressed NAb levels in international units per milliliter (IU/mL), calculated by using a commercially SARS-CoV-2 NAb standard curve. Samples were collected at various time points following the recommended vaccination schedule: after the first dose (T1), 15 to 75 days after the second dose (T2), 90 to 365 days after the second dose (T3), 15 to 75 days after the third dose (T4), 90 to 365 days after the third dose (T5), 15 to 75 days after the fourth dose (T6), and 90 to 365 days after the fourth dose (T7). The total number of volunteers per group and the average time intervals for each time point are summarized in Figure 3A. In Brazil, heterologous booster doses (using a different vaccine platform than the initial regimen) were prioritized. Moreover, CoronaVac was less commonly used for boosters. Most booster doses for ChAdOx1 recipients were BNT162b2, and contrariwise. For the CoronaVac group, both ChAdOx1 and BNT162b2 were administered as boosters.

The first booster dose (third vaccine dose) was crucial in increasing NAb levels shortly after that dose, particularly in

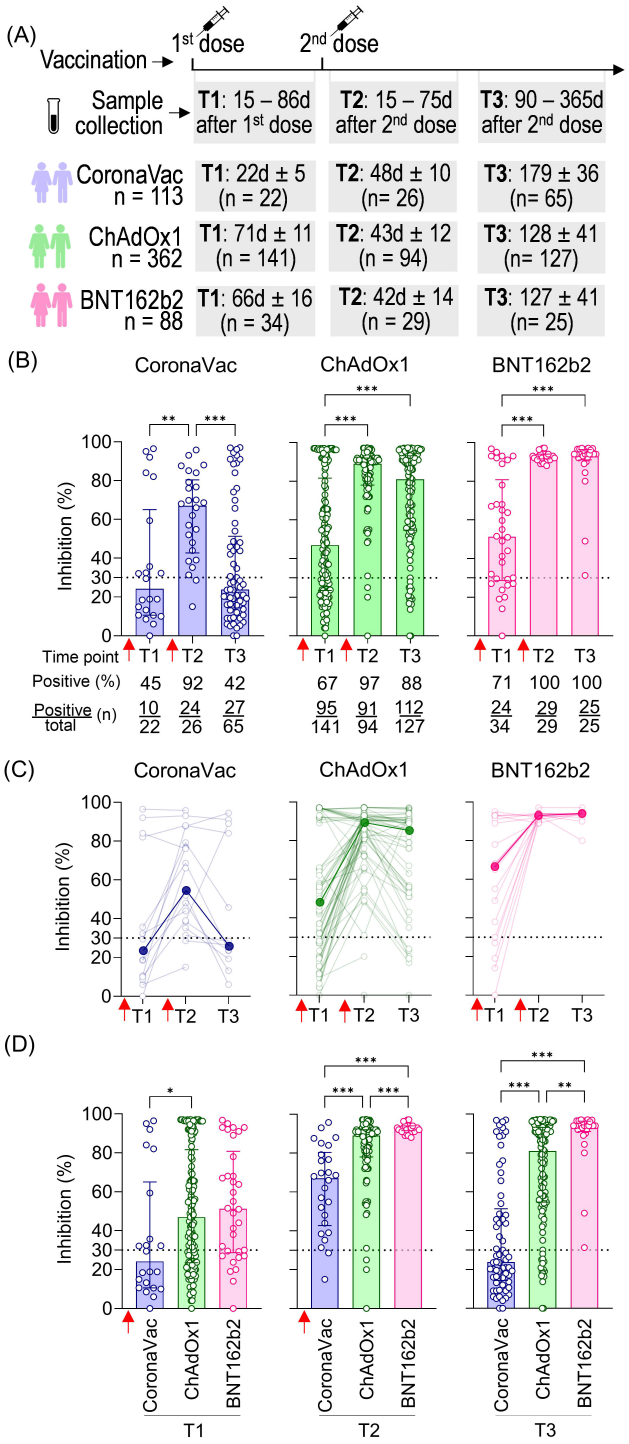

FIGURE 1
SARS-CoV-2 NAb response induced by two homologous doses of CoronaVac, ChAdOx1, and BNT162b2 vaccination. **(A)** Timeline of sample collection of vaccinated volunteers who received standard two-dose vaccine regimens with CoronaVac, ChAdOx1, or BNT162b2. Plasma samples were collected at the following time points: T1—15 to 86 days after the first dose; T2—15 to 75 days after the second dose; T3—90 to 365 days after the second dose. The average time for T1 varied according to the recommended schedule for each vaccine, being shorter for CoronaVac (average of 23 days) and longer for ChAdOx1 (average of 71 days) or BNT162b2 (average of 66 days). The number of volunteers per group and the average time of collection ± standard deviation are detailed. **(B)** Percentage of NAb in individuals vaccinated with one or two homologous doses of CoronaVac, ChAdOx1, or BNT162b2 vaccines. **(C)** Longitudinal follow-up of vaccinated volunteers with at least two subsequent collections through time points. Medians for each time point were connected by a bold line to better represent the results. **(D)** Comparison of NAb percentages at each time point according to the three different vaccine regimens. **(B–D)** Specific NAb percentages were assessed using the cPass™ SARS-CoV-2 Neutralization Antibody with the RBD from the original SARS-CoV-2 strain (Wuhan isolate). The dashed line at 30% indicates the test positivity threshold. Red arrows indicate vaccine doses. The bars indicate the median and IQR. Non-parametric Kruskal–Wallis test was used for statistical analyses. *$p < 0.05$, **$p < 0.01$, ***$p < 0.001$. Sample sizes of **(C)**—CoronaVac: T1 (n = 14), T2 (n = 19), and T3 (n = 13); ChAdOx1: T1 (n = 62), T2 (n = 75), and T3 (n = 49); BNT162b2: T1 (n = 19), T2 (n = 22), and T3 (n = 10). Samples sizes of **(B, D)** are detailed in **(A)**.

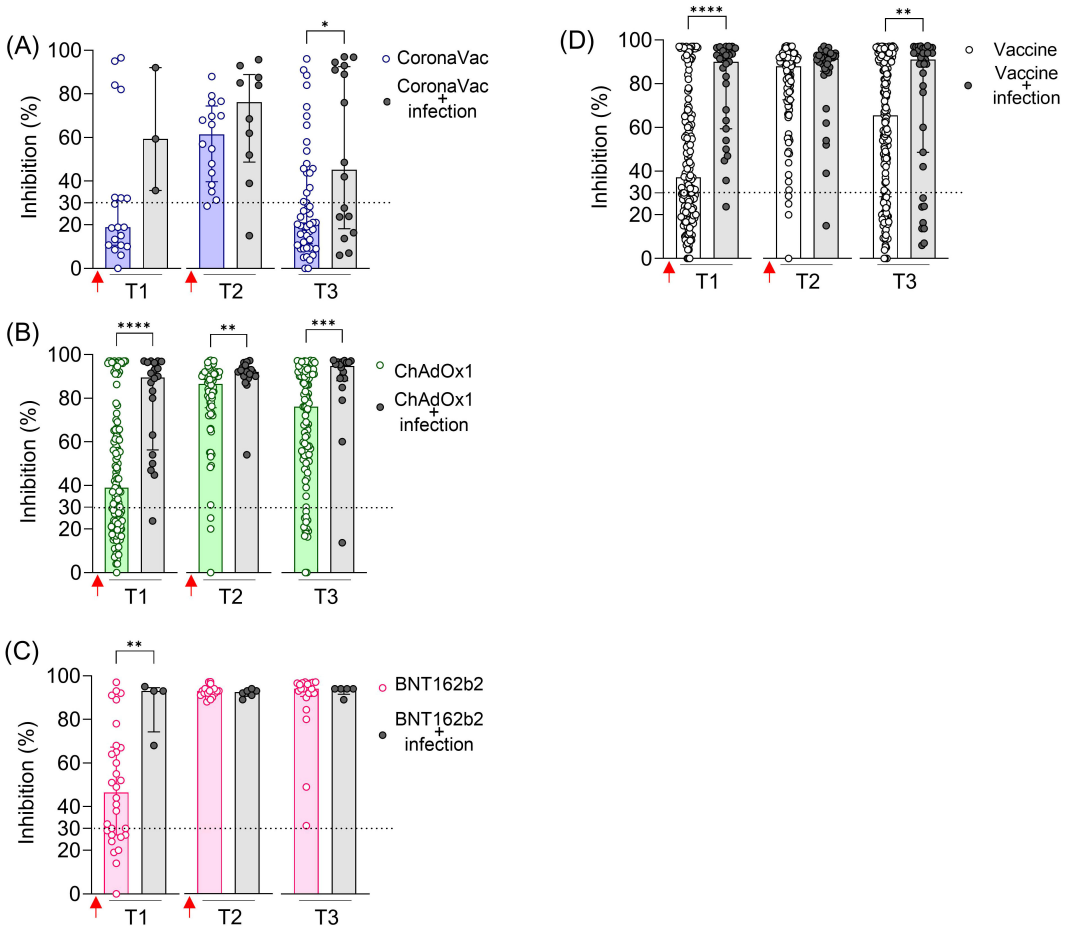

FIGURE 2
SARS-CoV-2 NAb in individuals vaccinated with CoronaVac, ChAdOx1, or BNT162b2, with and without previous SARS-CoV-2 infection. Percentage (%) of NAb in individuals vaccinated with the standard two-dose regimen with CoronaVac **(A)**, ChAdOx1 **(B)**, BNT162b2 **(C)**, and all vaccines together **(D)**. Specific NAb percentages were assessed using the cPass™ SARS-CoV-2 Neutralization Antibody with the RBD from the original SARS-CoV-2 strain (Wuhan isolate). Previous SARS-CoV-2 infection was determined by self-reported positive results from PCR and/or rapid tests, as well as specific seroconversion to the viral nucleocapsid protein. The dashed line at 30% indicates the test positivity threshold. Red arrows represent vaccine doses. The bars indicate the median and IQR. Non-parametric Mann–Whitney test was used for statistical analyses. *$p< 0.05$; **$p< 0.01$; ***$p< 0.001$; ****$p< 0.0001$. Sample sizes: T1—CoronaVac (n = 19/3), ChAdOx1 (n = 121/20), and BNT162b2 (n = 30/4); T2—CoronaVac (n = 16/10), ChAdOx1 (n = 76/18), and BNT162b2 (n = 23/6); T3—CoronaVac (n = 49/16), ChAdOx1 (n = 109/18), and BNT162b2 (n = 20/5); values indicate number of vaccine-only/vaccine + infection participants.

individuals who received CoronaVac (479.7-fold increase) or ChAdOx1 (14.1-fold increase) as the initial vaccine regimen, where T4 was statistically higher than T3. Although not statistically significant in the BNT162b2 group, NAb levels showed a 4.4-fold increase shortly after the first booster dose (third vaccine dose) between T3 and T4. The short-term impact of the second booster dose (fourth vaccine dose) seems less prominent regarding the NAb response against the original virus, as there was no significant statistical increase in values observed at T6 (shortly after the fourth dose) compared to the values observed both shortly and long after the third dose (T3 and T4, respectively) (Figure 3B). Longitudinal analysis of vaccinees showed a similar pattern of responses, with a prominent increase in NAb levels shortly after the first booster dose, especially for CoronaVac and ChAdOx1, followed by high and uniform NAb levels (Figure 3C).

The long-term persistence of NAb following vaccination is evident in the extended collection times, ranging from 90 to 365 days after each dose: T3 (after the second dose), T5 (after the third dose), and T7 (after the fourth dose) (Figure 3D). Comparatively, we observe much lower NAb levels long after the second dose (T3) compared to long after the third dose (T5) in the CoronaVac and ChAdOx1 vaccinees, underscoring the importance of the first booster dose in enhancing the durability of NAb responses against SARS-CoV-2 regarding these vaccines. In the CoronaVac group, NAb levels were approximately 386.1-fold lower in T3 (average of 179 days after the second dose) compared to T5 (average of 178 days after the third dose). However, the fourth dose resulted in a non-significant small decrease comparing NAb in T5 (average of 178 days after the third dose T5) and T7 (average of 249 days after the fourth dose). Regarding the ChAdOx1 vaccine,

NAb levels were statistically 7.3-fold lower in T3 (average of 128 days after the second dose) compared to T5 (average of 167 days after the third dose), with a less pronounced increase (1.3-fold) in T7 (average of 206 days after the fourth dose) compared to T5. In contrast, individuals who initially received the BNT162b2 regimen maintained consistently high and long-lasting NAb levels, with no significant difference observed between T3 (average of 127 days after the second dose), T5 (average of194 days after the third dose), and T7 (average of 200 days after the fourth dose) (Figure 3D).

We assessed the influence of sex and age on the NAb response. Owing to the limited number of individuals in some subgroups, we combined all vaccinated individuals at different time points and also separated them by the first vaccine regimens (the first two homologous doses) (Supplementary Figure S2). The influence of

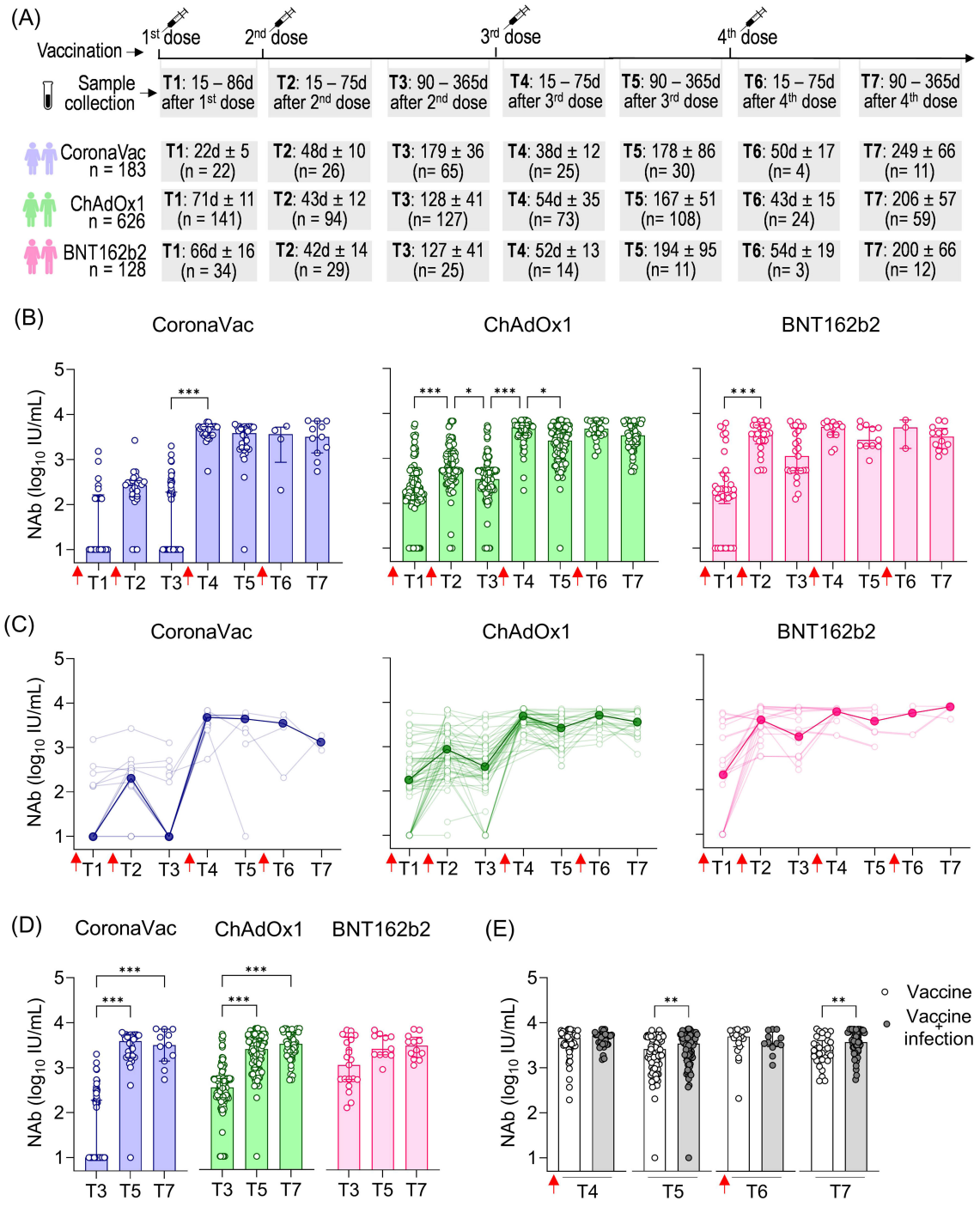

FIGURE 3 (Continued)

FIGURE 3 (Continued)
SARS-CoV-2 NAb response induced by two homologous doses of CoronaVac, ChAdOx1, and BNT162b2 vaccination followed by booster doses. **(A)** Timeline of sample collection of vaccinated volunteers who received the first standard two-dose vaccine regimen with CoronaVac, ChAdOx1, or BNT162b2 vaccines followed by the booster doses. Plasma samples were collected at the following time points: T1—15 to 86 days after the first dose; T2—15 to 75 days after the second dose; T3—90 to 365 days after the second dose. The average time for T1 varied according to the recommended schedule for each vaccine, being shorter for CoronaVac (average of 23 days) and longer for ChAdOx1 (average of 71 days) or BNT162b2 (average of 66 days). The number of volunteers per group and the average time of collection ± standard deviation are detailed. **(B)** Concentration (IU/mL) of NAb against the original SARS-CoV-2 strain (Wuhan isolate) in volunteers who received the initial vaccine regimen of CoronaVac, ChAdOx1, or BNT162b2, followed by one or two booster doses of any of these vaccines. **(C)** Longitudinal follow-up of the NAb concentration (IU/mL) for participants with two or more consecutive sample collections from T1 to T7. Medians for each time point were connected by a bold line to better represent the results. **(D)** Concentration (IU/mL) of NAb against the original SARS-CoV-2 strain (Wuhan isolate) in vaccinees at long-term time points (T3, T5, and T7). Concentrations (IU/mL) of NAb were assessed using the cPass™ SARS-CoV-2 Neutralization Antibody with the RBD from the original SARS-CoV-2 strain (Wuhan isolate) and a standard monoclonal antibody curve (GenScript). **(E)** Concentration of NAb in vaccinated individuals (CoronaVac, ChAdOx1, and BNT162b2) followed by booster doses with or without previous SARS-CoV-2 infection. **(B–D)** The bars indicate the median and IQR. Red arrows indicate vaccine doses. **(B, D)** Non-parametric Kruskal–Wallis test was used for statistical analyses. *$p < 0.05$, ***$p < 0.001$. **(E)** Non-parametric Mann–Whitney test was used for statistical analyses. **$p < 0.01$. Sample sizes of **(C)**—CoronaVac: T1 (n = 20), T2 (n = 23), T3 (n = 15), T4 (n = 8), T5 (n = 6), T6 (n = 3), and T7 (n = 3); ChAdOx1: T1 (n = 70), T2 (n = 75), T3 (n = 70), T4 (n = 56), T5 (n = 54), T6 (n = 25), and T7 (n = 23); BNT162b2: T1 (n = 14), T2 (n = 19), T3 (n = 29), T4 (n = 20), T5 (n = 10), T6 (n = 4), and T7 (n = 2). Sample sizes of **(E)**—Vaccine only: T4 (n = 73), T5 (n = 76), T6 (n = 19), and T7 (n = 31); Vaccine + infection: T4 (n = 39), T5 (n = 73), T6 (n = 12), and T7 (n = 51). Samples sizes of **(B, D)** are detailed in **(A)**.

sex was only evident shortly after the second booster dose (T6), where male individuals had higher NAb levels than female individuals (Supplementary Figure S2A). Regarding age, we observed that individuals aged 60 years or older had lower NAb levels only at the longest time point after vaccination (T3), but this difference was not seen in either shortly (T4 and T6) or long (T5 and T7) after booster doses (Supplementary Figure S2A).

To assess the influence of prior SARS-CoV-2 infection on NAb dynamics after booster doses, we analyzed data from all vaccinated individuals together (CoronaVac, ChAdOx1, and BNT162b2). While no significant impact of prior infection was observed in the shorter follow-up times after the third (T4) and fourth (T6) vaccine doses, we found statistically higher NAb levels in vaccinated individuals and individuals previously infected with SARS-CoV-2 at the longer time points (T5 and T7) (Figure 3E). This suggests that prior infection mainly affects the durability of NAb responses rather than their magnitude.

Taken together, these results highlight the importance of booster doses in enhancing the antibody response to the original SARS-CoV-2 strain. The first booster played a significant role in increasing the NAb levels both shortly and long after vaccination, while the second booster was slightly more relevant in promoting greater durability of these antibodies (Abs), which was also correlated with the impact of prior SARS-CoV-2 infection.

3.5 Cross-reactivity of NAb response induced by CoronaVac, ChAdOx1, or BNT162b2 vaccination directed to Gamma, Delta, and Omicron variants

A major difficulty in COVID-19 vaccination is promoting a robust and durable cross-protective immune response against emerging SARS-CoV-2 VOCs leading to ongoing infection waves and prolonging the pandemic. To assess antibody cross-reactivity, we examined their neutralization capacity against Gamma (P.1), Delta (B.1.617.2), and Omicron (B.1.1.529) VOCs.

A standard vaccination regimen with two homologous doses of CoronaVac, ChAdOx1, or BNT162b2 showed a greater capacity to neutralize the original SARS-CoV-2 strain compared to the Gamma, Delta, and Omicron variants shortly after vaccination (T2) (Figure 4). The NAb median response against the Gamma and Delta variants was above the positive threshold for all three vaccines, though it remained lower compared to the original strain. For Gamma, the NAb percentages were approximately 47.9% for CoronaVac, 41.9% for ChAdOx1, and 82.9% for BNT162b2 groups. Against Delta, the averages were 55.9%, 45.6%, and 81.4%, respectively. However, none of the regimens demonstrated effective neutralization against the highly mutated Omicron variant, which exhibited the lowest average NAb levels (CoronaVac: 12.8%, ChAdOx1: 2.6%, and BNT162b2: 16.3%) and the largest reduction ratio relative to the original strain (CoronaVac: 5.3-fold, ChAdOx1: 29.9-fold, and BNT162b2: 5.6-fold). Comparatively, CoronaVac and BNT162b2 groups showed the lowest rates of antibody reduction against VOCs, while the ChAdOx1 vaccinees exhibited the highest reduction (Figure 4).

Given the widespread prevalence of Omicron since late 2021, the cross-reactivity of Ab induced by booster doses was evaluated exclusively against this variant shortly after vaccination. Statistically, all vaccine regimens showed lower levels of NAb against Omicron compared to the original strain, both after the second (T2) and third doses (T4). While a reduction in NAb levels was observed after the fourth dose, it was statistically significant only in the ChAdOx1 group (Figure 5A). Over time (T2 to T6), NAb levels showed a tendency to increase. To investigate whether this rise was driven solely by the booster doses or also by natural infections with ongoing Omicron waves, samples from all vaccine groups were analyzed, distinguishing between vaccination alone and vaccination with SARS-CoV-2 infection before collection. A clear increase in NAb levels against both the original strain and Omicron was observed after booster doses compared to the initial response from the homologous vaccine regimen (Figure 5B). Antibody levels against Omicron were higher in individuals who had both been vaccinated and infected with SARS-CoV-2, with

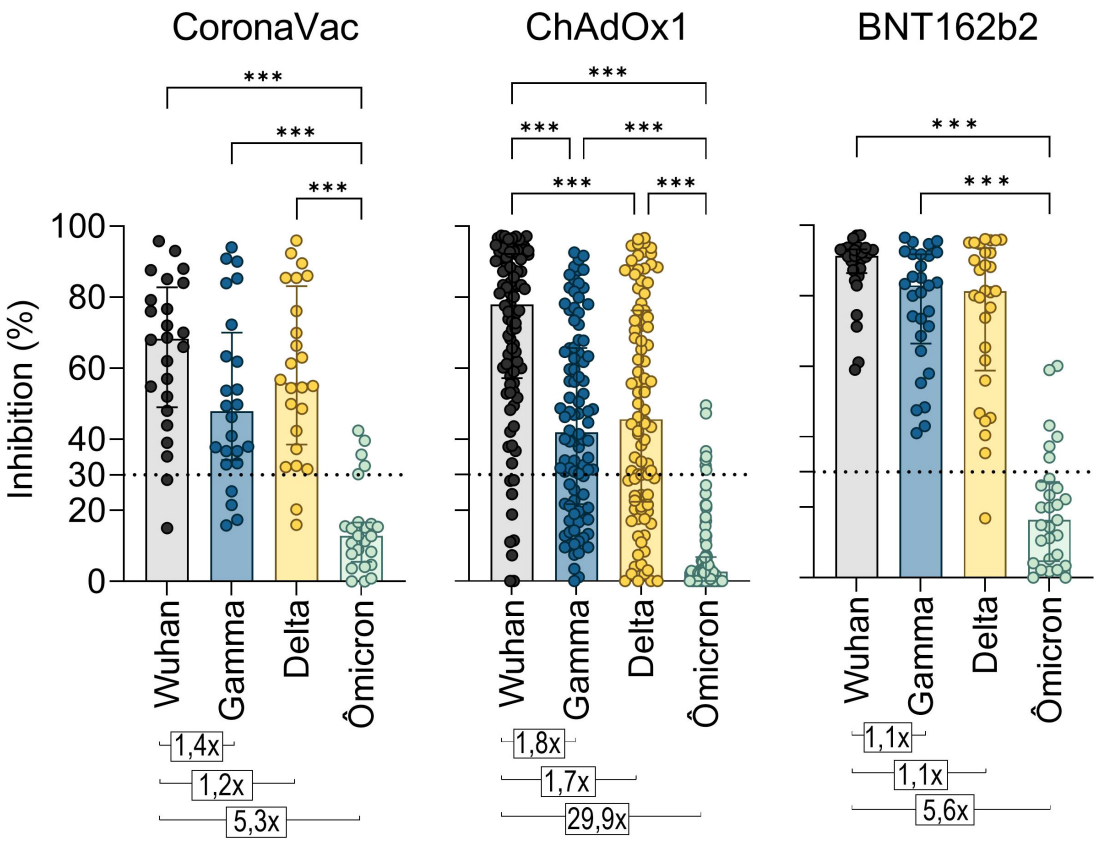

FIGURE 4
Neutralizing antibody response to SARS-CoV-2 Gamma, Delta, and Omicron variants induced by two homologous doses of CoronaVac, ChAdOx1, and BNT162B2 vaccination. Percentage (%) of NAb in individuals shortly after vaccination with CoronaVac, ChAdOx1, or BNT162b2, against the original virus RBD or its VOCs Gamma, Delta, and Omicron. The bars represent the median and IQR. Different plasma dilutions were used for samples of each vaccination regimens: CoronaVac, 10-fold; AstraZeneca, 50-fold; Pfizer, 100-fold. The dashed line at 30% represents the positivity detection threshold of the test. Values above the bars represent the average ratios between the NAb percentage against the original virus RBD and against the RBDs of the Gamma, Delta, and Alpha VOCs. The Kruskal–Wallis non-parametric test was used for statistical analysis. ***$p < 0.001$. Sample sizes—CoronaVac (n = 24), ChAdOx1 (n = 94), and BNT162b2 (n = 29).

statistically significant differences at T2 and T4 (Figure 5C). After the second dose of the homologous regimen (T2), SARS-CoV-2 infection increased the Omicron NAb response, even though the Omicron variant was not circulating when these samples were collected. This increase was more evident after the third (T4) dose, with NAb levels rising from 76% to 87.2% (Figure 5C).

4 Discussion

The unprecedented development of COVID-19 vaccines has been crucial in combating the pandemic. The ongoing accumulation of population-based vaccination data provides valuable insights to understand how to optimize vaccine use in the future. Although not exclusively, the development of COVID-19 vaccines prioritized inducing a NAb response, primarily targeting the highly antigenic S protein, which is crucial for viral entry. Several studies with individuals vaccinated against COVID-19 demonstrate a positive correlation between high levels of NAb and vaccine protective efficacy (17–19). In Brazil, the population was primarily vaccinated with three COVID-19 vaccines: CoronaVac (inactivated virus), ChAdOx1 (viral vector), and BNT162b2 (mRNA). Since different vaccine platforms can induce varying immune responses, this study aimed to evaluate the magnitude and durability of NAb up to 365 days after the vaccination following booster doses and its ability to neutralize viral variants.

While PRNT50 is the gold standard for measuring NAb against SARS-CoV-2 (20) and other viruses, its complexity limits its use (costly, time-consuming, and the need for a BSL3 facility). As an alternative, this study used a commercially available Food and Drug Administration (FDA)-approved immunoenzymatic assay (cPass Neutralizing Antibody kit) that measures ACE2-RBD binding inhibition as a surrogate for NAb levels (13, 21). Previous studies correlate well such an assay with PRNT results (22–26), which was also seen here with a subset of our vaccinated cohort.

Our initial data show that the two-dose homologous regimen of the BNT162b2 vaccine generated higher and long-lasting NAb levels against SARS-CoV-2, followed by ChAdOx1 and finally CoronaVac. Direct comparisons of our findings with the literature are challenging, as COVID-19 vaccination worldwide involved not only these vaccines but also several others,

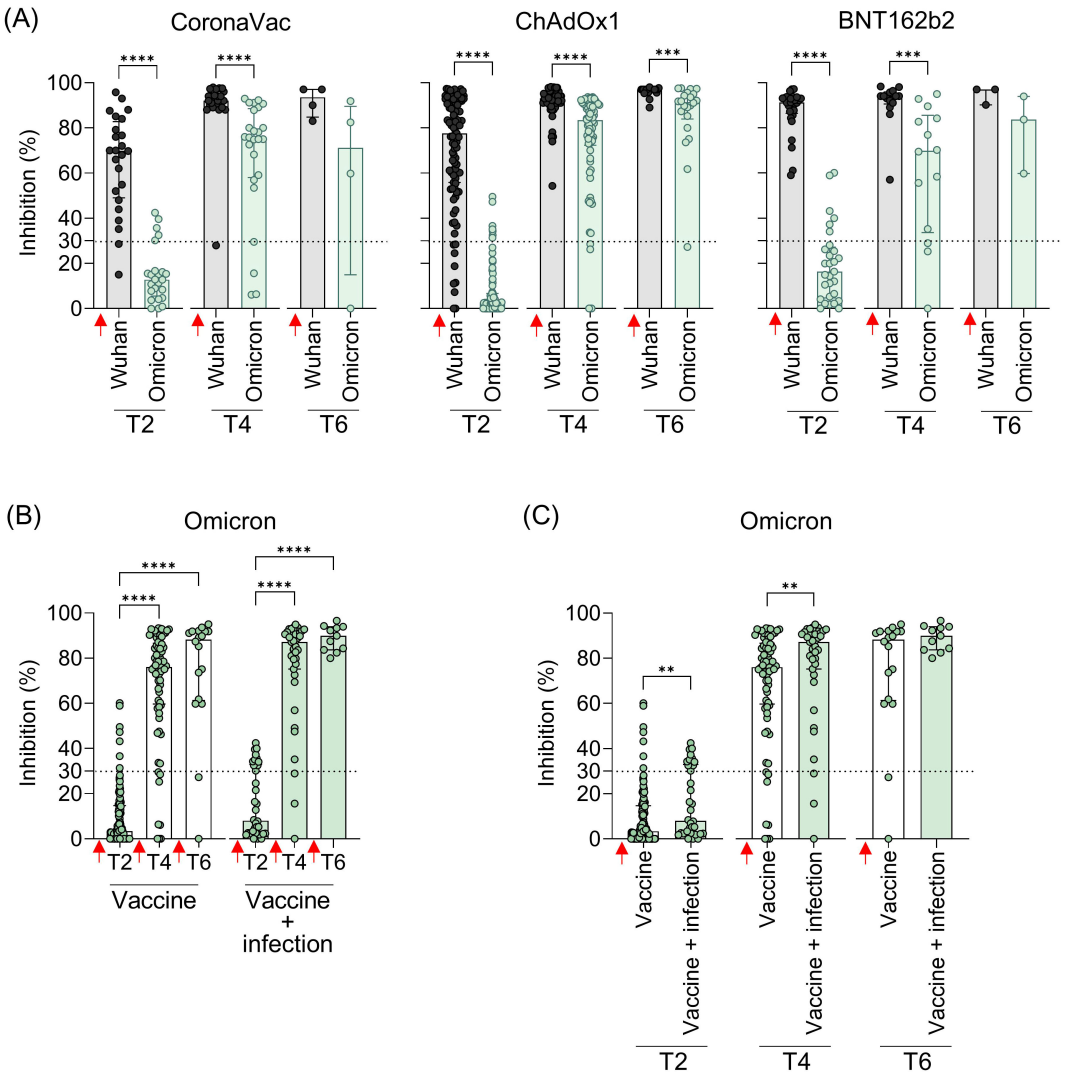

FIGURE 5
Neutralizing antibodies against the original virus and the Omicron VOC in individuals vaccinated with CoronaVac, ChAdOx1, or BNT162b2 followed by booster doses, with and without previous SARS-COV-2 infection. **(A)** Percentage (%) of NAb against the original SARS-CoV-2 virus and Omicron variant at the different time points. **(B, C)** Percentage (%) of NAb against the Omicron variant in vaccinated individuals with and without previous virus infection. Plasma samples were collected at the following time points: T2—15 to 75 days after the second dose; T4—15 to 75 days after the third dose; T6—15 to 75 days after the fourth dose. Specific NAb percentages were assessed using the cPass™ SARS-CoV-2 Neutralization Antibody with the RBD from the original SARS-CoV-2 strain (Wuhan isolate) or Omicron (B.1.529.1). Previous SARS-CoV-2 infection was determined by self-reported positive results from PCR and/or rapid tests, as well as specific seroconversion to the viral nucleocapsid protein. The bars represent the median and IQR. Red arrows indicate vaccine doses. Non-parametric Mann–Whitney test was used for statistical analyses. $^{**}p< 0.01$; $^{***}p< 0.001$; **** $p< 0.0001$. Sample size of **(A)**—CoronaVac: T2 (n = 24), T4 (n = 25), and T6 (n = 4); ChAdOx1: T2 (n = 94), T4 (n = 73), and T6 (n = 22); BNT162b2: T2 (n = 29), T4 (n = 14), and T6 (n = 3). Sample size of **(B, C)**—Vaccine only: T2 (n = 113), T4 (n = 73), and T6 (n = 18); Vaccine + infection: T2 (n = 34), T4 (n = 39), and T6 (n = 11).

administered in varying orders and schedules. Similar results were seen comparing these three different vaccine platforms (27, 28). Healthcare workers vaccinated with mRNA vaccines (mRNA-1273 and BNT162b2) exhibited significantly higher NAb titers after the first dose, and these levels remained elevated 6 months after the second dose, compared to those vaccinated with ChAdOx1 or Sinopharm (28). Similar patterns have been reported in Mexico (29), Thailand (30), Chile (31), Indonesia (32), and Brazil (33, 34), where studies consistently showed that BNT162b2 induced superior NAb responses compared to other vaccine platforms. Other studies have shown that vaccine-induced SARS-CoV-2 NAb tends to decrease over time (8–10, 35), affecting the long-lasting protective immunity against this virus. One multicentric study conducted in Brazil and Mexico has shown that BNT162b2 offers a more sustained SARS-CoV-2 Spike IgG response in a 6-month follow up (36). Our results, in addition to others (36–38), revealed that CoronaVac induced lower and less durable levels of NAbs than BNT162b2 and ChAdOx1, indicating that the platform of the inactivated virus is less effective. Furthermore, the immunogenic epitopes of the spike protein may undergo structural changes during the virus inactivation process, potentially affecting and reducing its immunogenicity (39). However, it is important to

note that the CoronaVac and its platform was of extreme importance at the beginning of the pandemic in Brazil, by inducing protection against severe COVID-19 and deaths, being applied to health workers and the elderly (40), as well as in other countries around the world (4–6). The mRNA vaccines, in turn, mimic natural infection, leading to high-affinity antibody production and prolonged antigen protein production, which sustained the immune response (41).

Initially, vaccines were administered in a single vaccination schedule with two homologous doses, followed by booster doses in response to the observed decline in antibody neutralization over time and the ongoing evolution of viral variants capable of evading vaccine-induced immunity. In Brazil, boosters were primarily BNT162b2 for the CoronaVac and ChAdOx1 groups, and mainly ChAdOx1 for the BNT162b2 group. The first booster dose (third vaccination) significantly strengthened and sustained the NAb response over time, especially for CoronaVac and ChAdOx1 initial regimens. Booster doses of COVID-19 vaccines, particularly with heterologous regimens, have been shown to enhance antibody responses, including against emerging variants responsible for new infection waves (42–45). According to our findings, the mRNA vaccines (BNT162b2 and mRNA-1273) have been especially effective in reinforcing immunity initially induced by inactivated or viral vector vaccines (46–48). Studies from Brazil (49), Chile (50), and Thailand (51) show a robust increase in vaccine-induced NAb response when the BNT162b2 vaccine was administered as booster for individuals initially vaccinated with CoronaVac. These findings are important for designing future vaccine guidelines in low- and middle-income countries that relied on CoronaVac for their vaccination campaigns.

Several factors can alter the production and durability of NAb generated by COVID-19 vaccines, such as age, sex, and previous infections (52). In general, vaccines have lower efficacy in older individuals due to age-related immunosenescence (53, 54). However, our results showed similar immunogenicity regardless of age, in accordance with other vaccination studies (55, 56). Elderly individuals showed lower NAb levels in long-term follow-up after the initial vaccination regimen, suggesting an age-related impact in sustaining the vaccine's immunogenicity, but this difference was no longer apparent after booster doses. A single difference emerged after the booster dose, with men demonstrating higher NAb titers. This sex-specific difference, though not widely observed, has been reported previously (57) and may be related to factors not investigated here such as hormonal factors, genetic variations, or testosterone's impact on immune response activation (58).

The challenge of evaluating COVID-19 vaccine immunogenicity is that vaccination has occurred alongside waves of breakthrough infections likely caused by VOCs with high capacity to evade vaccine-induced immunity (59). Therefore, assessing the NAb response against these VOCs and the impact of natural infection on vaccine immunity is essential. Our findings demonstrate that regardless of the initial vaccine (CoronaVac, ChAdOx1, or BNT162b2), the Gamma, Delta, and especially Omicron variants showed reduction in NAb recognition. The reduced recognition of NAb against SARS-CoV-2 VOCs has been demonstrated for all vaccines, highlighting mutations mainly in the RBD as potent mediators of immune escape from the vaccine response (60–62). Even with NAb evasion, individuals infected with Omicron, which presents substantial differences compared to the original virus (63), typically experience mild disease (64), suggesting the involvement of other immune mechanisms, such as the T-cell response, in disease control and modulation.

One of the major benefits of administering booster doses against COVID-19 was the increase in protection against SARS-CoV-2 VOCs (65, 66). We observed an increase in NAb against Omicron booster doses, which may be associated with the stimulation of the immune system following antigen re-exposure, either from natural infection or from an additional vaccine booster dose. We showed that individuals previously infected with SARS-CoV-2 exhibited higher NAb levels after COVID-19 vaccination and that this prior infection had a significant impact on the long-term sustainability of the antibody response after booster doses, according to other studies (29, 31, 33, 67–69). Our data support that not only the effect of booster doses was responsible for increasing vaccine-induced immunity against the Omicron VOC, but also natural breakthrough infections occurring concomitantly with the immunization period, even when another VOC was circulating. These findings align with previous studies showing higher NAb production, including an enhanced ability to recognize VOCs (70, 71), probably due to an amplification of vaccine-induced memory immune response either by hybrid immunity from natural infection or by booster vaccination. In line with our findings where the majority of vaccinees received BNT162b2 as a heterologous booster dose, the use of mRNA vaccines has been of important value in strengthening immunity against SARS-CoV-2 VOCs (72–74).

This study has limitations. First, sample sizes were uneven across time points and participant subgroups, with relatively fewer elderly individuals and a higher proportion of women than men. Similarly, the representation of previously infected individuals varied across time points. Sample size for stratification based on the different vaccines used for booster doses (ChAdOx1 or BNT162b2) was also insufficient to clearly determine whether the results observed were associated with the vaccine platforms or even the impact of homologous boosters. Second, we were unable to follow all participants longitudinally, which constrained our ability to assess individual-level antibody dynamics over time. Third, we did not assess comorbidities, medication use, or other medical factors, as this information was not available for all volunteers, preventing us from establishing their potential impact on the NAb vaccine-induced response. Finally, the study focused exclusively on humoral immune responses, without evaluating cellular immunity, which plays a crucial role in vaccine-induced protection and long-term immune memory. Our population-based data indicate that the two-dose mRNA BNT162b2 vaccine generated stronger and more durable NAb responses compared with inactivated and vector-based vaccines. The booster doses, particularly the third vaccination, were essential, especially for CoronaVac and ChAdOx1, significantly increasing NAb levels, including against VOCs like Omicron, which was previously undetectable. This enhanced response was attributed to booster doses and/or natural

infection. The mRNA platform proved more effective in generating a stronger and more durable NAb response and played a highly effective role as a booster vaccine.

Data availability statement

The data of this study can be provided but not the confidential information about the participants. Requests to access the datasets should be directed to ada@ioc.fiocruz.br.

Ethics statement

The studies involving humans were approved by Ethics Committee of Oswaldo Cruz Institute (CEP-IOC) - Fiocruz (license numbers: CAAE 51345021.5.1001.5248 and CAAE 56246022.1.0000.5248) and of Federal University of Rio de Janeiro (license number: 35.303.120.5.0000.5257). The studies were conducted in accordance with the local legislation and institutional requirements. The participants provided their written informed consent to participate in this study.

Author contributions

BC: Data curation, Formal Analysis, Investigation, Methodology, Validation, Writing – original draft. PP: Conceptualization, Data curation, Formal Analysis, Investigation, Methodology, Validation, Visualization, Writing – original draft. ARP: Data curation, Investigation, Methodology, Writing – original draft. AL: Data curation, Investigation, Methodology, Writing – original draft. ASGP: Data curation, Methodology, Writing – original draft, Investigation. AN: Data curation, Investigation, Methodology, Writing – original draft. TRM: Data curation, Investigation, Methodology, Writing – original draft. APA: Data curation, Investigation, Methodology, Writing – original draft. TLM: Investigation, Methodology, Writing – original draft. LF-S: Investigation, Methodology, Writing – original draft, Data curation. AD: Investigation, Writing – original draft, Resources. IH: Investigation, Writing – original draft, Methodology. ASA: Investigation, Methodology, Writing – original draft. SC: Investigation, Methodology, Writing – original draft, Conceptualization, Data curation, Formal Analysis, Validation. AMBA: Conceptualization, Data curation, Formal Analysis, Investigation, Methodology, Validation, Funding acquisition, Project administration, Resources, Supervision, Visualization, Writing – review & editing.

Funding

The author(s) declare that financial support was received for the research and/or publication of this article. This research was funded by the Brazilian National Research Council (CNPq) (grants numbers: 302639/2022-5; 312650/2021-3), the Carlos Chagas Filho Foundation for Research Support of the State of Rio de Janeiro (FAPERJ) (grants numbers: E-26-210.244/2020; E-26/210.784/2021; E-26/211.134/2021; E-26/210.090/2023; E-26/211.128/2021; E-26/204.287/2024), the Oswaldo Cruz Institute and Oswaldo Cruz Foundation, Inova Program (grant number: 135951354149900), the National Institute of Science and Technology in Vaccines (INCTV) (grant number: 573547/2013), the Coordination of Improvement of Higher Education Personnel (CAPES) (grant number: 88887.694977/2022-00).

Acknowledgments

We would like to thank all the volunteers who agreed to participate in this study. Without them, we could not perform such a study. We also acknowledge Dr. Luzia M. O. Pinto (Viral Immunology Laboratory, IOC, Fiocruz – RJ, Brazil) for providing pre-pandemic, non-SARS-CoV-2 exposed samples.

Conflict of interest

The authors declare that the research was conducted in the absence of any commercial or financial relationships that could be construed as a potential conflict of interest.

The author(s) declared that they were an editorial board member of Frontiers, at the time of submission. This had no impact on the peer review process and the final decision.

Generative AI statement

The author(s) declare that no Generative AI was used in the creation of this manuscript.

Publisher's note

Supplementary material

The Supplementary Material for this article can be found online at: https://www.frontiersin.org/articles/10.3389/fimmu.2025.1603612/full#supplementary-material

References

1. Gao Q, Bao L, Mao H, Wang L, Xu K, Yang M, et al. Development of an inactivated vaccine candidate for SARS-CoV-2. *Science*. (2020) 369:77–81. doi: 10.1126/science.abc1932

2. Folegatti PM, Ewer KJ, Aley PK, Angus B, Becker S, Belij-Rammerstorfer S, et al. Safety and immunogenicity of the ChAdOx1 nCoV-19 vaccine against SARS-CoV-2: a preliminary report of a phase 1/2, single-blind, randomised controlled trial. *Lancet*. (2020) 396:467–78. doi: 10.1016/S0140-6736(20)31604-4

3. Polack FP, Thomas SJ, Kitchin N, Absalon J, Gurtman A, Lockhart S, et al. Safety and efficacy of the BNT162b2 mRNA covid-19 vaccine. *N Engl J Med*. (2020) 383:2603–15. doi: 10.1056/NEJMoa2034577

4. Palacios R, Patiño EG, de Oliveira Piorelli R, Conde MTRP, Batista AP, Zeng G, et al. Double-Blind, Randomized, Placebo-Controlled Phase III Clinical Trial to Evaluate the Efficacy and Safety of treating Healthcare Professionals with the Adsorbed COVID-19 (Inactivated) Vaccine Manufactured by Sinovac - PROFISCOV: A structured summary of a study protocol for a randomised controlled trial. *Trials*. (2020) 21:853. doi: 10.1186/s13063-020-04775-4

5. Fadlyana E, Rusmil K, Tarigan R, Rahmadi AR, Prodjosoewojo S, Sofiatin Y, et al. A phase III, observer-blind, randomized, placebo-controlled study of the efficacy, safety, and immunogenicity of SARS-CoV-2 inactivated vaccine in healthy adults aged 18–59 years: An interim analysis in Indonesia. *Vaccine*. (2021) 39:6520–8. doi: 10.1016/j.vaccine.2021.09.052

6. Tanriover MD, Doğanay HL, Akova M, Güner HR, Azap A, Akhan S, et al. Efficacy and safety of an inactivated whole-virion SARS-CoV-2 vaccine (CoronaVac): interim results of a double-blind, randomised, placebo-controlled, phase 3 trial in Turkey. *Lancet*. (2021) 398:213–22. doi: 10.1016/S0140-6736(21)01429-X

7. Voysey M, Clemens SAC, Madhi SA, Weckx LY, Folegatti PM, Aley PK, et al. Safety and efficacy of the ChAdOx1 nCoV-19 vaccine (AZD1222) against SARS-CoV-2: an interim analysis of four randomised controlled trials in Brazil, South Africa, and the UK. *Lancet*. (2021) 397:99–111. doi: 10.1016/S0140-6736(20)32661-1

8. Fonseca MHG, de Souza T de FG, de Carvalho Araújo FM, de Andrade LOM. Dynamics of antibody response to CoronaVac vaccine. *J Med Virol*. (2022) 94:2139–48. doi: 10.1002/jmv.27604

9. Mishra SK, Pradhan SK, Pati S, Sahu S, Nanda RK. Waning of anti-spike antibodies in AZD1222 (ChAdOx1) vaccinated healthcare providers: A prospective longitudinal study. *Cureus*. (2021) 13:e19879. doi: 10.7759/cureus.19879

10. Naaber P, Tserel L, Kangro K, Sepp E, Jürjenson V, Adamson A, et al. Dynamics of antibody response to BNT162b2 vaccine after six months: a longitudinal prospective study. *Lancet Reg Health Eur*. (2021) 10:100208. doi: 10.1016/j.lanepe.2021.100208

11. Feikin DR, Higdon MM, Abu-Raddad LJ, Andrews N, Araos R, Goldberg Y, et al. Duration of effectiveness of vaccines against SARS-CoV-2 infection and COVID-19 disease: results of a systematic review and meta-regression. *Lancet*. (2022) 399:924–44. doi: 10.1016/S0140-6736(22)00152-0

12. SChad F, Thronicke A. Real-world evidence—Current developments and perspectives. *Int J Environ Res Public Health*. (2022) 19:10159. doi: 10.3390/ijerph191610159

13. Food and Drug Administration (FDA). *Guidance for Industry: cPass SARS-CoV-2 Neutralization Antibody Detection Kit* . Available online at: https://www.fda.gov/media/143584/download (Accessed December 16, 2021).

14. Jung J, Rajapakshe D, Julien C, Devaraj S. Analytical and clinical performance of cPass neutralizing antibodies assay. *Clin Biochem*. (2021) 98:70–3. doi: 10.1016/j.clinbiochem.2021.09.008

15. Horbach IS, de Souza Azevedo A, Schwarcz WD, Alves NDS, de Moura Dias B, Setatino BP, et al. Plaque reduction neutralization test (PRNT) accuracy in evaluating humoral immune response to SARS-coV-2. *Diseases*. (2024) 12:29. doi: 10.3390/diseases12010029

16. Fernandes-Siqueira LO, Ferreira FAP, Sousa BG, Mebus-Antunes NC, Neves-Martins TC, Almeida FCL, et al. On the caveats of a multiplex test for SARS-CoV-2 to detect seroconversion after infection or vaccination. *Sci Rep*. (2022) 12:10366. doi: 10.1038/s41598-022-14294-8

17. Khoury DS, Cromer D, Reynaldi A, Schlub TE, Wheatley AK, Juno JA, et al. Neutralizing antibody levels are highly predictive of immune protection from symptomatic SARS-CoV-2 infection. *Nat Med*. (2021) 27:1205–11. doi: 10.1038/s41591-021-01377-8

18. Cromer D, Steain M, Reynaldi A, Schlub TE, Wheatley AK, Juno JA, et al. Neutralising antibody titres as predictors of protection against SARS-CoV-2 variants and the impact of boosting: a meta-analysis. *Lancet Microbe*. (2022) 3:e52–61. doi: 10.1016/S2666-5247(21)00267-6

19. Carpp LN, Hyrien O, Fong Y, Benkeser D, Roels S, Stieh DJ, et al. Neutralizing antibody correlate of protection against severe-critical COVID-19 in the ENSEMBLE single-dose Ad26.COV2.S vaccine efficacy trial. *Nat Commun*. (2024) 15:9785. doi: 10.1038/s41467-024-53727-y

20. Perera RA, Mok CK, Tsang OT, Lv H, Ko RL, Wu NC, et al. Serological assays for severe acute respiratory syndrome coronavirus 2 (SARS-CoV-2), March 2020. *Eurosurveillance*. (2020) 25:2000421. doi: 10.2807/1560-7917.ES.2020.25.16.2000421

21. GenScript USA Inc. *Nanjing GenScript Diagnostics Technology Co., Ltd. cPass SARS-CoV-2 Neutralization Antibody Detection Kit - Instructions for Use*. (2022). Available at: https://www.genscript.com/gsfiles/techfiles/GS%2dSOP%2dCPTS001G%2d05_L00847%2dC.pdf

22. Taylor SC, Hurst B, Martiszus I, Hausman MS, Sarwat S, Schapiro JM, et al. Semi-quantitative, high throughput analysis of SARS-CoV-2 neutralizing antibodies: Measuring the level and duration of immune response antibodies post infection/vaccination. *Vaccine*. (2021) 39:5688–98. doi: 10.1016/j.vaccine.2021.07.098

23. Zhu F, Althaus T, Tan CW, Costantini A, Chia WN, Van Vinh Chau N, et al. WHO international standard for SARS-CoV-2 antibodies to determine markers of protection. *Lancet Microbe*. (2022) 3:e81–2. doi: 10.1016/S2666-5247(21)00307-4

24. Graninger M, Jani CM, Reuberger E, Prüger K, Gaspar P, Springer DN, et al. Comprehensive comparison of seven SARS-coV-2-specific surrogate virus neutralization and anti-spike igG antibody assays using a live-virus neutralization assay as a reference. *Microbiol Spectr*. (2023) 11:e0231422. doi: 10.1128/spectrum.02314-2

25. Tan CW, Chia WN, Qin X, Liu P, Chen MI-C, Tiu C, et al. A SARS-CoV-2 surrogate virus neutralization test based on antibody-mediated blockage of ACE2-spike protein-protein interaction. *Nat Biotechnol*. (2020) 38:1073–8. doi: 10.1038/s41587-020-0631-z

26. Valcourt EJ, Manguiat K, Robinson A, Chen JC-Y, Dimitrova K, Philipson C, et al. Evaluation of a commercially-available surrogate virus neutralization test for severe acute respiratory syndrome coronavirus-2 (SARS-CoV-2). *Diagn Microbiol Infect Dis*. (2021) 99:115294. doi: 10.1016/j.diagmicrobio.2020.115294

27. Adjobimey T, Meyer J, Sollberg L, Bawolt M, Berens C, Kovačević P, et al. Comparison of igA, igG, and neutralizing antibody responses following immunization with moderna, bioNTech, astraZeneca, sputnik-V, johnson and johnson, and sinopharm's COVID-19 vaccines. *Front Immunol*. (2022) 13:917905. doi: 10.3389/fimmu.2022.917905

28. Maher S, Assaly NME, Aly DM, Atta S, Fteah AM, Badawi H, et al. Comparative study of neutralizing antibodies titers in response to different types of COVID-19 vaccines among a group of Egyptian healthcare workers. *Virol J*. (2024) 21:277. doi: 10.1186/s12985-024-02546-0

29. Morales-Núñez JJ, Muñoz-Valle JF, MaChado-Sulbarán AC, Díaz-Pérez SA, Torres-Hernández PC, Panduro-Espinoza BV, et al. Comparison of three different COVID-19 vaccine platforms (CoronaVac, BTN162b2, and Ad5-nCoV) in individuals with and without prior COVID-19: Reactogenicity and neutralizing antibodies. *Immunol Lett*. (2022) 251–252:20–8. doi: 10.1016/j.imlet.2022.10.002

30. Sudjaritruk T, Mueangmo O, Saheng J, Winichakoon P, Salee P, Wongjak W, et al. Comparison of Immunogenicity and Reactogenicity of Five Primary Series of COVID-19 Vaccine Regimens against Circulating SARS-CoV-2 Variants of Concern among Healthy Thai Populations. *Vaccines*. (2023) 11:564. doi: 10.3390/vaccines11030564

31. Muena NA, García-Salum T, Pardo-Roa C, Avendaño MJ, Serrano EF, Levican J, et al. Induction of SARS-CoV-2 neutralizing antibodies by CoronaVac and BNT162b2 vaccines in naïve and previously infected individuals. *eBioMedicine*. (2022) 78:103972. doi: 10.1016/j.ebiom.2022.103972

32. Fadlyana E, Setiabudi D, Kartasasmita CB, Putri ND, Rezeki Hadinegoro S, Mulholland K, et al. Immunogenicity and safety in healthy adults of full dose versus half doses of COVID-19 vaccine (ChAdOx1-S or BNT162b2) or full-dose CoronaVac administered as a booster dose after priming with CoronaVac: a randomised, observer-masked, controlled trial in Indonesia. *Lancet Infect Dis*. (2023) 23:545–55. doi: 10.1016/S1473-3099(22)00800-3

33. do Nascimento TA, Nogami PY, de Oliveira CF, Neto WFF, da Silva CP, Ribeiro ACS, et al. Equal maintenance of anti-SARS-coV-2 antibody levels induced by heterologous and homologous regimens of the BNT162b2, chAdOx1, coronaVac and ad26.COV2.S vaccines: A longitudinal study up to the 4th dose of booster. *Vaccines (Basel)*. (2024) 12:792. doi: 10.3390/vaccines12070792

34. Daher IP, Almeida B da S, de Souza-Silva GA, Marques RF, Soares GHC, Andreata-Santos R, et al. Neutralizing antibody responses after a two-dose regimen with BNT162b2, CoronaVac or ChAdOx1-S in Brazil: Differential neutralization of SARS-CoV-2 omicron variants. *Clin Immunol*. (2025) 276:110492. doi: 10.1016/j.clim.2025.110492

35. Levin EG, Lustig Y, Cohen C, Fluss R, Indenbaum V, Amit S, et al. Waning immune humoral response to BNT162b2 covid-19 vaccine over 6 months. *New Engl J Med*. (2021) 385:e84. doi: 10.1056/NEJMoa2114583

36. Romero-Ibarguengoitia ME, Rivera-Salinas D, Sarti R, Levi R, Mollura M, Garza-Silva A, et al. Efficacy of six different SARS-coV-2 vaccines during a six-month follow-up and five COVID-19 waves in Brazil and Mexico. *Vaccines (Basel)*. (2023) 11:842. doi: 10.3390/vaccines11040842

37. Mok CKP, Cohen CA, Cheng SMS, Chen C, Kwok K, Yiu K, et al. Comparison of the immunogenicity of BNT162b2 and CoronaVac COVID-19 vaccines in Hong Kong. *Respirology*. (2022) 27:301–10. doi: 10.1111/resp.14191

38. Jantarabenjakul W, Chantasrisawad N, Puthanakit T, Wacharapluesadee S, Hirankarn N, Ruenjaiman V, et al. Short-term immune response after inactivated SARS-CoV-2 (CoronaVac®, Sinovac) and ChAdOx1 nCoV-19 (Vaxzevria®, Oxford-AstraZeneca) vaccinations in health care workers. *Asian Pac J Allergy Immunol*. (2022) 40:269–77. doi: 10.12932/AP-250721-1197

39. Kordyukova LV, Moiseenko AV, Serebryakova MV, Shuklina MA, Sergeeva MV, Lioznov DA, et al. Structural and immunoreactivity properties of the SARS-coV-2 spike protein upon the development of an inactivated vaccine. *Viruses*. (2023) 15:480. doi: 10.3390/v15020480

40. Victora PC, Castro PMC, Gurzenda S, Medeiros AC, França GVA, Barros PAJD. Estimating the early impact of vaccination against COVID-19 on deaths among elderly people in Brazil: Analyses of routinely-collected data on vaccine coverage and mortality. *EClinicalMedicine*. (2021) 38:101036. doi: 10.1016/j.eclinm.2021.101036

41. Verbeke R, Hogan MJ, Loré K, Pardi N. Innate immune mechanisms of mRNA vaccines. *Immunity*. (2022) 55:1993–2005. doi: 10.1016/j.immuni.2022.10.014

42. Flaxman A, Marchevsky NG, Jenkin D, Aboagye J, Aley PK, Angus B, et al. Reactogenicity and immunogenicity after a late second dose or a third dose of ChAdOx1 nCoV-19 in the UK: a substudy of two randomised controlled trials (COV001 and COV002). *Lancet*. (2021) 398:981–90. doi: 10.1016/S0140-6736(21)01699-8

43. Zeng G, Wu Q, Pan H, Li M, Yang J, Wang L, et al. Immunogenicity and safety of a third dose of CoronaVac, and immune persistence of a two-dose schedule, in healthy adults: interim results from two single-centre, double-blind, randomised, placebo-controlled phase 2 clinical trials. *Lancet Infect Dis*. (2022) 22:483–95. doi: 10.1016/S1473-3099(21)00681-2

44. Costa Clemens SA, Weckx L, Clemens R, Almeida Mendes AV, Ramos Souza A, Silveira MBV, et al. Heterologous versus homologous COVID-19 booster vaccination in previous recipients of two doses of CoronaVac COVID-19 vaccine in Brazil (RHH-001): a phase 4, non-inferiority, single blind, randomised study. *Lancet*. (2022) 399:521–9. doi: 10.1016/S0140-6736(22)00094-0

45. Meeraus W, Stuurman AL, Durukal I, Conde-Sousa E, Lee A, Maria AS, et al. COVID-19 vaccine booster doses provide increased protection against COVID-19 hospitalization compared with previously vaccinated individuals: Interim findings from the REFORCO-Brazil real-world effectiveness study during Delta and Omicron. *Vaccine*. (2023) 41:6366–78. doi: 10.1016/j.vaccine.2023.08.085

46. Ranzani OT, Hitchings MDT, de Melo RL, de França GVA, Fernandes C de FR, Lind ML, et al. Effectiveness of an inactivated Covid-19 vaccine with homologous and heterologous boosters against Omicron in Brazil. *Nat Commun*. (2022) 13:5536. doi: 10.1038/s41467-022-33169-0

47. Glatman-Freedman A, Bromberg M, Hershkovitz Y, Sefty H, Kaufman Z, Dichtiar R, et al. Effectiveness of BNT162b2 vaccine booster against SARS-coV-2 infection and breakthrough complications, Israel. *Emerg Infect Dis*. (2022) 28:948–56. doi: 10.3201/eid2805.220141

48. Campos GRF, Almeida NBF, Filgueiras PS, Corsini CA, Gomes SVC, de Miranda DAP, et al. Booster dose of BNT162b2 after two doses of CoronaVac improves neutralization of SARS-CoV-2 Omicron variant. *Commun Med (Lond)*. (2022) 2:76. doi: 10.1038/s43856-022-00141-4

49. Cerqueira-Silva T, Katikireddi SV, de Araujo Oliveira V, Flores-Ortiz R, Júnior JB, Paixão ES, et al. Vaccine effectiveness of heterologous CoronaVac plus BNT162b2 in Brazil. *Nat Med*. (2022) 28:838–43. doi: 10.1038/s41591-022-01701-w

50. Acevedo J, Acevedo ML, Gaete-Argel A, Araos R, Gonzalez C, Espinoza D, et al. Neutralizing antibodies induced by homologous and heterologous boosters in CoronaVac vaccines in Chile. *Clin Microbiol Infect*. (2023) 29:541.e1–7. doi: 10.1016/j.cmi.2022.11.017

51. Takheaw N, Liwsrisakun C, Laopajon W, Pata S, Chaiwong W, Inchai J, et al. Levels and durability of neutralizing antibodies against SARS-CoV-2 Omicron and other variants after ChAdOx-1 or BNT162b2 booster in CoronaVac-primed elderly individuals. *Heliyon*. (2023) 9:e15653. doi: 10.1016/j.heliyon.2023.e15653

52. Excler J-L, Saville M, Privor-Dumm L, Gilbert S, Hotez PJ, Thompson D, et al. Factors, enablers and challenges for COVID-19 vaccine development. *BMJ Glob Health*. (2023) 8:e011879. doi: 10.1136/bmjgh-2023-011879

53. Tartof SY, Slezak JM, Fischer H, Hong V, Ackerson BK, Ranasinghe ON, et al. Effectiveness of mRNA BNT162b2 COVID-19 vaccine up to 6 months in a large integrated health system in the USA: a retrospective cohort study. *Lancet*. (2021) 398:1407–16. doi: 10.1016/S0140-6736(21)02183-8

54. Ward H, Whitaker M, Flower B, Tang SN, Atchison C, Darzi A, et al. Population antibody responses following COVID-19 vaccination in 212,102 individuals. *Nat Commun*. (2022) 13:907. doi: 10.1038/s41467-022-28527-x

55. Walsh EE, Frenck RW, Falsey AR, Kitchin N, Absalon J, Gurtman A, et al. Safety and immunogenicity of two RNA-based covid-19 vaccine candidates. *N Engl J Med*. (2020) 383:2439–50. doi: 10.1056/NEJMoa2027906

56. Ramasamy MN, Minassian AM, Ewer KJ, Flaxman AL, Folegatti PM, Owens DR, et al. Safety and immunogenicity of ChAdOx1 nCoV-19 vaccine administered in a prime-boost regimen in young and old adults (COV002): a single-blind, randomised, controlled, phase 2/3 trial. *Lancet*. (2020) 396:1979–93. doi: 10.1016/S0140-6736(20)32466-1

57. Boedecker-Lips SC, Lautem A, Runkel S, Klimpke P, Kraus D, Keil P, et al. Six-month follow-up after vaccination with BNT162b2: SARS-coV-2 antigen-specific cellular and humoral immune responses in hemodialysis patients and kidney transplant recipients. *Pathogens*. (2022) 11:67. doi: 10.3390/pathogens11010067

58. Mori M, Yokoyama A, Shichida A, Sasuga K, Maekawa T, Moriyama T. Impact of sex and age on vaccine-related side effects and their progression after booster mRNA COVID-19 vaccine. *Sci Rep*. (2023) 13:19328. doi: 10.1038/s41598-023-46823-4

59. Mistry P, Barmania F, Mellet J, Peta K, Strydom A, Viljoen IM, et al. SARS-coV-2 variants, vaccines, and host immunity. *Front Immunol*. (2022) 12:809244. doi: 10.3389/fimmu.2021.809244

60. Kuzmina A, Khalaila Y, Voloshin O, Keren-Naus A, Boehm-Cohen L, Raviv Y, et al. SARS-CoV-2 spike variants exhibit differential infectivity and neutralization resistance to convalescent or post-vaccination sera. *Cell Host Microbe*. (2021) 29:522–528.e2. doi: 10.1016/j.chom.2021.03.008

61. Garcia-Beltran WF, Lam EC, St Denis K, Nitido AD, Garcia ZH, Hauser BM, et al. Multiple SARS-CoV-2 variants escape neutralization by vaccine-induced humoral immunity. *Cell*. (2021) 184:2372–2383.e9. doi: 10.1016/j.cell.2021.03.013

62. Dejnirattisai W, Huo J, Zhou D, Zahradník J, Supasa P, Liu C, et al. SARS-CoV-2 Omicron-B.1.1.529 leads to widespread escape from neutralizing antibody responses. *Cell*. (2022) 185:467–484.e15. doi: 10.1016/j.cell.2021.12.046

63. Wang Q, Iketani S, Li Z, Liu L, Guo Y, Huang Y, et al. Alarming antibody evasion properties of rising SARS-CoV-2 BQ and XBB subvariants. *Cell*. (2023) 186:279–286.e8. doi: 10.1016/j.cell.2022.12.018

64. Goldblatt D, Alter G, Crotty S, Plotkin SA. Correlates of protection against SARS-CoV-2 infection and COVID-19 disease. *Immunol Rev*. (2022). 6–26. doi: 10.1111/imr.13091

65. Pérez-Then E, Lucas C, Monteiro VS, Miric M, Brache V, Cochon L, et al. Neutralizing antibodies against the SARS-CoV-2 Delta and Omicron variants following heterologous CoronaVac plus BNT162b2 booster vaccination. *Nat Med*. (2022) 28:481–5. doi: 10.1038/s41591-022-01705-6

66. Yorsaeng R, Suntronwong N, Phowatthanasathian H, Assawakosri S, Kanokudom S, Thongmee T, et al. Immunogenicity of a third dose viral-vectored COVID-19 vaccine after receiving two-dose inactivated vaccines in healthy adults. *Vaccine*. (2022) 40:524–30. doi: 10.1016/j.vaccine.2021.11.083

67. Anichini G, Terrosi C, Gandolfo C, Gori Savellini G, Fabrizi S, Miceli GB, et al. SARS-coV-2 antibody response in persons with past natural infection. *N Engl J Med*. (2021) 385:90–2. doi: 10.1056/NEJMc2103825

68. Bates TA, McBride SK, Leier HC, Guzman G, Lyski ZL, Schoen D, et al. Vaccination before or after SARS-CoV-2 infection leads to robust humoral response and antibodies that effectively neutralize variants. *Sci Immunol*. (2022) 7:eabn8014. doi: 10.1126/sciimmunol.abn8014

69. Srivastava K, Carreño JM, Gleason C, Monahan B, Singh G, Abbad A, et al. SARS-CoV-2-infection- and vaccine-induced antibody responses are long lasting with an initial waning phase followed by a stabilization phase. *Immunity*. (2024) 57:587–599.e4. doi: 10.1016/j.immuni.2024.01.017

70. Lake DF, Roeder AJ, Gonzalez-Moa MJ, Koehler M, Kaleta E, Jasbi P, et al. Third COVID-19 vaccine dose boosts neutralizing antibodies in poor responders. *Commun Med*. (2022) 2:1–7. doi: 10.1038/s43856-022-00151-2

71. Zheng Y, Pan J, Jin M, Wang J, Tung T-H, Chen S, et al. Efficacy of the neutralizing antibodies after the booster dose on SARS-CoV-2 Omicron variant and a two-year longitudinal antibody study on Wild Type convalescents. *Int Immunopharmacol*. (2023) 119:110151. doi: 10.1016/j.intimp.2023.110151

72. Monge S, Rojas-Benedicto A, Olmedo C, Mazagatos C, José Sierra M, Limia A, et al. Effectiveness of mRNA vaccine boosters against infection with the SARS-CoV-2 omicron (B.1.1.529) variant in Spain: a nationwide cohort study. *Lancet Infect Dis*. (2022) 22:1313–20. doi: 10.1016/S1473-3099(22)00292-4

73. Zedan HT, Nasrallah GK. Effectiveness of mRNA booster doses against the omicron variant. *Lancet Infect Dis*. (2022) 22:1257–8. doi: 10.1016/S1473-3099(22)00319-X

74. Grewal R, Nguyen L, Buchan SA, Wilson SE, Nasreen S, Austin PC, et al. Effectiveness of mRNA COVID-19 vaccine booster doses against Omicron severe outcomes. *Nat Commun*. (2023) 14:1273. doi: 10.1038/s41467-023-36566-1

frontiers | Frontiers in Immunology

TYPE Original Research
PUBLISHED 18 August 2025
DOI 10.3389/fimmu.2025.1639825

OPEN ACCESS

EDITED BY
Fabio Fiorino,
LUM University Giuseppe Degennaro, Italy

REVIEWED BY
Hauke Thomsen,
Medical School Berlin, Germany
Jianming James Tang,
University of Alabama at Birmingham,
United States

*CORRESPONDENCE
Juan Francisco Gutiérrez-Bautista
juanfry@ugr.es
Juan Sainz
jsainz@ugr.es

†These authors have contributed equally to this work

RECEIVED 02 June 2025
ACCEPTED 28 July 2025
PUBLISHED 18 August 2025
CORRECTED 21 August 2025

CITATION
Cabrera-Serrano AJ, Ruiz-Durán L, Gutiérrez-Bautista JF, Carretero-Fernández M, ter Horst R, Li Y, Reyes-Zurita FJ, García-Verdejo FJ, Netea MG, Sánchez-Rovira P, López-Nevot MÁ, Sampedro A and Sainz J (2025) A genome-wide association study identifies new loci associated with response to SARS-CoV-2 mRNA-1273 vaccine in a cohort of healthy healthcare workers. *Front. Immunol.* 16:1639825. doi: 10.3389/fimmu.2025.1639825

A genome-wide association study identifies new loci associated with response to SARS-CoV-2 mRNA-1273 vaccine in a cohort of healthy healthcare workers

Antonio José Cabrera-Serrano[1,2], Lucía Ruiz-Durán[1,2], Juan Francisco Gutiérrez-Bautista[1,2,3,4*†], María Carretero-Fernández[1,2], Rob ter Horst[5,6,7], Yang Li[5,8], Fernando Jesús Reyes-Zurita[9], Francisco José García-Verdejo[1,10], Mihai G. Netea[5,11], Pedro Sánchez-Rovira[1,10], Miguel Ángel López-Nevot[2,3,4], Antonio Sampedro[2,12] and Juan Sainz[1,2,9,13*†]

[1]Genomic Oncology Area, GENYO, Centre for Genomics and Oncological Research: Pfizer/University of Granada/Andalusian Regional Government, Parque Tecnológico de Ciencias de la Salud (PTS), Granada, Spain, [2]Instituto de Investigación Biosanitaria IBs.Granada, Granada, Spain, [3]Servicio de Análisis Clínicos e Inmunología, University Hospital Virgen de las Nieves, Granada, Spain, [4]Departamento de Bioquímica, Biología Molecular e Inmunología III, University of Granada, Granada, Spain, [5]Department of Internal Medicine and Radboud Center for Infectious Diseases, Radboud University Nijmegen Medical Center, Nijmegen, Netherlands, [6]CeMM Research Center for Molecular Medicine of the Austrian Academy of Sciences, Vienna, Austria, [7]Medical University of Vienna, Center for Medical Data Science, Institute of Artificial Intelligence, Vienna, Austria, [8]Centre for Individualised Infection Medicine (CiiM) & TWINCORE, joint ventures between the Helmholtz-Centre for Infection Research (HZI) and the Hannover Medical School (MHH), Hannover, Germany, [9]Department of Biochemistry and Molecular Biology I, Faculty of Sciences, University of Granada, Granada, Spain, [10]Department of Medical Oncology, Complejo Hospitalario de Jaén, Jaén, Spain, [11]Department for Immunology & Metabolism, Life and Medical Sciences Institute (LIMES), University of Bonn, Bonn, Germany, [12]Servicio de Microbiología, University Hospital Virgen de las Nieves, Granada, Spain, [13]Centro de Investigación Biomédica en Red de Epidemiología y Salud Pública (CIBERESP), Madrid, Spain

Introduction: The COVID-19 pandemic had significant global public health consequences, affecting over 200 countries and regions by 2020. The development and efficacy of specific vaccines, such as the mRNA-1273 (Spikevax®) vaccine developed by Moderna Inc., have substantially reduced the impact of the pandemic and mitigated its consequences. This study aims to identify novel genetic loci associated with the effectiveness of the mRNA-1273 vaccine, as measured by elevated anti-Spike (anti-S) IgG levels at multiple time points post-vaccination.

Materials and methods: We conducted three genome-wide association studies (GWAS) in a cohort of Spanish healthcare workers, analyzing anti-S IgG levels at one-month post-vaccination (n=567), at three months post-vaccination (n=447), and the difference in circulating anti-S IgG levels between these two time points (n=447).

Results: We identified fourteen novel loci associated with increasing concentrations of anti-S IgG post-vaccination (p=5.01x10^{-13} and p=2.81x10^{-8}). Functional results showed that some of the novel risk alleles influence the absolute counts of specific B cell subsets (p=2.57x10^{-5}-8.82x10^{-3}), which are

involved in immune signaling pathways and metabolic processes. Furthermore, these variants co-localize with multiple QTLs and epigenetic marks, suggesting that the GWAS hits may affect regulatory activity in promoters, enhancers, and transcriptional regions, thereby modulating gene expression relevant to the humoral immune response.

Discussion: In conclusion, this study highlights the complex interplay of genetic factors influencing the immune response to vaccination, particularly through modulation of B cell activity, immune signaling pathways, and metabolic processes. The identification of genetic variants could inform future strategies to enhance vaccine efficacy and provide a deeper understanding of individual variability in vaccine responses, especially for COVID-19 and other viral infections.

KEYWORDS

SARS-CoV-2, GWAS, circulating IgG levels, genetic variants, IgG decay

Introduction

The SARS-CoV-2 pandemic had a profound impact on the global population. As of June 2020, the virus spread to over 200 countries and territories, affecting diverse populations and communities (1). Since the emergence of the virus in 2019, more than 775 million infections and about 7 million deaths have been reported because of this infection (2), although these numbers are likely to be underestimated.

Advanced age and the presence of comorbidities such as hypertension, diabetes, and cardiovascular disease have been identified as significant risk factors for severe complications from SARS-CoV-2 infection (3). These underlying conditions can increase the vulnerability of individuals to the virus, as it enters host cells through the angiotensin-converting enzyme 2 (ACE2) receptor, which is present in a wide range of tissues and organs (4). Additionally, chronic lung diseases, including chronic obstructive pulmonary disease and interstitial lung diseases such as idiopathic pulmonary fibrosis, have been associated with a higher risk of hospitalization and mortality among SARS-CoV-2 patients (5). The evasion from the effects of the type I interferon response by SARS-CoV-2 is another critical factor contributing to its ability to cause severe disease (6). This immune evasion mechanism allows the virus to replicate and spread more efficiently, leading to the development of acute respiratory distress syndrome and other life-threatening complications (6).

Given the significant morbidity and mortality, the development and distribution of effective and safe vaccines have become a top priority (7). Vaccination efforts against SARS-CoV-2 have been rapid and widespread, with a significant proportion of the global population having received at least one vaccine dose. These vaccines, including those based on messenger RNA (mRNA), viral vectors, recombinant proteins, and inactivated virus platforms, primarily aim to generate a humoral immune response against the SARS-CoV-2 spike (S) protein, which plays a crucial role in the ability of the virus to infect host cells (8).

Numerous studies have investigated the response of different populations to SARS-CoV-2 vaccines (8–12). The immune response to the vaccines has been found to be generally robust in the general population, with the vaccines demonstrating high efficacy in reducing the risk of severe disease and hospitalization (8, 12). One of the most widely used SARS-CoV-2 vaccines is the mRNA-1273 vaccine (Spikevax®), developed by Moderna Inc. in collaboration with the National Institute of Allergy and Infectious Diseases (11). The mRNA-1273 vaccine, similar to the BNT162b2 vaccine developed by BioNtech and Pfizer, utilizes mRNA technology to enable the production of the full-length SARS-CoV-2 S protein, which triggers an immune response (10) While these mRNA vaccines have been shown to be highly effective in preventing SARS-CoV-2 infections and severe disease, there is growing interest in understanding the factors that may influence individual responses to these vaccines (9). Some studies have linked humoral and cellular responses to mRNA vaccination to human leukocyte antigen (HLA) molecules (13–15). However, relatively few studies have explored the association between genetic polymorphisms and vaccine response. Genome-wide association studies (GWAS) have emerged as a powerful tool for identifying genetic variants linked to various traits and diseases, including immune responses to vaccines (16, 17). With respect to SARS-CoV-2 infection, numerous studies have identified polymorphisms related to severity, infection, and disease susceptibility (18–20), but only a few have shown alterations in IgG responses and altered cytokine profiles post-vaccination (21–23).

Understanding the genetic factors that influence vaccine response is crucial for optimizing vaccination strategies and identifying individuals at risk of suboptimal immune responses. By elucidating the genetic architecture underlying the response to the mRNA-1273 vaccine, this study aims to provide insights that can facilitate and accelerate the development of improved vaccination approaches, contribute to ongoing efforts to combat SARS-CoV-2, and enhance our understanding of the response to mRNA vaccines. To this end, we conducted, for the first time, a

GWAS involving 601 Spanish healthcare workers, correlating their genetic data with their humoral immune response to the mRNA-1273 vaccine.

Materials and methods

Study population

The study included 601 healthy healthcare workers (399 women and 202 men) recruited from the Virgen de las Nieves University Hospital in Granada, Spain. All participants received the mRNA-1273 vaccine (Moderna). Eligibility criteria required the absence of prior SARS-CoV-2 infection, verified through review of clinical history, RT-PCR testing, and institutional serological screenings. Individuals with any previous positive PCR or serological result were excluded. A follow-up antibody determination was performed at 30 and 90 days after vaccination.

All biological samples were collected in accordance with local medical ethics regulations, following the provision of informed consent by the participants, their legal representatives, or both, in line with guidelines reported in the Declaration of Helsinki. The study protocol was reviewed and approved by the regional ethics committee (Portal de Ética de la Investigación Biomédica, Junta de Andalucía, code: 0297-N-21).

Antibodies against SARS-CoV-2 quantification

Participants underwent blood extraction at 1 month (30 days) and 3 months (90 days) after receiving the second vaccine dose of the mRNA-1273 vaccine. Quantitative determination of IgG antibodies against the SARS-CoV-2 Spike (S) protein was performed. Circulating anti-Spike IgG levels were quantified using chemiluminescent SARS-CoV-2 IgG assay (Alinity, Abbott, USA), following the manufacturer's instructions. Results are expressed in binding antibody units per milliliter (BAU/mL), with a positivity cutoff set at >7.5 BAU/mL.

It is important to note that anti-Spike IgG levels are used in this study as a surrogate marker of the humoral immune response. Although such measurements provide a standardized and widely accepted indication of prior immunologic exposure or response to vaccination, they do not directly measure neutralizing antibody activity or functional immune protection. Therefore, the results should be interpreted within the context of known limitations of binding antibody assays, and not as definitive correlates of vaccine-induced clinical protection against SARS-CoV-2 infection.

DNA extraction and quantification

All blood samples were stored at −80°C until analysis. DNA extraction was carried out at GENYO (Centre for Genomics and Oncological Research: Pfizer/University of Granada/Andalusian Regional Government, Granada, Spain) using QIAamp DNA Blood kits (Valencia, CA, USA) according to the manufacturer's instructions. DNA concentration and quality were measured using Qubit 4 Fluorometer (Thermo Fisher, Applied Biosystems, Waltham MA, USA).

Genome-wide associations analyses

All individuals included in the GWAS were genotyped using the Infinium™ Global Screening Array-24 v3.0 BeadChip (Illumina, San Diego, CA, USA). Extensive quality control metrics were applied to the data using R v3.3.1 and PLINK v1.90p software. Samples were excluded if there was sex discordance, a call rate of <90%, minimal or excessive heterozygosity (>3 SDs from the mean), estimated relatedness (Pihat≥0.2) or if they were identified as non-European based on principal components analysis (PCA). The PCA was performed with PLINK v1.90b, including the genotypes from phase 3 of the 1000 Genomes Project as the reference panel (24).

Genetic variants were excluded if they showed a significant deviation from Hardy–Weinberg equilibrium (HWE<1×10^{-5}), had minor allele frequency (MAF) of <0.05, or a genotype call rate of ≤90%. Genome-wide imputation was then performed using the Michigan Imputation Server (https://imputationserver.sph.umich.edu/index.html) and the Haplotype Reference Consortium reference haplotype panel (HRC V.r1.1; http://www.haplotype-reference-consortium.org/) (25). All variants with an imputation R^2<0.3 were excluded from subsequent analysis. PLINK v1.90p was used to perform all GWAS analysis. To identify independent SNPs, we utilized data from LDLink for European cohorts (https://ldlink.nih.gov/?tab=home). SNPs were considered independent if they met the criteria of r^2<0.1 and D'<0.2.

To ensure the accuracy and comparability of the genetic association analysis, the IgG phenotypes were normalized using Z-score transformation prior to conducting the GWAS. We conducted linear regression analysis to examine the association between SNPs and circulating IgG levels, adjusting for sex, age and the top ten principal components. Genomic control (GC) adjustment to ensure the robustness and validity of our analysis.

We conducted three GWAS to investigate genetic factors associated with IgG levels at different time points. Specifically, the first GWAS focused on IgG quantification measured during the first month, while the second analysis assessed IgG levels at the third month. A third GWAS was performed to analyze the absolute differences in IgG levels between these two time points. This design allowed us to capture both static and dynamic changes in IgG levels over time, enabling the identification of genetic variants potentially influencing baseline IgG production, temporal changes, and overall immune dynamics.

Functional effect of GWAS hits and cytokine quantitative trait loci, circulating levels of inflammatory proteins, blood-derived cell populations, and steroid hormones

To provide insight into the functional role of the novel SNPs identified through the GWAS, we performed *in vitro* stimulation experiments and measured cytokine production (IFNγ, IL1Ra, IL1β,

IL6, IL8, IL10, TNFα, IL17, and IL22) after stimulation of peripheral blood mononuclear cells (PBMCs), whole blood (WB) or monocyte-derived macrophages (MDMs) with LPS (1 or 100 ng/ml), PHA (10µg/ml), Pam3Cys (10µg/ml), CpG (ODN M362; 10µg/ml), *Escherichia coli*, and *Staphylococcus aureus*. Stimulation experiments were conducted on 408 healthy subjects of the 500FG of the Human Functional Genomics Project (HFGP) according to previously reported protocols (26, 27).

A proteomic analysis was also performed on serum and plasma samples from the 500FG cohort. Circulating protein concentrations were measured using the commercial Olink® Inflammation panel (Olink, Sweden), resulting in the quantification of 103 different biomarkers (Supplementary Table 1). Protein concentrations were expressed on a $\log_2$ scale as normalized protein expression values and were further normalized using bridging samples to correct for batch variation (27).

Additionally, we tested the association of GWAS hits with absolute numbers of 91 blood-derived cell populations (Supplementary Table 2). Blood-derived cell populations were measured by 10-color flow cytometry (Navios flow cytometer, Beckman Coulter, Miami, FL, USA) after blood sampling (2–3 h), and cell count analysis was performed using Kaluza software (Beckman Coulter, v.1.3). To reduce inter-experimental noise and increase statistical power, cell count analysis was performed by calculating parental and grandparental percentages, which were defined as the percentage of a certain cell type within the subpopulation of the cells from which it was isolated. Detailed laboratory protocols for cell isolation, reagents, gating strategies, and flow cytometry analysis, as well as methodological details of the functional experiments, have been reported elsewhere (28, 29).

Given the impact of sex on the response to mRNA vaccines for SARS-CoV-2A, as well as the influence of steroid hormones on immune responses, we also evaluated the association of GWAS markers with circulating concentrations of seven steroid hormones (androstenedione, cortisol, 11-deoxy-cortisol, 17-hydroxy-progesterone, progesterone, testosterone and 25-hydroxy vitamin D3) in a subset of the 500FG cohort, excluding individuals undergoing hormonal replacement therapy or taking oral contraceptives (n=279) (27).

Finally, in order to test if genetic markers were associated with baseline serum levels of immunoglobulin IgG and its subclasses were measured by immunonephelometry using Beckman Coulter reagents and a Beckman Coulter Imager according to previously reported protocols.

In order to account for multiple comparisons, we used a significance threshold of 4.62×10^{-4} (0.05/12 SNPs/9 cytokines), $p=4.04\times10^{-5}$ (0.05/12 SNPs/103 inflammatory proteins, $p=4.58\times10^{-5}$ (0.05/12 SNPs/91 blood cell types), 5.95×10^{-4} (0.05/12 SNPs/7 hormones) 4.16×10^{-3} (0.05/12 SNPs IgG levels) for the cytokine quantitative trait loci, proteomic, blood cell counts, steroid hormone analyses and IgG levels, respectively. All functional analyses were performed using R v4.2.2 software (https://www.r-project.org/) adjusted by age and sex as covariates, using custom scripts in the R programming language based on existing functions. Functional plots were displayed using Graphpad Prism v8.0.1 (Graphpad Software, San Diego, CA, USA). All data used in this project have been meticulously cataloged and archived in the BBMRI-NL data infrastructure (https://hfgp.bbmri.nl/) using the MOLGENIS open-source platform for scientific data (30). This allows flexible data querying and download, including sufficiently rich metadata and interfaces for machine processing (R statistics, REST API) and using FAIR principles to optimize Findability, Accessibility, Interoperability, and Reusability (31).

Bioinformatic and in silico analyses

Annotation and biological interpretation of genome-wide significant association results were performed using publicly available bioinformatic tools, including the FUMA-GWAS platform (https://fuma.ctglab.nl/) (32) and the Open Targets Platform (https://platform.opentargets.org/) (33). We also tested whether the associated SNPs could represent expression quantitative trait loci (eQTL) acrossdifferent cell types and tissues using data from the GTEx portal (https://gtexportal.org/home/) (34) and QTLbase (http://www.mulinlab.org/qtlbase) (35), which aggregates functional QTL data from sources such as TCGA, GTEx, Pancan-MNVQTLdb, and DICE. To complete these functional analyses, meta-scores were developed, integrating diverse annotations or individual scores into a single quantitative score using Combined Annotation Dependent Depletion (CADD) (36) and Regulome DB (https://regulomedb.org/) (37).

These in silico analyses were conducted in an exploratory framework, and we emphasize that they do not constitute direct experimental validation.Annotations were considered of potential interest if they met a nominal significance threshold ($p<1\times10^{-3}$) and/or were supported by at least two independent tools among FUMA-GWAS, Open Targets Platform, GTEx, QTLbase, CADD, and RegulomeDB, in order to increase the reliability of the functional prioritization. The GC value was calculated using the "QCEWAS" (38) package from R v4.2.2 software to estimate the inflation rate for each GWAS. Quantile-quantile (Q-Q) plots and Manhattan plots were generated using "qqplot" (39) and "qqman" (40) procedures in R v3.3.1.

Results

A total of 601 healthy healthcare workers were recruited at the Virgen de las Nieves University Hospital (Granada, Spain), including 399 women and 202 men. After applying quality control filters, antibody determination during the first 30 days was conducted in a cohort of 567 individuals (366 women and 201 men). The overall mean age was 48.1 years (range: 21-68 years), with a mean of 48.8 years for women (range: 21-66 years) and 46.6 years for men (range: 23-68 years). At the time of the second antibody determination, conducted 90 days after vaccination, 447 participants were included (294 women and 153 men). The mean age was 49.5 years (range: 22–68 years), with 50.0 years for men (range: 22–66) and 47.8 years for women (range: 23–68 years) (Table 1). While most participants showed a decline in IgG levels between the first and second determinations, only 2

individuals (0.45%) exhibited increased IgG titers at 90 days, indicating minimal upward variation at the individual level.

We also evaluated the potential effect of age and sex on IgG concentrations at both time points (Supplementary Table 3). Sex had a statistically significant impact on antibody levels: men showed higher median IgG titers than women at both 1 month (3570.5 vs. 2697.3 AU/mL; p = 0.00079) and 3 months (1305.8 vs. 991.6 AU/mL; p = 0.00048) post-vaccination. A slight difference in age between sexes was observed at 1 month (p = 0.035), but not at 3 months (p = 0.309), and we found no strong overall correlation between age and IgG levels. Based on these findings, all GWAS analyses were adjusted for age and sex to account for their potential confounding effects.

Genome-wide genetic analyses

After quality control, three GWAS were conducted. The first included a total of 567 individuals and corresponded to data collected one month after vaccination. The second GWAS included 447 individuals, a subset of the original cohort, and was based on data collected three months after vaccination. The third GWAS, also with 447 individuals, compared antibody responses between 1- and 3-months post-vaccination. The GC factor (lambda) was adjusted to 1.001 for all GWAS, indicating minimal inflation of test statistics due to population structure. The Q-Q plot did not show evidence of systematic inflation (Supplementary Figures 1A–C), confirming the absence of hidden population substructure or cryptic relatedness.

GWAS at 1-month post-vaccination

In the GWAS at 1-month post-vaccination, nine novel independent genetic signals were identified associated with circulating IgG concentrations (Table 2, Figure 1).

GWAS analyses were conducted using linear regression with PLINK software. Estimates calculated according to a log-additive model of inheritance and adjusted for age, sex and 10 first principal components.

The two most statistically significant associations were *ENSG00000295231|ALDH1A2*$_{rs1350209880}$ and *CYP26B1*$_{rs72845602}$ (Table 2), which map to a LncRNA gene upstream *ALDH1A2* (Aldehyde Dehydrogenase 1 Family Member A2 gene, 15q21.3) and downstream of the CYP26B1 (Cytochrome P450 Family 26 Subfamily B Member 1 gene, 2p13.2, Supplementary Figure 2A). The other seven novel associations were for the *SLC6A11|LINC00606*$_{rs4088054}$, *TMOD1*$_{rs117643807}$, *CDK14*$_{rs7792239}$, *SMASR|SMAD3-DT*$_{rs28485994}$, *CCDC172|PNLIPRP3*$_{rs7907582}$, *GRIN2A|LOC105371076*$_{rs34340658}$ and *SNX24|LOC124901213*$_{rs55770715}$ SNPs (Table 2, Supplementary Figures 2B–H). At functional level, we found, for the first time, a significant association of the *CDK14*$_{rs7792239A}$ allele with increased absolute numbers of IgD^-CD5^+ immature memory B lymphocytes (p=2.57×10^{-5}, Figure 2A) and potential associations with increased absolute numbers of other immature memory B lymphocytes, including IgD^-IgM^-, $CD24^+CD38^+$ and IgD^-IgM^+ (p=2.38×10^{-3}; p=2.99×10^{-3} and p=8.82×10^{-3}, respectively, Figures 2B, 4D).

In addition, carriers of the *SNX24|LOC124901213*$_{rs55770715A}$ allele had lower expression levels of *SNX24* mRNAs in different tissues (p=9.63×10^{-6}-2.60×10^{-4}, Supplementary Table 4, Supplementary Figures 2C, 5A, B). Interestingly, we also identified 19 novel potentially interesting associations with increased circulating concentrations of IgG at 1-month post-vaccination, which remained borderline significant. These association signals were located near the *ENSG00000307057*, *TNFSF4|LOC100506023*, *THOC1|COLEC12*, *METTL8*, *UOX*, *ZNF516*, *PLCB1*, *SOCS3*, *ENSG00000232855|ENSG00000307297*, *CACNA1A*, *PLXNC1*, *ENSG00000234703|RUNX1*, *LYZL1*, *ENSG00000300202*, *LOC105369715*, *ENSG00000226566|ENSG00000307505*, *ENSG00000229618*, *PLAT* and *RNU6-1326P|USP25 loci* (p=7.76×10^{-8} – 5.41×10^{-7}, Supplementary Table 5).

TABLE 1 Description of study cohorts.

Variable	*Cohort for 1 month (N=567)*	*Cohort for 3 months (N=447)*	*Cohort for 1-3 months (N=447)*
Age (years)	48.19 ± 11.49	49.50 ± 11.10	49.50 ± 11.10
Sex ratio (female/male)	1.82 (366/201)	1.92 (294/153)	1.92 (294/153)
*Anti-S IgG (BAU/mL)**	2424.31 (1543.41-3891.87)	892.09 (520.63-1469.24)	1526.62 (998.3-2401.49)

*Values are presented as Median (IQR). IQR, Interquartile Range.

GWAS at 3 months post-vaccination

In the GWAS at 3 months post-vaccination, two novel independent genetic signals were identified associated with increased circulating IgG levels (Figure 3). These two significant associations were the *SMASR|SMAD3-DT*$_{rs28485994}$ and *ATP2B2*$_{rs55725269}$ (OR=2.15, p=3.66×10^{-12} and OR=2.25, p=7.62×10^{-9}, respectively, Table 2).

The first signal maps between two LncRNA genes on chromosome 15q21.3 while the second is located downstream of the ATPase Plasma Membrane Ca^{2+} Transporting 2 gene on chromosome 3p25.3 (Supplementary Figure 3). Interestingly, these signals were previously identified in the GWAS after 1 month vaccine, with the first being identified directly and the second associated with *SLC6A11|LINC00606*$_{rs4088054}$, which shows modest LD (D'=1.00 and r^2 = 0.584). Additionally, we identified nine novel potential associated signals with borderline significance in the *NUAK1|CKAP4*, *ST6GALNAC3*, *LOC105379385*, *GPRC5A*, *GTDC1*, *FILNC1*, *CEP128*, *LOC105376235* and *COL25A1 loci* associated with de increased levels of IgG after third month vaccine (p=1.58×10^{-7}-9.58×10^{-7}, Supplementary Table 5).

GWAS for differential antibody responses at 1 vs 3 months post-vaccination

In the third GWAS, conducted to evaluate the differences in circulating IgG levels between 1 and 3 months we identified nine

TABLE 2 Genome-wide significant associations with antibody production identified in GWASs.

GWASs	SNP	Chr	Position	Alt/Ref	Nearest gene(s)	Consequence	MAF	MAF (1,000 Genomes)	Beta	Standard error	P_{value}
GWAS 1	rs1350209880	15	58183817	A/T	*ENSG00000295231* | *ALDH1A2*	LncRNA | Upstream gene variant	0.060	0.00004	0.785	0.113	1.12×10^{-11}
	rs72845602 δ	2	72347224	T/C	*CYP26B1*	Downstream gene variant	0.053	0.040	0.845	0.126	5.72×10^{-11}
	rs4088054 γ	3	10808633	T/A	*SLC6A11* | *LINC00606*	Intergenic | Upstream gene variant	0.093	0.088	0.654	0.106	1.71×10^{-09}
	rs117643807	9	100352774	T/C	*TMOD1*	Intron variant	0.068	0.067	0.724	0.121	4.37×10^{-09}
	rs7792239	7	90808856	A/G	*CDK14*	Intron variant	0.067	0.105	0.773	0.130	5.93×10^{-09}
	rs28485994	15	67257395	C/T	*SMASR* | *SMAD3-DT*	Intergenic variant	0.097	0.094	0.588	0.100	8.13×10^{-09}
	rs7907582	10	118144424	C/G	*CCDC172* | *PNLIPRP3*	Intergenic variant	0.069	0.087	0.674	0.117	1.41×10^{-08}
	rs34340658	16	10129731	T/C	*GRIN2A* | *LOC105371076*	Intron variant	0.124	0.095	0.539	0.094	2.04×10^{-08}
	rs55770715	5	122347325	A/G	*SNX24* | *LOC124901213*	Intergenic variant	0.061	0.041	0.738	0.130	2.78×10^{-08}
GWAS 2	rs28485994	15	67257395	C/T	*SMASR* | *SMAD3-DT*	Intergenic variant	0.097	0.094	0.768	0.110	3.66×10^{-12}
	rs55725269 γ	3	10799545	A/G	*ATP2B2*	Downstream gene variant	0.057	0.054	0.812	0.140	7.62×10^{-09}
GWAS 3	rs1350209880	15	58183817	A/T	*ENSG00000295231* | *ALDH1A2*	LncRNA | Upstream gene variant	0.060	0.00004	0.915	0.122	5.01×10^{-13}
	rs117643807	9	100352774	T/C	*TMOD1*	Intron variant	0.068	0.067	0.932	0.139	1.04×10^{-10}
	rs75197984 δ	2	54765683	T/C	*SPTBN1*	Intron variant	0.059	0.063	0.863	0.131	1.97×10^{-10}
	rs7907582	10	118144424	C/G	*CCDC172* | *PNLIPRP3*	Intergenic variant	0.069	0.087	0.779	0.126	2.15×10^{-09}
	rs7792239	7	90808856	A/G	*CDK14*	Intron variant	0.067	0.105	0.873	0.145	5.65×10^{-09}
	rs1125991	2	172263448	A/T	*METTL8*	Intron variant	0.083	0.072	0.706	0.118	7.71×10^{-09}
	rs34340658	16	10129731	T/C	*GRIN2A* | *LOC105371076*	Intron variant	0.124	0.095	0.669	0.112	8.64×10^{-09}
	rs4630616	17	76330484	A/G	*LOC105371912*	Intron variant	0.153	0.176	0.626	0.107	1.78×10^{-08}
	rs55919500	20	8072501	A/G	*PLCB1*	Intron variant	0.065	0.101	0.805	0.140	2.81×10^{-08}

SNP, single nucleotide polymorphism; Chr, Chromosome; Alt, alternative allele; Ref, reference allele; MAF, minor allele frequency; OR, odds ratio; CI, confidence interval; P, P-value; Phet, P-value of heterogeneity.

[δ]rs72845602 and rs75197984 are in modest linkage disequilibrium (D' = 0.601; r^2 = 0.001).

[γ]rs4088054 and rs55725269 are in complete linkage disequilibrium with the rs3745990 (D' = 1.00; r^2 = 0.584).

GWAS 1: The GWAS analysis of IgG levels measured at the first month after mRNA-1273 vaccination.

GWAS 2: The GWAS analysis of IgG levels measured at the third month after mRNA-1273 vaccination.

GWAS 3: The GWAS analysis of the difference in IgG levels between the first and third months after mRNA-1273 vaccination.

10.3389/fimmu.2025.1639825

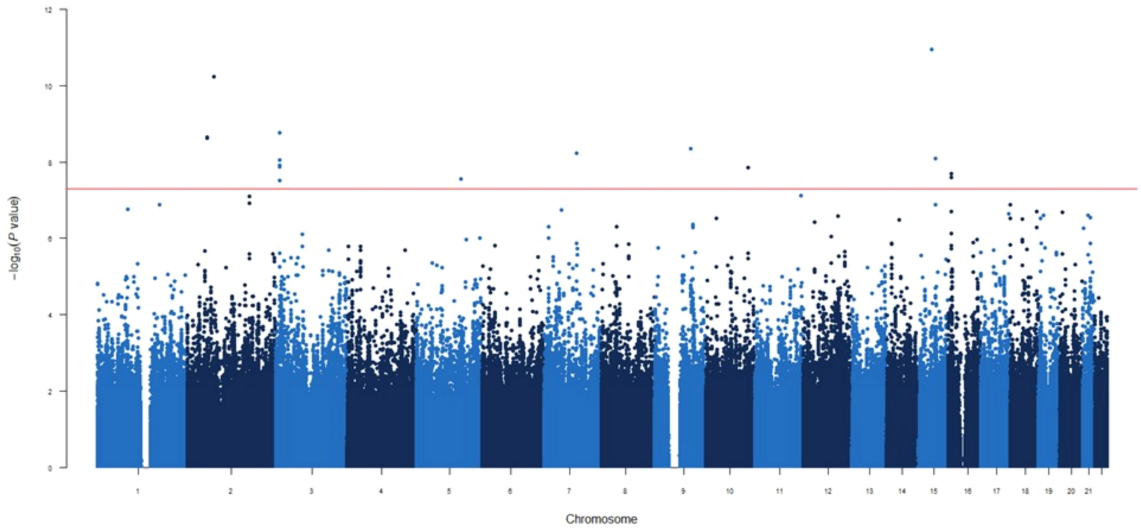

FIGURE 1
Manhattan plot for the GWAS analysis for IgG levels measured one month after mRNA-1273 vaccine.

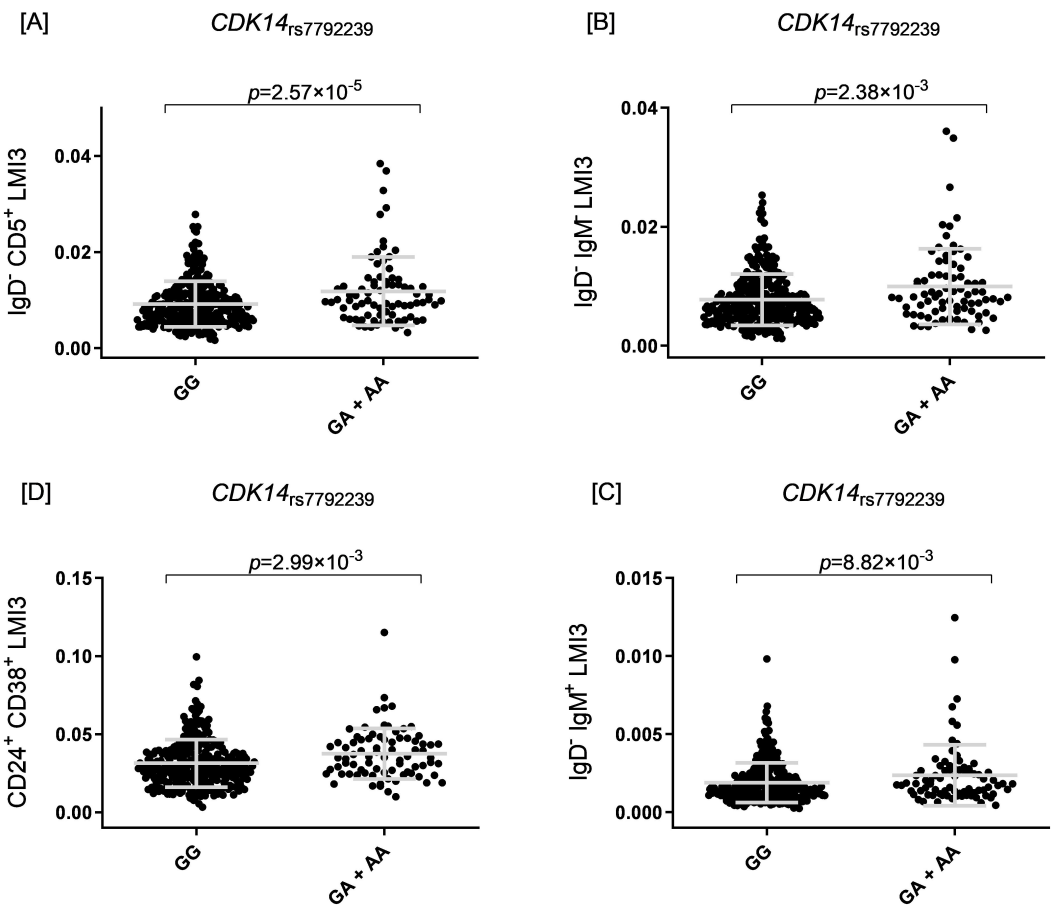

FIGURE 2
Four scatter plots labeled **(A–D)** show data for CDK14 rs7792239. [A] Plot for IgD^{-} $CD5^{+}$ LMI3, comparing GG and GA + AA, with p = 2.57×10^{-5}. [B] Plot for IgD^{-} IgM LMI3, comparing GG and GA + AA, with p = 2.38×10^{-3}. [C] Plot for IgD^{-} IgM^{+} LMI3, comparing GG and GA + AA, with p = 8.82×10^{-3}. [D] Plot for $CD24^{+}$ $CD38^{+}$ LMI3, comparing GG and GA + AA, with p = 2.99×10^{-3}.

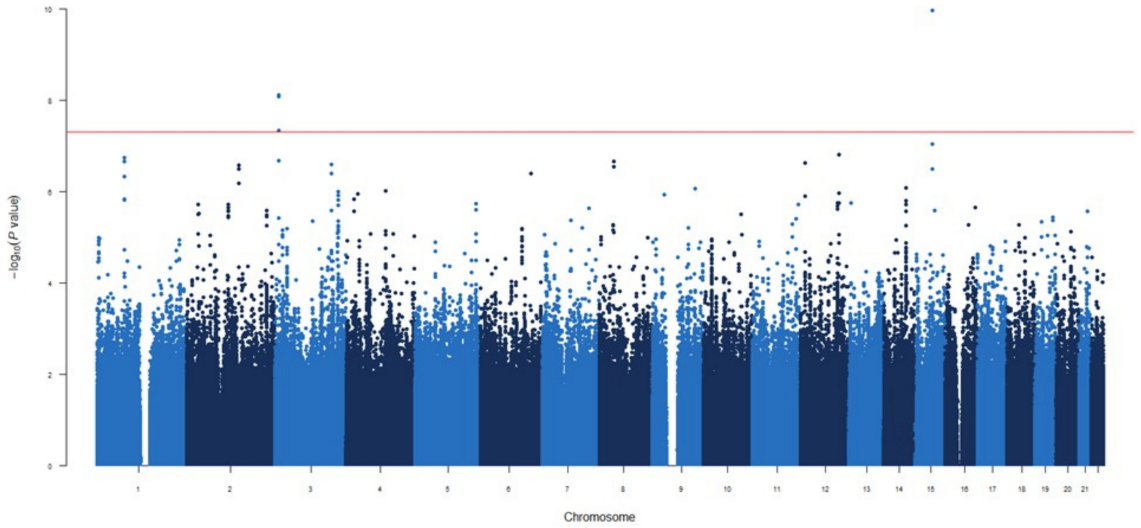

FIGURE 3
Manhattan plot for the GWAS analysis for IgG levels measured three months after mRNA-1273 vaccine.

novel genetic variants associated with the different IgG levels (Figure 4). Similar to the first GWAS, the most statistically significant association was the *ENSG00000295231|ALDH1A2*$_{rs1350209880}$ SNP (OR=2.50, p=5.01×10^{-13}, Table 2) which maps on LncRNA gene and upstream *ALDH1A2* gene on chromosome 15q21.3. The next five significant associations were *TMOD1*$_{rs117643807}$, *SPTBN1*$_{rs75197984}$, *CCDC172|PNLIPRP3*$_{rs7907582}$, *CDK14*$_{rs7792239}$ and *GRIN2A|LOC105371076*$_{rs34340658}$ SNPs (OR=2.54, p=1.04×10^{-10}; OR=2.37, p=1.97×10^{-10} OR=2.18, p=2.15×10^{-09}; OR=2.39, p=5.65×10^{-09} and OR=1.95, p=8.64×10^{-09}, respectively, Table 2, Supplementary Table 5) were also directly identified in the first GWAS, with the exception of *SPTBN1*$_{rs75197984}$ which shows slight linkage disequilibrium (LD) with *CYP26B1*$_{rs72845602}$ (D'=0.601 and r^2 = 0.001). In addition, the other three significant associations were *METTL8*$_{rs1125991}$, *LOC105371912*$_{rs4630616}$ and *PLCB1*$_{rs55919500}$ (OR=2.03, p=7.71×10^{-09}; OR=1.87, p=1.78×10^{-08} and OR=2.24, p=2.81×10^{-08}, respectively, Table 2, Supplementary Table 5) which were identified for the first time, in this GWAS. Besides the functional impact of the *CDK14* SNP on absolute numbers of different immature memory B lymphocytes mentioned previously, we found that carriers of the *PLCB1*$_{rs55919500A}$ allele had increased absolute numbers of IgD$^+$IgM$^+$CD27$^+$ memory B cells and natural effector CD24$^+$CD38$^+$IgD$^+$IgM$^+$ B cells (p=1.07×10^{-3} and p=2.15×10^{-3},

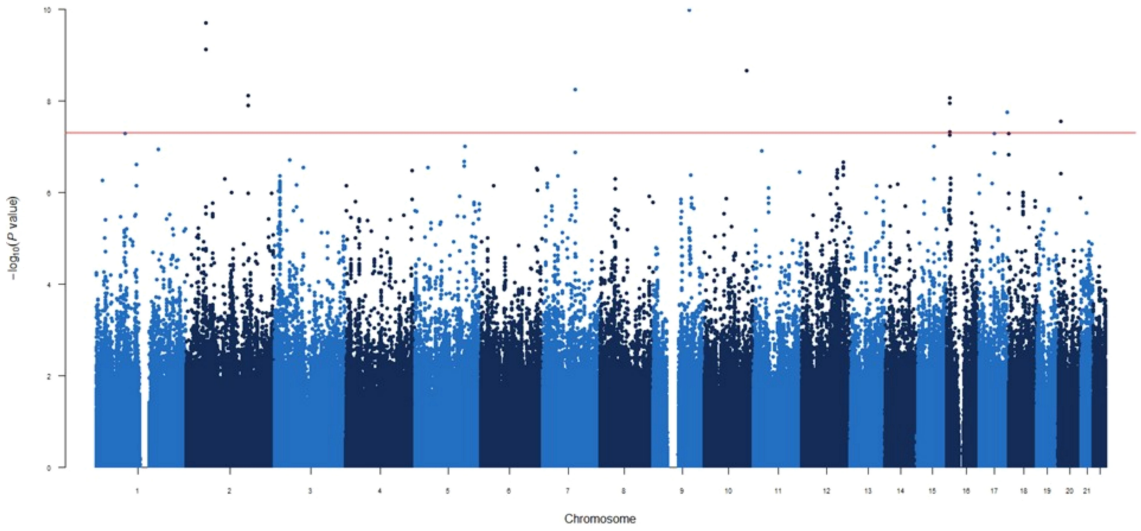

FIGURE 4
Manhattan plot for the GWAS analysis for difference IgG levels between one and three months after mRNA-1273 vaccine.

10.3389/fimmu.2025.1639825

respectively, Figures 5A, B). Intriguingly, carriers of the *PLCB1*$_{rs55919500A}$ allele also had decreased absolute numbers of naïve IgD$^+$IgM$^+$CD27$^-$ B cells (p=2.38×10^{-3}, Figure 5C).

Finally, we identified 28 novel potential associated signals with borderline significance (5×10^{-8}<p<1×10^{-6}) in the *THOC1|COLEC12*, *ENSG00000301718|ENSG00000295563*, *SMASR|SMAD3-DT*, *ETF1*, *TNFSF4 | LOC100506023*, *lnc-LUZP2-3|HSALNG0143151*, *RN7SKP216|ENSG00000258254*, *LOC105378072|LOC101928923*, *LOC101928923*, *ENSG00000258272*, *ENSG00000299420*, *ENSG00000307057*, *BAAT*, *ENSG00000294440|ENSG00000308043*, *BTD*, *HAL*, *ENSG00000309019|MYL9*, *LINC01918|ENSG00000293860*, *LOC105371757*, *ENSG00000300202*, *PTPRG*, *TMIGD3*, *PCGF3-AS1*, *GPC5*, *LOC105376642|HNRNPKP3*, *LINC00606|ENSG00000230599*, *HACL1* and *CNTNAP5 loci* associated with difference circulating levels of IgG between first and third month vaccine (p=5.10×10^{-8}-9.87×10^{-7}, Supplementary Table 5).

Of note, none of the genetic signals identified in these GWASs showed association with baseline IgG levels measured in the 500FG cohort of the HFGP, which confirms that the reported associations are specific to the immune response elicited by vaccination (Supplementary Table 5).

Discussion

This comprehensive study identified, for the first time, 14 genetic variants significantly associated with increased circulating IgG levels at 1 month and 3 months post-vaccination with the mRNA-1273 vaccine or in the GWAS assessing differential antibody responses between 1- and 3-months post-vaccination.

The strongest association was for the *ENSG00000295231|ALDH1A2*$_{rs1350209880}$ SNP, located within a LncRNA gene and upstream of *ALDH1A2* gene on chromosome 15q21.3. This variant showed the most significant association in the first GWAS, at 1-month post-vaccination, and in third GWAS to differences in circulating IgG levels between months 1 and 3 post-vaccination, suggesting a role in sustaining IgG production and possibly influencing the magnitude or persistence of the humoral immune response. While rs1350209880 is annotated as a rare variant in external databases, it exhibited a minor allele frequency above 0.05 in our cohort, likely reflecting population-specific enrichment. This justified its retention following standard GWAS quality control thresholds. Genotyping quality metrics were robust and supported the validity of this signal; however, we acknowledge that associations involving population-enriched or low-frequency variants should be interpreted with caution and warrant replication in independent cohorts.

Although *ENSG00000295231* LncRNA remains uncharacterized, several studies have shown that LncRNAs are important regulators in immune diseases (41–43), cancer (44–46) and various biological pathways (47, 48). *ALDH1A2* encodes Aldehyde Dehydrogenase 1 Family Member A2, which catalyzes the NAD-dependent oxidation of retinaldehyde to retinoic acid, a key signaling molecule involved in immune genes regulation (49–51). Retinoic acid, a metabolite of vitamin A, is essential for enhancing and sustaining IgG immune responses in B cell (52) and *in vivo* (53). It is also used as an adjuvant to boost mucosal/systemic immune responses and cytokine production (52, 54, 55). Specifically, retinoic acid may help reduce respiratory complications and aid epithelial repair after SARS-CoV-2 infection, due to its immune-modulating and anti-inflammatory properties (56, 57).

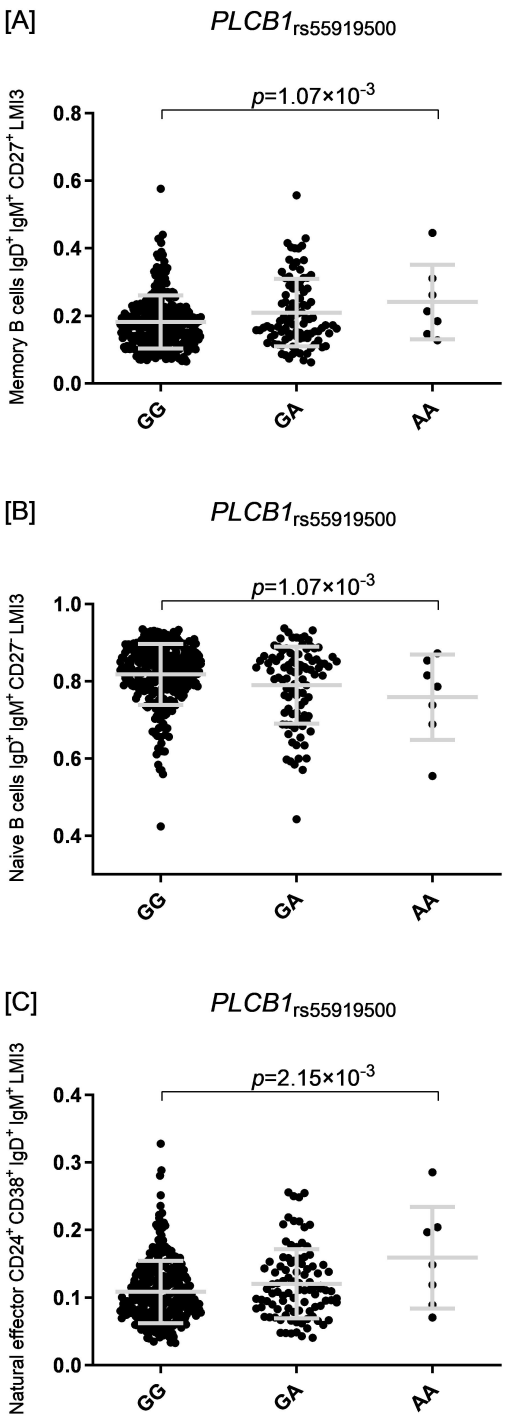

FIGURE 5
Three dot plots display B cell subsets associated with the PLCB1 rs55919500 genotype: GG, GA, and AA. Plot **(A)** shows memory B cells with a p-value of 1.07×10^{-3}. Plot **(B)** presents naïve B cells with a similar p-value. Plot **(C)** illustrates natural effector B cells with a p-value of 2.15×10^{-3}. Each plot includes individual data points and median lines.

Supporting this role, we found *CYP26B1*$_{rs72845602}$ SNP significantly associated with higher concentrations of circulating IgG levels 1-month post-vaccination. This SNP lies within *CYP26B1* gene, which encodes a cytochrome P450 enzyme that metabolizes all-trans retinoic acid and influences T cell differentiation and inflammation (54, 58–60). Another SNP, *SPTBN1*$_{rs75197984}$, in moderate LD with *CYP26B1*$_{rs72845602}$, was associated with increased circulating concentrations of IgG at 3 months post-vaccination. This genetic variant maps to Spectrin Beta, Non-Erythrocytic 1 (SPTBN1), encoding βII-spectrin, a cytoskeletal protein involved in cell shape, membrane organization, and protein sorting (61–63). Though not directly linked to circulating IgG levels or SARS-CoV-2, *SPTBN1* is involved in modulating immune regulating and viral infections, including HIV-1 (64–66). *In silico* analyses showed both SNPs are associated with several QTLs in blood, $CD4^+$ naïve T cells, and $CD14^+$ monocytes, and alter regulatory motifs in Gfi1, a transcription factor essential for B cell differentiation and IgG class switching (67–69). Gfi1-deficient B cells produce more IgG2a and IgG2b, likely via increased TGF-β1 expression, which regulates IgG subclass production (69). These findings suggest that *CYP26B1*$_{rs72845602}$ and *SPTBN1*$_{rs75197984}$ may influence IgG production by modulating immune cell function and response to vaccination.

Likewise, *SLC6A11*|*LINC00606*$_{rs4088054}$ maps to a validated LncRNA and the Solute Carrier Family 6 Member 11 (SLC6A11) genes, which encodes a sodium-dependent gamma-aminobutyric acid (GABA) transporter. GABA, an inhibitory neurotransmitter, is involved in modulation of immune cell activation via its transporters in T cells and macrophages (70). At 3 months post-vaccination, *ATP2B2*$_{rs55725269}$ SNP, in complete LD with *SLC6A11*|*LINC00606*$_{rs4088054}$, was also associated with elevated circulating levels of IgG. This SNP lies downstream of the ATPase Plasma Membrane Ca2+ Transporting 2 (ATP2B2), encoding PMCA2, a plasma membrane calcium ATPase critical for restoring calcium balance in T cells (71, 72) thus regulating immune response intensity and duration (73). These results suggest that both SNPs may elevate IgG concentrations through immune modulation, possibly via calcium-dependent effects of ATP2B2 on SLC6A11 function. Supporting this, a recent study associated genetic variants within *ATP2B2* with higher mortality in severe SARS-CoV-2 cases (74), while GWAS have associated the *SLC6A11* locus with gut microbiome composition (75, 76). Given the microbiome's role in SARS-CoV-2 infection (77–79), and vaccine efficacy (80, 81), *SLC6A11* may impact circulating IgG concentrations via microbiome modulation.

Another noteworthy finding from the 1-month post-vaccination GWAS was the association of *SNX24*|*LOC124901213*$_{rs55770715}$ with higher circulating concentrations of IgG. This SNP maps *SNX24* and a small nucleolar RNA gene at 5q23.2. SNX24, a member of the Sorting Nexin family, is involved in regulating protein trafficking through the endocytic pathway (82). Variants in *SNX24* have been linked to platelet indices (83, 84), and upregulation in megakaryocytes with ploidy (85). Our data and the finding that *SNX24* is downregulated in FLI1-deficient platelets support a role in platelet formation. *SNX24* is also required for α-granule biogenesis and cargo trafficking in megakaryocytes (86). This SNP overlaps histone marks in blood and lung cells, suggesting it may act as a regulatory element. It is also associated with *SNX24* expression in lung and spleen and constitutes an mQTL in blood, indicating a potential regulatory role in immune response gene expression.

In addition to *ENSG00000295231*|*ALDH1A2*$_{rs1350209880}$ five other SNPs were associated with antibody responses from 1 to 3 months post-vaccination (*CDK14*$_{rs7792239}$, *CCDC172*|*PNLIPRP3*$_{rs7907582}$, *TMOD1*$_{rs117643807}$, *GRIN2A*|*LOC105371076*$_{rs34340658}$, and *LOC105371912*$_{rs4630616}$), indicating their likely involvement in regulating antibody production over time.

The *CDK14*$_{rs7792239}$ SNP maps to Cyclin Dependent Kinase 14 (CDK14) gene, which regulates the G2/M cell cycle and supports endothelial and epithelial proliferation and migration (87, 88). A recent mouse study linked CDK14 with interferon-gamma (IFN-γ) pathways, suggesting a key role in lung immune repair (89). The *CDK14*$_{rs7792239A}$ allele was associated with increased absolute numbers of IgD^-CD5^+ immature memory B lymphocytes, and trends (though not significant) towards increases in absolute numbers of IgD^-IgM^-, $CD24^+CD38^+$ and IgD^-IgM^+ immature memory B cells. Previous studies have reported shifts in B cell memory populations, especially increased IgG^+ memory B cells, after SARS-CoV-2 infection and vaccination (90–92). Given CDK14's link to IFN-γ/STAT1 signaling and its potential to promote IgG production, this variant may support humoral responses. Notably, *CDK14*$_{rs7792239}$ affects the E2A_2 regulatory motif, which is crucial for B cell development, germinal center formation, and IgG production (93–95). CDK14 thus appears vital for effective humoral immunity and protection against SARS-CoV-2.

The *CCDC172*|*PNLIPRP3*$_{rs7907582}$ SNP is located between the *CCDC172* and *PNLIPRP3* genes on chromosome 10q25.3. *CCDC172* participates in protein-protein interactions and structural integrity, while *PNLIPRP3* encodes for a pancreatic lipase-like protein. Though their roles in SARS-CoV-2 are unclear, *in silico* analyses catalogued the SNP as probably malignant, with effects on regulatory motifs like CEBPB_known4 and Maf_known3/4, which showed altered activity in monocytes from hospitalized SARS-Cov-2 patients (96) and are activated in respiratory epithelial cells during severe infection (97). This suggests a potential role of CEBPB in modulating immune responses in the context of severe viral infection. Additionally, its paralog, CEBPD, has been implicated in driving immune cell responses in monocytes through IL-6-associated survival pathways (98). In support of this hypothesis, it has been found that the Maf_known3/4 motif is a transcription factor MAFB family member, which shows survival-associated upregulation in monocytes (98).

On the other hand, the *TMOD1*$_{rs117643807}$ SNP maps to the Tropomoduling 1 (*TMOD1*) gene, which encodes an acting-capping protein that regulates cytoskeleton dynamics and is involved in cell shape, motility and signaling. *TMOD1* is essential in erythroid and cardiac cells, but recent studies suggest it also plays

a role in immune regulation by maintaining cytoskeletal structure during immune cell activation and trafficking (99). In dendritic cells, it is also critical for proper maturation and function, reducing the ability of these cells to stimulate T cells and shifts cytokine secretion toward immune tolerance (100). While not directly linked to IgG levels or SARS-CoV-2, this variant could influence B cell activation and function via cytoskeletal remodeling and modulation of phagocyte's activities.

The *GRIN2A|LOC105371076*$_{rs34340658}$ SNP is located between *GRIN2A* gene, which encodes a subunit of the N-methyl-D-aspartate (NMDA) receptor involved in synaptic signaling, and a LncRNA at 16p13.2. While *GRIN2A* has mainly been studied in neurological disorders, growing evidence indicates cross-talk between neurotransmission and host immunity (101–103). Some studies have shown that non-neutralizing anti-SARS-CoV-2 IgG antibodies, particularly those against the S protein, can alter central nervous system (CNS) gene expression in mice, including upregulation of *GRIN2A* in the hippocampus. This suggests that such antibodies may influence neuronal activity and contribute to neurological symptoms seen in SARS-CoV-2 patients and vaccinated individuals. Given *GRIN2A*'s role in synaptic plasticity, preventing the production of anti-S1-111 IgG or similar antibodies could help reduce CNS manifestations of SARS-CoV-2 infection and vaccination (104). Interestingly, these observations are consistent with *in silico* findings linking this SNP—and similarly, the marker identified in *CKD14*—to altered E2A_2 and E2A_5 regulatory motifs. These motifs are bound by E2A and, as mentioned above, are involved in modulating B cell development, germinal center formation, and IgG production (93–95). Therefore, *GRIN2A|LOC105371076*$_{rs34340658}$ likely contributes to effective humoral responses and protection against SARS-CoV-2.

Lastly, the *LOC105371912*$_{rs4630616}$ SNP maps an uncharacterized ncRNA gene. Although its specific role in SARS-Cov-2 remains unknown, growing evidence suggests that lncRNAs are key regulatory elements in diverse biological processes, including the modulation and effectiveness of the immune responses during infection and following vaccination. Nonetheless, further studies are warranted to explore the potential involvement of this gene in SARS-CoV-2 pathogenesis.

At this point, it is also important to note that we found an association of the *SMASR|SMAD3-DT*$_{rs28485994}$ SNP with increased circulating IgG concentrations in the GWAS conducted at 1 and 3 months post-vaccination, suggesting a role of this marker in sustaining antibody production over time. This SNP maps to *SMASR* and *SMAD3-DT*, lncRNA genes associated with the *SMAD3* gene. *SMAD3* encodes a key protein that cooperates with FOSL2 in the TGF-β signaling pathway, which suppresses type I IFN responses and promotes immune evasion (105–107). Recent studies have revealed a role for SMAD3 in SARS-CoV-2 pathogenesis. The SARS-CoV-2 N protein binds to SMAD3, enhancing TGF-β/SMAD3 signaling, which leads to G1 cell cycle arrest and tubular epithelial cell death via necroptosis (108–110). SMAD3 also downregulates Cystic Fibrosis Transmembrane Conductance Regulator (CFTR), increasing intracellular chloride levels and triggering the release of pro-inflammatory cytokines. In line with this, some studies have shown that SMAD3 suppresses miR-145, exacerbating CFTR dysfunction and inflammation (111), and that in severe SARS-CoV-2, there is an increase in polymorphonuclear myeloid-derived suppressor cells (PMN-MDSCs) that suppress T-cell activity through reactive oxygen species (ROS) (112). These findings suggest that the role of TGF-β/SMAD3 in immune regulation could potentially influence B-cell responses, particularly by modulating IgG levels after vaccination.

Finally, another noteworthy finding of this study was the identification of three SNPs—*PLCB1*$_{rs55919500}$, *METTL8*$_{rs1125991}$, and *LOC105371912*$_{rs4630616}$—associated with differential antibody responses. These variants point toward potentially important molecular mechanisms that link genetic regulation with immune cell function, particularly in the context of viral infections such as SARS-CoV-2. *PLCB1* encodes phospholipase C beta 1, an enzyme involved in intracellular signaling pathways that regulate inflammation and immune responses through modulation of proinflammatory cytokines such as IL-1β, IL-6, and IL-8 (113, 114). Consistent with this function, *in vitro* analysis showed that carriers of the *PLCB1*$_{rs55919500A}$ allele had an increased absolute number of memory B cells ($IgD^+IgM^+CD27^+$) and natural effector B cells ($CD24^+CD38^+IgD^+IgM^+$), as well as fewer naïve B cells ($IgD^+IgM^+CD27^-$). These subsets have been implicated in the response to SARS-CoV-2 infection and vaccination (115, 116), with unswitched memory B cells ($IgD^+IgM^+CD27^+$) found to be increased in individuals recovering from severe SARS-CoV-2 compared to those with milder disease (115). *METTL8*, on the other hand, encodes a mitochondrial RNA methyltransferase responsible for installing 3-methylcytidine (m3C) modifications in specific mitochondrial tRNAs, a process essential for efficient mitochondrial translation and respiratory chain activity (117, 118). RNA methylation, including by METTL family enzymes, has been recognized as a key regulator of immune cell function, differentiation, and tumor immune evasion (119, 120). In addition, *METTL8*$_{rs1125991}$ was associated with changes in the regulatory motif of FOXO1, a transcription factor crucial for B cell development, tolerance, and function. Supporting a functional role, this SNP was strongly linked to increased expression of CYBRD1 mRNA in blood and was identified as an mQTL in both blood and naïve $CD4^+$ T cells. CYBRD1 encodes an iron-regulated ferric reductase, and altered expression may modulate immune responses by affecting iron metabolism, ferroptosis (iron-dependent cell death), and the tumor microenvironment (121). Notably, components of mitochondrial cytochrome systems have been found to be elevated in the plasma of SARS-CoV-2 patients, reflecting mitochondrial dysfunction and apoptosis during severe infection (122). Moreover, METTL8 itself has been implicated in $CD8^+$ T cell infiltration in lung squamous cell carcinoma, suggesting a broader role in regulating immune responses within tissue microenvironments (123). Taken together, these findings suggest that genetic variation in *PLCB1* and *METTL8* influences immune cell profiles and functions through distinct molecular mechanisms, namely, inflammatory signaling, mitochondrial RNA modification, and transcriptional regulation. These mechanisms converge to shape the host's antibody responses and may modulate the outcome of SARS-CoV-2.

In summary, this study identified fourteen genetic variants linked to increased circulating IgG levels following mRNA-1273 vaccination, with the most notable being *ENSG00000295231|ALDH1A2*$_{rs1350209880}$, a variant associated with immune regulation and enhanced IgG production over time. Other key variants mapped to genes like *CYP26B1*, *SPTBN1*, and *SMASR|SMAD3-DT*, which influences cytokine production, T cell differentiation, and IgG subclass production, were crucial for optimizing immune responses. Variants in *CDK14* and *GRIN2A* were directly linked to B cell activation and memory, further shaping the humoral immune response. Despite other variants map on LncRNAs that may regulate IgG production through mechanisms like neurotransmission and calcium signaling and need further investigation. Finally, variants including *TMOD1*$_{rs117643807}$ and *PLCB1*$_{rs55919500}$, suggest immune modulation via cell signaling pathways, while variants like *ATP2B2*$_{rs55725269}$ and *METTL8*$_{rs1125991}$ highlight the role of metabolism and the microbiome in vaccine responses.

Although this study provides valuable insights into the genetic predisposition to increase IgG levels after vaccination, it also has several limitations. First, our analysis was restricted to individuals of the Spanish cohort, which limited our ability to replicate previous findings from studies in other ethnic populations. This decision was based on both scientific and logistical considerations. Focusing on a genetically homogeneous population increases internal consistency and reduces confounding due to population structure and environmental heterogeneity, thereby enhancing the robustness of GWAS findings. Additionally, we did not have access to large-scale, individual-level data from other vaccinated cohorts, which limited the feasibility of multi-cohort or trans-ethnic analyses. While we do not assume fundamental differences in immune function between European populations, replication in independent cohorts will be essential to validate and generalize our results.

Second, we were unable to confirm the association of several potentially relevant *loci*. This could be attributed to the relatively limited statistical power of our study. Differences in the vaccine platform used (e.g., mRNA-1273 in our study versus BNT162b2 or mixed vaccine platforms in other studies), distinct timepoints for sample collection, population-specific allele frequencies, and varying analytical strategies may also explain these discrepancies. For instance, recent large-scale GWAS such as the UK Biobank study (124) analyzed combined data from different vaccine types without distinguishing between platforms like BNT162b2 and ChAdOx1, while our study focused specifically on the mRNA-1273 vaccine, providing greater homogeneity in immune stimulus and timing. Additionally, some of the previously identified variants may have modest effect sizes that require larger sample sizes or meta-analyses to achieve statistical significance. The absence of overlapping associations therefore does not rule out the relevance of these loci but underscores the complexity of genetic regulation of vaccine responses and the importance of harmonized designs across studies for robust cross-cohort validation. Finally, while our functional and *in silico* analyses offer an initial understanding of the potential effects of GWAS hits, further experimental validation is needed to definitively establish the biological roles of these markers. Additionally, while our functional and *in silico* analyses offer an initial understanding of the potential effects of GWAS hits, further experimental validation is needed to definitively establish the biological roles of these markers.

Third, although age and sex are known factors influencing immune responses, we did not perform stratified analyses by sex or age strata due to limited statistical power, which would reduce the reliability of such subgroup analyses. Notably, previous studies have consistently reported that vaccine-induced antibody titers tend to be statistically higher in women than in men, highlighting sex as an important biological variable in immune responses (125, 126). For example, Demombreun et al. demonstrated higher SARS-CoV-2 antibody titers post-vaccination in women compared to men (125), while Jensen et al. also reported sex differences favoring stronger humoral responses in females (126). However, our findings did not replicate this trend, as shown in Supplementary Table 3, where no statistically significant difference or even a trend toward higher titers in men was observed. These discrepancies may be explained by several factors. Our cohort consisted exclusively of individuals of European ancestry, whereas Demombreun et al. included a more diverse racial and ethnic population including Hispanic/Latinx, Non-Hispanic Asian, Non-Hispanic Black, among others. Moreover, women in our study were slightly older and represented a larger sample size than men, which could influence antibody levels. In addition, differences in antibody measurements may contribute to the contrasting results. Our study measured anti-Spike IgG antibodies, reflecting a broader antibody response, whereas the cited studies focused on anti-RBD IgG antibodies, which target a specific region of the spike protein. Although related, these assays are not directly comparable. On the other hand, the referenced studies assessed immune responses at baseline, after the first dose, and after the second dose, while our measurements were performed at one and three months post full vaccination, capturing a later phase of the immune response, which may display different sex-related patterns. Furthermore, biological and immunological factors likely contribute to these differences. It is well established that innate and adaptive immune responses tend to be stronger and faster in women, which can lead to higher antibody titers but also increased susceptibility to autoimmune diseases and more frequent vaccine adverse reactions (127). However, some studies have demonstrated no evidence of stronger vaccine-induced immunity in females compared to males (128), suggesting that sex differences may vary by context and methodology. Hormonal differences, such as higher estrogen levels in women and testosterone in men, modulate immune responses and may partially explain sex differences in vaccine efficacy and reactogenicity. Age also interacts with sex in shaping vaccine responses; while some vaccines are more effective in younger women (127), sex differences in adverse reactions may persist regardless of age.

Considering all the above, age and sex were included as covariates in all GWAS models, helping to control for their potential confounding effects. Future studies with larger cohorts are needed to rigorously assess the impact of age and sex on immune outcomes and genetic associations.

Finally, it is important to note that our study design included antibody measurements at only two post-vaccination time points, 1

and 3 months, which limits the ability to fully characterize the longitudinal dynamics of the IgG response. While our GWAS comparing differences between these time points partially captures interindividual variability in antibody kinetics, the use of static snapshots may overlook important temporal patterns such as early peaks, delayed responses, or rapid waning. Future studies incorporating denser longitudinal sampling, particularly in the early and late phases post-vaccination, will be essential to better understand the genetic regulation of humoral values over time.

These findings underscore the complex interplay of genetic factors influencing the immune response to vaccination, particularly through modulation of B cell activity, immune signaling pathways, and metabolic processes. These insights could inform future strategies to enhance vaccine efficacy, especially for SARS-CoV-2 and other viral infections. The identification of genetic variants provides a novel and deeper understanding of individual variability in vaccine responses and opens new avenues for personalized vaccine strategies.

Data availability statement

The datasets presented in this study can be found in online repositories. The names of the repository/repositories and accession number(s) can be found below: https://hfgp.bbmri.nl/, BBMRI-NL data infrastructure ftp.genyo.es, GENYO repository.

Ethics statement

The studies involving humans were reviewed and approved by the regional ethics committee (Portal de Ética de la Investigación Biomédica, Junta de Andalucía, code: 0297-N-21). The studies were conducted in accordance with the local legislation and institutional requirements. The participants provided their written informed consent to participate in this study. The HFGP study was approved by the Arnhem-Nijmegen Ethical Committee (no. 42561.091.12), and biological specimens were collected after informed consent was obtained.

Author contributions

AC: Formal Analysis, Investigation, Methodology, Writing – original draft. LR: Formal Analysis, Investigation, Methodology, Writing – review & editing. JG: Investigation, Methodology, Resources, Writing – review & editing. MC: Formal Analysis, Investigation, Methodology, Writing – review & editing. Rt: Data curation, Formal Analysis, Investigation, Methodology, Resources, Writing – review & editing. YL: Funding acquisition, Investigation, Methodology, Resources, Writing – review & editing. FR: Investigation, Methodology, Software, Writing – review & editing. FG: Investigation, Methodology, Resources, Writing – review & editing. MN: Investigation, Methodology, Resources, Writing – review & editing. PS: Investigation, Methodology, Resources, Writing – review & editing. ML: Investigation, Methodology, Resources, Supervision, Writing – review & editing. AS: Funding acquisition, Investigation, Methodology, Resources, Writing – review & editing. JS: Conceptualization, Funding acquisition, Investigation, Methodology, Project administration, Resources, Supervision, Writing – original draft.

Funding

The author(s) declare that financial support was received for the research and/or publication of this article. This study was supported by grants PI20/01845, PI21/01708, and DTS23/00030 from Fondo de Investigaciones Sanitarias (Madrid, Spain), by intramural funds of GENYO and FIBAO foundation (Granada, Spain) and by "Investigación y Desarrollo (I + D) del Sistema Andaluz de Salud (SAS)". Our group at GENYO was also supported by a Senior Post-Doctoral Fellowship, funded by the Consejería de Salud y Familias of the Government of Andalusia (RH-0061-2020). YL was supported by an ERC Starting Grant (948207) and the Radboud University Medical Centre Hypatia Grant (2018) for Scientific Research.

Conflict of interest

The authors declare that the research was conducted in the absence of any commercial or financial relationships that could be construed as a potential conflict of interest.

Correction note

This article has been corrected with minor changes. These changes do not impact the scientific content of the article.

Generative AI statement

The author(s) declare that no Generative AI was used in the creation of this manuscript.

Publisher's note

Supplementary material

The Supplementary Material for this article can be found online at: https://www.frontiersin.org/articles/10.3389/fimmu.2025.1639825/full#supplementary-material

References

1. Iyanda AE, Adeleke R, Lu Y, Osayomi T, Adaralegbe A, Lasode M, et al. A retrospective cross-national examination of COVID-19 outbreak in 175 countries: a multiscale geographically weighted regression analysis (January 11-June 28, 2020). *J Infect Public Health*. (2020) 13:1438–45. doi: 10.1016/j.jiph.2020.07.006

2. WHO. Coronavirus (COVID-19) dashboard. Available online at: https://covid19.who.int/ (Accessed August 14, 2024).

3. Contini C, Caselli E, Martini F, Maritati M, Torreggiani E, Seraceni S, et al. COVID-19 is a multifaceted challenging pandemic which needs urgent public health interventions. *Microorganisms*. (2020) 8:1228. doi: 10.3390/microorganisms8081228

4. Maiti BK. Potential role of peptide-based antiviral therapy against SARS-CoV-2 infection. *ACS Pharmacol Transl Sci*. (2020) 3:783–5. doi: 10.1021/acsptsci.0c00081

5. Bui LT, Winters NI, Chung MI, Joseph C, Gutierrez AJ, Habermann AC, et al. Chronic lung diseases are associated with gene expression programs favoring SARS-CoV-2 entry and severity. *Nat Commun*. (2021) 12:4314. doi: 10.1038/s41467-021-24467-0

6. Xia H, Cao Z, Xie X, Zhang X, Chen JY-C, Wang H, et al. Evasion of type I interferon by SARS-CoV-2. *Cell Rep*. (2020) 33. doi: 10.1016/j.celrep.2020.108234

7. Hao Y-J, Wang Y-L, Wang M-Y, Zhou L, Shi J-Y, Cao J-M, et al. The origins of COVID-19 pandemic: A brief overview. *Transbound Emerg Dis*. (2022) 69:3181–97. doi: 10.1111/tbed.14732

8. Yang R, Deng Y, Huang B, Huang L, Lin A, Li Y, et al. A core-shell structured COVID-19 mRNA vaccine with favorable biodistribution pattern and promising immunity. *Signal Transduct Target Ther*. (2021) 6:213. doi: 10.1038/s41392-021-00634-z

9. Verheul MK, Nijhof KH, de Zeeuw-Brouwer MI, Duijm G, ten Hulscher H, de Rond L, et al. Booster immunization improves memory B cell responses in older adults unresponsive to primary SARS-CoV-2 immunization. *Vaccines (Basel)*. (2023) 11:1196. doi: 10.3390/vaccines11071196

10. Krauson AJ, Casimero FVC, Siddiquee Z, Stone JR. Duration of SARS-CoV-2 mRNA vaccine persistence and factors associated with cardiac involvement in recently vaccinated patients. *NPJ Vaccines*. (2023) 8:141. doi: 10.1038/s41541-023-00742-7

11. Anderson EJ, Rouphael NG, Widge AT, Jackson LA, Roberts PC, Makhene M, et al. Safety and immunogenicity of SARS-CoV-2 mRNA-1273 vaccine in older adults. *New Engl J Med*. (2020) 383:2427–38. doi: 10.1056/NEJMoa2028436

12. Zhang H, Xu N, Xu Y, Qin P, Dai R, Xu B, et al. Safety and immunogenicity of Ad5-nCoV immunization after three-dose priming with inactivated SARS-CoV-2 vaccine in Chinese adults. *Nat Commun*. (2023) 14:4757. doi: 10.1038/s41467-023-40489-2

13. Gutiérrez-Bautista JF, Sampedro A, Gómez-Vicente E, Rodríguez-Granger J, Reguera JA, Cobo F, et al. HLA class II polymorphism and humoral immunity induced by the SARS-CoV-2 mRNA-1273 vaccine. *Vaccines (Basel)*. (2022) 10:402. doi: 10.3390/vaccines10030402

14. Esposito M, Minnai F, Copetti M, Miscio G, Perna R, Piepoli A, et al. Human leukocyte antigen variants associate with BNT162b2 mRNA vaccine response. *Commun Med*. (2024) 4:63. doi: 10.1038/s43856-024-00490-2

15. Magri C, Marchina E, Sansone E, D'Adamo AP, Cappellani S, Bonfanti C, et al. Genome-wide association studies of response and side effects to the BNT162b2 vaccine in Italian healthcare workers: Increased antibody levels and side effects in carriers of the HLA-A* 03: 01 allele. *HLA*. (2023) 102:707–19. doi: 10.1111/tan.15157

16. Li P, Shi D, Shen W, Shi S, Guo X, Li J, et al. Pilot genome-wide association study of antibody response to inactivated SARS-CoV-2 vaccines. *Front Immunol*. (2022) 13:1054147. doi: 10.3389/fimmu.2022.1054147

17. Bian S, Guo X, Yang X, Francis SS, Shu Y, Liu S, et al. Genetic determinants of IgG antibody response to COVID-19 vaccination. *Am J Hum Genet*. (2024) 111:181–99. doi: 10.1016/j.ajhg.2023.12.005

18. Cruz R, Diz-de Almeida S, López de Heredia M, Quintela I, Ceballos FC, Pita G, et al. Novel genes and sex differences in COVID-19 severity. *Hum Mol Genet*. (2022) 31:3789–806. doi: 10.1093/hmg/ddac132

19. The COVID-19 Host Genetics Initiative. A second update on mapping the human genetic architecture of COVID-19. *Nature*. (2023) 621:E7–E26. doi: 10.1038/s41586-023-06355-3

20. Pairo-Castineira E, Rawlik K, Bretherick AD, Qi T, Wu Y, Nassiri I, et al. GWAS and meta-analysis identifies 49 genetic variants underlying critical COVID-19. *Nature*. (2023) 617:764–8. doi: 10.1038/s41586-023-06034-3

21. Fukushima K, Kubo T, Ito Y, Oda Y, Nagayoshi Y, Fukuda M, et al. Humoral and cellular immune responses to mRNA COVID-19 vaccinations in the elderly: A longitudinal study in Japan. *J Infect Chemother*. (2025) 31. doi: 10.1016/j.jiac.2025.102695

22. Akhtar M, Islam MR, Khaton F, Rahman F, Sami TA, Tauheed I, et al. Spike specific IgG3 and nucleocapsid IgG response in serum serve as distinguishing immunological markers between SARS-CoV-2 infection and vaccination. *Front Immunol*. (2025) 16. doi: 10.3389/fimmu.2025.1518915

23. Noé A, Dang TD, Axelrad C, Burrell E, Germano S, Elia S, et al. BNT162b2 COVID-19 vaccination in children alters cytokine responses to heterologous pathogens and Toll-like receptor agonists. *Front Immunol*. (2023) 14:1242380. doi: 10.3389/fimmu.2023.1242380

24. The 1000 Genomes Project Consortium. A map of human genome variation from population-scale sequencing. *Nature*. (2010) 467:1061–73. doi: 10.1038/nature09534

25. The Haplotype Reference Consortium. A reference panel of 64,976 haplotypes for genotype imputation. *Nat Genet*. (2016) 48:1279–83. doi: 10.1038/ng.3643

26. Li Y, Oosting M, Smeekens SP, Jaeger M, Aguirre-Gamboa R, Le KTT, et al. A functional genomics approach to understand variation in cytokine production in humans. *Cell*. (2016) 167:1099–110.e14. doi: 10.1016/j.cell.2016.10.017

27. ter Horst R, Jaeger M, Smeekens SP, Oosting M, Swertz MA, Li Y, et al. Host and environmental factors influencing individual human cytokine responses. *Cell*. (2016) 167:1111–24.e13. doi: 10.1016/j.cell.2016.10.018

28. Aguirre-Gamboa R, Joosten I, Urbano PCM, van der Molen RG, van Rijssen E, van Cranenbroek B, et al. Differential effects of environmental and genetic factors on T and B cell immune traits. *Cell Rep*. (2016) 17:2474–87. doi: 10.1016/j.celrep.2016.10.053

29. Orrù V, Steri M, Sole G, Sidore C, Virdis F, Dei M, et al. Genetic variants regulating immune cell levels in health and disease. *Cell*. (2013) 155:242. doi: 10.1016/j.cell.2013.08.041

30. Van Der Velde KJ, Imhann F, Charbon B, Pang C, van Enckevort D, Slofstra M, et al. MOLGENIS research: Advanced bioinformatics data software for non-bioinformaticians. *Bioinformatics*. (2019) 35:1076–8. doi: 10.1093/bioinformatics/bty742

31. Wilkinson MD, Dumontier M, Aalbersberg IJ, Appleton G, Axton M, Baak A, et al. Comment: The FAIR Guiding Principles for scientific data management and stewardship. *Sci Data*. (2016) 3:1–9. doi: 10.1038/sdata.2016.18

32. Watanabe K, Taskesen E, Van Bochoven A, Posthuma D. Functional mapping and annotation of genetic associations with FUMA. *Nat Commun*. (2017) 8. doi: 10.1038/s41467-017-01261-5

33. Ochoa D, Hercules A, Carmona M, Suveges D, Baker J, Malangone C, et al. The next-generation Open Targets Platform: reimagined, redesigned, rebuilt. *Nucleic Acids Res*. (2023) 51:D1353–9. doi: 10.1093/nar/gkac1046

34. Lonsdale J, Thomas J, Salvatore M, Phillips R, Lo E, Shad S, et al. The genotype-tissue expression (GTEx) project. *Nat Genet*. (2013) 45:580–5. doi: 10.1038/ng.2653

35. Zheng Z, Huang D, Wang J, Zhao K, Zhou Y, Guo Z, et al. QTLbase: an integrative resource for quantitative trait loci across multiple human molecular phenotypes. *Nucleic Acids Res*. (2020) 48:D983–91. doi: 10.1093/nar/gkz888

36. Rentzsch P, Witten D, Cooper GM, Shendure J, Kircher M. CADD: predicting the deleteriousness of variants throughout the human genome. *Nucleic Acids Res*. (2019) 47:D886–94. doi: 10.1093/nar/gky1016

37. Boyle AP, Hong EL, Hariharan M, Chen Y, Schaub MA, Kasowski M, et al. Annotation of functional variation in personal genomes using RegulomeDB. *Genome Res*. (2012) 22:1790–7. doi: 10.1101/gr.137323.112

38. Van Der Most PJ, Küpers LK, Snieder H, Nolte I. QCEWAS: automated quality control of results of epigenome-wide association studies. *Bioinformatics*. (2017) 33:1243–5. doi: 10.1093/bioinformatics/btw766

39. Wickham H. ggplot2. *Wiley Interdiscip Rev Comput Stat*. (2011) 3:180–5. doi: 10.1002/wics.147

40. Turner SD. qqman: an R package for visualizing GWAS results using Q-Q and manhattan plots. *J Open Source Softw*. (2018) 3:731. doi: 10.21105/joss.00731

41. Taheri M, Noroozi R, Sadeghpour S, Omrani MD, Ghafouri-Fard S. The rs4759314 SNP within Hotair lncRNA is associated with risk of multiple sclerosis. *Mult Scler Relat Disord*. (2020) 40:101986. doi: 10.1016/j.msard.2020.101986

42. Zhang R-X, Zhang Z-X, Zhao X-Y, Liu Y-H, Zhang X-M, Han Q, et al. Mechanism of action of lncRNA-NEAT1 in immune diseases. *Front Genet*. (2025) 16. doi: 10.3389/fgene.2025.1501115

43. Seyedi D, Espandar N, Hojatizadeh M, Mohammadi Y, Sadri F, Rezaei Z. Noncoding RNAs in rheumatoid arthritis: modulators of the NF-κB signaling pathway and therapeutic implications. *Front Immunol*. (2024) 15. doi: 10.3389/fimmu.2024.1486476

44. Huang X, Zhang W, Shao Z. Association between long non-coding RNA polymorphisms and cancer risk: a meta-analysis. *Biosci Rep*. (2018) 38:BSR20180365. doi: 10.1042/BSR20180365

45. Mu D, Shi Y, Sun R, Han B, Zhong K, Ye Y, et al. The acidic microenvironment promotes pancreatic cancer progression via the lncRNA-LOC100507424/E2F1/FOXM1 axis. *BMC Cancer*. (2025) 25:655. doi: 10.1186/s12885-025-14073-4

46. Kwas K, Szubert M, Wilczyński JR. Latest update on lncRNA in epithelial ovarian cancer-A scoping review. *Cells*. (2025) 14:555. doi: 10.3390/cells14070555

47. Lin Y, Pang Q, Shi Y, Chen X, Tu F. Long noncoding RNA MALAT1 promotes angiogenesis through the caveolin-1/VEGF pathway after cerebral ischemic injury. *Neuroreport*. (2025) 36:350–63. doi: 10.1097/WNR.0000000000002157

48. Lu Y. Blocking lncRNA NOP14-AS1 overcomes 5-Fu resistance of colon cancer cells by modulating miR-30a-5p-LDHA-glucose metabolism pathway. *Discover Oncol.* (2025) 16:458. doi: 10.1007/s12672-025-02156-4

49. Chen Y, Zhu J-Y, Hong KH, Mikles DC, Georg GI, Goldstein AS, et al. Structural basis of ALDH1A2 inhibition by irreversible and reversible small molecule inhibitors. *ACS Chem Biol.* (2018) 13:582–90. doi: 10.1021/acschembio.7b00685

50. Beecroft SJ, Ayala M, McGillivray G, Nanda V, Agolini E, Novelli A, et al. Biallelic hypomorphic variants in ALDH1A2 cause a novel lethal human multiple congenital anomaly syndrome encompassing diaphragmatic, pulmonary, and cardiovascular defects. *Hum Mutat.* (2021) 42:506–19. doi: 10.1002/humu.24179

51. Oliveira LDM, Teixeira FME, Sato MN. Impact of retinoic acid on immune cells and inflammatory diseases. *Mediators Inflammation.* (2018) 2018:3067126. doi: 10.1155/2018/3067126

52. Erbs G, Jakobsen JT, Schmidt ST, Christensen D, Bailey M, Jungersen G. Retinoic acid-adjuvanted vaccine induces antigen-specific secretory IgA in the gut of newborn piglets. *Vaccine.* (2025) 46:126672. doi: 10.1016/j.vaccine.2024.126672

53. Chun TY, Carman JA, Hayes CE. Retinoid repletion of vitamin A-Deficient mice restores IgG responses. *J Nutr.* (1992) 122:1062–9. doi: 10.1093/jn/122.5.1062

54. Hao X, Zhong X, Sun X. The effects of all-trans retinoic acid on immune cells and its formulation design for vaccines. *AAPS J.* (2021) 23:32. doi: 10.1208/s12248-021-00565-1

55. Riccomi A, Piccaro G, Christensen D, Palma C, Andersen P, Vendetti S. Parenteral vaccination with a tuberculosis subunit vaccine in presence of retinoic acid provides early but transient protection to M. Tuberculosis infection. *Front Immunol.* (2019) 10:437157. doi: 10.3389/fimmu.2019.00934

56. Sadeghzadeh-Bazargan A, Behrangi E, Goodarzi A. Systemic retinoids in the COVID-19 era – are they helpful, safe, or harmful? a comprehensive systematized review. *Iranian J Dermatol.* (2020) 23:9–12. doi: 10.22034/ijd.2020.114847

57. Elkazzaz M, Abo-Amer YE-E, Ahmed A, Haydara T. 13 cis retinoic acid improved the outcomes of COVID-19 patients. *A randomized Clin trial. medRxiv.* (2022). doi: 10.1101/2022.03.05.22271959

58. Silveira KC, Fonseca IC, Oborn C, Wengryn P, Ghafoor S, Beke A, et al. CYP26B1-related disorder: expanding the ends of the spectrum through clinical and molecular evidence. *Hum Genet.* (2023) 142:1571. doi: 10.1007/s00439-023-02598-2

59. Takeuchi H, Yokota A, Ohoka Y, Iwata M. Cyp26b1 regulates retinoic acid-dependent signals in T cells and its expression is inhibited by transforming growth factor-β. *PloS One.* (2011) 6:e16089. doi: 10.1371/journal.pone.0016089

60. Chenery A, Burrows K, Antignano F, Underhill TM, Petkovich M, Zaph C, et al. The retinoic acid-metabolizing enzyme cyp26b1 regulates CD4 T cell differentiation and function. *PloS One.* (2013) 8:e72308. doi: 10.1371/journal.pone.0072308

61. Ogawa Y, Schafer DP, Horresh I, Bar V, Hales K, Yang Y, et al. Spectrins and ankyrinB constitute a specialized paranodal cytoskeleton. *J Neurosci.* (2006) 26:5230–9. doi: 10.1523/JNEUROSCI.0425-06.2006

62. Zhang C, Susuki K, Zollinger DR, Dupree JL, Rasband MN. Membrane domain organization of myelinated axons requires βII spectrin. *J Cell Biol.* (2013) 203:437–43. doi: 10.1083/jcb.201308116

63. Tang Y, Katuri V, Dillner A, Mishra B, Deng C-X, Mishra L. Disruption of transforming growth factor-beta signaling in ELF beta-spectrin-deficient mice. *Science.* (2003) 299:574–7. doi: 10.1126/science.1075994

64. Nihei Y, Haniuda K, Higashiyama M, Asami S, Iwasaki H, Fukao Y, et al. Identification of IgA autoantibodies targeting mesangial cells redefines the pathogenesis of IgA nephropathy. *Sci Adv.* (2023) 9:eadd6734. doi: 10.1126/sciadv.add6734

65. Havlicek MG. The role of the host factor SPTBN1 in HIV-1 infection of the role of the host factor SPTBN1 in HIV-1 infection of microglial cells microglial cells.

66. Dai L-P, Xu X-D, Yang T-T, Yin Z-H, Ye Z-Z, Wei Y-Z. SPTBN1 attenuates rheumatoid arthritis synovial cell proliferation, invasion, migration and inflammatory response by binding to PIK3R2. *Immun Inflammation Dis.* (2022) 10:e724. doi: 10.1002/iid3.724

67. Van Der Meer LT, Jansen JH, van der Reijden BA. Gfi1 and Gfi1b: key regulators of hematopoiesis. *Leukemia.* (2010) 24:1834–43. doi: 10.1038/leu.2010.195

68. Möröy T, Khandanpour C. Growth factor independence 1 (Gfi1) as a regulator of lymphocyte development and activation. *Semin Immunol.* (2011) 23:368–78. doi: 10.1016/j.smim.2011.08.006

69. Igwe E, Kosan C, Khandanpour C, Sharif-Askari E, Brüne B, Möröy T. The zinc finger protein Gfi1 is implicated in the regulation of IgG2b production and the expression of Igamma2b germline transcripts. *Eur J Immunol.* (2008) 38:3004–14. doi: 10.1002/eji.200838251

70. Xia Y, He F, Wu X, Tan B, Chen S, Liao Y, et al. GABA transporter sustains IL-1β production in macrophages. *Sci Adv.* (2021) 7:eabe9274. doi: 10.1126/sciadv.abe9274

71. Street VA, McKee-Johnson JW, Fonseca RC, Tempel BL, Noben-Trauth K. Mutations in a plasma membrane Ca2+-ATPase gene cause deafness in deafwaddler mice. *Nat Genet.* (1998) 19:390–4. doi: 10.1038/1284

72. Ficarella R, Di Leva F, Bortolozzi M, Ortolano S, Donaudy F, Petrillo M, et al. A functional study of plasma-membrane calcium-pump isoform 2 mutants causing digenic deafness. *Proc Natl Acad Sci U.S.A.* (2007) 104:1516–21. doi: 10.1073/pnas.0609775104

73. Merino-Wong M, Niemeyer BA, Alansary D. Plasma membrane calcium ATPase regulates stoichiometry of CD4+ T-cell compartments. *Front Immunol.* (2021) 12:687242. doi: 10.3389/fimmu.2021.687242

74. López-Bielma MF, Falfán-Valencia R, Fierro-Piña A, Abarca-Rojano E, Córdoba-Lanus E, Fricke-Galindo I, et al. Genetic variants in ATP2B2 as risk factors for mortality in patients unrelated but not associated with families with severe COVID-19. *Heliyon.* (2024) 10:e29493. doi: 10.1016/j.heliyon.2024.e29493

75. Ishida S, Kato K, Tanaka M, Odamaki T, Kubo R, Mitsuyama E, et al. Genome-wide association studies and heritability analysis reveal the involvement of host genetics in the Japanese gut microbiota. *Commun Biol.* (2020) 3:686. doi: 10.1038/s42003-020-01416-z

76. Rühlemann MC, Hermes BM, Bang C, Doms D, Moitinho-Silva L, Thingholm LB, et al. Genome-wide association study in 8,956 German individuals identifies influence of ABO histo-blood groups on gut microbiome. *Nat Genet.* (2021) 53:147–55. doi: 10.1038/s41588-020-00747-1

77. Weaver D, Gago S, Bassetti M, Ciacobbe DR, Prattes J, Hoenigl M, et al. Mycobiome analyses of critically ill COVID-19 patients. *Microbiol Spectr.* (2025) 13:e0411023. doi: 10.1128/spectrum.04110-23

78. Guha SK, Niyogi S. Microbial dynamics in COVID-19: unraveling the impact of human microbiome on disease susceptibility and therapeutic strategies. *Curr Microbiol.* (2024) 82:59. doi: 10.1007/s00284-024-04041-9

79. Bhanu P, Buchke S, Hemandhar-Kumar N, Varsha P, Kiran SKR, Vikneswaran G, et al. Comparative metagenomic analysis of the oral microbiome in COVID-19 patients and healthy individuals. *Sci Rep.* (2025) 15:10303. doi: 10.1038/s41598-024-81864-3

80. Ng HY, Liao Y, Cheung CL, Zhang R, Chan KH, Seto W-K, et al. Gut microbiota is associated with persistence of longer-term BNT162b2 vaccine immunogenicity. *Front Immunol.* (2025) 16. doi: 10.3389/fimmu.2025.1534787

81. Dutta S, Chatterjee N, Gallina NLF, Kar S, Koley H, Nanda PK, et al. Diet, microbiome, and probiotics establish a crucial link in vaccine efficacy. *Crit Rev Microbiol.* (2025) 20:1–26. doi: 10.1080/1040841X.2025.2480230

82. Worby CA, Dixon JE. Sorting out the cellular functions of sorting nexins. *Nat Rev Mol Cell Biol.* (2002) 3:919–31. doi: 10.1038/nrm974

83. Astle WJ, Elding H, Jiang T, Allen D, Ruklisa D, Mann AL, et al. The allelic landscape of human blood cell trait variation and links to common complex disease. *Cell.* (2016) 167:1415–29.e19. doi: 10.1016/j.cell.2016.10.042

84. Vuckovic D, Bao EL, Akbari P, Lareau CA, Mousas A, Jiang T, et al. The polygenic and monogenic basis of blood traits and diseases. *Cell.* (2020) 182:1214–31.e11. doi: 10.1016/j.cell.2020.08.008

85. Choudry FA, Bagger FO, Macaulay IC, Farrow S, Burden F, Kempster C, et al. Transcriptional characterization of human megakaryocyte polyploidization and lineage commitment. *J Thromb Haemost.* (2021) 19:1236–49. doi: 10.1111/jth.15271

86. Lacey J, Webster SJ, Heath PR, Hill CJ, Nicholson-Goult L, Wagner BE, et al. Sorting nexin 24 is required for α-granule biogenesis and cargo delivery in megakaryocytes. *Haematologica.* (2022) 107:1902. doi: 10.3324/haematol.2021.279636

87. Kaldis P, Pagano M. Wnt signaling in mitosis. *Dev Cell.* (2009) 17:749–50. doi: 10.1016/j.devcel.2009.12.001

88. Davidson G, Niehrs C. Emerging links between CDK cell cycle regulators and Wnt signaling. *Trends Cell Biol.* (2010) 20:453–60. doi: 10.1016/j.tcb.2010.05.002

89. Chen J-W, Wang Y-X, Gao R-R, Ma L-Y, Zhong J, Yang J-X, et al. CDK14 regulates the development and repair of lung. *Cell Death Discov.* (2025) 11:1–14. doi: 10.1038/s41420-025-02292-4

90. Chen S, Guan F, Candotti F, Benlagha K, Camara NOS, Herrada AA, et al. The role of B cells in COVID-19 infection and vaccination. *Front Immunol.* (2022) 13:988536. doi: 10.3389/fimmu.2022.988536

91. Rajamanickam A, Kumar NP, Nancy P A, Selvaraj N, Munisankar S, Renji RM, et al. Recovery of memory B-cell subsets and persistence of antibodies in convalescent COVID-19 patients. *Am J Trop Med Hyg.* (2021) 105:1255. doi: 10.4269/ajtmh.21-0883

92. Ciabattini A, Pastore G, Fiorino F, Polvere J, Lucchesi S, Pettini E, et al. Evidence of SARS-CoV-2-specific memory B cells six months after vaccination with the BNT162b2 mRNA vaccine. *Front Immunol.* (2021) 12:740708. doi: 10.3389/fimmu.2021.740708

93. Lin YC, Jhunjhunwala S, Benner C, Heinz S, Welinder E, Mansson R, et al. A global network of transcription factors, involving E2A, EBF1 and Foxo1, that orchestrates the B cell fate. *Nat Immunol.* (2010) 11:635. doi: 10.1038/ni.1891

94. Wöhner M, Tagoh H, Bilic I, Jaritz M, Kostanova D, Fischer M, et al. Molecular functions of the transcription factors E2A and E2-2 in controlling germinal center B cell and plasma cell development. *J Exp Med.* (2016) 213:1201. doi: 10.1084/jem.20152002

95. Wikström I, Forssell J, Goncalves M, Colucci F, Holmberg D. E2-2 regulates the expansion of pro-B cells and follicular versus marginal zone decisions. *J Immunol.* (2006) 177:6723–9. doi: 10.4049/jimmunol.177.10.6723

96. Zhang B, Zhang Z, Koeken VACM, Kuman S, Aillaud M, Tsay H-C, et al. Altered and allele-specific open chromatin landscape reveals epigenetic and genetic

regulators of innate immunity in COVID-19. *Cell Genomics*. (2023) 3:100232. doi: 10.1016/j.xgen.2022.100232

97. Zhang L, Nishi H, Kinoshita K. Single-cell RNA-seq public data reveal the gene regulatory network landscape of respiratory epithelial and peripheral immune cells in COVID-19 patients. *Front Immunol*. (2023) 14. doi: 10.3389/fimmu.2023.1194614

98. Amrute JM, Perry AM, Anand G, Cruchaga C, Hock KG, Farnsworth CW, et al. Cell specific peripheral immune responses predict survival in critical COVID-19 patients. *Nat Commun*. (2022) 13:882. doi: 10.1038/s41467-022-28505-3

99. Geng X, Xia X, Liang Z, Li S, Yue Z, Zhang H, et al. Tropomodulin1 exacerbates inflammatory response in macrophages by negatively regulating LPS-induced TLR4 endocytosis. *Cell Mol Life Sci*. (2024) 81:402. doi: 10.1007/s00018-024-05424-8

100. Liu X, Xia X, Wang X, Zhou J, Sung LA, Long J, et al. Tropomodulin1 expression increases upon maturation in dendritic cells and promotes their maturation and immune functions. *Front Immunol*. (2021) 11:587441. doi: 10.3389/fimmu.2020.587441

101. Camp CR, Vlachos A, Klöckner C, Krey I, Banke TG, Shariatzadeh N, et al. Loss of Grin2a causes a transient delay in the electrophysiological maturation of hippocampal parvalbumin interneurons. *Commun Biol*. (2023) 6. doi: 10.1038/s42003-023-05298-9

102. Strehlow V, Heyne HO, Vlaskamp DRM, Marwick KFM, Rudolf G, de Bellescize J, et al. GRIN2A-related disorders: genotype and functional consequence predict phenotype. *Brain*. (2019) 142:80–92. doi: 10.1093/brain/awy304

103. Yasmin F, Marwick KFM, Hunter DW, Nawaz S, Marshall GF, Booker SA, et al. Absence of GluN2A in hippocampal CA1 neurons leads to altered dendritic structure and reduced frequency of miniature excitatory synaptic events. *Brain Commun*. (2025) 7:fcaf124. doi: 10.1093/braincomms/fcaf124

104. Xu J, Wei H, You P, Sui J, Xiu J, Zhu W, et al. Non-neutralizing antibodies to SARS-Cov-2-related linear epitopes induce psychotic-like behavior in mice. *Front Mol Neurosci*. (2023) 16. doi: 10.3389/fnmol.2023.1177961

105. Wang J, Sun D, Wang Y, Ren F, Pang S, Wang D, et al. FOSL2 positively regulates TGF-β1 signalling in non-small cell lung cancer. *PLoS One*. (2014) 9:e112150. doi: 10.1371/journal.pone.0112150

106. Yang X, Letterio JJ, Lechleider RJ, Chen L, Hayman R, Gu H, et al. Targeted disruption of SMAD3 results in impaired mucosal immunity and diminished T cell responsiveness to TGF-β. *EMBO J*. (1999) 18:1280–91. doi: 10.1093/emboj/18.5.1280

107. Malhotra N, Kang J. SMAD regulatory networks construct a balanced immune system. *Immunology*. (2013) 139:1. doi: 10.1111/imm.12076

108. Zhao X, Nicholls JM, Chen YG. Severe acute respiratory syndrome-associated coronavirus nucleocapsid protein interacts with smad3 and modulates transforming growth factor-β Signaling. *J Biol Chem*. (2021) 283:3272. doi: 10.1074/jbc.M708033200

109. Liang L, Wang W, Chen J, Wu W, Huang X-R, Wei B, et al. SARS-CoV-2 N protein induces acute kidney injury in diabetic mice via the Smad3-Ripk3/MLKL necroptosis pathway. *Signal Transduction Targeted Ther*. (2023) 8:1–4. doi: 10.1038/s41392-023-01410-x

110. Wang W, Chen J, Hu D, Pan P, Lliang L, Wu W, et al. SARS-CoV-2 N protein induces acute kidney injury via Smad3-dependent G1 cell cycle arrest mechanism. *Advanced Sci*. (2021) 9:2103248. doi: 10.1002/advs.202103248

111. Chen M, Yao C, Qin Y, Cui X, Li P, Ji Z, et al. SARS-CoV-2 nucleocapsid protein triggers hyperinflammation via protein-protein interaction-mediated intracellular Cl– accumulation in respiratory epithelium. *Signal Transduction Targeted Ther*. (2022) 7:1–13. doi: 10.1038/s41392-021-00710-4

112. Mukund K, Nayak P, Ashokkumar C, Rao S, Almeda J, Betancourt-Garcia MM, et al. Immune response in severe and non-severe coronavirus disease 2019 (COVID-19) infection: A mechanistic landscape. *Front Immunol*. (2021) 12:738073. doi: 10.3389/fimmu.2021.738073

113. Klenke S, Rump K, Buschkamp K, Engler A, Peters J, Siffert W, et al. Characterization of the PLCB1 promoter and regulation by early growth response transcription factor EGR-1. *Eur J Pharmacol*. (2014) 742:8–14. doi: 10.1016/j.ejphar.2014.08.026

114. Lin Y-J, Chang J-S, Liu X, Tsang H, Chien W-K, Chen J-H, et al. Genetic variants in PLCB4/PLCB1 as susceptibility loci for coronary artery aneurysm formation in Kawasaki disease in Han Chinese in Taiwan. *Sci Rep*. (2015) 5:1–12. doi: 10.1038/srep14762

115. Reyes RA, Clarke K, Gonzales SJ, Cantwell AM, Garza R, Catano G, et al. SARS-CoV-2 spike-specific memory B cells express higher levels of T-bet and FcRL5 after non-severe COVID-19 as compared to severe disease. *PLoS One*. (2021) 16:e0261656. doi: 10.1371/journal.pone.0261656

116. García-Vega M, Llamas-Covarrubias MA, Loza M, Reséndiz-Sandoval M, Hinojosa-Trujillo D, Melgoza-González E, et al. Single-cell transcriptomic analysis of B cells reveals new insights into atypical memory B cells in COVID-19. *J Med Virol*. (2024) 96:e29851. doi: 10.1002/jmv.29851

117. Kleiber N, Lemus-Diaz N, Stiller C, Heinrichs M, Mai MM-Q, Hackert P, et al. The RNA methyltransferase METTL8 installs m3C32 in mitochondrial tRNAsThr/Ser (UCN) to optimise tRNA structure and mitochondrial translation. *Nat Commun*. (2022) 13:1–19. doi: 10.1038/s41467-021-27905-1

118. Huang M-H, Peng G-X, Mao X-L, Wang J-T, Zhou J-B, Zhang J-H, et al. Molecular basis for human mitochondrial tRNA m3C modification by alternatively spliced METTL8. *Nucleic Acids Res*. (2022) 50:4012. doi: 10.1093/nar/gkac184

119. Li Y, Jin H, Li Q, Shi L, Mao Y, Zhao L. The role of RNA methylation in tumor immunity and its potential in immunotherapy. *Mol Cancer*. (2024) 23:130. doi: 10.1186/s12943-024-02041-8

120. Zhang K, Eldin P, Ciesla JH, Briant L, Lentini JM, Ramos J, et al. Proteolytic cleavage and inactivation of the TRMT1 tRNA modification enzyme by SARS-CoV-2 main protease. *Elife*. (2024) 12:RP90316. doi: 10.7554/eLife.90316.2

121. Chen R, Cao J, Jiang W, Wang S, Cheng J. Upregulated expression of CYBRD1 predicts poor prognosis of patients with ovarian cancer. *J Oncol*. (2021) 2021:7548406. doi: 10.1155/2021/7548406

122. Chen ZZ, Johnson L, Trahtemberg U, Baker A, Huq S, Dufresne J, et al. Mitochondria and cytochrome components released into the plasma of severe COVID-19 and ICU acute respiratory distress syndrome patients. *Clin Proteomics*. (2023) 20:17. doi: 10.1186/s12014-023-09394-0

123. Tang M, Li Y, Luo X, Xiao J, Wang J, Zeng X, et al. Identification of biomarkers related to CD8+ T cell infiltration with gene co-expression network in lung squamous cell carcinoma. *Front Cell Dev Biol*. (2021) 9:606106. doi: 10.3389/fcell.2021.606106

124. Xie J, Mothe B, Alcalde Herraiz M, Li C, Xu Y, Jödicke AM, et al. Relationship between HLA genetic variations, COVID-19 vaccine antibody response, and risk of breakthrough outcomes. *Nat Commun*. (2024) 15:4031. doi: 10.1038/s41467-024-48339-5

125. Demonbreun AR, Sancilio A, Velez ME, Ryan DT, Pesce L, Saber R, et al. COVID-19 mRNA vaccination generates greater immunoglobulin G levels in women compared to men. *J Infect Dis*. (2021) 224:793–7. doi: 10.1093/infdis/jiab314

126. Jensen A, Stromme M, Moyassari S, Chadha AS, Tartaglia MC, Szoeke C, et al. COVID-19 vaccines: Considering sex differences in efficacy and safety. *Contemp Clin Trials*. (2022) 115:106700. doi: 10.1016/j.cct.2022.106700

127. Bachmann M, Gültekin N, Stanga Z, Fehr JS, Ülgür II, Schlagenhauf P. Disparities in response to mRNA SARS-CoV-2 vaccines according to sex and age: A systematic review. *New Microbes New Infect*. (2024) 63:101551. doi: 10.1016/j.nmni.2024.101551

128. Jay C, Adland E, Csala A, Lim N, Longet S, Ogbe A, et al. Age- and sex-specific differences in immune responses to BNT162b2 COVID-19 and live-attenuated influenza vaccines in UK adolescents. *Front Immunol*. (2023) 14:1248630. doi: 10.3389/fimmu.2023.1248630

frontiers | Frontiers in Immunology

TYPE Original Research
PUBLISHED 05 September 2025
DOI 10.3389/fimmu.2025.1657082

OPEN ACCESS

EDITED BY
Fabio Fiorino,
LUM University Giuseppe Degennaro, Italy

REVIEWED BY
Maria Hristianova Nikolova,
National Center of Infectious and Parasitic Diseases (NCIPD), Bulgaria
Ritthideach Yorsaeng,
Chulalongkorn University, Thailand

*CORRESPONDENCE
Stefania Varchetta
stefania.varchetta@policlinico.mi.it

†These authors share last authorship

RECEIVED 30 June 2025
ACCEPTED 12 August 2025
PUBLISHED 05 September 2025

CITATION
Varchetta S, Golfetto FS, Bono P, Callegaro A, Fabbris T, Favalli A, Crosti M, De Feo TM, Iannotti N, Bozzi G, Castelli V, Mariani B, Muscatello A, Abrignani S, Grifantini R, Bandera A and Lombardi A (2025) Reduced spike specific T-cell responses in COVID-19 vaccinated subjects undergoing SARS-CoV-2 breakthrough infection.
Front. Immunol. 16:1657082.
doi: 10.3389/fimmu.2025.1657082

Reduced spike specific T-cell responses in COVID-19 vaccinated subjects undergoing SARS-CoV-2 breakthrough infection

Stefania Varchetta[1*], Federica Sole Golfetto[1], Patrizia Bono[2], Annapaola Callegaro[2], Tanya Fabbris[3], Andrea Favalli[3], Mariacristina Crosti[3], Tullia Maria De Feo[4], Nathalie Iannotti[1], Giorgio Bozzi[1], Valeria Castelli[1], Bianca Mariani[1], Antonio Muscatello[1], Sergio Abrignani[3,5], Renata Grifantini[3], Alessandra Bandera[1,6†] and Andrea Lombardi[1,6†]

[1]Infectious Diseases Unit, Department of Internal Medicine, Fondazione IRCCS Ca' Granda Ospedale Maggiore Policlinico, Milan, Italy, [2]Microbiology and Virology Unit, Foundation IRCCS Ca' Granda Ospedale Maggiore Policlinico, Milan, Italy, [3]INGM, Istituto Nazionale Genetica Molecolare "Romeo ed Enrica Invernizzi", Milan, Italy, [4]North Italy Transplant program (NITp). Transplant Coordination Unit, Fondazione IRCSS Ca' Granda Ospedale Maggiore Policlinico, Milan, Italy, [5]Department of Clinical Sciences and Community Health, Università degli Studi di Milano, Milan, Italy, [6]Department of Pathophysiology and Transplantation, University of Milan, Milan, Italy

Introduction: T-cell responses to SARS-CoV-2 remain largely preserved across variants despite waning neutralizing antibodies. However, T-cell immunity may vary with the host's immune status, and data on T-cell responses in post-vaccine infections (PVI) are limited.

Methods: We assessed Spike-specific T-cell responses in 32 vaccinated individuals, 16 of whom experienced PVI. Immune responses were evaluated at three time points: 1 month after the second vaccine dose (T1), 1 month after the booster dose (T2), and, in the PVI group, 1–3 months after the first positive nasal swab (T3). Additionally, we evaluated anti-spike antibody levels, T-cell exhaustion markers, and natural killer cell subsets, focusing on memory-like $CD57^+$ $NKG2C^+$ cells.

Results: Subjects who developed PVI exhibited significantly reduced Spike-specific CD4 T-cell responses following the booster dose compared to vaccinated individuals who remained uninfected. This was accompanied by increased frequencies of $LAG\text{-}3^+$ $CD4^+$ and $CD8^+$ T-cells. A positive correlation was observed between AIM^+ $CD4^+$ T-cells and $NKG2C^+$ NK cells at T2 in PVI subjects. Following natural infection, T-cell responses were enhanced and associated with an expansion of $NKG2C^+$ NK cells.

Conclusions: Individuals experiencing PVI displayed impaired booster-induced $CD4^+$ T-cell responses and increased expression of the immune checkpoint LAG-3. Natural infection restored and enhanced cellular immunity, particularly

through the expansion of Spike-specific T-cells and memory NK cell populations. This study identifies an immune profile characterized by low spike-specific responses, which are associated with an increased susceptibility to breakthrough infections.

KEYWORDS

SARS-CoV-2, vaccine, breakthrough infection, T cell immune responses, natural killercells, LAG-3

1 Introduction

Five years after the COVID-19 pandemic, significant data have been collected regarding the breadth and durability of the T-cell responses following SARS-CoV-2 infection or COVID-19 vaccination (1, 2). One significant discovery is the ability of T-cells to cross-recognize SARS-CoV-2 variants, including those with extensive mutations in the spike protein (3, 4). Indeed, despite the immune evasion observed in neutralizing antibody responses, T-cell responses have remained largely preserved across variants (5–8).

This preservation of T-cell functionality may explain the effectiveness of vaccines against severe disease, even when breakthrough infections occur with antigenically distinct variants (9). This cross-reactivity is particularly evident in $CD4^+$ T-cells, which target conserved epitopes in the spike protein (10, 11). While $CD8^+$ T-cell responses are more variable, these cells can adapt by generating *de novo* responses to mutated epitopes following breakthrough infections (12, 13). Tarke et al. demonstrated that over 80% of $CD4^+$ and $CD8^+$ T-cell epitopes are conserved across variants of concern, suggesting a robust cellular immune memory that is less susceptible to viral escape than humoral immunity (14).

Multiple studies have identified breakthrough infections as potentially beneficial immunological events that broaden the immune response beyond that achieved by vaccination alone (15, 16). These infections may function as natural boosters, especially against emerging variants not represented in the original vaccine formulations (17).

However, the precise immunological profile characterizing subjects who undergo breakthrough infections, particularly at the T-cell level, remains incompletely characterized.

Notably, Natural killer (NK) cells have been identified as essential components in the orchestration of vaccine-induced immune responses and are considered a promising target for enhancing vaccination strategies (18). These cells rapidly produce cytokines, such as IFN-γ, which can induce T-cell activation, promote dendritic cell maturation and the priming of virus-specific T-cells. In particular, increasing data support a critical role for "memory-like" NK cells in both the induction and the effector phases in response to vaccines (19–23). This subset of NK cells, identified in CMV-positive individuals, is characterized by the expression of the $NKG2C^+$ activating receptor (19, 24). Memory-like NK cells may recognize peptide-HLA-E complex through binding to NKG2C (25). The therapeutic potential of these cells is recognized by their employment in many clinical trials for viral infections and cancer (23, 26–29).

In this study, we conducted a comprehensive analysis of NK and T-cell immunomodulation, including Spike-specific T-cell responses in 32 COVID-naïve individuals vaccinated with three doses of the original (Wuhan-Hu-1) mRNA or adenoviral vaccine. Among them, 16 experienced a breakthrough infection following booster dose during the December 2021-April 2022 period, when the Omicron sublineage BA.1 was the predominant SARS-CoV-2 variant in Italy (30, 31).

Our findings reveal unexpected dynamics in the $CD4^+$ and $CD8^+$ T-cell compartments following booster vaccination and breakthrough infection and provide essential insights into the complex interplay between vaccination and breakthrough infection in shaping T and NK-cell immunity against SARS-CoV-2.

2 Materials and methods

2.1 Study design and participants

Healthcare workers from Fondazione IRCCS Ca' Granda Policlinico in Milan, Italy, were enrolled during the initial COVID-19 vaccination campaign. All participants received their first COVID-19 vaccination schedule with one of the following vaccines as primary regimen: BNT162b2 (Comirnaty, Pfizer–BioNTech), ChAdOx1-S (Vaxzevria, AstraZeneca–Oxford) or mRNA-1273 (Spikevax, Moderna–NIAID). Booster doses consisted of BNT162b2 (Comirnaty, Pfizer–BioNTech) or mRNA-1273 (Spikevax, Moderna–NIAID). Table 1 shows the demographic and vaccination features of the subjects included in the study.

Among them, we identified 16 subjects with SARS-CoV-2 infection between 1–3 months after the third vaccine dose (post-vaccine infection, PVI) group. SARS-CoV-2 infection was identified through positive PCR on nasal swab, performed in all study participants reporting symptoms compatible with influenza-like illness. Sixteen control subjects of the same sex and similar age were also included in the study (CTRL group). We included in the

10.3389/fimmu.2025.1657082

TABLE 1 Demographic data and vaccination schedule in controls and PVI subjects.

Demographic and vaccination features	CTRL (N=16)	PVI (N=16)	Total (N=32)
Age, median (range)	45.5 (25-64)	43.5 (26-58)	44.5 (25-64)
Female gender, n (%)	8 (50.0)	9 (56.2)	17 (53.1)
1° -2° vaccine dose			
BNT162b2 (Comirnaty, Pfizer–BioNTech) n (%)	7 (43.7)	3 (18.7)	10 (31.2)
ChAdOx1-S (Vaxzevria, AstraZeneca–Oxford n (%)	9 (56.2)	10 (62.5)	19 (59.3)
mRNA-1273 (Spikevax, Moderna–NIAID) n (%)	0	3 (18.7)	3 (9.3)
3° vaccine dose			
BNT162b2 (Comirnaty, Pfizer–BioNTech) n (%)	15 (93.7)	12 (75.0)	27 (84.3)
ChAdOx1-S (Vaxzevria, AstraZeneca–Oxford), n (%)	0	0	0
mRNA-1273 (Spikevax, Moderna–NIAID) n (%)	1 (6.2)	4 (25.0)	5 (15.6)
Days between booster dose and PVI; median(IQR)	–	54 (38 - 123)	–
Days between PVI and T3; median (IQR)	–	49 (28-62)	–

PVI, Post Vaccine Infection.

survey only subjects who tested negative for SARS-CoV-2 anti-nucleocapsid IgG and provided informed consent for the study. Immune responses were examined in peripheral blood mononuclear cells (PBMC) collected at the following time points: 1 month after the second dose (T1), 1 month after the third dose (T2, booster) and 15–90 days following the first positive swab (only for IPV group) (T3). Figure 1 shows time sampling and time of infection.

All subjects signed an informed consent. The study protocol adhered to the ethical guidelines outlined in the 1975 Declaration of Helsinki. It was approved by the Ethics Committee Lombardia 3 (document number 878, date of approval 18/03/2021).

2.1.1 Isolation of peripheral blood mononuclear cells

Peripheral blood mononuclear cells (PBMC) were isolated by density gradient centrifugation (1.077 g/ml) using Ficoll-Plaque (Cedarlane, Burlington, Canada) according to the manufacturer's instructions. Briefly, whole blood was diluted with an equal volume of phosphate-buffered saline (PBS) and layered on the Ficoll gradient. PBMC were isolated after centrifugation at 500 x g for 30 min at room temperature without brakes. PBMC were resuspended in PBS-EDTA and centrifuged at 400 × g for 10 min. Pellets were resuspended in PBS containing 2% FBS and washed by centrifugation at 250 × g for 10' at room temperature. Cell numbers

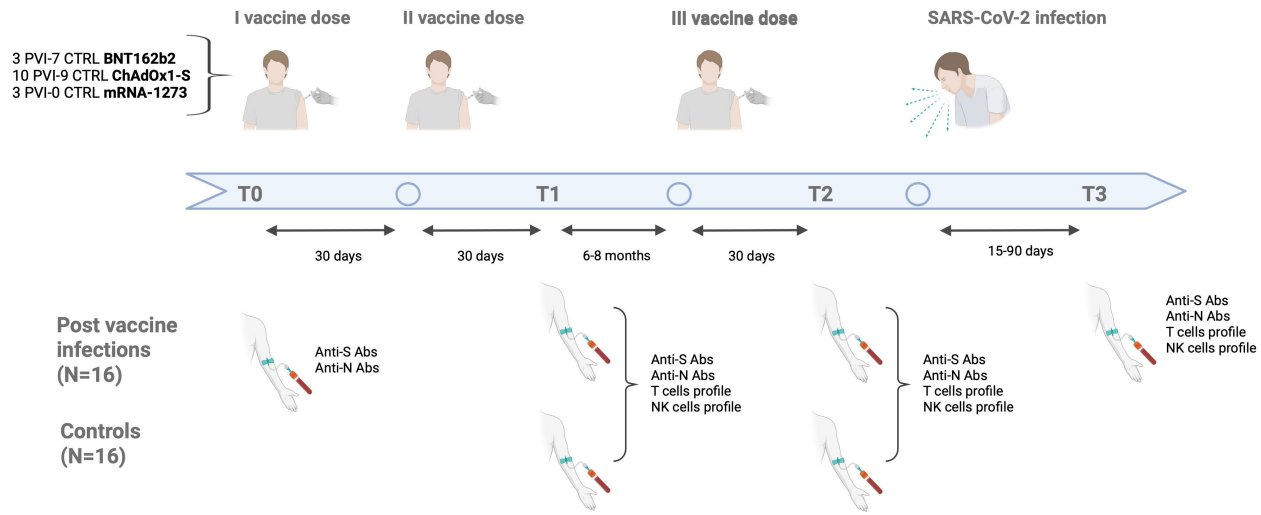

FIGURE 1
Time of vaccination and blood sampling scheme.

were determined by light microscopy count in a Burker chamber. Nonviable cells were identified by staining with trypan blue. Isolated PBMC were frozen in fetal bovine serum (FBS) with 10% dimethyl sulfoxide (DMSO) and stored in liquid nitrogen until use.

2.2 Peptide pools

A total of 53 synthetic 15-mer peptide pools, overlapping by 11 amino acid residues, covering the full-length Spike protein of the ancestral Wuhan strain (GenBank: MN_908947), were used as part of the PepTivator® SARS-CoV-2 Prot_S Complete, premium grade (Miltenyi Biotec, Bergisch Gladbach, Germany). The peptide pools were dissolved following the manufacturer's directions in sterile water. As a positive control, cells were stimulated with staphylococcal enterotoxin B (1 µg/mL, Sigma-Aldrich).

2.3 Activation-induced marker assay

Cryopreserved PBMC were thawed, resuspended in complete medium (RPMI 1640 containing 10% FBS, 1% L-glutamine, and 1% penicillin/streptomycin) and rested at 2×10^6 cells for 2 hours at 37° C. Then, 1×10^6 PBMC/well were plated in 96 well U-plates in complete medium in the presence/absence of 1µg/ml of Spike overlapping peptides. After 18 hours, PBMCs were washed and stained with CD3 BUV395 (clone UCHT1), CD56 RB613 (clone B159), CD4 APC (clone SK3), CD8 BUV737 (clone SK1), CD134 (OX40) RY586 (clone ACT35), CD137 (41BB) (RB744 (clone 4B4-1), CD69 BV480 (clone FN50), CD45RA RB545 (clone HI100), CD45RO BV786 (clone UCHL1), CCR7 BV711 (clone 2-L1-A), CD14 BUV496 (clone MφP9), CD19 BUV496 (clone SJ25C1) (BD Biosciences, CA, USA). A LIVE/DEAD® Fixable Near-IR Dead Cell Stain Kit (Thermo Fisher Scientific, Waltham, MA, USA) was used to determine cell viability. After washing, cells were fixed with 2% paraformaldehyde in PBS and acquired with a FACS Symphony (BD Biosciences) flow cytometer. Spike-specific T cells were identified by activation-induced markers (AIM), measured as $CD134^+$ $CD137^+$ co-expression in $CD4^+$ and as $CD69^+CD137^+$ co-expression in $CD8^+$ T cell subsets (gating strategy shown in Supplementary Figure 1. The frequency of AIM^+ T cells in Spike-stimulated samples was determined by subtracting the frequency of AIM^+ T cells observed in the corresponding unstimulated (negative control) samples Three PVI subjects missed PBMC from timepoint 1. Staphylococcal enterotoxin B (SEB) 1 mg/ml) was used as positive control.

2.4 NK cell immunophenotype

Natural killer cell phenotype was assessed on thawed PBMC after resting for 2 hours at 37°C. A LIVE/DEAD® Fixable Near-IR Dead Cell Stain Kit (Thermo Fisher Scientific) was used to determine cell viability. To identify NK cell subsets, the following antibodies were used: CD56 RB613 (clone B159), CD3 BUV563 (clone SK7), CD8 BUV737 (clone SK1), CD16 RY775 (clone 3G8), CD57 BUV395 (clone NK-1), CD69 BV480 (clone FN50), NKp46 BV786 (clone 9E2/NKp46), NKp30 BUV661 (clone p30-15), NKG2D BV711 (clone 1D11), CD127 RB744 (clone HIL-7R-M21), TIGIT BV650 (cloneTgMab-2), KLRG1 BV750 (clone Z7-205.rMAb), NKG2C BV421 (clone 134591) (BD Biosciences), NKG2AVio Bright B515 (clone REA1100) (Miltenyi Biotec, Bergisch Gladbach, Germany), Siglec-7 PE (clone QA79) ThermoFisher, MA, USA). After washing, cells were fixed with 2% paraformaldehyde in PBS and acquired with a FACSymphony A5 (BD Biosciences) flow cytometer. FlowJo software (v10.10) (BD Biosciences) was used to analyze data. An unsupervised approach was performed using the FlowJo plugin Uniform Manifold Approximation and Projection (UMAP) analysis on concatenated live NK cells. A total of 1260 NK cells for each individual were downsampled and concatenated before applying UMAP. Concatenated cells were clustered using FlowSom analysis. The cluster explorer plugin was used to identify cell clusters. In detail, 1260 NK cells were concatenated and analyzed with the FlowJo UMAP plugin. UMAP was run with the default settings (Euclidean distance function, nearest neighbors: 15 and minimum distance: 0.5). UMAP projections were obtained for concatenated cells from controls (n=16) and PVI subjects (n=16).

2.5 Antibody measurement

Elecsys Anti-SARS-CoV-2 S kit (Roche Diagnostics, Mannheim, Germany) was used to assess the development of total anti-Spike antibodies following SARS-CoV-2 vaccination. Precisely, this assay predominantly detects anti-RBD antibodies. Elecsys Anti-SARS-CoV-2 kit (Roche) was used to evaluate the development of total anti-N antibodies following SARS-CoV-2 infection. The threshold values were 1.0 Cut-Off Index (COI) for anti-N and 0.8 U/mL for anti-S.

2.6 Statistical analysis

Statistical analysis and graphical presentations were performed using GraphPad Software version 10.5.0 (GraphPad Software Inc, La Jolla, CA). Statistical differences between data within the same group were assessed by the non-parametric Friedman test followed by Dunn's multiple comparisons or by the Wilcoxon matched-pairs signed-rank test. A mixed-effects model (REML) with Holm-Sidak's multiple comparisons test was used, accounting for missing data. The Mann-Whitney U test was used to compare the differences between the two groups. The Shapiro-Wilk test was used to determine whether the data were normally distributed. The Fisher's exact test was used to compare frequencies of responders to stimulation above the cut-off threshold (median values obtained after stimulation with the vehicle control for the AIM assay, 2 for the stimulation index).

10.3389/fimmu.2025.1657082

3 Results

3.1 Study participants

This monocentric study recruited 32 COVID-19-naïve subjects who were vaccinated against COVID-19 at the Policlinico of Milan between January and December 2021. Seventeen subjects (53.1%) were female. The median age was 44.5 (range 25-64) years. The age of the control group ranged from 25 to 64 years, and the PVI group from 26 to 58 years. Only one subject, in the control group, was over 60. None of the subjects had comorbidities, except one control with obesity (Table 2). All patients received COVID-19 vaccination with a primary regimen of two vaccine doses followed by a third booster dose. The vaccines employed were BNT162b2, ChAdOx1-S or mRNA-1273. The adenoviral Chadox1-S vaccine was administered only as

TABLE 2 Individual demographic characteristics, comorbidities and vaccine type.

Subject ID	Sex	Age (years)	Comorbidities	Vaccine type (1st/2nd dose)	Vaccine type (3rd dose)
CTRL 0004	M	32	None	BNT162b2	BNT162b2
CTRL 0009	F	64	None	BNT162b2	BNT162b2
CTRL 0011	F	53	None	BNT162b2	BNT162b2
CTRL 0012	F	45	Obesity	BNT162b2	BNT162b2
CTRL 0028	F	59	None	BNT162b2	BNT162b2
CTRL 0029	M	58	None	BNT162b2	BNT162b2
CTRL 0034	F	57	None	BNT162b2	BNT162b2
CTRL 0037	F	30	None	ChAdOx1 S	BNT162b2
CTRL 0040	F	51	None	ChAdOx1 S	BNT162b2
CTRL 0043	M	47	None	ChAdOx1 S	BNT162b2
CTRL 0052	M	46	None	ChAdOx1 S	BNT162b2
CTRL 0053	F	37	None	ChAdOx1 S	BNT162b2
CTRL 0068	M	25	None	ChAdOx1 S	mRNA - 1273
CTRL 0069	M	25	None	ChAdOx1 S	BNT162b2
CTRL 0072	M	33	None	ChAdOx1 S	BNT162b2
CTRL 0077	M	40	None	ChAdOx1 S	BNT162b2
PVI 0013	F	43	None	BNT162b2	BNT162b2
PVI 0030	M	58	None	BNT162b2	BNT162b2
PVI 0032	F	56	None	BNT162b2	BNT162b2
PVI 0035	F	52	None	ChAdOx1 S	BNT162b2
PVI 0039	M	38	None	ChAdOx1 S	BNT162b2
PVI 0044	M	50	None	ChAdOx1 S	BNT162b2
PVI 0055	M	38	None	ChAdOx1 S	BNT162b2
PVI 0059	M	47	None	ChAdOx1 S	BNT162b2
PVI 0065	F	30	None	ChAdOx1 S	BNT162b2
PVI 0076	M	31	None	ChAdOx1 S	mRNA - 1273
PVI 0078	F	33	None	ChAdOx1 S	BNT162b2
PVI 0084	F	35	None	ChAdOx1 S	BNT162b2
PVI 0087	M	26	None	ChAdOx1 S	BNT162b2
PVI 0127	F	58	None	mRNA - 1273	mRNA - 1273
PVI 0251	F	44	None	mRNA - 1273	mRNA - 1273
PVI 0264	F	46	None	mRNA - 1273	mRNA - 1273

a primary regimen in 19 individuals and given in two doses separated by 4–6 weeks. The mRNA vaccines BNT162b2 and mRNA-1273 were used as primary regimens in 13 subjects and for boosting in all participants. When used as a primary regimen, these vaccines required two doses separated by 4–6 weeks. Among the 16 subjects with ascertained SARS-CoV-2 infection, none required hospitalization or oxygen supplementation with all belonging to WHO ordinal clinical severity scale 1 and 2. Figure 1 shows time sampling and time of infection.

3.2 Anti-spike and anti-nucleocapsid antibodies

All subjects were tested for serum levels of anti-N and anti-Spike antibodies at T0 (before vaccination) and at the subsequent timepoints (T1, T2 and T3) (Figure 2).

All sera were negative for anti-N antibodies at T0, T1 and T2, confirming the naïve status of all individuals during the study (Figures 2A, B). All PVI subjects except one developed anti-N antibodies at T3 following natural infection. However, there was substantial variation in anti-N antibody levels, ranging from 0 to 52 Cut-Off Index (COI) levels (Figure 2B). Anti-Spike antibodies were significantly increased along time points in both groups (Figures 2C, D), and their level was comparable in the two groups at all time points (Figure 2E).

3.3 T-cell maturation subsets

We investigated the immunophenotypic dynamics of $CD4^+$ and $CD8^+$during vaccine follow-up using multiparametric flow cytometry. The analysis of $CD4^+$ T-cell maturation subsets revealed a consistent decline in naïve cells at T2 compared to T1 across both study groups. In contrast, central memory (CM) $CD4^+$ T-cells increased significantly in the control group, with a similar trend in PVI subjects ($p = 0.054$). A trend toward a significant reduction of the frequency of CM CD4 T-cells was observed at T2 in PVI compared with controls ($p= 0.08$) (Supplementary Figures 2A, B). Notably, the PVI group exhibited a significant increase in effector memory (EM) and terminally differentiated effector memory T cells re-expressing CD45RA (EMRA) $CD4^+$ T-cells at T3 (Supplementary Figures 2C, D).

Among $CD8^+$ T-cells, controls exhibited a marked decrease in naïve and EMRA subsets at T2 (Supplementary Figure 2D), as well as a significant expansion of central memory cells (Supplementary Figure 2E). A considerable reduction of EMRA CD8 T-cells was present at T2 in the control group only (Supplementary Figure 2G),

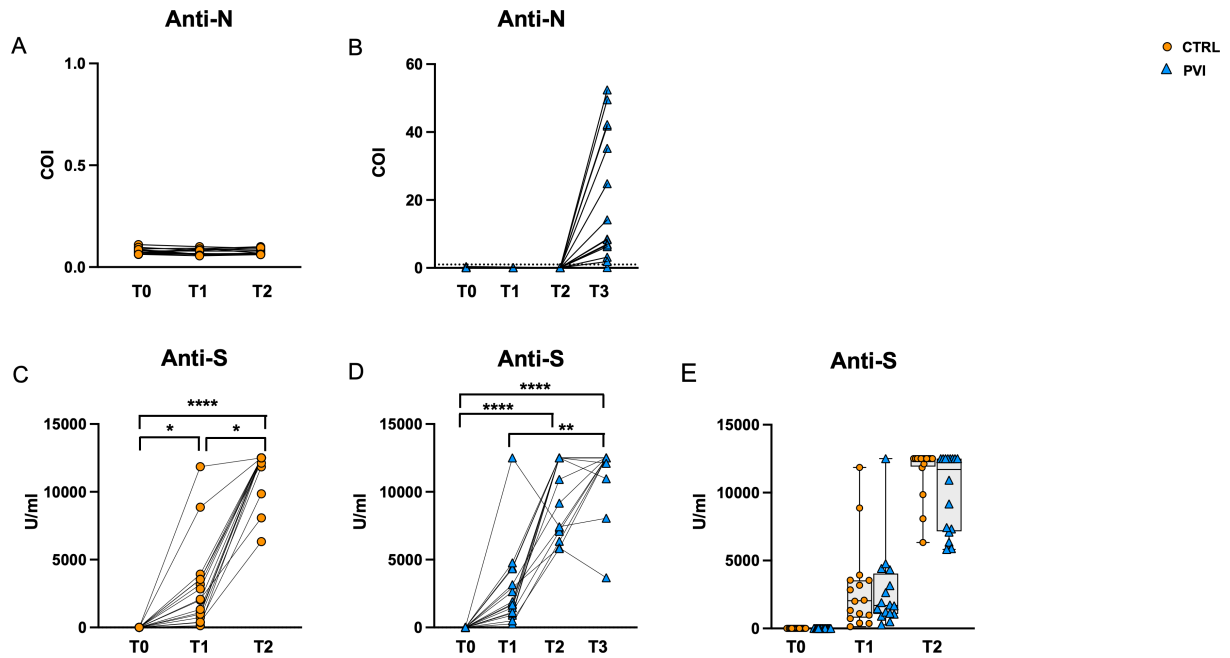

FIGURE 2
Antibody secretion following vaccination. Anti-N IgG tested negative in controls **(A)** and PVI **(B)** subjects at T0, T1 and T2. All PVI subjects except one developed anti-N antibodies following natural infection at T3 **(B)**. Anti-S antibodies were significantly increased among timepoints in control- **(C)** as well as IPV subjects **(D)**. Comparable anti-S antibodies were observed between IPVs (blue triangle) and CTRLs (orange circle) during vaccine timepoint follow-up **(E)**. Anti-N, anti nucleocapsid antibodies; anti-S, anti-Spike antibodies; COI, Cut-Off Index. The one-way Friedman with Dunn's multiple comparison test was used to compare data within the same group. The non-parametric Mann–Whitney U test was used to assess statistical differences between groups. *$p < 0.05$; **$p<0.01$; ****$p<0.0001$.

while no differences were observed among EM CD8 T-cells Supplementary Figure 2F).

3.4 COVID-19 vaccination was unable to induce an effective CD4$^+$ and CD8$^+$ T-cell response following the booster dose

To assess Spike-specific recall responses, AIM analysis was performed on T-cells following stimulation with overlapping peptides (OP) spanning the Spike protein. Co-expression of OX40 (CD134) and 4-1BB (CD137) was used to identify Spike-specific CD4$^+$ T-cell activation. CD4$^+$ T-cells exhibited significantly increased activation following OP stimulation compared to the negative control (unstimulated cells) at all time points in both groups (Figures 3A, B). After background subtraction of AIM responses observed in the negative controls, the control group showed a significant increase in the frequencies of AIM$^+$ CD4$^+$ T-cells at T2 compared to T1. At T1, the comparison between the two groups showed similar frequencies of Spike-specific CD4$^+$ T-cells. However, at T2, the PVI group exhibited a reduced frequency of AIM$^+$ CD4 T-cells compared to controls (Figure 3C); furthermore, the proportion of subjects with responses above the threshold (defined as the median of negative control values) was also significantly lower in the PVI group at T2.

Additionally, the stimulation index (SI), calculated as the ratio of AIM$^+$ CD4$^+$ T-cell frequencies in stimulated versus unstimulated cells, was significantly increased at T2 compared to T1 in the control group only. Notably, at T2, the IPV group had a considerably lower SI compared to controls (Figure 3D). Consistently, the proportion of subjects with a ≥2-fold SI response was significantly reduced in the PVI group at T2 (Figure 3D). Representative CD4+ AIM dot plots are shown in Figures 3E, F.

Spike-specific CD8$^+$ T-cell responses were assessed through CD69 and CD137 co-expression analysis. Following stimulation with Spike OP, CD8$^+$ T-cell responses were significantly increased compared to the negative control at all time points in both groups. (Figures 4A, B). No differences in antigen-specific AIM responses were observed between the two groups after subtracting the AIM responses in negative control (Figures 4C). However, a significantly increased frequency of Spike-specific CD8$^+$ T-cells was observed at T2 compared to T1 in the control group only. Similarly, a significant increase in the SI was observed at T2 compared to T1 in the control group only (Figure 4D). No significant differences were observed among the frequency of subjects responding above the AIM or SI threshold (Figures 4C, D). Representative CD8+ AIM dot plots are shown in Figures 4E, F.

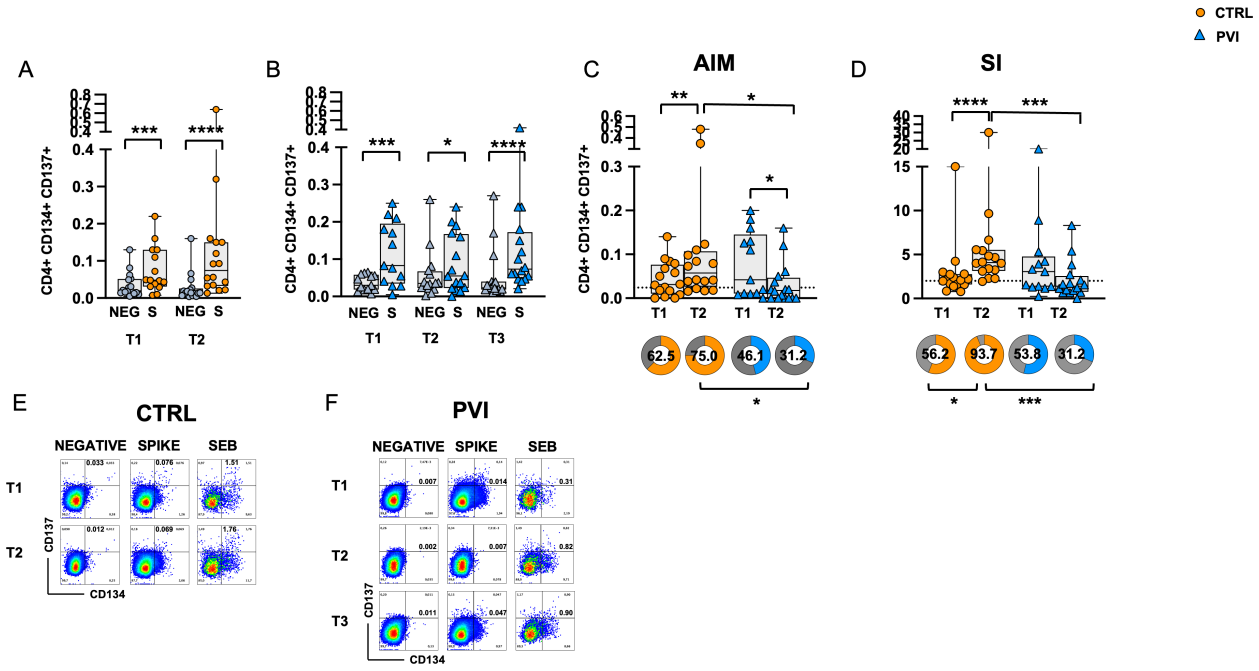

FIGURE 3
Expression of Activation-Induced Markers (AIMs) in CD4$^+$ T-cells following stimulation with Spike overlapping peptides. Frequency of AIM-expressing CD4$^+$ T-cells in unstimulated cells (grey symbol) or following stimulation with Spike (orange symbol) overlapping peptides in **(A)** the control group (circles) and **(B)** in the PVI group (triangles). **(C)** Spike-reactive CD4$^+$ T-cells following stimulation with Spike overlapping peptides in controls and PVI subjects after subtraction of the negative control. Donut graph shows the frequency of subjects responding above the threshold in the two groups. **(D)** Stimulation Index in the control group and in the PVI group. Donut graph shows the frequency of subjects responding 2-fold above the stimulation index. Representative AIM dot plots from **(E)** one control and **(F)** one PVI subject. SI—Stimulation Index; SEB- Staphylococcal enterotoxin **(B)** Statistical differences between data within the same group were assessed by the Wilcoxon matched-pairs signed-rank test. Statistical differences between groups were assessed by the non-parametric Mann–Whitney U test. Fisher's exact test was used to compare proportions. *p < 0.05; **p<0.01; ***p < 0.001; ****p<0.0001.

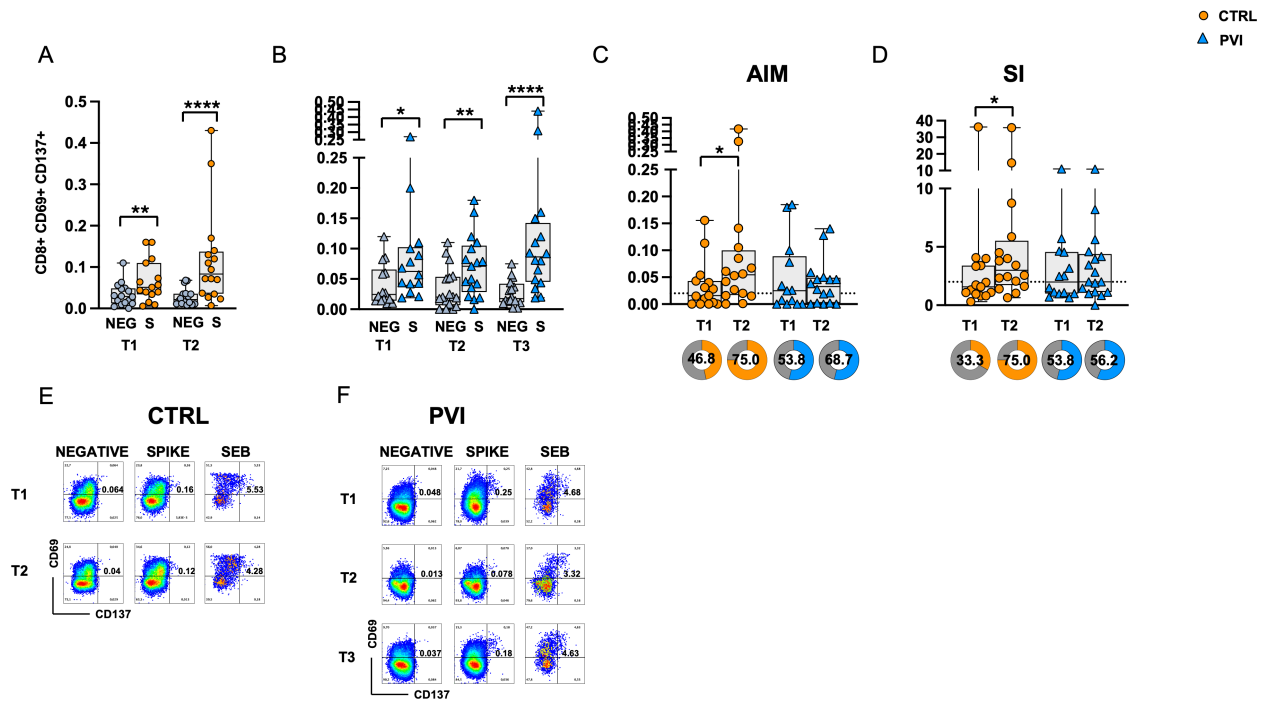

FIGURE 4
Expression of Activation-Induced Markers (AIMs) in CD8$^+$ T-cells following stimulation with Spike overlapping peptides. Frequency of AIM-expressing CD8$^+$ T-cells in unstimulated cells (grey symbol) or following stimulation with Spike (orange symbol) overlapping peptides in **(A)** the control group (circles) and **(B)** in the PVI group (triangles). **(C)** Spike-reactive CD8$^+$ T-cells following stimulation with Spike overlapping peptides in controls and PVI subjects after subtraction of the negative control. Donut graph shows the frequency of subjects responding above the threshold in the two groups. **(D)** Stimulation index in the control group and in the PVI group. Donut graph shows the frequency of subjects responding 2-fold above the stimulation index. Representative AIM dot plots from **(E)** one control and **(F)** one PVI subject. SI—Stimulation Index; SEB- Staphylococcal enterotoxin **(B)** Statistical differences between data within the same group were assessed by the Wilcoxon matched-pairs signed-rank test. Statistical differences between groups were assessed by the non-parametric Mann–Whitney U test. Fisher's exact test was used to compare proportions. *p < 0.05; **p<0.01; ****p<0.0001.

3.5 Natural infection restores spike-specific T-cell immunity

Comparison of CD4 and CD8 T-cell responses before (T2) and after (T3) COVID breakthrough infection revealed a significant increase in AIM expression in both CD4$^+$ and CD8$^+$ T-cells at T3 compared to T2 (Figures 5A, B). The proportion of subjects with AIM$^+$ CD4$^+$ T-cell responses above the threshold (defined by the median of negative controls) was significantly higher at T3 compared to T2. Additionally, the SI was significantly elevated in CD8$^+$ T-cells at T3, while a trend toward significance was observed in CD4$^+$ T-cells (p = 0.083) (Figures 5C, D).

3.6 Increased LAG-3 expression in CD4 and CD8 T-cells

To investigate the potential involvement of T-cell dysfunction in the reduced CD4$^+$ T-cell response, we assessed the expression of several co-inhibitory receptors commonly associated with exhaustion, including LAG-3, PD-1, TIM-3, TIGIT, CTLA-4, and BTLA on CD4$^+$ and CD8$^+$ T-cells. A significant increase in the proportion of LAG-3-positive CD4$^+$ and CD8$^+$ T-cells was observed in the PVI group at T2, following the booster dose, compared to T1 (Figures 6A, G).

Upregulation of exhaustion-associated markers can occur as part of the normal T-cell activation process, for example after vaccination. However, the level of expression is generally expected to remain comparable across successive doses and between individuals mounting similarly effective responses. In this context, the increase in LAG-3 expression, particularly among CD8+ T-cells, was more pronounced in individuals who subsequently experienced a breakthrough infection. This could suggest a qualitative difference in the immune response, potentially reflecting a state of early or functional exhaustion. However, given that these markers can also reflect recent activation, further functional assays would be necessary to distinguish between activation-associated expression and true exhaustion. No significant differences were detected for the other exhaustion markers analyzed (Figure 6).

3.7 Memory-like NK cell expansion in PVI

Fifteen different antibodies (listed in Materials and Methods) were used to analyze the immunophenotype of NK cells by flow cytometry. The frequency of total CD56$^+$ CD3$^-$ NK cells was

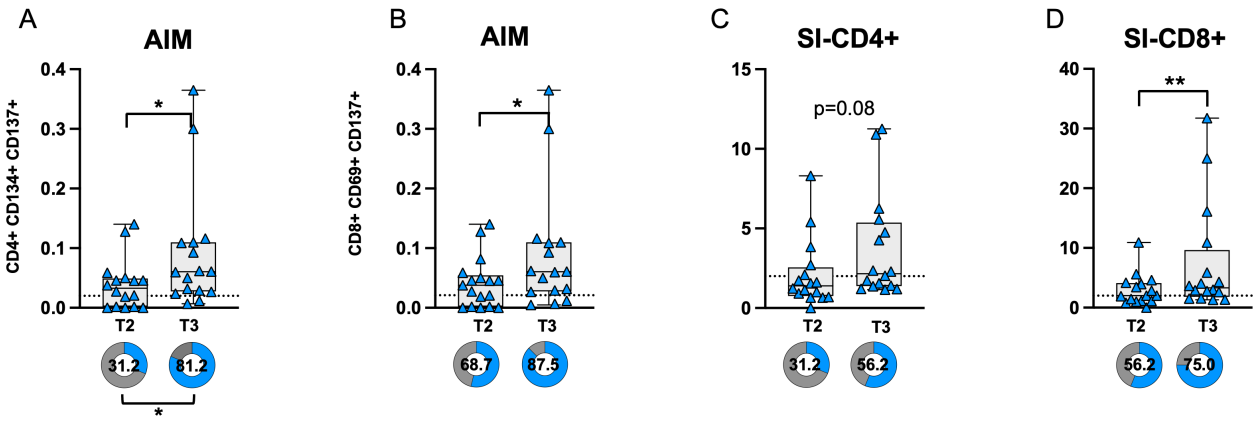

FIGURE 5
AIM expression in CD4 **(A)** and CD8 **(B)** T-cells before (T2) and after (T3) breakthrough infection in PVI subjects. Donut graph shows the frequency of subjects responding above the threshold in the two groups. Stimulation index in CD4 **(C)** and CD8+ **(D)** T-cells. Donut graph shows the frequency of subjects responding 2-fold above the stimulation index. SI—Stimulation Index; Statistical differences were assessed by the Wilcoxon matched-pairs signed-rank test. Fisher's exact test was used to compare proportions. *p < 0.05; **p<0.01.

significantly reduced at T2 in both PVI and controls. Additionally, a significant decrease was observed at T3 compared to T1 in the PVI group (Figure 7A). The immune profiling of NK cells revealed a marked reduction in the expression of the cell activation marker CD16 in both groups at T2, followed by a significant increase at T3 in PVI subjects (Figure 7B). Similarly, the frequencies of the activating receptor NKp46 and the maturity marker CD57 were reduced at T2 compared to T1 in both groups, with both markers showing a significant increase at T3 in the PVI group (Figures 7C, D). The frequency of the inhibitory receptor NKG2A increased at T2 compared to T1 in both groups (Figure 7E). Notably, NKG2C$^+$ and CD57$^+$ NKG2C$^+$ memory-like NK cells were significantly increased at T3 in PVI subjects (Figures 7F, G). Unsupervised analysis identified 12 distinct NK cell clusters; among these, Cluster 2 showed increased frequency in the PVI group and exhibited a phenotype consistent with memory-like NK cells (CD57$^+$,

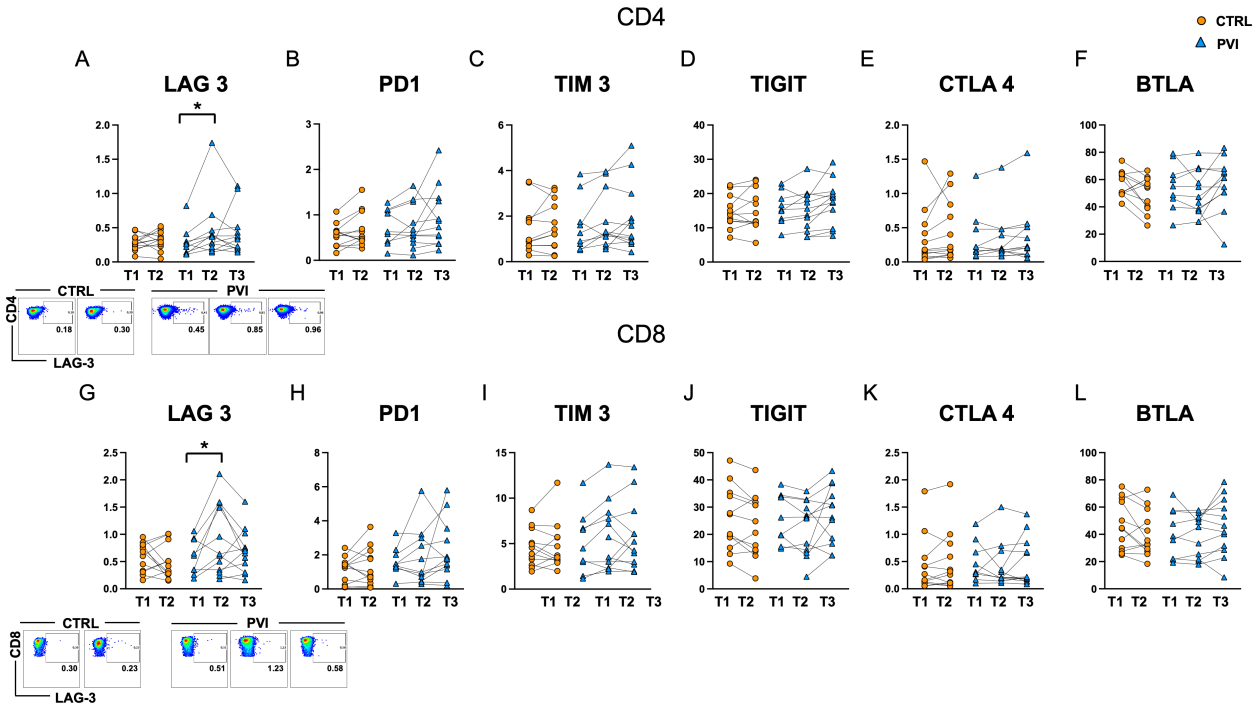

FIGURE 6
Levels of exhaustion markers in CD4$^+$ **(A-F)** and CD8$^+$ **(G-L)** T-cells in controls (orange circles) and PVI subjects (blue triangles). LAG-3 representative dot plots are shown for CD4$^+$ (upper panel) and CD8$^+$ (lower panel) cells. Statistical differences were assessed by the Wilcoxon matched-pairs signed-rank test and Holm-Šídák's multiple comparisons test. *p < 0.05.

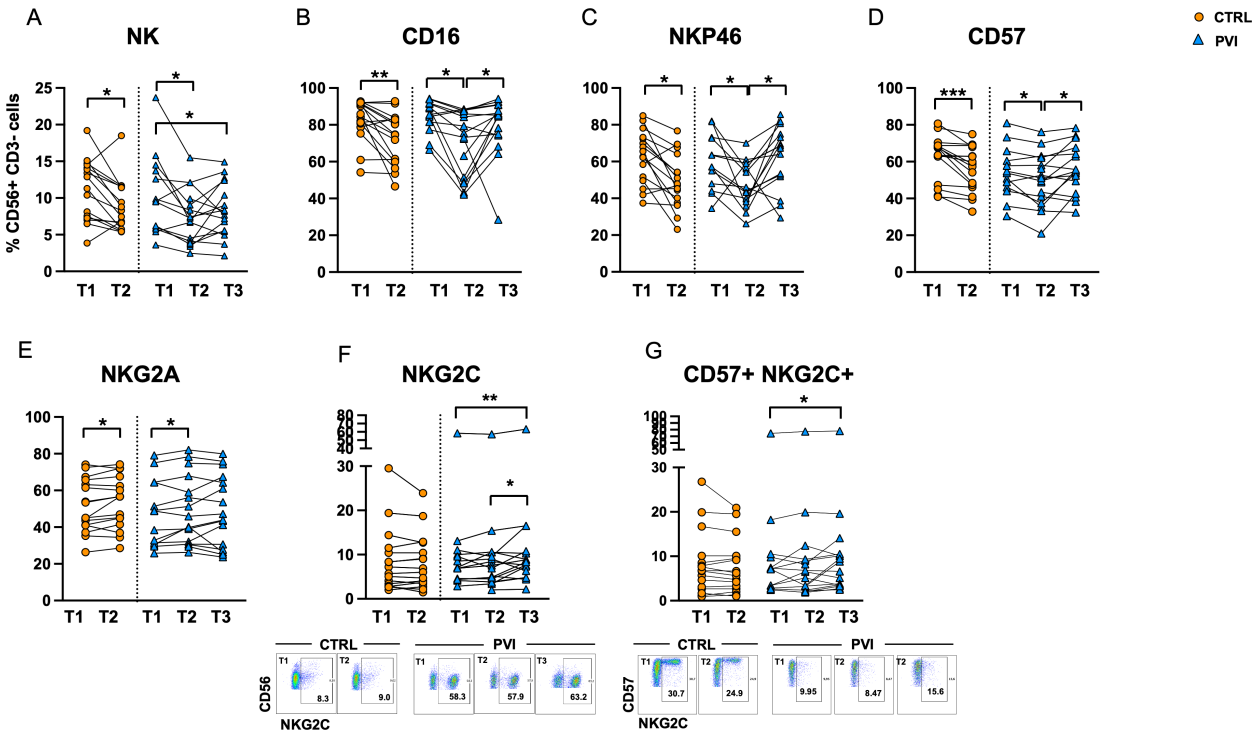

FIGURE 7
NK cell frequency in controls (orange circles) and PVI subjects (blue triangles) **(A)**. Proportion of NK cells expressing CD16$^+$ **(B)**, NKp46$^+$ **(C)**, CD57 **(D)**, NKG2A **(E)**, NKG2C **(F)** and CD57$^+$ NKG2C$^+$ memory-like NK cells **(G)** in controls (orange circles) and PVI (blue triangles) subjects. NKG2C$^+$ and CD57$^+$ NKG2C$^+$ representative dot plots are shown. Statistical differences were assessed by the Wilcoxon matched-pairs signed-rank test and Holm-Šídák's multiple comparisons test. *p < 0.05; **p<0.01; ***p < 0.001.

NKG2C$^+$, NKG2A$^-$, Siglec-7^{low}, NKp46^{low}) (Supplementary Figure 3). Interestingly, a comparison of Cluster 2 between the two groups revealed a distinct receptor expression pattern associated with PVI, characterized by a reduced proportion of CD56$^+$CD8$^+$ NK cells and increased expression of NKp46 (Supplementary Figure 3E).

Furthermore, the frequencies of memory-like CD57$^+$NKG2C$^+$ and NKG2C$^+$ NK cells at T3 were positively correlated with anti-N antibody levels at the same time point (Figures 8A, B). Additionally, in PVI subjects only, the proportion of memory-like NK cells at T2 was positively correlated with the frequency of AIM$^+$CD4$^+$ T-cells at the corresponding time point (Figures 8C, D).

4 Discussion

This study provides a comprehensive analysis of Spike-specific T-cell responses in a cohort of SARS-CoV-2-unexposed subjects who experienced breakthrough infection following the booster dose of the COVID-19 vaccine. Notably, in the period following the third

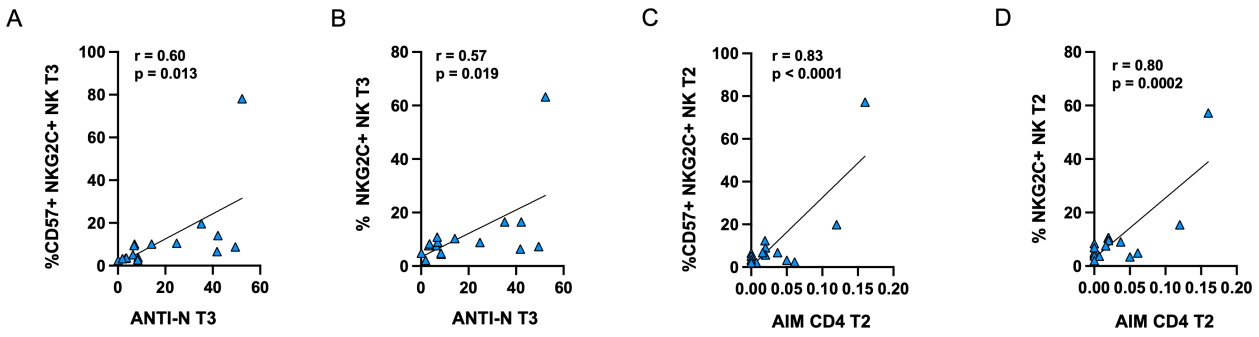

FIGURE 8
Positive correlations between anti-N antibodies and the frequency of CD57$^+$NKG2C$^+$ **(A)** or NKG2C **(B)** memory-like NK cells in PVI subjects at T3. Positive correlations between the frequency of AIM$^+$ CD4$^+$ T-cells and CD57$^+$NKG2C$^+$ **(C)** or NKG2C **(D)** memory-like NK cells in PVI subjects at T2. Correlations between variables were analyzed by Pearson's rank correlation coefficient.

vaccine dose, individuals who later developed PVI exhibited a distinct immunological profile characterized by significantly reduced Spike-specific $CD4^+$ T-cell responses. This impaired cellular immunity was restored after natural infection, as demonstrated by enhanced antigen-specific $CD4^+$ and $CD8^+$ T-cell activation post-infection.

Our findings are consistent with a previous study, which reported reduced spike-specific T-cell responses in individuals who subsequently developed COVID-19 compared to those who remained uninfected (32). Another study showed that older adults who later experienced PVI displayed significantly lower vaccine-induced spike-specific $CD4^+$ and $CD8^+$ T-cell responses compared to those who remained uninfected; however, in contrast to our data, they did not observe any significant differences in the frequency of spike-specific T-cells among younger population suggesting that host-related factors such as age and immune competence may influence susceptibility to PVI (33).

Similarly, Rovida et al. reported no significant differences in T-cell responses between PVI and non-PVI individuals after two doses of the BNT162b2 vaccine (34). However, it is essential to note that immune responses were assessed during acute infection (within 48 hours of diagnosis), potentially masking pre-infection differences due to infection-induced immune activation. This methodological difference may explain the discordant results and emphasizes the importance of timing in immunological assessments.

Interestingly, we found that the reduction in T-cell responses after booster vaccination in PVI subjects was accompanied by increased expression of the immune checkpoint receptor LAG-3, particularly in $CD8^+$ T cells. LAG-3 is typically associated with T cell exhaustion, particularly in the context of chronic infection or persistent antigen exposure. Indeed, prior studies have linked high LAG-3 expression to both mild and severe COVID-19 cases (35) and dysfunctional antiviral responses (36). However, co-inhibitory markers are also known to be transiently upregulated following T-cell activation. Therefore, the increased LAG-3 expression observed in individuals who later experienced breakthrough infection may indicate an altered immune profile, potentially indicative of early dysfunction, or reflect recent activation. Further functional studies are needed to better understand its significance.

In line with this, our data show a trend towards decreased central memory $CD4^+$ T-cells in PVI subjects. Central memory T-cells have a prominent role in peptide-induced recall responses and are enriched following effective vaccination or infection (2, 37). The reduction of the CM T-cell pool may contribute to weaker T-cell recall responses to Spike peptides post-booster, as confirmed by lower AIM^+ $CD4^+$ T-cell frequencies and stimulation index in the PVI group.

In contrast to T-cells, the anti-Spike antibody levels were comparable between groups at all time points, suggesting that antibody titers alone may not predict protection against PVI. These findings are supported by previous work demonstrating that T-cell immunity is critical for long-term protection and disease control (38).

The evaluation of NK cell immunophenotype during vaccination revealed modulation within the memory-like NK cell compartment following vaccination and infection, with a significant increase in $NKG2C^+$ NK cells post-infection in PVI individuals. These cells have been previously associated with robust antiviral responses in convalescent individuals (26) and have been shown to improve outcomes in SARS-CoV-2 infection. Indeed, the deletion of the NKG2C receptor has been associated with the development of severe COVID-19 (39). Moreover, recent data have shown that memory-like natural killer cells exhibit protective activity against lung invasion during SARS-CoV-2 infection (40). Emerging evidence suggests that memory-like $NKG2C^+$ NK cells play a crucial role in shaping effective vaccine responses, as they contribute to orchestrating T-cell immunity following COVID-19 vaccination, underscoring their importance in the development of vaccine-induced immunity (40).

A positive correlation between memory-like NK cell frequencies and both anti-N antibodies and AIM^+ $CD4^+$ T-cells was observed, suggesting a coordinated innate and adaptive antiviral immune activation. This finding aligns with previous reports showing that cooperation between innate lymphoid cells and vaccine-induced antibodies contributes to the regulation of vaccine-elicited T-cell responses, further supporting the idea of integrated crosstalk between innate and adaptive immunity during antiviral responses (41, 42).

Finally, in agreement with previous studies (15, 43, 44) our results confirm that natural infection boosts cellular immunity more robustly than vaccination alone, likely due to broader epitope exposure and higher antigenic load.

This study has several limitations. First, the small sample size limits the statistical power and applicability of the findings, particularly for subgroup comparisons. Second, while we assessed antigen-specific T-cell activation using AIM assays, we did not evaluate functional parameters such as cytokine production, which would provide deeper insights into the quality and breadth of the T-cell response. Third, immune responses were not tested against specific SARS-CoV-2 variants, which could have influenced susceptibility to breakthrough infection. Moreover, all the PVI included were of limited severity, not requiring hospitalization or oxygen supplementation. It cannot be ruled out that in more severe clinical manifestations the difference detected in our study can be more pronounced. Additionally, the study focused on circulating immune cells and did not assess mucosal immunity, a key component of protection against respiratory viruses. The use of different vaccine types among participants introduces heterogeneity, and potential confounders. Although the majority received either BNT162b2 or ChAdOx1-S for the initial two doses, a small subset received mRNA-1273. Similarly, the third dose included both BNT162b2 and mRNA-1273, with different distributions between the PVI and control groups. Given known differences in immunogenicity between vaccine platforms and mRNA dose, this variation could influence immune responses. Due to the limited sample size, stratified subgroup analyses were not feasible; thus, this heterogeneity should be considered when interpreting the findings. Finally, although multiple time points were analyzed, some immune dynamics may have been missed due to the limited sampling frequency, particularly after infection.

In summary, our study provides evidence that COVID-naïve, vaccinated individuals who later experience breakthrough infection display impaired Spike-specific $CD4^+$ T-cell responses after the third vaccine dose, despite comparable antibody levels. This reduced cellular response may contribute to increased susceptibility to SARS-CoV-2 infection. Following natural infection, both T-cell and NK cell responses were restored or enhanced, indicating that natural exposure can overcome initial vaccine-induced immune limitations.

These findings underscore the importance of evaluating cellular immunity to predict vaccine efficacy and the risk of breakthrough infections. Moreover, they emphasize the need for additional research into host factors, including LAG-3, and the potential role of memory-like NK cells as biomarkers of immune competence.

Data availability statement

The raw data supporting the conclusions of this article will be made available by the authors, without undue reservation.

Ethics statement

The study was conducted in accordance with the Declaration of Helsinki, and approved by the Ethics Committee of Fondazione IRCCS Cà Granda Policlinico of Milan, document n. 878, date of approval 18/03/21. The studies were conducted in accordance with the local legislation and institutional requirements. The participants provided their written informed consent to participate in this study.

Author contributions

SV: Formal analysis, Writing – review & editing, Investigation, Writing – original draft, Conceptualization. FG: Visualization, Writing – review & editing, Investigation. PB: Investigation, Writing – review & editing. AC: Writing – review & editing, Investigation. TF: Writing – review & editing, Data curation, Investigation. AF: Investigation, Data curation, Writing – review & editing. MC: Methodology, Writing – review & editing. TD: Resources, Writing – review & editing. NI: Writing – review & editing, Resources. GB: Resources, Writing – review & editing. VC: Writing – review & editing, Resources. BM: Writing – review & editing, Resources. AM: Writing – review & editing, Resources. SA: Writing – review & editing, Supervision, Resources. RG: Resources, Supervision, Writing – review & editing. AB: Conceptualization, Writing – review & editing, Funding acquisition, Project administration. AL: Writing – review & editing, Funding acquisition, Conceptualization, Project administration.

Funding

The author(s) declare financial support was received for the research and/or publication of this article. This research was supported by EU funding within the NextGeneration EU-MUR PNRR Extended Partnership initiative on Emerging Infectious Diseases (Project no. PE00000007, INF-ACT).

Acknowledgments

We are grateful to all the individuals who participated in the study.

Conflict of interest

The authors declare that the research was conducted in the absence of any commercial or financial relationships that could be construed as a potential conflict of interest.

The author(s) declared that they were an editorial board member of Frontiers, at the time of submission. This had no impact on the peer review process and the final decision.

Generative AI statement

The author(s) declare that no Generative AI was used in the creation of this manuscript.

Any alternative text (alt text) provided alongside figures in this article has been generated by Frontiers with the support of artificial intelligence and reasonable efforts have been made to ensure accuracy, including review by the authors wherever possible. If you identify any issues, please contact us.

Publisher's note

Supplementary material

The Supplementary Material for this article can be found online at: https://www.frontiersin.org/articles/10.3389/fimmu.2025.1657082/full#supplementary-material

References

1. Sette A, Crotty S. Adaptive immunity to SARS-coV-2 and COVID-19. *Cell*. (2021) 184:861–80. doi: 10.1016/j.cell.2021.01.007

2. Grifoni A, Weiskopf D, Ramirez SI, Mateus J, Dan JM, Moderbacher CR, et al. Targets of T cell responses to SARS-CoV-2 coronavirus in humans with COVID-19 disease and unexposed individuals. *Cell*. (2020) 181(7):1489–1501.e15. doi: 10.1016/j.cell.2020.05.015

3. Reynolds CJ, Pade C, Gibbons JM, Butler DK, Otter AD, Menacho K, et al. Prior SARS-CoV-2 infection rescues B and T cell responses to variants after first vaccine dose. *Science*. (2021) 372:1418–23. doi: 10.1126/science.abh1282

4. Geers D, Shamier MC, Bogers S, Den Hartog G, Gommers L, Nieuwkoop NN, et al. SARS-CoV-2 variants of concern partially escape humoral but not T cell responses in COVID-19 convalescent donors and vaccine recipients. *Sci Immunol*. (2021) 6: eabj1750. doi: 10.1126/sciimmunol.abj1750

5. Redd AD, Nardin A, Kared H, Bloch EM, Pekosz A, Laeyendecker O, et al. CD8+ T-cell responses in COVID-19 convalescent individuals target conserved epitopes from multiple prominent SARS-coV-2 circulating variants. *Open Forum Infect Dis*. (2021) 8: ofab143. doi: 10.1093/ofid/ofab143

6. Bertoletti A, Le Bert N, Tan AT. SARS-CoV-2-specific T cells in the changing landscape of the COVID-19 pandemic. *Immunity*. (2022) 55:1764–78. doi: 10.1016/j.immuni.2022.08.008

7. Binayke A, Zaheer A, Vishwakarma S, Sharma P, Dandotiya J, Raghavan S, et al. Understanding the landscape of the SARS-CoV-2-specific T cells post-omicron surge. *J Med Virol*. (2024) 96:e29877. doi: 10.1002/jmv.29877

8. Rubio R, Yavlinsky A, Escalera Zamudio M, Molinos-Albert LM, Martín Pérez C, Pradenas E, et al. Initial antigen encounter determines robust T-cell immunity against SARS-CoV-2 BA.2.86 variant three years later. *J Infection*. (2025) 90:106402. doi: 10.1016/j.jinf.2024.106402

9. Keeton R, Tincho MB, Ngomti A, Baguma R, Benede N, Suzuki A, et al. T cell responses to SARS-CoV-2 spike cross-recognize Omicron. *Nature*. (2022) 603:488–92. doi: 10.1038/s41586-022-04460-3

10. Grifoni A, Sidney J, Vita R, Peters B, Crotty S, Weiskopf D, et al. SARS-CoV-2 human T cell epitopes: Adaptive immune response against COVID-19. *Cell Host Microbe*. (2021) 29:1076–92. doi: 10.1016/j.chom.2021.05.010

11. Mateus J, Dan JM, Zhang Z, Rydyznski Moderbacher C, Lammers M, Goodwin B, et al. Low-dose mRNA-1273 COVID-19 vaccine generates durable memory enhanced by cross-reactive T cells. *Science*. (2021) 374:eabj9853. doi: 10.1126/science.abj9853

12. Minervina AA, Komech EA, Titov A, Bensouda Koraichi M, Rosati E, Mamedov IZ, et al. Longitudinal high-throughput TCR repertoire profiling reveals the dynamics of T-cell memory formation after mild COVID-19 infection. *eLife*. (2021) 10:e63502. doi: 10.7554/eLife.63502

13. Sahin U, Muik A, Vogler I, Derhovanessian E, Kranz LM, Vormehr M, et al. BNT162b2 vaccine induces neutralizing antibodies and poly-specific T cells in humans. *Nature*. (2021) 595:572–7. doi: 10.1038/s41586-021-03653-6

14. Tarke A, Sidney J, Methot N, Yu ED, Zhang Y, Dan JM, et al. Impact of SARS-CoV-2 variants on the total CD4+ and CD8+ T cell reactivity in infected or vaccinated individuals. *Cell Rep Med*. (2021) 2:100355. doi: 10.1016/j.xcrm.2021.100355

15. Collier A ris Y, Brown CM, McMahan KA, Yu J, Liu J, Jacob-Dolan C, et al. Characterization of immune responses in fully vaccinated individuals after breakthrough infection with the SARS-CoV-2 delta variant. *Sci Transl Med*. (2022) 14:eabn6150. doi: 10.1126/scitranslmed.abn6150

16. Bates TA, McBride SK, Leier HC, Guzman G, Lyski ZL, Schoen D, et al. Vaccination before or after SARS-CoV-2 infection leads to robust humoral response and antibodies that effectively neutralize variants. *Sci Immunol*. (2022) 7:eabn8014. doi: 10.1126/sciimmunol.abn8014

17. Reynolds CJ, Gibbons JM, Pade C, Lin KM, Sandoval DM, Pieper F, et al. Heterologous infection and vaccination shapes immunity against SARS-CoV-2 variants. *Science*. (2022) 375:183–92. doi: 10.1126/science.abm0811

18. Cox A, Cevik H, Feldman HA, Canaday LM, Lakes N, Waggoner SN. Targeting natural killer cells to enhance vaccine responses. *Trends Pharmacol Sci*. (2021) 42:789–801. doi: 10.1016/j.tips.2021.06.004

19. Lee J, Zhang T, Hwang I, Kim A, Nitschke L, Kim M, et al. Epigenetic modification and antibody-dependent expansion of memory-like NK cells in human cytomegalovirus-infected individuals. *Immunity*. (2015) 42(3):431–42. doi: 10.1016/j.immuni.2015.02.013

20. Sun JC, Lopez-Verges S, Kim CC, DeRisi JL, Lanier LL. NK cells and immune "memory". *J Immunol*. (2011) 186(4):1891–7. doi: 10.4049/jimmunol.1003035

21. Market M, Angka L, Martel AB, Bastin D, Olanubi O, Tennakoon G, et al. Flattening the COVID-19 curve with natural killer cell based immunotherapies. *Front Immunol*. (2020) 11:1512. doi: 10.3389/fimmu.2020.01512

22. Herrera L, Martin-Inaraja M, Santos S, Inglés-Ferrándiz M, Azkarate A, Perez-Vaquero MA, et al. Identifying SARS-CoV-2 'memory' NK cells from COVID-19 convalescent donors for adoptive cell therapy. *Immunology*. (2022) 165(2):234–49. doi: 10.1111/imm.13432

23. Shang QN, Yu XX, Xu ZL, Chen YH, Han TT, Zhang YY, et al. Expanded clinical-grade NK cells exhibit stronger effects than primary NK cells against HCMV infection. *Cell Mol Immunol*. (2023) 20(8):895–907. doi: 10.1038/s41423-023-01046-5

24. Schlums H, Cichocki F, Tesi B, Theorell J, Beziat V, Holmes TD, et al. Cytomegalovirus infection drives adaptive epigenetic diversification of NK cells with altered signaling and effector function. *Immunity*. (2015) 42:443–56. doi: 10.1016/j.immuni.2015.02.008

25. Sun JC, Lopez-Verges S, Kim CC, DeRisi JL, Lanier LL. NK cells and immune "Memory. *J Immunol*. (2011) 186:1891–7. doi: 10.4049/jimmunol.1003035

26. Herrera L, Martin-Inaraja M, Santos S, Inglés-Ferrándiz M, Azkarate A, Perez-Vaquero MA, et al. Identifying SARS-CoV-2 'memory' NK cells from COVID-19 convalescent donors for adoptive cell therapy. *Immunology*. (2022) 165:234–49. doi: 10.1111/imm.13432

27. Dong H, Ham JD, Hu G, Xie G, Vergara J, Liang Y, et al. Memory-like NK cells armed with a neoepitope-specific CAR exhibit potent activity against NPM1 mutated acute myeloid leukemia. *Proc Natl Acad Sci USA*. (2022) 119:e2122379119. doi: 10.1073/pnas.2122379119

28. Berrien-Elliott MM, Cashen AF, Cubitt CC, Neal CC, Wong P, Wagner JA, et al. Multidimensional analyses of donor memory-like NK cells reveal new associations with response after adoptive immunotherapy for leukemia. *Cancer Discovery*. (2020) 10:1854–71. doi: 10.1158/2159-8290.CD-20-0312

29. Haroun-Izquierdo A, Vincenti M, Netskar H, Van Ooijen H, Zhang B, Bendzick L, et al. Adaptive single-KIR$^+$ NKG2C$^+$ NK cells expanded from select superdonors show potent missing-self reactivity and efficiently control HLA-mismatched acute myeloid leukemia. *J Immunother Cancer*. (2022) 10:e005577. doi: 10.1136/jitc-2022-005577

30. Stefanelli P, Trentini F, Petrone D, Mammone A, Ambrosio L, Manica M, et al. Tracking the progressive spread of the SARS-CoV-2 Omicron variant in Italy, December 2021 to January 2022. *Eurosurveillance*. (2022) 27(45):2200125. doi: 10.2807/1560-7917.ES.2022.27.45.2200125

31. Bergna A, Lai A, Sagradi F, Menzo S, Mancini N, Bruzzone B, et al. Genomic epidemiology of the main SARS-coV-2 variants circulating in Italy during the omicron era. *J Med Virol*. (2025) 97:e70215. doi: 10.1002/jmv.70215

32. Paniskaki K, Anft M, Meister TL, Marheinecke C, Pfaender S, Skrzypczyk S, et al. Immune response in moderate to critical breakthrough COVID-19 infection after mRNA vaccination. *Front Immunol*. (2022) 13:816220. doi: 10.3389/fimmu.2022.816220

33. Datwani S, Kalikawe R, Mwimanzi F, Speckmaier S, Liang R, Sang Y, et al. Dynamics of T-cell responses following COVID-19 mRNA vaccination and breakthrough infection in older adults. *PAI*. (2023) 8:117–35. doi: 10.20411/pai.v8i1.613

34. Rovida F, Cassaniti I, Paolucci S, Percivalle E, Sarasini A, Piralla A, et al. SARS-CoV-2 vaccine breakthrough infections with the alpha variant are asymptomatic or mildly symptomatic among health care workers. *Nat Commun*. (2021) 12:6032. doi: 10.1038/s41467-021-26154-6

35. Rendeiro AF, Casano J, Vorkas CK, Singh H, Morales A, DeSimone RA, et al. Profiling of immune dysfunction in COVID-19 patients allows early prediction of disease progression. *Life Sci Alliance*. (2021) 4:e202000955. doi: 10.26508/lsa.202000955

36. Blackburn SD, Shin H, Haining WN, Zou T, Workman CJ, Polley A, et al. Coregulation of CD8+ T cell exhaustion by multiple inhibitory receptors during chronic viral infection. *Nat Immunol*. (2009) 10:29–37. doi: 10.1038/ni.1679

37. Dan JM, Mateus J, Kato Y, Hastie KM, Yu ED, Faliti CE, et al. Immunological memory to SARS-CoV-2 assessed for up to 8 months after infection. *Science*. (2021) 371:eabf4063. doi: 10.1126/science.abf4063

38. Lu Z, Laing ED, Pena DaMata J, Pohida K, Tso MS, Samuels EC, et al. Durability of SARS-coV-2–specific T-cell responses at 12 months postinfection. *J Infect Diseases*. (2021) 224:2010–9. doi: 10.1093/infdis/jiab543

39. Vietzen H, Zoufaly A, Traugott M, Aberle J, Aberle SW, Puchhammer-Stöckl E. Deletion of the NKG2C receptor encoding KLRC2 gene and HLA-E variants are risk factors for severe COVID-19. *Genet Med*. (2021) 23:963–7. doi: 10.1038/s41436-020-01077-7

40. Zheng H, Chen Y, Li J, Zhang Y, Li H, Zhao X, et al. Essential role of CD56dimNKG2C + NK cells trained by SARS-CoV-2 vaccines in protecting against COVID-19. *Mol Ther*. (2025) S1525-0016(25):00401-0. doi: 10.1016/j.ymthe.2025.05.031

41. Cherrier M, Ramachandran G, Golub R. The interplay between innate lymphoid cells and T cells. *Mucosal Immunol*. (2020) 13:732–42. doi: 10.1038/s41385-020-0320-8

42. Eberl G, Colonna M, Di Santo JP, McKenzie ANJ. Innate lymphoid cells: A new paradigm in immunology. *Science*. (2015) 348:aaa6566. doi: 10.1126/science.aaa6566

43. Koutsakos M, Reynaldi A, Lee WS, Nguyen J, Amarasena T, Taiaroa G, et al. SARS-CoV-2 breakthrough infection induces rapid memory and *de novo* T cell responses. *Immunity*. (2023) 56:879–892.e4. doi: 10.1016/j.immuni.2023.02.017

44. Tarke A, Ramezani-Rad P, Alves Pereira Neto T, Lee Y, Silva-Moraes V, Goodwin B, et al. SARS-CoV-2 breakthrough infections enhance T cell response magnitude, breadth, and epitope repertoire. *Cell Rep Med*. (2024) 5:101583. doi: 10.1016/j.xcrm.2024.101583

frontiers | Frontiers in Immunology

TYPE Opinion
PUBLISHED 30 September 2025
DOI 10.3389/fimmu.2025.1655969

OPEN ACCESS

EDITED BY
Sonia Jangra,
The Rockefeller University, United States

REVIEWED BY
Ekaterini Simoes Goudouris,
Federal University of Rio de Janeiro, Brazil

*CORRESPONDENCE
Manuela Berto Pucca
manuela.pucca@unesp.br

RECEIVED 29 June 2025
ACCEPTED 15 September 2025
PUBLISHED 30 September 2025

CITATION
Filardi ETM, Carbonell RCC, Pavan FR, Cerni FA and Pucca MB (2025) One hundred years of BCG: the journey of tuberculosis vaccination in Brazil.
Front. Immunol. 16:1655969.
doi: 10.3389/fimmu.2025.1655969

One hundred years of BCG: the journey of tuberculosis vaccination in Brazil

Eloise Trostdorf Monteiro Filardi[1], Roberto Carlos Cruz Carbonell[1,2], Fernando Rogério Pavan[1], Felipe Augusto Cerni[2] and Manuela Berto Pucca[1]*

[1]Graduate Program in Bioscience and Biotechonology Applied to Pharmacy, School of Pharmaceutical Sciences, São Paulo State University (UNESP), Araraquara, São Paulo, Brazil, [2]Medical School, Federal University of Roraima, Boa Vista, Brazil

KEYWORDS

BCG, bacillus Calmette-Guérin, vaccine, *Mycobacterium tuberculosis*, immunization

Vaccines represent one of the most significant achievements in medical science, constituting safe preparations or substances developed with the primary purpose of stimulating the immune system (1, 2). Their central function is to protect the human body against a myriad of infectious diseases that can be prevented through immunization. From an educational perspective, vaccines can be described as biological preparations that "train" the immune system to recognize and mount an effective defense against specific pathogens (e.g., viruses or bacteria) prior to natural exposure, thereby preventing the onset of disease (3).

The relevance of vaccines transcends individual protection, extending to a considerable socioeconomic impact. When employed as a public health strategy, vaccines are widely considered one of the best investments available, primarily due to their exceptional cost-effectiveness (4). The benefits of vaccination extend far beyond the immediate prevention of disease in individuals. By enabling large-scale disease control, vaccines significantly reduce the burden on healthcare systems, leading to fewer hospital admissions, diminished reliance on high-cost medical interventions, and reduced demand for long-term care services. Moreover, individuals protected through immunization are generally healthier and more capable of contributing to the workforce, thereby enhancing economic productivity at both community and national levels (5, 6).

The history of vaccination is a narrative of scientific triumphs and transformative impact on global health. Over the past five decades, global immunization efforts have resulted in an extraordinary achievement. It is estimated that at least 154 million lives have been saved, the vast majority of them (approximately 101 million) being children (7). A particularly eloquent testament to this success is the impact of measles vaccination, which alone accounted for about 60% of those lives saved, equivalent to approximately 94 million children protected since 1974 (8, 9).

This year marks a significant milestone, a century of the Bacillus Calmette–Guérin (BCG) vaccination in Brazil, a pivotal tool in the fight against tuberculosis (TB), a disease responsible for thousands of deaths worldwide. Officially introduced in Brazil in 1925, the BCG vaccine became a symbol of prevention and public health advancement against one of the most lethal infectious diseases globally (10, 11). However, the vaccine's origin dates to

1921 (ie., four years before), when French scientists Albert Calmette and Camille Guérin, working at the Pasteur Institute in Paris, developed the immunizing agent after years of dedicated research. The scientists attenuated a strain of *Mycobacterium bovis*, a close relative of *M. tuberculosis*, the pathogen responsible for human tuberculosis. Over the course of 13 years, they subjected the bacterium to 231 serial passages in subcultures containing bile, gradually reducing its virulence while retaining its immunogenic capacity. The outcome was a live attenuated vaccine capable of inducing protective immunity without causing disease, first administered to humans in 1921 and subsequently adopted worldwide (12).

In Brazil, before the introduction of BCG vaccine (1925) and, later, the development of effective therapeutics from the mid-20th century onwards, the tuberculosis scenario in Brazil was critical. The disease, often called the "white plague," was one of the leading causes of death, surrounded by fear and social stigma (13). In the absence of specific treatments, therapeutic approaches were largely palliative and of limited efficacy. In that time, the main strategy for managing patients consisted of isolation in sanatoria, institutions typically built in locations considered healthy climates (mountains or coast), where prolonged rest, enhanced nutrition, and exposure to fresh air, known as "climatotherapy", were prescribed (14). Although these represented an effort to care for patients and attempt to contain disease spread, sanatoria were insufficient to meet demand and inaccessible to most of the affected population, especially the poor. The effectiveness of these measures in curing the disease was questionable, serving more as palliation and a form of segregation (15).

The introduction of the BCG vaccine in Brazil occurred relatively soon after its development in France, demonstrating a proactive response from the Brazilian scientific and medical community to the serious tuberculosis problem. The protagonist of this introduction was the physician and researcher Arlindo de Assis, who brought the BCG strain from Paris to Brazil in 1925 (Figure 1A). Linked to the Brazilian League against Tuberculosis, Assis initiated the production and application of the vaccine in the country, initially via the oral route, a method he advocated for many years (16). Subsequent production and research efforts involved renowned institutions such as the Oswaldo Cruz Institute (Fiocruz) (17), consolidating the vaccine's presence in the national scenario from the late 1920s and early 1930s. Brazil's early engagement with BCG technology, facilitated by figures like Arlindo de Assis and institutions like Fiocruz, signaled recognition of the magnitude of the TB problem and an openness to incorporating new scientific interventions, laying the foundation for the future integration of BCG into national immunization programs. Despite significant progress in the fight against TB, the disease remains a major global health challenge. The variable efficacy of BCG vaccine, particularly in adults, and the increasing prevalence of *M. tuberculosis* strains resistant to first-line drugs are critical concerns (18). These biomedical challenges are further compounded by persistent social determinants of health, including overcrowded living conditions, malnutrition, and limited access to timely diagnosis and effective treatment in underserved populations (19, 20).

Another important historical milestone in Brazil occurred in 1975, when tuberculosis was officially included among the diseases subject to compulsory notification. This was established by Federal Law No. 6,259, enacted on October 30, 1975, which organized the national system of epidemiological surveillance. The law was later regulated by Decree No. 78,231 of August 12, 1976 (21, 22). From that point on, all diagnosed cases of tuberculosis had to be reported to health authorities. This measure played a crucial role in strengthening public health efforts, allowing for more accurate monitoring of the disease, improved resource allocation, and the implementation of more effective tuberculosis control strategies nationwide (23–25).

Although TB is a preventable and curable disease, it remains one of the leading causes of death from infectious diseases worldwide, second only to COVID-19 during certain periods. In 2023, it is estimated that approximately 1.25 million people died from TB globally (26). In Brazil, 5,845 TB-related deaths were reported in 2022, corresponding to a mortality rate of 2.72 per 100,000 inhabitants, the highest recorded in over two decades of surveillance (27, 28). The high lethality of TB is often associated with factors such as delayed diagnosis, treatment abandonment, social vulnerability, and coinfections, particularly TB-HIV, which significantly worsens patient prognosis (29). These indicators highlight the urgent need for integrated strategies focused on surveillance, early diagnosis, treatment adherence, and public policies aimed at reducing social inequalities.

A temporal analysis of new reported tuberculosis (TB) cases in Brazil from 2013 to 2023, together with national BCG vaccination coverage, is shown in Figure 1B. The data demonstrate that, despite a decline in vaccination coverage during the COVID-19 pandemic, there was no immediate proportional increase in TB notifications. However, a marked rise in reported cases is observed in 2022, likely related to the resumption of surveillance activities and improved case detection.

BCG vaccination coverage in Brazil remained consistently high until 2018, with rates above 95% (Figure 1). From 2019 onward, a gradual decline was observed, becoming more pronounced between 2020 and 2021, when coverage dropped below 80%, despite its mandatory status under Federal Law. This decrease is likely associated with disruptions in health services, logistical challenges, and vaccine hesitancy exacerbated by the COVID-19 pandemic, as previously discussed by Filardi et al. (37). Importantly, despite the drop in coverage, no immediate proportional increase in TB cases was evident during this period. This highlights the critical need to restore and maintain high BCG vaccination coverage and to strengthen epidemiological surveillance systems to ensure timely case detection and control. Encouragingly, coverage rose to 83.5% in 2023, and preliminary data for 2024 indicate a further increase to 92.8%, suggesting a recovery toward pre-pandemic vaccination levels (30).

Vaccination remains a crucial tool in the global fight against TB, particularly given the disease's persistent lethality and impact on vulnerable populations. The BCG vaccine, although not fully effective in preventing pulmonary TB in adults, plays a fundamental role in protecting children against the most severe

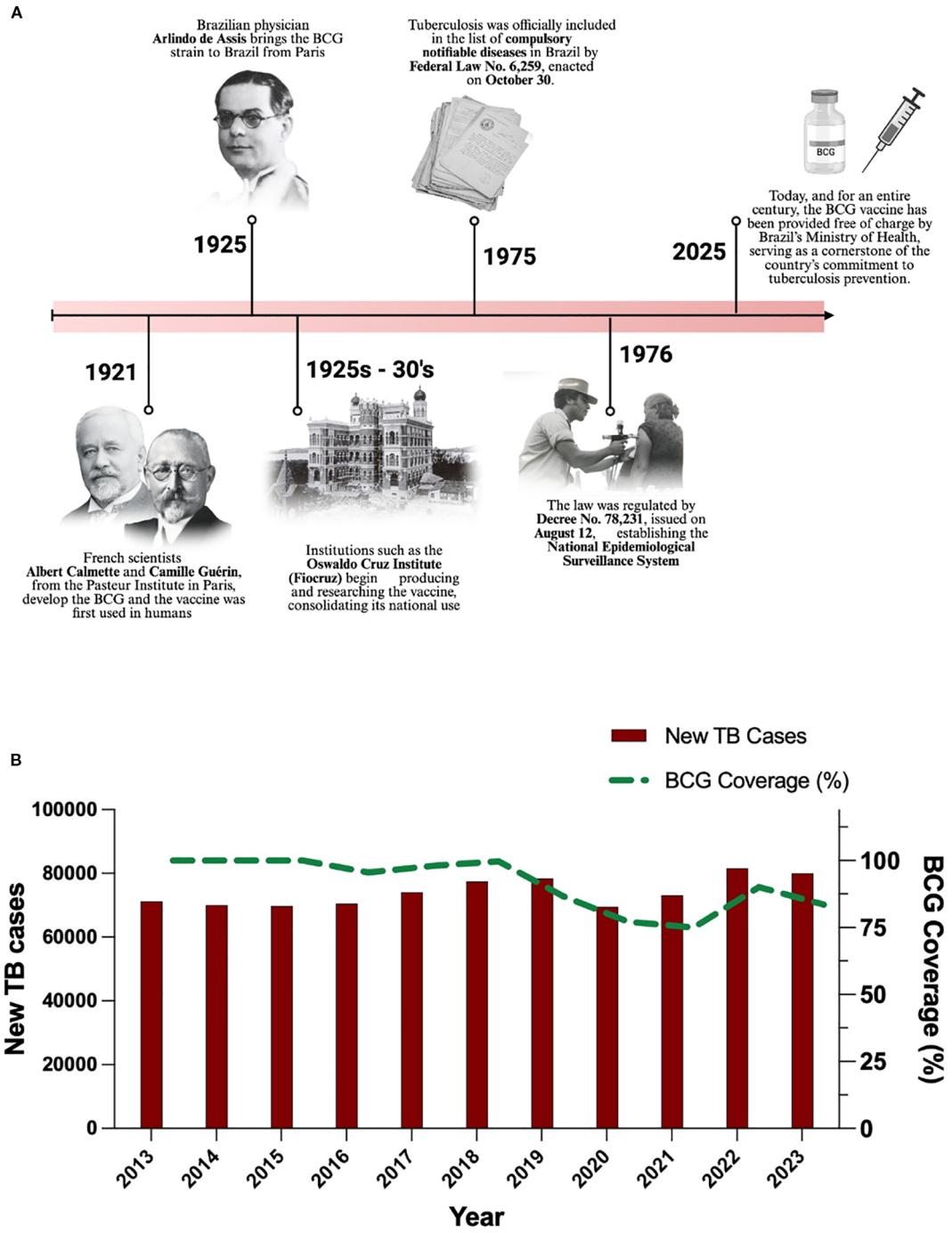

FIGURE 1
Historical and epidemiological context of BCG vaccination and tuberculosis in Brazil. **(A)** Timeline illustrating key milestones in BCG implementation in Brazil. **(B)** Temporal trends in new reported tuberculosis (TB) cases and national BCG vaccination coverage (2013–2023).

and life-threatening forms of the disease, such as tuberculous meningitis and miliary TB. By reducing the incidence of these severe manifestations, BCG contributes directly to lowering TB-associated mortality and alleviating the overall burden on public health systems. Mass immunization programs, therefore, are essential to prevent avoidable deaths and to control the progression of TB, especially in high-risk communities (31, 32).

Although BCG vaccination coverage is not universal and has shown a concerning decline in several regions over recent years, it remains the most effective public health intervention for preventing severe forms of TB in children, particularly extrapulmonary manifestations. Robust evidence from observational studies and meta-analyses supports the vaccine's efficacy, with protection ranging from 70% to 80% against these critical forms. A

systematic review by the Cochrane Collaboration (2014) demonstrated a 73% reduction in the risk of tuberculous meningitis and a 77% reduction in the incidence of miliary TB among vaccinated individuals. These findings reinforce the importance of maintaining high BCG vaccination coverage as a cornerstone of global TB control strategies, particularly in endemic regions. As illustrated in the graphs for Brazil, while BCG coverage remained above 95% until 2015, a subsequent decline may jeopardize these public health gains and is potentially associated with the observed fluctuations in TB mortality. Together, these data emphasize the urgent need to strengthen immunization efforts to ensure sustained protection against severe TB and prevent a resurgence in disease-related mortality (33).

Looking ahead, scientific innovation stands as a crucial driver in the global effort to eliminate TB. Promising candidates for next-generation vaccines are in advanced stages of development, aiming to provide broader and more durable protection across age groups and geographic settings (34). In parallel, advances in molecular diagnostics and digital health technologies are enhancing early detection, while targeted public health campaigns are raising awareness and promoting adherence to treatment regimens. Together, these integrated strategies are essential for accelerating progress toward TB control and, ultimately, eradication (35, 36).

As Brazil marks a century of tuberculosis vaccination (1925–2025), this milestone serves not only as a testament to the progress achieved but also as a call to address the persistent challenges that remain. Sustained investment in public health infrastructure, research, and equitable access to healthcare, combined with ongoing scientific innovation, will be essential to ensuring that, in the coming century, tuberculosis is no longer a threat to public health in Brazil or across the globe.

Author contributions

EF: Conceptualization, Writing – review & editing, Writing – original draft, Investigation. RC: Investigation, Writing – review & editing. FP: Investigation, Writing – review & editing. FC: Writing – review & editing, Investigation. MP: Investigation, Writing – original draft, Writing – review & editing, Resources, Conceptualization, Supervision.

Funding

The author(s) declare financial support was received for the research and/or publication of this article. We thank Fundação de Amparo à Pesquisa do Estado de São Paulo (FAPESP; scholarship to ETMF. No. 2024/13258–0).

Conflict of interest

The authors declare that the research was conducted in the absence of any commercial or financial relationships that could be construed as a potential conflict of interest.

The author(s) declared that they were an editorial board member of Frontiers, at the time of submission. This had no impact on the peer review process and the final decision.

Generative AI statement

The author(s) declare that no Generative AI was used in the creation of this manuscript.

Any alternative text (alt text) provided alongside figures in this article has been generated by Frontiers with the support of artificial intelligence and reasonable efforts have been made to ensure accuracy, including review by the authors wherever possible. If you identify any issues, please contact us.

Publisher's note

References

1. *Vaccines and immunization: What is vaccination?* . Available online at: https://www.who.int/news-room/questions-and-answers/item/vaccines-and-immunization-what-is-vaccination (Accessed May 8, 2025).

2. National Research Council (US) Division of Health Promotion and Disease Prevention. Vaccine Supply and Innovation Washington (DC): National Academies Press (US). (1985) 2, Vaccines: Past, Present, and Future. Available online at: https://www.ncbi.nlm.nih.gov/books/NBK216821.

3. Ghattas M, Dwivedi G, Lavertu M, Alameh M-G. Vaccine technologies and platforms for infectious diseases: current progress, challenges, and opportunities. *Vaccines (Basel).* (2021) 9:1490. doi: 10.3390/vaccines9121490

4. Nandi A, Shet A. Why vaccines matter: understanding the broader health, economic, and child development benefits of routine vaccination. *Hum Vaccin Immunother.* (2020) 16:1900–4. doi: 10.1080/21645515.2019.1708669

5. Rodrigues CMC, Plotkin SA. Impact of vaccines; health, economic and social perspectives. *Front Microbiol.* (2020) 11:1526. doi: 10.3389/fmicb.2020.01526

6. Quilici S, Smith R, Signorelli C. Role of vaccination in economic growth. *J Mark Access Health Policy.* (2015) 3:10. doi: 10.3402/jmahp.v3.27044

7. *Global immunization efforts have saved at least 154 million lives over the past 50 years*. Available online at: https://www.who.int/news/item/24-04-2024-global-immunization-efforts-have-saved-at-least-154-million-lives-over-the-past-50-years (Accessed May 8, 2025).

8. Minta AA. Progress toward measles elimination — Worldwide, 2000–2023. *MMWR Morb Mortal Wkly Rep.* (2024) 73:1036–42. doi: 10.15585/mmwr.mm7345a4

9. UNICEF. (2025). *Measles cases are spiking globally*. UNICEF. Available online at: https://www.unicef.org/stories/measles-cases-spiking-globally (Accessed April 23, 2025).

10. Institut Pasteur. *BCG vaccine: the first tuberculosis vaccination took place a century ago*. Institut Pasteur (2021). Available online at: https://www.pasteur.fr/en/home/research-journal/news/bcg-vaccine-first-tuberculosis-vaccination-took-place-century-ago (Accessed September 23, 2025).

11. BCG. Ministério da Saúde. Available online at: https://www.gov.br/saude/pt-br/assuntos/saude-de-a-a-z/b/bcg/bcg (Accessed May 12, 2025).

12. Vacina BCG: a primeira vacinação contra tuberculose ocorreu há um século. Available online at: https://www-pasteur-fr.translate.goog/en/home/research-journal/news/bcg-vaccine-first-tuberculosis-vaccination-took-place-century-ago?_x_tr_sl=en&_x_tr_tl=pt&_x_tr_hl=pt&_x_tr_pto=sge (Accessed May 12, 2025).

13. Bertolli Filho C. *Social history of tuberculosis and the tuberculous: 1900–1950*. Rio de Janeiro: FIOCRUZ Press. (2001). Available online at: https://books.scielo.org/id/4 (Accessed September 23, 2025).

14. Diniz JPFD. A Climatoterapia e o tratamento sanatorial. A busca pelo tratamento da tuberculose em Belo Horizonte – MG (1920-1950). *Contraponto*. (2021) 10:404.

15. Hijjar MA, Gerhardt G, Teixeira GM, Procópio MJ. Retrospecto do controle da tuberculose no Brasil. *Rev Saúde Pública*. (2007) 41:50–7. doi: 10.1590/S0034-89102007000800008

16. Agência Brasil. *BCG: 100 years – how the vaccine changed the history of tuberculosis control*. Agência Brasil (2021). Available online at: https://agenciabrasil.ebc.com.br/saude/noticia/2021-07/bcg-100-anos-como-vacina-mudou-historia-no-combate-tuberculose (Accessed September 23, 2025).

17. Rosemberg J. Tuberculose - Aspectos históricos, realidades, seu romantismo e transculturação. *Boletim Pneumologia Sanitária*. (1999) 7:5–29. doi: 10.5123/S0103-460X1999000200002

18. Bloom BR, Atun R, Cohen T, Dye C, Fraser H, Gomez GB, et al. Tuberculosis. In: Holmes KK, Bertozzi S, Bloom BR, Jha P, editors. *Major Infectious Diseases*. The International Bank for Reconstruction and Development/The World Bank, Washington (DC (2017). Available online at: http://www.ncbi.nlm.nih.gov/books/NBK525174/.

19. . *The urgency of investing in health systems in Latin America and the Caribbean*. (United Nations, Paho). (2024). Available online at: https://www.paho.org/en/documents/urgency-investing-health-systems-latin-america-and-caribbean-reduce-inequality-and

20. Gulumbe BH, Abdulrahim A, Ahmad SK, Lawan KA, Danlami MB. WHO report signals tuberculosis resurgence: Addressing systemic failures and revamping control strategies. *Decoding Infect Transm*. (2025) 3:100044. doi: 10.1016/j.dcit.2025.100044

21. Teixeira M da G, Penna GO, Risi JB, Penna ML, Alvim MF, de MJC, et al. Seleção das doenças de notificação compulsória: critérios e recomendações para as três esferas de governo. *Informe Epidemiol do Sus*. (1998) 7:7–28. doi: 10.5123/S0104-16731998000100002

22. BRASIL. *Dispõe sobre a organização das ações de Vigilância Epidemiológica, o Programa Nacional de Imunizações, estabelece a obrigatoriedade de notificação compulsória de doenças e dá outras providências*. (Brazil: National Immunization Program (PNI)) (1975).

23. Notificação Compulsória. Ministério da Saúde. Available online at: https://www.gov.br/saude/pt-br/composicao/svsa/notificacao-compulsoria/notificacao-compulsoria (Accessed May 20, 2025).

24. Bartholomay P, Oliveira GPd, Pinheiro RS, Vasconcelos AMN. Melhoria da qualidade das informações sobre tuberculose a partir do relacionamento entre bases de dados. *Cad Saúde Pública*. (2014) 30:2459–70. doi: 10.1590/0102-311X00116313

25. Bartholomay P, Oliveira GPde, Pinheiro RS, Vasconcelos AMN. Melhoria da qualidade das informações sobre tuberculose a partir do relacionamento entre bases de dados. *Cadernos De Saúde Pública*. (2014) 30(11):2459–70. doi: 10.1590/0102-311X00116313

26. Miranda G. (2024). *Tuberculosis surpasses COVID-19 and becomes the leading cause of death from infectious disease worldwide*. Medscape. Available online at: https://portugues.medscape.com/verartigo/6511893?form=fpf (Accessed September 23, 2025).

27. Associação Paulista de Medicina. *Eighty thousand people fall ill from tuberculosis annually in Brazil*. APM (2024). Available online at: https://www.apm.org.br/oitenta-mil-pessoas-adoecem-por-tuberculose-anualmente-no-brasil/ (Accessed September 23, 2025).

28. CNN Brasil. *Almost 16 people died from tuberculosis per day in Brazil in 2022*. CNN Brasil (2024). Available online at: https://www.cnnbrasil.com.br/saude/quase-16-pessoas-morreram-de-tuberculose-por-dia-no-brasil-em-2022/ (Accessed September 23, 2025).

29. Leite OH. *Tuberculosis deaths in Brazil reach a record number in nearly two decades*. Jornal da USP (2023). Available online at: https://jornal.usp.br/atualidades/mortes-por-tuberculose-no-brasil-atingem-numero-recorde-em-quase-duas-decadas/ (Accessed September 23, 2025).

30. Vacinação do Calendário Nacional. Ministério da Saúde do Brasil(2024). Available online at: https://infoms.saude.gov.br/extensions/SEIDIGI_DEMAS_VACINACAO_CALENDARIO_NACIONAL_MENU_COBERTURA/SEIDIGI_DEMAS_VACINACAO_CALENDARIO_NACIONAL_MENU_COBERTURA.html (Accessed June 28, 2025).

31. BUTANTAN. *BCG vaccine: Immunization should be administered within the first hours of life and is the best strategy to protect children from severe forms of tuberculosis*. Instituto Butantan. (2024). Available online at: https://butantan.gov.br/noticias/vacina-bcg-imunizante-deve-ser-aplicado-nas-primeiras-horas-de-vida-e-e-melhor-estrategia-para-proteger-criancas-das-formas-graves-da-tuberculose (Accessed September 23, 2025).

32. Pereira SM, Dantas OMS, Ximenes R, Barreto ML. Vacina BCG contra tuberculose: efeito protetor e políticas de vacinação. *Rev Saúde Pública*. (2007) 41:59–66. doi: 10.1590/S0034-89102007000800009

33. Trunz BB, Fine P, Dye C. Effect of BCG vaccination on childhood tuberculous meningitis and miliary tuberculosis worldwide: a meta-analysis and assessment of cost-effectiveness. *Lancet*. (2006) 367:1173–80. doi: 10.1016/S0140-6736(06)68507-3

34. Junqueira-Kipnis AP, Leite LC de C, Croda J, Chimara E, Carvalho ACC, Arcêncio RA. Advances in the development of new vaccines for tuberculosis and Brazil's role in the effort forward the end TB strategy. *Mem Inst Oswaldo Cruz*. (2024) 119:e240093. doi: 10.1590/0074-02760240093

35. Ahmed MM, Okesanya OJ, Olaleke NO, Adigun OA, Adebayo UO, Oso TA, et al. Integrating digital health innovations to achieve universal health coverage: promoting health outcomes and quality through global public health equity. *Healthcare*. (2025) 13:1060. doi: 10.3390/healthcare13091060

36. National Academies of Sciences, Engineering, and Medicine, Health and Medicine Division, Board on Global Health, and Forum on Microbial Threats, Nicholson A, Liao J, Biffl C. Detection. In: *Innovations for Tackling Tuberculosis in the Time of COVID-19: Proceedings of a Workshop*. National Academies Press (US (2022). Available online at: https://www.ncbi.nlm.nih.gov/books/NBK587312/.

37. Filardi ETM, Pucca MB, Araujo Junior JP, Costa PId. Pandemic paradox: the impact of the COVID-19 on the global and Brazilian tuberculosis epidemics. *Front Public Health*. (2024) 12. doi: 10.3389/fpubh.2024.1399860

frontiers | Frontiers in Immunology

TYPE Original Research
PUBLISHED 01 October 2025
DOI 10.3389/fimmu.2025.1657235

OPEN ACCESS

EDITED BY
Sonia Jangra,
The Rockefeller University, United States

REVIEWED BY
Florencia Rammauro,
Pasteur Institute of Montevideo, Uruguay
Sara S. El Zahed,
Icahn School of Medicine at Mount Sinai, United States

*CORRESPONDENCE
Jingxin Li
jingxin42102209@126.com
Yuxin Chen
yuxin.chen@nju.edu.cn
Xiangjun Zhai
jszxj@jscdc.cn

†These authors have contributed equally to this work and share first authorship

RECEIVED 01 July 2025
ACCEPTED 15 September 2025
PUBLISHED 01 October 2025

CITATION
Gan M, Han W, Li C, Li S, Huang Z, Xu L, Xu X, Zhai X, Chen Y and Li J (2025) Impact of an aerosolized or intramuscular adenovirus type 5-vectored COVID-19 vaccine on Fc-mediated immune effector functions in a hybrid immunity population. *Front. Immunol.* 16:1657235. doi: 10.3389/fimmu.2025.1657235

Impact of an aerosolized or intramuscular adenovirus type 5-vectored COVID-19 vaccine on Fc-mediated immune effector functions in a hybrid immunity population

Mingzhi Gan[1,2†], Weiwei Han[1†], Chuang Li[3†], Simin Li[4], Zhuangzhuang Huang[1], Lingjie Xu[5], Xiaoyu Xu[5], Xiangjun Zhai[1,6*], Yuxin Chen[7*] and Jingxin Li[1,2*]

[1]School of Public Health, National Vaccine Innovation Platform, Nanjing Medical University, Nanjing, China, [2]Jiangsu Provincial Medical Innovation Center, National Health Commission Key Laboratory of Enteric Pathogenic Microbiology, Jiangsu Provincial Center for Disease Control and Prevention (Jiangsu Provincial Academy of Preventive Medicine), Nanjing, China, [3]Department of Laboratory Medicine, Nanjing Drum Tower Hospital Clinical College of Nanjing University of Chinese Medicine, Nanjing, Jiangsu, China, [4]School of Public Health, Southeast University, Nanjing, China, [5]Vazyme Biotech Co., Ltd, Nanjing, China, [6]Major Project Executive Office, Jiangsu Provincial Center for Disease Control and Prevention, Nanjing, Jiangsu, China, [7]Department of Laboratory Medicine, Nanjing Drum Tower Hospital, Nanjing University Medical School, Nanjing, Jiangsu, China

Background: Beyond the role of neutralizing antibodies in protecting against SARS-CoV-2, Fc-mediated antibodies functions may offer additional immune defense. This study aimed to evaluate the Fc-mediated immune responses elicited by aerosolized and intramuscular Ad5-nCoV vaccines in a Chinese population with hybrid immunity.

Methods: Serum samples were collected from the immunogenicity sub-cohort within a multicenter, partially randomized platform trial comparing aerosolized and intramuscular adenovirus type 5-vectored COVID-19 vaccine (Ad5-nCoV) boosters in adults in China. Participants were enrolled approximately six months after an Omicron wave in late 2022, and randomized to receive a booster dose with aerosolized or intramuscular Ad5-nCoV. Fc-mediated immune responses to wild-type and XBB.1.16 variant spike proteins were assessed by measuring antibody-dependent cellular phagocytosis (ADCP), antibody-dependent neutrophil phagocytosis (ADNP), and antibody-dependent cellular cytotoxicity (ADCC) before vaccination, and at 14 days, 3 months, 6 months post-booster. Correlations between Fc-mediated responses (ADCP, ADNP, ADCC) and neutralizing antibodies, IgG, and IgA levels responses were also analyzed.

Results: Intramuscular Ad5-nCoV vaccination significantly induced Fc-mediated effector functions against wild-type spike protein, with peak responses at 14 days post-booster, including ADCP score of 107.21 (95% CI: 84.43-129.99), ADNP score of 133.96 (95% CI: 112.81-155.11), and ADCC fold induction of 9.64 (95% CI: 8.57-10.70). These responses gradually waned over time. In contrast, aerosolized Ad5-nCoV did not significantly enhance ADCP or ADNP, but did elicit notable ADCC responses, peaking at 3 months post-vaccination (fold induction: 7.85,95% CI: 6.66-9.04). Fc-mediated responses to XBB.1.16 were lower than those to the

wild-type spike. Notably, the fold reductions in ADCP, ADNP, and ADCC against XBB.1.16 were less pronounced than the corresponding reduction in neutralizing antibody titers.

Conclusions: Intramuscular Ad5-nCoV vaccination elicited robust ADCP, ADNP, and ADCC responses, while the aerosolized formulation primarily induced ADCC activity. Fc-mediated effector functions exhibited greater cross-reactivity against emerging variants compared to neutralizing antibodies, but correlated only weakly with neutralizing antibody titers.

KEYWORDS

COVID-19, Fc-mediated immune effector functions, ADCP, ADNP, ADCC

Introduction

Widespread vaccination against severe acute respiratory syndrome coronavirus 2 (SARS-CoV-2) has significantly reduced global morbidity and mortality associated with COVID-19 (1). Most current vaccines were developed based on the ancestral SARS-CoV-2 strain. However, the emergence of SARS-CoV-2 variants with immune escape properties has challenged the effectiveness of both vaccine-induced or infection-acquired humoral immunity, as these variants can partially or fully evade neutralizing antibodies (2). Beyond neutralization, antibodies exert additional antiviral effects through interaction between their Fc region and Fc receptors (FcRs) on immune cells (3, 4). These Fc-mediated effector functions, including antibody-dependent cellular cytotoxicity (ADCC), antibody-dependent cellular phagocytosis (ADCP), and antibody-dependent neutrophil phagocytosis (ADNP), might also play crucial role in antiviral function independent of direct neutralization (5, 6). However, the immunological and clinical relevance of Fc-mediated responses remains underexplored, as most COVID-19 vaccine studies have focused primarily on neutralizing antibody titers.

Fc-dependent immune responses have been shown to play a crucial role in protection against a wide range of viral infections, including influenza, HIV, and Ebola (3). In the context of SARS-CoV-2, vaccines have been demonstrated to elicit Fc-mediated effector functions that contribute to viral clearance. For instance, three-dose regimen of CoronaVac significantly induced ADCP and ADNP responses against Omicron subvariants (7). Similarly, mRNA-1273 vaccine generated spike-specific antibodies with robust FcR-binding capacity and functional activity, even when neutralization was diminished by viral evolution (8). Furthermore, Fc-mediated antibody function, particularly those involving Fcγ receptor (FcγR) engagement, have been linked to improved clinical outcomes in COVID-19 (9).

In China, over 90% of the population has completed the primary COVID-19 vaccination series (10), and a large-scale national survey reported that 82.4% of individuals have been infected with SARS-CoV-2 between December 2022 and February 2023 (11). This had led to widespread hybrid immunity. Recent evidence suggests that hybrid immunity enhances FcR-binding antibody responses compared to vaccination alone, potentially promoting stronger activation of macrophages and natural killer (NK) cells, and augmenting ADCP, ADNP, and ADCC activity (12). Previously, we demonstrated that a booster dose of aerosolized or intramuscular adenovirus type 5-vectored COVID-19 vaccine (Ad5-nCoV) could enhance the humoral immunity against SARS-CoV-2 variants in individuals with a hybrid immunity (13). However, whether these booster strategies can also elicit robust Fc-mediated immune functions against emerging variants remains unclear.

In this study, we evaluate Fc-mediated immune responses elicited by aerosolized and intramuscular Ad5-nCoV booster vaccines in individuals with hybrid immunity. Specifically, we assessed their capacity to induce ADCP, ADNP and ADCC activity against SARS-CoV-2 wild-type strain and XBB.1.16 variants. These findings may provide new perspectives into optimizing booster vaccination strategies for population with hybrid immunity.

Materials and methods

Study cohort and serum sample collection

We did a multicenter, partially randomized platform clinical trial (ClinicalTrials.gov identifier: NCT05855408), to assess the efficacy of aerosolized (inhaled, IH) versus intramuscular (IM) administration of a booster dose of an Ad5-nCoV in adults aged ≥18 years with hybrid immunity, which has been reported previously (13).

Briefly, eligible participants were adults ≥18 years, with or without underlying medical conditions. Other key inclusion criteria included ≥4 months since SARS-CoV-2 infection or confirmation of no prior infection, and ≥6 months since the last COVID-19 vaccination. Participants provided written informed consent and were randomly assigned to receive either IH or IM Ad5-nCoV. Exclusion criteria included: suspected COVID-19

symptoms at enrollment, a positive SARS-CoV-2 antigen test, receipt of a second booster dose, history of severe adverse vaccine reactions or anaphylaxis, and pregnancy or lactation.

The first 60 individuals from each vaccination group were included in the immunogenetic subcohort. Blood samples were collected at baseline (pre-booster), and on day 14, month 3, and month 6 post-vaccination for serum and peripheral blood mononuclear cell (PBMC) isolation.

The study was approved by the Ethics Committee of the Jiangsu Provincial Center for Disease Control and Prevention and conducted in accordance with the Declaration of Helsinki and Good Clinical Practice (GCP) guidelines.

Measurement of the antibody responses

Fc-mediated effector functional assays

ADCP and ADNP assay

ADNP and ADCP assays were carried out as previously study described (7). Spike proteins from SARS-CoV-2 Wild-type (WT) (Vazyme, Cat# CG202, Nanjing, China) and Omicron XBB.1.16 (Vazyme, Cat# CG282, Nanjing, China) variants were used. Proteins were biotinylated using Sulfo-NHS-LC biotin (Thermo Fisher Scientific, cat# A39257, MA, USA), with excess biotin removed via Zeba Spin Desalting Columns (Thermo Fisher Scientific, cat# A44300, MA, USA). Botinylated antigens were then coupled to 1 µm yellow-green fluorescent NeutrAvidin beads (Invitrogen, cat# F8776, MA, USA) in a 1:1 ratio and incubated at 37°C for 2 hours, followed by centrifugation (16,000 g, 15 min) and resuspension in Phosphate-Buffered Saline (PBS) with 0.5% Bovine Serum Albumin (BSA).

For the ADCP assay, THP-1 cells were used. Serum samples were diluted 1:25 in PBS containing 0.5% Tween-20 and 1% BSA, and incubated with antigen-coupled beads at 4°C overnight. After washing, 25,000 THP-1 cells were added per well in R10 medium and incubated at 37°C, 5% CO_2 for 1 hour. Cells were then washed with PBS and fixed with 4% paraformaldehyde (PFA) (Leagene, cat# DF0135, Beijing, China) for 30 min. The fixed cells were then analyzed by flow cytometry. Serum samples from healthy archived individuals from 2019, who were unexposed and unvaccinated, served as negative controls, which were assayed in parallel with the test samples.

For the ADNP assay, ADNP granulocytes were isolated from the whole blood of healthy adult donors using a lysis method (8). Immune complexes were prepared by incubating the 25-fold diluted serum with antigen-coupled beads (Invitrogen, cat# F8776, MA, USA), as described above. After incubation, unbound immunoglobulins were removed by washing with sterile PBS. Granulocytes were resuspended in R10 medium at a concentration of 5 00,000 cells/mL. A total of 50,000 cells were added to each well containing immune complexes, mixed by gentle shaking, and incubated for 1 hour at 37°C with 5% CO_2. Following incubation, cells were washed and stained for neutrophil identification using an APC-conjugated anti-CD66b antibody (BioLegend, cat# 17-0666-42, CA, USA). Fixation was carried out using 4% PFA (Leagene, cat# DF0135, Beijing, China) for 30 minutes. Flow cytometric analysis was subsequently performed. The same negative control sera used in the ADCP assay were included and assayed in parallel with the test samples.

To assess the phagocytic efficacy, the geometric mean fluorescence intensity (gMFI) and percentage of bead-positive cells (THP-1 or neutrophils) were measured by flow cytometry. The phagoscore was calculated as: Phagoscore = (% positive cells × gMFI)/100,000. The corrected phagoscore was defined as the actual phagoscore derived from the sample minus phagoscore derived from the blank control. If the phagoscore was calculated to be less than zero, it was assigned a value of zero.

ADCC assay

ADCC assay was carried out as previously study described (14). Two sets of 293F cell lines were constructed, each stably expressing the spike protein of either the SARS-CoV-2 wild-type (WT) strain or the XBB.1.16 variant. These cell lines were established by transfecting the respective plasmids and selecting stable clones, which were then used as target cells in the ADCC assay. Jurkat-FcγRIII-NFAT-Luc reporter cells (Vazyme, cat# DD1301-1, Nanjing, China) were used as effector cells. These cells stably express the FcγRIIIa (CD16) receptor and contain a functional NFAT transcription factor that regulates the expression of the Lucia luciferase gene. When antibodies bind to FcγRIIIa, the NFAT pathway is activated, resulting in NFAT translocation to the nucleus and subsequent binding to the promoter of the Lucia luciferase gene, driving luciferase expression (15).

Serum samples were diluted 1:60 in R10 medium and incubated with 25,000 target 293F cells per well at 37°C and 5% CO_2 for 1 hour. After incubation, 75,000 Jurkat reporter cells were added to each well, gently mixed, and further incubated under the same conditions for 12 hours. Luciferase substrate (Vazyme, cat# DD1201-03, Nanjing, China) was then added, and the wells were shaken to ensure a complete reaction. Relative light units (RLU) were measured using the protocol provided by PerkinElmer (Waltham, MA). Serum samples from healthy adult donors collected in 2019, identical to those used in the ADCP assay, were included as negative controls. ADCC activity was calculated as the fold induction of luciferase activity relative to the negative control sera.

Pseudovirus neutralization assay and IgG/IgA testing

Neutralizing antibody responses against wild-type SARS-CoV-2, XBB.1.16, and BA.4/5 variants were assessed using pseudovirus neutralization tests, employing a human immunodeficiency virus pseudovirus system expressing the spike glycoprotein. In the experiment, serum samples were incubated with pseudoviruses expressing the spike glycoprotein of the aforementioned variants, and then the mixture was added to HEK293-ACE2 cells. The viral infectivity was assessed by measuring the expression level of the reporter gene using the Bio-Lite luciferase reporter assay kit. The neutralizing antibody activity was quantified by calculating the half-maximal inhibitory concentration (IC50). To ensure sensitivity, the cutoff titer for detection was set at 1:30.

The RBD-specific IgG and IgA antibody responses were evaluated using ELISA kits from Vazyme Biotech (Nanjing,

TABLE 1 Demographic characteristics of the participants in this study.

Characteristic	IM Ad5-nCoV (n=60)	IH Ad5-nCoV (n=61)	P value
Age, years			
Mean (SD)	47.33(13.4)	47.85(13.8)	0.834
Sex, n (%)			
Female	40(66.7)	36(59.0)	0.384
Male	20(33.3)	25(41.0)	
BMI, kg/m^2			
Mean (SD)	24.3(3.8)	24.1(3.1)	0.660
Vaccination history before booster, n (%)			
ICV+ICV+ICV	58(96.7)	60(98.4)	0.619
ICV+ICV	1(1.7)	0(0.0)	
ICV+ICV+Ad5-IM	0(0.0)	1(1.6)	
CHO+CHO+CHO	1(1.7)	0(0.0)	

Data are n (%) or mean (SD). BMI=Body-mass index. IM Ad5-nCoV (Ad5-IM) =adenovirus type 5 vectored COVID-19 vaccine through intramuscular injection. IH Ad5-nCoV=adenovirus type 5 vectored COVID-19 vaccine through oral inhalation. ICV=inactivated COVID-19 vaccine. CHO=SARS-CoV-2 recombinant protein vaccine (CHO cell).

China). For IgG detection, a quantitative ELISA kit was used, where the optical density (OD) was calculated by subtracting the OD value at 630 nm from that at 450 nm. The lower limit of quantification for the IgG assay was 0.125 BAU/mL. The final concentration of IgG antibodies was determined by multiplying the detected OD value by the serum dilution factor. IgG antibodies were assessed against both wild-type (WT) SARS-CoV-2 and BA.4/5 variants. For IgA detection, an indirect ELISA method was used with the RBD-specific IgA ELISA kit. After a two-step incubation and color development, the absorbance at a specific wavelength was positively correlated with the concentration of SARS-CoV-2 RBD IgA antibodies targeting the XBB.1.5 variant. The antibody concentration was then calculated by referencing a standard curve.

Statistical analysis

The χ^2-test or Fisher's exact test was used for categorical demographic data. Student's t-test was used for continuous demographic data. For comparisons of ADCP, ADNP, and ADCC responses at different time points, mixed-effect models was performed, followed by Tukey's correction for multiple comparisons. Single-variable comparisons between the two vaccine groups, were conducted using the Mann-Whitney U test. Spearman correlation analysis was used to evaluate the relationships between ADCP, ADNP, ADCC, NAb, IgG, and IgA. A correlation heatmap was generated using ChiPlot (https://www.chiplot.online/correlation_heatmap.html). For comparisons of ADCP, ADNP, ADCC, NAbs, and IgG responses specific to the COVID-19 wild-type strain versus Omicron subvariants, paired t-tests were performed. Data analysis was carried out using SPSS version 26 and GraphPad Prism version 9.5.1. All statistical tests were two-tailed, and a p-value of < 0.05 was considered statistically significant.

Results

Longitudinal Fc-mediated effector functions to WT and XBB.1.16 spikes in two vaccination groups

We assessed Fc-mediated effector functions (ADCP, ADNP, and ADCC) in 121 participants (60 from the IM Ad5-nCoV group and 61 from the IH Ad5-nCoV group) at four time points: baseline (pre-booster), day 14 (14 days post-booster), month 3 (3 months post-booster), and month 6 (6 months post-booster). There were no significant differences between groups in demographic characteristics, including age, sex, BMI and vaccination history (Table 1).

In the IM Ad5-nCoV group, WT spike-specific ADCP significantly increased at day 14, with a mean phagoscore of 107.21 (95% CI: 84.43-129.99) compared to baseline (62.15, 95% CI: 47.82-76.48). However, ADCP responses declined by month 3 (64.65, 95% CI: 50.78-78.51) and further by month 6 (54.77, 95% CI: 43.38-66.15). In contrast, IH Ad5-nCoV induce no significant changes in ADCP responses over time, with phagoscores remaining stable at 76.72 (95% CI: 62.47-90.96) at baseline, 83.70 (95% CI: 70.19-97.20) at day 14, 83.55 (95% CI: 67.41-99.70) at month 3, and 75.12 (95% CI: 65.21-89.04) at month 6 (Figure 1A). In contrast to ADCP responses against wild-type SARS-CoV-2, those against XBB.1.16 were observed at lower levels across all time points, with the peak phagoscore at day 14 of 78.84 (95% CI: 60.35-97.32) in IM Ad5-nCoV group. Similarly, IH Ad5-nCoV did not induce significant changes in ADCP responses against XBB.1.16, with responses showing a gradual decline at month 3 and month 6 (Figure 1B).

IM Ad5-nCoV significantly induced ADNP responses for WT Spike, with phagoscores of 102.81 (95% CI: 82.97-122.65) at baseline, 133.96 (95% CI: 112.81-155.11) at day 14, and followed by a gradual decline at month 3 (85.64, 95% CI: 71.30-99.98) and month 6 (78.42, 95% CI: 66.29-90.55). In comparison, IH Ad5-nCoV did not elicit a significant enhancement in ADNP responses. A significant decline was observed over time, with the mean phagocytic score decreasing to 92.90 (95% CI: 77.62-108.17) at month 3 and 88.86 (95% CI: 75.96-101.77) at month 6, relative to the response level on day 14 post-vaccination (131.0, 95% CI: 110.4-151.7). (Figure 1C). For the XBB.1.16 Spike, a similar trend was observed. In contrast to ADNP responses against wild-type SARS-CoV-2, those against XBB.1.16 were observed at lower levels across all time points, with the peak phagoscore at day 14 of 97.61(95% CI: 77.80-117.41) in IM Ad5-nCoV group. Similarly, IH Ad5-nCoV did not elicit significant ADNP responses against XBB.1.16, and a significant decline was observed at month 6 (58.94,95% CI: 45.80-72.07) compared to day 14 (87.47, 95% CI: 68.47-106.47). (Figure 1D).

Both vaccines induced ADCC responses against WT spike. IM Ad5-nCoV vaccination induced a peak response at day 14 (9.64-fold, 95% CI: 8.57-10.70), which declined by month 3 (7.98, 95% CI: 6.66-9.30) and returned to near-baseline levels by month 6

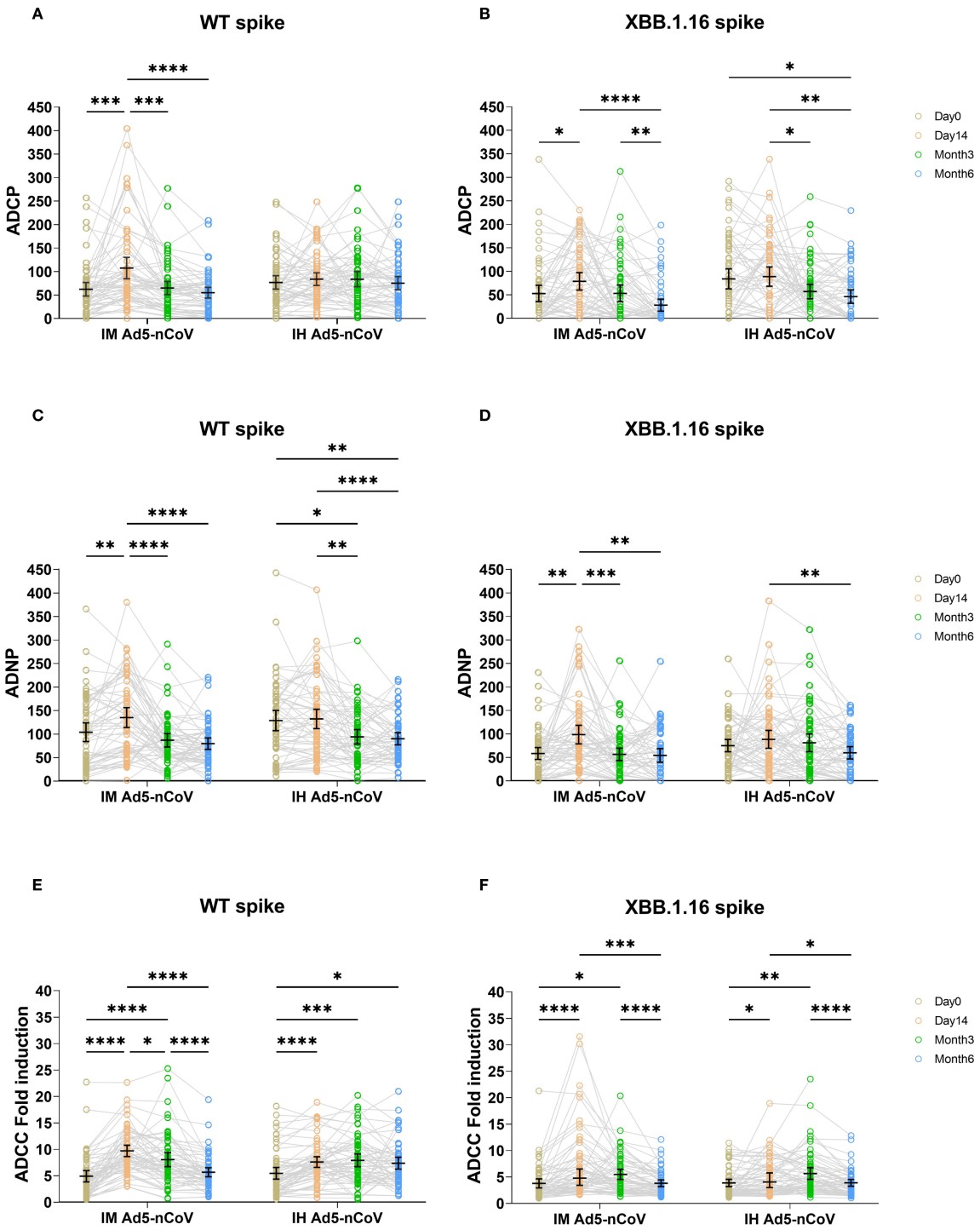

FIGURE 1
ADCP, ADNP, and ADCC specific to WT and XBB.1.16 spike proteins across four time points in two vaccination groups. ADCP **(A, B)**, ADNP **(C, D)**, and ADCC **(E, F)** specific to WT and XBB.1.16 spike proteins were measured before the booster dose, and at day 14, month 3, and month 6 post-booster. Trends over time were compared across the two groups using two-sided mixed-effects models, followed by Tukey's correction for multiple comparisons. IM Ad5-nCoV=adenovirus type 5 vectored COVID-19 vaccine through intramuscular injection. IH Ad5-nCoV=adenovirus type 5 vectored COVID-19 vaccine through oral inhalation. Significant differences are indicated by asterisks: *p < 0.05, **p < 0.01, ***p < 0.001, ****p <0.0001.

(5.60, 95% CI: 4.73-6.46). By comparison, IH Ad5-nCoV elicited more durable ADCC responses, peaking at month 3 (7.85, 95% CI: 6.66-9.04) and remaining stable at month 6 (7.30, 95% CI: 6.17-8.42) (Figure 1E). In contrast to ADCC responses against wild-type spike, ADCC responses against XBB.1.16 followed a similar kinetics pattern, albeit with lower magnitudes (Figure 1F). Specifically, IM Ad5-nCoV group generated a peak fold increase at day 14 (7.22,95% CI: 5.51-8.92), whereas the IH Ad5-nCoV group peaked at month 3 (5.67, 95% CI: 4.57-6.77) followed by a significant decline at month 6 (3.90, 95% CI: 3.26-4.54).

IM Ad5-nCoV induces more pronounced Fc-mediated effector functions than IH Ad5-nCoV

To account for baseline variability, the Fc-mediated immune effector functions at day 14, month 3, and month 6 were standardized by calculating fold changes relative to each individual's own baseline, with pre-booster levels used for comparison. After standardization, we compared the ADCP, ADNP, and ADCC responses across these three time points. For ADCP and ADNP responses against both WT and XBB.1.16 strains, IM Ad5-nCoV group and IH Ad5-nCoV group showed a decrease at month 3 relative to day 14, with further decline at month 6 (Supplementary Figures S1A, B). In the case of ADCC responses to both WT and XBB.1.16 strains, IM Ad5-nCoV group exhibited a decrease at month 3 relative to day 14, with further reduction at month 6. However, for the WT spike-specific ADCC response, IH Ad5-nCoV group did not show a downward trend, whereas for XBB.1.16 variant, the response at month 6 was lower than a month 3 (Supplementary Figure S1C). These findings confirm that the trends observed in both raw and standardized data are consistent.

Then, we compared the fold changes in Fc-mediated immune effector functions between the two vaccines. Against WT spike, IM Ad5-nCoV induced 1.85-fold greater ADCP responses at day 14, compared to 1.22-fold increase for IH Ad5-nCoV (P = 0.0003). No significant differences were observed between the two vaccines at month 3 and month 6(Figure 2A). For the XBB.1.16 spike, a modest but significant improvement was observed at day 14 (1.17 vs. 1.06, P = 0.047) (Figure 2B), with no significant differences at later timepoints.

A similar pattern was observed for ADNP responses. IM Ad5-nCoV also induced 1.34-fold increase for wild-type spike specific ADNP responses at day 14 versus 1.11 for IH Ad5-nCoV group (P = 0.002), and there was no significant differences were observed at month 3 and month 6 (Figure 2C). For the XBB.1.16 spike, the fold increase for ADNP responses at 14 days was 1.41 for IM Ad5-nCoV versus 1.20 for IH Ad5-nCoV (P = 0.023), with no significant differences at month 3 and month 6 (Figure 2D).

Similarly, IM Ad5-nCoV also outperformed IH Ad5-nCoV in ADCC responses. For the WT spike, the mean fold increase at day 14 was 3.86 for IM Ad5-nCoV versus 2.03 for IH Ad5-nCoV (P = 0.001), with no significant differences at later timepoints (Figure 2E). For the XBB.1.16 spike, the mean fold increase in ADCC at day 14 was 2.20 for IM Ad5-nCoV versus 1.65 for IH Ad5-nCoV (P = 0.001). There were no statistical differences at subsequent timepoints (Figure 2F).

Correlation between Fc-mediated immune effector functions and antibody responses

We previously analyzed the levels of IgG, IgA, and neutralizing antibodies (NAbs) in both cohorts (13). IH Ad5-nCoV group showed peak NAbs against wild-type SARS-CoV-2 at month 3 (GMT:1026.2, 95% CI 792.7-1328.6) and slightly declined at month 6 (880.9, 95% CI 700.9-1107.2). In comparison, the IM Ad5-nCoV group exhibited similar levels at day 14 (796.4, 95% CI 635.3-998.2), but decreased at month 3 (681.6, 95% CI 542.2-856.9) and month 6 (520.0, 95% CI 413.1-654.6) (Supplementary Figure S2A). Both groups showed comparable NAbs against BA.4/5 (Supplementary Figure S2B), with the peak GMTs at month 3 of 1061.0 (95% CI 800.1-1405.5) in the IH Ad5-nCoV group and 883.0 (95% CI 670.1-1163.4) in the IM Ad5-nCoV group. However, NAbs against XBB.1.16 were lower in both groups compared to WT SARS-CoV-2 and BA.4/5 variants, though GMTs significantly increased post-booster (Supplementary Figure S2C).

RBD-specific IgG responses followed a similar pattern to NAbs. WT-specific IgG geometric mean concentrations (GMCs) rose from 1071.2 (95% CI: 833.1-1377.3) to 2174.1 (95% CI: 1890.4-2500.5) BAU/mL at day 14 in the IM Ad5-nCoV group, and from 1635.9 (95% CI: 1339.0-1998.7) to 2779.8 (95% CI: 2432.1-3177.2) BAU/mL at month 3 in the IH Ad5-nCoV group (Supplementary Figure S3A). Both vaccines significantly increased IgG against BA.4/5 despite of modest magnitude (Supplementary Figure S3B). Additionally, IgA antibodies against the XBB.1.5 variant peaked at month 3 post-vaccination in IM Ad5-nCoV group, followed by a slight decline at month 6, with the peak GMCs at month 3 of 456.9 (95% CI: 296.9-615.8) U/mL, and the IH Ad5-nCoV group showed a peak at day 14 of 477.4 (364.7-625.0) U/mL, which decreased by month 3 and declined further by month 6 (Supplementary Figure S4).

Spearman correlation analysis showed moderate correlations between ADCP and ADNP for the wild-type spike (IM: r = 0.50; IH: r = 0.56, both $P < 0.0001$) and XBB.1.16 spike (IM: r = 0.30; IH: r = 0.46, both $P < 0.0001$). Nevertheless, ADCC correlated weakly with ADCP and ADNP. Correlation between Fc effector functions and antibody levels were generally weak for ADCP/ADNP, and IgG, but moderate-to-strong for ADCC and IgG. Specifically, WT spike-specific ADCC was correlated with WT RBD-specific IgG antibodies (r = 0.63 in IM, r=0.48 in IH, both $P < 0.0001$), and also correlated with BA.4/5 RBD-specific IgG (IM: r = 0.64; IH: r = 0.49; both $P < 0.0001$). For the XBB.1.16 spike, ADCC in the IH group demonstrated a moderate correlation with WT RBD-specific IgG antibodies (r = 0.51; $P < 0.0001$), whereas the correlation in the IM group was weaker (r = 0.34; $P < 0.0001$). Correlations between ADCC and BA.4/5 RBD-specific IgG antibodies were moderate in both groups (IM: r = 0.51; IH: r = 0.52; both $P < 0.0001$). IgA correlated moderately with ADCC responses, but weakly with ADCP and ADNP. In particular, XBB 1.16 spike-specific ADCC effects exhibited a moderate positive correlation with XBB.1.5 RBD-specific IgA antibodies (r = 0.42 in IM, r = 0.50 in IH, both $P <$ 0.0001). Correlation with NAbs were weak across all Fc functions in both vaccine groups (Figures 3A, B).

Fc-mediated effector functions demonstrate stronger cross-reactivity than the IgG and neutralizing antibodies

We further compared the fold reduction in Fc effector function and NAbs from WT spike to XBB.1.16 spike as well as spike-specific IgG responses from WT to BA.4/5. In the IM Ad5-nCoV group

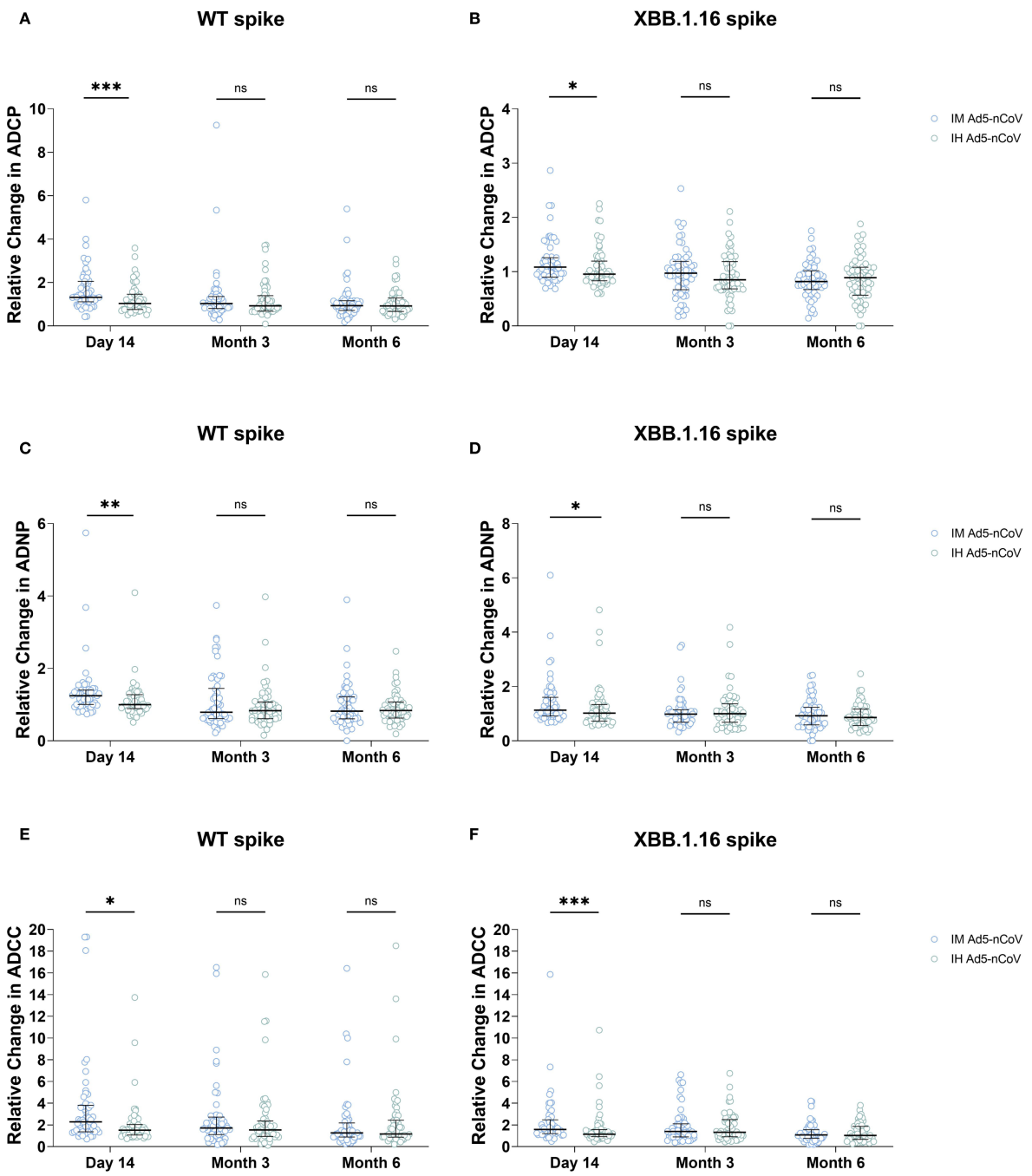

FIGURE 2
Fold-change comparison of ADCP, ADNP, and ADCC responses between two vaccines at three time points. Panels show the relative change in **(A, B)** ADCP, **(C, D)** ADNP, and **(E, F)** ADCC responses specific to the SARS-CoV-2 wild-type (WT) spike **(A, C, E)** and XBB.1.16 spike **(B, D, F)** at day 14, month 3, and month 6 post-booster, compared between the IM Ad5-nCoV and IH Ad5-nCoV groups. Statistical comparisons between the two vaccine groups at each time point were performed using the Mann-Whitney U test. IM Ad5-nCoV=adenovirus type 5 vectored COVID-19 vaccine through intramuscular injection. IH Ad5-nCoV=adenovirus type 5 vectored COVID-19 vaccine through oral inhalation. Asterisks indicate statistically significant differences between the groups at each time point: *p < 0.05, **p < 0.01, ***p < 0.001. ns indicates no significant difference.

(Figure 4A), the GMT of WT-specific NAb dropped from 796.4 (95% CI: 635.3-998.2) to 201.3 (95% CI: 130.5-310.6) against XBB.1.16 (8.87-fold reduction, $P < 0.0001$). The GMC of WT-specific IgG decreased from 2174.1 (95% CI: 1890.4-2500.5) BAU/mL to 632.4 (95% CI: 527.1-758.8) BAU/mL (3.42-fold, $P < 0.0001$). In contrast, the fold reduction was remarkably smaller for ADCP, ADNP and ADCC. The mean phagocytic score of WT-specific ADCP dropped from 107.21 (95% CI: 84.43-129.99) to 78.84 (95% CI: 60.35-97.32) against XBB.1.16 (2.05-fold, $P < 0.0001$). The mean phagocytic score of WT-specific ADNP dropped from 133.96 (95% CI: 112.81-155.11) to 97.61 (95% CI: 77.80-117.41) against XBB.1.16 (2.01-fold, $P = 0.0008$). The mean fold induction of

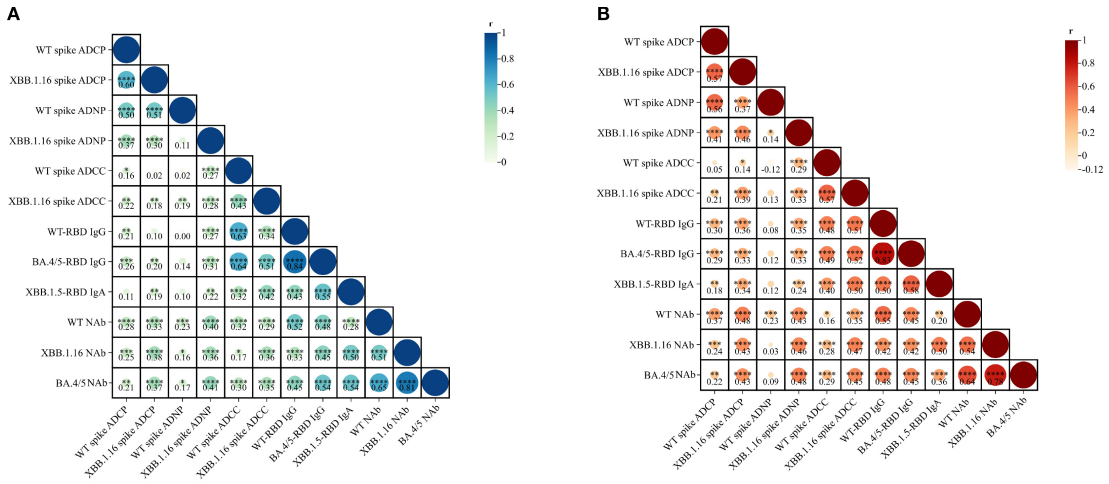

FIGURE 3
Correlation analysis of ADCP, ADNP, ADCC, IgG, IgA, and neutralization activity elicited by IM Ad5-nCoV **(A)** and IH Ad5-nCoV **(B)**. Statistics were analyzed using Spearman correlation analysis. Spearman correlation coefficients (r) are displayed within the matrix, with significant correlations indicated by asterisks (*p < 0.05, **p < 0.01, ***p < 0.001, ****p < 0.0001). IM Ad5-nCoV=adenovirus type 5 vectored COVID-19 vaccine through intramuscular injection. IH Ad5-nCoV=adenovirus type 5 vectored COVID-19 vaccine through oral inhalation.

WT-specific ADCC dropped from 9.64 (95% CI: 8.57-10.70) to 7.22 (95% CI: 5.51-8.92) against XBB.1.16 (2.12-fold, $P = 0.0005$).

Similarly, in the IH Ad5-nCoV group (Figure 4B), the GMT of WT-specific NAb dropped from 796.9 (95% CI: 635.6-999.1) to 170.5 (95% CI: 114.7-253.4) against XBB.1.16 (8.94-fold reduction, $P < 0.0001$). The GMC of WT-specific IgG decreased from 2779.8 (95% CI: 2432.1-3177.2) BAU/mL to 589.3 (95% CI: 478.5-725.8) BAU/mL against BA.4/5 (3.62-fold, $P < 0.0001$). Again, the fold reduction in Fc-mediated functions was considerably smaller. The mean phagocytic score for WT-specific ADCP remained almost unchanged, from 83.70 (95% CI: 70.19-97.20) to 88.94 (95% CI: 68.5-109.4) against XBB.1.16 (1.28-fold, $P = 0.54$). The mean phagocytic score of ADNP dropped from 131.0 (95% CI: 110.4-151.7) to 87.5 (95% CI: 68.5-106.5), a 2.97-fold reduction ($P < 0.0001$). The mean fold induction of ADCC dropped from 7.5 (95% CI: 6.5-8.5) to 5.1 (95% CI: 4.2-6.0), a 1.83-fold reduction ($P < 0.0001$). Collectively, these findings indicate that Fc-mediated effector functions retain broader cross-reactivity against emerging variants compared to NAb and IgG responses.

Discussion

In this study, we demonstrate that intramuscular administration of Ad5-nCoV booster, based on the ancestral strain, elicits robust Fc-mediated effector functions, with ADCP, ADNP, and ADCC responses peaking at 14 days post-boost. These findings align with previous studies reporting that both inactivated and mRNA vaccines encoding the ancestral spike protein can effectively induce potent Fc-dependent immune responses (12, 14).

While the aerosolized Ad5-nCoV vaccine effectively induced ADCC responses, it showed limited capacity to stimulate ADCP and ADNP activities. Furthermore, Fc-mediated effector functions were consistently lower in IH group than IM group. This discrepancy may be attributable to the distinct immunological microenvironments and mechanisms active by two delivery routes. Aerosolized vaccines primarily stimulate mucosal immunity in the respiratory tract, whereas intramuscular vaccination induces more robust systemic immunity (16). Of note, systemic vaccination triggers strong cytokine responses, including IFN-γ, TNF-α, and IL-2 from activated immune cells. Of particular importance is IFN-γ, which enhances macrophage and NK cell function and upregulates Fc receptor expression, thereby amplifying Fc-mediated immune activity (17). These immunological mechanisms likely underpin the superior Fc-effector responses observed following IM vaccination. In addition, our results showed that in the IH group, XBB.1.16 spike-specific ADCP and WT spike-specific ADNP at month 6 post-booster declined to below baseline levels. A plausible explanation is that at baseline, participants were in a state of hybrid immunity. Previous studies have shown that hybrid immunity elicits stronger Fc-mediated effector functions compared with vaccination alone (12, 18). By contrast, the aerosolized Ad5-nCoV booster failed to induce robust ADCP and ADNP responses, which likely contributed to the sub-baseline levels observed at 6 months post-booster in the IH group.

We also observed only weak to moderate correlations between Fc-mediated effector functions and levels of NAbs, IgG or IgA. This finding is consistent with prior studies, including those identifying ADCC responses in convalescent individuals post SARS-CoV-2 infection (18). The spike glycoprotein remains the primary target of SARS-CoV-2 antibody responses, with dominant neutralizing epitopes localized in the RBD of the S1 subunit (19). However, evidence suggests that, in hybrid immunity, antibodies targeting the S2 subunit can exhibit enhanced Fc receptor-binding capacity and more effectively mediate immune cell activation, particularly via

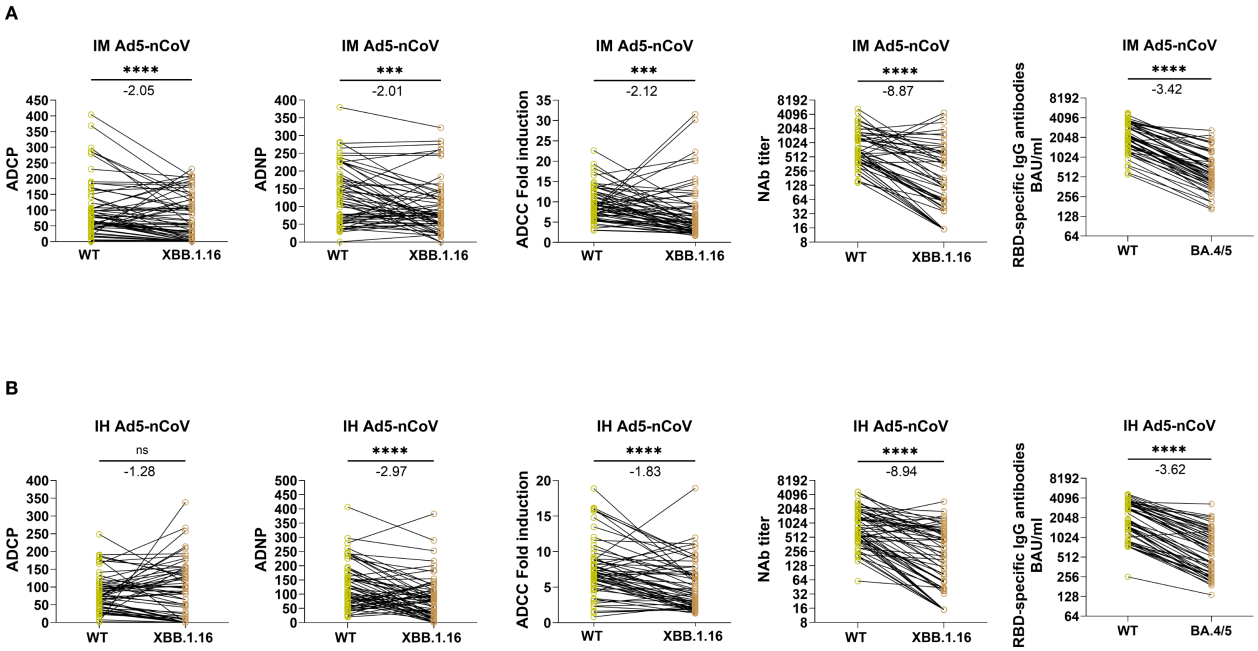

FIGURE 4
Paired comparisons of Fc-mediated effector functions and antibody responses to SARS-CoV-2 wild-type and Omicron subvariants at day 14 following IM Ad5-nCoV or IH Ad5-nCoV vaccination. Panels **(A, B)** present data from IM and IH Ad5-nCoV groups, respectively. Immune responses to the WT and Omicron variant spikes were compared at day 14 post-booster, including ADCP, ADNP, ADCC, NAb titers, and RBD-specific IgG. Statistical analyses were performed using the Wilcoxon matched-pairs signed-rank test. Fold reductions in immune responses from WT to variant were calculated for each individual, and the group mean values are annotated above each plot. IM Ad5-nCoV=adenovirus type 5 vectored COVID-19 vaccine through intramuscular injection. IH Ad5-nCoV=adenovirus type 5 vectored COVID-19 vaccine through oral inhalation. Asterisks indicate statistical significance: ***p < 0.001, ****p < 0.0001. ns indicates no significant difference.

ADCP, ADNP, and ADCC responses (12). This functional divergence may explain the limited correlation between Fc effector functions and conventional humoral markers. Indeed, Fc activity appears to reply more on the structural properties of the antibody Fc domain than on neutralizing potency, suggesting that even antibodies with limited neutralizing capacity may provide meaningful protection via Fc-driven mechanisms.

Our data also provide important insights into cross-variant immune responses. Previous work has shown that infection with Beta and Delta variant induces more broadly cross-reactive Fc-mediated antibodies, compared to infection with D614G strain or Ad26.COV2.S vaccination (20). Similarly, in our study, ADCP, ADNP, and ADCC responses against XBB.1.16 variant, while lower than those against WT spike, declined less sharply than NAbs and IgG levels. These observations echo the finding from mRNA-1273 vaccine studies, which demonstrated the sustained Fc-mediated immunity across a wide range of SARS-CoV-2 variants (8). The broader Fc cross-reactivity might be explained by two principal factors. First, most mutations in variants of concerns (VOCs) cluster in the RBD and N-terminal domain (NTD), limiting their impact on Fc-epitope recognition (21). Secondly, Fc-mediated functions are less affected by mutations that alter ACE2 receptor binding, which primarily influence neutralization capacity (22, 23).

This study has several limitations. First, we focused on Fc-mediated effector responses against the XBB.1.16 variant, and did not assess other currently circulating variants. Second, all vaccines administered targeted the ancestral strain, precluding direct comparison with variant-adapted vaccines. Third, the follow up duration was limited to six months post-vaccination, restricting conclusions regarding the long-term immune durability. Finally, the relatively small cohort size (n=121) may limit the generalizability across broader populations.

In conclusion, this study provides a comprehensive evaluation of Fc-mediated immune responses following IM and IH administration of Ad5-nCoV. Our findings show that IM vaccination induces significantly stronger ADCP, ADNP, and ADCC activity, while IH vaccination effectively elicits ADCC responses. Importantly, Fc-mediated effector functions displayed broader cross-reactivity against emerging variants compared to NAbs and IgG responses. These results not only underscore the pivotal role of Fc effector functions in vaccine-mediated immunity, but also highlight the necessity of optimizing Fc-mediated immunity in future vaccine design strategies, particularly against rapidly evolving viral pathogens.

Data availability statement

Individual participant data underlying the results reported in this article are available under restricted access due to requirements imposed by the Chinese Human Genetic Resources Administration regarding the public disclosure of clinical trial data. Researchers who provide a scientifically sound proposal will be allowed access to the de-identified individual participant data. Individual participant data can be obtained by submitting a request to the corresponding authors.

Ethics statement

The studies involving humans were approved by Scientific Review Committee and the Ethics Committee of Jiangsu Provincial Center for Disease Control and Prevention. The studies were conducted in accordance with the local legislation and institutional requirements. The participants provided their written informed consent to participate in this study.

Author contributions

MG: Investigation, Writing – original draft. CL: Writing – review & editing. SL: Investigation, Writing – review & editing. ZH: Writing – review & editing, Investigation. LX: Writing – review & editing, Resources. XX: Resources, Writing – review & editing. YC: Writing – review & editing, Methodology. JL: Conceptualization, Writing – review & editing. WH: Data curation, Writing – review & editing. XZ: Methodology, Writing – review & editing.

Funding

The author(s) declare financial support was received for the research and/or publication of this article. This work is supported by the National Key Research and Development Program (grant number 2023YFC2309100) and the National Natural Science Foundation of China (grant numbers 92269118, 92269205).

Acknowledgments

We thank CanSino Biologics for providing the investigational vaccines for this study. We also thank all the participants for their involvement in this study.

Conflict of interest

Author LX and XX were employed by the company Vazyme Biotech Co., Ltd.

The remaining authors declare that the research was conducted in the absence of any commercial or financial relationships that could be construed as a potential conflict of interest.

Generative AI statement

The author(s) declare that no Generative AI was used in the creation of this manuscript.

Any alternative text (alt text) provided alongside figures in this article has been generated by Frontiers with the support of artificial intelligence and reasonable efforts have been made to ensure accuracy, including review by the authors wherever possible. If you identify any issues, please contact us.

Publisher's note

Supplementary material

The Supplementary Material for this article can be found online at: https://www.frontiersin.org/articles/10.3389/fimmu.2025.1657235/full#supplementary-material

References

1. Feikin DR, Higdon MM, Abu-Raddad LJ, Andrews N, Araos R, Goldberg Y, et al. Duration of effectiveness of vaccines against SARS-CoV-2 infection and COVID-19 disease: results of a systematic review and meta-regression. *Lancet*. (2022) 399:924–44. doi: 10.1016/S0140-6736(22)00152-0

2. Liang D, Zhang G, Huang M, Wang L, Hong W, Li A, et al. Progress of the COVID-19: persistence, effectiveness, and immune escape of the neutralizing antibody in convalescent serum. *Pathogens*. (2022) 11(12):1531. doi: 10.3390/pathogens11121531

3. Lu LL, Suscovich TJ, Fortune SM, Alter G. Beyond binding: antibody effector functions in infectious diseases. *Nat Rev Immunol*. (2018) 18:46–61. doi: 10.1038/nri.2017.106

4. Bates TA, Lu P, Kang YJ, Schoen D, Thornton M, McBride SK, et al. BNT162b2-induced neutralizing and non-neutralizing antibody functions against SARS-CoV-2 diminish with age. *Cell Rep*. (2022) 41:111544. doi: 10.1016/j.celrep.2022.111544

5. Tauzin A, Nayrac M, Benlarbi M, Gong SY, Gasser R, Beaudoin-Bussières G, et al. A single dose of the SARS-CoV-2 vaccine BNT162b2 elicits Fc-mediated antibody effector functions and T cell responses. *Cell Host Microbe*. (2021) 29:1137–50.e6. doi: 10.1016/j.chom.2021.06.001

6. Mercado NB, Zahn R, Wegmann F, Loos C, Chandrashekar A, Yu J, et al. Single-shot Ad26 vaccine protects against SARS-CoV-2 in rhesus macaques. *Nature*. (2020) 586:583–8. doi: 10.1038/s41586-020-2607-z

7. Wang L, Li C, Li W, Zhao L, Zhao T, Chen L, et al. Coronavac inactivated vaccine triggers durable, cross-reactive Fc-mediated phagocytosis activities. *Emerg Microbes Infect*. (2023) 12:2225640. doi: 10.1080/22221751.2023.2225640

8. Kaplonek P, Fischinger S, Cizmeci D, Bartsch YC, Kang J, Burke JS, et al. mRNA-1273 vaccine-induced antibodies maintain Fc effector functions across SARS-CoV-2 variants of concern. *Immunity*. (2022) 55:355–65.e4. doi: 10.1016/j.immuni.2022.01.001

9. Mackin SR, Desai P, Whitener BM, Karl CE, Liu M, Baric RS, et al. Fc-γR-dependent antibody effector functions are required for vaccine-mediated protection against antigen-shifted variants of SARS-CoV-2. *Nat Microbiol*. (2023) 8:569–80. doi: 10.1038/s41564-023-01359-1

10. Zheng L, Liu S, Lu F. Impact of National Omicron Outbreak at the end of 2022 on the future outlook of COVID-19 in China. *Emerg Microbes Infect*. (2023) 12:2191738. doi: 10.1080/22221751.2023.2191738

11. Fu D, He G, Li H, Tan H, Ji X, Lin Z, et al. Effectiveness of COVID-19 vaccination against SARS-coV-2 omicron variant infection and symptoms - China, December 2022-February 2023. *China CDC Wkly*. (2023) 5:369–73. doi: 10.46234/ccdcw2023.070

12. Bowman KA, Stein D, Shin S, Ferbas KG, Tobin NH, Mann C, et al. Hybrid immunity shifts the fc-effector quality of SARS-coV-2 mRNA vaccine-induced immunity. *mBio*. (2022) 13:e0164722. doi: 10.1128/mbio.01647-22

13. Jia S, Liu Y, He Q, Pan H, Liang Z, Zhou J, et al. Effectiveness of a booster dose of aerosolized or intramuscular adenovirus type 5 vectored COVID-19 vaccine in adults: a multicenter, partially randomized, platform trial in China. *Nat Commun*. (2025) 16:2969. doi: 10.1038/s41467-025-58327-y

14. Li C, Yu J, Issa R, Wang L, Ning M, Yin S, et al. CoronaVac-induced antibodies that facilitate Fc-mediated neutrophil phagocytosis track with COVID-19 disease resolution. *Emerg Microbes Infect*. (2025) 14:2434567. doi: 10.1080/22221751.2024.2434567

15. Dufloo J, Grzelak L, Staropoli I, Madec Y, Tondeur L, Anna F, et al. Asymptomatic and symptomatic SARS-CoV-2 infections elicit polyfunctional antibodies. *Cell Rep Med*. (2021) 2:100275. doi: 10.1016/j.xcrm.2021.100275

16. Jeyanathan M, Fritz DK, Afkhami S, Aguirre E, Howie KJ, Zganiacz A, et al. Aerosol delivery, but not intramuscular injection, of adenovirus-vectored tuberculosis vaccine induces respiratory-mucosal immunity in humans. *JCI Insight*. (2022) 7(3): e155655. doi: 10.1172/jci.insight.155655

17. Park-Min KH, Serbina NV, Yang W, Ma X, Krystal G, Neel BG, et al. FcgammaRIII-dependent inhibition of interferon-gamma responses mediates suppressive effects of intravenous immune globulin. *Immunity*. (2007) 26:67–78. doi: 10.1016/j.immuni.2006.11.010

18. Zedan HT, Smatti MK, Al-Sadeq DW, Al Khatib HA, Nicolai E, Pieri M, et al. SARS-CoV-2 infection triggers more potent antibody-dependent cellular cytotoxicity (ADCC) responses than mRNA-, vector-, and inactivated virus-based COVID-19 vaccines. *J Med Virol*. (2024) 96:e29527. doi: 10.1002/jmv.29527

19. Izadi A, Nordenfelt P. Protective non-neutralizing SARS-CoV-2 monoclonal antibodies. *Trends Immunol*. (2024) 45:609–24. doi: 10.1016/j.it.2024.06.003

20. Richardson SI, Manamela NP, Motsoeneng BM, Kaldine H, Ayres F, Makhado Z, et al. SARS-CoV-2 Beta and Delta variants trigger Fc effector function with increased cross-reactivity. *Cell Rep Med*. (2022) 3:100510. doi: 10.1016/j.xcrm.2022.100510

21. Amanat F, Thapa M, Lei T, Ahmed SMS, Adelsberg DC, Carreño JM, et al. SARS-CoV-2 mRNA vaccination induces functionally diverse antibodies to NTD, RBD, and S2. *Cell*. (2021) 184:3936–48.e10. doi: 10.1016/j.cell.2021.06.005

22. Kaplonek P, Cizmeci D, Fischinger S, Collier AR, Suscovich T, Linde C, et al. mRNA-1273 and BNT162b2 COVID-19 vaccines elicit antibodies with differences in Fc-mediated effector functions. *Sci Transl Med*. (2022) 14:eabm2311. doi: 10.1126/scitranslmed.abm2311

23. Ullah I, Beaudoin-Bussières G, Symmes K, Cloutier M, Ducas E, Tauzin A, et al. The Fc-effector function of COVID-19 convalescent plasma contributes to SARS-CoV-2 treatment efficacy in mice. *Cell Rep Med*. (2023) 4:100893. doi: 10.1016/j.xcrm.2022.100893

frontiers | Frontiers in Immunology

TYPE Brief Research Report
PUBLISHED 13 October 2025
DOI 10.3389/fimmu.2025.1663819

OPEN ACCESS

EDITED BY
Sonia Jangra,
The Rockefeller University, United States

REVIEWED BY
Roberta Marzi,
Institute for Research in Biomedicine, Spain
Keon-Il Im,
LucasBio, Republic of Korea

*CORRESPONDENCE
Zhen Zeng
zzeng22@jhmi.edu
Joel N. Blankson
jblanks@jhmi.edu

†These authors have contributed equally to this work

‡These authors have contributed equally to this work

RECEIVED 11 July 2025
ACCEPTED 15 September 2025
PUBLISHED 13 October 2025

CITATION
Mercado A, Sop J, Amanat S, Zhang L, Chida NM, Basseth CR, Gebo KA, Antar AAR, Smith KN, Zeng Z and Blankson JN (2025) SARS-CoV-2 vaccines induce a diverse spike-specific CD4+ T cell receptor repertoire in people living with HIV with low CD4 nadirs.
Front. Immunol. 16:1663819.
doi: 10.3389/fimmu.2025.1663819

SARS-CoV-2 vaccines induce a diverse spike-specific CD4+ T cell receptor repertoire in people living with HIV with low CD4 nadirs

Alicia Mercado[1†], Joel Sop[1†], Steven Amanat[2,3†], Li Zhang[2,3], Natasha M. Chida[1], Christie R. Basseth[1], Kelly A. Gebo[1], Annukka A. R. Antar[1], Kellie N. Smith[2,3], Zhen Zeng[2,3*‡] and Joel N. Blankson[1,4*‡]

[1]Department of Medicine, Johns Hopkins Medicine, Baltimore, MD, United States, [2]Bloomberg~Kimmel Institute for Cancer Immunotherapy, Johns Hopkins Medicine, Baltimore, MD, United States, [3]Sidney Kimmel Comprehensive Cancer Center, Johns Hopkins Medicine, Baltimore, MD, United States, [4]Department of Molecular and Comparative Pathobiology, Johns Hopkins Medicine, Baltimore, MD, United States

People living with HIV with low CD4 T cell nadirs on antiretroviral therapy have suboptimal responses to immunization. We analyzed the SARS-CoV-2 spike-specific CD4+ T cell repertoire in individuals with CD4 nadirs of less than 100 cells/ul who received a primary SARS-CoV-2 mRNA vaccine series as well as the bivalent ancestral/BA.5 spike mRNA vaccine. We tested the hypothesis that antigenic imprinting would result in the preferential expansion of pre-existing cross-reactive T cells that were primed against the 4 common cold coronaviruses. We found that these individuals made robust effector and memory T cell responses to the SARS-CoV-2 spike protein that exceeded the responses to spike proteins from the common cold coronaviruses. Furthermore, in 4 individuals, the number of SARS-CoV-2 specific TCRs far exceeded the number of common cold coronavirus-specific T cell receptors. TCRs that were cross-reactive for common cold coronaviruses and SARS-CoV-2 comprised less than 10% of the total detected SARS-CoV-2 specific T cells. The diversity of the SARS-CoV-2 spike-specific repertoire in 6 study participants was comparable to that of the repertoire in vaccinated HIV healthy donors. Our data suggests people living with HIV with low CD4 nadirs can have significant functional immune reconstitution with little evidence of antigenic imprinting due to pre-existing T cell responses to common cold coronaviruses.

KEYWORDS

CD4 T cell, SARS-CoV-2, HIV, T cell receptor (TCR), common cold coronaviruses

Introduction

People living with HIV (PLWH) with low CD4 nadirs have limited responses to immunization with antigens and some vaccines (1, 2). Lange et al. found that the CD4 nadir predicted T cell responses to immunization with tetanus toxoid, diphtheria-toxoid, and keyhole limpet hemocyanin in PLWH on antiretroviral therapy (1). Similarly, Tebas et al. found that PLWH with low CD4 nadirs on antiretroviral therapy were less likely to respond to an H1N1 vaccine (2). The mechanisms responsible for this are unknown but disruptions in the T cell receptor (TCR) repertoire that are not fully restored with antiretroviral therapy have been reported in these individuals (3). The presence of a restricted naïve TCR repertoire could potentially lead to the phenomenon of antigenic imprinting which is also called the original antigenic sin. The latter term was coined by Thomas Francis in 1960 to describe the observation that infection with a new strain of Influenza boosted the antibody responses against strains of the virus that an individual had been previously exposed to (4). A similar phenomenon has been observed with T cell responses (5), and recent observations suggest that in some cases, the expansion of pre-existing cross-reactive responses can come at the expense of the development of mono-reactive responses. This is important as mono-reactive T cells may have higher affinity for the novel antigen they are primed against (6, 7). Many studies have shown some degree of pre-existing T cell immunity to SARS-CoV-2 due to cross recognition of SARS-CoV-2 by T cells that were primed against the 4 common-cold coronaviruses (8). In this study we tested the hypothesis that patients with low CD4 nadirs with variable degrees of immune reconstitution on antiretroviral therapy would show evidence of antigenic imprinting and thus would not have a robust mono-reactive T cell response to immunization with SARS-CoV-2 mRNA vaccines. We achieved this by using the functional expansion of specific T cells (FEST) assay to compare the T cell receptor repertoire after stimulating peripheral blood mononuclear cells (PBMCs) with spike protein from SARS-CoV-2 or the 4 common cold coronaviruses (7–12). This assay sequences the CDR3 region of the beta chain of the T cell receptor (TCR) of cells that have been cultured with antigens and therefore can identify expanded antigen-specific clones (13, 14). It can also distinguish between TCRs that cross-recognize SARS-CoV-2 and common cold coronavirus spike proteins versus those that are mono-reactive for a specific spike protein (7). Our data suggest that the SARS-CoV-2 specific T cell response in PLWH with low CD4 nadirs was mostly mono-reactive in nature. Thus, antigenic imprinting does not appear to play a major role in the T cell responses to SARS-CoV-2 in these patients.

Methods

Study participants

The study was approved by the Johns Hopkins University Institutional Review Board. Written informed consent was obtained from all participants prior to their inclusion in the study. The clinical characteristics of the study participants studied are summarized in Supplementary Table 1. The healthy donors were described in a prior study (11). Blood for the initial SARS-CoV-2 ELISpot and FEST assays was drawn a median of 189 days after receipt of the bivalent ancestral spike/BA.5 spike mRNA vaccine (range 127–278 days) and the participants had a median age of 45 years (range 29–57 years). The PLWH had blood drawn a median of 174 days post vaccination (range 54 to 307 days) and had a median age of 55 years (range 37 to 63 years). The median CD4 nadir was 36 cells/ul (range 1-90). One study participant (CP100) had a CD4 nadir of 2 cells/ul and prolonged SARS CoV-2 shedding prior to initiating ART (15). For the SARS-CoV2 and common cold coronavirus FEST assays, blood was obtained a median of 436 days after the bivalent ancestral spike/BA.5 spike mRNA vaccine was given (range 426–487 days, Supplementary Table 2). CP100, had also received the monovalent XBB1.5 vaccine 106 days prior to the blood draw.

Serology

Multi-array electrochemiluminescence detection technology from MesoScale Diagnostics V-Plex SARS-CoV-2 Panel 31 were used to evaluate IgG binding antibodies to SARS-CoV-2 spike protein in a prior study (11). PLWH with low CD4 nadirs were also tested for antibodies against HCoV-NL63, HCoV-OC43, HCoV-229E, and HCoV-HKU1. Antibody responses were evaluated using ELISA kits purchased from Alpha Diagnostics International following the manufacturer's instructions as previously described (9).

Peptides and ELISpot assays

The ELISpot data in Figure 1A were previously obtained (11). The SARS-CoV2 ancestral spike peptide pool consisted of a pool of 315 peptides derived from 15 mers with 11 amino acid overlaps obtained from JPT Peptide Technologies. Peptide pools for the spike proteins of HCoV-NL63, HCoV-229E, HCoV-OC43, and SARS-Cov-2, shown in Figure 1B were obtained from BEI Resources and were reconstituted with DMSO at a concentration of 10 mg/mL. The HCoV-229E S protein peptide pool has 195 peptides consisting of 17 mer with 11 amino acid overlaps. The HCoV-NL63 S protein peptide pool has 226 peptides made up of 14–17 mer with 11–13 amino acid overlaps. The HCoV-OC43 S protein peptide pool has 226 peptides made up of 17 or 18 mer with 11 amino acid overlaps. The SARS-CoV-2 peptides are 12 mer, 13 mer, or 17 mer, with 10 amino acid overlaps. IFN-γ ELISpot assays were performed as previously described (11). Briefly ELISpot Pro and ELISpot Plus kits with precoated plates were purchased from Mabtech. The wells were plated with unfractionated PBMCs or CD8 + T cell–depleted PBMCs at 130,000-250,000 cells/well, and the cells were cultured for 20 hours with HCoV peptides at a concentration of 1 μg/mL. The plates were then processed according to the manufacturer's protocol and read by a blinded independent investigator using an automated reading system.

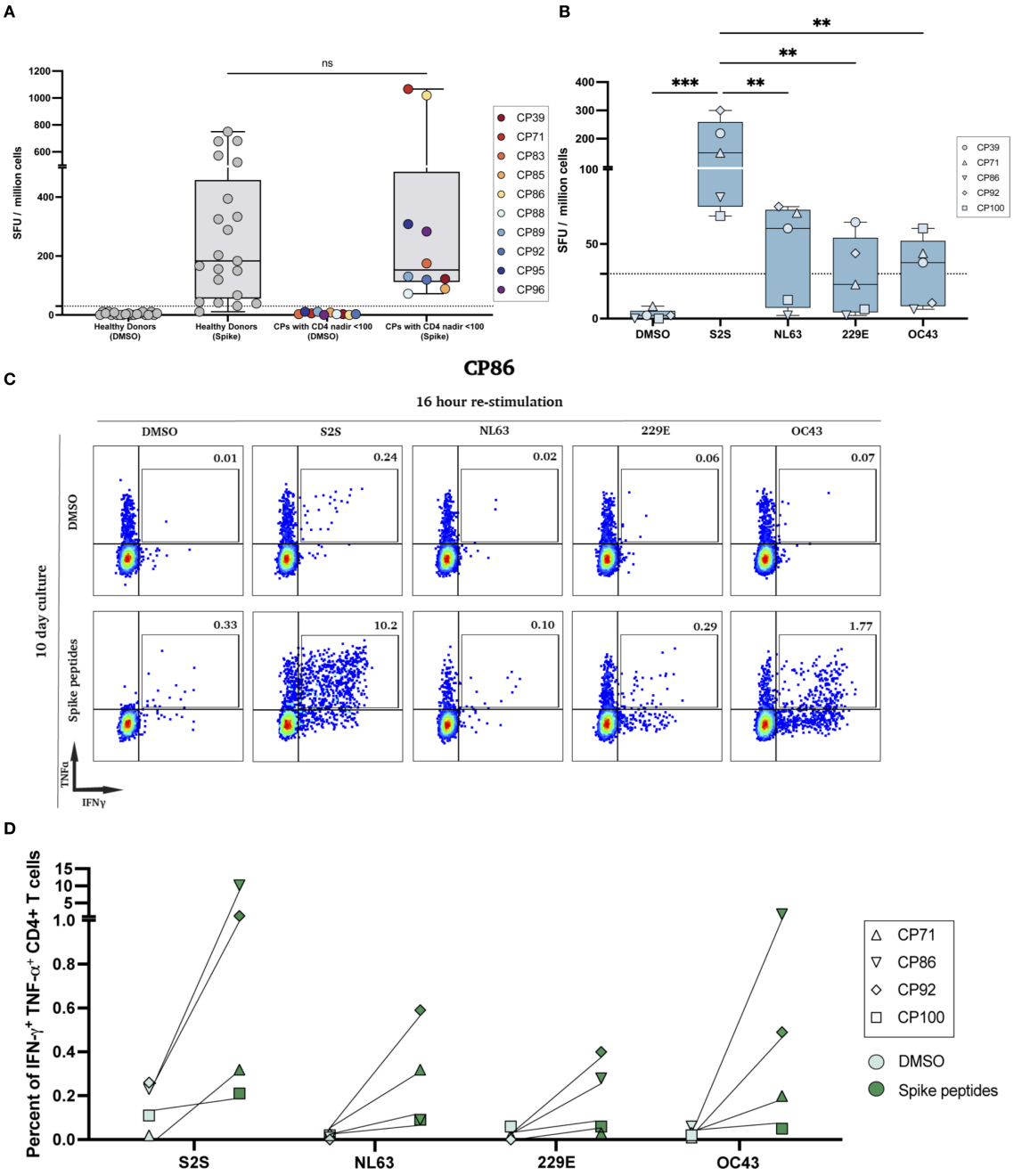

FIGURE 1
SARS-CoV-2 ELISpot responses and polyfunctional responses after peptide expansion. **(A)** IFN-γ ELISpot with the SARS-CoV-2 spike peptide pool (S2S) on PBMCs from HIV-seronegative donors and PLWH with historical CD4 nadir <100; DMSO controls shown for each cohort (ns, not significant). **(B)** Low-nadir CP IFN-γ ELISpot responses to DMSO, S2S, and common-cold coronavirus pools (HCoV-NL63, -229E, -OC43). (**p<0.01, ***p<0.001). **(C)** Representative flow cytometry plots for CP86. Day-10 spike-expanded $CD4^+$ T-cells were re-stimulated for 16 hours with DMSO (top row) or the indicated peptide pools (bottom row); numbers indicate % IFN-γ^+TNF-α^+ of $CD4^+$ T cells. **(D)** Quantification of IFN-γ^+TNF-α^+ $CD4^+$ T cells across low-nadir CPs after 7-day (CP71, CP100) or 10-day (CP86, CP92) culture with each peptide pool vs DMSO. Each pair represents the same participant; lines connect paired conditions.

Expansion culture assay

PBMCs were cultured in RPMI with 10% fetal calf serum with 10 U/mL IL-2 and raltegravir (4uM) and 1 µg/mL of peptide pools or DMSO for either 7 (CP71, CP100) or 10 days (CP86, CP92) as previously described (9). Half of the media was removed and replaced with fresh media with 10 U/ml IL2 on day 3 and day 7. The cells were then washed and replated in fresh media and rested for 6 hours before they were stimulated again with 5 µg/mL of either the same peptide pool or DMSO with protein transport inhibitors (GolgiPlug, 1 µg/mL; GolgiStop, 0.7 µg/mL) and 1ug/ml of antibodies against CD28 and CD49d (all from BD Biosciences).

After a 16-hour incubation, the cells were washed and stained with antibodies against CD3 (APC-Cy-7, BioLegend), and CD4 (PerCP-CY-5.5, BioLegend). The cells were then fixed, permeabilized, and stained intracellularly for TNF-α (PE-Cy-7, BD Biosciences, 557647) and IFN-γ (APC, BD Biosciences).

FEST assay

The FEST assay utilized ancestral SARS-CoV-2, HCoV-NL63, HCoV-229E and HCoV-OC43 spike peptide pools from BEI resources (NIAID, NIH) as well as HCoV-HKU1 spike peptides from JPT Peptide Technologies (Berlin, Germany), to activate CD8 + T cell-depleted PBMCs from the 4 participants as previously described. One participant, CP88, had 2 assays performed. One with SARS-CoV-2, HCoV-NL63, HCoV-229E and HCoV-OC43 spike peptides, and another with SARS-CoV-2 and HCoV-HKU1 spike peptides alone. All peptide pools were used at a concentration of 1 ug/ml. On day 10, cells were harvested, and DNA was extracted using the QIAmp micro-DNA kit (QIAGEN). TCR-Seq was conducted at the Johns Hopkins FEST and TCR Immunogenomics Core Facility (FTIC) using the Ampliseq TCR Beta Short-Read Assay, sequenced on the Illumina sequencer platform (iSeq100, MiSeq and NextSeq1000) with unique dual indexes as previously described (7). Data was uploaded to the MANAFEST analysis tool (http://www.stat-apps.onc.jhmi.edu/FEST/) to identify antigen-specific T cell clonotypes. Positive responses were required to have a mean frequency of greater than 0.1% in at least two replicates, with at least a 5-fold increase over the DMSO controls. Mono-reactive responses were identified if these criteria were met and the mean frequency was 5-fold higher than responses to other spike proteins. Individual receptors analyzed are detailed in Supplementary Table 3.

Spike-specific repertoire diversity

From the three replicate experiments performed for each patient in the FEST assay, frequencies of spike-specific clonotypes were normalized to the spike-specific subset. Shannon's diversity index (log2 base) was calculated for each individual replicate of each patient. Then, the indices for each patient were averaged and the patient groups were compared using the Mann-Whitney U test. $P < 0.05$ was considered statistically significant. It is noted that Shannon's diversity index is a metric conventionally used for entire TCR repertoires, while it is used here to compare antigen-specific subsets.

Levenshtein distances for sequence homology

The spike-specific TCR sequences for the two patient groups were pooled together to assess homology across groups. To obtain the non-redundant region of the TCR sequences, the first three and last three amino acids were removed from the TCR Vβ CDR3 sequence. Then, the Levenshtein distances were computed for every pair of TCR sequences across the pooled dataset using the stringdist R package (16). An unrooted phylogenetic tree was generated to visualize sequence homology using the ape R package, with each leaf representing a TCR Vβ CDR3 sequence (17). From the overall tree, branches were manually selected by node number and visualized as heatmaps using the pheatmap R package (18). In the heatmaps, each row represented a TCR Vβ CDR3 sequence and the color scale was fixed across maps. All analyses were performed using R version 4.4.2.

Results

PLWH with low CD4 nadirs have robust SARS-CoV-2-specific effector and memory T cell responses

In a prior study, we used the IFN-γ ELISpot assay to measure the frequency of ancestral SARS-CoV-2 spike-specific effector T cell responses in PLWH and healthy donors after they received the bivalent ancestral/BA.5 spike mRNA vaccine (11). As shown in Figure 1A, there was no significant difference in the frequency of effector T cells in the 2 groups of study participants. In order to compare the frequency of effector T cells that recognized spike peptides from SARS-CoV-2 versus 3 of the 4 common cold coronaviruses, we again performed an ELISpot assay. As shown in Figure 1B, the frequency of ancestral SARS-CoV-2 spike peptide-specific T cells was significantly higher than the frequency of T cells specific for spike peptides from HCoV-OC43, HCoV-NL63, and HCoV-229E.

To determine the frequency of memory T cells that recognized the spike peptides from each virus, we performed an expansion assay where PBMCs were cultured with either DMSO or spike peptide pools from each virus for 7 to 10 days and then restimulated the cells for 16 hours with the same peptide pool. As shown for CP86 in Figure 1C, there was an expansion of SARS-CoV-2 and HCoV-OC43 spike-specific memory CD4+ T cells that co-expressed IFN-γ and TNF-α. However, the frequency of the SARS-CoV-2 specific memory cells was 5-fold greater. In all 4 participants tested, the frequency of SARS-CoV-2 spike-specific memory CD4+ T cells was higher than the frequency of memory CD4+ T cells specific for the common cold coronavirus spike peptides (Figure 1D).

The number of detected TCRs specific for SARS-CoV-2 greatly exceeds the number of TCRs specific for the common cold coronavirus in PLWH with low CD4 nadirs

The ELISpot and expansion assays measure the frequency of the antigen-specific T cells but not the breadth of the response. In order to measure this parameter, we performed the FEST assay to

determine the breadth of TCRs that were specific for spike proteins from SARS-CoV-2 versus the common cold coronaviruses. As seen in Figure 2, the number of total SARS-CoV-2 specific TCRs detected ranged from 82 to 115 TCRs with a median of 100.5 TCRs. In contrast, the numbers of TCRs specific for each of the common cold coronaviruses detected ranged from 7 to 54 TCRs with a median of 14 TCRs for HCoV-NL63, 3 to 13 TCRs with a median of 8.5 TCRs for HCoV-229E, 5 to 29 TCRs with a median of 11 TCRs for HCoV-OC43, and 6 to 28 TCRs with a median of 19.5 TCRs for HCoV-HKU1.

The percentage of SARS-CoV-2 spike mono-reactive TCRs greatly exceeds those of SARS-CoV-2 and common cold coronavirus cross-reactive TCRs

Functional assays cannot distinguish between individual T cells with receptors that cross-recognize different antigens versus separate populations of T cells that recognize each antigen. Thus, we used the FEST assay to determine the frequency of TCRs that cross-recognized spike peptides from SARS-CoV-2 and the common cold coronaviruses. We identified TCRs that recognized SARS-CoV-2 spike alone and others that cross-recognized SARS-CoV-2 and common cold coronavirus spike peptides in each participant. Three representative mono-reactive and cross-reactive TCRs are each shown for CP100 in Figure 3A. Across all 4 participants, the percentage of mono-reactive TCRs (median of 96.4%, range from 90.1% to 97.4%) greatly exceeded that of cross-reactive TCRs (median of 4.5% range from 2.6% to 9.9%) (Figure 3B). Of the cross-reactive TCRs specific for SARS-CoV-2 and at least 1 common cold coronavirus, the majority cross-recognized SARS-CoV-2 and HKU1 spike peptides (Supplementary Figure 2). There were a few TCRs that cross-recognized spike peptides from SARS-CoV-2 and 2 or more common cold coronaviruses (Supplementary Figure 2).

Diversity of the SARS-CoV-2 spike-specific TCRs is similar to that seen in vaccinated healthy donors

In order to determine whether the total TCR diversity was different in healthy donors versus PLWH with low CD4 nadirs, we analyzed the CD4 TCR repertoire from 5 age matched individuals from each group and analyzed the CD4+ TCR repertoire. Diversity was measured with the Shannon index. As shown in Figure 4A, the TCR repertoire from healthy donors was more diverse than TCR

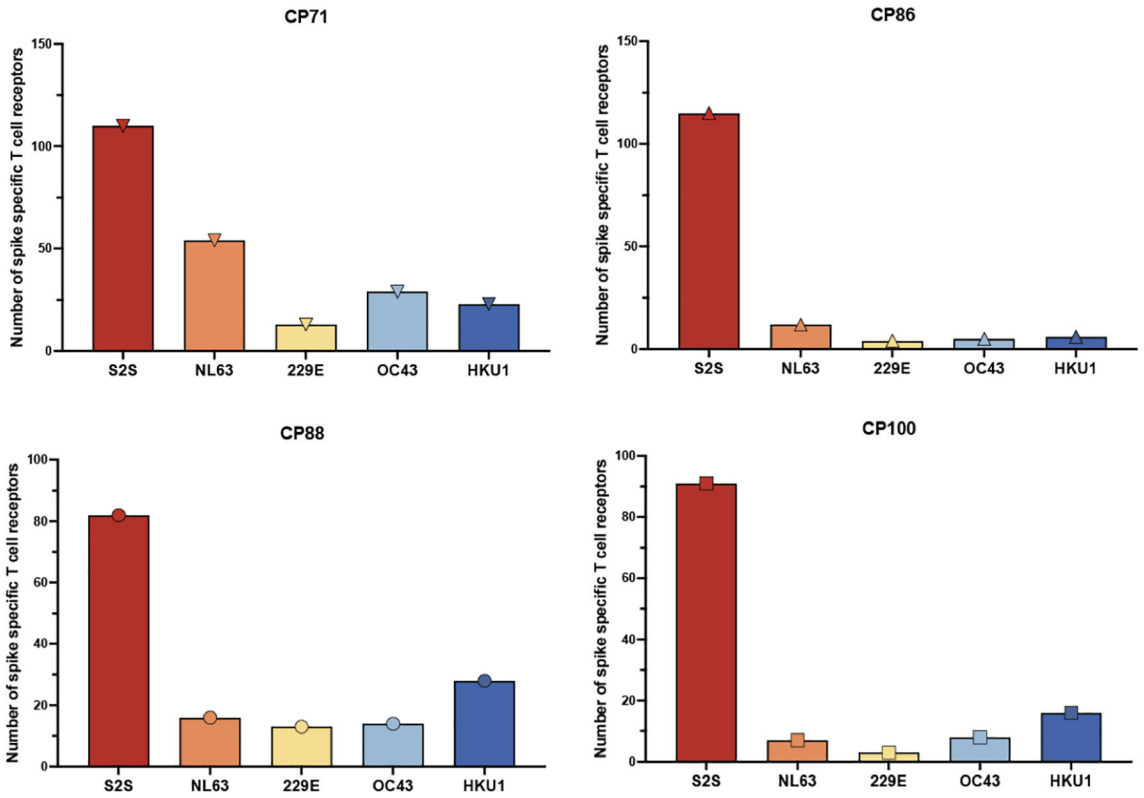

FIGURE 2
Frequency of spike-specific CD4$^+$ T cell receptors recognizing SARS-CoV-2 and common cold coronavirus peptides. The total number of spike-specific CD4$^+$ TCR clonotypes identified by the FEST assay is shown for four CPs with low CD4 nadirs. TCRs were classified based on their expansion following stimulation with spike peptide pools derived from SARS-CoV-2 (S2S) or common cold human coronaviruses HCoV-NL63, HCoV-229E, HCoV-OC43, and HCoV-HKU1. Each bar represents the total number of unique spike-specific TCRs detected per condition, with error bars indicating standard deviation across three technical replicates.

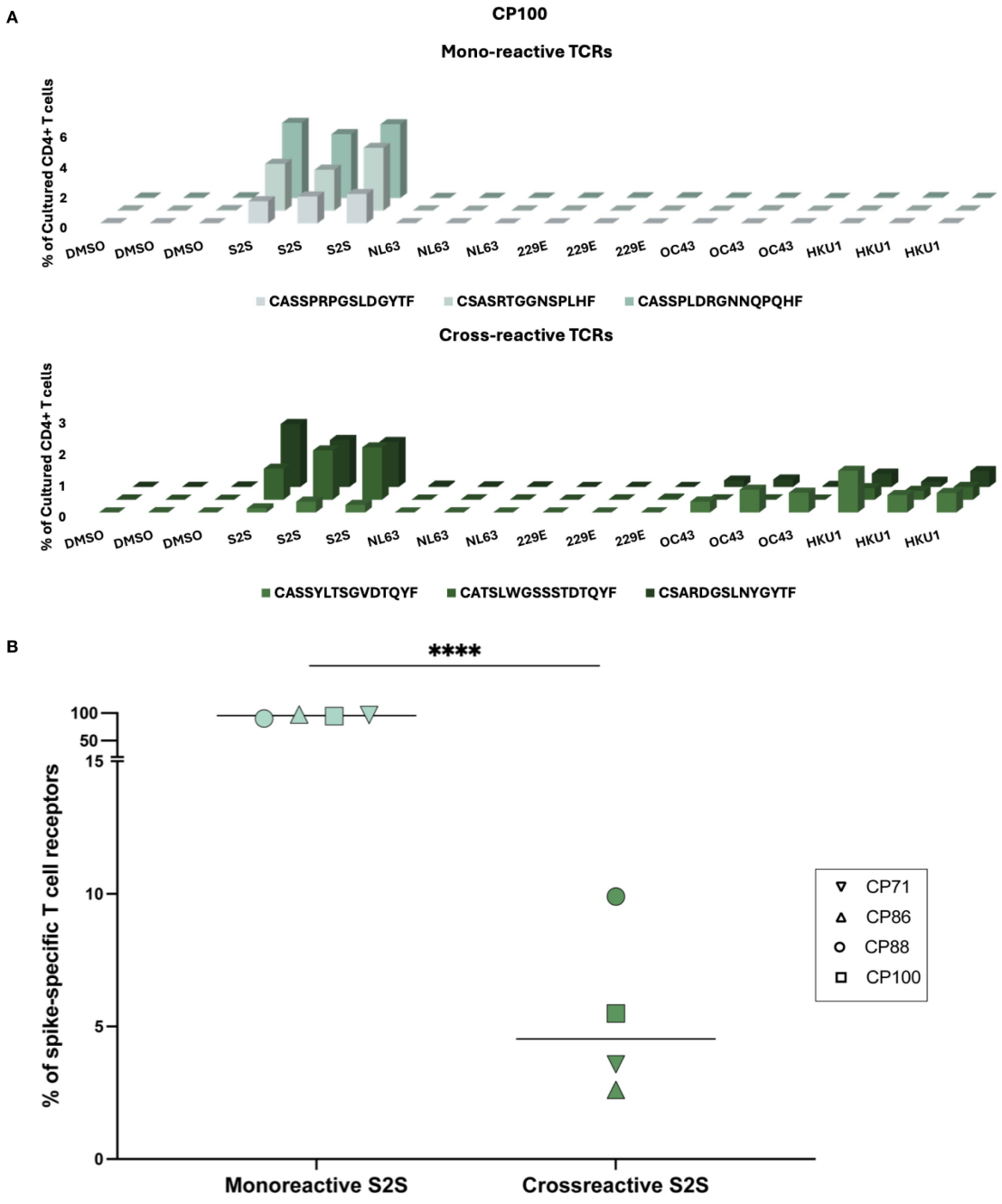

FIGURE 3
Cross-reactivity of spike-specific CD4$^+$ TCRs following in vitro peptide stimulation. **(A)** Representative expansion profiles of three mono-reactive (CASSPRPGSLDGYTF, CSASRTGGNSPLHF, CASSPLDRGNNQPQHF) and three cross-reactive (CASSYLTSGVDTQYF, CATSLWGSSSTDTQYF, CSARDGSLNYGYTF) CD4$^+$ TCR clonotypes from participant CP100. TCRs were identified using the FEST assay. The frequencies (% of cultured CD4$^+$ T cells, y-axis) of distinct TCR clonotypes (z-axis) across peptide conditions (x-axis), including SARS-CoV-2 spike (S2S) and common cold coronavirus (HCoV-NL63, HCoV- 229E, HCoV-OC43, HCoV-HKU1) peptide pools. Three technical replicates were performed for each condition. **(B)** Quantification of the proportion of mono-reactive versus cross-reactive S2S-specific CD4$^+$ TCR clonotypes for four CPs. Horizontal lines indicate group medians. Mono-reactive TCRs were defined as those expanding only in response to S2S peptides, while cross-reactive TCRs expanded to both S2S and at least one common cold coronavirus peptide pool. ****$p < 0.0001$.

repertoire from the PLWH with low CD4 nadirs. There was no correlation between either the nadir or current CD4 count and the Shannon Index (Supplementary Figure 3A).

To investigate whether the spike-specific TCR repertoire was also different in the 2 groups of participants, we compared the previously described SARS-CoV-2 spike-specific T cell repertoire in 4 PLWH with low CD4 nadirs (CP88, CP89, CP100, CP104) and 10 healthy donors who received bivalent ancestral/BA.5 spike COVID mRNA vaccines (11). We also analyzed the spike-specific T cell repertoire from 2 PLWH with low CD4 nadirs in the current study (CP71 and CP86). We found there were no significant differences in the diversity of the spike-specific TCR repertoire in PLWH with low CD4 nadirs and healthy donors (Figure 4B). Furthermore, in a prior study of healthy donors, we showed that SARS-CoV-2 spike-specific TCRs share sequence homology within and among participants. We performed a similar analysis and showed that there was significant homology of spike-specific TCRs in patients with low CD4 nadirs and healthy donors (Figure 4C). There was no correlation between either the nadir or current CD4 counts and the Shannon Index (Supplementary Figure 3B).

Discussion

In this study, we analyzed TCRs specific for SARS-CoV-2 and the 4 common cold coronaviruses spike proteins in PLWH with low

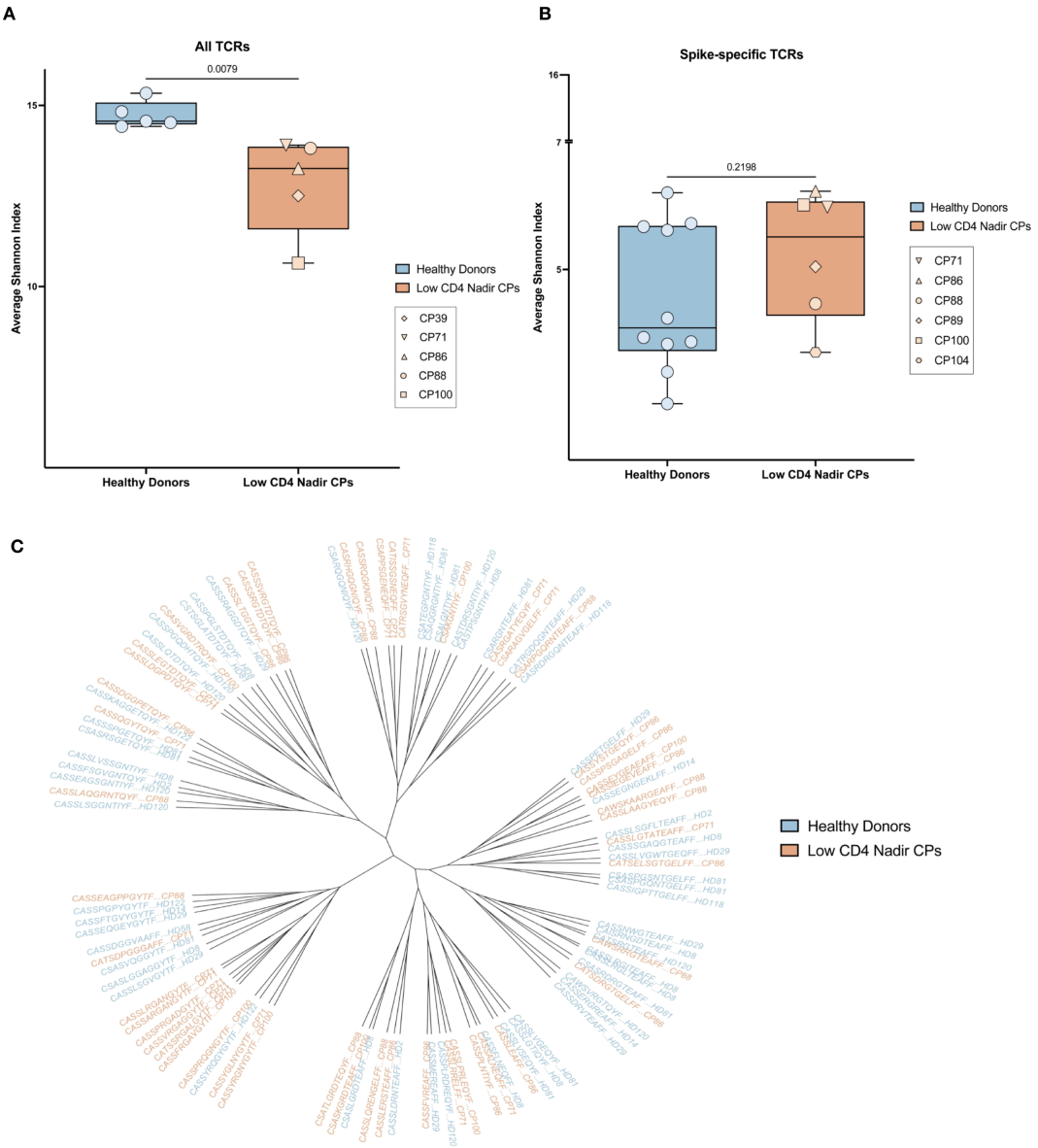

FIGURE 4
Diversity and sequence homology of T receptors. **(A)** Shannon index of the diversity of all TCRs from PLWH with low CD4 nadirs (orange) and HIV seronegative donors (blue). **(B)** Shannon index of the diversity of SARS-CoV-2-specific TCRs from PLWH with low CD4 nadirs (orange) and HIV seronegative donors (blue). **(C)** Phylogenetic tree showing SARS-CoV-2-specific TCRs from PLWH with low CD4 nadirs (orange) and HIV seronegative donors (blue).

CD4 nadirs who had received monovalent and bivalent COVID mRNA vaccines. These individuals responded well to vaccination with antibody titers and CD4+ T cell responses that were similar to healthy donors. The frequencies of SARS-CoV-2 spike-specific effector and memory T cells in these individuals exceeded the frequencies of effector and memory T cells that recognized spike peptides from common cold coronaviruses. We used the FEST assay to distinguish between TCRs that were mono-reactive for SARS CoV-2 versus those that cross-recognized spike proteins from common cold coronaviruses. We previously validated the FEST assay by transferring cloned TCRs into Jurkat cells and demonstrated that TCRs that were identified as cross-reactive in the FEST assay recognized spike peptides from SARS-CoV-2 and HCoV-NL63, whereas TCRs that were identified as being mono-reactive only recognized spike peptides from SARS-CoV-2 (7).

Disruptions of the TCR repertoire in PLWH with low CD4 nadirs are not completely reversed with antiretroviral therapy (3). This could explain the suboptimal responses to immunization that are generally seen in these individuals (1, 2). A skewed TCR repertoire could potentially lead to antigenic imprinting where there is preferential expansion of pre-existing, cross-reactive T cells. This would be pertinent in recipients of COVID vaccines as cross-reactive TCRs have a lower functional avidity for SARS-CoV-2 spike peptides than mono-reactive T cells (6, 7). We reasoned that if antigenic imprinting was occurring in these patients, the spike-specific T cell response would consist predominantly of TCRs primed against the common cold coronaviruses that cross-reacted with SARS-CoV-2. Instead, we found that in all 4 individuals we analyzed, more than 90% of the total SARS-CoV-2 spike specific TCRs were mono-reactive for SARS-CoV-2. We found a similar phenomenon in healthy donors who were vaccinated after experiencing natural infection in a prior study (10), and here we show that in spite of lower total TCR diversity, the diversity of the spike-specific TCR repertoire in the PLWH with low CD4 nadirs we analyzed is comparable to that of healthy donors. Furthermore, we demonstrated that SARS-CoV-2 spike-specific TCRs share sequence homology within and among healthy donors and PLWH with low CD4 nadirs suggesting similar immune responses in these individuals.

Our study is limited by sample size. We evaluated 4 participants with low CD4 nadirs for cross-reactive TCRs, however, we analyzed large numbers of TCRs for each participant, and we saw the same dramatic finding in each of the 4 participants. It is possible that our assay may not detect low frequency clones that could potentially have been cross-reactive. Our diversity analysis is limited by the fact the PLWH with low CD4 nadirs were older and 2 of the 6 individuals were further removed from the time of vaccination compared to the healthy donors. In spite of this, we saw comparable levels of diversity. Interestingly, there appeared to be lower diversity in the SARS-CoV-2 spike specific T cell responses in a subset of the healthy donors, but larger studies will be needed to confirm this finding. Our results suggest that in spite of having CD4 nadirs as low as 2 cells/ul, PLWH can make robust T cell responses in response to SARS-CoV-2 vaccination that are not due to an expansion of pre-existing cross-reactive TCRs. The high titer of SARS-CoV-2 spike-specific antibodies seen in these individuals is most likely a manifestation of this robust functional CD4+ T cell immune reconstitution. CP100, who had undetectable SARS-CoV-2 specific antibodies despite receiving the first dose of the primary mRNA vaccine series and having prolonged SARS-CoV-2 shedding when he had a CD4 count of 2 cells/ul (15), seroconverted after initiating ART and receiving subsequent mRNA vaccine doses. It will be important to analyze TCR repertoire responses to other vaccines in these participants to determine whether this phenomenon is unique to COVID mRNA vaccine induced T cell responses.

Data availability statement

The original contributions presented in the study are publicly available. This data can be found here: https://doi.org/10.6084/m9.figshare.c.8075320.v1.

Ethics statement

The studies involving humans were approved by JHU Institutional Review Board. The studies were conducted in accordance with the local legislation and institutional requirements. The participants provided their written informed consent to participate in this study.

Author contributions

AM: Writing – review & editing. JS: Writing – review & editing. SA: Writing – review & editing. LZ: Writing – review & editing. NC: Writing – review & editing. CB: Visualization, Writing – review & editing. KG: Writing – review & editing. AA: Writing – review & editing. KS: Writing – review & editing. ZZ: Writing – review & editing. JB: Conceptualization, Writing – original draft.

Funding

The author(s) declare financial support was received for the research and/or publication of this article. JB is supported by NIH grant R21AI172542 and the Johns Hopkins University CFAR (P30AI094189). AM was supported by R25 GM109441 granted to the Post-baccalaureate Research Education Program at Johns Hopkins. JS is supported by the Vivien Thomas Scholars Initiative. SA, KS, and ZZ are supported by the Bloomberg Kimmel Institute for Cancer Immunotherapy, Mark Foundation for Cancer Research, and Cancer Research Institute.

Acknowledgments

We deeply thank the study participants for their commitment in volunteering in this study.

Conflict of interest

The authors declare that the research was conducted in the absence of any commercial or financial relationships that could be construed as a potential conflict of interest.

Generative AI statement

The author(s) declare that no Generative AI was used in the creation of this manuscript.

Any alternative text (alt text) provided alongside figures in this article has been generated by Frontiers with the support of artificial intelligence and reasonable efforts have been made to ensure accuracy, including review by the authors wherever possible. If you identify any issues, please contact us.

Publisher's note

Supplementary material

The Supplementary Material for this article can be found online at: https://www.frontiersin.org/articles/10.3389/fimmu.2025.1663819/full#supplementary-material

References

1. Lange CG, Lederman MM, Medvik K, Asaad R, Wild M, Kalayjian R, et al. Nadir CD4+ T-cell count and numbers of CD28+ CD4+ T-cells predict functional responses to immunizations in chronic HIV-1 infection. *AIDS*. (2003) 17:2015–23. doi: 10.1097/00002030-200309260-00002

2. Tebas P, Frank I, Lewis M, Quinn J, Zifchak L, Thomas A, et al. Poor immunogenicity of the H1N1–2009 vaccine in well controlled HIV-infected individuals. *AIDS*. (2010) 24:2187–92. doi: 10.1097/QAD.0b013e32833c6d5c

3. Connors M, Kovacs JA, Krevat S, Gea-Banacloche JC, Sneller MC, Flanigan M, et al. HIV infection induces changes in CD4+ T-cell phenotype and depletions within the CD4+ T-cell repertoire that are not immediately restored by antiviral or immune-based therapies. *Nat Med*. (1997) 3:533–40. doi: 10.1038/nm0597-533

4. Francis T. On the doctrine of original antigenic sin. *Proc Am Philos Soc*. (1960) 104:572–8.

5. Good MF, Zevering Y, Currier J, Bilsborough J. 'Original antigenic sin', T cell memory, and malaria sporozoite immunity: an hypothesis for immune evasion. *Parasite Immunol*. (1993) 15:187–93. doi: 10.1111/j.1365-3024.1993.tb00599.x

6. Bacher P, Rosati E, Esser D, Martini GR, Saggau C, Schiminsky E, et al. Low-avidity CD4+ T cell responses to SARS-coV-2 in unexposed individuals and humans with severe COVID-19. *Immunity*. (2020) 53:1258–71. doi: 10.1016/j.immuni.2020.11.016

7. Dykema AG, Zhang B, Woldemeskel BA, Garliss CC, Cheung LS, Choudhury D, et al. Functional characterization of CD4+ T cell receptors crossreactive for SARS-CoV-2 and endemic coronaviruses. *J Clin Invest*. (2021) 131:e146922. doi: 10.1172/JCI146922

8. Sette A, Crotty S. Pre-existing immunity to SARS-CoV-2: the knowns and unknowns. *Nat Rev Immunol*. (2020) 20:457–8. doi: 10.1038/s41577-020-0389-z

9. Woldemeskel BA, Dykema AG, Garliss CC, Cherfils S, Smith KN, Blankson JN. CD4+ T cells from COVID-19 mRNA vaccine recipients recognize a conserved epitope present in diverse coronaviruses. *J Clin Invest*. (2022) 132:e156083. doi: 10.1172/JCI156083

10. Dykema AG, Zhang B, Woldemeskel BA, Garliss CC, Rashid R, Westlake T, et al. SARS-CoV-2 vaccination diversifies the CD4+ spike-reactive T cell repertoire in patients with prior SARS-CoV-2 infection. *EBioMedicine*. (2022) 80:104048. doi: 10.1016/j.ebiom.2022.104048

11. Sop J, Traut CC, Dykema AG, Hunt JH, Beckey TP, Basseth CR, et al. Bivalent mRNA COVID vaccines elicit predominantly cross-reactive CD4+ T cell clonotypes. *Cell Rep Med*. (2024) 5:101442. doi: 10.1016/j.xcrm.2024.101442

12. Sop J, Mercado A, Figueroa A, Beckey TP, Traut CC, Zhang L, et al. The XBB.1.5 mRNA booster vaccine does not significantly increase the percentage of XBB.1.5 mono-reactive T cells. *Front Immunol*. (2025) 16:1513175. doi: 10.3389/fimmu.2025.1513175

13. Danilova L, Anagnostou V, Caushi JX, Sidhom JW, Guo H, Chan HY, et al. The mutation-associated neoantigen functional expansion of specific T cells (MANAFEST) assay: A sensitive platform for monitoring antitumor immunity. *Cancer Immunol Res*. (2018) 6:888–99. doi: 10.1158/2326-6066.CIR-18-0129

14. Caushi JX, Zhang J, Ji Z, Vaghasia A, Zhang B, Hsiue EH, et al. Transcriptional programs of neoantigen-specific TIL in anti-PD-1-treated lung cancers. *Nature*. (2021) 596:126–32. doi: 10.1038/s41586-021-03752-4

15. Peters JL, Fall A, Langerman SD, El Asmar M, Nakazawa M, Mustapha A, et al. Prolonged severe acute respiratory syndrome coronavirus 2 delta variant shedding in a patient with AIDS: case report and review of the literature. *Open Forum Infect Dis*. (2022) 9:ofac479. doi: 10.1093/ofid/ofac479

16. van der Loo M. The stringdist package for approximate string matching. *R J*. (2014) 6:111–22. doi: 10.32614/RJ-2014-011

17. Paradis E, Schliep K. ape 5.0: an environment for modern phylogenetics and evolutionary analyses in R. *Bioinformatics*. (2019) 35:526–8. doi: 10.1093/bioinformatics/bty633

18. Kolde R. pheatmap: pretty heatmaps. In: *R package version 1.0.13*. (2025). doi: 10.32614/CRAN.package.pheatmap

Frontiers in Immunology

Explores novel approaches and diagnoses to treat immune disorders.

The official journal of the International Union of Immunological Societies (IUIS) and the most cited in its field, leading the way for research across basic, translational and clinical immunology.

Discover the latest Research Topics

See more →

Frontiers

Avenue du Tribunal-Fédéral 34
1005 Lausanne, Switzerland
frontiersin.org

Contact us

+41 (0)21 510 17 00
frontiersin.org/about/contact